Instytut Paleobiologii Polskiej Akademii Nauk

OSTEOLOGY, LIFESTYLE, AND BIOMECHANICS OF THE TRIASSIC ARCHOSAUROMORPH *TANYSTROPHEUS* FROM MIEDARY

Osteologia, tryb życia i biomotoryka triasowego archozauromorfa *Tanystropheus* z Miedar

Adam Aleksander Rytel

Dissertation for the degree of PhD at the Institute of Paleobiology, Polish Academy of Sciences. The research was conducted under the supervision of dr hab. Tomasz Sulej, prof. IPal PAS, and dr Mateusz Tałanda (University of Warsaw)

Rozprawa doktorska wykonana w Instytucie Paleobiologii PAN pod kierunkiem Dra hab. Tomasza Suleja, prof. IPal PAN, oraz Dra Mateusza Tałandy (Uniwersytet Warszawski)

Warszawa, marzec 2026

Table of contents

Acknowledgments **4**

Abstract **7**

Streszczenie **9**

Introduction **11**

Institutional abbreviations **13**

Chapter I

***Tanystropheus* still conspicuous – an osteological redescription of the first tanystropheid** **14**

Chapter II

Unique internal anatomy of vertebrae as a key factor for neck elongation in Triassic archosauromorphs **150**

Chapter III

Biomechanics of the extremely elongated neck of the Triassic archosauromorph *Tanystropheus* **187**

Chapter IV

Bone infills reveal the parautochtonous origin of the Middle Triassic Miedary vertebrate assemblage **207**

Conclusions of the thesis **233**

References **235**

Appendix I **269**

Appendix II **325**

Oświadczenia **326**

Acknowledgments

First, I would like to thank my mother Bożena for her support of my academic pursuits. I warmly thank my supervisors, T. Sulej and M. Tałanda, for the help and inspiration they have given me during this journey. S. Spiekman and T. Scheyer also had an immense impact on this thesis, for which I am extremely grateful. I thank all the colleagues that provided input into this work, and especially those that lead the excavations in Miedary: Ł. Czepiński, W. Pawlak and P. Świś. I thank the coauthors of the chapters, whose contribution made my studies possible. I also wanted to express my deepest appreciation to all my family members and friends for being willing to ask and listen about *Tanystropheus*. I thank my teachers, who guided me through all the stages of my education: A. Kreft-Zwara, A. Dempc, B. Fręśko, W. Kotowski, D. Moskalewicz, and S. Fedorowicz. I also thank the workers of the Institute of Paleobiology, as well as the fellow PhD students, with whom I shared the ups and downs of our academic fate. I am greatly indebted to the reviewers and editors for helpful comments and corrections, which significantly improved the contents of Chapters I and II, and especially the late H.-D. Sues, for whom Chapter I was one of the last manuscripts he reviewed. I also thank the late M. Kowal-Linka, whose research inspired me to invent the study contained within Chapter IV, and who provided me with invaluable advice for as long as she could.

I wholeheartedly thank K. Przestrzelska, I. Janicki, E. Hara, P. Bajdek, U. Chatys and J. Kraski for masterful specimen preparation, and A. Zaremba, J. Kraski, M. Gardocki, G. Widlicki, and G. Kaproń for creating the thin and polished sections. I thank K. De Baets, P. Gorzelak, W. Łaska, and J. Stolarski for access to the hardware used for thin-section imaging. I acknowledge J. Zalewski for creating one of the illustrations included in this work. I extend my thanks to P. Duda, K. Janiszewska, M. Binkowski, G. Kaczmarczyk and D. Wałach for their help in the 3D data acquisition through CT-scanning. I thank P. Bącal for obtaining the SEM images of the reptile teeth surface.

I am grateful to T. Kollaske and A. Ehling (both BGR), B. Gaitzsch (FG), S. Meng (GG), Jiang D. (GMPKU), U. Kotthoff (GPIH), I. Werneburg (GPIT), F. Bach (GPUL) and M. Henniger (GPUL alumni), A. Gehler and L. Leschner (both GZG), Li C. and Wang W. (both IVPP), D. Schwarz and D. Ware (both MB), R. Stockar and F. Magnani (both MCSN), F. M. Dalla Vecchia, L. Simonetto and P. Visentini (both MFSN), P. Raczyński and A. Setlik (both MGUWr), K. and H. Hagdorn (MHI), M. Albrecht and R. Rozzi (both MLU), T. Hübner (MNG), M. Buchwitz and F. Trostheide (both MNM), C. Dal Sasso and S. Nosotti (both MSNM), T. Woroncowa-Marcinowska (Muz. PGI-NRI), R. Werneburg and G. Sommer (both

NHMS), M. Jones (NHMUK), U. Göhlich (NHMW), C. Becher (NME), M. Krüger, B. Bock and G. Brehm (all three PMJ), Ch. Klug, B. Scheffold and T. M. Scheyer (all three PIMUZ), G. Niedźwiedzki (PMU), A. Reisdorf and H. Weber (both RE), R. Brocke (SMF), J. Kimmig and D. Grabow (both SMNK), E. Mujal, R. Schoch and S. N. F. Spiekman (all three SMNS), M. Kellermann and O. Rauhut (both SNSB-BSPG), M. Wilmsen and R. Winkler (both SNSD), E. Głuszek and K. Suchodolska (both SUT-MG), U. Albert, S. Eggmaier and J. Rabold (all three U-MO), V. Beyer Rodrigues, D. Carobene, and A. Schwermann (all three WMNM), and J. Kobylińska (ZPAL) for their hospitality and help during the visits and examination of their respective collections.

I thank A. Brignon, G. Niedźwiedzki, K. Janneau, T. Keinerknecht (MAN), R. Kosma, C. Kurz (NMK), B. Lathuilière and S. Radecker for their help in the search for *Tanystropheus* specimens. I am grateful to Ż. Bartosińska, J. Gumowska, H. Hagdorn, R. Niedźwiedzki, M. Supel, T. M. Scheyer, S. N. F. Spiekman, T. Szczygielski, R. Werneburg and M. Wilmsen for their help in the acquisition of historic literature. I thank R. Wild and H. Hagdorn for their help in deciphering the topographic data concerning some specimens. I thank C. Kurz (NMK), G. Niedźwiedzki, A. Ősi for sharing their photographs of relevant *Tanystropheus* specimens. I thank W. Kocik for his donation of the *Pistosaurus* tooth illustrated herein to ZPAL.

I want to express my gratitude to the authorities of the Zbrosławice municipality, as well as the community of the Miedary village, especially W. Nawrocki, H. Kupka, I. Hryckiewicz, S. Szczygiel, K. Rode for their long-standing hospitality. I thank K. Pielka, owner of the Miedary claypit area, for support during the excavations. I warmly thank T. Szczygielski, and D. Dróżdż for discussions and help with data acquisition, M. Dziewiński and J. Jabłoński, for specimen transportation and photography, and all the students and volunteers taking part in the fieldwork in the Miedary site since 2014, particularly those who directly contributed to the discovery of the specimens described in this study: K. Banasiak, M. Baranowska, A. Betiuk, M. Bieniaszewski, M. Biernat, O. Godlewska, M. Granica, D. Hałubek, A. Kawińska, A. Kowalewska, T. Kozyk, S. Kugler, K. Nawrot, R. Nowakowski, G. Opoka, K. Paszek, J. Piwowarczyk, M. Piwowarczyk, K. Porębna, P. Rozwalak, M. Ruminowicz, M. Samborska, D. Sieradz, K. Sosnowska, K. Szuper, M. Taşdemir, S. Tymińska, D. Wężyk, and I. Zębik.

And finally, I wanted to thank my wife Monia for always being there for me and supporting me at every step.

This study was supported by the Polish National Science Centre grants 2017/27/B/NZ8/01543, 2020/39/O/NZ8/02301 (both awarded to T. Sulej), 2019/32/C/NZ4/00150 (awarded to D. Surmik), 2019/35/N/NZ8/03806 (awarded to Ł. Czepiński), and the National Agency for Academic Exchange grant BPN/PRE/2022/1/00009. Coauthors of the chapters also received funding from the Deutsche Forschungsgemeinschaft (SCHO 791/7-1, MU 5245/1-1) and the Foundation for Polish Science (FNP).

Abstract

The Triassic was a key period in the evolution of vertebrates, and reptiles in particular, giving rise to a plethora of successful lineages, some of which are still extant. One of the groups that flourished during the early Mesozoic were the tanysaurians (Archosauromorpha: Tanysauria). The scientific goal of this thesis is to unravel the biology of the long-necked tanysaurian *Tanystropheus*. With the new material being excavated in Miedary (Upper Silesia, Poland), an opportunity arose for solving the long-standing debate over several aspects of life of this remarkable animal. These subjects are covered within this dissertation, which consists of an Introduction, four chapters, Conclusions, and an Appendix. Chapters II, III, and IV were created in collaboration with teams consisting of both Polish and foreign scientists, among whom I was the leading author.

Chapter I focuses on the anatomy, taxonomy, and environmental preferences of *Tanystropheus*. I describe the osteology of *Tanystropheus conspicuus* in detail, based on the abundant and diverse remains from Miedary. These include several hundreds of specimens, mostly isolated elements, but with some articulated individuals, and including the first unambiguous cranial remains referred to this species, providing valuable insights into its biology. I provide a new diagnosis for *Tanystropheus conspicuus*, which differentiates it from other *Tanystropheus* species. Several newly observed anatomical features contribute to the dispute on the lifestyle of *Tanystropheus*, which is confirmed to have been an aquatic ambush predator that hunted in shallow nearshore settings.

Chapter II includes the first comprehensive description of the internal structure of the extremely elongate cervical vertebrae of tanysaurians. Through computed tomography and sectioning, we were able to reveal some intriguing features comparable to those seen in pterosaurs and birds. However, contrary to what we see in pneumatic bones, cervicals of tanysaurians contain a singular voluminous cavity. This results in a cylindrical structure in these vertebrae, which likely provided durability, while contributing less to the weight of the neck. Our insights are relevant for better understanding of a unique and extreme anatomy among tetrapods, which evolved as a result of very strict selection for some particular function. Importantly, these findings demonstrate that major modifications of the internal anatomy of vertebrae were not unique to derived avemetatarsalians (pterosaurs and dinosaurs), but more widespread among reptiles. This chapter has already been published.

Chapter III presents the first digital biomechanical analysis of the neck of *Tanystropheus*. We assessed its range of motion and performed finite element analysis on the individual cervical ribs and the neck model in different configurations. Our results indicate that the neck of *Tanystropheus* was not extremely stiff, as previously postulated, and the ribs likely did not impair its movements. They transferred tensile forces towards the base of the neck, similar to what was hypothesised for sauropods. This study elucidates the bauplan of this extremely specialised animal and brings us closer to understand the functionality of neck elongation in vertebrates.

Chapter IV describes some of the taphonomic features of the Miedary assemblage. Fossilised bones can preserve characteristics that are otherwise not recorded in the surrounding rock, and their histotaphonomic features and sedimentary infill can serve as a basis for unravelling the origin of fossil bonebeds. We used a suite of analytical methods on a broad sample of thin sections made from bones of reptiles, amphibians and fishes, to assess the diversity of their taphonomic characteristics. The remains of *Tanystropheus* do not differ in their preservation from those of aquatic taxa, supporting its interpretation as a water-dwelling animal. Our results demonstrate that some Middle Triassic ecosystems combined faunistic elements usually found in different environments, underlining transitional nature of these habitats.

The new material from Miedary allowed for studying the biology of *Tanystropheus* with a holistic approach. Traditional palaeontological methods, numeric analyses, modern imaging techniques, and digital reconstructions gave us new insights into various aspects of life of this animal. *Tanystropheus conspicuus* turned out to be a valid taxon endemic to the Central European Basin. It inhabited shallow near-shore waters. Its extremely elongated neck was composed of vertebrae that were tube-like in structure, which increased their durability. Hyperelongate ribs extended along them, but they did not constrain the movements of the neck, but rather transferred tensile forces.

Streszczenie

Trias był kluczowym okresem w ewolucji kręgowców, a szczególnie gadów, dając początek wielu liniom filogenetycznym, z których część przetrwała do dziś. Jedną z grup, które odniosły sukces ewolucyjny we wczesnym mezozoiku, były tanyzaury (Archosauromorpha: Tanysauria). Celem niniejszej rozprawy jest zbadanie biologii długoszyjego tanyzaura *Tanystropheus*. Dzięki nowemu materiałowi kopalnemu wydobytemu w Miedarach (Górny Śląsk, Polska) pojawiła się jedyna w swoim rodzaju szansa na rozwiązanie wieloletnich dyskusji dotyczących różnych aspektów życia tego niezwykłego zwierzęcia. Zagadnienia te zostały omówione w niniejszej pracy, która składa się ze Wstępu, czterech rozdziałów, Podsumowania i Załączników. Rozdziały II, III i IV powstały we współpracy z zespołami naukowców z ośrodków krajowych i zagranicznych, w których ja byłem wiodącym autorem.

Rozdział I koncentruje się na anatomii, taksonomii oraz preferencjach środowiskowych *Tanystropheus*. W tym rozdziale przedstawiam szczegółowy opis osteologii *Tanystropheus conspicuus*, dokonany na podstawie bogatego i zróżnicowanego materiału z Miedar. Obejmuje on kilkaset okazów, głównie izolowane elementy, ale także częściowo artykułowane osobniki, jak również pierwsze elementy pochodzące z czaszki tego gatunku, dostarczające cennych informacji o jego biologii. Przedstawiam nową diagnozę *Tanystropheus conspicuus*, pozwalającą odróżnić go od innych gatunków rodzaju *Tanystropheus*. Kilka nowo zaobserwowanych cech anatomicznych wnosi istotny wkład w dyskusję nad trybem życia tego gada, którego uznaję za drapieżnika polującego z zasadzki w płytkich, przybrzeżnych środowiskach.

Rozdział II zawiera pierwszy rozbudowany opis budowy wewnętrznej silnie wydłużonych kręgów szyjnych tanyzaurów. Dzięki zastosowaniu tomografii komputerowej oraz przekrojów przez okazy udało się ujawnić intrygujące cechy porównywalne z tymi obserwowanymi u pterozaurów i ptaków. W przeciwieństwie do kości pneumatycznych, kręgi szyjne tanyzaurów zawierają pojedynczą, obszerną pustkę. Skutkuje to cylindryczną budową tych kręgów, która prawdopodobnie zapewniała im wytrzymałość przy jednoczesnym zmniejszeniu masy szyi. Wyniki te mają znaczenie dla lepszego zrozumienia wyjątkowej wśród czworonogów anatomii, która wyewoluowała w wyniku silnej presji selekcyjnej. Co istotne, wyniki te pokazują, że znaczące modyfikacje wewnętrznej budowy kręgów nie były unikatowe dla pterozaurów i dinozaurów, lecz były znacznie szerzej rozpowszechnione wśród wczesnych archozauromorfów. Ten rozdział już został opublikowany.

Rozdział III przedstawia pierwszą cyfrową analizę biomechaniczną szyi *Tanystropheus*. Oceniliśmy zakres jej ruchomości oraz przeprowadziliśmy analizę elementów skończonych dla pojedynczych żeber szyjnych i modelu całej szyi w różnych konfiguracjach. Wyniki wskazują, że szyja *Tanystropheus* nie była tak sztywna, jak wcześniej sugerowano, a żebra prawdopodobnie nie miały aż tak dużego wpływu na zakres jej ruchów. Przenosiły one siły rozciągające ku podstawie szyi, podobnie jak proponowano wcześniej dla zauropodów. Badanie to zbliża nas znacznie do zrozumienia budowy skrajnie wyspecjalizowanego zwierzęcia jakim jest *Tanystropheus*, jak również wartości adaptacyjnej wydłużania szyi u kręgowców.

Rozdział IV opisuje wybrane cechy tafonomiczne miedarskiej tafocenozy. Skamieniałe kości mogą zachowywać informacje, które nie zawsze są zachowane w otaczającej skale, a ich cechy histotafonomiczne oraz wypełniający je osad mogą pomóc w ustaleniu genezy nagromadzeń szczątków. W badaniach wykorzystano kilka metod analitycznych, zastosowanych na dużym zbiorze szlifów cienkich wykonanych z kości gadów, płazów i ryb, co pozwoliło na ocenę różnorodności ich cech tafonomicznych. Szczątki *Tanystropheus* nie różnią się pod względem zachowania od szczątków organizmów wodnych, co wspiera interpretację tego zwierzęcia jako formy wodnej. Uzyskane wyniki pokazują, że w środkowym triasie niektóre ekosystemy łączyły elementy faunistyczne zwykle znajdowane w odmiennych środowiskach, podkreślając przejściowy charakter tych siedlisk.

Nowy materiał z Miedar umożliwił kompleksowe zbadanie biologii *Tanystropheus*. Połączenie tradycyjnych metod paleontologicznych, analiz numerycznych, nowoczesnych technik obrazowania oraz rekonstrukcji cyfrowych dostarczyło wielu nowych informacji dotyczących różnych aspekty życia tego zwierzęcia. *Tanystropheus conspicuus* okazał się być ważnym taksonem, endemicznym dla Basenu Środkowoeuropejskiego. Zamieszkiwał płytkie wody w pobliżu morskich wybrzeży. Jego ekstremalnie wydłużona szyja składała się z kręgów przypominających w budowie tuby, co zwiększało ich odporność. Wzdłuż nich ciągnęły się niezwykle długie żebra, które nie ograniczały ruchów szyi, a raczej przenosiły siły rozciągające.

Introduction

Archosauromorphs were the dominant clade of terrestrial vertebrates during the Mesozoic (Foth et al. 2016; Ezcurra and Butler 2018; Ezcurra et al. 2020). Extant birds and crocodilians represent only a small remnant of their morphological diversity. Especially in the Triassic, following the end-Permian mass extinction, archosauromorphs rapidly diversified into various forms with striking anatomical characteristics and disparate modes of life (Foth et al. 2016; Ezcurra and Butler 2018; Ezcurra et al. 2020). Among these are the long-necked tanysaurians, which includes the remarkable *Tanystropheus*, characterised by its extreme body proportions (Wild 1973; Spiekman et al. 2024*b*).

Unlike other long-necked reptiles, *Tanystropheus* has only 13 cervical vertebrae, which are, however, extraordinarily elongated instead, resulting in morphology unseen in any other vertebrate (Rytel et al. 2024*a*). These elements, together with rod-like cervical ribs, form a bauplan that puzzled researchers for over a century. Despite its long history of research, functional anatomy and ecology of *Tanystropheus* remained poorly understood. Whereas some studies interpreted *Tanystropheus* as a largely land-based animal with an extremely mobile neck (e.g., Peyer 1931; Wild 1973; Renesto 2005), other suggested that it was aquatic, and its neck was rather stiff (Tschanz 1986, 1988; Nosotti 2007; Spiekman et al. 2020*a*, *b*). Several recent works have contributed much to our understanding of *Tanystropheus*, clarifying the taxonomic status of most of its material (Spiekman and Scheyer 2019), bringing an end to the discussion on the conspecificity of the small and large morphotypes from Monte San Giorgio (Spiekman et al. 2020*a*), presenting the first digital skull reconstruction (Spiekman et al. 2020*b*), a detailed phylogenetic analysis of related forms (Spiekman et al. 2021), and evidence for predatory interactions (Spiekman and Mujal 2023). Despite these major contributions, many aspects of biology of *Tanystropheus* still remained enigmatic, due to the best preserved specimens being diagenetically flattened and spatially limited to the Monte San Giorgio area (Italy/Switzerland) and China (Peyer 1931; Wild 1973; Nosotii 2007; Rieppel et al. 2010).

The recent discovery of a diverse Ladinian vertebrate assemblage site in Miedary, Poland, was an important development for the studies on *Tanystropheus* (see Czepiński et al. 2023). A series of excavation campaigns have yielded hundreds three-dimensionally preserved isolated elements and articulated portions of several skeletons that together comprise most of the skeleton. More *Tanystropheus* material has originated from Miedary than from the entire rest of the Central European Basin, offering us a unique opportunity of studying this

remarkable animal. This work aims to tackle several major issues that affect our interpretation of biology of *Tanystropheus*. These include the role of the empty cervical vertebrae, the osteology and taxonomic status of the type species (*T. conspicuus*), the mobility of its neck, and finally, the environment of origin of the remains of *Tanystropheus*. Gaining insights into these subjects will have an impact on our perception of the complex Middle Triassic ecosystems, in which such specialised forms like *Tanystropheus* could evolve and thrive.

Institutional abbreviations:

BGR, Bundesanstalt für Geowissenschaften und Rohstoffe, Berlin, Germany; **FG**, Geowissenschaftliche Sammlungen, TU Bergakademie Freiberg, Freiberg, Germany; **GG**, Institut für Geographie und Geologie der Universität Greifswald, Greifswald, Germany; **GIUS**, Institute of Earth Sciences, University of Silesia, Sosnowiec, Poland; **GMPKU**, Geological Museum of Peking University, Beijing, China; **GPIH**, Geologisch-Paläontologischen Sammlungen, Leibniz-Institut zur Analyse des Biodiversitätswandels, Hamburg, Germany; **GPIT**, Geologisch-Paläontologisches Institut, Universität Tübingen, Tübingen, Germany; **GPUL**, Geologisch-Paläontologische Sammlung, Universität Leipzig, Leipzig, Germany; **GZG**, Geowissenschaftlichen Zentrum, Georg-August-Universität Göttingen, Göttingen Germany; **IVPP,** Institute of Vertebrate Paleontology and Paleoanthropology, Beijing, China; **MAN**, Muséum-Aquarium de Nancy, Nancy, France; **MB**, Museum für Naturkunde Berlin, Berlin, Germany; **MFSN**, Museo Friulano di Scienze Naturali, Udine, Italy; **MCSN**, Museo Cantonale di Scienze Naturali, Lugano, Switzerland; **MGUWr**, Henryk Teisseyre Museum of Geology, University of Wrocław, Wrocław, Poland; **MHI**, Muschelkalk Museum Hagdorn, Ingelfingen, Germany; **MLU**, Geologisch-Paläontologischen Sammlungen, Martin-Luther-Universität Halle-Wittenberg, Halle/Saale, Germany; **MNG**, Museum der Natur Gotha, Gotha, Germany; **MNM**, Museum für Naturkunde Magdeburg, Magdeburg, Germany; **MSBO**, Museum am Schöler Berg für Natur und Umwelt, Osnabrück, Germany; **MSNM**, Museo di Storia Naturale, Milan, Italy; Muz. **PGI-NRI**, Polish Geological Institute Geological Institute – National Research Institute, Warsaw, Poland; **NHMS**, Naturhistorisches Museum Schleusingen, Schleusingen, Germany; **NHMUK**, Natural History Museum, London, United Kingdom; **NHMW**, Naturhistorisches Museum Wien, Vienna, Austria; **NME**, Naturkundemuseum Erfurt, Erfurt, Germany; **NMK**, Naturkundemuseum Kassel, Kassel, Germany; **PIMUZ**, Paläontologisches Institut der Universität Zürich, Zurich, Switzerland; **PMJ**, Phyletisches Museum Jena, Jena, Germany; **PMU**, Museum of Evolution, Uppsala University, Uppsala, Sweden; **RE**, Ruhr Museum Essen, Essen, Germany; **SMF**, Senckenberg Naturmuseum Frankfurt, Frankfurt a. M., Germany; **SMNK**, Staatliches Museum für Naturkunde Karlsruhe, Karlsruhe, Germany; **SMNS**, Staatliches Museum für Naturkunde Stuttgart, Stuttgart, Germany; **SNSB-BSPG**, Staatliche Naturwissenschaftliche Sammlungen Bayerns – Bayerische Staatssammlung für Paläontologie und Geologie, Munich, Germany; **SNSD**, Senckenberg Naturhistorische Sammlungen Dresden, Dresden, Germany; **SUT-MG**, Czesław Poborski Museum of Mineral Deposit Geology, Faculty of Mining and Geology, Silesian University of Technology, Gliwice, Poland; **U-MO**, Urwelt-Museum Oberfranken, Bayreuth, Germany; **WMNM**, LWL-Museum für Naturkunde, Münster, Germany; **WNoZ**, Earth Science Museum, University of Silesia, Sosnowiec, Poland; **ZPAL**, Institute of Paleobiology, Polish Academy of Sciences, Warsaw, Poland.

Chapter I

Tanystropheus still conspicuous – an osteological redescription of the first tanystropheid

Adam Rytel[1,*]

[1]Institute of Paleobiology, Polish Academy of Sciences, Twarda 51/55, 00-818 Warsaw, Poland

* – adam.rytel@twarda.pan.pl

Introduction

Archosauromorphs were the dominant clade of terrestrial vertebrates during the Mesozoic. They had a diverse size range, evolved into a plethora of lineages with disparate ecological characteristics, and gained a virtually global spatial range of occurrence (Foth et al. 2016; Ezcurra and Butler 2018; Ezcurra et al. 2020). Extant archosauromorphs, birds and crocodilians, despite being evolutionarily successful and diverse, represent only a fraction of the previous diversity of the clade. These forms are members of Archosauriformes, which was the only clade of archosauromorphs surviving to the Jurassic. Although in the Triassic the archosauriforms were already the dominant archosauromorph group, non-archosauriform archosauromorphs also spread quickly and diversified into several distinct lineages, each characterised by the presence of highly derived anatomical traits (Foth et al. 2016; Ezcurra and Butler 2018; Ezcurra et al. 2020). These included the allokotosaurians, mostly herbivorous, stoutly built land dwellers; the rhynchosaurians, a group of relatively small, stocky, herbivorous reptiles; and lastly, the tanysaurians, which were long-necked and ecologically extremely diverse (Ezcurra 2016; Foth et al. 2016; Ezcurra and Butler 2018; Ezcurra et al. 2020; Spiekman et al. 2021, 2024*b*). Tanysauria comprises two families – Tanystropheidae Gervais, 1859 and Trachelosauridae Abel, 1919. Whereas extensive adaptations to an aquatic lifestyle are extremely rare among archosauromorphs throughout their entire history, intriguingly in the Middle Triassic such adaptations appear separately in both groups of the Tanysauria – in the tanystropheid *Tanystropheus* von Meyer, 1849, and convergently in the trachelosaurids *Dinocephalosaurus* Li, 2003 and *Trachelosaurus* Broili and Fischer, 1918 (Wild 1973; Nosotti 2007; Spiekman et al. 2020*a*, *b*, 2024*a*, *b*). This further underlines the fast pace of diversification and acquisition of specialised anatomical traits in the early-branching archosauromorphs during the Early and Middle Triassic (Foth et al. 2016). *Tanystropheus* and its relatives are, therefore, important taxa, which can help us understand the dynamic evolutionary changes taking place during this period.

Tanystropheus is an animal that in the past has been the subject of special interest for the scientific community (see bibliography in the Synonymy List below), due to its peculiar bauplan. The elongate neck constitutes nearly half of the total body length of some individuals (Wild 1973; pers. obs. AR). Whereas similar proportions have appeared convergently in several other reptile groups (sauropterygians, choristoderans, trachelosaurids), in all of them the presacral vertebrae count increased (Rytel et al. 2024*a*). In tanystropheids this number seems to have been constrained to 25, and hence in *Tanystropheus* the neck elongation proceeded mostly via the elongation of the cervical vertebrae and the 'cervicalisation' of some of the dorsal vertebrae (Wild 1973; Rytel et al. 2024*a*). The cervical vertebrae of *Tanystropheus* reached proportions unseen in any other animal, being superficially similar to limb bones. They were associated with straight, rod-like cervical ribs, which extended posteriorly across several succeeding intervertebral articulations. This cervical anatomy is unparallelled among known vertebrates, including both terrestrial and aquatic long-necked reptiles (Rytel et al. 2024*a*). This resulted in difficulties in deciphering the lifestyle of *Tanystropheus*. Moreover, the studies on *Tanystropheus* have been severely constrained due to the nature of its preservation – isolated three-dimensionally preserved bones were scarce, usually fragmentary, and of limited element diversity, whereas the relatively complete and articulated skeletons were compressed and often essentially two-dimensional. This contributed to the difficulties in understanding its unique bauplan and resulted in *Tanystropheus* being considered "enigmatic", despite a very long history of research.

The first species of *Tanystropheus* – *Tanystropheus conspicuus* von Meyer, 1852 was described based on isolated cervical vertebrae from modern-day Germany and Poland, which were then considered to likely be caudal vertebrae (von Meyer 1847-1855). It was not until the 1930s that the true identity of these elements was revealed by the articulated specimens of *Tanystropheus hydroides* Spiekman, Neenan, Fraser, Fernandez, Rieppel, Nosotti, Scheyer, 2020 and *Tanystropheus longobardicus* (Bassani, 1886) recovered from the Besano Formation of Monte San Giorgio (Italy/Switzerland; Peyer 1930, 1931). Later studies predominantly focused on this material, culminating in the monograph of Wild (1973), which served as the basis for most of the studies on *Tanystropheus* for over half a century. Whereas the contribution of Wild (1973) to understanding and illustrating the osteology of *Tanystropheus* is indisputable, the comparative part of this work has become largely outdated. Wild (1973) considered tanystropheids as squamates, but they are now unequivocally regarded as archosauromorphs, with many new forms closely related to *Tanystropheus* being described in

the interim (Evans 1988; Ezcurra 2016; Spiekman et al. 2021). The discovery of aquatic trachelosaurids, a sister group to tanystropheids, is especially worthy of notice in that context (Li 2003; Spiekman et al. 2021, 2024*a*, *b*). The bauplan of these animals demonstrates that some archosauromorphs were able to adapt well to life in Middle Triassic marine environments, evolving flipper-like limbs, viviparity and serpentine vertebral columns (Li 2003; Li et al. 2017b; Liu et al. 2017; Spiekman et al. 2024*a*, *b*).

Since the publication of Wild (1973) further studies have brought to light new details on the postcranial anatomy of *Tanystropheus*, but they were all hampered by the relatively two-dimensional preservation of the novel specimens which are diagenetically flattened or still partially embedded in matrix (Wild 1980*a*; Renesto 2005; Li 2007; Nosotti 2007; Rieppel et al. 2010). The isolated bones of *Tanystropheus* sp. found in Canada (Sues and Olsen 2015), Hungary (Ősi et al. 2020), Israel (Peyer 1955; Rieppel 2001), Italy (Dalla Vecchia 2000, 2006, 2008; Dalla Vecchia and Avanzini 2002; Dalla Vecchia and Simonetto 2018), Romania (Jurcsak 1973, 1975, 1978), and Saudi Arabia (Vickers-Rich et al. 1999) have provided additional insight into the spatiotemporal distribution of the genus, as well as some ontogenetic and morphological aspects, but this material was not found to be diagnostic because these parts of the postcranium were considered to exhibit a lot of intraspecific variation (Spiekman and Scheyer 2019). Previously there were also no cranial elements of *Tanystropheus* known from outside of the Monte San Giorgio region (Peyer 1931; Wild 1973, 1980*a*; Nosotti 2007; Spiekman et al. 2020*b*). Wild (1973) stated that *T. conspicuus* might be conspecific with *T. longobardicus* (and *T. hydroides*), but this can only be confirmed or refuted after more of the material of the former species is reported. With virtually no diagnostic remains of *T. conspicuus* having been reported in the subsequent period, Spiekman and Scheyer (2019) considered it a *nomen dubium*.

The discovery and description of the new site in Miedary (Upper Silesia, southern Poland) provided an unprecedented opportunity for the further meaningful studies of *Tanystropheus*, in particular *T. conspicuus* (see Czepiński et al. 2023). At this locality, remains of at least 20, predominantly large (i.e. ontogenetically mature) individuals of *Tanystropheus* were excavated, together with some scarce remains of juveniles and subadults. The abundant and diverse remains from Miedary permit for a broad analysis of three-dimensionally preserved specimens of *Tanystropheus*. Previously the majority of postcranial elements of *Tanystropheus* could have not been studied from this perspective. Of particular interest are the bones comprising the transitional cervico-dorsal region of the skeleton, as this region of the

body was not well preserved in accessible specimens, and it is key to understanding the role and mobility of the neck. Moreover, cranial remains of *T. conspicuus* have been identified for the first time. Due to the presence of articulated and three-dimensionally preserved remains, the material from Miedary allows us not only to examine the osteology of most of the skeleton of *T. conspicuus*, but also combines the preservation characteristics of isolated finds from around the world and the diagenetically flattened individuals of *Tanystropheus* from Monte San Giorgio and China, constituting a key to their future comparisons, and further analyses.

The aim of this study is to:

1) Analyse the currently accessible material of *Tanystropheus*, with an emphasis on the Miedary material, and carry out an osteological redescription of *Tanystropheus conspicuus*;

2) Compare the material of *Tanystropheus conspicuus* to other species of *Tanystropheus* and establish the taxonomic status of the former;

3) Interpret the functional anatomy of *Tanystropheus* based on the new three-dimensional material, and elucidate some enigmatic aspects its biology, including its mode of life, its habitat and the role of the extremely elongated neck;

4) Explain the unexpected abundance of remains of *Tanystropheus conspicuus* in the Miedary site.

Historical Background

Several elongate vertebrae were collected from the Upper Muschelkalk of the area around Bayreuth (Upper Franconia, Germany) in the first half of the 19th century (Fig. 1A–E, F–J). Originally some were stored in the collection of Count Georg zu Münster, whereas others were reposited in the local state-owned collection in Bayreuth. Although some of the latter specimens were already illustrated by Braun (1840), their first description was incorporated within the voluminous monograph of von Meyer (1847-1855). While working on this publication, H. von Meyer had access to several other collections, including the specimens collected by C. Mentzel from the Muschelkalk localities in Upper Silesia (present-day Poland), which were partially published in a separate work (von Meyer 1849). The material from Silesia contained an elongate vertebra (MB.S. 11, Fig. 1E) that, together with eight specimens from Franconia, served as a basis for a description of the genus *Tanystropheus* von Meyer, 1849 and its type species *Tanystropheus conspicuus* von Meyer, 1852. U-MO BT

3079, a humerus from Bayreuth was also illustrated by Braun (1840) and von Meyer (1847-1855), but first referred to *T. conspicuus* by Diedrich (2012); hence only the nine elongate cervical vertebrae constitute the type series of *T. conspicuus* (see Appendix I). Another cervical vertebra from the Silesian Upper Muschelkalk of Laryszów (Larischhof) was reported by Langenhan (1903, 1911). Skawiński et al. (2017) suggested that more than one syntype of *T. conspicuus* originated from Silesia, and that MB.S. 11 might have been gathered from the Lettenkeuper strata of Miedary instead, but Czepiński et al. (2023) saw no clear evidence for these claims and considered Miedary a newly discovered locality.

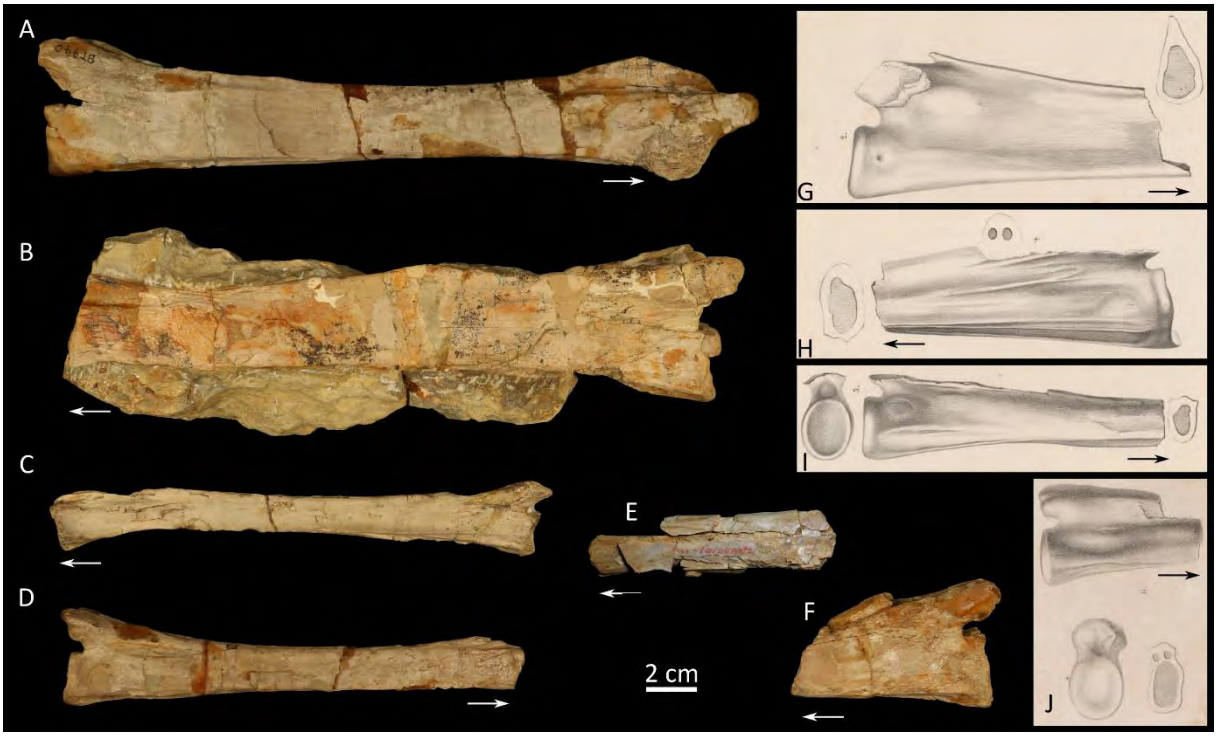

Fig. 1. Photographs (A–F) and lithographs (G–J) of the type series of *Tanystropheus conspicuus*, consisting of ten middle cervical vertebrae: U-MO BT 740 (**A**; the lectotype), U-MO BT 737 (**B**), U-MO BT 732 (**C**), U-MO BT 733 (**D**), MB.S.11 (**E**), U-MO BT 734 (**F**), and the four lost specimens illustrated in von Meyer 1847-1855 (plate 30, fig. 6 – **J**; plate 46, figs. 2–4 – **G–I**). A, D, G, I–J in right lateral view, rest in left lateral view. A–D and F–J from the Upper Muschelkalk (upper Anisian) of Bayreuth (Germany). E from the Upper Muschelkalk (upper Anisian) of Laryszów (Poland). Arrows indicate anterior direction.

Some additional individual vertebrae of *T. conspicuus* (see Appendix I) were reported by Broili (1915), Edinger (1924), Peyer (1931), Lang and von Huene (1952), Adam (1953), Spiekman and Scheyer (2019), and Schwermann et al. (2025). The overwhelming majority of the historic specimens referred to *T. conspicuus* were described in various publications authored by F. von Huene. Von Huene (1902) erected several new reptile taxa based on the isolated remains from the Upper Muschelkalk-Lower Keuper strata of Germany. These included: *Procerosaurus cruralis*, based on a large isolated femur GPIT-PV-60009; *Pectenosaurus strunzi*, represented by a partial vertebra (GPIT-PV-60014); and a new testudine genus *Chelyzoon*, encompassing two species – *Ch. blezingeri* and *Ch. latum*, both based on singular isolated vertebrae (with SMNS 8728 being the holotype of *Ch. blezingeri*). The type specimens of *Procerosaurus cruralis, Ch. blezingeri*, *Ch. latum*, and a "sauropterygian" sacral vertebra of von Huene (1902, p. 45; GPIT-PV-60011) were regarded as belonging to *T. conspicuus* by Wild (1973). The vertebra of *Pectenosaurus strunzi* was referred to *Tanystropheus* by Kuhn (1963) and to *T. conspicuus* by Spiekman and Scheyer (2019). Thus, four of the taxa erected by von Huene (1902) were at some point considered subjective junior synonyms of *T. conspicuus*, although Spiekman and Scheyer (2019) mentioned that the type specimens of both species of *Chelyzoon* appear to be morphologically disparate from the known vertebrae of *Tanystropheus*. Von Huene (1907-1908) described some previously unpublished vertebrae of *T. conspicuus*, including a cervical originating from present-day France (see Appendix I), and erected several new taxa of what he considered dinosaurs. These included a second species of *Tanystropheus* – *Tanystropheus antiquus* (herein not considered a species of *Tanystropheus*; see Rytel et al. 2024*b* for the most recent comment on the status of this taxon), and *Thecodontosaurus latespinatus*, with the type series for both consisting solely of isolated vertebrae. The temporal and spatial ranges of occurrence for the latter species have largely overlapped with *Tanystropheus conspicuus*.

After the articulated skeletons from Monte San Giorgio were described by Peyer (1931), von Huene (1931) reevaluated the previous interpretations of the material from the Central European Basin (CEB; also known as the Germanic Basin), stating that the vertebrae of *Zanclodon laevis*, the holotype of *Procerosaurus cruralis* and the entirety of the material assigned to *Thecodontosaurus latespinatus* should likely be referred to *Tanystropheus*. *Zanclodon laevis* Plieninger, 1846 was described on the basis of several isolated elements, of which only the lectotype jaw fragment (not belonging to *Tanystropheus*) survives to this day (see Plieninger 1846*a*, *b*; Wild 1973; Schoch 2011). Wild (1973) concurred with von Huene

(1931), synonymising *Procerosaurus cruralis* and *Thecodontosaurus latespinatus* with *Tanystropheus conspicuus*, referring all the described material to the latter species, together with three other vertebrae from the Upper Muschelkalk/Lettenkeuper (see Appendix I) illustrated by von Huene (1931). Moreover, Wild (1973) provided a discussion on the status of *Zanclodon laevis* and deemed a part of its type series, the two lost vertebrae, to likely belong to *Tanystropheus conspicuus*. Von Huene (1920) described a humerus, SMF R 4034, found near Bayreuth, and interpreted it as belonging to a "parasuchian". Wild (1973) also referred this specimen to *T. conspicuus*. A specimen of similar morphology served as the basis for the description of *Megacnemus grandis* von Huene, 1954. Von Huene (1954) interpreted the relatively large (21.6 cm in length) limb bone as a femur of a new "protorosaurian". Skawiński et al. (2015) pointed out that the specimen represents a humerus, rather than a femur, and that its morphology is nearly identical to the humeri of tanystropheids. Unfortunately, the specimen lost its original label during the Second World War, making its taxonomic interpretation difficult, due to the lack of stratigraphic and topographic data.

Corroy (1928) described a partial articulated hindlimb, originating from the Upper Muschelkalk of Mont-sur-Meurthe (France), that he referred to *Thecodontosaurus latespinatus*. Following the original interpretation, the specimen preserved a distal end of a femur, a fibula, and a potential tibia. It was stored at the University of Strasbourg, and later at the Museum and Aquarium Nancy under the number MAN 2016.0.213, but its current location is unknown (pers. comm. T. Keinerknecht). Wild (1973) and Spiekman and Scheyer (2019) considered the partial limb bone to belong to *T. conspicuus*, but this hypothesis cannot be fully corroborated for as long as the specimen remains missing.

Teeth of *Tanystropheus* were described for the first time by Fraas (1896), who erected a new species of *Nothosaurus*, *N. blezingeri*, on the basis of several isolated teeth (currently under a joint specimen number SMNS 52478) collected from the Grenzbonebed near Crailsheim (Germany) by R. Blezinger. Fraas (1896) noted the similarity between the tooth morphology of the new species and that of *Pistosaurus grandaevus* von Meyer, 1855, a junior synonym of *P. longaevus* von Meyer, 1839 (see Sues 1987). Additional isolated teeth (MAN 2016.0.201 and MAN 2016.0.202) were described from the Muschelkalk localities of Lorraine (France) by Corroy (1928), who regarded *N. blezingeri* as a junior synonym of *P. grandaevus*. Finally, the teeth of *N. blezingeri* were considered to belong to *Tanystropheus* by Rieppel and Wild (1996) and Rieppel (2000). Schoch et al. (2018) were the first to delineate

the morphological differences between the teeth of *Tanystropheus* and *Nothosaurus*, describing both morphotypes in more detail.

Wild (1973) summarised the state of knowledge on the genus *Tanystropheus* in an extensive monograph, providing a description of both historic and novel material, synonymy lists, diagnoses and establishing the types for each of the species of *Tanystropheus*. U-MO BT 740, one of the original specimens of von Meyer (1847-1855) was designated as the lectotype of *T. conspicuus*. More recently, several unpublished isolated bones and teeth of *T. conspicuus* from Germany (see Appendix I) were mentioned or illustrated in the studies of Diedrich (2009, fig. 12; 2015, fig. 10C:2), Ezcurra et al. (2014, figs. 16D, 18C), Ezcurra (2016, figs. 14a–b, 33B), Jaquier and Scheyer (2017), Spiekman and Scheyer 2019 (see supp. tab. 1 therein), and Schwermann et al. (2025) but were not described osteologically. Spiekman and Scheyer (2019) expanded the work of Wild (1973), providing the most up-to-date list of known specimens referred to this species, including their historic background and the current location of individual elements.

Sites in Germany remained the main source of material of *T. conspicuus* for the last century, until the Miedary fauna was reported by Czepiński et al. (2023), which provided a description of a vertebra referred therein to *Tanystropheus* sp. Several more isolated cervical vertebrae from this site were analysed in the studies of Rytel et al. (2024*a*, *b*). Until now, however, only a fraction of the total tanystropheid material excavated in Miedary had been published. Consequently, the hypodigm of *T. conspicuus* was restricted to postcranial remains (vertebrae, humeri, femora) and some tentatively referred teeth – in sum a little over 100 individual elements, of which roughly only one half has been described.

Materials and methods

To assess the presence of specimens referable to *Tanystropheus conspicuus* based on personal observations, I visited collections in Austria, Germany, Poland, Switzerland, and the United Kingdom. Therein, I have collected topographic and stratigraphic data for each element, the literature sources referring to it, as well as some morphometric measurements. These data are contained within the Appendix I, which also includes a list of specimens that are currently lost or no longer considered to belong to *T. conspicuus*. Photographs and three-dimensional models of all specimens illustrated herein have been uploaded to MorphoSource, where they can be accessed: https://www.morphosource.org/projects/000774422.

The novel specimens from Miedary were collected during annual excavations coordinated by the Institute of Paleobiology, Polish Academy of Sciences, and the Institute of Evolutionary Biology, University of Warsaw, during the 2014-2024 field seasons. The material originated mostly from the M2, but also the M1 and M4 layers of Unit 1 of Czepiński et al. (2023). No fossils from the M3 layer, or the strata overlaying Unit 1 in the Miedary site, can currently be referred to *Tanystropheus*. The excavated remains were treated with cyanoacrylate adhesive and secured with plaster jackets to ensure the structural stability of the fossils during transport. Their preparation was carried out mainly with pneumatic needles.

Due to the lack of *in situ* association, an overwhelming majority of the analysed specimens could not be confidently regarded as originating from the same individual. Only a few articulated finds preserve larger portions of a skeleton. Isolated elements of *T. conspicuus* that were not a part of these associations, nor directly comparable with them, were identified based on morphological similarity with the largely complete individuals of *T. hydroides* and *T. longobardicus*. Only specimens presenting the original morphology most closely (i.e. the most complete and/or least distorted examples of each respective element) were illustrated, but the descriptions of individual skeletal elements are based on all accessible material.

Simple measurements were taken from all bones referred to *T. conspicuus* preserving at least one of the measured characteristics. For the anterior postaxial cervical vertebrae these included: maximum total length (the distance between the distal tips of corresponding zygapophysis and epipophysis), centrum length, height at mid-point, and maximum height (see further below). The same measurements were taken for other postaxial vertebrae, except for height at mid-point, as it is roughly equal to their maximum height. For non-vertebral elements only two characters were measured: maximum length and maximum height. All

measurements were recorded using digital callipers with an original resolution of 0.1 mm, rounded to the nearest millimetre half up. Photographs of ZPAL V. 36/584 were taken with a NIKON D5 camera, whereas all other photographs presented here were taken with a NIKON D5300 camera by the author.

Computed tomographic (CT) scans were generated for the maxilla ZPAL V. 36/1213 and the skull roof ZPAL V. 36/1244. To obtain the serial images of these specimens, a GE phoenix v|tomex|m device (GE Sensing and Inspection Technologies Phoenix|x-ray, Wunstorf, Germany) located in the Laboratory of X-ray Computed Tomography, Department of Geomechanics, Civil Engineering and Geotechnics, AGH University of Kraków, Poland, was used. For ZPAL V. 36/1213 it was operating at a voltage of 200 kV and a tube current of 240 μA, acquiring 3000 projections. For ZPAL V. 36/1244 voltage was set to 190 kV and tube current to 190 μA, and 2600 projections were generated. The spectrum was hardened with an additional copper filter. Isometric voxel size for both specimens equalled 0.07499975 mm. Avizo Lite 2020.3.1 (Thermo Fisher Scientific, USA) was used to create the models of individual bones. The surface of the ZPAL V. 36/1213 model was smoothed and simplified in MeshLab v.2023.12 (Cignoni et al. 2008), using Scale Dependant Laplacian Smooth tool with default settings and Simplification: Quadric Edge Collapse Decimation tool, reducing the model surface to 200 000 faces.

Surface scans of the analysed specimens were obtained using a Shining 3D EinScan Pro 2X 3D scanner fixed on a tripod, located in ZPAL, with an EinTurntable and EXScan Pro 3.7.4.0 software. The morphological data was acquired by either using the Ein-Turntable (alignment based on features) or without a turntable, by scanning the specimen manually. The number of turntable steps was varied, chosen dependent upon the specimen. The models were meshed using the Watertight Model and Medium Detail presets. Due to the large size of the semiarticulated cervical series ZPAL V. 36/100, its model was acquired through photogrammetry.

Snapshots of the models of specimens illustrated in the figures were captured in MeshLab v.2023.12 using the Save snapshot tool in orthographic view, with the ‘xray’, Lit Sphere Radiance Scaling or Lambertian Radiance Scaling shader enabled.

Scanning electron microscope (SEM) imaging was used to compare selected, well-preserved teeth of *T. conspicuus* (ZPAL V. 36/163, ZPAL V. 36/1204), *Nothosaurus* sp. (ZPAL V. 36/233, ZPAL V. 36/254), both from Miedary, and of *Pistosaurus* sp. (ZPAL V. 84/LA/001)

from the Upper Muschelkalk of Laryszów (Poland). The non-sputtered samples were analysed in Low Vacuum mode and the water pressure in the SEM chamber was maintained at 50 Pa. The used Field Emission SEM was a Thermo Fisher Quattro S Environmental Electron Microscope (ESEM located in ZPAL). The samples were mounted using conductive carbon tape adhesive and aluminium foil casing directly attached to a standard SEM stub. Large-area mapping was conducted using MAPS 3 software, which automates the acquisition of large overviews by stitching multiple images.

Following Rytel et al. (2024*a*, *b*) in the differentiation of the morphological subregions in the neck of *Tanystropheus*, I refer to the three last cervical vertebrae as "posterior", and to the rest of the postaxial cervical vertebrae (three to ten) as "middle". For the anatomical description I followed the terminology used by Ezcurra (2016) and Spiekman et al. (2021), with some minor differences. For example, when considering the vertebral elongation in archosauromorphs Ezcurra (2016) and Spiekman et al. (2021) used the ratio of centrum length to its anterior articular surface dorsoventral height. However, in the articulated specimens the dorsal part of the anterior end of the centrum is usually obscured by the prezygapophysis and centroprezygapophyseal lamina (see Wild 1973; Wild 1980*a*; Renesto 2005; Li 2007; Nosotti 2007; Rieppel et al. 2010). Instead, vertebral elongation is here defined as a ratio of centrum length to the height at the anteroposterior midpoint of the vertebra. This measurement can be taken consistently from virtually all complete *Tanystropheus* cervical vertebrae in lateral view. In the middle cervical vertebrae of *Tanystropheus* the maximal vertebral height is not reached near the midpoint of anteroposterior length due to the strong reduction of the neural spine here. Instead, the middle cervical vertebrae are taller near the anterior and posterior ends of the neural spine instead. To be able to quantitatively analyse this characteristic morphology, I recorded maximal height of complete vertebral specimens, and this was defined as the largest distance between the dorsal extent of the neural spine and the ventralmost point located on the ventral keel at same section of anteroposterior length of the vertebra (see Appendix I).

Systematic palaeontology

Class Reptilia Laurenti, 1768

Clade Archosauromorpha von Huene, 1946

Order Protorosauria Huxley, 1871

Clade Tanysauria Spiekman, Ezcurra, Rytel, Wang, Mujal, Buchwitz, and Schoch, 2024

Family Tanystropheidae Gervais, 1859

Genus *Tanystropheus* von Meyer, 1849

Type species: *Tanystropheus conspicuus* von Meyer, 1852

Referred species: *Tanystropheus hydroides* Spiekman, Neenan, Fraser, Fernandez, Rieppel, Nosotti, Scheyer, 2020; *Tanystropheus longobardicus* (Bassani, 1886)

Previous diagnosis

The most recent previous diagnosis was provided by Spiekman and Scheyer (2019): "Long-necked tanystropheid archosauromorphs distinguished from other genera by the following combination of characters (autapomorphy among non-archosauriform archosauromorphs marked with an asterisk): 1) the absence of shagreen-like teeth on the vomers and palatines; 2) mid-cervical vertebrae with a vertebral centrum length more than 2.5 times their minimum height; 3) a low neural spine of the cervical vertebrae; 4) very long and extremely thin cervical ribs, being approximately three times the length of their corresponding vertebra in the mid-cervical region, bearing short free ending anterior processes; 5) ribs of second sacral vertebrae not bifurcated; 6) curved anterior margin of scapular blade, which is consequently directed posteriorly; 7) the absence of hyperphalangy; 8) only two ossified distal carpals*; and 9) a thyroid fenestra present between the pubis and ischium."

Additionally, the phylogenetic analysis of Spiekman et al. (2021) found the following synapomorphies present within *Tanystropheus*: postaxial anterior or mid-cervical neural spines are only present at the anterior and posterior ends of the vertebrae but are completely or virtually lost at their anteroposterior midpoints; lengths of the fourth or fifth cervical centra versus the heights of their anterior articular surfaces between 14.58 and 15.58 or between 17.08 and 18.67; total length of the humerus versus the total length of the femur between 0.84 and 0.91.

Emended diagnosis

Long-necked tanystropheid archosauromorph distinguished from other genera by the following combination of characters (autapomorphy among non-archosauriform archosauromorphs marked with an asterisk): 1) the absence of shagreen-like teeth on the vomers and palatines; 2) ratio of centrum length of middle cervical vertebrae to height at midpoint of their anteroposterior length equal to or more than four, and in some specimens reaching more than 15*; 3) neural spines of the third to ninth cervical vertebrae well outlined only in their anterior and posterior portions, and virtually completely reduced in the middle section of their anteroposterior length; 4) one or two large subcentral foramina present on the ventral surface of the postaxial cervical vertebrae, near the mid-point of their anteroposterior length*; 5) very long and extremely thin cervical ribs, being approximately three to four times the length of their corresponding vertebra in the mid-cervical region, and bearing a distinct anterior free ending processes; 6) curved anterior margin of scapular blade, which is directed posteriorly; 7) absence of an ossified interclavicle; 8) deltopectoral crest extremely reduced; 9) presence of only two ossified distal carpals*; 10) a thyroid fenestra present between the pubis and ischium; and 11) sexual dimorphism indicated by the presence of two pairs of elongate ossifications in the postcloacal region in individuals of one of the sexes.

Species *Tanystropheus conspicuus* von Meyer, 1852

https://zoobank.org/urn:lsid:zoobank.org:act:478F90B7-32A3-4DFD-8B94-BBEC5C82A7CA

Lectotype: U-MO BT 740, isolated middle cervical vertebra.

Paralectotypes: MB.S.11, U-MO BT 732, U-MO BT 733, U-MO BT 734, U-MO BT 737 – five middle cervical vertebrae. The remaining paralectotypes (four middle cervical vertebrae) are ostensibly lost.

Type locality: Bindlacher Berg near Bayreuth (after Wild, 1973), Upper Franconia, Germany.

Type horizon: Upper Muschelkalk, upper Trochitenkalk Formation or lower Meißner Formation, upper Anisian (see Klein et al. 2022).

Stratigraphic occurrence: lower Upper Muschelkalk (lower Trochitenkalk Formation) to uppermost Lower Keuper (Grenzdolomit, uppermost Erfurt Formation); upper Anisian to upper Ladinian.

Geographic distribution: France (Alsace, Lorraine); Germany (Baden-Württemberg, Bavaria, ?Hesse, Lower Saxony, North Rhine-Westphalia, Thuringia); Poland (?Lesser Poland, Upper Silesia).

Material: Hundreds of isolated bones and teeth, as well as several incomplete articulated individuals, altogether comprising a majority of the skeleton (lacking some of the cranial and autopodial elements). For the full list of referred specimens see Appendix I.

Previous diagnosis.

The most recent diagnosis for *Tanystropheus conspicuus* was provided in Wild (1973, p. 149; translated from German after Spiekman and Scheyer 2019): "Up to six(?) meters long species, that can be distinguished from *T. longobardicus* by the wider attachment sites of the cervical ribs and the split anterior end of the neural spine for the attachment of the dorsal ligament." Note that Wild (1973) considered both the small and large sized individuals of *Tanystropheus* from the Monte San Giorgio to be conspecific (and belong to *T. longobardicus*), which was disproven by Spiekman et al. (2020*a*).

Emended diagnosis

Tanystropheus conspicuus is distinguished from all other *Tanystropheus* species by the following combination of characters: 1) premaxilla lacking distinct prenarial and postnarial processes (shared with *T. hydroides*); 2) single-cusped marginal teeth (shared with *T. hydroides*); 3) no dentary tooth piercing through a foramen in the maxilla (shared with *T. longobardicus*); 4) number of dentary teeth reaching up to 26 or more in some specimens; 5) dentary bearing a distinct ventral keel at its anterior end (shared with *T. hydroides*); 6) frontal semi-trapezoidal in outline in dorsal view, with its transverse width notably greater than its anteroposterior length; 7) lack of a shelf-like ridge on the dorsolateral surface of the 13th cervical rib; 8) dorsal and sacral vertebrae at least two times taller than long; 9) distal region of the neural spine laterodistally expanded and bulbous in appearance along the vertebral column from the 10th cervical to the anterior caudal vertebrae; 10) scapula with a distinct dorsoventral constriction located at its anteroposterior midpoint and a significantly posteriorly expanded scapular blade; and 11) dorsolateral surface of the first three dorsal ribs anteroposteriorly expanded, forming a plate-like extension radiating distally from the tuberculum-capitulum conjunction.

Synonymy list

1840	"Saurus" (partim)	Braun p. 81–83; plate 9, figure 5; plate 11 figures 1, 6; plate 12, post-cloacal bone, lowermost figure on the left; plate 20, figure 3; plate 21, figure 6
1846*a*	*Smilodon laevis* (partim) gen. nov. sp. nov.	Plieninger, p. 153, 247; plate 3, figure 4
1846*b*	*Zanclodon [laevis]* (partim)	Plieninger, p. 247-248, 254
1849	*Tanystropheus* gen. nov.	von Meyer, p. 219
1847-1855 [1852]	*Tanystropheus conspicuus* sp. nov.	von Meyer throughout text; plate 27, figures 19–20; plates 30, 46; plate 49, figure 3
1854	*Tanystropheus*	von Meyer, p. 52
1860	*Tanystropheus*	von Meyer, p. 17, 48
1860	*Tanystrophaeus conspicuus*	Owen, p. 220–222
1862	*Tanystropheus*	Braun, p. 11
1864	*Tanistropheus conspicuus*	von Alberti, p. 234
1865	*Tanystropheus conspicuus*	Eck, p. 122, 126
1870	*Tanystropheus conspicuus*	Roemer, p. 147
1884	*Tanystropheus*	Gürich, p. 141
1887	*Tanystrophaeus conspicuus*	Cope, p. 221
1887-1890	*Tanystrophaeus conspicuus*	Zittel, p. 567, 733, 767; figure 514
1894	*Tanystropheus*	Fritsch, p. 277
1896	*Nothosaurus Blezingeri* sp. nov. (partim)	Fraas, p. 11; figure 4
1896	*Tanystropheus conspicuus*	Fraas, p. 5, 14–15
1901	*Tanystropheus conspicuus*	Nopcsa, p. 256
1902	*Chelyzoon Blezingeri* gen. nov. sp. nov.	von Huene, p. 51; plate 7, figure 1
1902	*Chelyzoon latum* gen. nov. sp. nov.	von Huene, p. 50–51; plate 7, figure 2
1902	*Procerosaurus cruralis* gen. nov. sp. nov.	von Huene, p. 64–65; plate 9, figure 1
1902	*Tanystrophaeus* (partim)	von Huene, throughout text; text-figure 50; plate 6, figure 6
1903	*Tanystrophaeus conspicuus*	Langenhan, p. 19; plate 15, figure 8
1905	*Thecodontosaurus latespinatus* sp. nov. (*nomen nudum*)	von Huene, p. 349
1905	*Tanystrophaeus conspicuus*	von Huene, p. 349
1906	*Tanystrophaeus conspicuus*	von Huene, p. 118
1907-1908	*Thecodontosaurus latespinatus* sp. nov.	von Huene, throughout text; text-figures 237–243; plates 91–92
1907-1908	*Tanystrophaeus conspicuus*	von Huene, throughout text; text- figures 250–251, 351; plate 94, figures 6–9; plates 95–96
1907-1908	*Zanclodon laevis* (partim)	von Huene, p. 187–190; text-figures 201–202

1910	*Procerosaurus cruralis*	von Huene, p. 321
1911	*Tanystrophaeus conspicuus*	Langenhan, plate 20, figure 30
1913	*Tanystropheus conspicuus*	Assmann, p. 337
1914*a*	*Procerosaurus*	von Huene, p. 157
1914*b*	*Procerosaurus cruralis*	von Huene, p. 12
1914*b*	*Tanystrophaeus conspicuus*	von Huene, p. 12
1914*b*	*Thecodontosaurus latespinatus*	von Huene, p. 12
1914*c*	*Procerosaurus cruralis*	von Huene, p. 672
1915	*Tanystrophaeus conspicuus*	Broili, throughout text; plate 2; plate 3, figures 4–5
1915	*Thecodontosaurus primus*	Broili, p. 57–58; plate 3, figure 3
1915	*Chelyzoon Blezingeri*	Drevermann, p. 404
1915	*Chelyzoon latum*	Drevermann, p. 404
1915	*Tanystrophaeus conspicuus*	Drevermann, p. 404
1916	*Chelyzoon Blezingeri*	Jaekel, p. 89
1916	*Chelyzoon latum*	Jaekel, p. 89
1919	*Tanystrophaeus conspicuus*	Abel, p. 580
1920*a*	"Parasuchier aus dem oberen Muschelkalk von Bayreuth"	von Huene, throughout text; figure 1
1920*b*	*Procerosaurus*	von Huene, p. 162
1921	*Nothosaurus Blezingeri* (partim)	Edinger, p. 17–19
1923	*Tanystrophaeus conspicuus*	Edinger, p. 143
1924	*Tanystrophaeus conspicuus*	Edinger, throughout text; figures 1–4
1928	*Pistosaurus grandaevus* (partim)	Corroy, p. 121; plate 3, figures 2, 7
1928	*Chelyzoon blezingeri*	Schmidt, p. 414; figure 1161
1928	*Chelyzoon latum*	Schmidt, p. 413–414; figure 1160
1928	*Nothosaurus Blezingeri*	Schmidt, p. 398; figure 1115
1928	*Procerosaurus cruralis*	Schmidt, p. 425; figure 1190
1928	*Tanystrophaeus conspicuus* (partim)	Schmidt, p. 424–425; figure 1188 a–c
1928	*Thecodontosaurus latespinatus*	Schmidt, p. 434; figure 1213
1931	*Tanystropheus conspicuus*	Edinger, p. 846–847
1931	*"Procerosaurus cruralis"*	von Huene, p. 66, 69
1931	*"Thecodontosaurus latespinatus"*	von Huene, throughout text
1931	*Tanystropheus conspicuus*	von Huene, throughout text; figures 1–3, 6
1931	*Zanclodon laevis* (partim)	von Huene, throughout text
1931	*Tanystropheus conspicuus*	Peyer, throughout text; text–figures 1–2, 24–25
1932	*Chelyzoon blezingeri*	Case, p. 88
1932	*Chelyzoon latum*	Case, p. 88
1932	*Procerosaurus cruralis*	von Huene, p. 33
1932	*Tanystropheus conspicuus*	von Huene, throughout text
1932	*Tanystropheus conspicuus*	von Zittel, p. 270
1934	*Macroscelosaurus conspicuus*	Kuhn, p. 118–119
1934	*Nothosaurus blezingeri*	Kuhn, p. 37
1937	*Tanystropheus conspicuus*	Peyer, p. 84; figure 1
1938	*Tanystropheus conspicuus*	Schmidt, p. 75–76; figure 1188a
1938	*Tanystropheus* sp.	Schmidt, p. 76; figure 1188b
1939*a*	*Chelyzoon*	Kuhn, throughout text

1939*b*	*Procerosaurus cruralis*	Kuhn, p. 35
1939*b*	*Thecodontosaurus latespinatus*	Kuhn, p. 12
1941	*Chelyzoon*	Kuhn, p. 10
1944	*Tanystrophaeus conspicuus*	Assmann, 84–85
1944	*Tanystropheus conspicuus*	von Huene, p. 127
1944	*Tanystropheus conspicuus*	Peyer, p. 65; figure 49
1952	*Tanystrophaeus conspicuus*	Lang and von Huene, p. 27
1953	*Tanystropheus conspicuus*	Adam, throughout text; figure 1
1954	*Megacnemus grandis* gen. nov. sp. nov.	Huene, throughout text; figure 1
1955	*Chelyzoon*	Bergounioux, p. 521
1955	*Thecodontosaurus latespinatus*	De Lapparent and Lavocat, p. 933
1955	*Tanystropheus conspicuus*	Peyer, p. 489
1955	*Macrosclerosaurus*	Peyer and Kuhn-Schnyder, p. 578
1955	*Tanystropheus conspicuus*	Peyer and Kuhn-Schnyder, p. 578; figures 1, 21
1956	*Megacnemus*	von Huene, p. 648
1956	*Tanystropheus* (partim)	von Huene, figure 657e
1956	*Tanystropheus* (partim)	Romer, figure 122M
1958	"Parasuchier" (partim)	von Huene, p. 66; figure 4
1961*a*	*Megacnemus*	Kuhn, p. 5
1961*b*	*Chelyzoon*	Kuhn, p. 32
1963	*Megacnemus grandis*	Kuhn, p. 9
1963	*Tanystropheus conspicuus*	Kuhn, p. 6
1965	*Tanystropheus conspicuus*	Kuhn, p. 45
1965	*"Thecodontosaurus" latespinatus*	Kuhn, p. 45
1969	*Megacnemus grandis*	Kuhn, p. 70; plate 24, figure 3
1969	*Tanystropheus conspicuus*	Kuhn, p. 71
1969	*Tanystropheus* (partim)	Kuhn, plate 19, figure 18
1969	*Thecodontosaurus* (partim)	Kuhn, plate 21, figure 22
1970	*Thecodontosaurus latespinatus*	Colbert, p. 31–33
1971	*Chelyzoon blezingeri*	Kuhn, p. 10
1971	*Chelyzoon latum*	Kuhn, p. 10; plate 17, figure 1
1971	*Megacnemus grandis*	Kuhn, p. 12
1971	*Tanystropheus conspicuus*	Kuhn, p. 11; plate 21a, figure 1a–c; plate 41b, figures 11–12
1971	*Tanistropheus longobardicus* (partim)	Kuhn plate 21, figure 11
1971	*Thecodontosaurus latespinatus*	Kuhn, p. 17; plate 21, figure 26
1972	*Tanystropheus conspicuus*	Emmert and von Horstig, plate 2, figure 4
1973	*Tanystropheus conspicuus*	Wild, throughout text; figures 38–62, 67, 73, 97b–c
1973	*Megacnemus grandis*	Wild, p. 119; plate 21, figure 1
1974	*Tanystropheus conspicuus*	Kuhn-Schnyder, p. 55–56
1975	*Tanystropheus conspicuus*	Jurcsak, p. 46–48
1975	*Tanystropheus* sp.	Kuhn, p. 9–10
1975*a*	*Tanystropheus conspicuus*	Wild, p. 153; figure 1
1975*b*	*Tanystropheus conspicuus*	Wild, throughout text

1976	*Tanystropheus latespinatus*	Galton and Cluver, p. 153
1976*a*	*Tanystropheus conspicuus*	Wild, p. 125
1976*b*	*Tanystropheus conspicuus*	Wild, p. 15, 20; figure 3
1977	*Tanystropheus conspicuus*	Wild, p. 675; figure 1
1980*a*	*Tanystropheus conspicuus*	Wild, throughout text
1980*b*	*Tanystropheus conspicuus*	Wild, p. 201, 204–205
1981	*Tanystropheus conspicuus*	Melville, p. 188
1986	*Tanystropheus conspicuus*	Benton, p. 296–297
1986	*Tanystropheus conspicuus*	Chatterjee, p. 311
1986	*Tanystropheus conspicuus*	Tschanz, throughout text
1987	*Tanystropheus conspicuus*	Wild, p. 37, 39, 42
1988	*Megacnemus*	Carroll, p. 619
1988	*Tanystropheus conspicuus*	Hagdorn and Reif, p. 130
1988	*Tanystropheus conspicuus*	Tschanz, p. 997–998, 1002
1988	*Tanystropheus conspicuus*	Evans, p. 227
1989	*Tanystropheus conspicuus*	Wild, p. 40
1990	*Tanystropheus conspicuus*	Hagdorn, p. 86
1991	*Tanystropheus conspicuus*	Olshevsky, p. 106, 181–182
1995	*Tanystropheus conspicuus*	Lucas, p. 94
1996	*Tanystropheus*	Rieppel and Wild, p. 61
1997	*Tanystropheus conspicuus*	Benton and Allen, p. 945, 947
1999	*Tanystropheus conspicuus*	Hagdorn and Rieppel, p. 662, 664, 667
1999	*Tanystropheus conspicuus*	Hauschke and Wilde, p. 332, 340, 590
1999	*Tanystropheus conspicuus*	Rieppel et al., p. 75
1999	*Tanystropheus conspicuus*	Schoch, p. 14
2000	*Tanystropheus conspicuus*	Dalla Vecchia, p. 136, 138–139
2001	*Tanystropheus conspicuus*	Rieppel, throughout text
2003	*Tanystropheus conspicuus*	Oosterink et al., p. 42
2005	*Tanystropheus conspicuus*	Renesto, p. 386
2005	*Megacnemus*	Sennikov, p. 200, 206
2005	*Tanystropheus conspicuus*	Sennikov, p. 207
2006	*Tanystropheus conspicuus*	Dalla Vecchia, p. 40–42
2006	*Tanystropheus conspicuus*	Fraser and Rieppel, p. 866, 870
2007	*Tanystropheus conspicuus*	Nosotti, throughout text
2008	*"Tanystropheus conspiquus"*	Dalla Vecchia, p. 81
2009	*Tanystropheus conspicuus*	Spielmann et al., p. 307; fig. 13
2009	*Tanystrophaeus longibardicus* (partim)	Diedrich, p. 1, 6, 12; figure 12
2011	*Tanystropheus conspicuus*	Sennikov, p. 100
2012	*Tanystrophaeus conspicuus*	Diedrich, throughout text; figure 14: 2–15
2014	*Tanystropheus longobardicus* (partim)	Ezcurra et al., throughout text, figures 16D, 18C
2014	*Tanystropheus conspicuous*	Ezcurra et al., p. 25
2015	*Tanystropheus conspicuus/ Tanystrophaeus conspicuus*	Diedrich, throughout text; figure 10C:2
2015	*Tanystropheus conspicuus*	Pritchard et al., p. 4, 9, 15
2015	*Tanystropheus conspicuus*	Nesbitt et al., throughout text
2015	*Tanystropheus conspicuus*	Schoch, p. 243, figure 10.7a–b

2015	*Tanystropheus* sp.	Schoch, p. 243, figure 10.13l
2015	*Tanystropheus*	Hagdorn et al., p. 336, 350, 354, 356
2016	*Tanystropheus longobardicus* (partim)	Ezcurra, throughout text; figures 14A–B, 31B, 33B, 35A, 43A–B
2017	*Tanystropheus conspicuus*	Beardmore and Furrer, p. 2
2017	*Tanystropheus* sp. (partim)	Jaquier and Scheyer, figures 1B–C; 2A, E–H;
2017	*Tanystropheus conspicuus*	Jaquier and Scheyer, figures 1E; 2D;
2017	*Tanystropheus conspicuus*	Skawiński et al., p. 4, 14–15; figure 5O–P
2017	*Tanystropheus conspicuus*	Sues, p. 129–130
2018	*Tanystropheus conspicuus*	Renesto and Saller, p. 23
2018	*Tanystropheus* (partim)	Schoch et al. 2018, p. 630; figure 4q
2019	*Tanystropheus conspicuus*	Rieppel, throughout text
2019	*Tanystropheus conspicuus*	Spiekman and Scheyer, throughout text
2019	*Tanystropheus conspicuus*	Spiekman et al., throughout text
2020	*Tanystropheus conspicuus*	Dalla Vecchia, throughout text
2020	*Tanystropheus longobardicus* (partim)	Ezcurra et al., figure 1D
2020	*Tanystropheus conspicuus*	Ősi et al., p. 266
2020*b*	*Tanystropheus 'conspicuus'*	Spiekman et al., p. 7, 59, 63
2021*a*	*Tanystropheus conspicuus*	Brignon, p. 33
2021*b*	*Tanystropheus* sp.	Brignon, throughout text; figure 34B
2021	*Tanystropheus conspicuus*	Hauschke et al., p. 334
2021	*Megacnemus grandis*	Spiekman et al., p. 11
2021	*Tanystropheus "conspicuus"*	Spiekman et al., throughout text
2022	*Tanystropheus conspicuus*	Klein et al., p. 9–10
2022	*Tanystropheus conspicuus*	Sues et al., p. 7
2023	*Tanystropheus "conspicuus"*	Czepiński et al., p. 6
2024*a*	*Tanystropheus 'conspicuus'*	Rytel et al., throughout text
2024*b*	*Tanystropheus 'conspicuus'*	Rytel et al., throughout text
2024*b*	*Tanystropheus "conspicuus"*	Spiekman et al., p. 14, 28
2024	*Tanystropheus conspicuus*	Sues, p. 4
2025	*Tanystropheus conspicuus*	Dalle-Laste et al., p. 7-9
2025	*Tanystropheus conspicuus*	Schubul et al., p. 106, 114
2025	*Tanystropheus*	Schwermann et al., figure 1
2025	*Tanystropheus conspicuus*	Sues and Schoch, p. 441, figure 8C
2025	*'Chelyzoon'*	Szczygielski et al., p. 23

Nomenclatural clarification

The available generic name *Tanystropheus* was first mentioned in 1849 by von Meyer (1849), who attributed elongate vertebrae from Laryszów and Bayreuth to this animal. Following Article 11.4.1 of the International Commission on Zoological Nomenclature (ICZN), this usage was valid, despite not being associated with any nominal species. Some of the soon-to-become syntypes from Bayreuth were illustrated even earlier, by Braun (1840), but not named. The first comprehensive description encompassing the remains from both Franconia and Silesia was included in von Meyer (1847-1855), who introduced *Tanystropheus*

conspicuus, the type species of the genus. The investigation of Quenstedt (1963) has shown that this combination seems to have appeared in print in 1852, even though some of the plates including the lithographs of the type material could have been delivered as early as 1847 (contents of this publication were printed gradually, in instalments). According to Article 21.6 of the ICZN, 1852 is adopted as the year of publication containing the first valid usage of the specific name. Some authors (Broili 1915; Kuhn 1934) have argued that the genus name *Macroscelosaurus* Münster, 1834 has precedence over *Tanystropheus* von Meyer, 1852 (see Nosotti 2007). As a result of the requests of Wild (1975*a*, 1976*a*), the ICZN suppressed *Macroscelosaurus* Münster, 1834 and conserved the generic name *Tanystropheus* von Meyer, 1849 (Melville 1981). *Tanystropheus conspicuus* von Meyer, 1852 was designated as the type species by monotypy. Spiekman and Scheyer (2019) considered this species a *nomen dubium*, arguing that it is represented by material that is diagnostic on the genus level, but insufficient to distinguish it convincingly from other *Tanystropheus* species. The taxonomic status of *Tanystropheus conspicuus* is further explored in this work, on the basis of the newly identified remains.

The authorship of family-group name Tanystropheidae was historically nearly unequivocally attributed to Gervais (1858) or Gervais (1859). Recently Spiekman et al. (2020*a*, supplemental information – methods S1) argued that this name does not appear in either of the two sources, but instead is mentioned for the first time in Camp (1945), with an incorrect spelling, as Tanystrophaeidae. According to ICZN Article 35.4.1, the emended name would be Tanystropheidae Camp, 1945. There are, however, at least two cases of older family-group names based upon synonyms of *Tanystropheus* – Tribelesodontidae von Nopsca, 1923 and Macrosclerosauridae Kuhn, 1934. As the type genus of the latter taxon has been suppressed (Melville 1981), this name is no longer valid, according to ICZN Article 39. *Tribelesodon* Bassani, 1886 was considered a junior synonym of *Tanystropheus* von Meyer, 1849 by Peyer (1930), and Tribelesodontidae von Nopsca, 1923 has been in disuse since then. According to ICZN Article 40, Tanystropheidae Camp, 1945 should be maintained instead, due to its overwhelming prevailing usage, with Tribelesodontidae von Nopsca, 1923 as its senior synonym. According to ICZN Recommendation 40A, the family-group name should be cited with its original author and date followed by the date of its priority – Tanystropheidae Camp, 1945 (1923). That is, if we consider the name used by Gervais (1859) as not valid. Gervais (1859), page 485, mentions “Les *Tanystrophes*” as one of the extinct “reptile” **families** not yet observed in France (the list also included taxonomic names of

relatively higher ranks: dicynodonts, rhynchosaurs, thecodontosaurs etc.), clearly using it as a scientific name to denote a suprageneric taxon. Even though only the vernacular form of the taxon was mentioned, it is available as a family-group name with its original author and date, according to ICZN Article 11.7 (more explicitly, Article 11.7.2), as it has been latinised by later authors and has been generally accepted as valid by researchers interested in the group (e.g., Wild 1973; Rieppel 2001; Renesto 2005; Fraser and Rieppel 2006; Nosotti 2007; Sennikov 2011; Skawiński et al. 2017; Formoso et al. 2019; Dalla Vecchia 2020; Ősi et al. 2020; Sues and Schoch 2025). Before the publication of Spiekman et al. (2020*a*), virtually all authors attributed the authorship of Tanystropheidae to Paul Gervais, with some citing Gervais (1858) instead of Gervais (1859), albeit mistakenly, as there is no mention of *Tanystropheus* or "Les *Tanystrophes*" in Gervais (1858). For the sake of taxonomic stability, in accordance with the rules of ICZN, I propose to conserve the uniform usage of **Tanystropheidae Gervais, 1859** as the name of the family with *Tanystropheus* as its type genus.

Protorosauria Huxley, 1871 has been widely used as a suprafamiliar group name that encompasses Tanystropheidae, usually at the rank of an Order. The monophyly and composition of Protorosauria has been extensively studied and discussed (e.g., Dilkes 1998; Rieppel et al. 2003; Gottmann-Quesada and Sander 2009; Ezcurra et al. 2014; Pritchard et al. 2015; Ezcurra 2016; but see Spiekman et al. 2021 for a summary). Most recently, Spiekman et al. (2021) conducted a detailed phylogenetic analysis focusing on the group, and argued against its usage, due to its possible polyphyly. Yet, if defined as an order encompassing all non-crocopodan archosauromorphs, it is a grade (see Ezcurra et al. 2025 and Schoch et al. 2025 for the latest iterations of the phylogenetic analyses focusing on early archosauromorphs). Paraphyletic groups are an important and still widely used part of biological classification, and they can convey useful phylogenetic and evolutionary information (see Hörandl 2006; Hörandl and Stuessy 2010; Carter et al. 2015). It is beyond the scope of this work, however, to formally draw the boundaries of what is a protorosaur. In the absence of a non-obscure alternative, Protorosauria is regarded as the order-rank taxon including *Tanystropheus*.

Description

Cranial elements of *Tanystropheus conspicuus* are described only on a preliminary basis, as the Miedary site is still yielding new skull bones. A detailed comparative description of the cranial material of *T. conspicuus*, including a reconstruction of the skull, will be carried out in the future. Herein I describe the cranial features due to their usefulness in the species differentiation within *Tanystropheus*.

Skull

Premaxilla

The premaxilla of *Tanystropheus conspicuus* is an elongate, flat, element (Fig. 2). Similar to the other species of *Tanystropheus*, it bears six circular alveoli, from which the anterior five are subequal in size (Fig. 2B; Wild 1973; Nosotti 2007; Spiekman and Scheyer 2019, Spiekman et al. 2020*b*). As in *T. hydroides*, the posteriormost alveolus is slightly smaller (Spiekman et al. 2020*b*). The alveoli are aligned in a single row, with the openings of the anterior three being more laterally oriented than the posterior three, which are predominantly ventral-facing (Fig. 2 B_1). They are evenly spaced along the anterolateral margin of the premaxilla, and clearly outlined in dorsal view (Fig. 2 A_2), being marked by a labial expansion of the dorsal alveolar wall, as in *T. hydroides* but unlike *T. longobardicus* (Fig. 2B; Nosotti 2007; Spiekman et al. 2020*b*). Tooth implantation was anisothecodont (="subthecodont", see "Dentition" below). Lingually, the premaxillary teeth were separated by triangular interdental plates (Fig. 2 B_2). This represents the first known occurrence of interdental plates outside of Archosauriformes (Nesbitt 2011; Ezcurra 2016), in which this character occurs broadly, suggesting a considerably earlier origin of this trait than previously considered among Archosauromorpha. Between the interdental plates, the lingual margin of each alveolus is distomesially constricted, but widens gradually towards its rounded lingual margin in ventral view, forming a deep, droplet shaped notch (Fig. 2 B_2).

At the base of the lingual side of the alveoli, there is a distinct, sharp, medial ridge, which projects ventrally, roughly at the mid-point of the premaxilla. The symphysial contact of the premaxilla with its antimere (i.e. corresponding, symmetrical element) was along a straight line. Posterior to it, an incipient prenarial process was identified by Spiekman et al. (2020*b*) in *T. hydroides*. A similar, ventromedially oriented ridge is present in the premaxillae of *T. conspicuus*, but it does not extend posteriorly nor does it possess a nasal facet. Therefore, as in *T. hydroides*, it is here interpreted as the posterior extension of the symphysial margin instead. The dorsal surface of the premaxilla is rugose and bears no foramina, as in *T.*

hydroides, but not in *T. longobardicus* (Nosotti 2007; Spiekman et al 2020*b*). Compared to the symphysial margin, the posterior premaxillary edge, which articulated with the maxilla, retains a similar transverse width, but it is more inclined. The postnarial process is absent, similar to *T. hydroides* but unlike *T. longobardicus* (Nosotti 2007; Spiekman et al 2020*b*). As in *T. hydroides*, the dorsomedial edges of the premaxillae constituted the anterior margin of a single, dorsally oriented external naris (Fig. 2A). Overall, the maxilla of *T. conspicuus* closely resembles the maxilla of *T. hydroides*, but appears to be relatively more dorsoventrally flattened and anteroposteriorly elongate.

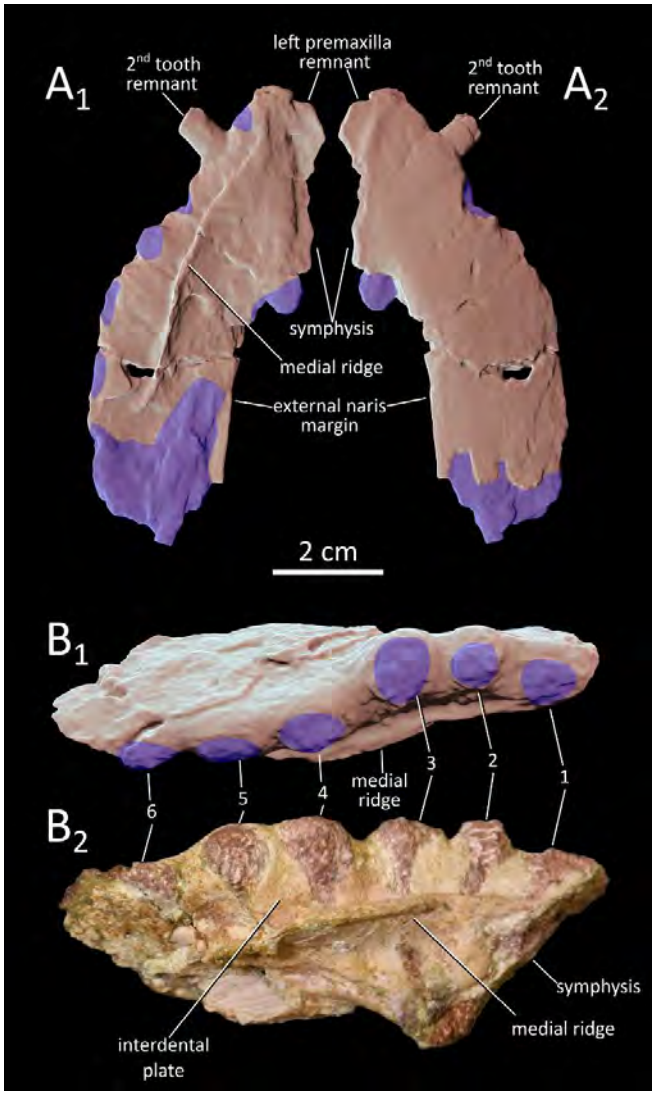

Fig. 2. Right premaxillae of *Tanystropheus conspicuus* from the Lower Keuper (lower Ladinian) of Miedary (Poland) – ZPAL V. 36/179 (**A**) and ZPAL V. 36/2487 (**B**). A photograph (B_2) and three-dimensional model snapshots with Lit Sphere Radiance Scaling shader enabled (A, B_1), in ventral (A_1, B_2), dorsal (A_2), and anterolateral (B_1) views. Numerals indicate the alveoli. Areas covered with sediment marked with blue hue.

Maxilla

The maxilla of *Tanystropheus conspicuus* is a relatively flat and slender element (Fig. 3). Thirteen or fourteen alveoli are present in the complete maxilla ZPAL V. 36/2474 (Fig. 3B). Although some intraspecific variation seems to exist, presence of a similar number of maxillary teeth has been reported for *T. longobardicus* (11-15, Wild 1973; Nosotti 2007) and *T. hydroides* (12-15, see Wild 1973; Spiekman et al. 2020*b*). Characteristics of the alveoli are similar to those described for the premaxilla. In ventral view they are all circular, and densely packed along a single, straight line (Fig. $3A_5$, B_1). Lingually, the maxillary teeth were separated by triangular interdental plates. Between the interdental plates, the lingual margin of each alveolus is formed as a deep, droplet-shaped notch. Unlike on the premaxilla, there is a considerable alveolus (tooth) size difference. The middle (sixth-seventh) maxillary teeth were likely comparable in size to the premaxillary teeth, but the maxillary teeth size gradually decreased both anteriorly and posteriorly to these teeth (Fig. $3A_1$, B_1). In *T. hydroides* this configuration is identical (Spiekman et al. 2020*b*).

The anterior edge of the maxilla is straight in lateral view (Fig. $3A_{2-3}$, B_2), and its articulation with the premaxilla seems to have been relatively simple. The dorsal surface of the anterior portion of the maxilla is flat and medially expanded, forming a distinct, ventromedially projecting dorsomedial shelf. Around the mid-length of the maxilla, the dorsal margin extends dorsomedially, forming the ascending process. It is triangular in lateral view, short, and composed of a thin bony plate that forms a rounded distal end.

A prominent longitudinal canal is present within the anterior portion of the maxilla, directly ventral to the dorsally rounded dorsal apex (Fig. $3A_1$). Its diameter is constant and there are no branchings. Anteriorly, this canal continues at least to the articulation surface of the premaxilla. Posteriorly, it terminates as a foramen on the medial side of the ascending process. In *T. hydroides* a canal of nearly identical morphology is present in the same relative location, posteriorly terminating at the articulation surface of the lacrimal (pers. obs. AR). Its occurrence was not mentioned by Spiekman et al. (2020*b*), but it was segmented within the left maxilla of PIMUZ T 2790. The lacrimal in this specimen is pierced by a large foramen for the nasolacrimal duct (Spiekman et al. 2020*b*), which corresponds with its size and location to the canal present in the maxilla. The canal present in the maxillae of both *T. conspicuus* and *T. hydroides* was likely a part of the nasolacrimal duct. Alternatively, it could be interpreted as the maxillary canal. However, this less likely, as in other Permo-Triassic diapsids the maxillary canal is located ventral to the nasolacrimal duct, ventrally along the edge of the

dental margin, and has branchings (Ford and Benson 2018; Benoit et al. 2021). The tube-like canal in the maxilla of *T. conspicuus* and *T. hydroides* is located parallel to the dorsal margin of the bone, but its dorsoventral distance from the alveoli changes significantly along its length (Fig. $3A_1$).

The ventral maxillary edge is relatively straight in lateral view, being only slightly convex at mid-length (Fig. $3A_{2-3}$, B_2). Its posterior portion forms a triangular process, which tapers to a point (Fig. $3B_2$). On the dorsolateral surface of the posterior process of the maxilla, an elongate groove is present, marking the location of the jugal facet. Along the same section of the posterior process, but on its medial surface, a slightly medially extended shelf is present, which formed the articular facet for the palatine. Between the jugal and the palatine facets, an anteroposteriorly oriented ridge is located. It is lateromedially thin and extends dorsally. The lacrimal articulated between the posterior edge of the ascending process, and the anterior portion of the posterior process. The surface of the maxilla is generally smooth, but with a slightly rugose texture. No large foramina are present.

The morphology of the maxilla of *Tanystropheus conspicuus* is generally congruent with that of *T. hydroides*. Both species are different in similar respects to *T. longobardicus*. The latter has a proportionally much taller maxilla bearing tricuspid teeth that are homodont in size and a much more dorsally expanded ascending process (Nosotti 2007; Spiekman et al. 2020*b*). The overall configuration of the alveoli makes it likely that *T. hydroides* also possessed interdental plates, although the nature of the reconstructed CT data makes it difficult to identify these structures unambiguously (see Spiekman et al. 2020*b*, fig. 7). The maxilla of *T. conspicuus* is nevertheless distinct from that of *T. hydroides* in several features. Importantly, the maxilla of *T. conspicuus* lacks the foramen for a dentary tooth, the presence of which was considered an autapomorphy of *T. hydroides* by Spiekman et al. (2020*b*). In addition, the main character serving as a basis for differentiating the maxillae of *T. conspicuus* and *T. hydroides* is the relative height of the posterior process. In the former species it is much taller, being anteriorly nearly as tall as the portion of the maxilla anterior to the ascending process.

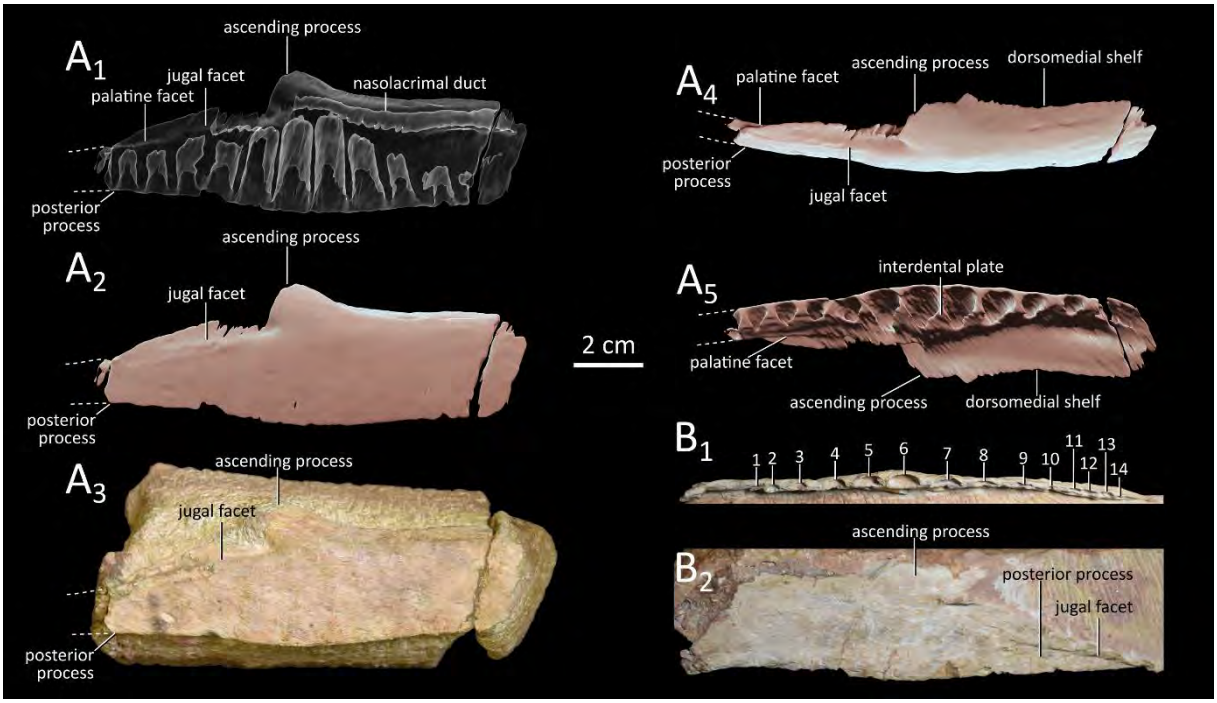

Fig. 3. Maxillae of *Tanystropheus conspicuus* from the Lower Keuper (lower Ladinian) of Miedary (Poland) – right ZPAL V. 36/1213 (**A**) and left ZPAL V. 36/2474 (**B**) element. Photographs (A_3, B) and three-dimensional segmented model snapshots with X-ray (A_1) and Lit Sphere Radiance Scaling (A_2, $A_{4–5}$) shaders enabled, in lateral ($A_{1–3}$, B_2), dorsal (A_4), and ventral (A_5, B_1) views. Numerals indicate the alveoli.

Skull roof

The skull roof of *Tanystropheus conspicuus* is known only from one specimen, ZPAL V. 36/1244, which preserves the frontals, fused parietals, and partial postorbitals (Fig. 4). The postfrontals are seemingly absent, as in *T. hydroides* (see Spiekman et al. 2020*b*), but this is equivocal as the posterolateral portions of the preserved skull roof are damaged. The preserved elements are in tight articulation and therefore did not disassociate during postmortem transport, contrary to the great majority of vertebrate fossils from Miedary.

Frontal

The frontals are flat, dorsoventrally thin, and transversely wide elements. They are trapezoidal in dorsal view, with their posterior portions more expanded laterally than the anterior portions, and their transverse width notably greater than anteroposterior length (Fig. 4A–F). The anterior frontal margin is concave in dorsal view and bears a short, rounded anterior process on its medial side (Fig. 4A–G). Posterior to it, there is a distinct ridge on the dorsal surface of the frontal, which parallels the anterior edge in its curvature, with a crescent-

shaped, flat, and relatively smooth surface formed between them (Fig. 4E). This is the facet for the nasal, which would have dorsally overlapped the frontal. In anterior view, the portion of the anterior margin of the frontal adjacent to the midline suture is slightly concave (Fig. 4G). As in *T. hydroides*, this concavity marks the anterior edge of the broad, obliquely oriented medial depression of the frontal, which extends towards the posteromedial corner of the bone (Fig. 4E; Spiekman et al. 2020*b*). Further laterally, the anterior margin is convex in dorsal view, forming the anterolateral corner of the frontal and the attachment area for the prefrontal. Posterior to it, the lateral margin of the frontal is dorsoventrally thickened and slightly convex in lateral view (Fig. 4I–J).

The posterior frontal margin is relatively straight in dorsal view and somewhat ventrally expanded, constituting the articulation surface for the medial process of the postorbital along its entire length. The posteromedial corner of the frontal tapers posteriorly to a point, forming the ventral portion of the anterior edge of the parietal foramen. The anterolateral process of the parietal articulated on top of the posteromedial region of the frontal, overlapping the distal portion of the medial process of the postorbital dorsally (Fig. 4B). The midline suture between the frontals is relatively straight, but interdigitating over part of its length, with several transversely extending laminae overlapping similar structures projecting from the antimere (Fig. 4B–F). The dorsal surface of the frontals displays longitudinal grooves radiating from the centre of growth, with the orbital rim being especially rugose. On the ventral surface of the frontal, a poorly defined ridge, *crista cranii*, extends from the posteromedial corner of the bone, parallel to the midline suture (Fig. 4F). It tapers anteriorly, terminating approximately at mid-length of the element. Spiekman et al. (2020*b*) interpreted this feature as the posterior portion of the margin of the olfactory tract. As for *T. hydroides* but unlike *T. longobardicus*, there is no depression accommodating the olfactory bulb (Nosotti 2007; Spiekman et al. 2020*b*).

The overall anatomy of the skull roof is very reminiscent to the description for *T. hydroides* by Spiekman et al. (2020*a*, *b*), and the comparisons to other archosauromorph taxa (including *T. longobardicus*) made therein are valid for *T. conspicuus* as well. There are, however, several significant differences in the proportions of the frontals between the three known specimens of *T. hydroides* preserving them (PIMUZ T 2787, PIMUZ T 2790, PIMUZ T 2819) and *T. conspicuus* (Fig. 5). In the former the elements taper anteriorly, and their transverse width increases posteriorly at a relatively constant rate. Thus, in dorsal view they are roughly triangular (Fig. 5C). By contrast in *T. conspicuus* they are trapezoidal, with their

anterior margin being slightly concave along the articulation with the nasals. Furthermore, because their anterior margin is more latero-medially oriented, the frontals of *T. conspicuus* are relatively shorter anteroposteriorly than in *T. hydroides* (Fig 5B–C). *T. conspicuus* exhibits an even more transversely wide interorbital region of the skull roof than the already remarkably expanded interorbital region of *T. hydroides* (see Spiekman et al. 2020*b*). Whereas in the latter the transverse width of the frontal is roughly equal to its anteroposterior length, in the former it is about 1.2-1.3 wider than long. The articulation facets for the nasals, well-marked in *T. conspicuus*, are not visible in the currently known specimens of *T. hydroides* (see Wild 1973; Spiekman et al. 2020*b*). The midline suture in *T. hydroides* is straight in all specimens in which it can be observed (PIMUZ T 2787, PIMUZ T 2790, PIMUZ T 2819; Spiekman et al. 2020*a*, *b*), and in contrast to the condition of *T. longobardicus* (Fig. 5; Nosotti 2007; Spiekman and Scheyer 2019; Spiekman et al. 2020*b*). As for *T. longobardicus*, in *T. conspicuus* the midline suture is interdigitating, especially along its posterior portion (Fig. 5A, C). Although this specific feature might change during ontogeny, the remaining aspects of the cranial morphology of *T. conspicuus* allow for its clear differentiation from other species of *Tanystropheus*.

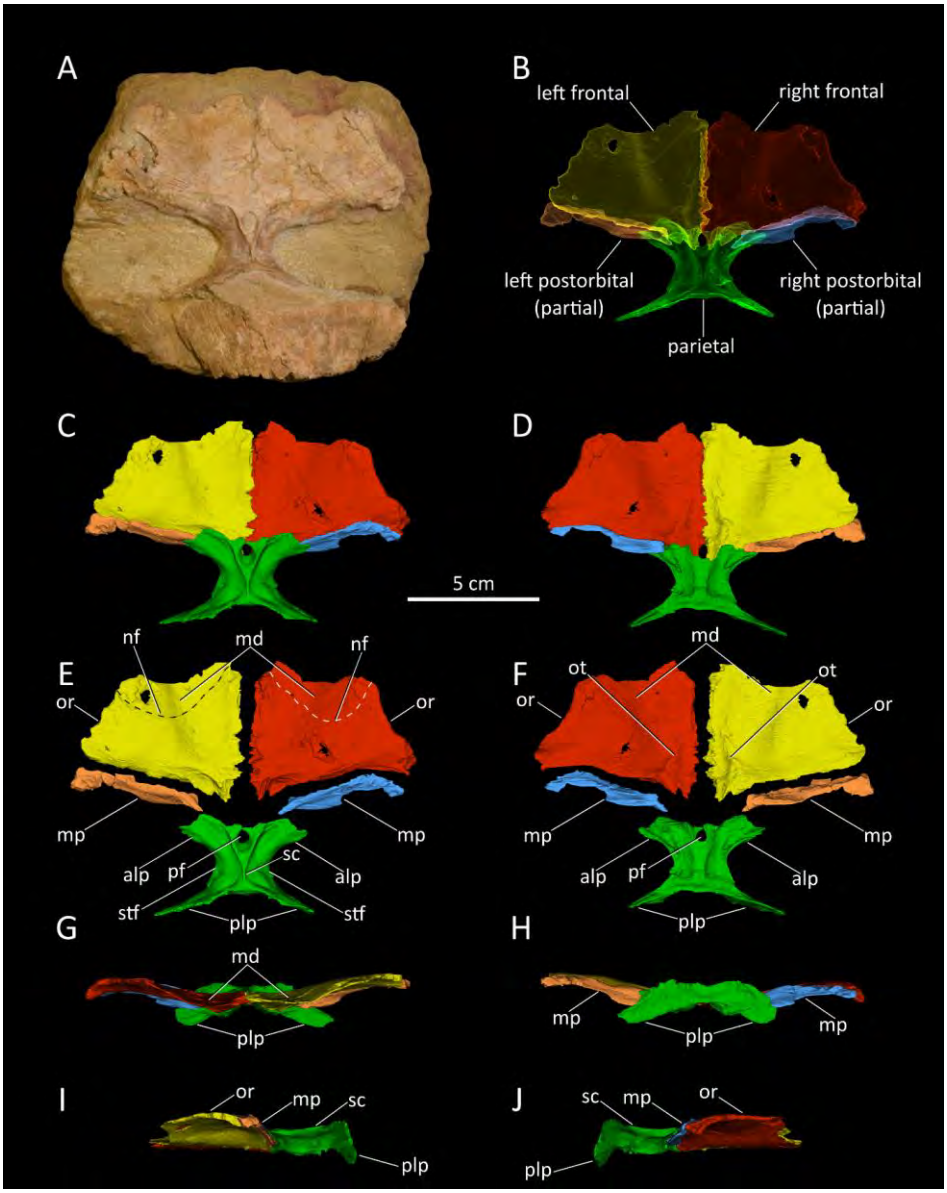

Fig. **4**. Skull roof ZPAL V. 36/1244 of *Tanystropheus conspicuus* from the Lower Keuper (lower Ladinian) of Miedary (Poland). A photograph of the original specimen (A) and three-dimensional segmented model snapshots with X-ray (B) and Lambertian Radiance Scaling (C–J) shaders enabled, in dorsal (**A–C, E**), ventral (**D, F**), anterior (**G**), left lateral (**I**), posterior (**H**), and right lateral (**J**) views, in natural articulation (A–D, G–J) and manually disarticulated (E–F). The left frontal was slightly damaged post-CT scanning, hence the difference in its morphology between the photograph (A) and the segmented model snapshots (B–J). Different colours demark different bones (see B). Dashed lines outline the posterior margin of the nasal facet. Abbreviations: alp, anterolateral process; md, medial depression; mp, medial process of a postorbital; nf, nasal facet (posterior extent); ot, olfactory tract margin (*crista cranii*); or, orbital rim; pf, parietal foramen; plp, posterolateral process; sc, sagittal crest; stf, supratemporal fossa.

Postorbital

The morphology of the postorbital in *Tanystropheus conspicuus* is only partially known, as ZPAL V. 36/1244 only preserves the medial processes of both postorbitals. They are in tight articulation with the corresponding frontals and parietals (Fig. 4B). The medial process of the postorbital in *T. conspicuus* partially dorsally overlaps the posterior margin of the frontal and is more ventrally expanded, forming a vertically oriented, flat, plate-like projection, which tapers distally to a point. The base of the process is thickened and has a rugose dorsal surface. The medial process constituted the anterior margin of the supratemporal fenestra, separating it completely from the frontals. Whereas the morphology of the medial process of the postorbital in *T. hydroides* cannot be fully discerned from the holotype (Spiekman et al. 2020*b*), the referred specimen PIMUZ T 2819 exhibits both nearly identical proportions and an identical position for this process as in *T. conspicuus*.

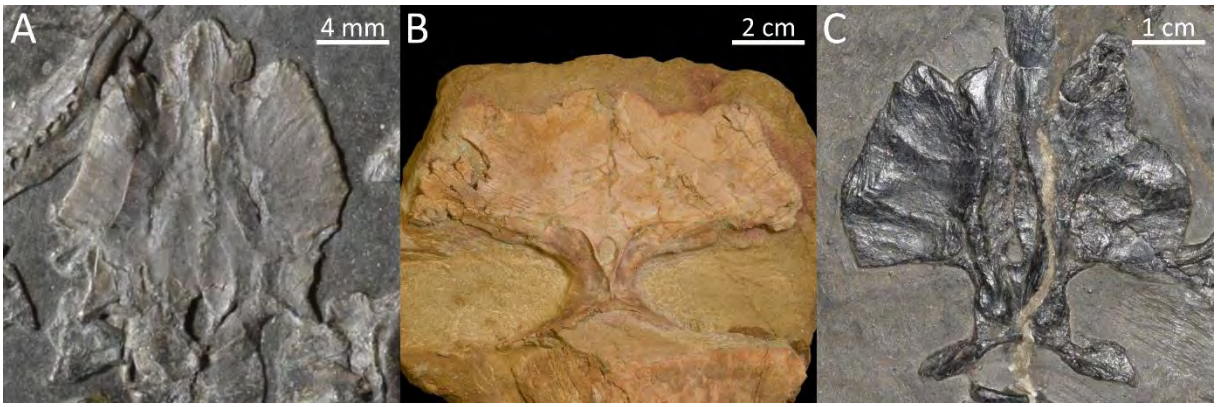

Fig. 5. Comparison of the skull roof morphology in tree species of *Tanystropheus*. Photographs of the frontals in: *T. longobardicus* from the Besano Formation (upper Anisian to lower Ladinian) of Monte San Giorgio (Switzerland) – PIMUZ T 2484 in dorsal view (**A**); *T. conspicuus* from the Lower Keuper (lower Ladinian) of Miedary (Poland) – ZPAL V. 36/1244 in dorsal view (**B**); and *T. hydroides* from the Besano Formation (upper Anisian to lower Ladinian) of Monte San Giorgio (Switzerland) – PIMUZ T 2787 in ventral view (**C**).

Parietal

The parietals are seamlessly fused, forming a single element that is X-shaped in dorsal view. The anterior end of the parietal is composed of a complex set of pits, ridges, and grooves, which are bilaterally symmetrical, forming an intricate, tight articulation with the postorbitals and the frontals anteriorly (Fig. 4F). The anterolateral process of the parietal dorsally overlaps the posteromedial corner of the corresponding frontal and the distal portion

of the medial process of the postorbital, which is enclosed by them. The parietal foramen is relatively large, subcircular, and well outlined. The frontals contributed only to the ventral portion of its anterior margin, with the parietals fully enclosing it along its dorsal rim (Fig. 4C–D).

The foramen is posterolaterally flanked by ridges that merge posteriorly to it, forming a low but well defined sagittal crest, which runs along the midline of the parietals (Fig. 4E). The surface of the parietals is bilaterally concave, forming the supratemporal fossae, which constituted the entire medial margin of the supratemporal fenestrae. The portion of the fenestra enclosed by the parietal is semicircular, with the anterolateral parietal process contributing to its anteromedial edge and the posterolateral process contributing to its posteromedial edge (Fig. 4B–D). The posterolateral process is longer than the anterolateral process, forming an anteroposteriorly thin projection with a distal portion that is seemingly rounded in posterior view (Fig. 4H, although the distal tip itself is not preserved in ZPAL V. 36/1244). As for *Tanystropheus hydroides*, it is dorsoventrally tall and almost entirely transversely oriented (Spiekman et al. 2020*b*). In fact, the parietal of *T. conspicuus* does not seem to differ from *T. hydroides* in any major feature (see Wild 1973; Nosotti 2007; Spiekman and Scheyer 2019; Spiekman et al. 2020*b*).

Quadrate

The quadrate of *Tanystropheus conspicuus* strongly resembles the quadrate of *T. hydroides* (compare Fig. 6 and fig. 14 of Spiekman et al. 2020*b*). The shaft is formed as a longitudinal, vertical thickening located along the transverse mid-width of the bone (Fig. 6). Its dorsal portion is nearly vertical (Fig. 6A_1). More ventrally it slopes gently posteriorly, with the middle portion of the shaft being slightly concave in lateral view and the ventral portion ventromedially directed (Fig. 6A_1, A_3, A_6). The dorsal margin of the quadrate is convex in posterior view, with the thickened dorsal portion of the shaft projecting posterodorsally from it (Fig. 6A_5–A_6, B).

The dorsolateral tip of the shaft has a rough surface, forming a distinct, slightly laterally expanded tuberosity. In *T. hydroides* this tuberosity forms a dorsal hook, which was considered to be one of the autapomorphic features of this taxon by Spiekman et al. (2020*a, b*). All known quadrates of *T. conspicuus* (ZPAL V. 36/574, ZPAL V. 36/1350, ZPAL V. 36/1764) are relatively well preserved, but the dorsal tuberosity in all of them is eroded and

likely missing its tip, which was originally more laterally extended, possibly forming the conspicuous hook, as in *T. hydroides*.

Two thin plates of bone project from the shaft, anterolaterally and anteromedially, respectively, with a right angle formed between them (Fig. 6A$_3$). The anteromedial extension is the pterygoid ramus. It is roughly semicircular in medial view, although it is not fully preserved in any of the known specimens (Fig. 6A–B). On the posterior surface of the quadrate, near the pterygoid ramus, a faint elliptical concavity is present. On the opposite side of the ramus, a corresponding convexity is present (Fig. 6B). The anterolateral edge of the quadrate is constricted laterally at mid-height, with the two resulting triangular projections being separated by the posterior margin of the quadrate foramen (Fig. 6A$_5$–A$_6$, B). The one located dorsally to the notch bears the tympanic crest.

The lateral condyle is present ventrally to the tympanic crest and projects more strongly from the shaft (Fig. 6A$_5$–A$_6$, B). As in *T. hydroides*, its dorsolateral surface is occupied by an elliptical facet which receives the ventral portion of the quadratojugal (Fig. 6A$_6$; Spiekman et al. 2020*b*). Posterior to the lateral condyle, the ventral surface of the quadrate is concave in posterior view, forming a groove, which demarcates the boundary between the lateral and medial condyles of the ventral quadrate end (Fig. 6A$_5$–A$_6$, B). In ventral view, their distal margins are thickened anteromedially, with an anteroposterior constriction of the ventral margin of the quadrate separating them (Fig. 6A$_4$). The medial condyle is more robust than the lateral condyle, and projects posteroventrally. Its posterior margin is confluent with the ventral portion of the shaft. A “Foramen quadrati” was previously considered present in *T. hydroides* and *T. longobardicus* by Wild (1973, p. 12) but was not identified in either species in the study of Spiekman et al. (2020*b*) and is also absent in *T. conspicuus*.

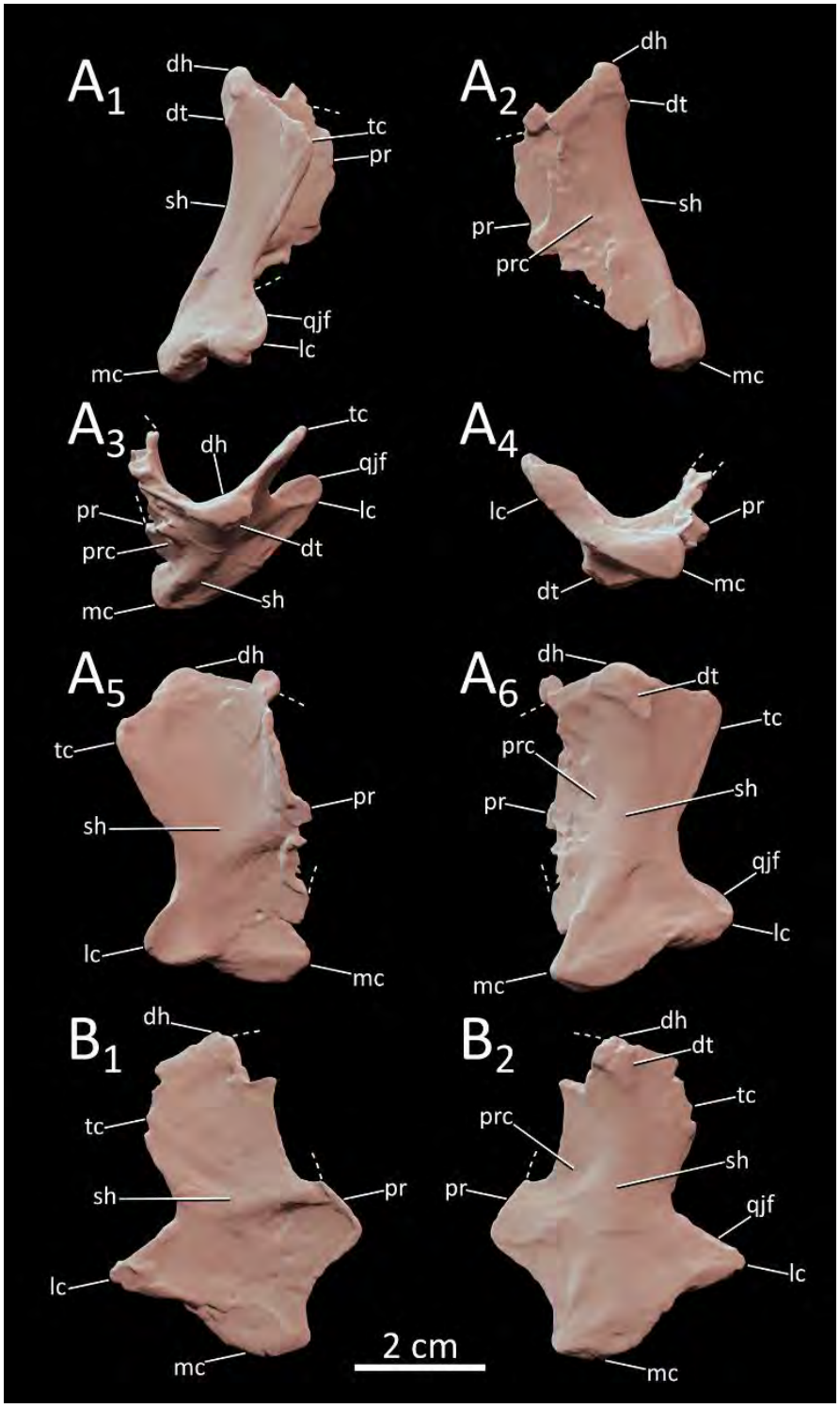

Fig. 6. Right quadrates of *Tanystropheus conspicuus* from the Lower Keuper (lower Ladinian) of Miedary (Poland) – ZPAL V. 36/574 (**A**) and ZPAL V. 36/1764 (**B**). Three-dimensional model snapshots with Lit Sphere Radiance Scaling shader enabled, in lateral (A_1), medial (A_2), dorsal (A_3), ventral (A_4), anterior (A_5, B_1), posterior (A_6, B_2) views. Abbreviations: dh, dorsal head; dt, dorsal tuberosity; lc, lateral condyle; mc, medial condyle; pr, pterygoid ramus; prc, pterygoid ramus concavity; qjf, quadratojugal facet; sh, shaft; tc, tympanic crest.

Pterygoid

The pterygoid of *Tanystropheus conspicuus* is known only from the incomplete specimen ZPAL V. 36/2541, which is missing the entire palatal ramus, but preserves most of the details of its posterior portion (Fig. 7). As most of the other cranial elements of *T. conspicuus*, the pterygoid is nearly indistinguishable from the pterygoid of *T. hydroides* as described by Spiekman et al. (2020*b*). The main difference is the more transversely concave dorsal surface of the pterygoid body in *T. conspicuus*, but this might be due to diagenetic changes. The bone is dorsoventrally thin and lateromedially slender, with the exception of the laterally extending transverse flange, which thickens considerably towards its distal end (Fig. 7F). As in *T. hydroides*, the articular surface of the transverse flange is rugose, flat, and spindle shaped in dorsolateral view (Fig. 7; Spiekman et al. 2020*b*).

The quadrate ramus projects strongly posteriorly, as a morphologically complex process. Between it and the transverse flange the posterior edge of the pterygoid is strongly concave in dorsal view, forming a wide, semi-circular embayment (Fig. 7A–B). The medial portion of the quadrate ramus is strongly concave in anterior or posterior view, with a deep groove flanked by two ridges – dorsally by an extremely thin dorsal flange, and ventrally by the ventromedially projecting arcuate flange (Fig. 7D). Both ridges are similar in height. The anterior portion of the groove, a circular basipterygoid facet, is distinctly outlined, with a dorsoventrally oriented ridge constituting its posterior margin.

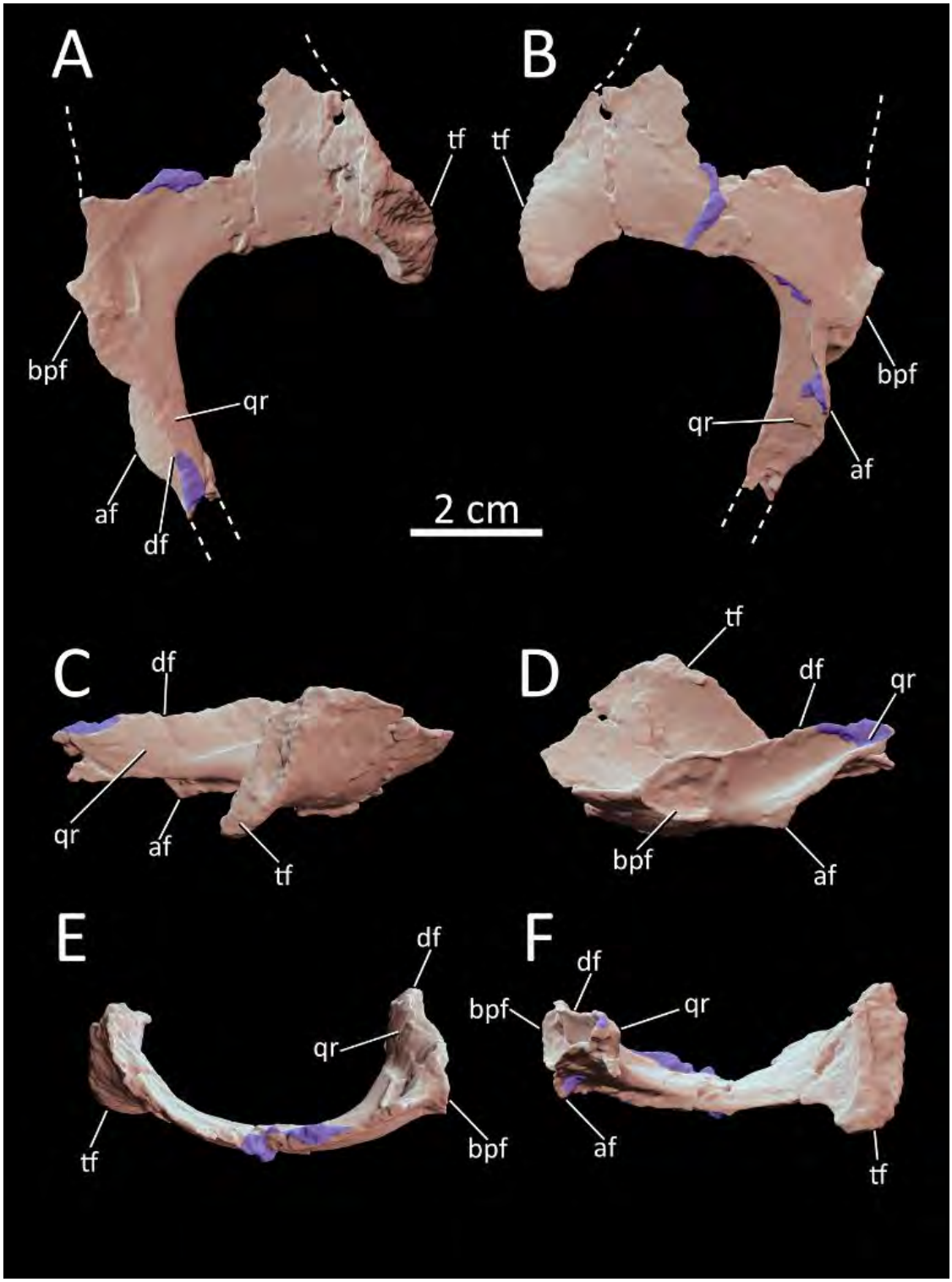

Fig. 7. Posterior portion of the right pterygoid of *Tanystropheus conspicuus* from the Lower Keuper (lower Ladinian) of Miedary (Poland) – ZPAL V. 36/2541. Three-dimensional model snapshots with Lit Sphere Radiance Scaling shader enabled, in dorsal (**A**), ventral (**B**), lateral (**C**), medial (**D**), anterior (**E**), and posterior (**F**) views. Areas covered with sediment marked with blue hue. Abbreviations: af, arcuate flange; bpf; basipterygoid facet; df, dorsal flange; qr, quadrate ramus; tf, transverse flange.

Dentary

The elements constituting the posterior portion of the mandibular rami of *Tanystropheus conspicuus* have still to been identified. Most of the length of the lower jaw is, however, preserved in several dentaries (e.g., ZPAL V. 36/2428). The dentary of *T. conspicuus* is a slender, elongate, and labiolingually thin element (Fig. 8). It bears at least 26 tooth alveoli (Fig. 8C), although no complete specimen has been found so far. As in the maxilla, the alveoli are all circular in dorsal view and densely packed in a single, continuous row along the entire preserved length of the dentary (Fig. 8C). As in the other jaw elements described here, the dentary teeth were lingually separated by triangular interdental plates (Fig. 8A–B). Between the interdental plates, the lingual margin of the anteriormost alveoli is formed as a deep, droplet-shaped notch (8A–B). Similar to the maxilla, there are size differences in the alveoli (Fig. 8B). The anterior three alveoli are especially large, bearing teeth similar in size to the premaxillary teeth. Posterior to them, there is a series of about seven teeth which are much smaller. Continuing further posteriorly, the size of the alveoli changes in a manner similar to the maxilla, with some larger ones around the mid-length of the dentary and then decreasing in size towards its posterior end. Although the alveoli are distributed in a single row, they are not located in a straight line in lateral view. Instead, their position changes labiolingually and dorsoventrally, undulating in two dimensions (Fig. 8B, D). The large anteriormost and middle teeth are located on the convexities of the dorsal margin of the dentary, thus being placed more labially and dorsally. All dentary teeth projected dorsally, with only the three anterior "fangs" being more anterodorsally oriented. In dorsal view, most of the length of the dentary is relatively straight, with only the middle section, which bore the larger teeth, being slightly labially expanded.

At the level of the maxilla-premaxilla contact, the anterior thickened portion of the dentary bends towards the contact with its antimere, following the curvature present in the premaxilla. The symphysial surface is ventrally expanded, forming a ventral keel (Fig. 8D). The suture between the mandibular rami is interdigitating, with multiple longitudinal grooves and ridges being present (Fig. 8E). On the lingual surface of the dentary a plate-like portion of the bone is ventrally and dorsally limited by grooves that extend along the whole length of the dentary (Fig. 8E). The splenial articulated with this area. In medial view the anteriormost extent of the splenial facet is marked by a faint ridge, which extends obliquely (anteroventrally-posterodorsally) to the longitudinal axis of the bone, as in *T. hydroides* (Fig. 8E; Spiekman et al. 2020*b*). The preserved posterior portion of the dentary tapers in lateral

view. Its posteroventral margin is formed as a lateromedially thin ridge (incompletely preserved in ZPAL V. 36/2428 in Fig. 8) which constituted the ventrolateral surface of the Meckelian groove (Fig. 8E). The middle section of the dentary, which bore the larger teeth, is dorsoventrally expanded and convex in lateral view. Between the middle expansion and the anterior portion, along the section that bears the smallest teeth, the dentary is dorsoventrally constricted. The lateral surface of the dentary is relatively smooth, with a slightly rugose texture. There are some foramina present along its anterior portion.

As with the maxilla, the anterior portion of the mandibular ramus of *T. conspicuus* is more similar in its morphology to *T. hydroides* than to *T. longobardicus*, but with some distinct differences. The ventral keel, which was considered a unique feature of *T. hydroides* by Spiekman et al. (2020*b*), and later described also for *Dinocephalosaurus orientalis* by Spiekman et al. (2024*a*), is also present in *T. conspicuus*. Both *T. hydroides* and *T. longobardicus* have less than 20 dentary teeth, with the exact number being difficult to ascertain (Wild 1973; Nosotti 2007; Spiekman et al. 2020*a*, *b*). Even though the teeth positions and their size changes along the dentary are similar to what has been reported for *T. hydroides* (see Spiekman et al. 2020*b*), the incomplete dentary of *T. conspicuus* bears 26 alveoli, with some additional ones likely being present in its missing posterior portion. Thus, *T. conspicuus* probably had a considerably higher number of dentary teeth than other species of *Tanystropheus*.

Despite the general morphological similarity, the dentaries of *T. conspicuus* and *T. hydroides* differ in proportions. In the former the dentary is relatively lower and more dorsoventrally constricted along its anterior portion than the latter (Wild 1973; Spiekman et al. 2020*b*). In both species the dorsal surface of the dentary is undulating in lateral view, with a convexity mid-way along its length (Fig. 8B; Wild 1973; Spiekman et al. 2020*b*). There seems to be some variation in the relative differences of height changes of the dentary along its length in various *T. hydroides* individuals (undulating in fig. 17 of Wild 1973 and relatively straight in fig. 28 of Spiekman et al. 2020*b*), but in *T. conspicuus* the dorsal surface of the dentary is even more undulating.

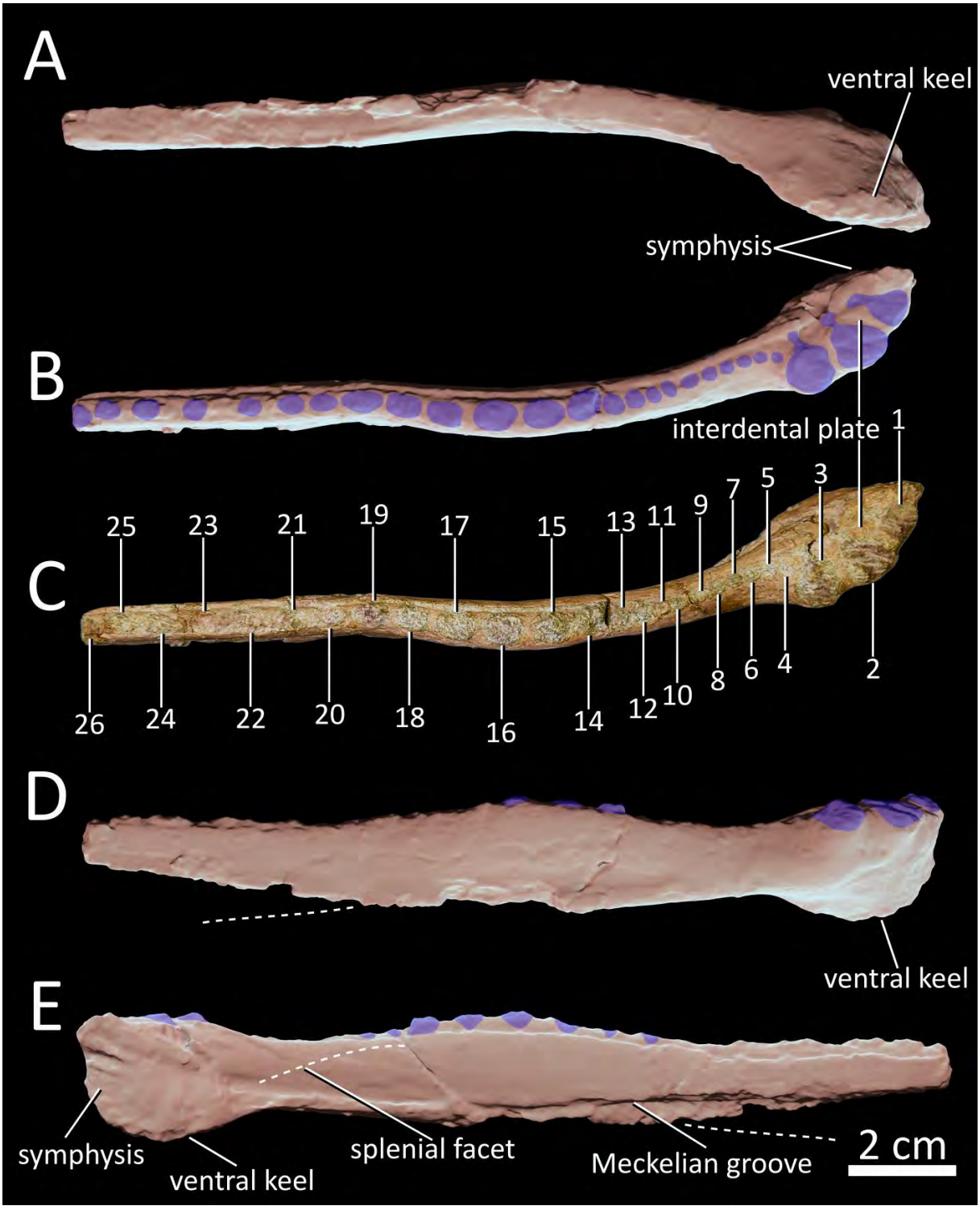

Fig. 8. Partial right dentary of *Tanystropheus conspicuus* from the Lower Keuper (lower Ladinian) of Miedary (Poland) – ZPAL V. 36/2428. Photograph (C) and three-dimensional model snapshots with Lit Sphere Radiance Scaling shader enabled (A–B, D–E), in ventral (**A**), dorsal (**B–C**), lateral (**D**), and medial (**E**) views. Numerals indicate the alveoli. Areas covered with sediment marked with blue hue.

Dentition

Although teeth referred here to *Tanystropheus conspicuus* are only found isolated (excluding a fragment still preserved in an alveolus within the ZPAL V. 36/179 premaxilla), they are extremely similar to the teeth preserved in the jaws of *T. hydroides* and can be easily distinguished from the teeth of the other contemporaneous aquatic reptiles. Moreover, their relatively high frequency in Miedary corresponds to the large number of *T. conspicuus* bones found at that site. Due to the previous absence of cranial material of *T. conspicuus*, the published descriptions of its dentition were limited. Fraas (1896) mentioned that the teeth of *N. blezingeri* (junior synonym of *T. conspicuus*) are slender, slightly curved, and originated from the premaxilla. The apical half of their tooth crown was smooth, and the basal half had only a few shallow grooves, in contrast to other species of *Nothosaurus* in which the grooves are very close together and deep. Corroy (1928) mentioned that the "anterior" part of the crown of these teeth possess ridges, whereas the "posterior" side is smooth. The first extensive description of these teeth was provided by Schoch et al. (2018). It closely corresponds to the observations provided here.

The teeth of *T. conspicuus* are slender, tall, conical, and lingually curved (Fig. 9A, C). The longest known specimens reach about seven cm in total preserved length, of which less than a half can be considered the crown (not including the worn apex). The long root has a smooth surface and transitions into the crown without a change of tooth diameter. Although it is difficult to assign an exact position of an isolated tooth within a jaw ramus exclusively based on its morphology, the largest and most curved teeth of *T. conspicuus* ("fangs") likely originated from the premaxillae and the anterior part of the dentary, as in *T. hydroides* (Wild, 1973; Spiekman et al. 2020*b*). More posteriorly originating teeth are usually relatively shorter and straighter. All teeth referred to *T. conspicuus* herein share the same crown surface characteristics and general morphology (homodonty) with those of *T. hydroides*, but contrast to the heterodont dentition in *T. longobardicus* (Wild, 1973; Spiekman et al. 2020*a*, *b*). The crown is lingually curved, with its apex frequently lingually worn. Low apicobasal ridges (see McCurry et al. 2019) are present on all surfaces of the crown. They are not strictly parallel to each other, with some ridges merging or bifurcating along their apicobasal length. On the labial side of the crown they are much more sparsely and unevenly distributed, with finer secondary ridges being present between the main ones (pattern similar to *Tanystropheus* teeth reported by Dalla Vecchia 2006). The ridges are relatively taller, much better defined and organised. There are no carinae or serrations. SEM imaging reveals that the crown surface is

covered with a network of microscopic ridges and grooves that are oriented semi-parallel to the apicobasal axis of the tooth (Fig. 9 C_2). The implantation of all premaxillary, maxillary and dentary teeth in *T. conspicuus* was subthecodont (*sensu* Bertin et al. 2018) or anisothecodont (*sensu* Mestriner et al. 2025), in the sense that the tooth sockets are asymmetric and cover much more of the length of the tooth labially than lingually. The almost complete absence of teeth preserved in the jaws of *T. conspicuus* indicates that the teeth were not ankylosed to the jaw.

Teeth of *T. conspicuus* have long been confused with the teeth of sauropterygians, especially *Nothosaurus* and *Pistosaurus*, with several works providing a brief comparison between them (Fraas 1896; Corroy 1928; Dalla Vecchia and Avanzini 2002; Dalla Vecchia 2006; Schoch et al. 2018). Results from a SEM analysis provide more definitive criteria to distinguish them from each other. By comparison with *T. conspicuus*, the apicobasal ridges are much more evenly distributed and regularly arranged in the teeth of *Nothosaurus* sp. from Miedary (compare Fig. 9 B_1 and C_1). The SEM results show that at micro-scale the crown surface in *Nothosaurus* sp. is smooth and lacks any secondary ridges (Fig. $9B_2$). Moreover, the teeth of *T. conspicuus* are much more frequently preserved with a root. These characteristics demonstrate that the teeth of *T. conspicuus* and *Nothosaurus* sp. can be readily distinguished, despite being somewhat similar at first glance.

As previously noted by Fraas (1896) and Corroy (1928), the teeth of *T. conspicuus* closely correspond in their morphology to those of *P. longaevus*. Even recently, Diedrich (2012, fig. 14.1) described a specimen U-MO BT 3078 as belonging to *T. conspicuus*, whereas in fact it is indistinguishable from the teeth of *P. longaevus*. A specimen referred to "*Tanystrophaeus longibardicus*" (sic!) by Diedrich (2009, "MSB No. Pal 327— 534") is likely of the same affinities. Although the tooth crowns of both reptiles share the convergently acquired tall, slender, conical shape, those of *Pistosaurus* sp. are devoid of large, well-defined ridges, instead being covered with densely distributed, irregular, shallow grooves (compare Fig. 9 C and D). On the microscopic scale their crown surface is also relatively smooth, similar to *Nothosaurus* sp. (Fig. 9 B and D) The miniscule grooves and ridges scattered across the tooth crown surface in *T. conspicuus* do not seem to be present in Middle Triassic sauropterygians, but instead are likely characteristic of some Triassic archosauromorphs. The surface of the teeth of *T. conspicuus* is reminiscent in its morphology to that illustrated by Dorka (2002) for the specimens originating from the Ladinian deposits of Schöningen (Germany). The morphotypes 12 and 13, and some of the teeth referred to morphotype 1

(Dorka 2002, fig. 2C) bear a striking resemblance to the Miedary material despite the size difference. A similar morphology was also described by Ősi et al. (2020, morphotype 2) for the teeth from the Ladinian Templomhegy Dolomite in Hungary, which has yielded material of *Tanystropheus* sp. More microscopic scale analyses are needed to better understand the morphological disparity of the teeth in early archosauromorphs and possibly permit their confident identification.

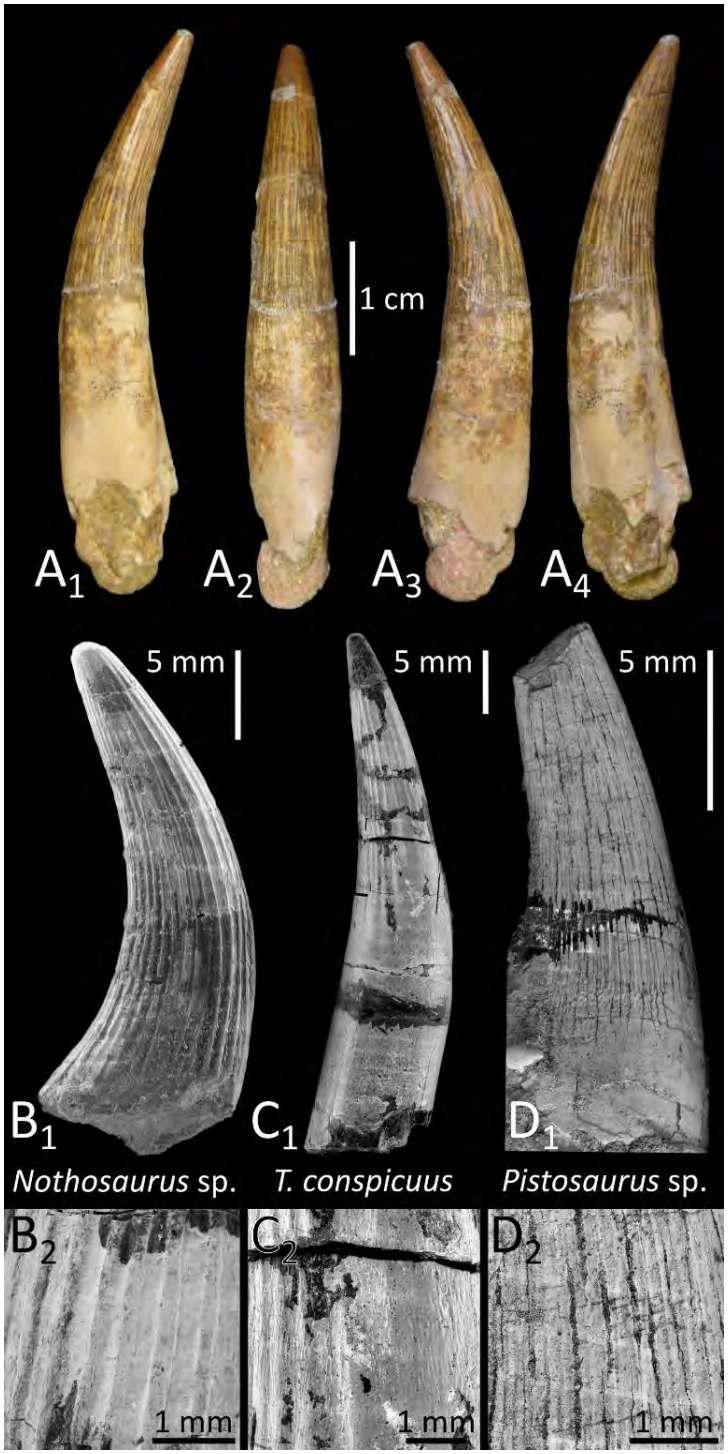

Fig. 9. Photographs (A) and stitched SEM images (B–D) of teeth of *Tanystropheus conspicuus* from the Lower Keuper (lower Ladinian) of Miedary, Poland (ZPAL V. 36/1204 – **A**; ZPAL V. 36/163 – **C**), *Nothosaurus* sp. from the Lower Keuper (lower Ladinian) of Miedary, Poland (ZPAL V. 36/254 – **B**), and *Pistosaurus* sp. from the Upper Muschelkalk (upper Anisian to lower Ladinian) of Laryszów, Poland (ZPAL V. 84/LA/001 – **D**), in mesial/distal (A_1, A_3, B_1, C_1, D_1), labial (A_2), and lingual (A_4) views, and their surface under higher magnification (B_2, C_2, D_2).

Postcranium

Axis

The axis of *Tanystropheus conspicuus* is an elongate, slender element (Fig. 10). As in all the succeeding vertebrae, its centrum is amphicoelous but not notochordal and its articular surfaces are roughly circular in anterior and posterior views. The centrum is roughly two to three times longer than the vertebra is tall at its anteroposterior midpoint. Its ventral margin is formed as an extremely thin lamina – the ventral keel, which, compared to the other cervical vertebrae, is especially strongly developed in the axis (Fig. 10A). The anterior portion of the ventral keel is deeply concave in lateral view, but the curvature of its distal margin changes around the mid-length of the centrum, becoming convex in its posterior portion (Fig. 10A). A pair of longitudinal laminae runs roughly parallel to the ventral margin of the axis on either side of the keel. There are no subcentral foramina on the ventral surface of the centrum. The articular surface for the rib occupies the anteroventral corner of the centrum, but it is not delimited in any way other than a change in bone texture.

The openings of the neural canal are rhomboidal. The prezygapophyses are strongly reduced – their distal margin does not extend beyond the anterior edge of the centrum (Fig. 10B_1–B_2). They are formed as slight anterolateral projections of the longitudinal laminae that mark the base of the neural spine (Fig. 10B_2). Their articular surfaces are small, elliptical in dorsal view and dorsolaterally oriented. The postzygapophyses are long and relatively slender. They extend far beyond the posterior edge of the centrum (Fig. 10B_2). Their elliptical articular surfaces are roughly ventral-facing (Fig. 10B_3). A thin plate-like lamina (=transpostzygapophyseal lamina, =Horizontallamelle *sensu* Wild, 1973) spans the area between the postzygapophyses, constituting the posteriormost portion of the neural canal roof, and forming a triangular shelf in dorsal view (Fig. 10B_1). In posterior view this shelf extends anteriorly below the posterior overhang of the neural spine (postzygapophyseal trough *sensu* Rieppel 2001). The dorsal portion of both postzygapophyses is formed as a distinct ridge, which projects posteriorly as a process (epipophysis). The neural spine is low, especially in its posterior portion, and tapers posterodorsally to form a long, conical process, which is similar in its orientation and size to the distal tips of the epipophyses (Fig. 10B_1–B_2). The anterior portion of the neural spine is strongly convex in lateral view (Fig. 10A, B_2). Its anterior margin is nearly vertical and merges with its dorsal margin dorsal to the prezygapophyses, forming an anterior overhang. The anterodistal portion of the neural spine is distinctly transversely expanded and rugose (Fig. 10B_1).

The axis of *T. conspicuus* is similar in its proportions to the axes known for *T. hydroides* (e.g., PIMUZ T 2790, PIMUZ T 2819 – see Wild 1973; Spiekman et al. 2020*b*) but it is relatively more elongate than the same element in *T. longobardicus* (e.g., MSNM BES SC 265, PIMUZ T 2791, PIMUZ T 3901 – see Wild 1973, 1980*a*; Nosotti 2007). The high dorsal extent of the distal expansion of the anterior portion of the neural spine is, however, a feature shared by *T. conspicuus* and *T. longobardicus*, but in contrast with *T. hydroides*, in which the anterodistal margin of the neural spine is only slightly convex (Wild 1973; Spiekman et al. 2020*b*). Moreover, the axis of *T. conspicuus* is distinct from other species of *Tanystropheus* in the presence of a ventral keel with a convex distal margin (which is relatively straight and less well developed in both *T. hydroides* and *T. longobardicus* – compare Wild 1973, 1980*a*; Nosotti 2007; Spiekman et al. 2020*b*).

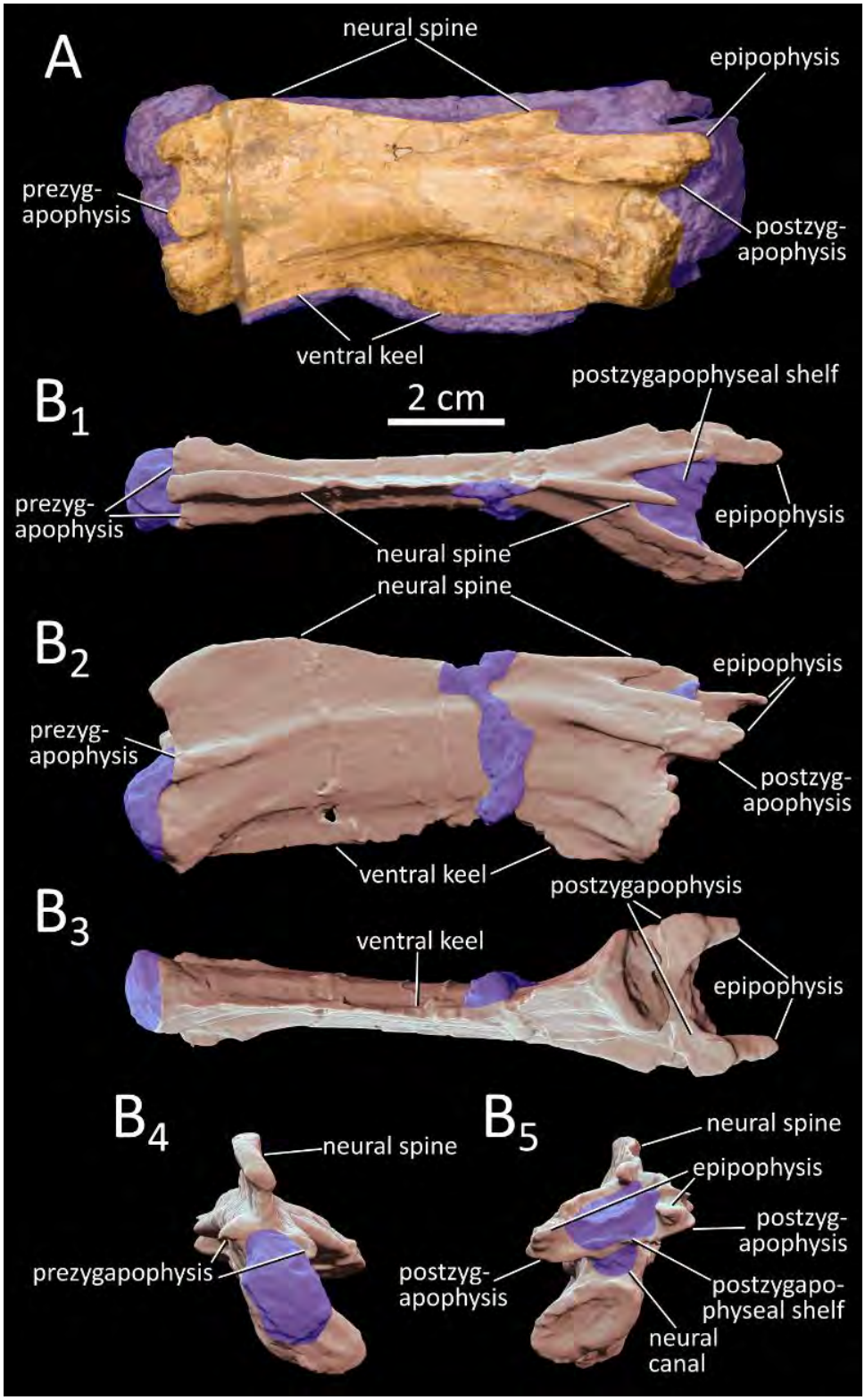

Fig. 10. Axes of *Tanystropheus conspicuus* from the Lower Keuper (lower Ladinian) of Miedary (Poland) – ZPAL V. 36/1170 (**A**) and ZPAL V. 36/847 (**B**). A photograph (A) and three-dimensional model snapshots with Lit Sphere Radiance Scaling shader enabled (B), in left lateral (A, B_2), dorsal (B_1), ventral (B_3), anterior (B_4), and posterior (B_5) views. Areas covered with sediment marked with blue hue.

Middle cervical vertebrae

Due to their elongation, the middle cervical vertebrae are the most striking element of the osteology of *Tanystropheus*. They are the most elongate vertebrae among all known animals, with only azhdarchid pterosaurs reaching similar proportions (Renesto 2005; Rytel et al. 2024*b*). In all middle cervical vertebrae of *Tanystropheus* the elongation ratio (centrum length versus height at midpoint) exceeds four (pers. obs. AR, but see Wild 1973; Spiekman et al. 2021). This ratio varies highly between individuals, reaching up to about 20 in PIMUZ T 2790, the holotype of *Tanystropheus hydroides* (pers. obs. AR). In cervical vertebrae three to eight in *Tanystropheus longobardicus* and T. *hydroides* it usually remains relatively constant, with an average value of around 13 (pers. obs. AR). In comparison, the same vertebrae in *Tanystropheus conspicuus* are usually taller and more robust, with their average elongation ratio of around nine (see measurements in Appendix I). Whereas Wild (1973) was very specific in attributing each particular isolated cervical vertebra described by him to its original location in the vertebral column, the morphometric study of Rytel et al. (2024*a*) showed that the differences in shape within cervical vertebrae three to eight are marginal. Their morphology changes gradually along the vertebral column, and consequently, attributing any isolated cervical from this section to its exact place in the sequence is highly equivocal, as knowledge on the ontogenetic and intraspecific variation of skeletal morphology in *T. conspicuus* is limited. By contrast, the posterior-most cervical vertebrae nine to thirteen can be easily differentiated due to their markedly changing proportions and neural spine shape and are described separately.

Nevertheless, although it is difficult to refer isolated middle cervical vertebrae to their original position, some distinct differences between them are present. The anterior-most middle cervical vertebrae are generally more slender and elongate than the succeeding vertebrae, as can be determined from the only known series of cervical vertebrae from the same individual of *T. conspicuus*, ZPAL V. 36/100 (see. Fig. 11). However, the neural spine height varies substantially among the isolated middle cervical vertebrae referred to *T. conspicuus* (see measurements in Appendix I), and to a much larger extent than present in the articulated series of ZPAL V. 36/100 (see. Fig. 11). This is likely due to a complex combination of several factors, and therefore the neural spine shape represents a poor proxy for identifying the position of isolated vertebrae. Importantly, the length changes of succeeding cervical vertebrae of *T. conspicuus* follow the pattern recorded for other species of *Tanystropheus* by Peyer (1931, fig. 27), Wild (1973, fig. 29), and Nosotti (2007, fig. 54). In

ZPAL V. 36/100 (see. Fig. 11), vertebrae three to six have a relatively constant centrum length, with the seventh cervical vertebra being only slightly longer (Appendix I). The ninth and tenth cervical vertebrae are the longest vertebrae of *T. conspicuus*, whereas the cervical vertebrae posterior to these are much shorter. This corresponds to the configuration in *T. hydroides* and *T. longobardicus* (pers. obs. AR; Peyer 1931; Wild 1973; Nosotti 2007).

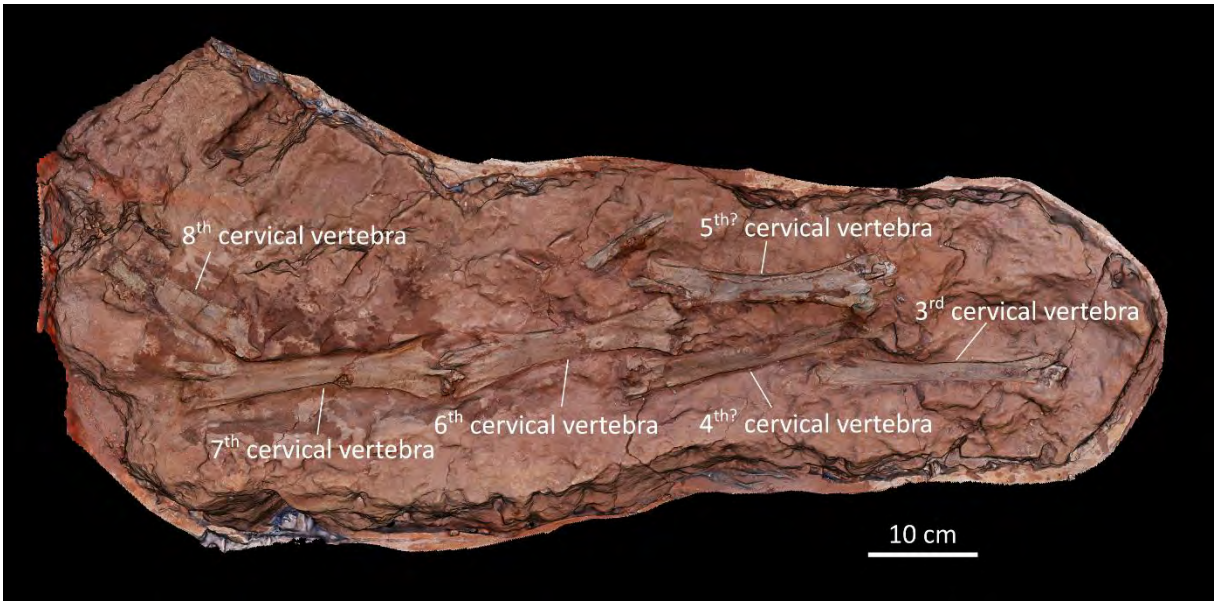

Fig. 11. Snapshot of a photogrammetric model of a plaster jacket ZPAL V. 36/100 preserving a semiarticulated series of middle cervical vertebrae of *Tanystropheus conspicuus* from the Lower Keuper (lower Ladinian) of Miedary (Poland), with Lambertian Radiance Scaling shader enabled. Cervicals fours and five are in the left lateral view, and the rest in the right lateral view. Model courtesy of T. Szczygielski.

The description of the cervical vertebrae three to eight is based on the lectotype specimen of *T. conspicuus* – U-MO BT 740 (Fig. 12), with some additional complementary data gathered from the newly referred specimens from Miedary (Fig. 13), including the semi-articulated cervical series ZPAL V. 36/100 (Fig. 11).

As in all other vertebrae, the centrum in the cervical vertebrae of *T. conspicuus* is deeply amphicoelous but not notochordal. Its circular articular surfaces are slightly ventrally tilted from the vertical plane and thus not fully parallel to each other (Fig. 13C). The centrum is elliptical to triangular in transverse cross-section (see Rytel et al. 2024*b* for a detailed description of the internal anatomy). On its ventral surface, an intricate array of bifurcating and merging laminae is present (Figs. 12E, 13E). The lamina that runs along the midline of the ventral surface of the vertebra forms a well-defined but low ventral keel. It is laterally

flanked by deep, symmetrical grooves, which in turn are laterally constrained by the ventrolateral laminae (lateroventral margins *sensu* Nosotti 2007). These ventrolateral laminae demarcate the margin between the ventral and lateral surface of the bone. A pair of subcentral foramina is present near the mid-length of the vertebra (Figs. 12E, 13E), with one foramen present on either side of the ventral keel. Intervertebral arteries penetrated the centrum through these foramina (see Rytel 2024*b*). The openings of the foramina are usually elliptical, but differ slightly in shape and location, even within the same pair. Posterior to the foramina, on the ventral surface of the centrum, two pairs of laminae are present – the ventromedial and posteroventral laminae (Figs. 12C, E, 13C, E). The ventromedial laminae extend obliquely between the ventral keel and the ventrolateral laminae. The posteroventral laminae are located posteriorly to them, along the midline between the posterior portion of the ventral keel and the ventrolateral laminae. Both anteroventral and posteroventral laminae are present in all middle cervical vertebrae of *T. conspicuus* in which this character can be assessed, as well as in the three-dimensionally preserved specimens from Romania and north-eastern Italy (pers. obs. AR; Jurcsak 1975; Dalla Vecchia 2006). They are seemingly absent in the specimens from Monte San Giorgio and China, but this might be due to the differences in preservation (i.e., diagenetic compression, pers. obs. AR).

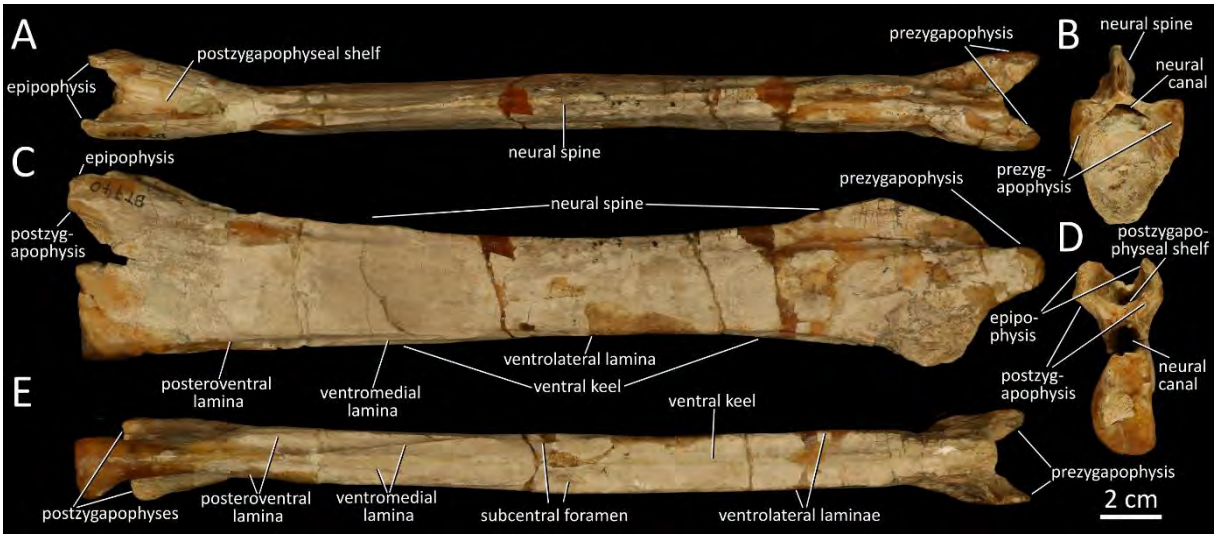

Fig. 12. Photographs of a middle cervical vertebra U-MO BT 740 from the Upper Muschelkalk (upper Anisian) of Bayreuth (Germany), the lectotype *Tanystropheus conspicuus*, in dorsal (**A**), anterior (**B**), right lateral (**C**), posterior (**D**), and ventral (**E**) views.

The lateral surface of the centrum is smooth with no noticeable foramina. The parapophysis and diapophysis are extremely reduced and essentially confluent with each other, forming triangular rib attachment sites on the anterolateral corners of the centrum (Figs. 12C, 13C). They barely project from the centrum surface, with the associated ribs being located very close to the vertebra when compared to other archosauromorphs. The rib attachment site is partially located on a lamina, which connects the anteroventral corner of the centrum with the base of the prezygapophysis, extending beyond the anterior edge of the centrum.

The neural canal openings differ in shape, with the anterior one being triangular and the posterior one roughly circular (Figs. 12B, D). The prezygapophyses project strongly anteriorly and are triangular in transverse cross-section (Fig. 13B). Their distal end is formed as a rounded, non-tapering expansion in lateral view, which extends anteriorly from the lamina that connects the centrum and the prezygapophyseal articular surface. The dorsal surface of the prezygapophyses is confluent with the base of the neural spine (Figs. 12C, 13 C). The prezygapophyseal articular surfaces are almost dorsally facing, with only a slight medial tilting (Figs. 12B, 13B). The postzygapophyses extend far beyond the posterior edge of the centrum and in lateral view are separated from it by a deep notch (Figs. 12C, 13C). Massive, tall epipophyses project posterodorsally from them. Contrasting with the morphology of the epipophyses of the axis, their distal tips are rounded and non-tapering in lateral view (Figs. 12C, 13 C). Between the epipophyses, a broad shelf is located. It covers the entire surface between the neural spine and the posterior ends of the postzygapophyses (Figs. 12A, D, 13A, D). The postzygapophyseal articular surfaces are well outlined, elliptical, and oriented corresponding to the prezygapophyseal articular surfaces – nearly parallel to the horizontal plane, but with their lateral surface only slightly raised (Figs. 12D, 13D).

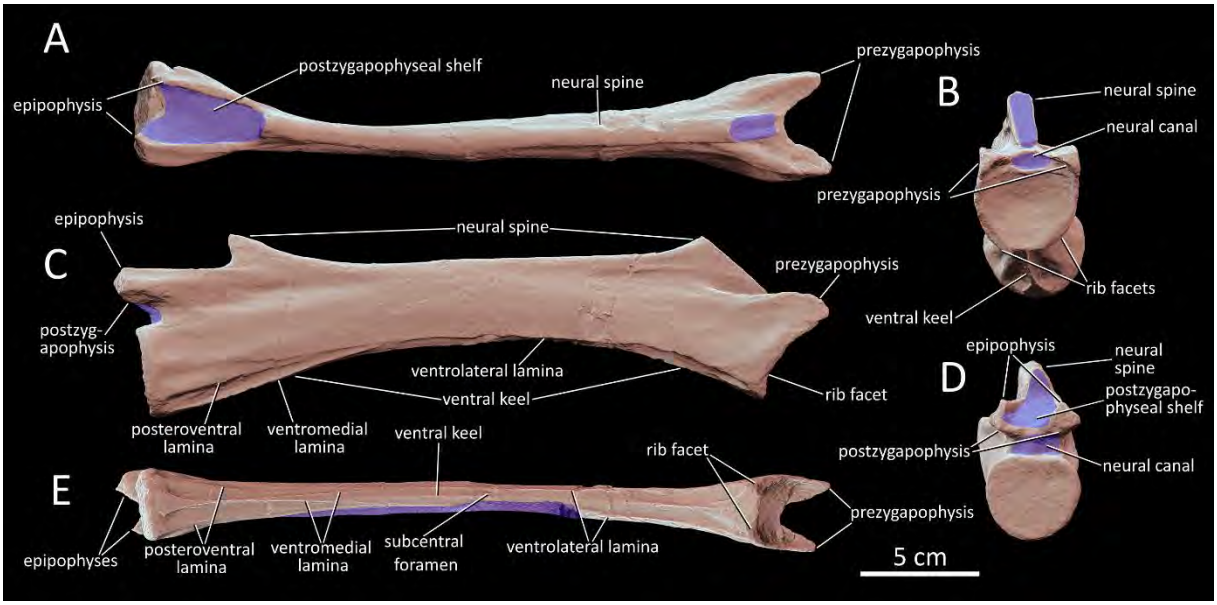

Fig. 13. Middle cervical vertebra of *Tanystropheus conspicuus* from the Lower Keuper (lower Ladinian) of Miedary (Poland) – ZPAL V. 36/1078. Three-dimensional model snapshots with Lit Sphere Radiance Scaling shader enabled, in dorsal (**A**), anterior (**B**), right lateral (**C**), posterior (**D**), and ventral (**E**) views. Areas covered with sediment marked with blue hue.

The neural spine is extremely low, being barely discernible in its middle section, with only its anterodistal and posterodistal portions projecting from the dorsal surface of the vertebra (Figs. 12C, 13C). In some of the middle cervical vertebrae (e.g., U-MO BT 740) the neural spine is a distinct keel, running along most of the length of the vertebra, but histological studies indicate that neural spine height might, to some extent, change during ontogeny (Jaquier and Scheyer 2017; Rytel et al. 2024*b*). The shape of the anterior portion of the neural spine varies highly between different specimens, mostly because only a few cervical vertebrae preserving its distal tip due to their fragility (e.g., ZPAL V. 36/101, see Czepiński et al. 2023). In those most completely preserved specimens, the anterior portion of the neural spine is roughly triangular in lateral view. Its anterior edge is split, with two laminae running from its base merging distally, thus forming a deep, triangular concavity (Figs. 12B, 13B), which was interpreted as an attachment for the dorsal ligament by Wild (1973). The anterodorsal tip of the neural spine is anteriorly oriented. The posterior portion of the neural spine exhibits a similar morphology, but it is usually lower, and projects posteriorly as a tapering, conical process overhanging the postzygapophyseal shelf (Fig. 13C).

All known cervical vertebrae three to eight of *Tanystropheus* share the neural spine morphology (von Meyer 1847-1855; von Huene 1907-1908; Peyer 1931; Wild 1973, 1980*a*; Jurcsak 1975; Renesto 2005; Dalla Vecchia 2006; Li 2007; Nosotti 2007; Rieppel et al. 2010)

and hence they are not diagnostic at the species level, being differentiated mostly on the basis of size and provenance. The ninth cervical vertebra is the anteriormost postaxial vertebra of *Tanystropheus conspicuus* in which the neural spine shape changes distinctly (Fig. 14), marking the beginning of the cervico-dorsal transition. Whereas in the preceding middle cervical vertebrae the neural spine is nearly completely reduced in its middle section, in the ninth cervical vertebra it forms a low, narrow, but continuous ridge (Fig. 14C). Its height changes along its length, forming a slight but distinct crest near the middle of the vertebral length.

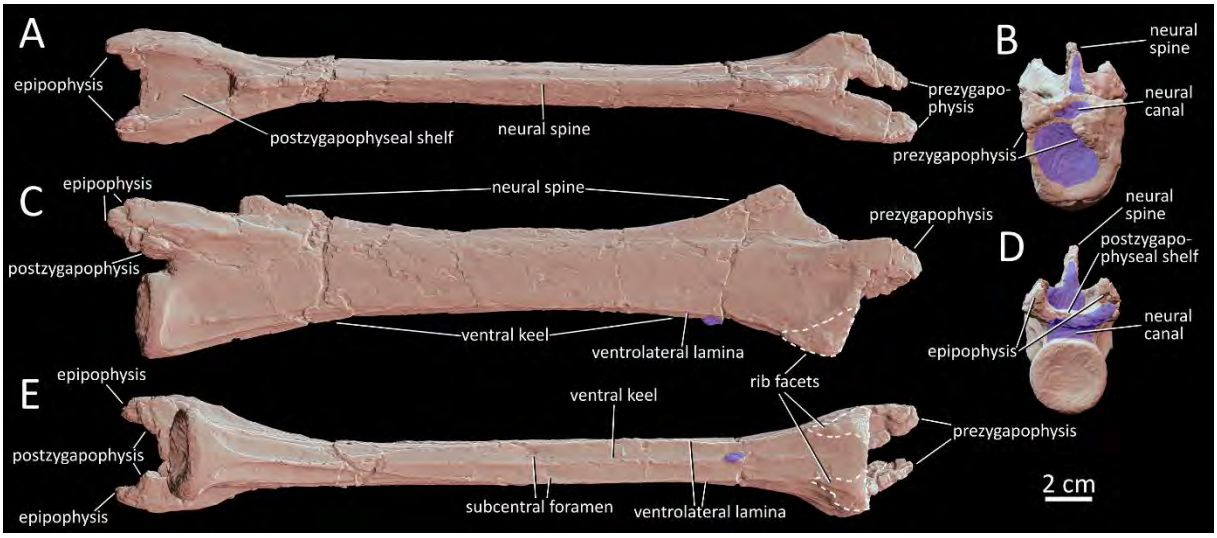

Fig. 14. Ninth cervical vertebra of *Tanystropheus conspicuus* from the Lower Keuper (lower Ladinian) of Miedary (Poland) – ZPAL V. 36/1202. Three-dimensional model snapshots with Lit Sphere Radiance Scaling shader enabled, in dorsal (**A**), anterior (**B**), right lateral (**C**), posterior (**D**), and ventral (**E**) views. Areas covered with sediment marked with blue hue.

The succeeding tenth cervical vertebra shares this morphology but with the neural spine height increased by a magnitude in its anteroposterior middle portion (Fig. 15). Whereas in the more anterior postaxial vertebrae the neural spine is concave (e.g., Fig. 13C), in the tenth cervical vertebra it is formed predominantly as a convex ridge in lateral view (Fig. 15A, B_3). Anterior to the mid-length of the vertebra, its neural spine becomes concave in lateral view, reaching the point of its minimum height, and then rises again to form the anterior extension found also in the preceding elements (Fig. 15A, B_3). The dorsal margin of the neural spine of the tenth cervical vertebra of *T. conspicuus* is, therefore, undulating in lateral view (Fig. 15A, B_3). The tenth cervical vertebra in other species of *Tanystropheus* has a much lower neural spine with a straight distal margin (see Wild 1973; Renesto 2005; Li 2007; Nosotti 2007; Rieppel et al. 2010). Moreover, in *T. conspicuus* the distal margin is distinctly

transversely expanded, forming a distal thickening (Fig. 15B$_5$), which is also present in all succeeding vertebrae up to the anterior caudal vertebrae. A lamina is present on the anterior part of the lateral surface of the neural spine of the 10th vertebra. It runs parallel to its distal margin. Only present in this cervical, it can serve as a basis for the identification of partially preserved, isolated vertebrae. In the ninth and tenth cervical vertebrae the rib articulation surface is more prominent ventrally, but it is not until the eleventh cervical vertebra that the parapophysis and diapophysis can be unequivocally regarded as functionally separate, with the capitulum and tuberculum of the corresponding rib also being distinctly separated (contra Wild (1973), who differentiated them in the two preceding cervical vertebrae as well).

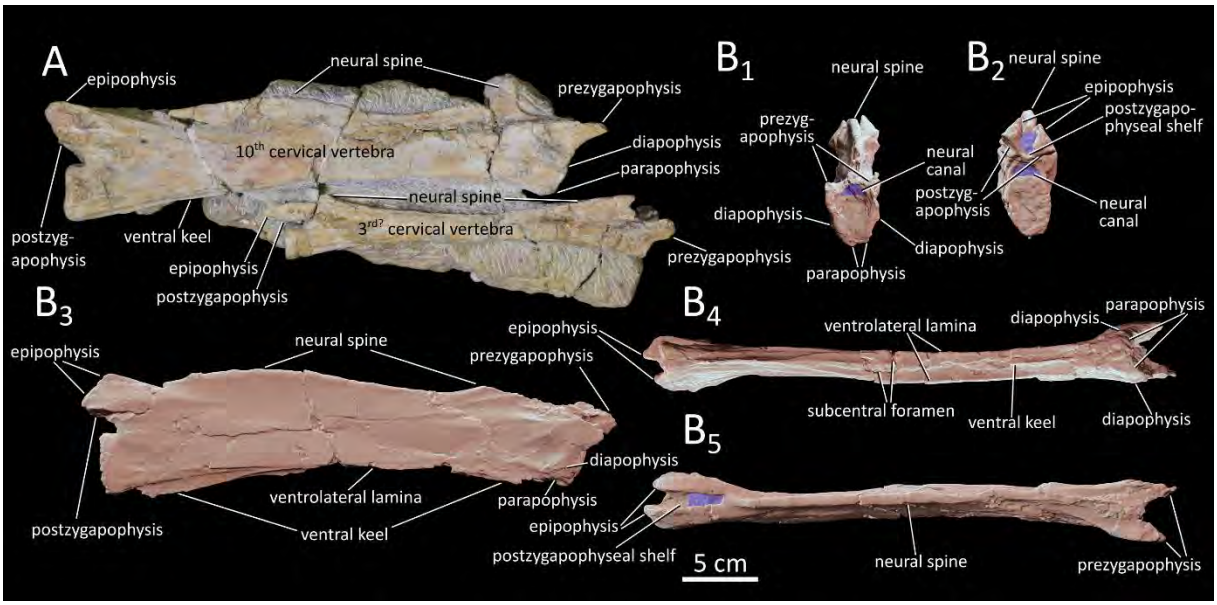

Fig. 15. Tenth cervical vertebrae of *Tanystropheus conspicuus* from the Lower Keuper (lower Ladinian) of Miedary (Poland) – ZPAL V. 36/186 (**A**) and ZPAL V. 36/105 (**B**). A photograph (A) and three-dimensional model snapshots with Lit Sphere Radiance Scaling shader enabled (B), in right lateral (A, B$_3$), anterior (B$_1$), posterior (B$_2$), ventral (B$_4$), and dorsal (B$_5$) views. Areas covered with sediment marked with blue hue.

Posterior cervical vertebrae

Between the tenth and eleventh cervical vertebrae of *Tanystropheus* there is considerable morphological disparity, probably caused by the expression of different sets of *hox*-genes (Rytel et al. 2024*a*). As a result, each of the three cervical vertebrae succeeding the tenth is less elongate than its predecessor. One of the newly referred specimens of *Tanystropheus conspicuus*, ZPAL V. 36/584, preserves all three elements in close association, confirming their correct identification (Fig. 16).

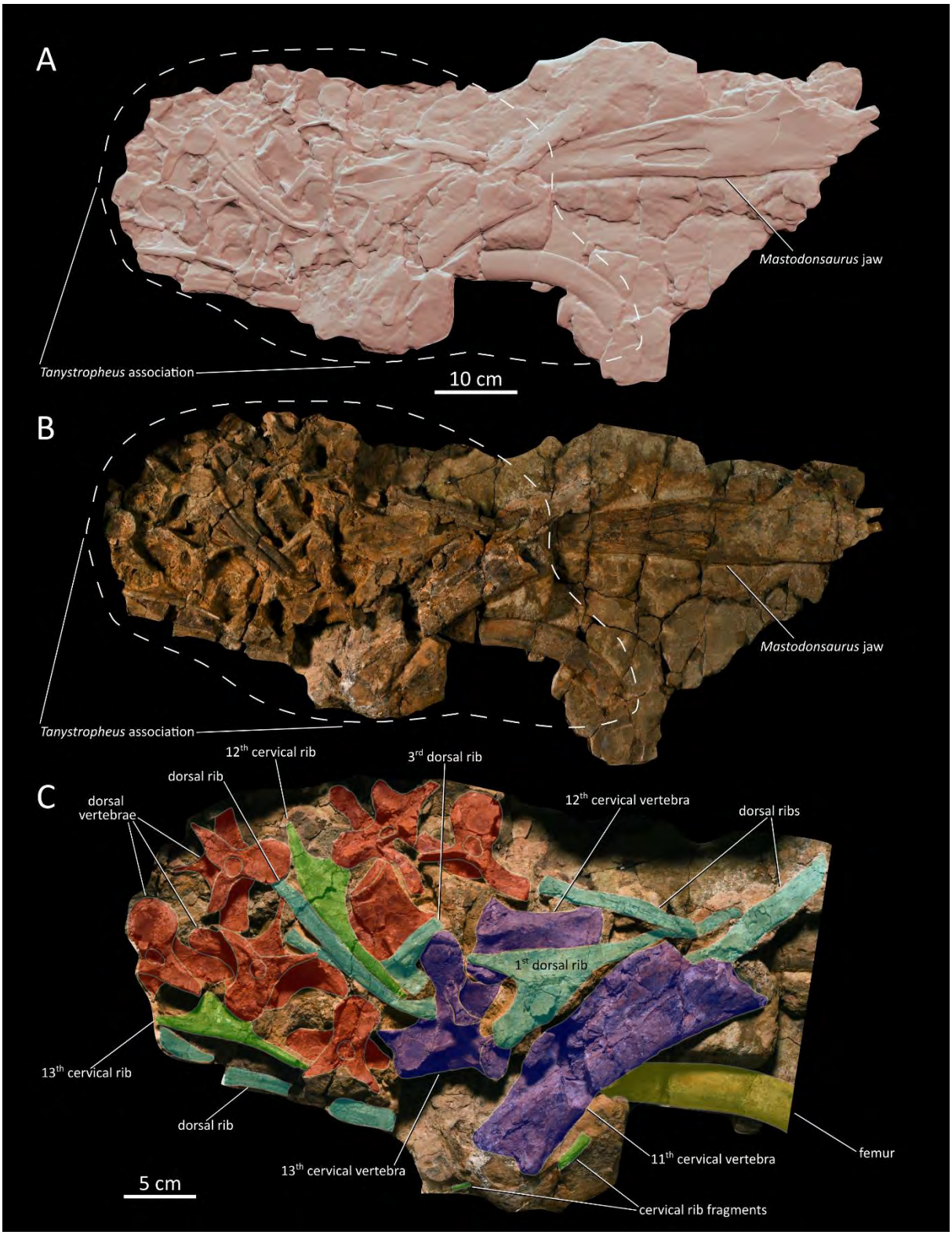

Fig. 16. Association of elements from the cervico-dorsal transition of a single individual of *Tanystropheus conspicuus* from the Lower Keuper (lower Ladinian) of Miedary (Poland) – ZPAL V. 36/584. A three-dimensional model snapshot with Lit Sphere Radiance Scaling shader enabled (**A**), and photographs (**B–C**), with individual elements marked with different colours (**C**).

The eleventh cervical vertebra, described in detail by Wild (1973), is still relatively elongate (Fig. 17). The characteristics of its centrum, other than the relative length, are generally similar to the middle cervical vertebrae. The subcentral foramina are located posterior to the mid-length of the vertebra (Fig. 17E). The ventral keel as well as the ventrolateral and posteroventral laminae are present (Fig. 17E). Importantly, although the articular surfaces of the centrum are vertical oriented and lie on parallel planes, the anterior articular surface is located much more dorsally than the posterior one (Fig. 17C). The ventral surface of the centrum is, therefore, inclined, as was also reported for the twelfth cervical vertebra of *T. longobardicus* by Renesto (2005). In *T. conspicuus* this features is much more pronounced than in other species of *Tanystropheus* (see Wild 1973; Renesto 2005; Li 2007; Nosotti 2007; Rieppel et al. 2010). The articular surfaces of the centrum are elliptical, being taller than wide (Fig. 17B, D). The diapophyses and parapophyses are separate and formed as robust, but weakly projecting tuberosities in the anteroventral portion of the centrum (Fig. 17B–C).

The openings of the neural canal are semicircular, with a flattened ventral margin (Fig. 17D). The pre- and postzygapophyses are relatively much shorter than in the preceding vertebrae, but they still extend beyond the corresponding end of the centrum (Fig. 17C). The anteroventral margin of the prezygapophysis is more dorsally located than in the middle cervical vertebrae, thus only covering the dorsalmost portion of the anterior articular surface of the centrum in lateral view (Fig. 17C). The anterodorsal margin of this lamina is convex, forming a mound-like tuberosity, which projects further anteriorly than the prezygapophyseal facet. All zygapophyseal articular surfaces are elliptical and sub-vertical, with their lateral margins slightly raised (Fig. 17B, D). The epipophyses are much more robust and taller, but anteroposteriorly shorter, than in the middle cervical vertebrae (Fig. 17C–D). They delimit the postzygapophyseal shelf bilaterally as tall, thick ridges and do not extend posteriorly beyond the postzygapophyses (Fig. 17A, C).

The concavity formed at the base of the posterior portion of the neural spine is deep. The neural spine is continuous and convex in lateral view. By contrast with the undulating distal margin observed in the neural spine of the tenth cervical vertebra, in the eleventh cervical vertebra the distal margin is expressed as a gradually sloping, crescent-shaped curve (Fig. 17C). It reaches its maximum height posterior to the mid-length of the vertebra. The anterodorsal margin of the neural spine is not bifurcated, and thus, the anterior concavity

observed in the preceding vertebrae is absent (Fig. 17B). The distal margin of the neural spine is transversely expanded and thickened, especially in its tallest part (Fig. 17A). In some specimens the anterior portion of this expansion is marked by the presence of an anterodorsally projecting tuberosity (Fig. 17A–C). The posterior portion of the neural spine forms as a posteriorly projecting tapering process that overhangs the postzygapophyseal shelf (Fig. 17C). In the eleventh cervical vertebra of other species of *Tanystropheus* the neural spine is much lower, and its distal margin is straight, or even slightly concave, in lateral view (see Wild 1973; Renesto 2005; Li 2007; Nosotti 2007; Rieppel et al. 2010). Additionally, in *T. conspicuus* the height of the neural spine increases gradually along its anterior portion, whereas in other species of *Tanystropheus* it rises sharply and remains relatively constant along its entire length.

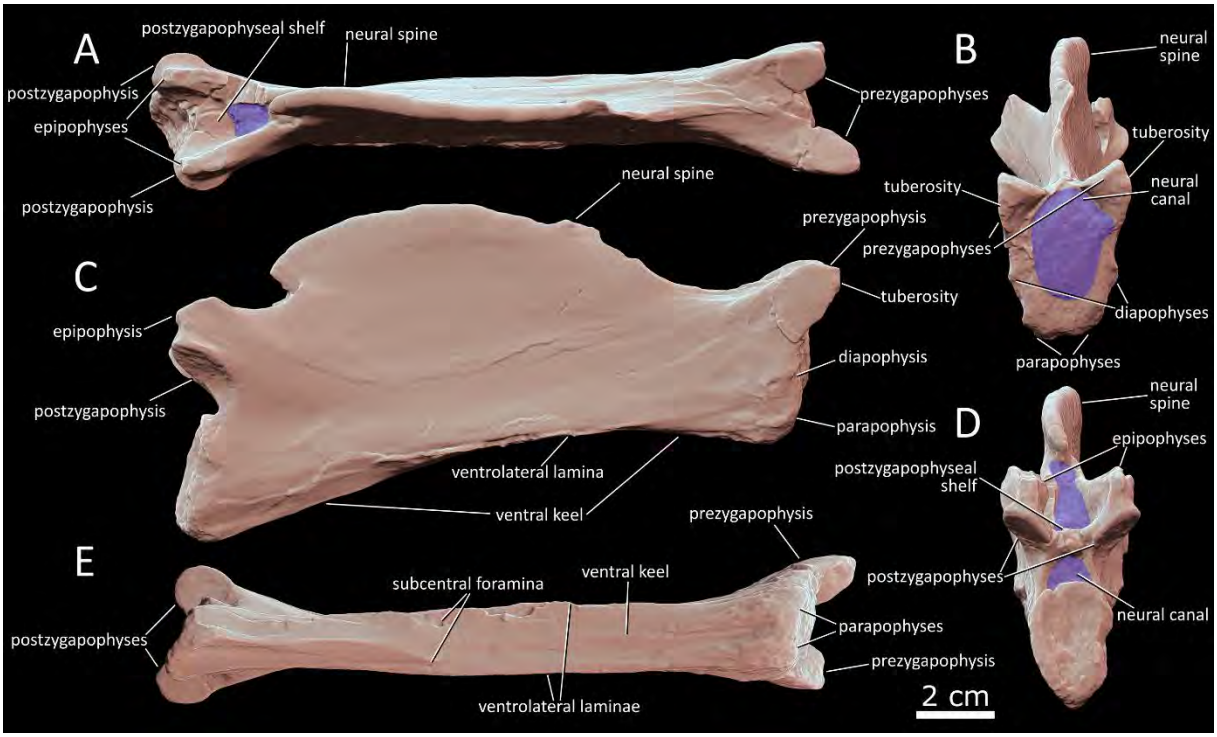

Fig. 17. Eleventh cervical vertebra of *Tanystropheus conspicuus* from the Lower Keuper (lower Ladinian) of Miedary (Poland) – ZPAL V. 36/1171. Three-dimensional model snapshots with Lit Sphere Radiance Scaling shader enabled, in dorsal (**A**), anterior (**B**), right lateral (**C**), posterior (**D**), and ventral (**E**) views. Areas covered with sediment marked with blue hue.

The twelfth cervical vertebra of *Tanystropheus conspicuus* is a relatively robust element compared to the preceding cervical vertebrae (Fig. 18). Its height at mid-length is subequal to the length of the centrum (Fig. 18A, B_3). As for the eleventh cervical vertebra, the

ventral surface of the twelfth cervical vertebra is inclined (Fig. 18A, B_3), corresponding to the condition reported for *T. longobardicus* by Renesto (2005). The centrum itself is parallelogram-shaped in lateral view, with its ventral surface being distinctly concave and marked by the presence of a weakly outlined keel (Fig. 18A, B_3). At least one of the pair of subcentral foramina is usually present, situated lateral to the keel, but they are much smaller than in the preceding vertebrae (Fig. $18B_1$). The anterior articular surface of the centrum is circular in anterior view (Fig. $18B_2$). The posterior surface is ventrally expanded, appearing sub-triangular in posterior view (Fig. $18B_5$). The centrum is spool-shaped in ventral view (Fig. $18B_1$), with its middle section being laterally constricted, and its anterior portion being considerably expanded transversely due to the presence of robust, stout diapophyses and parapophyses. Their articular surfaces are elliptical and predominantly ventrally oriented (Fig. 18A, B_1, B_3). The parapophyses lie directly adjacent to each other, being separated only by the anterior portion of the ventral keel (Fig. $18B_1$–B_2).

The anterior neural canal opening is triangular and the posterior one is subrectangular (Fig. $18B_2$, B_5). The prezygapophyses are stocky, barely extending beyond the anterior articular surface of the centrum (Fig. 18A, B_3). Similar to the condition observed in the eleventh cervical vertebra, they bear distinct mound-like anteriorly projecting tuberosities (Fig. 18A, B_2, B_3), which are shorter but more robust than in the middle cervical vertebrae. The prezygapophyseal articular surfaces are positioned dorsal to the mound-like tuberosities, with an obtuse angle between them in anterior view (Fig. $18B_2$). In contrast to the preceding vertebrae, they are transversely broad and anteroposteriorly short. The anteromedial surface of each prezygapophysis is formed as a thin lamina, which joins the prespinal lamina in a triradiate connection above the anterior neural canal opening (Fig. $18B_2$). The postzygapophyses are similar in their characteristics to the prezygapophyses. They are robust and extend slightly beyond the posterior articular surface of the centrum (Fig. 18A, B_3). Their articular surfaces are broad and transversely wide. The angle formed between them is slightly obtuse (Fig. $18B_5$). They are aligned with the floor of the postzygapophyseal shelf (Fig. $18B_5$). The weakly posterodorsally projecting epipophyses are much smaller than in the preceding vertebrae and do not extend posteriorly beyond the postzygapophyses (Fig. 18A, B_3). The concavity formed at the base of the posterior portion of the neural spine is deep and flanked bilaterally by the postzygapophyses (Fig. $18B_5$). A distinct postspinal lamina runs along the midline of its dorsal surface, becoming confluent with the neural spine near its posterodorsal corner (Fig. $18B_3$, B_5).

The morphology of the neural spine itself can vary considerably between specimens (compare Fig. 18A and B_3). In some individuals the height of the thin prespinal lamina increases gradually before reaching the distal surface of the neural spine (Fig. 18B), whereas in others the anterior margin of the neural spine is deeply concave in lateral view and nearly vertical, with the neural spine being relatively taller but much shorter anteroposteriorly (Fig. 18A). All known vertebrae 12 of *T. conspicuus* share the characteristics of the distal surface of the neural spine, which is rounded, slightly transversely expanded, and with a more dorsally raised posterior portion, so that in lateral view it is anteroventrally inclined (Fig. 18A, B_3, B_4). Moreover, all known twelfth cervical vertebrae of *T. conspicuus* have a neural spine that is considerably taller than in the corresponding vertebrae of other species of *Tanystropheus* (pers. obs. AR; Wild 1973; Renesto 2005; Nosotti 2007; Rieppel et al. 2010).

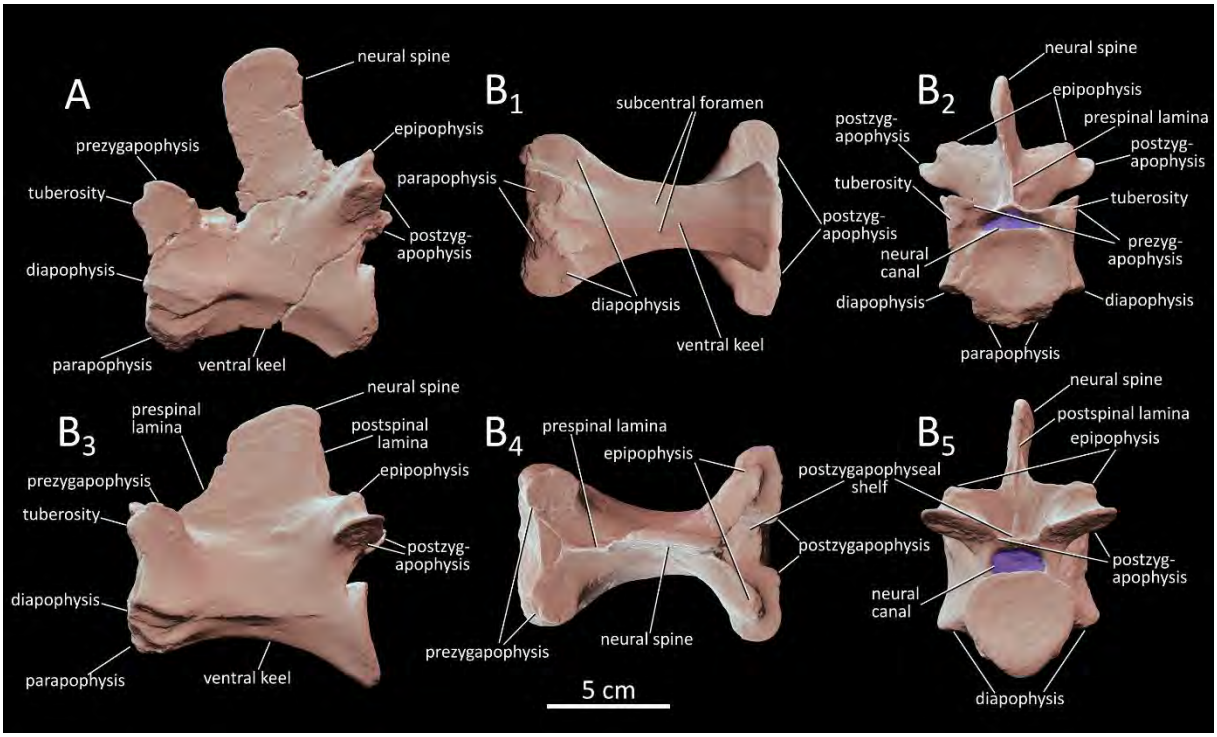

Fig. 18. Twelfth cervical vertebrae of *Tanystropheus conspicuus* from the Lower Keuper (lower Ladinian) of Miedary (Poland) – ZPAL V. 36/108 (**A**) and ZPAL V. 36/1209 (**B**). Three-dimensional model snapshots with Lit Sphere Radiance Scaling shader enabled, in left lateral (A, B_3), ventral (B_1), anterior (B_2), dorsal (B_4), and posterior (B_5) views. Areas covered with sediment marked with blue hue.

The thirteenth cervical vertebra is proportionally more similar to the succeeding dorsal vertebrae than the preceding cervical vertebrae (Fig. 19). The length of its centrum is always shorter than the height of the vertebra (Fig. 19A). The centrum is considerably constricted

bilaterally and ventrally, being slightly concave in lateral view and hourglass-shaped in ventral view (Fig. 19A–B). The midline of the ventral surface is marked by the presence of a weakly developed ventral keel (Fig. 19B). On its sides, near the anteroposterior midpoint are up to two subcentral foramina. In some instances there may only be one, or none at all, and they are always much smaller than the corresponding foramina in the preceding cervical vertebrae.

The neural canal openings are semicircular, with the anterior one being much lower but transversely broader than the posterior one (Fig. 19D–E). The articular surfaces of the centrum are circular and very weakly amphicoelous. The anterior one is larger and more ventrally located (Fig. 19A, D–E). The parapophyses are directly adjacent to each other, being separated only by the anterior portion of the ventral keel (Fig. 19B). The diapophyses are intermediate in length between those of the cervical vertebrae and the dorsal vertebrae. They are especially massive, projecting lateroventrally from the anterolateral portion of the centrum as stout processes, with a deep, broad concavity between them and the parapophyses (Fig. 19A–B). The rib articular surfaces of the parapophyses are flat, subcircular, and more anteriorly oriented than the elliptical, rounded, lateroventrally oriented articular surfaces of the diapophyses (Fig. 19B). The lateral surface of the vertebra is concave between the diapophysis and the distal tip of the prezygapophysis, with its margin being semicircular in anterior view (Fig. 19D–E).

The prezygapophyses are relatively long, broad, and laterally projecting. They do not extend anteriorly beyond the articular surface of the centrum (Fig. 19A). The mound-like anterior tuberosities, present in the preceding cervical vertebrae, are absent, but the corresponding anteroventral surface of the prezygapophyses is rugose (Fig. 19D). The prezygapophyseal articular surfaces are elliptical. Their longer axis is sub-transversely oriented (Fig. 19C). The angle formed between them is obtuse (Fig. 19D). The postzygapophyses are longer than the prezygapophyses, with their articular surfaces also being transversely wider (Fig. 19C). They project dorsolaterally but do not extend posteriorly beyond the articular surface of the centrum (Fig. 19A). The angle formed between them is obtuse but to a lesser extent than between the prezygapophyses (Fig. 19E). The epipophyses are nearly completely reduced, being developed as minute projections on the dorsal surface of the postzygapophyses (Fig. 19E).

The base of the neural spine is anteriorly and posteriorly constricted by concavities in lateral view, with the posterior one being larger and deeper (Fig. 19D–E). These concavities

are flanked by the laminae that connect the zygapophyses to the neural spine and ventrally floored by the laminae that constitute the roof of the neural canal. As for the twelfth vertebra, there is some disparity in the neural spine morphology in the last cervical of *T. conspicuus*, with its relative length varying considerably. In most specimens the neural spine is anteroposteriorly short but dorsoventrally tall and relatively straight, with distinct prespinal and postspinal laminae extending along its anterior and posterior margins (Fig. 19A). The distal surface of the neural spine is rounded in lateral view and slightly transversely expanded. As for most other vertebrae, the neural spine morphology is the main feature distinguishing *T. conspicuus* from *T. hydroides* and *T. longobardicus*, with the two latter exhibiting considerably shorter neural spines with a flat, straight distal surface (see Wild 1973; Renesto 2005; Nosotti 2007; Rieppel et al. 2010). However, all species of *Tanystropheus* share the characteristically robust diapophyses (see Wild 1980*a*; Rieppel et al. 2010).

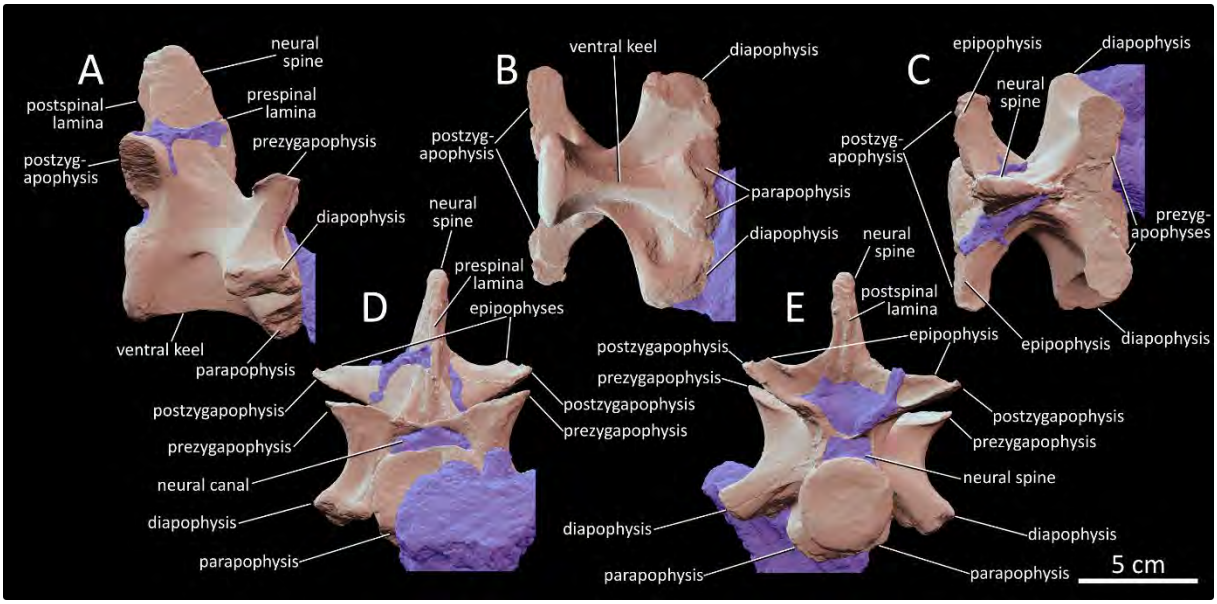

Fig. 19. Thirteenth cervical vertebra of *Tanystropheus conspicuus* from the Lower Keuper (lower Ladinian) of Miedary (Poland) – ZPAL V. 36/2485. Three-dimensional model snapshots with Lit Sphere Radiance Scaling shader enabled, in right lateral (**A**), ventral (**B**), dorsal (**C**), anterior (**D**), and posterior (**E**) views. Areas covered with sediment marked with blue hue. The vertebra could not be fully prepared due to its association with a delicate skull bone.

Dorsal vertebrae

Similar to other species of *Tanystropheus*, twelve dorsal vertebrae are present in *Tanystropheus conspicuus*, although no specimen preserves a full series (see Discussion). Specimen ZPAL V. 36/125 includes eleven dorsal vertebrae still in articulation, as well as the two sacral vertebrae, several caudal vertebrae, the left scapula, the left pubis, and the left ilium, as well as many ribs and gastralia (Fig. 20). All dorsal vertebrae of *T. conspicuus* are amphicoelous and lack any trace of the neurocentral suture.

The anterior dorsal vertebrae are similar in their morphology to the last cervical vertebra (compare Fig. 19 and Fig. 21). In *Tanystropheus* the dorsal vertebrae differ, however, from the cervical vertebrae in the complete absence of two major features – the subcentral foramina and the epipophyses. Moreover, in the anterior dorsal vertebrae the diapophyses are longer and laterally oriented, the postzygapophyses are shorter and more posteriorly projecting, and the anterior articular surface of the centrum is relatively smaller compared to the posterior cervical vertebrae. In the anteriormost dorsal vertebrae the centrum is parallelogram-shaped in lateral view and relatively longer than in the succeeding vertebrae (Fig. 21C). Its circular articular surfaces are roughly on the same dorsoventral level, with the anterior one being relatively larger. In ventral view the centrum is hourglass-shaped, with a median keel forming its ventral edge (Fig. 21E). The parapophyses are located in the ventrolateral corner of the anterior articular surface. Their bases nearly touch, being separated only by the ventral keel (Fig. 21E). They are short and sturdy, weakly ventrally expanded, and ventrolaterally oriented (Fig. 21C, E). The diapophyses originate from the lateral surface of the vertebra, roughly at the boundary between the centrum and the neural arch (Fig. 21C). They are relatively long and robust, extending laterally far beyond the zygapophyses. Their distal ends are elliptical in lateral view and thickened (Fig. 21C). Three distinct laminae are present along most of the length of the diapophysis (Fig. 21A, C, E) – a lamina extending to the corresponding prezygapophysis (prezygodiapophyseal lamina), a lamina extending towards the corresponding parapophysis (anterior centrodiapophyseal/paradiapophyseal lamina), and finally a lamina extending towards the posteroventral corner of the centrum (posterior centrodiapophyseal lamina). Moreover, the posterolateral portion of the base of the diapophysis is connected to the base of the corresponding postzygapophysis by a weakly developed postzygodiapophyseal lamina (Fig. 21C). Between the diapophyseal laminae, there are deep, triangular pits (fossae), of which the fossa located anteriorly to the diapophysis (the prezygocentrodiapophyseal fossa) is the deepest (Fig. 21A).

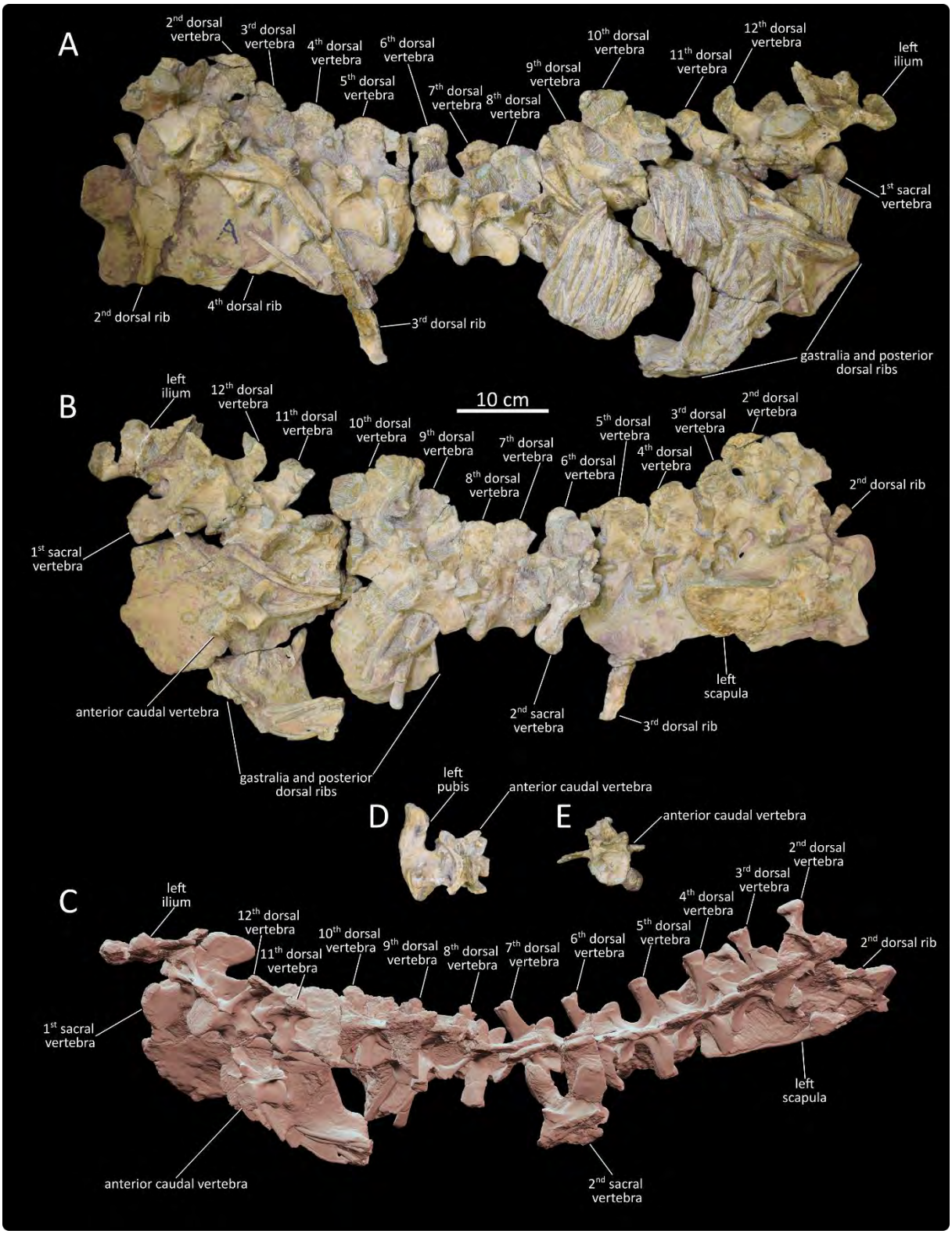

Fig. 20. Partial skeleton of *Tanystropheus conspicuus* from the Lower Keuper (lower Ladinian) of Miedary (Poland) – ZPAL V. 36/125, including most of the torso of one individual (**A**, **B**, **C**) and some associated elements (**D**, **E**). Photographs (A–B, D–E) and a three-dimensional model snapshot with Lit Sphere Radiance Scaling shader enabled (C), in left lateral (A), right lateral, (B), dorsal (C–D), and anterior (E) views.

The prezygapophyses are relatively large and transversely wide (Fig. 21A, D). Their distal margin is rounded and confluent with the edge of the corresponding articular surface (Fig. 21A). The prezygapophyseal articular surfaces are elliptical in dorsal view and have their lateral edges slightly raised, with an obtuse angle of around 150° being formed between the prezygapophyses (Fig. 21A, D). They connect to the centrum through centroprezygapophyseal laminae, which laterally flank the elliptical opening for the neural canal (Fig. 21A). Between the prezygapophysis and the neural spine there is a shelf (transprezygapophyseal lamina), which also constitutes the roof of the neural canal (Fig. 21A, D). This shelf is posteriorly delimited by the neural spine and the spinoprezygapophyseal laminae. The postzygapophyses are shorter than the prezygapophyses, and posterolaterally oriented (Fig. 21D). As in the prezygapophyses, they meet in an obtuse angle (Fig. 21B). Their articular surfaces are elliptical. The postzygapophyses connect to the centrum through the vertical centropostzygapophyseal laminae, which flank the posterior, rectangular, opening for the neural canal (Fig. 21B). The posterior portion of the neural canal is roofed by the transpostzygapophyseal lamina, which extends between the postzygapophyses and the base of the neural spine, forming a shelf that is anteriorly delimited by the spinopostzygapophyseal laminae (Fig. 21B, D).

The neural spine is tall. Its base is anteroposteriorly constricted through the presence of deep pits formed between the zygapophyses (Fig. 21A–C). From those pits, two laminae extend towards the distal end of the neural spine – the anterior, prespinal lamina, and the posterior, postspinal lamina (Fig. 21A–C). They expand the anteroposterior width of the neural spine in lateral view, forming well outlined attachment sites for ligaments. The distal portion of the neural spine is posteriorly displaced relative to its base and the neural spine is consequently posteriorly curved (Fig. 21C). On its laterodistal surface, a tuberosity is present bilaterally, possibly forming a weakly laterally projecting mammillary process on both sides (Fig. 21B–C). The distal portion of the neural spines is convex in lateral view, transversely expanded, and bulbous. Its surface is distinctly rugose and covered with a dense network of grooves, pits, and ridges (Fig. 21C–D).

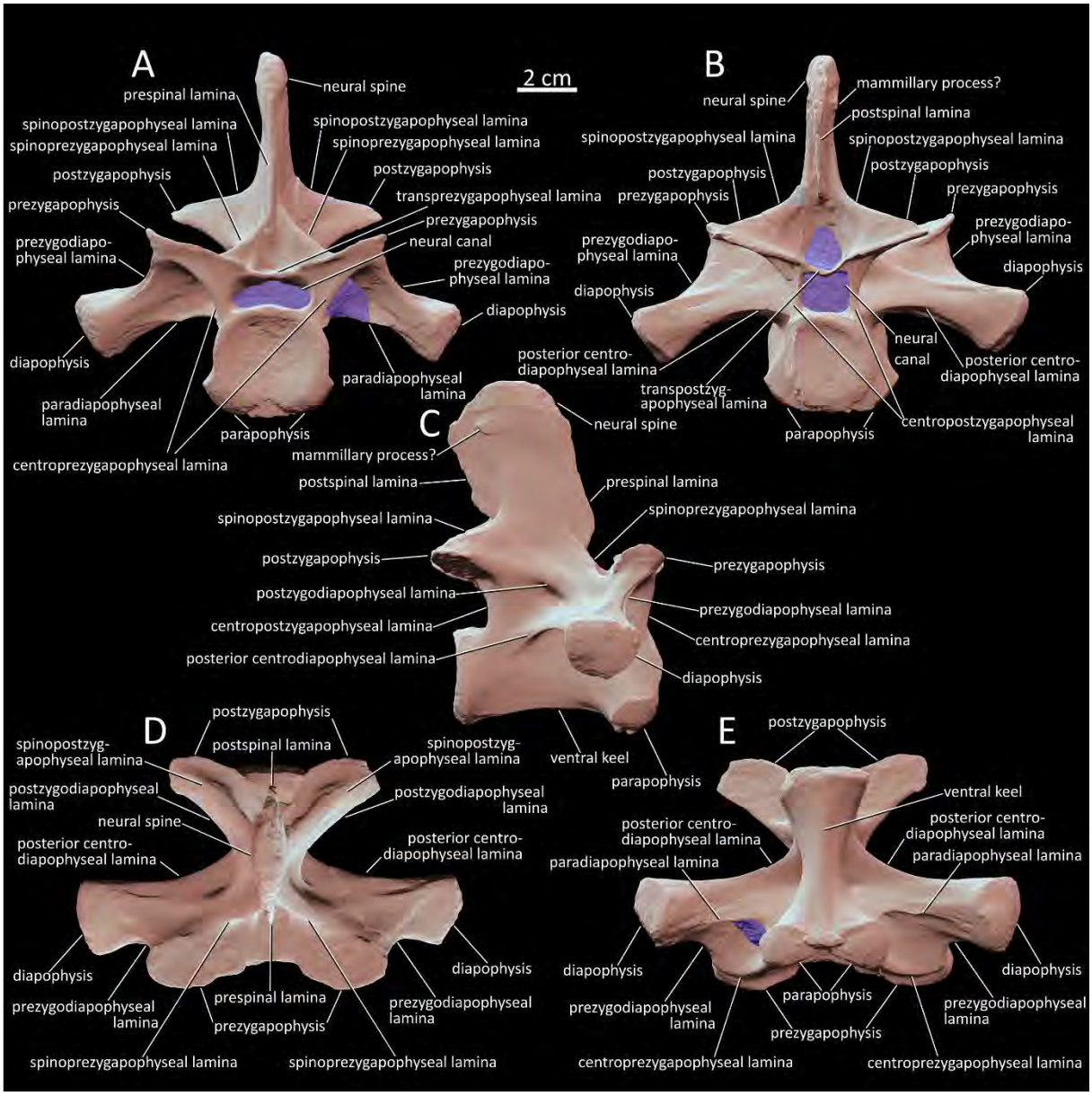

Fig. 21. Anterior dorsal vertebra of *Tanystropheus conspicuus* from the Lower Keuper (lower Ladinian) of Miedary (Poland) – ZPAL V. 36/1249/. Three-dimensional model snapshots with Lit Sphere Radiance Scaling shader enabled, in anterior (**A**), posterior (**B**), right lateral (**C**), dorsal (**D**), and ventral (**E**) views. Areas covered with sediment marked with blue hue.

The morphology of the succeeding dorsal vertebrae corresponds closely with that of the anterior ones, although several features change gradually along the length of the vertebral column (see Fig. 20). The centrum length remains relatively constant, with only the last three dorsal vertebrae being considerably shorter (Fig. 20B). Parapophyses are present up to the fourth dorsal vertebra, and in each succeeding vertebrae after the first one, they are slightly more distant from each other and the ventral keel (Fig. 20A). The transverse processes retain their length and anteroposterior width up to the tenth dorsal (Fig. 20C). In dorsal vertebrae three to ten, the transverse processes are situated near the anteroposterior mid-point of the centrum, with the prezygodiapophyseal lamina not extending towards the anterior edge of the prezygapophyses, and this lamina being nearly completely reduced in the last two dorsal vertebrae (Fig. 20A–C). From the third dorsal vertebra onwards, the shape of the diapophyseal articular surface for the rib attachment changes from elliptical to triangular, becoming dorsoventrally taller in lateral view (Fig. 20A–B). The zygapophyses become successively shorter and more anteroposteriorly projecting in each consecutive vertebra. The angle between their articular surfaces remains relatively constant and similar to that observed in the anterior dorsal vertebrae. Their articular surfaces are elliptical and transversely wide. The neural spine is posteriorly curved only in the first two dorsal vertebrae (Fig. 20A–B). In all succeeding elements it is relatively straight in lateral view. Dorsal to the ridge extending between the prespinal and postspinal laminae in dorsal vertebrae five to ten the distal margin of the neural spine is anteroposteriorly expanded (Fig. 20A–B). As a result, the distal portion of their neural spines is rhomboidal in lateral view. All dorsal vertebrae share the presence of a rugose distal surface of the neural spine, although the exact morphology and the extent of this distal expansion are highly variable, sometimes differing between vertebrae from the same position in the vertebral column. The last two dorsal vertebrae differ from the preceding ones in several features, as previously documented in *Tanystropheus* by Wild (1973) and Nosotti (2007) who considered them as “lumbar” vertebrae. Their centra are relatively much shorter and lack the ventral keel, their neural spines are relatively taller, anteroposteriorly short, and distally less expanded (Fig. 22). Moreover, their diapophyses are more anteriorly located, occupying the space directly between the prezygapophyses and the centrum.

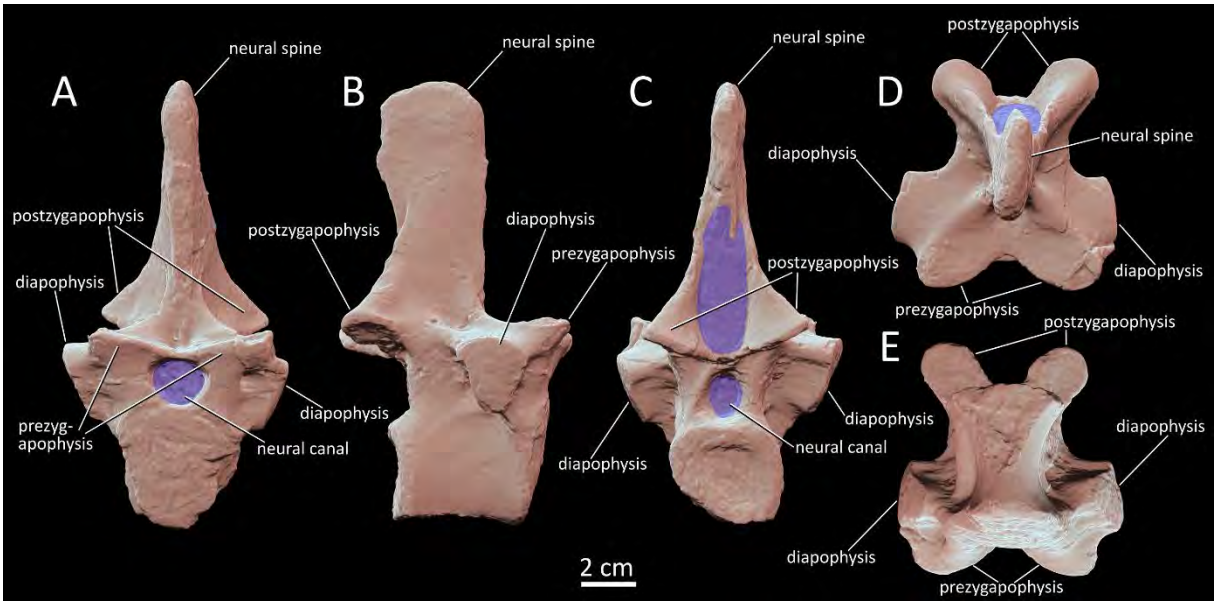

Fig. 22. Posterior (eleventh?) dorsal vertebra of *Tanystropheus conspicuus* from the Lower Keuper (lower Ladinian) of Miedary (Poland) – ZPAL V. 36/1033. Three-dimensional model snapshots with Lit Sphere Radiance Scaling shader enabled, in anterior (**A**), right lateral (**B**), posterior (**C**), dorsal (**D**), and ventral (**E**) views. Areas covered with sediment marked with blue hue.

There are several morphological differences present between the dorsal vertebrae of *Tanystropheus conspicuus* and other *Tanystropheus* species. For example, the diapophyses being much longer and more robust in the former (compare Figs. 20–21 with the vertebrae illustrated by Wild 1973, 1980*a*; Renesto 2005; Nosotti 2007). Only a few of the vertebrae of *T. conspicuus* that Wild (1973) had access to preserved the distal portion of the neural spine, and with it, the distal rugose expansion and convex outline in lateral view. It is only evident now, through the discovery of further, complete, elements that *T. conspicuus* differs in neural spine morphology from the other *Tanystropheus* species. Among non-crocopodan archosauromorphs, this condition is present to a similar extent in only one other tanysaurian, *Trachelosaurus fischeri*. This taxon is also characterised by the presence of the rugose, convex thickening of the distal portion of the neural spine in most of its precaudal vertebrae, and with well-developed transverse striations marking its surface (Spiekman et al. 2024*b*). By contrast with the vertebrae known from the CEB referred to *T. conspicuus*, all other published dorsal vertebrae of *Tanystropheus* have a shorter neural spine, with a distal expansion formed as a straight, flat spine table (pers. obs. AR; Wild 1973; Wild 1980*a*; Renesto 2005; Dalla Vecchia 2006, 2008; Nosotti 2007; Rieppel et al. 2010; Ezcurra 2016; Dalla Vecchia and Simonetto 2018; Renesto and Saller 2018; Spiekman et al. 2021). In the dorsal vertebrae of

these forms the vertebral height at the midpoint is usually subequal, or slightly larger than the length of the corresponding centrum (pers. obs. AR, see Wild, 1973; Nosotti 2007; Fig. 23). In *T. conspicuus* the dorsal vertebrae are always about two to three times taller than long. There is some overlap of the centrum length between the largest known dorsal vertebrae of *T. hydroides* and the smallest measured dorsal vertebrae of *T. conspicuus*, but the neural spines of the latter are much taller (Fig. 23).

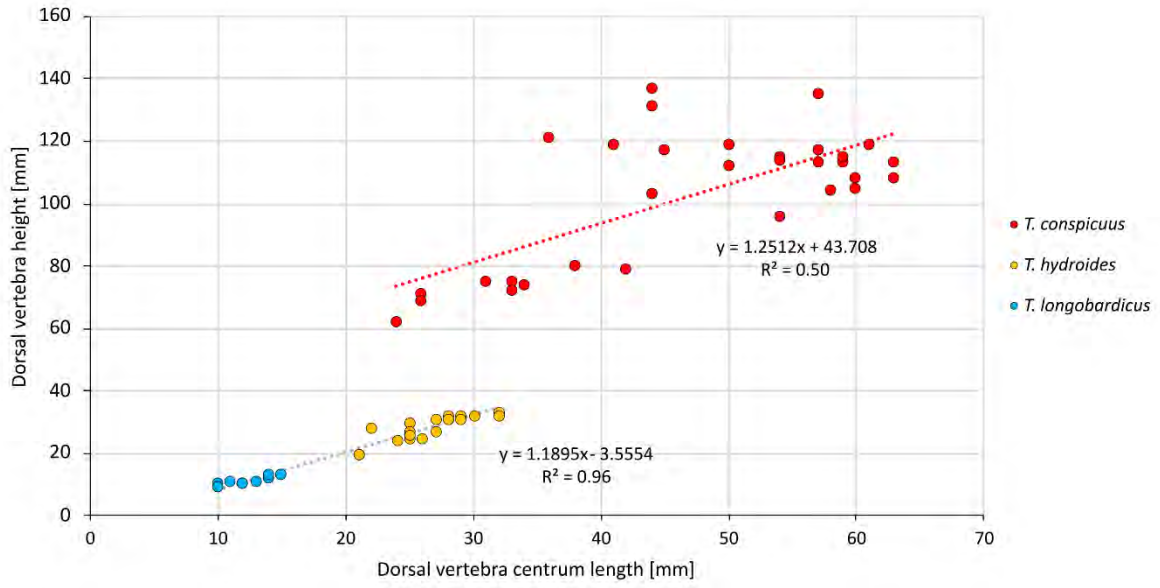

Fig. 23. Comparison of length to height ratio in the dorsal vertebrae of three species of *Tanystropheus*. See Appendix I for the list of specimens used and the respective measured values. Dashed lines represent the linear regression fitted lines, one for *T. conspicuus* and one treating *T. hydroides and T. longobardicus* as one population, with respective regression equation and coefficient of determination value provided next to them.

Sacral vertebrae

As in other species of *Tanystropheus*, there are two unfused sacral vertebrae present in *Tanystropheus conspicuus* (Wild, 1973; Nosotti 2007). Aside from the presence of the sacral ribs, they are morphologically similar to the posteriormost dorsal vertebra, and are of nearly identical size (Fig. 20). The centrum of the first sacral vertebra is relatively short, slightly amphicoelous, and does not have a ventral constriction nor a ventral keel (Fig. 24E). Its articular surfaces are round, with the posterior one being relatively smaller (Fig. 24A, C). The sacral ribs are fully fused to the transverse processes without a discernible suture line. The ribs extend laterally from the anterodorsal corner of the lateral surfaces of the centrum (Fig. 24B). They anteroposteriorly widen distally, with their anterior portion being further laterally

extended (Fig. 24D). Their distal margin is oriented obliquely to the longitudinal axis of the vertebra, with the articular surface for the ilium being ventrolaterally and slightly posteriorly facing. In lateral view the articular surface of the rib is elliptical (Fig. 24B). In anterior view, the sacral ribs have a straight dorsal and convex ventral margin (Fig. 24A). The neural canal openings are relatively small and circular (Fig. 24A, C). The prezygapophyses project dorsolaterally, with their articular surfaces being elliptical and transversely broad (Fig. 24D). The angle between them is obtuse in anterior view (Fig. 24A) and does not differ from the condition noted in the dorsal vertebrae. The postzygapophyses are relatively short and posterolaterally projecting (Fig. 24D). Their articular surfaces share the characteristics of the prezygapophyseal articular surfaces. The neural spine is tall and slightly anteroposteriorly expanded towards its distal end (Fig. 24B).

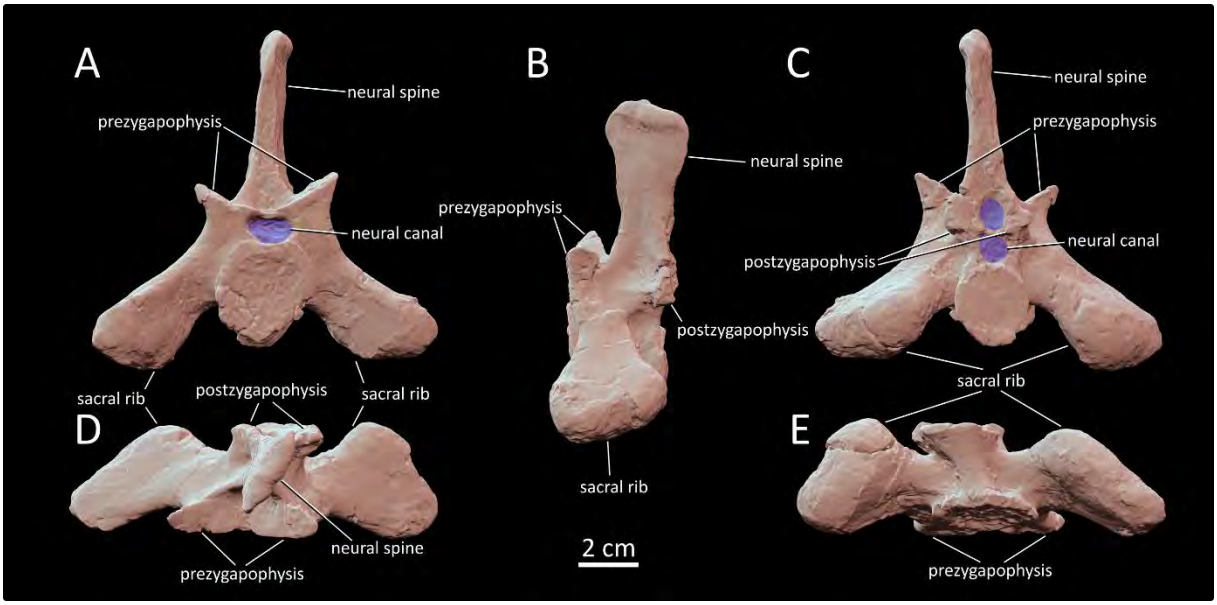

Fig. 24. First sacral vertebra of *Tanystropheus conspicuus* from the Lower Keuper (lower Ladinian) of Miedary (Poland) – ZPAL V. 36/1187. Three-dimensional model snapshots with Lit Sphere Radiance Scaling shader enabled, in anterior (**A**), left lateral (**B**), posterior (**C**), dorsal (**D**), and ventral (**E**) views. Areas covered with sediment marked with blue hue.

The second sacral vertebra differs from the first one mainly in the characteristics of the ribs. The second pair of dorsal ribs is ventrolaterally and somewhat anteriorly oriented, shorter, and they widen distally to a lesser extent than the first pair (Fig. 25). The anterior margin of the second sacral rib is flat in lateral view (Fig. 25B), forming an articulation surface for the posterolateral tip of the first sacral rib. On the posterodorsal margin of each of the second sacral ribs, at the level of the most dorsal extent of the posterior articular surface of the centrum, a posteriorly projecting, anteroposteriorly flattened process is present. It is triangular in dorsal view and tapers to a point (Fig. 25D). Further differences between the first and the second sacral vertebrae of *T. conspicuus* include the presence of a weakly pronounced ventral keel on the centrum (Fig. 25E) and a more anteroposteriorly expanded neural spine in the latter (Fig. 25B). Moreover, the prezygapophyses in the second sacral vertebra are positioned more ventrally than the postzygapophyses, conversely to the first sacral vertebra (compare Figs. 24 and 25).

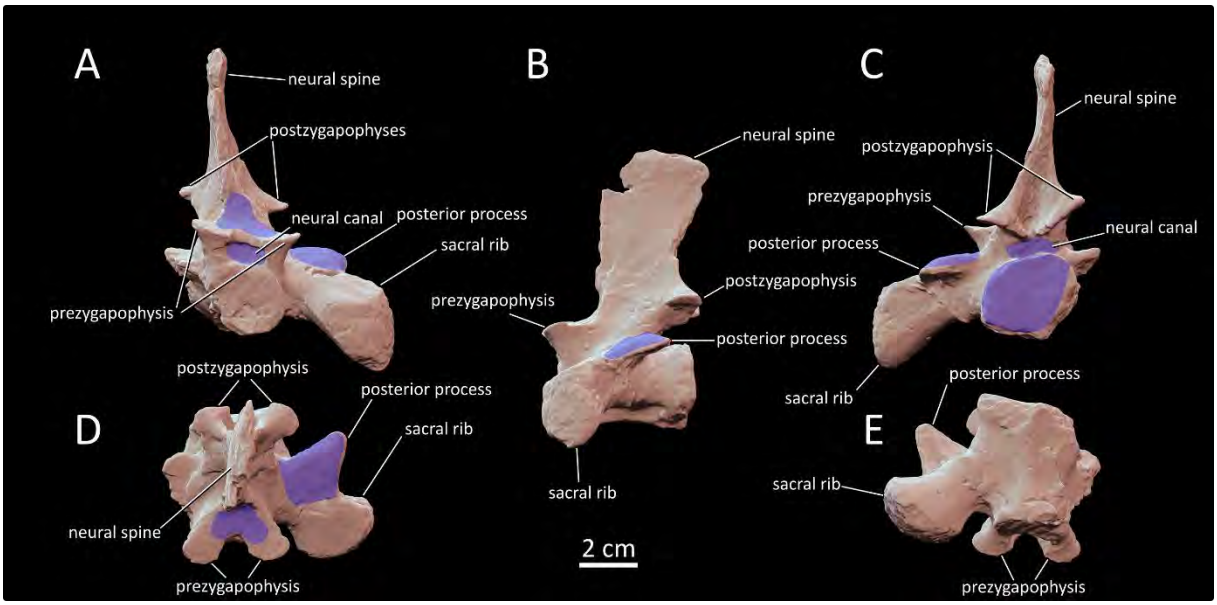

Fig. 25. Second sacral vertebra of *Tanystropheus conspicuus* from the Lower Keuper (lower Ladinian) of Miedary (Poland) – ZPAL V. 36/1037. Three-dimensional model snapshots with Lit Sphere Radiance Scaling shader enabled, in anterior (**A**), left lateral (**B**), posterior (**C**), dorsal (**D**), and ventral (**E**) views. Areas covered with sediment marked with blue hue.

Caudal vertebrae

In all known caudal vertebrae of *Tanystropheus conspicuus* the transverse processes are seamlessly fused with ribs. In the text I refer to the whole fused element as a transverse process. They are present in approximately the first fourteen caudal vertebrae in *T. hydroides* (Wild 1973) – these can be considered the proximal caudal vertebrae. The inferred distal caudal vertebrae therefore lack a transverse process. The first caudal vertebra in *T. hydroides*

and *T. longobardicus* can be distinguished by the presence of posterolaterally oriented, distally tapering, wing-like transverse processes (Wild 1973, 1980*a*). Further posteriorly, the proximal caudal vertebrae possess a non-tapering transverse processes with a relatively constant anteroposterior width, and hence when dealing with isolated vertebrae, it is only the first caudal vertebra that can be assigned to its original position in the vertebral column with any certainty in these two species. However, no caudal with such posterolaterally oriented and distally tapering transverse processes is known from Miedary. Wild (1973) identified a fragmentary vertebra as the first caudal of *T. conspicuus*, but due to the missing transverse processes, this identification is equivocal. The only specimen that can be regarded as a likely first caudal vertebra of *T. conspicuus* is MHI 2199/2, in which the transverse processes are reminiscent of butterfly wings - they are relatively short, triangular in dorsal view, and possess two extensions, one projecting posterolaterally and the other anteriorly. The former extension tapers slightly. This anteriorly projecting extension is present, but much less pronounced, in the first caudal vertebra of other *Tanystropheus* species (e.g., PIMUZ T 1270, PIMUZ T 2483, MCSN 4451). MHI 2199/2 does not possess a median groove, associated with the presence of the chevron, both of which are absent in the anteriormost caudal vertebrae of *Tanystropheus* (see Fig. 26E), but present along most of the length of the tail (see Wild 1973; Renesto and Saller 2018).

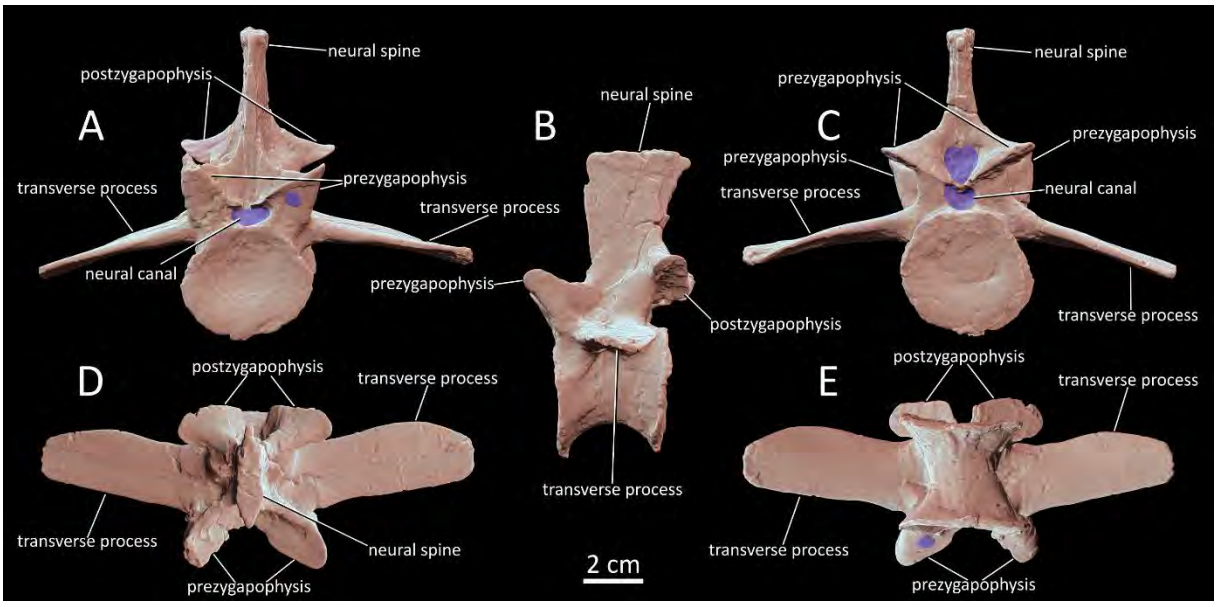

Fig. 26. Anterior caudal vertebra of *Tanystropheus conspicuus* from the Lower Keuper (lower Ladinian) of Miedary (Poland) – ZPAL V. 36/114. Three-dimensional model snapshots with Lit Sphere Radiance Scaling shader enabled, in anterior (**A**), left lateral (**B**), posterior (**C**), dorsal (**D**), and ventral (**E**) views. Areas covered with sediment marked with blue hue.

The proximal caudal vertebrae of *Tanystropheus conspicuus* possess a relatively short, ventrally and laterally constricted centrum, corresponding to the preceding sacral and posterior dorsal vertebrae (Fig. 26B, E). Its articular surfaces are moderately amphicoelous and circular (Fig. 26A, C). The openings of the neural canal are heart-shaped, with a bilobed dorsal margin (Fig. 26A, C). The transverse processes project laterally from the boundary between the centrum and the neural arch at mid-length (Fig. 26B). They are dorsoventrally thin and flat, and anteroposteriorly wide. In the proximal caudal vertebrae, apart from the first, the transverse processes have a blunt end, with a rounded distal margin (Fig. 26D–E). Their anterior and posterior margins curve slightly posteriorly relative to their base in dorsal view (Fig. 26D–E).

The prezygapophyses in the proximal caudal vertebrae are longer, more slender, and further dorsally projecting than in the sacral vertebrae (Fig. 26B, D). Their articular surfaces are elliptical in dorsal view. In anterior view the angle between them is considerably smaller than in all the preceding dorsal and sacral vertebrae, but still obtuse (Fig. 26A). Unlike in nearly all the preceding vertebrae, the transprezygapophyseal and transpostzygapophyseal laminae are absent, with the corresponding zygapophyses separated by a notch in dorsal view (Fig. 26A, C–D). The postzygapophyses project further laterally than the prezygapophyses, with the longitudinal axes of their articular surfaces being nearly parallel to each other and perpendicular to the sagittal plane of the vertebra (Fig. 26D).

As for the preceding elements, the base of the neural spine is anteroposteriorly constrained by deep, triangular grooves located between the zygapophyses (Fig. 26A, C). The neural spine is positioned relatively further posteriorly than in the preceding vertebrae (Fig. 26B). It is relatively shorter than in the dorsal and sacral vertebrae but still considerably taller in relative terms than in the corresponding elements of other *Tanystropheus* species (compare to Wild 1973; Dalla Vecchia 2000; Nosotti 2007). In lateral view its anterior and dorsal margins are straight, and the posterior edge is concave (Fig. 26B). The distal edge is spindle-shaped in dorsal view (Fig. 26D). It lacks the anteroposteriorly convex expansion present in the preceding elements but is formed as a rugose, flat “spine table” (see Ezcurra 2016; Renesto and Saller 2018; Spiekman et al. 2021), with the laterodistal surfaces of the neural spine also having a rough texture.

Posteriorly along the caudal column, the characters described above change gradually. The centrum retains its length or becomes slightly longer in the more posterior proximal vertebrae (Fig. 27). Distal to the first caudal vertebra, the centrum becomes more hourglass-

shaped in ventral view, with its articular surfaces becoming less transversely expanded, but more concave. The most distal caudal vertebrae have an approximately constant centrum height along their length (Fig. 27F–G). A median groove is present, along with the hemal arches, in one of the first proximal caudal vertebrae, and also occurs on the ventral surface of most, if not all, succeeding caudal centra. The groove is flanked by well-defined lateral ridges, which decrease in height near the anteroposterior midpoint of the centrum. At the midpoint, a deep notch of the ventral centrum margin is visible in lateral view (Fig. 27B–G). This ventral notch is absent in the caudal vertebrae of *T. hydroides* and *T. longobardicus* (pers. obs. AR; see Wild 1973; 1980*a*). The articulation surfaces for the hemal arches are poorly defined. The transverse processes decrease in length and anteroposterior width posteriorly along the caudal column to become a cone-shaped, tapering, laterally oriented projection in the posteriormost proximal caudal vertebrae (Fig. 27B–C). They are always located at the mid-length of the vertebra on the boundary between the centrum and the neural arch.

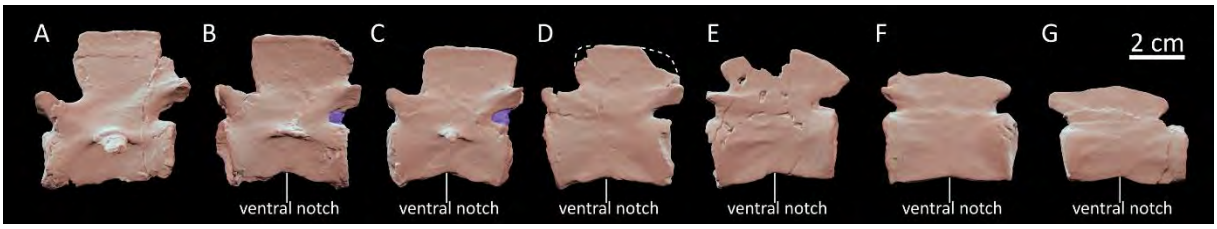

Fig. 27. A sequence of isolated middle-distal caudal vertebrae of *Tanystropheus conspicuus* from the Lower Keuper (lower Ladinian) of Miedary (Poland) – ZPAL V. 36/2489 (**A**), ZPAL V. 36/2490 (**B**), ZPAL V. 36/2491 (**C**), ZPAL V. 36/139 (**D**), ZPAL V. 36/116 (**E**), ZPAL V. 36/115 (**F**), and ZPAL V. 36/1070 (**G**). Three-dimensional model snapshots with Lit Sphere Radiance Scaling shader enabled, in left lateral (A, C, E, G) and right lateral (mirrored – B, D, F) views.

As in all other vertebrae of *Tanystropheus*, the fusion of the neural arch and the centrum is seamless in all caudal vertebrae. In all proximal caudal vertebrae of *T. conspicuus* the pre- and postzygapophyses extend slightly beyond the centrum (Fig. 27A–C). Distally along the caudal series, the zygapophyses become relatively smaller, and increasingly slender, dorsally projecting, and tapering (Fig. 27E–F). In the posterior proximal and anterior distal caudal vertebrae, the angle between the zygapophyseal articular surfaces changes from obtuse to acute. In the distal-most caudal vertebrae the postzygapophyses become confluent with the posterior margin of the neural spine (Fig. 27F–G). The prezygapophyses, which decrease in size along the caudal series less than the postzygapophyses, change from anteriorly oriented,

minute projections, to slight thickenings on the anterolateral surfaces of the neural spine (Fig. 27F–G).

Although the neural spine height decreases distally in the tail of *T. conspicuus*, all caudal vertebrae of this species seem to be distinctly taller than the corresponding vertebrae of *T. hydroides* and *T. longobardicus*. The distal margin of the neural spine in the latter two species is relatively straight in lateral view (see Wild 1973, 1980*a*; Nosotti 2007) or slightly concave in the distal caudal vertebrae of *T. hydroides* (PIMUZ T 2817, pers. obs. AR). In the distal caudal vertebrae of *T. conspicuus* the neural spine is distinctly convex, with its distalmost expansion point being located around the mid-length (Fig. 27D–G). The neural spine in the distal caudal vertebrae of both *T. conspicuus* and *T. hydroides* is positioned relatively much further anteriorly (see Peyer 1931, plate 11 - PIMUZ T 2793; Fig. 27) than in *T. longobardicus* (including the neotype specimen PIMUZ T 2791, "Exemplar a" of Wild 1973). In the distal-most vertebrae of *T. conspicuus*, in which only remnants of the zygapophyses can be identified, the anterodistal and posterodistal margins of the low neural spine are rounded in lateral view (Fig. 27). The anterior portion of the neural spine in *T. conspicuus* extends beyond the centrum anteriorly, overhanging it (Fig. 27G).

Hemal arches similar to those known from the articulated specimens of *T. hydroides* and *T. longobardicus* (see Wild 1973; Nosotti 2007) have been found in Miedary, but they are not diagnostic enough to unequivocally refer them to *Tanystropheus*.

Cervical ribs

Only the two posteriormost, shortest, cervical ribs of *Tanystropheus conspicuus* have been found as complete specimens. The longest preserved fragments of cervical ribs found in Miedary measure around 25 cm in length, but almost certainly reached over 100 cm when complete. All cervical ribs found in Miedary so far are dicephalous, with a narrow canal partitioning the articular head of the rib into capitulum and tuberculum (Fig. 28). Thus, in all species of *Tanystropheus* the cervical ribs were only functionally single-headed (contra Wild 1973 and following Nosotti 2007).

As in other species of *Tanystropheus*, the articular portion (anterior to the shaft) in all anterior and middle cervical ribs is exceedingly small when compared to the total length of the element. In contrast to the posterior cervical ribs, the anteromedially oriented free ending process is blunt, short, and does not taper (Fig. 28). Tuberculum and capitulum are dorsoventrally very short but well defined. The tuberculum is anteroposteriorly longer, with

its articular surface being narrow, elongate, and oriented obliquely to the shaft (Fig. 28A). The dorsal edge of the tuberculum is concave in lateral view, with its anterior and posterior portions located more dorsally than the middle section, thereby forming a gentle curve in outline (Fig. 28C). The capitulum extends medially as a short, rounded, process (Fig. 28A–B, D). It is more robust, wider, and shorter than the tuberculum but its longitudinal axis is also oblique to the shaft (Fig. 28A). The articular surface of the capitulum is concave in medial view, forming a V-shaped depression (Fig. 28A). The space between the articular heads is restricted to a narrow and shallow canal (Fig. 28A). The shaft is formed as an extremely elongate, thin, tapering rod, with a semicircular cross section.

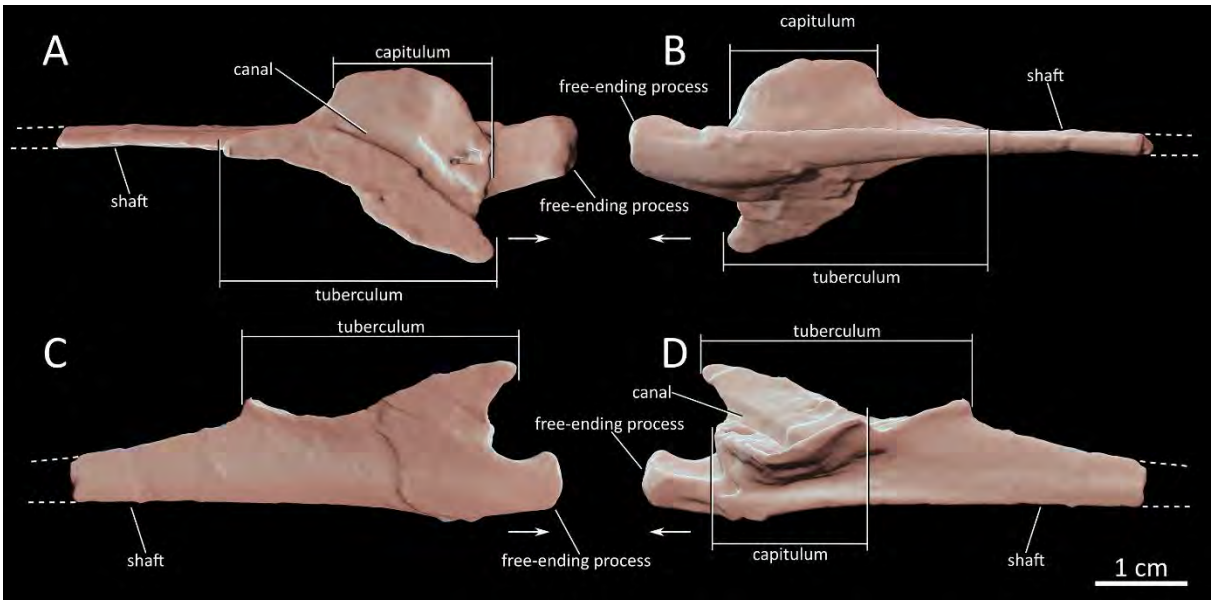

Fig. 28. Anterior portion of a right middle cervical rib head of *Tanystropheus conspicuus* from the Lower Keuper (lower Ladinian) of Miedary (Poland) – ZPAL V. 36/2433. Three-dimensional model snapshots with Lit Sphere Radiance Scaling shader enabled, in dorsal (**A**), ventral (**B**), lateral (**C**), and medial (**D**) views. Arrows indicate anterior direction.

The cervical rib morphology changes markedly near the base of the neck, with the pair of ribs articulating with the eleventh cervical vertebra being shorter and more massive (Fig. 29A). Its anterior free-ending process tapers to a point and is dorsomedially oriented (Fig. 29A$_3$). Both articular heads are stocky but taller than in the preceding ribs (Fig. 29A$_4$). Their articular surfaces are semicircular and flat (Fig. 29A$_1$). The dorsally oriented tuberculum is slightly larger and more elongate than the dorsomedially oriented capitulum (Fig. 29A$_1$). Between them, there is relatively much more space than in the more anterior ribs. Low, thin,

laminae extend posteriorly from the articular heads, along the shaft, expanding its edge dorsally (Fig. 29A$_3$–A$_4$).

The twelfth cervical vertebra bears the first pair of relatively short ribs (Fig. 29B). They are also characterised by the presence of a long, tapering, dorsomedially oriented free-ending anterior process, and a highly curved, convex, ventral surface (Fig. 29B$_3$). Compared to the preceding ribs, the pair of ribs associated with the twelfth cervical vertebra has a more posteriorly located tuberculum, which is also taller and possesses a larger articular surface. The ventrally curved lamina that extends from the posterodorsal edge of the tuberculum reaches nearly to the end of the shaft (Fig. 29B$_1$, B$_3$). In contrast to the preceding ribs, the posterior end of the shaft is blunt, and does not taper (Fig. 29B$_3$).

The last pair of cervical ribs, associated with the thirteenth vertebra, differs from the preceding elements with its relatively straight ventral surface, and the presence of a shorter, relatively posteriorly recurved anterior free-ending process (Fig. 29C$_3$). Cervical ribs from the posteriormost pair are also relatively the shortest and the tallest (Fig. 29, compare C to A and B). Their articular heads are also much longer, and oriented anterodorsally, with acute angles formed between them and the anterior free-ending process (Fig. 29C$_3$). Similar to the preceding rib pairs, there are thin laminae extending between the articular heads and the posterior portion of the shaft (Fig. 29C$_1$, C$_3$–C$_4$). The one associated with the tuberculum is much taller (Fig. 29C$_4$). Radial striations are present on its lateral surface. They are more pronounced near the relatively straight dorsal edge of this lamina (Fig. 29C$_3$). The general morphology of the last cervical rib is shared between *T. conspicuus* and *T. hydroides* but not *T. longobardicus* (see Wild 1973; Nosotti 2007; Rieppel et al. 2010). In the latter, the lamina projecting from the tuberculum is not posterodorsally expanded. Intriguingly, there is a feature that is present in both the *T. hydroides* specimen PIMUZ T 2787 from Monte San Giorgio and a *Tanystropheus* specimen from China GPKU P 1527 but not in any of the ribs of *T. conspicuus*: on the dorsolateral surface of the lamina connecting the tuberculum and the shaft in the last cervical rib of the two latter forms there is a horizontal shelf-like ridge parallel to the shaft. In *T. conspicuus* this surface is flat.

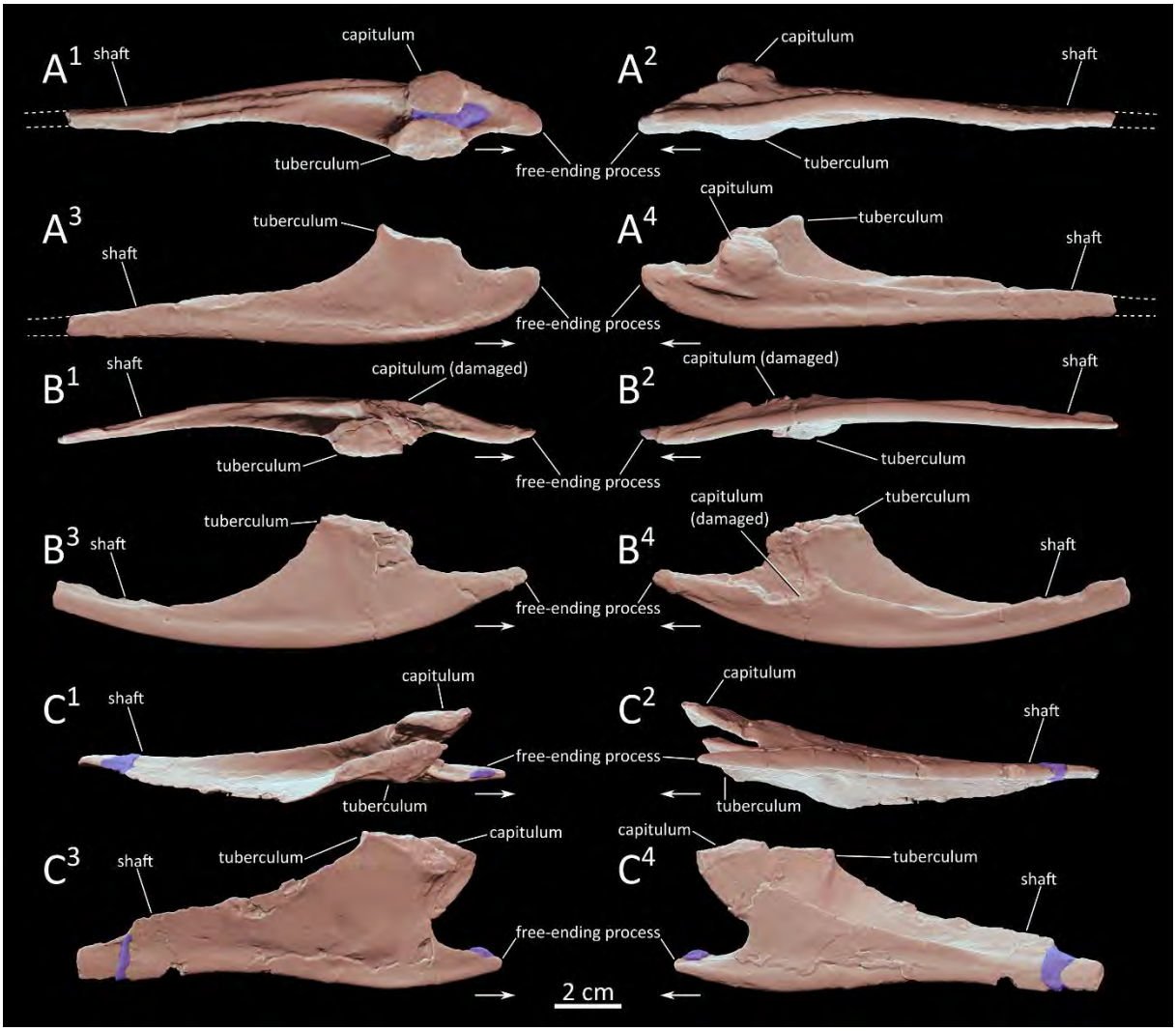

Fig. 29. Posterior cervical ribs of *Tanystropheus conspicuus* from the Lower Keuper (lower Ladinian) of Miedary (Poland) – anterior portion of the left (mirrored) eleventh cervical rib ZPAL V. 36/1019 (**A**), left (mirrored) twelfth cervical rib ZPAL V. 36/1000 (**B**), and right thirteenth cervical rib ZPAL V. 36/1251 (**C**). Three-dimensional model snapshots with Lit Sphere Radiance Scaling shader enabled, in ventral (A_1, B_1, C_1), dorsal (A_2, B_2, C_2), lateral (A_3, B_3, C_3), and medial (A_4, B_4, C_4) views. Arrows indicate anterior direction. Areas covered with sediment marked with blue hue. Note that the capitulum in ZPAL V. 36/1000 is largely missing and the tuberculum and capitulum in ZPAL V. 36/1251 are nearly touching due to diagenetic deformation.

Dorsal ribs

As in many other archosauromorphs, the dorsal ribs of *Tanystropheus conspicuus* are long, slender, and lateromedially curved elements (Fig. 30). Their morphology is clearly visible in the partial skeletons ZPAL V. 36/125 (Figs. 20, 30) and ZPAL V. 36/584 (Fig. 16). Whereas I generally consider most isolated dorsal ribs from Miedary as non-diagnostic for *Tanystropheus*, the dicephalous anterior dorsal ribs are distinct in their shape (see below) and can be referred to *T. conspicuus* with high confidence.

Among the dorsal ribs of other species of *Tanystropheus*, the first two or three pairs were identified as dicephalous (Wild 1973; Renesto 2005; Nosotti 2007), whereas the rest are holocephalous. Three dicephalous dorsal ribs are associated with their corresponding consecutive vertebrae within ZPAL V. 36/125 (Fig. 30). They were likely preceded by a not unpreserved first dorsal vertebra (see Discussion), which implies that the four anteriormost pairs of dorsal ribs were dicephalous in *T. conspicuus*. They bear a well-separated, relatively long and slender capitulum and a stubby tuberculum, which becomes more massive in the more posterior elements. Dorsal ribs from the first pair, of which an example is preserved in isolation but identified based on its morphology, are similar in the morphology of their proximal portion to the posteriormost cervical ribs, and possess a large, triangular anterior free-ending process (Fig. 30A). It is nevertheless identified as a dorsal rib based on its shaft morphology. In the second dorsal rib pair the anterior free-ending process is very much reduced, and in the succeeding ribs it is completely absent (Fig. 30A).

The dicephalous anterior dorsal ribs of *T. conspicuus* bear a distinct feature – their dorsolateral surface is anteroposteriorly expanded along the shaft distal to the tuberculum-capitulum conjunction, forming a very thin plate-like extension (Fig. 30). Its lateral surface is relatively smooth but covered with radial striations. A similar structure is present in the posteriormost cervical ribs, but in the first dorsal ribs it is more distally expanded (compare Fig. 29C and Fig. 30A). In the first two dorsal rib pairs this extension is roughly triangular in lateral view, with laminae extending from the tuberculum and the free-ending process. Their anteroposterior width diminishes distally, as they terminate around the middle of the length of the shaft (Fig. 30). The third dorsal rib preserves only a slightly expanded anterolateral ridge, a remnant of the plate-like extension found in the preceding elements (Fig. 30B). In the fourth dorsal rib, in which the capitulum and the tuberculum become nearly confluent, this ridge is reduced to a weakly projecting tuberosity on the posterolateral edge of the rib (Fig. 30B). A similar morphology can be noted for the ribs associated with the first dorsal vertebra of *T.*

hydroides (e.g., PIMUZ T 2787, PIMUZ T 2793, PIMUZ T 2817, PIMUZ T 2818), *T.* cf. *T. longobardicus* (e.g., MCSN 4451) and *Tanystropheus* sp. (e.g., IVPP V 14472), all bearing the plate-like extension in at least the first pair of dorsal ribs, which also possess the free ending anterior process (PIMUZ T 2787, MCSN 4451). Wild (1973, fig. 35 – "fourth" dorsal rib) misidentified this process as a rudimentary capitulum in the first pair of dorsal ribs of PIMUZ T 2787. The plate-like extension is relatively much less expanded in the other species of *Tanystropheus* than in *T. conspicuus*, and in the latter it is present also on the third pair of dorsal ribs, albeit in a much reduced form (Fig. 30B). This structure has not been reported in any other tanysaurian.

Posterior to the fourth dorsal vertebra the vertebrae bear holocephalous ribs, with each succeeding rib being shorter and less lateromedially curved. Wild (1973) interpreted the ribs of the last two dorsal vertebrae in *Tanystropheus* as pleurapophyses tightly fused with their corresponding vertebrae. ZPAL V. 36/125 demonstrates that this was not the case in *T. conspicuus*. Diapophyses in this specimen are clearly separate in even the last pair of dorsal ribs, which are individual short elements.

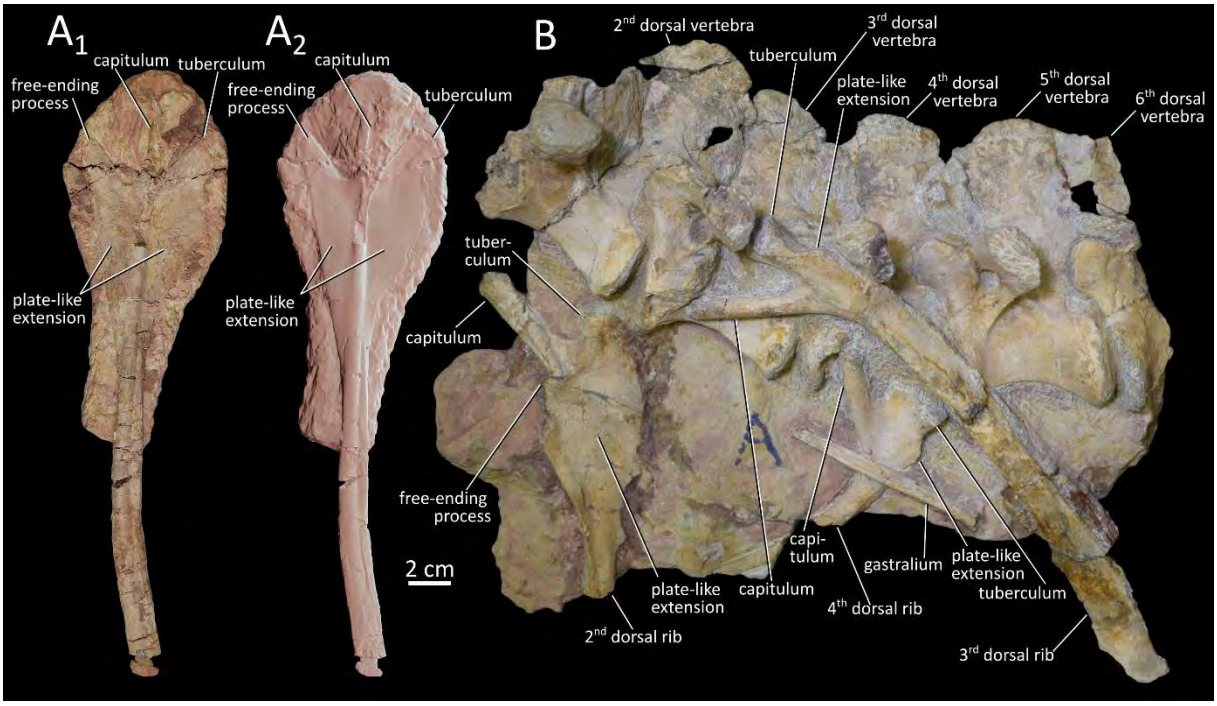

Fig. 30. Anterior dorsal ribs of *Tanystropheus conspicuus* from the Lower Keuper (lower Ladinian) of Miedary (Poland) – first right dorsal rib ZPAL V. 36/123 (**A**) and left anterior dorsal ribs associated within an anterior portion of a partial skeleton ZPAL V. 36/125 (**B**). Photographs (A_1, B) and a three-dimensional model snapshot with Lit Sphere Radiance Scaling shader enabled (A_2), in medial ($A_{1–2}$), and left lateral views (B).

Gastralia

Some isolated slender, elongate, roughly V-shaped elements similar to those known from the articulated specimens of *T. hydroides* and *T. longobardicus* have been found in Miedary, but they are not diagnostic enough to unequivocally identify them as gastralia of *Tanystropheus*. The only unequivocal gastralia of *T. conspicuus* are associated with the articulated partial skeleton ZPAL V. 36/125, which preserves a considerable number of intermingled, closely packed, relatively thin elements (Fig. 31) which in life would have formed an extensive gastral basket.

Consistent with the other species of *Tanystropheus*, there are two morphotypes of gastralia, which intertwined with each other (Wild 1973). The more laterodorsally located ones were gently bent to form an obtuse angle, thus being bow-like in their shape. The elements forming the medioventral part of the gastral basket were generally straight, with only their ventralmost portion mediodorsally curved roughly at a right angle. These gastralia met along the midline of the ventralmost part of the torso, with the hook-like ending interlocking with corresponding element originating from the contra-lateral side. Together they formed a transversely V-shaped structure, a condition widely distributed in other diapsids including tanysaurians (see Olsen 1979; Jaquier et al. 2017; Spiekman et al. 2024*a*, *b*).

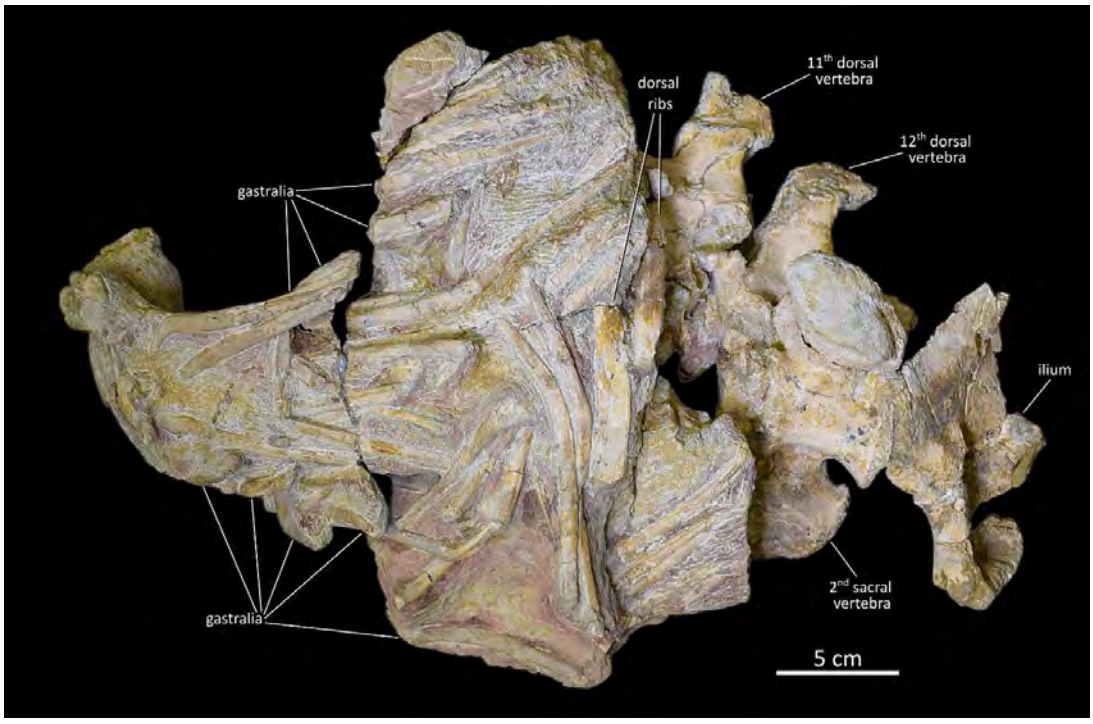

Fig. 31. Gastralia of *Tanystropheus conspicuus* from the Lower Keuper (lower Ladinian) of Miedary (Poland) – association within the posterior portion of the ZPAL V. 36/125 partial skeleton in left lateral-ventral view.

Clavicle

Prior to this study, no elements from the pectoral girdle of *Tanystropheus conspicuus* were known. Only a few non-archosaurian archosauromorphs have three-dimensionally preserved and complete clavicles. Comparative material is therefore limited and as a consequence the identification of isolated clavicles is often problematic. Wild (1973) interpreted the more widened blunt portion of the clavicle of *Tanystropheus* as articulating with the interclavicle, but this interpretation was challenged by Jaquier et al. (2017) who argued that it articulated with the scapula instead. Here I follow the latter study.

As in many other diapsids, the clavicle of *T. conspicuus* is an elongate sickle-shaped element (Fig. 32). The anteromedial portion of the element is rod-like, with its tapering end pointing ventromedially. Two well-defined parallel grooves extend for most of the length of the clavicle along its anteroventral surface, giving it a T-shaped transverse cross section (Fig. 32B$_4$). They are separated by an anteroventrally oriented ridge, which is especially expanded near the anteroposterior midpoint of the bone (Fig. 32B$_3$). As there is no evidence for the presence of an ossified interclavicle in *Tanystropheus* (see Discussion), the anteromedial portion of the clavicle was likely embedded in chondral tissue instead. The posterolateral end of the clavicle, which articulated with the scapula, is dorsoventrally widened, forming a triangular expansion deflected posterodorsally from the relatively straight anteromedial portion of the bone (Fig. 32B$_1$, B$_3$). Its surface is rugose and covered with striations that run perpendicular to the bone edge. Morphology of the posterior margin of the posterolateral portion of the clavicle varies between the two known specimens (ZPAL V. 36/1308 and ZPAL V. 36/2449) and might be a subject of high intraspecific variation. In ZPAL V. 36/1308 it is formed as a lateromedially thin ridge that is straight in lateral view, whereas in ZPAL V. 36/2449 this margin has an irregular profile (Fig. 32B$_1$, B$_3$).

Elements from Miedary, interpreted as clavicles of *T. conspicuus,* are morphologically nearly identical to those of *T. hydroides* (see Fig. 32A). At the same time, the clavicular morphology of both *T. conspicuus* and *T. hydroides* differs from MFSN 31553, a *Tanystropheus* sp. clavicle described by Dalla Vecchia (2006, fig. 15). This specimens is relatively more robust and straight. Its posterolateral portion is not transversely expanded, contrary to what we see in *T. conspicuus,* but similar to what can be observed in *T. hydroides* and *T. longobardicus* (Wild 1973; Nosotti 2007). With the currently accessible sample size it is difficult to assess to what extent some of these differences might be attributable to preservation characteristics or individual size difference.

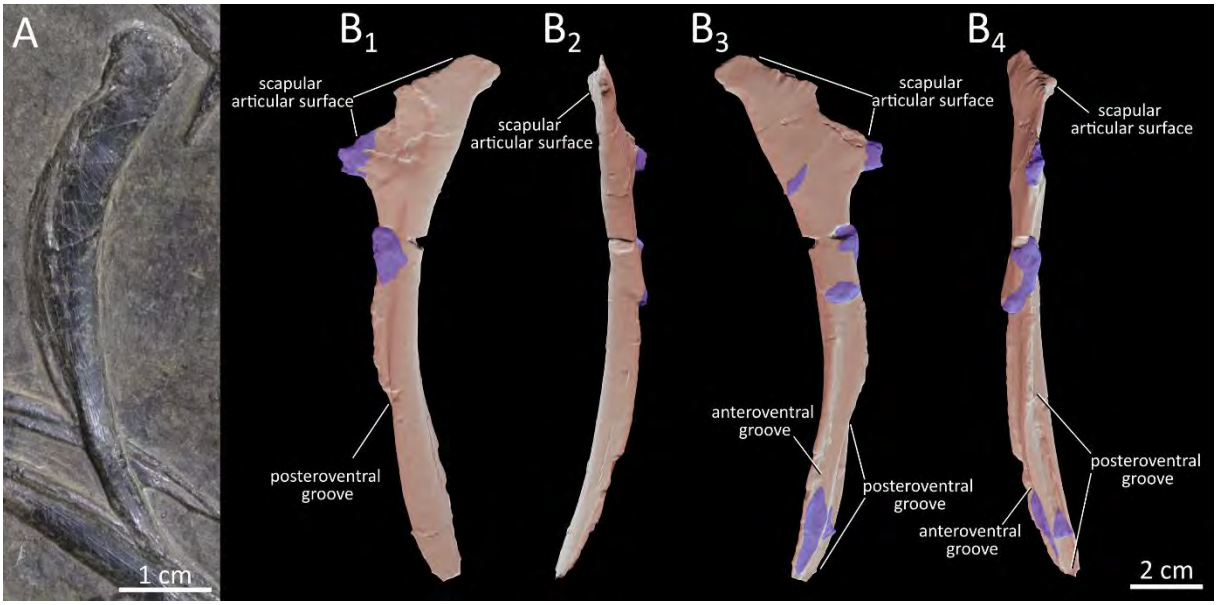

Fig. 32. Clavicles of *Tanystropheus* – left element of *Tanystropheus hydroides* from the Besano Formation (upper Anisian to lower Ladinian) of Monte San Giorgio (Switzerland) – PIMUZ T 2787 (**A**) and left element of *Tanystropheus conspicuus* from the Lower Keuper (lower Ladinian) of Miedary (Poland) – ZPAL V. 36/2449 (**B**). A photograph (A) and three-dimensional model snapshots with Lit Sphere Radiance Scaling shader enabled (B), in dorsomedial (A, B_1), anterodorsal (B_2), ventrolateral (B_3), and posteroventral (B_4) views. Areas covered with sediment marked with blue hue.

Scapula

The scapula in *Tanystropheus conspicuus* is an extremely lateromedially thin, anteroposteriorly broad and dorsoventrally elongate bone (Fig. 33A). Its lateral surface is smooth, with fine, straight striations radiating distally from the glenoid region (Fig. 33A). The glenoid peduncle is formed as a short but distinct process, with the glenoid fossa being located mainly ventrolaterally, and slightly posteriorly. Anterior to the glenoid, the anteroventral scapular edge is smoothly convex, forming a semicircular acromion process in lateral view (Fig. 33A). Posterodorsal to the acromion process and dorsal to the glenoid the anterodorsal edge of the scapula was slightly concave, forming a constriction near the middle of the anteroposterior length of the scapula in lateral view. Posterodorsal to the constriction, the scapula reached its dorsalmost extent, from which the dorsal scapular edge descended posteroventrally, forming the dorsal outline of the scapular blade in lateral view (Fig. 33A). Posterior to the glenoid, the edge of the scapula curved abruptly, at an angle close to 90°, and extended in a straight line posterodorsally, constituting the posteroventral outline of the scapular blade in lateral view. The scapular blade is similar to other species of *Tanystropheus*

in being subtriangular in lateral view (Fig. 33A). Whereas Wild (1973, 1987) interpreted the scapula and coracoid of *Tanystropheus* as being fused anteriorly and/or posteriorly, for *T. conspicuus* there is no indication for any contact between them other than at the glenoid region, similar to what was noted for *T. hydroides* and *T. longobardicus* by Spiekman et al. (2021).

One scapula of *T. conspicuus* from Miedary ZPAL V. 36/2426 has been found *in situ* in a vertical position, with the dorsal edge of the scapular blade pointing upwards. The scapular blade in this specimen is as thin as in the other scapulae of *T. conspicuus*, indicating that the extremely limited thickness of these elements is not diagenetically-induced.

The scapula of *Tanystropheus conspicuus* differs from other species of *Tanystropheus* in several features (see Fig. 33). In *T. longobardicus*, and possibly in *T. hydroides*, the acromion process is triangular in lateral view, tapering anteroventrally to a point (Fig. 33B–C). The ventral edge of this process is roughly parallel to the ventral edge of the scapular blade. This is unlike *T. conspicuus*, where they are close to being perpendicular (Fig. 33A) as a result of the acromion process being semicircular and more dorsally directed. The anteroposterior constriction of the scapular blade is deeper and more posteriorly located in *T. conspicuus* than in other species of *Tanystropheus* (Fig. 33). At the same time, the most dorsally extended point of the scapular edge is also relatively more posteriorly located. When compared to other species of *Tanystropheus* the posterior part of the scapula in *T. conspicuus* was much more elongate and occupied a much larger area than its anterior portion (Fig. 33A–C). A similar morphology is present in other tanystropheids (e.g., PIMUZ T 1559, a referred specimen of *Macrocnemus fuyuanensis* Li, Zhao, and Wang 2007), which share the constriction at the mid-length, semicircular acromion process and a long, triangular scapular blade (Jaquier et al. 2017). The scapula in *T. conspicuus* is, however, relatively more elongate and taller than in other tanysaurians, thus being distinct in its morphology. Moreover, the concavity present between the glenoid peduncle and the scapular blade in lateral view is much shallower than in its relatives (Fig. 33). These proportions are somewhat reminiscent to the scapular morphology of other early archosauromorphs, in which a fused scapulocoracoid is present (e.g., *Prolacerta broomi* Parrington, 1935, Protorosaurus speneri von Meyer, 1832; Gow 1975; Gottmann-Quesada and Sander 2009).

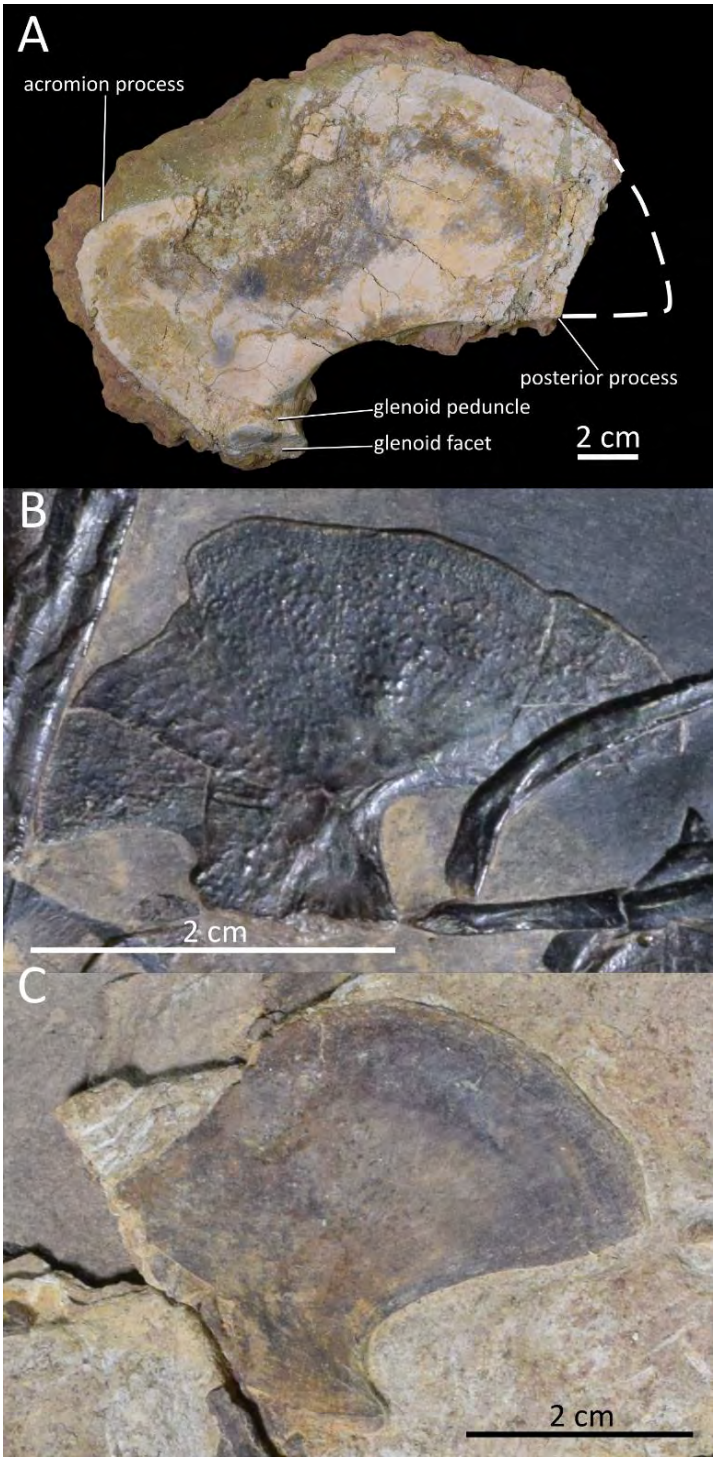

Fig. 33. Photographs of left scapulae of three species of *Tanystropheus* in left lateral view **–** a scapula of *Tanystropheus conspicuus* from the Lower Keuper (lower Ladinian) of Miedary (Poland) – ZPAL V. 36/811 (**A**, the posterior tip is missing), a scapula of *Tanystropheus longobardicus* from the Besano Formation (upper Anisian to lower Ladinian) of Monte San Giorgio (Italy) – MSNM BES SC 1018 (**B**), and a scapula of *Tanystropheus hydroides* from the Besano Formation (upper Anisian to lower Ladinian) of Monte San Giorgio (Switzerland) – PIMUZ T 1270 (**C**).

Coracoid

The coracoid in *Tanystropheus conspicuus* is a flat plate-like and dorsoventrally thin bone (Fig. 34). There are no osteological correlates for any other contact with the scapula other than a relatively reduced surface medial to the glenoid. When in articulation, the coracoid and scapula of *T. conspicuus* were seemingly not firmly fused and joined only at the glenoid, with their anterior and posterior portions being separated and forming a scapulocoracoidal fenestra (*sensu* Spiekman et al. 2021). The glenoid is located near the middle of the dorsolateral edge of the coracoid and is dorsolaterally oriented (Fig. 34). Anteromedial to it, a coracoid foramen is present. The portion of the coracoid anterior to the glenoid is more expanded than the postglenoid process, but both are similarly rounded and semicircular in shape in dorsal view. The ventromedial edge, which might have articulated with the unossified interclavicle, is anteroposteriorly straight in dorsal view and dorsoventrally thickened (Fig. 34). Both the dorsal and ventral surfaces of the coracoid are covered with radial striations. These are perpendicular to the concentric thickenings that mark the growth of the animal (Fig. 34).

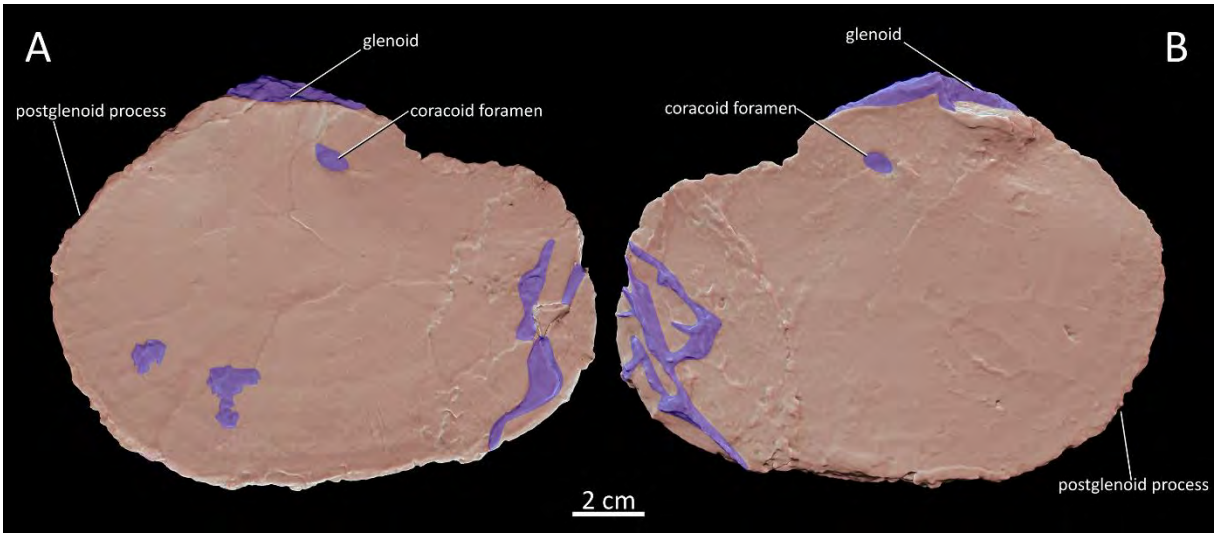

Fig. 34. Left coracoid of *Tanystropheus conspicuus* ZPAL V. 36/1177 from the Lower Keuper (lower Ladinian) of Miedary (Poland). Three-dimensional model snapshots with Lit Sphere Radiance Scaling shader enabled, in dorsal (**A**) and ventral (**B**) views. Areas covered with sediment marked with blue hue.

Humerus

All limb bones of *Tanystropheus conspicuus* are morphologically nearly identical to the corresponding elements of *T. hydroides*, although direct comparisons are difficult due to the differences in preservation and the resulting lack of three-dimensional information for the latter. As for other species of *Tanystropheus* (see Wild 1973; Nosotti 2007), the humerus of *T. conspicuus* is less elongate than the femur. Its lateral and anterior (dorsal) margins are relatively straight, and its medial and posterior (ventral) margins are concave (Fig. 35). Significant torsion, reaching more than 45°, can be observed between the well-ossified proximal and distal ends of the humerus(Fig. 35A_3, A_4).

The proximal portion of the humerus is posteromedially expanded when compared to the thickness of the shaft (Fig. 35A). Its articular surface is elliptical in proximal view (Fig. 35A_5). In anterior view it is convex, and slightly more proximally expanded on its lateral side (Fig. 35A_3–A_4). No clear tubers can be distinguished, with the outline of the articular surface being oval in proximal view (Fig. 35A_5). Adjacent to the proximal articular surface, distal to its anterolateral corner, a very poorly defined deltopectoral crest is present (Fig. 35A_2–A_5).

The shaft has a nearly constant thickness along its length. The distal portion of the humerus is medially and slightly laterally expanded and larger than the proximal one. On its anterolateral margin, the supinator process is present (Fig. 35A_1, A_6). It is formed as a longitudinal ridge parallel to the shaft, confluent with the anterior surface of the distal end of the humerus but distinctly separated from its posterior surface by a proximodistally oriented groove.

The distal end of the humerus is composed of two condyles (Fig. 35A_6) – the ectepicondyle (radial condyle) and the entepicondyle (ulnar condyle). They lie on two sides of a poorly outlined anteroposterior constriction of the distal portion of the humerus (Fig. 35A_6). The entepicondyle projects strongly medially from the shaft. Its medial and distal surfaces are roughly perpendicular, meeting in an obtuse angle. In distal view, the articular surface of entepicondyle is rounded and elliptical; it is separate from the ectepicondyle by an anteroposterior constriction and a poorly marked distal groove (Fig. 35A_6). Both condyles are distally expanded to a similar extent, forming a relatively straight distal margin of the humerus (Fig. 35A_2). The ectepicondyle is larger and more broadly rounded in proximal view than the entepicondyle. It lies along the longitudinal axis of the shaft whereas the entepicondyle is distinctly offset from it and mediodistally oriented (Fig. 35A_2).

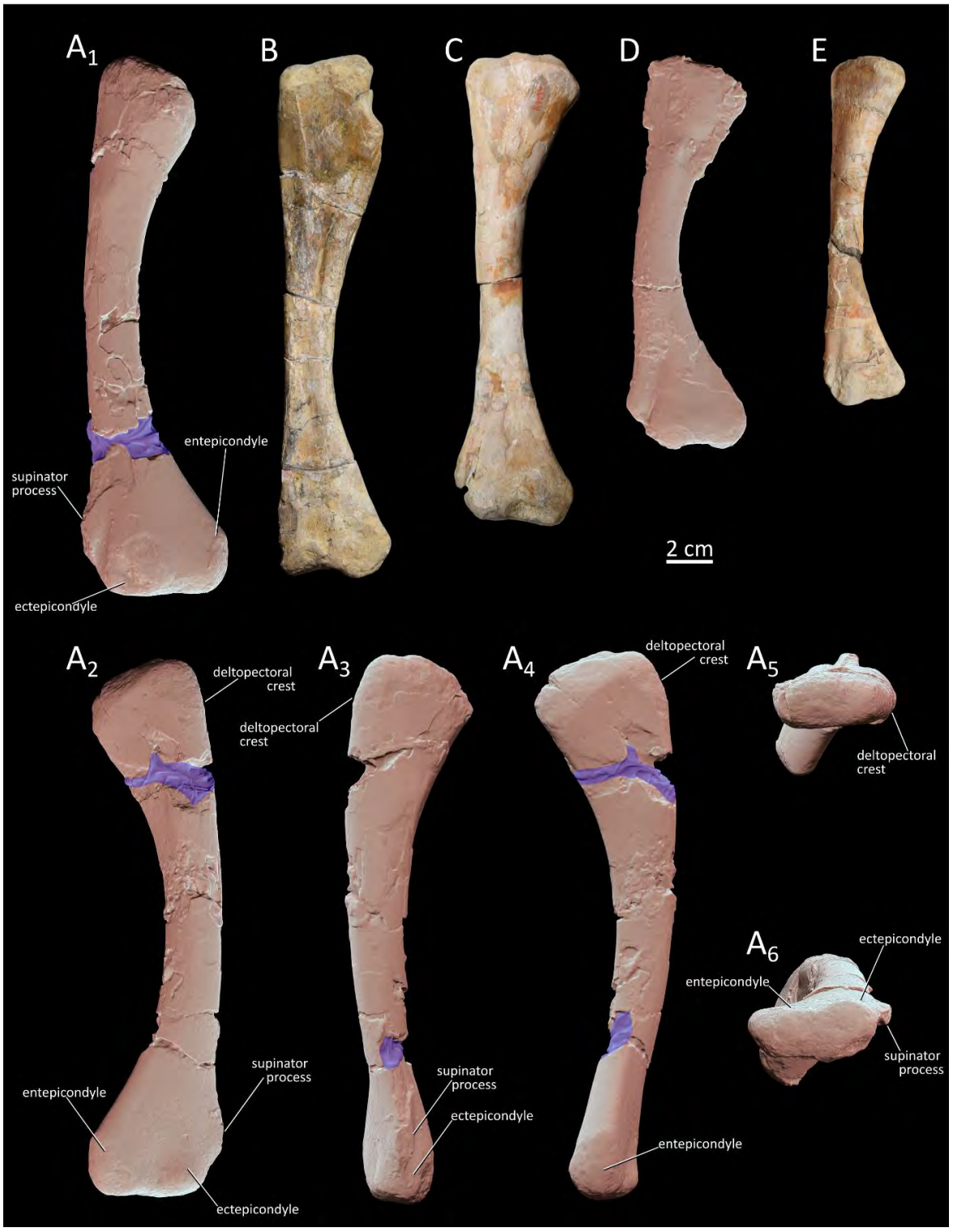

Fig. 35. Left humeri of *Tanystropheus conspicuus* from the Lower Keuper (lower Ladinian) of Miedary (Poland) – ZPAL V. 36/881 (**A**), GPIH 253 (**B**, the holotype of *Megacnemus grandis*), ZPAL V. 36/882 (**C**), SMF R 4034 (**D**), and U-MO BT 3079 (**E**). Photographs (B–C, E) and three-dimensional model snapshots with Lit Sphere Radiance Scaling shader enabled (A, D), in posterior/ventral (A_1, B–E), anterior/dorsal (A_2), lateral (A_3), medial (A_4), proximal (A_5), and distal (A_6) views. Areas covered with sediment marked with blue hue.

Ulna

The ulna of *Tanystropheus conspicuus* is a relatively straight element (Fig. 36). Its medial surface is slightly concave in anterior/dorsal view as a result of the lateromedial expansion of the proximal and distal ulnar ends (Fig. 36A, C). The ulna is virtually straight in medial view (Fig. 36B). In ZPAL V. 36/829, the only ulna referred to *T. conspicuus*, the articular surfaces are damaged but their margins are well outlined in anterior/dorsal view. The proximal portion of the ulna is more massive, with its articular surface being oriented obliquely to the longitudinal axis of the shaft in anterior/dorsal view (Fig. 36A, C). The olecranon process is absent. The lateral corner of the proximal end of the ulna is more proximally expanded than its medial corner (Fig. 36A, C). Distal to the proximal end of the ulna, a narrow, sharp ridge extends along the anteroposterior mid-width of the medial surface of bone (Fig. 36B). The distal end of the ulna in *T. conspicuus* is only slightly lateromedially expanded (Fig. 36A, C). It has a straight, nearly flat articular surface in anterior/dorsal view.

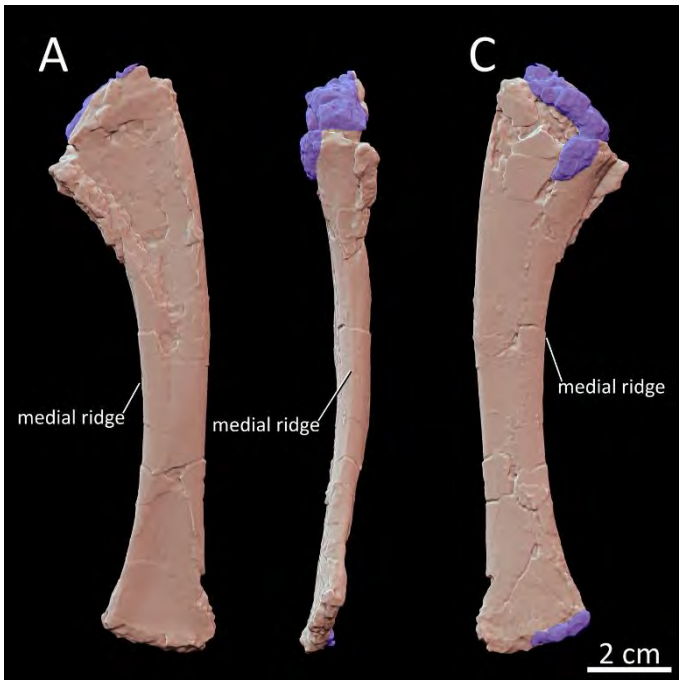

Fig. 36. Left (?) ulna of *Tanystropheus conspicuus* from the Lower Keuper (lower Ladinian) of Miedary (Poland) – ZPAL V. 36/829. Three-dimensional model snapshots with Lit Sphere Radiance Scaling shader enabled, in anterior/dorsal (**A**), medial (**B**), and posterior/ventral (**C**) views. Areas covered with sediment marked with blue hue.

Radius

The radius is similar in its proportions to the ulna but is considerably more curved, with its posterior margin being strongly concave in anterior/dorsal view (Fig. 37). It is virtually straight in lateral view (Fig. 37B). The known radii referred to *Tanystropheus conspicuus* do not have well preserved articular surfaces. The proximal articular surface is seemingly semi-triangular in proximal view, but this might be due to diagenetic alteration of its original morphology.

A fine ridge extends distal to the proximal portion along the posterolateral margin of the radius, parallel to the shaft (Fig. 37A–B). It becomes better defined and sharper in the middle section of the bone. An interosseous ligament likely stretched between this ridge, and the corresponding feature present on the ulna. Closer to the distal end of the radius, the ridge becomes wider but lower and more confluent with the shaft surface. On the opposite side of the shaft, a poorly outlined tuberosity is located (Fig. 37B–C). It might correspond to a similar feature present in other early archosauromorphs (e.g., *Malerisaurus robinsonae* Chatterjee, 1980 – see Sengupta et al. 2024, fig. 13). The distal end of the radius is only slightly less expanded than the proximal one, being marginally wider than the shaft (Fig. 37A, C). Its articular surface is elliptical in distal view and nearly straight in anterior/dorsal view.

Both the ulna and the radius of *T. conspicuus* are identical in their proportions to the corresponding elements of *T. hydroides*, being much more robust and thicker than the slender antebrachial bones of *T. longobardicus* (compare the “large” and “small” morphotypes of Wild 1973 and Nosotti 2007)

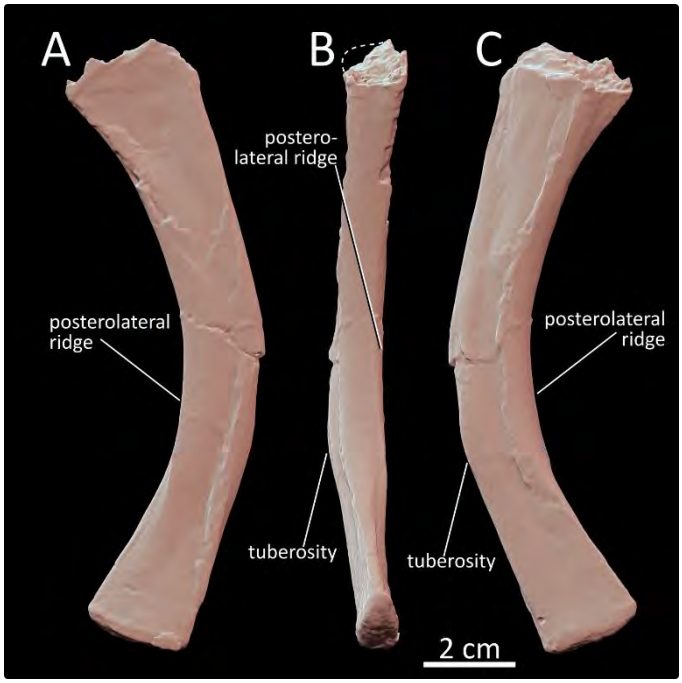

Fig. 37. Left (?) radius of *Tanystropheus conspicuus* from the Lower Keuper (lower Ladinian) of Miedary (Poland) – ZPAL V. 36/830. Three-dimensional model snapshots with Lit Sphere Radiance Scaling shader enabled, in posterior/ventral (**A**), lateral (**B**), and anterior/dorsal (**C**) views.

Autopodial elements

As for other Muschelkalk and Lettenkeuper sites, autopodial elements are scarce in Miedary. Several elongate bones from the site have been identified as reptile metatarsals and metacarpals, and it is highly likely that they belong to *Tanystropheus conspicuus* but they are not diagnostic enough for this referral, at least not before articulated manus or pedes are found in Miedary.

Ilium

The ilium of *Tanystropheus conspicuus* is relatively delicate for an animal of its size. It is composed of the acetabular region and the iliac blade, which are located on the opposite sides of the anteroposterior constriction of the ilium (Fig. 38). The majority of the acetabulum is located on the lateral surface of the ilium and the ischium, with only its anteroventral margin present on the lateroproximal portions of the pubis (Fig. 39). The pubic and ischial peduncles are similarly expanded anteroposteriorly, converging at an obtuse angle (Fig. 38A–B). The articular surface for the pubis is relatively straight and has a nearly uniform transverse width (Fig. 38B–C). The articular surface for the ischium is laterally concave, forming a lateroventrally oriented rhomboidal pit (Fig. 38B–C). Its triangular dorsal margin reaches

deep within the acetabulum, pointing towards the posterior end of the supraacetabular crest (Fig. 38B). The posterolateral corner of the ischial peduncle is laterally expanded, forming a cone-shaped projection (Fig. 38B–D). The morphology and location of this feature are reminiscent of the antitrochanter (raised surface at the posterior portion of the acetabulum, see Nesbitt 2011) seen in more crownward archosaurs, including some Triassic forms (Nesbitt 2011; Ezcurra 2016, Spiekman et al. 2024*c*). The acetabulum is anterodorsally framed by the supraacetabular crest, which extends from the anteriormost portion of the pubic peduncle, constituting the ventral part of the anterior edge of the ilium (Fig. 38B). More posterodorsally, the supraacetabular crest is formed as a distinct, laterally projecting, rugose tuberosity, which terminates dorsal to the acetabulum (Fig. 38B).

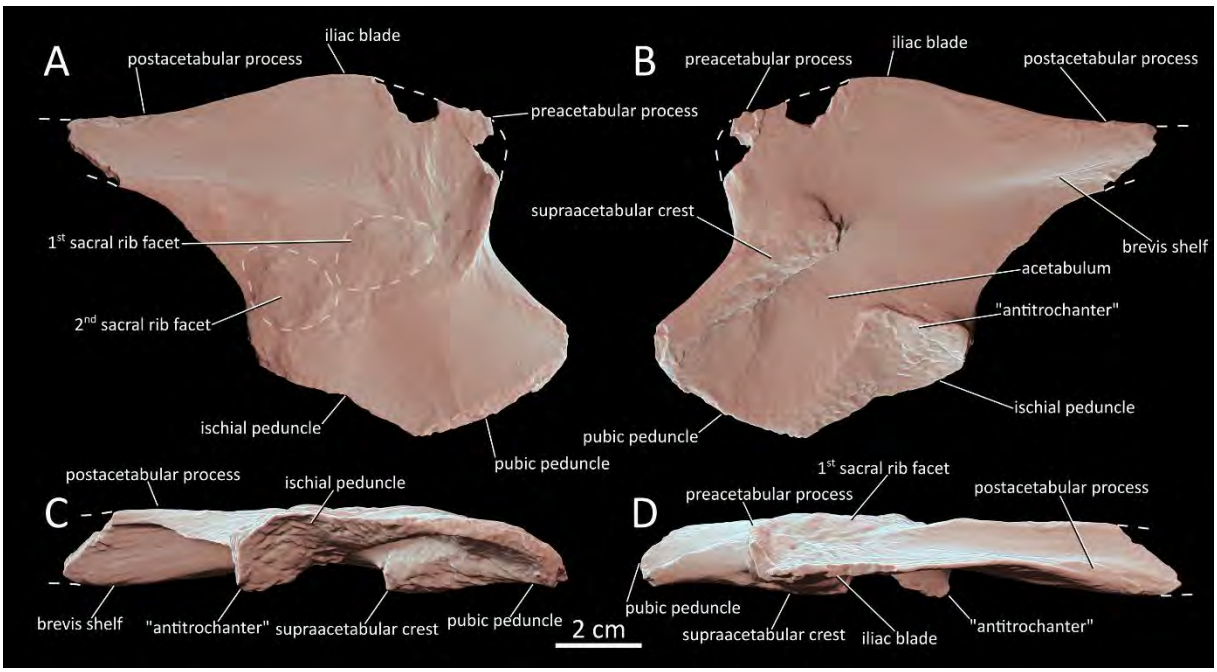

Fig. 38. Left ilium of *Tanystropheus conspicuus* from the Lower Keuper (lower Ladinian) of Miedary (Poland) – ZPAL V. 36/813. Three-dimensional model snapshots with Lit Sphere Radiance Scaling shader enabled, in dorsomedial (**A**), ventrolateral (**B**), ventromedial (**C**), and dorsolateral (**D**) views.

The iliac blade constitutes the dorsal region of the ilium in *T. conspicuus*, with the preacetabular process and the postacetabular process extending off of it. The anterior edge of the preacetabular process is relatively straight in lateral view, diverging anterodorsally from the supracetabular crest near its mid-length (Fig. 38A–B). More dorsally, the edge of the preacetabular process is convex, curving to become confluent with the dorsal margin of the iliac blade (Fig. 38A–B). As can be observed in *T. hydroides* (see Wild 1973, fig. 93) and

Tanystropheus sp. from north-eastern Italy (see Dalla Vecchia 2006, fig. 16), the minute anteriorly projecting extension of the preacetabular process described for *T. longobardicus* by Nosotti (2007) is absent in *T. conspicuus* (Fig. 38A–B). This character is, however, intraspecifically variable in *Tanystropheus* (see Spiekman et al. 2021). The iliac blade is composed of a lateromedially thin but ventrally thickened, plate of bone (Fig. 38D). The dorsal margin of the iliac blade is strongly convex in lateral view in its anterior portion, and its posterior portion is slightly concave (Fig. 38A–B). The postacetabular process is posterodorsally oriented and tapering (Fig. 38A–B). Its base is formed by a thin, concave, lamina extending from the ischial peduncle to the ventromedial edge of the postacetabular process in lateral view (Fig. 38A–C). Dorsolateral to it, the postacetabular process is slightly laterally expanded, forming a horizontal shelf on its dorsomedial side (Fig. 38A–B, D). This feature was interpreted by Ezcurra (2016) as homologous to the brevis shelf of Novas (1996), the origin of the *musculus caudifemoralis brevis*.

The medial side of the ilium is characterised by the presence of attachment sites for the sacral ribs (Fig. 38A). These are positioned posterodorsal to a curved ridge that extends posteroventrally from the notch in the anterior margin of the ilium (Fig. 38A). Both attachment sites for the sacral ribs are similar in size and elliptical in medial view. They are located at the neck of the ilium, which formed by its anteroposterior constriction. The first sacral rib facet is more centrally located, with the second one being positioned closer to the posterior margin of the ischial peduncle.

Prior to this study, no elements from the pelvic girdle of *T. conspicuus* were known. Von Huene (1958*a*) interpreted a specimen as an ilium of *Tanystropheus* sp. but this element is a nothosaurian scapula (Wild 1973, p. 114; pers. obs. AR). The ilium of *T. conspicuus* is very similar in its morphology to the ilia of other species of *Tanystropheus* (pers. obs. AR, but see Wild 1973; Dalla Vecchia 2006; Nosotti 2007), with the elements herein referred to *T. conspicuus* being relatively slightly taller. Moreover in *T. conspicuus* the postacetabular process is relatively more slender (dorsoventrally narrower) in lateral view and its ventral surface is less concave (compare Fig. 38 and fig. 93 of Wild 1973). The projection observed on the lateral surface of the ilium, posterior to the acetabulum (Fig. 38B–D), might also be present in *T. hydroides* and *T. longobardicus* (e.g., MSNM BES SC 1018, PIMUZ T 2483), but differences in preservation do not allow for a confident assessment. If this projection is interpreted as the antitrochanter, it would be its earliest occurrence (evolutionarily) within Archosauromorpha (Nesbitt 2011; Ezcurra 2016, Spiekman et al. 2021).

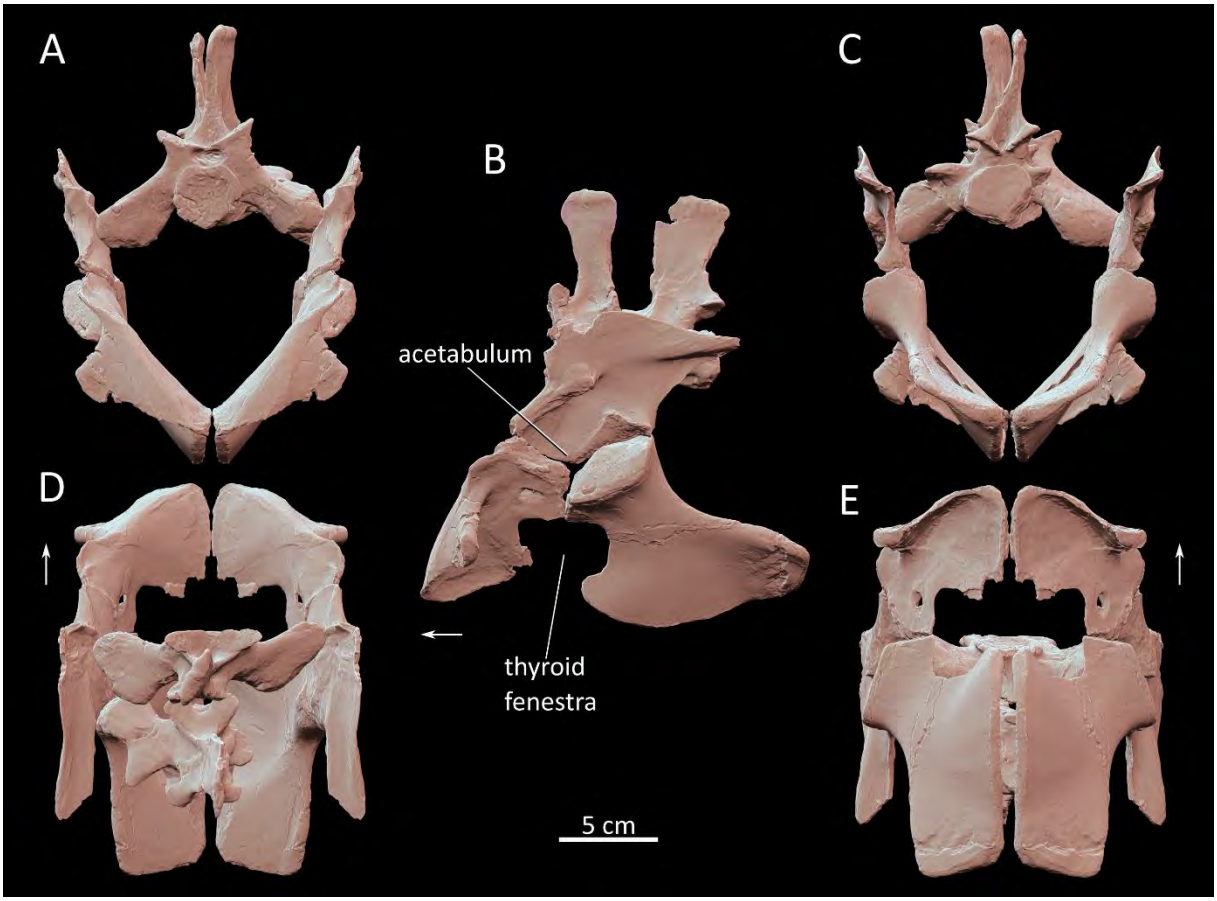

Fig. 39. The pelvis of *Tanystropheus conspicuus* from the Lower Keuper (lower Ladinian) of Miedary (Poland) – three-dimensional model snapshots with Lit Sphere Radiance Scaling shader enabled, in anterior (**A**), left lateral (**B**), posterior (**C**), dorsal (**D**), and ventral (**E**) views. The reconstructed model is composed of isolated specimens ZPAL V. 36/813, ZPAL V. 36/1006, ZPAL V. 36/1008, ZPAL V. 36/1037, ZPAL V. 36/1187, and their mirrored versions. The ZPAL V. 36/1006 ischium has been scaled down to about 80% of its original size. Note that none of the elements has been retrodeformed and some of their fragments are missing (e.g., right rib of the second sacral vertebra). Arrow indicates anterior direction.

Pubis

The pubis of *Tanystropheus conspicuus* is plate-like, but with a distinct lateral process (Fig. 40). Its dorsal region is the sturdiest portion of the bone and it is especially lateromedially thick near the acetabular contact with the ilium (Fig. 40). The straight posterodorsal margin of the pubis is equally divided between the articular surface for the pubic peduncle of the ilium, and, more laterally, the ventral portion of the acetabulum (Fig. 40A, C). The articular surface for the ischium occupies a much smaller area, positioned ventral to the posterior edge of the articular surface for the ilium, with an obtuse angle formed

between them (Fig. 40A, C). Anteroventral to this junction, the pubis is pierced by an obturator foramen (Fig. 40A, C). An anteriorly projecting, semi-circular ridge is present anterolateral to the ventral acetabulum margin (Fig. 40A–C). It forms the insertion point for the *musculus ambiens* (see Ezcurra 2016). Longitudinal striations covered the rugose surface of the pubis ventral to this process (Fig. 40B–C).

Distal to the articular portion of the bone, the pubis of *T. conspicuus* is composed of two plates of thin bone, the medial and the lateral plates, which meet roughly at a right angle along the edge of the pubic shaft (Fig. 40A). The lateral plate is triangular in anterior view and ventrolaterally oriented (Fig. 40A–B). Its dorsal edge is straight and projects from the pubic shaft at an obtuse angle (Fig. 40B). Similar to some other reptiles (Wild 1973, Ezcurra 2016), it is distally thickened, forming a distinct lateral process, which terminates sharply with an elliptical, laterally oriented muscle attachment surface (Fig. 40A). From the ventral edge of this surface the ventrolateral margin of the lateral plate descends to converge with the medial pubic margin, decreasing ventrally in its transverse width (Fig. 40B). The anteroposteriorly extending medial plate has a broad, almost completely flat surface (Fig. 40A–C). Its posterodorsal margin forms a semicircular notch in lateral view (Fig. 40A, C). A constriction perpendicular to the pubic shaft is formed between this notch and the dorsal surface of the base of the lateral process (Fig. 40A, C). The posterior edge of the medial plate is straight and converges with the ventromedial pubic margin at an acute angle (Fig. 40A, C). It contributes to the anterior margin of the thyroid fenestra between the pubis and the ischium. The pubes of *T. conspicuus* articulated along their straight symphysial margin, on the thickened ventral edge, and forming the pubic apron (Figs. 39, 40A, C).

Of the three bone pairs that formed the pelvic girdle of *Tanystropheus*, the pubes have the most three-dimensional features, due to the presence of the lateral process, and previously their original morphology could only be extrapolated from the diagenetically flattened individuals (Fig 39; Wild 1973). Nevertheless, all three valid species of *Tanystropheus* seem to share the same pubis morphology (pers. obs. AR).

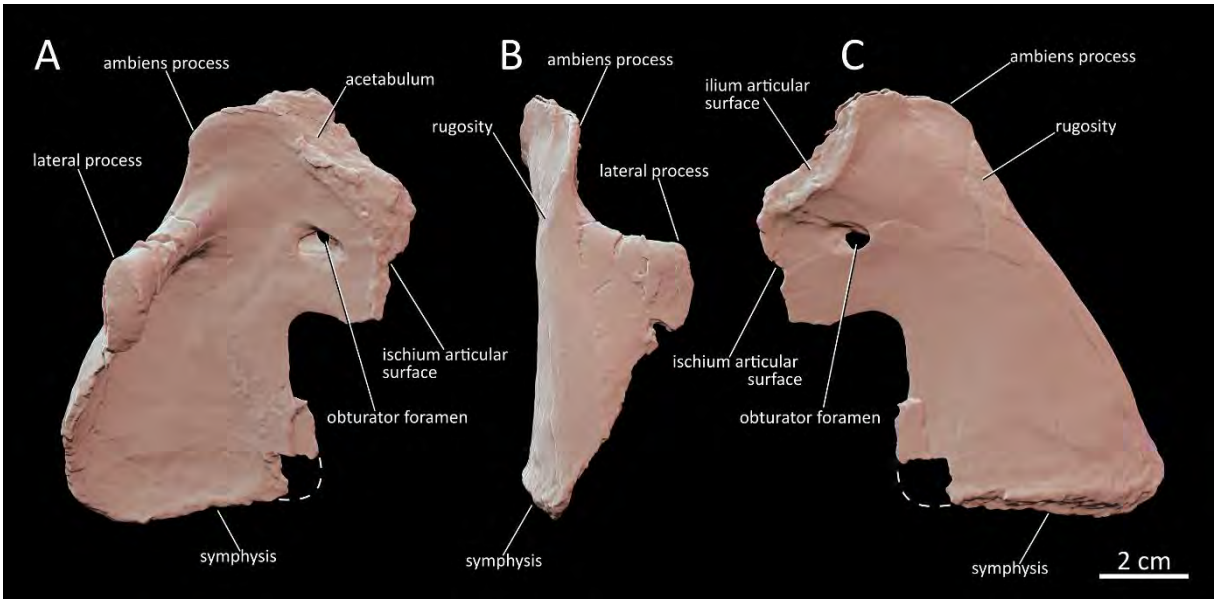

Fig. 40. Left pubis of *Tanystropheus conspicuus* from the Lower Keuper (lower Ladinian) of Miedary (Poland) – ZPAL V. 36/1008. Three-dimensional model snapshots with Lit Sphere Radiance Scaling shader enabled, in ventrolateral (**A**), anterior (**B**), and dorsomedial (**C**) views.

Ischium

The ischium of *Tanystropheus conspicuus* is composed of the robust articular region and the lateromedially flat, fan-shaped distal portion (Fig. 41). The proximal portion of the ischium is separated into the iliac and the pubic articular surfaces as well as the posteroventral margin of the acetabulum (Figs. 39, 41A–C). The more dorsally located surface, which articulated with the ischial peduncle of the ilium, is nearly confluent with the acetabulum, forming a virtually flat dorsoproximal portion of the ischium (Fig. 41C). This region is elliptical in dorsal view, with the acetabulum being more laterally located, and the articular surface for the ilium being posteromedially expanded, far beyond the plane of the plate-like distal portion of the ischium (Fig. 41B). The articular surface for the pubis constitutes the anteroproximal portion of the articular region, converging at an obtuse angle with the iliac articular surface (Fig. 41A, C). It is triangular in lateral view, projecting anteroventrally and tapering to a point. The posterodorsal portion of the articular surface of the ischium might have contributed to the "anitrochanter" present on the ischium (Figs. 39, 41)

Ventrodistal to the articular surface for the pubis, the anterior margin of the ischium forms the posterior edge of the thyroid fenestra, developed as a deep, rectangular notch in ventrolateral view (Figs. 39, 41A, C). The anterior process of the ischial fan is present ventral to it. The

lateromedially thin edge of the anterior process does not taper to a point, by contrast with some other archosauromorphs, including *T. hydroides* and *T. longobardicus* (Wild 1973; Ezcurra 2016). Instead, it is rounded in lateromedial view (Fig. 41A, C), and anteriorly expanded to a similar extent as the anteroventral corner of the pubic articular surface. The thyroid fenestra was ventrally open between the ischium and the pubis, albeit only with a narrow gap being present between the posterior process of the ischium, and the posteroventral edge of the pubis (Fig. 39). Ventral to the anterior process, the distal edge of the ischium is straight in lateral view, but concave in ventral view, due to its posteroventral corner being medially displaced (Fig. 41A, C–D). On the medial side of the ischial fan the distal edge of the ischium is convex, forming a distinct triangular and rugose thickening on which its antimere articulated along the ischial symphysis (Fig. 41A). The posterior process of the ischium is located posterodorsal to the symphysis. It is triangular in lateral view and does not taper to a point (Fig. 41A, C). Anterodorsal to this process, the posterodorsal edge of the ischium is concave in lateral view, and ascends towards the posterior corner of the articular region (Fig. 41A, C), expanding transversely in thickness.

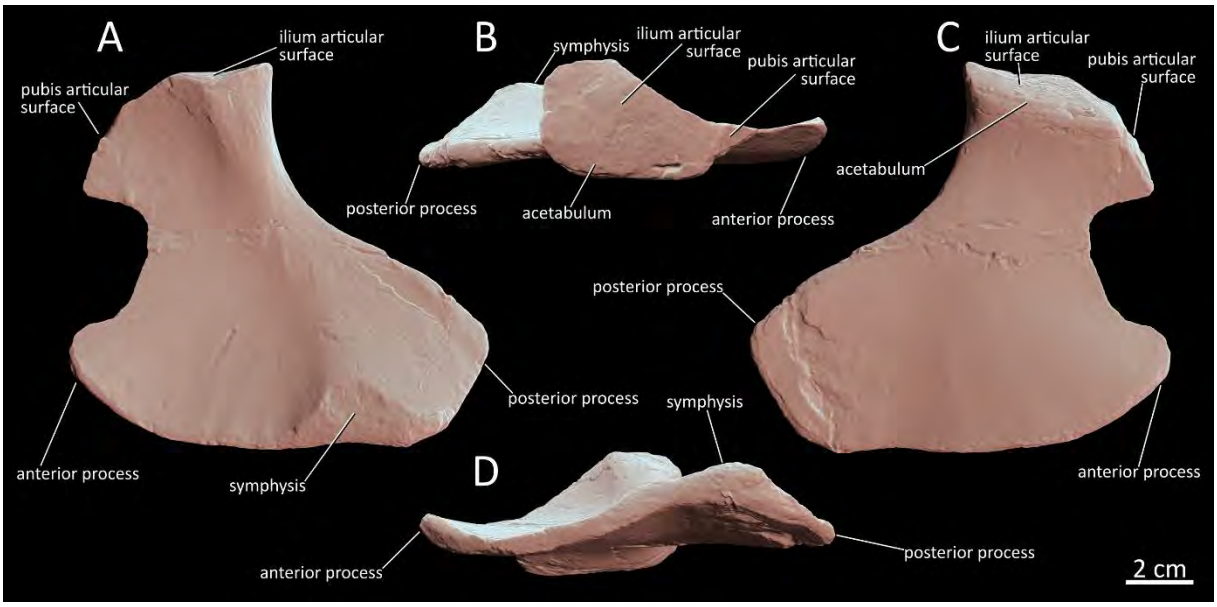

Fig. 41. Right ischium of *Tanystropheus conspicuus* from the Lower Keuper (lower Ladinian) of Miedary (Poland) – ZPAL V. 36/1006. Three-dimensional model snapshots with Lit Sphere Radiance Scaling shader enabled, in dorsomedial (**A**), dorsolateral (**B**), ventrolateral (**C**), and ventromedial (**D**) views.

The ischia of *T. conspicuus* and *T. hydroides* are nearly identical in shape, with the main difference being the slight difference in curvature of the posterior margin of the thyroid fenestra, which is rectangular in *T. conspicuus* and heart-shaped in *T. hydroides* (Fig. 39; Wild 1973). In *T. longobardicus* the ischium is relatively less expanded posteriorly and its anterior and posterior edges taper to a point (compare Fig. 41 and fig. 92 of Wild 1973). The ischial morphology described here is also reminiscent of the ischia reported by Dalla Vecchia (2006, fig. 4 A–B) from the Aupa Valley, which were interpreted as belonging to a eusauropterygian. These can now be referred to *Tanystropheus* sp. as well. Isolated eusauropterygian ischia, with the ones referred to *Nothosaurus* being the most common, have a more constricted "neck" distal to the articular region and their fan-shaped distal end is more symmetrical (see fig. 17 of Klein et al. 2022). Moreover, in both taxa there are some striations perpendicular to the distal edge of the ischium on its lateral and medial surfaces, but they are much more prominent in *Nothosaurus*.

Femur

The femur of *Tanystropheus conspicuus* is relatively much more elongate than the humerus. It is a slender, sigmoidally curved element that retains a constant width along most of its length (Fig. 42). The proximal half of its anterior margin is concave in lateral view, whereas the distal half is convex; the posterior margin mirrors this curvature (Fig. 42A, C). The femur is relatively straight in anterior (dorsal) and posterior (ventral) views, with the proximal end being medially expanded to a similar degree as the distal end (Fig. 42B, D). Its proximal and distal ends are well-ossified among the collected specimens. The shaft is elliptical in transverse cross-section, with the longer axis being anteroposteriorly oriented.

The proximal femoral head is marked by the presence of a well-defined, posteromedially oriented internal trochanter (=greater/major trochanter). It is formed as a thick, straight, ridge, which extends from the mid-length of the shaft to the proximal edge of the bone where it reaches its greatest height (Fig. 42A–C, E). The proximal edge of the internal trochanter projects perpendicularly from the proximal articular surface of the femur and meets the posterior edge of the internal trochanter at an obtuse angle (Fig. 42A, C). On both sides of the trochanteric ridge, there are deep and wide fossae (Fig. 42A–C, E). The medial one can be interpreted as the *fossa intertrochanterica* (*sensu* Novas 1996, but see Ezcurra 2016) as there is a slight depression anteroproximal to it, adjacent to the posterior margin of the proximal articular surface (Fig. 42C, E). The fossa located on the lateral side of the internal trochanter is broader, more clearly defined (Fig. 42A, E), and anterolaterally

flanked by the anterior trochanter (= lesser/minor trochanter). The anterior trochanter is formed as a narrow but proximally widening ridge on the proximal one-third of the bone (Fig. 42A–B, E). As for the internal trochanter, its distal edge reaches the proximal articular surface of the femur, but in contrast to it, it is confluent with the margin of the proximal surface, forming the anterolateral portion of the anterior tuber (Fig. 42A–B, D–E). The proximal articular surface is slightly convex in lateral view, rounded, and dorsomedially oriented. In proximal view it is rhomboidal in outline (Fig. 42E). Opposite the anterior tuber, anteromedial to the *fossa intertrochanterica*, a posterior tuber is present (Fig. 42E). On the anteromedial surface of the shaft, slightly proximal to its mid-length, a distinct, large nutrient foramen is present (Fig. 42C–D).

The distal femoral end is distinctly constricted anteroposteriorly, with grooves separating the lateral (fibular) and medial (tibial) tubers in distal view (Fig. 42F). These tubers are rounded, semi-circular in distal view, and subequally expanded in their respective direction, forming a relatively straight distal articular surface (Fig. 42B, D). There is a slight concavity between the condyles (Fig. 42B, F). Lateral to the posterior groove between the tubers, and posterior to the lateral tuber, the *crista tibiofibularis* (Nesbitt 2011) is located, forming a mound-like posterior extension (Fig. 42A–C, F). The femur of *T. conspicuus* does not differ from the femora of *T. hydroides* and *T. longobardicus* in its morphology.

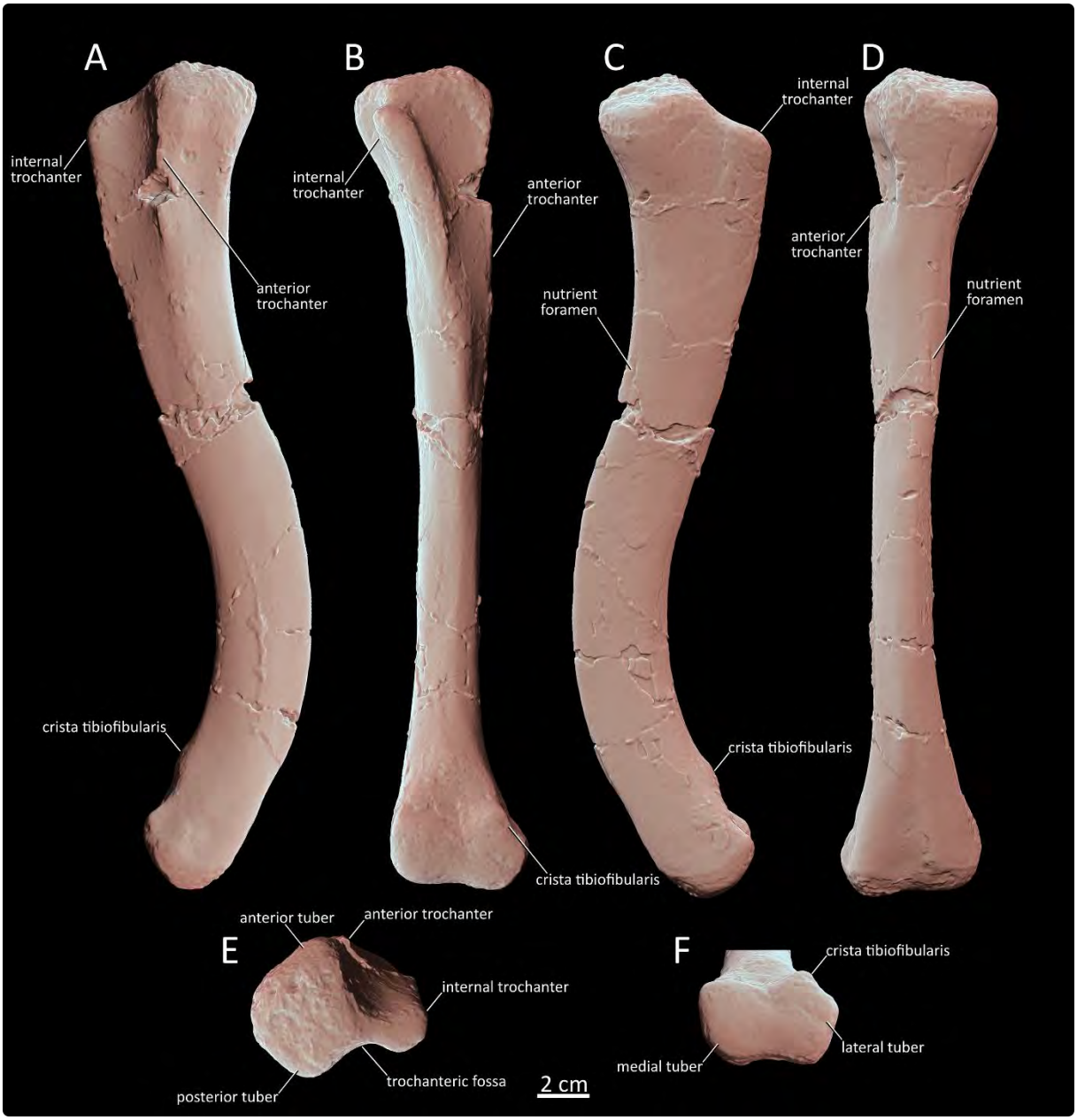

Fig. 42. Right femur of *Tanystropheus conspicuus* from the Lower Keuper (lower Ladinian) of Miedary (Poland) – ZPAL V. 36/838. Three-dimensional model snapshots with Lit Sphere Radiance Scaling shader enabled, in lateral (**A**), posterior/ventral (**B**), medial (**C**), anterior/dorsal **(D)**, proximal (**E**), and distal (**F**) views.

Tibia

The tibia of *Tanystropheus conspicuus* is a relatively straight and elongate element (Fig. 43). There is significant torsion between the proximal and distal ends although to some degree it might be partially due to diagenetic alteration. The proximal end of the tibia is transversely expanded and its articular surface is slightly convex and rounded in lateral view and elliptical in proximal view (Fig. 43B, D). Distal to the anterior edge of the proximal articular surface, a weakly outlined crest is present (Fig. 43B, D). On the lateral surface of the proximal end of the tibia, a faintly outlined fibular condyle is visible, forming a tuberosity (Fig. 43B, D). Distal to it, a distinct nutrient foramen is present (Fig. 43B).

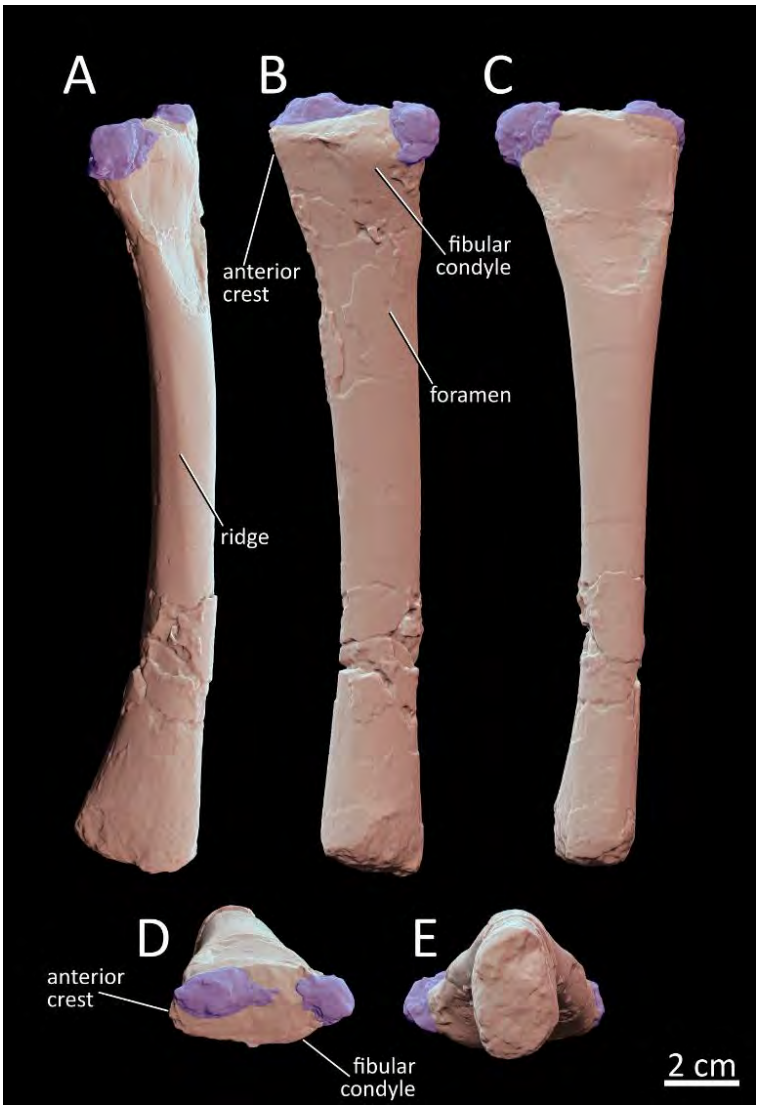

Fig. 43. Left tibia of *Tanystropheus conspicuus* from the Lower Keuper (lower Ladinian) of Miedary (Poland) – ZPAL V. 36/1200. Three-dimensional model snapshots with Lit Sphere Radiance Scaling shader enabled, in posterior (**A**), lateral (**B**), medial (**C**), proximal (**D**), and distal (**E**) views. Areas covered with sediment marked with blue hue.

The distal end of the tibia is anteroposteriorly expanded. Its articular surface is smaller and more oval in distal view than that of the proximal portion (Fig. 43E). The lateral edge of the shaft is slightly concave in posterior view, and its posterolateral section is marked by the presence of a subtle ridge (Fig. 43A). Aside from these features, the surface of the shaft is smooth and seemingly devoid of any other notable characters. The tibia of *T. conspicuus* is relatively more massive and thicker than the same element in other species of *Tanystropheus* (compare Wild 1973; Nosotti 2007). This characteristic might be partially due to individual size difference, as a large *T. hydroides* individual PIMUZ T 2818 also exhibits a relatively robust tibia comparable in its proportions to those of *T. conspicuus*.

A limb bone described by von Huene (1958*b*) as a "parasuchian" radius from the Upper Muschelkalk of Wesseln (Germany) bears a strong morphological resemblance to the tibiae referred to *T. conspicuus* and falls within the size range of the elements from Miedary. Unfortunately, the original specimen could not be located (pers. comm. R. Kosma).

Fibula

As in most other diapsids, the fibula of *Tanystropheus conspicuus* is much more slender and narrow at mid-length than tibia. It is also relatively straighter in anterior view, with both of its articular surfaces lying along the same axis (Fig. 44). In lateral view it is sigmoidally curved (Fig. 44A–B). The proximal articular surface is elliptical in proximal view and convex in lateral view, with rounded anterior and posterior margins (Fig. 44 A–B, D). At a point approximately one third down the length of the shaft, lies the insertion of the *musculus iliofibularis* (Fig. 44A, C). It forms as anteroposteriorly thick, low ridge, which separates an oval concavity on the lateral surface of the shaft from the anterior fibular margin (Fig. 44A). More distally, the anterolateral portion of the shaft is occupied by a deep groove, which is flanked anteriorly and posteriorly by distinct ridges (Fig. 44A, C). The anterior ridge extends parallel to the shaft, forming a thin lamina between the distal portion of the fibula and the insertion of *musculus iliofibularis* (Fig. 44A, C). Ezcurra (2016) stated that the shafts of the fibula and tibia in *Tanystropheus* are of approximately the same transverse width at about mid-length, but this is only due to the anterior fibular ridge appearing to increase the shaft thickness in lateral view (Fig. 44A). In all species of *Tanystropheus* the tibia is always the more robust of the two elements.

The distal portion of the illustrated fibula (Fig. 44) is thickened due to a pathological overgrowth (Fig. 44E). Compared to unaltered specimens, it is more anteroposteriorly expanded and distally concave. Another specimen, ZPAL V. 36/834, shows that the distal fibular end is rounded and convex in lateral view and elliptical in distal view (Fig. 44E). Its articular surface is only slightly larger than that of the proximal end. Whereas most of the surface of the fibula shaft in *T. conspicuus* is smooth, small pits and longitudinal striations appear near the articular ends, especially on the lateral side.

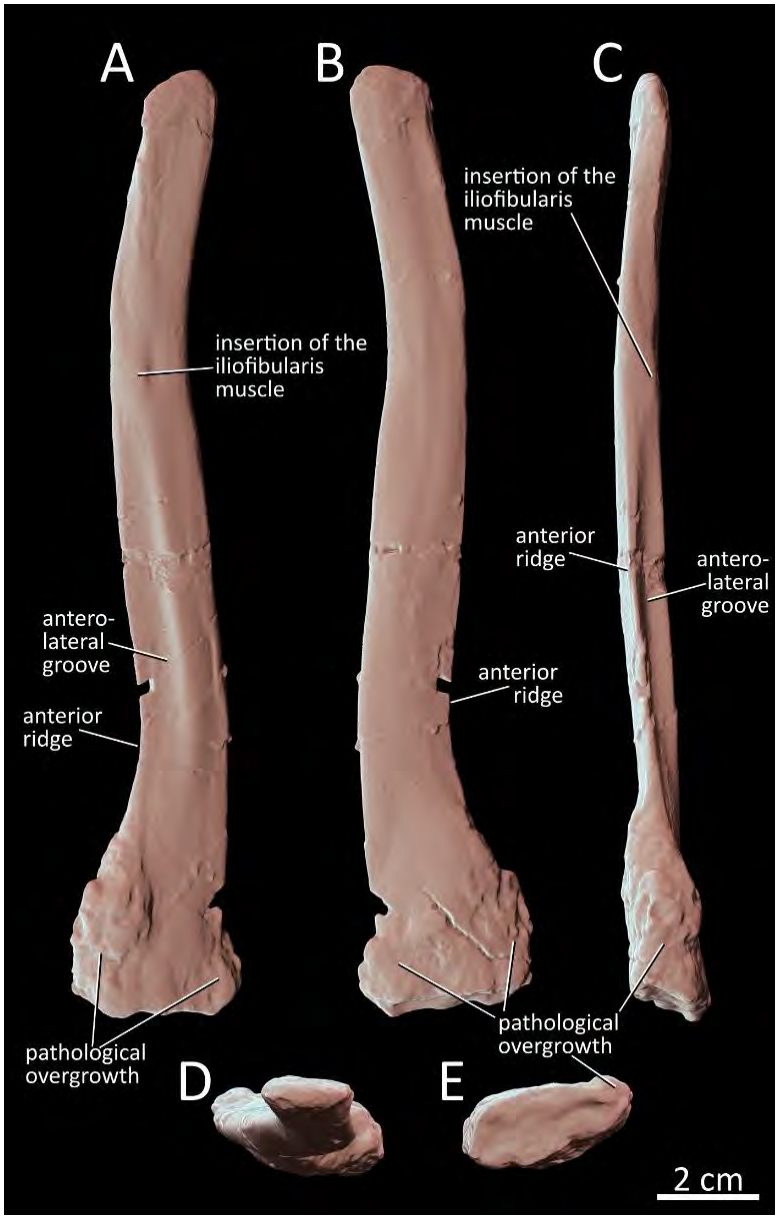

Fig. 44. Left fibula of *Tanystropheus conspicuus* from the Lower Keuper (lower Ladinian) of Miedary (Poland) – ZPAL V. 36/1176. Three-dimensional model snapshots with Lit Sphere Radiance Scaling shader enabled, in lateral (**A**), medial (**B**), anterior (**C**), proximal (**D**), and distal (**E**) views.

Postcloacal bones

Isolated postcloacal bones identical to those present in *T. hydroides* and *T. longobardicus* (see Discussion) have been identified at Miedary (Fig. 45). As can be discerned from articulated skeletons the postcloacal apparatus in *Tanystropheus* is composed of four elements – two anterior and two posterior bones. In vivo they were located posterior to the pelvis (around the cloaca as interpreted by Wild 1973, 1980*a*). The anterior portion of the posterior element articulated along the ventral surface of the corresponding anterior element, near the anteroposterior midpoint of its length. Both articulated pairs are always preserved in separation from each other, and from any other bones. They ran parallel to the main body axis.

Both elements are elongate, straight, with a rough, highly rugose surface (Fig. 45). Their internal structure is distinct, with the bone tissue forming them being highly cavernous and poorly organised (in agreement with the observations of Wild 1973). The anterior elements can be easily distinguished from the posterior ones based on their shape. The largest of these elements is over 30 cm long, so that in large individuals the whole apparatus might have reached approximately half a meter in length.

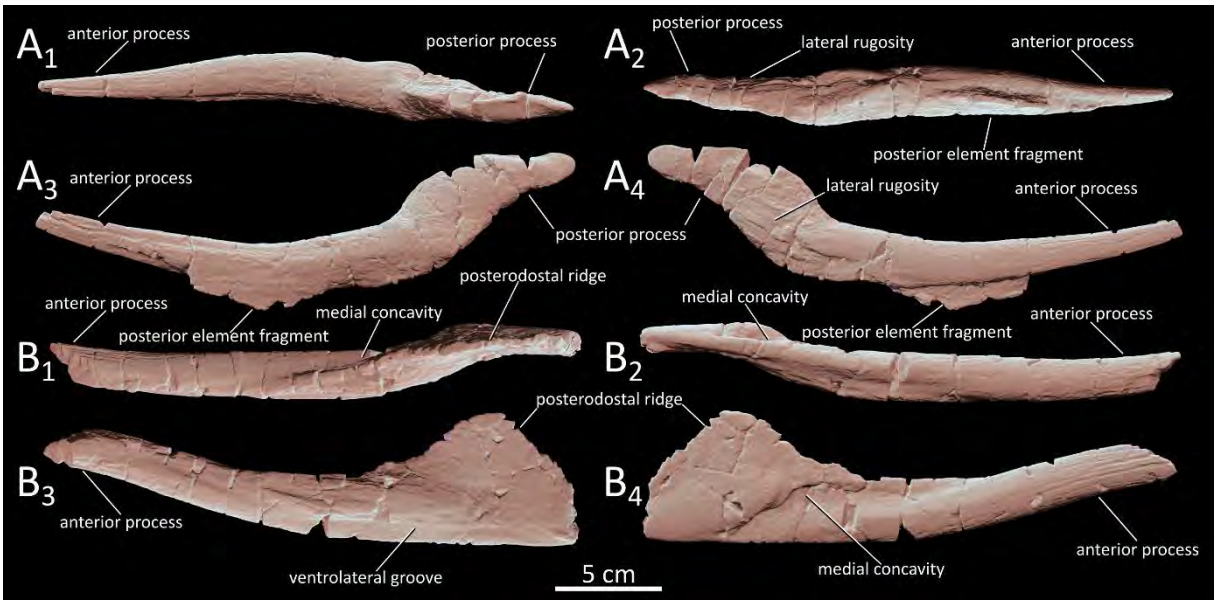

Fig. 45. Postcloacal bones of *Tanystropheus conspicuus* from the Lower Keuper (lower Ladinian) of Miedary (Poland) – left anterior element ZPAL V. 36/1147 (**A**) and right posterior element ZPAL V. 36/1148 (**B**). Three-dimensional model snapshots with Lit Sphere Radiance Scaling shader enabled, in dorsal (A_1, B_1), ventral (A_2, B_2), lateral (A_4, B_3), and medial (A_3, B_4) views.

The anterior element has two processes. The anterior process is rod-like, tapers anteriorly, and its surface is covered with deep, longitudinal, striations (Fig. 45A). Near the ventrolateral portion of its base, the posterior element articulated in a deep groove. Isolated anterior postcloacal bones are often preserved with a broken anteriormost portion of the corresponding posterior postcloacal bone still attached (Fig. 45A). The posterior process of the anterior element is shorter than the anterior process. Its base ascends sharply posterodorsally, but its distal tapering end is posterolaterally oriented with the dorsal surfaces of the anterior and posterior processes being nearly parallel (Fig. 45A_3–A_4). On the lateral surface of the base of the posterior process, the anterior postcloacal bone is especially rugose, being covered by a set of roughly longitudinal, deep grooves and distinct ridges (Fig. 45A_4).

The posterior element is similar to the anterior postcloacal bone. It has a rod-like, tapering anterior process, with its surface covered by deep, longitudinal, striations (Fig. 45B). The process is relatively more massive in the posterior element. The ventrolateral portion of its base is occupied by a deep groove, which is dorsally demarcated by a distinct broad ridge (Fig. 45B_3). The posterior portion of the posterior element is dorsally expanded, with a tall and straight ridge forming the posterodorsal edge of the bone (Fig. 45B_3–B_4). Ventromedial to it, a deep medial concavity is present, with its longitudinal axis extending obliquely to the anteroposterior axis of the whole element (Fig. 45B_4). When in articulation, the tip of the posterior process of the anterior element nearly reached the posterodorsal edge of the posterior element, thus creating an open embayment between the bones, as in other species of *Tanystropheus* (Wild 1973).

Discussion

Anatomy of the cervicodorsal region

The anatomy of the cervico-dorsal transition in *Tanystropheus* was poorly understood, because vertebrae from known specimens were either missing, damaged, or only partially visible (see Wild 1973; Renesto 2005; Nosotti 2007). However, based on a new specimen, Rieppel et al. (2010) were able to identify the transitional thirteenth presacral vertebra as the last cervical vertebra. From the newly described *Tanystropheus conspicuus* material, three specimens preserve articulated sections of the vertebral column but none of them includes a complete cervical and dorsal series. The number of presacral vertebrae in this species can, therefore, only be inferred indirectly.

Nine dorsal vertebrae and the first sacral vertebra are preserved in an unpublished vertebral series SMNS 13337. ZPAL V. 36/125 contains 11 dorsal vertebrae, two sacral vertebrae and several associated caudal vertebrae. Finally, ZPAL V. 36/100 includes six cervical vertebrae. In the latter specimen, the preserved section most likely represents the anteriormost postaxial cervical vertebrae (vertebrae three to eight). This interpretation is based on the presence of an axis consistent in size found in close proximity to the anterior end of the specimen, indicating that it likely derived from the same individual but was slightly disarticulated from the rest of the preserved series. Furthermore, the changes in centrum length between the consecutive elements in the articulated series follow the pattern observed by Wild (1973) for the first five postaxial cervical vertebrae of *Tanystropheus*, where the size of the first four elements is relatively constant and then increasing in the seventh cervical vertebra (see Appendix I). Morphotypes identified as the five posteriormost cervical vertebrae (cervical vertebrae nine to thirteen) can be distinguished from the other isolated remains of *T. conspicuus* as they strictly correspond in their morphology to the elements found in other species of *Tanystropheus* (see Wild 1973; Rytel et al. 2024*a*) and are partially preserved in the disarticulated but close association of bones of ZPAL V. 36/584 (Fig. 16). Moreover, this specimen preserves a characteristic dorsal rib with a broad plate-like expansion and two posteriormost cervical ribs in close proximity. This dorsal rib is virtually identical to that of ZPAL V. 36/123 (Fig. 30A) and morphologically distinct from the rib that articulated with the anteriormost preserved dorsal vertebra in ZPAL V. 36/125 (Fig. 30B). Moreover, the morphotype represented by ZPAL V. 36/123 is closer in shape to the last cervical rib than the anteriormost dorsal rib preserved in ZPAL V. 36/125. This clearly implies that in the latter specimen at least one more dorsal vertebra was present, with which the “transitional” first dorsal rib articulated. Thus, the combined morphological data gathered from both isolated and articulated specimens demonstrates that the presacral count in *T. conspicuus* is at least 13 cervical and at least 12 dorsal vertebrae, respectively. Importantly, the number of presacral vertebrae in tanystropheids seems to have been developmentally constrained to 25 (Rytel et al. 2024*a*), implying that these 25 vertebrae identified for *T. conspicuus* likely constituted the whole presacral section of the vertebral column. Based on several morphological characters and a similarity to closely related taxa, it can be assumed with high degree of confidence that *T. conspicuus* possessed 13 cervical and 12 dorsal vertebrae (see Rieppel et al. 2010; Spiekman et al. 2020*a*). The thirteenth cervical vertebra is more similar in its proportions to the succeeding dorsal vertebrae than the preceding cervical vertebrae. However, considering the morphology of the associated rib, which is tall, anteroposteriorly short, and horizontally

oriented, together with the presence of subcentral foramina (see Rytel et al. 2024*b*) and epipophyses (features absent in the dorsal vertebrae) on the vertebra, I concur with Rieppel et al. (2010) in identifying the thirteenth vertebra as the last cervical vertebra in all species of *Tanystropheus*.

The posture of the neck of *Tanystropheus* has long been a subject of debate, with previous studies suggesting various hypotheses – from fully horizontal and stiff to "swan-like" flexible S-shaped (Peyer 1931; Wild 1973; Kummer 1975; Tschanz 1986; Nosotti 2007; see Tschanz 1988 and Renesto 2005 for detailed summaries). The flexibility of the neck was undoubtedly highly dependent on the elasticity of the extremely elongate cervical ribs, assessment of which is outside the scope of this work, and should be addressed by biomechanical studies. Concerning the posture, Renesto (2005, p. 389) pointed out that the morphology of the twelfth cervical vertebra, in which the posterior articular surface of the centrum was "forward slanting", indicates that the base of the neck of this animal was dorsally inclined. This is reminiscent of the posture reconstructed by Wild (1973, plate 1). Nosotti (2007) argued against this interpretation, maintaining that the presence of an asymmetrical intervertebral disc or a slightly dorsally curved vertebral column in the trunk could have counteracted the inclination, and the neck was likely held horizontally, as demonstrated by Tschanz (1986). The specimens of *Tanystropheus conspicuus* described here provide new insights into the anatomy of the cervico-dorsal transition in *Tanystropheus* and the posture of the neck. In the thirteenth cervical vertebra the articular surfaces of the centrum are not parallel to each other, with the anterior one being slanted and facing slightly anterodorsally (Fig. 19A). In the preceding twelfth vertebra, the dorsal inclination of the ventral surface of the centrum is evident (Fig. 18B_3), in agreement with the observation of Renesto (2005) for *T. longobardicus* and also corresponding to MFSN 34727, a *Tanystropheus* sp. specimen from the Aupa Valley reported by Dalla Vecchia (2008, figs. 61C, 64A). In the eleventh cervical vertebra the articular surfaces of the centrum are, however, even more conspicuously located on different dorsoventral levels, with the anterior one being more dorsally positioned. In *T. conspicuus* this characteristic is much more pronounced than in other species of *Tanystropheus*, in which this vertebra is less inclined. This is possibly a function of the larger size of the former. In all middle cervical vertebrae of *T. conspicuus*, both articular surfaces of the centrum are either sub-parallel, or slightly downturned (Figs. 13–15).

Studies on the cervical anatomy of long necked animals, including sauropods, have shown that using purely osteological characters to reconstruct the neutral position of the neck

can be error-prone, but also that the inclusion of the intervertebral tissue usually “raises” the neutral position (Taylor and Wedel 2013; Taylor 2014). Morphology of the cervical vertebrae of *T. conspicuus* indicates that in the neutral position the posteriormost portion of its neck was likely dorsally inclined and the portion anterior to the eleventh cervical vertebra was held relatively horizontally, but with slight ventral bowing. Consequently, the skull and the base of the neck were positioned lower than the middle section of the neck (Fig. 46). This hypothesis combines the observations presented in previous studies (Wild 1973; Tschanz 1986; Renesto 2005; Nosotti 2007) and is further supported by cervical rib morphology. Whereas the ribs associated with the middle cervical vertebrae (Fig. 28) and the last cervical vertebra (Fig. 29C) have a relatively straight ventral margin and an anteriorly projecting anterior free-ending process, the ribs associated with the eleventh and twelfth vertebrae differ in this respect. The latter two have distinctly upturned anterior free-ending processes (Fig. 29A–B) and moreover, the twelfth rib is crescent-shaped. These morphological features imply the presence of some curvature in this section of the neck and support the hypothesised dorsal inclination (Renesto 2005).

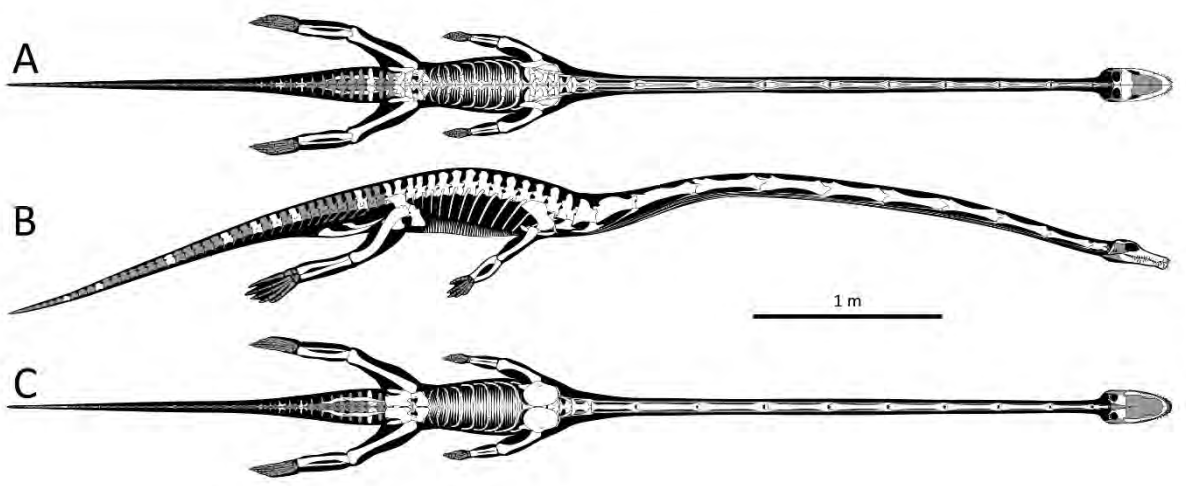

Fig. 46. An osteological reconstruction of a large individual of *Tanystropheus conspicuus* in dorsal (**A**), right lateral (**B**), and ventral (**C**) views. Bone outlines based on the specimens illustrated here (coloured in white), and the articulated specimens of *T. hydroides* (coloured in grey; for the skull see Spiekman et al. 2020*b*). Body proportions taken from the most complete known specimen of *T. hydroides*, PIMUZ T 2818.

Based on the reduced muscle attachment sites on the cervical vertebrae *Tanystropheus* Wild (1973) noted that the entire anterior and middle portions of neck of this animal were practically devoid of lateral musculature, but in turn the dorsal ligaments and ventral musculature were expanded. Tschanz (1986, 1988) hypothesised that the musculature was likely too weak to lift the neck beyond the horizontal level. Renesto (2005) argued that in conjunction with the inclined base of the neck, the cervical muscle/ligament system would be capable of raising the relatively light neck of *Tanystropheus*. Rieppel et al. (2010) reached similar conclusions concerning the vertical movements of the neck.

Although both a detailed range of motion analysis and a reconstruction of the myology of *T. conspicuus* are outside the scope of this work, the three-dimensional preservation of the new Miedary material allows for a preliminary re-assessment of this topic. Musculature on the lateral sides of the middle cervical vertebrae of *T. conspicuus* was apparently greatly reduced, with the cervical ribs located extremely close to the ventrolateral margin of the centrum and the zygapophyses projecting strongly anteroposteriorly. Attachment points for epaxial muscles and ligaments are especially well developed on the anterodorsal and posterodorsal portions of the middle cervical vertebrae. The free-ending processes of the ribs, expanded epipophyses, prominent anterior and posterior grooves at the base of the neural spine, together with the portions of the neural spine overhanging them, presumably supported an intricate muscle/ligament system.

In the four posteriormost cervical vertebrae these characteristics change – the centrum is shorter, the neural spine taller, and the vertebrae are more transversely expanded. In these vertebrae the epipophyses are less prominent, but distinct anteriorly projecting mound-like tuberosities on the prezygapophyses are more robust, forming additional attachment sites for the soft tissues of the more anterior portion of the neck. Posteriorly, the diapophyses and cervical ribs become much more massive and are located further from the centrum, implying the existence of expanded lateral musculature. The most striking feature of the posterior cervical vertebrae is the significant expansion of the distal end of the neural spine, which is developed as a bulbous thickening along its entire length. These would have served as attachment sites for the dorsal ligaments and muscles, providing stability for the neck, and allowing for the inclined posture.

Generally, the transitional cervicodorsal region in *T. conspicuus* is characterised by the presence of several broad, flat, plate-like bones (ribs associated with the transitional vertebrae, scapulae, coracoids). At least some of them could have served as large attachment sites for neck muscles and ligaments together with the distally expanded neural spines and possibly also the mammillary processes of the dorsal vertebrae. In *Tanystropheus*, the distal ends of most (up to seven pairs) cervical ribs reach to the section of the vertebral column between the eleventh cervical vertebra and the first dorsal vertebra, where they terminate essentially at the same point (Fig. 46; see PIMUZ T 2818). Their elongation served the purpose of not only stiffening the neck but also transmitting the attached muscles to the back of the neck (Tschanz 1986). Following Wild (1973), I hypothesise that the cervical muscle mass was relatively reduced in the middle portion of the neck of *Tanystropheus* but significantly expanded near the base of the neck. This would also explain the function of the anteroposteriorly projecting extensions of the anterior dorsal ribs. Regardless of the flexibility of the neck, but especially if it was as stiff as proposed by some (Tschanz 1986, 1988; Nosotti 2007), its movements would be mostly induced by the muscles and ligaments originating from the transitional cervicodorsal region.

Additional insights are provided by the change in the nature of the neural spine morphology. In the middle cervical vertebrae, the neural spine is well-developed in its posterior and anterior portions, but almost completely reduced in the middle. Moving the attachment points towards the peripheries of the extremely elongate vertebra could allow for finer control of the movement of the neck by providing a shorter lever. The middle section of the vertebra was reduced to a durable (but relatively light) tube-like structure described in detail by Rytel et al. (2024*b*). In the more posterior cervical vertebrae (10 to 13) the relative height of the middle section of the neural spine, as well as the height of the neural spine itself, increased markedly (these elements were held inclined in vivo), allowing for larger attachment areas for the muscles and ligaments originating from the torso. The proposed dorsally inclined posterior portion of the neck would allow for enhanced control of the movements of the neck (and the head) and thereby play a pivotal role in hunting (e.g., retraction during “kinetic inertial feeding” proposed by Tschanz 1986).

Miedary as a habitat of *Tanystropheus*

Insights concerning the environment of deposition for an animal carcass can be gained by assessing the frequency of occurrence of specific isolated skeletal elements as they have different hydrodynamic dispersal rates (Blob et al. 2022). To investigate this phenomenon, three sets of three-dimensionally preserved and isolated *Tanystropheus* bones can be compared – the material of *Tanystropheus conspicuus*, divided into Miedary (n=722) and the western part of the CEB (n=185), as well as the *Tanystropheus* sp. remains reported by Dalla Vecchia (2000, 2006, 2008), and Dalla Vecchia and Simonetto (2018) from the Aupa Valley in north-eastern Italy (n=204). All three collections have here been studied first-hand to minimise the possible effect of identification bias. Considerably fewer three-dimensionally preserved specimens have been published from sites in Canada (Sues and Olsen 2015), Hungary (Ősi et al. 2020), Israel (Rieppel 2001), Romania (Jurcsak 1975) and Saudi Arabia (Vickers-Rich et al. 1999). See Dalla Vecchia and Simonetto (2018) and Appendix I for a full list of analysed specimens.

In the western part of the CEB a taphonomic bias towards the preservation of large long bones (middle cervical vertebrae and stylopodial elements) seems to have existed when compared to the relative occurrence of other elements. This group of sites is nearly completely devoid of the elements from the pectoral and pelvic girdles. The Aupa Valley sites exhibit a much higher diversity of elements, with flat bones and short vertebrae being relatively much more common. This corresponds to the pattern from Miedary, which has the highest element diversity among these three sets, and is the least dominated by long bones (which are, however, still the most common).

Quantitative characteristics of the analysed material indicate that the remains of *T. conspicuus* from the western part of the CEB underwent significant sorting. Transport of the *Tanystropheus* bones in the Aupa Valley sites, and especially in Miedary, seems to have been over much shorter distances as the element diversity is much higher. Similar to the Upper Muschelkalk localities, autopodial elements and distal-most caudal vertebrae are scarce in Miedary, suggesting that the assemblage has undergone some hydraulic sorting, although, uniquely, some delicate cranial elements are also preserved from this site (although this could also be the result of a larger total number of bones having been found in Miedary), indicating the presence of specific conditions leading to their preservation in this depositional environment. The inferral of variable transport distances is supported by the results of a study by Blob et al. (2022), which implied that the presence of vertebrae with a wide diversity of

other skeletal elements is indicative of short transport distances whereas the presence of vertebrae as the primary preserved elements in an assemblage suggests a high likelihood of longer transport distances. It is, therefore, likely that *T. conspicuus* in Miedary lived, or at least died, in close proximity to the reservoir in which its remains were deposited.

The occurrences of the teeth of *Tanystropheus conspicuus* are stratigraphically and spatially concentrated. Among the accessioned collections in Germany, I have been able to identify over 100 teeth of *T. conspicuus* (see Appendix I). Roughly half of the known specimens have originated from the Grenzbonebed of the area around Crailsheim (Germany) – material collected mostly by R. Blezinger. The majority of the teeth of *T. conspicuus* are stored in SMNS and GPIT collections. The Grenzbonebed outcrops of the area around Crailsheim (Germany) are characterised by a high frequency of occurrence of vertebrate fossils, especially teeth (see Hagdorn and Reif 1988). It can be safely assumed that the high number of teeth of *T. conspicuus* originating from this stratum (compared to bone fragments) is due to pre-diagenetic sorting.

The reasons for the high relative (compared to other tetrapods) and absolute frequency of occurrence of *Tanystropheus conspicuus* in the Miedary site (see Czepiński et al. 2023) can be understood by comparing the characteristics of the assemblage and the locality itself to other outcrops within the local area and the broader region. In the western part of the CEB, where the remains of *Tanystropheus conspicuus* are rare, its fossils appear to be even more scarce in the Keuper strata above the Grenzbonebed, which marks the transition from marine to more terrestrial settings. In marked contrast, in the outcrops around Miedary a considerable fluctuation in the abundance of remains of *T. conspicuus* is recorded in the local rock sequence. Three stratigraphic units with significant vertebrate fossil content can be distinguished here: 1) the marine Upper Muschelkalk, 2) the Lettenkeuper glauconite beds deposited in shallow marine settings but with significant terrestrial influence, and 3) the marine Lettenkeuper dolomite beds (see Sulej et al. 2011; Pawlak et al. 2022; Czepiński et al. 2023). Only two vertebrae of *T. conspicuus* were reported from the Upper Muschelkalk, compared to hundreds of sauropterygian remains (pers. obs. AR; von Meyer 1847-1855; Langenhan 1903). The only the slightly younger Lettenkeuper strata of Miedary (Unit 1, see Czepiński et al. 2023 for stratigraphy) have yielded the massive vertebrate fossil accumulation described, in which elements of *T. conspicuus* were the most numerous throughout most of the layers (M1-M2 and M4, but not M3). The outcropping sediment sequence ends with the

strata directly overlying Unit 1, clays and dolomites, which so far seem to be completely devoid of remains of *T. conspicuus*.

Tanystropheus conspicuus is known from the late Anisian to the late Ladinian. The remains from Miedary date roughly from the middle of this interval – early Ladinian (Czepiński et al. 2023). Therefore, the extreme fluctuation of abundance of remains of *T. conspicuus* in the outcrops around Miedary is unlikely to be due to the emergence or extinction of the species in the region. The ages of the source strata fall well within the temporal range of occurrence for this animal in the western part of the Basin. Instead, the absolute and relative frequency of occurrences of *T. conspicuus* seems to be tightly controlled by environmental factors – a correlation can be observed between the presence of remains of *T. conspicuus* and differences in depositional settings. Sedimentation of the Upper Muschelkalk strata proceeded in a shallow, restricted, epicontinental basin with euryhaline to polyhaline salinity and limited terrestrial influence (see Korte et al. 2003; Franz et al. 2015; Pawlak et al. 2022). Similar conditions were present during the deposition of the dolomite beds in Miedary (Pawlak et al. 2022). Layers M1-M2 and M4 of Miedary were deposited in a very shallow, brackish, restricted reservoir with significant terrestrial input, and the M3 layer in (sub)terrestrial settings (Pawlak et al. 2022; Czepiński et al. 2023).

Combining the aforementioned factors concerning the occurrence of remains of *Tanystropheus conspicuus* in Miedary – high variability within the local stratigraphic column and the relatively high element diversity and short transport in the layers in which *T. conspicuus* is prevalent – it becomes clear that this taxon had relatively strict environmental preferences. The data reported here imply that *T. conspicuus* was rare or absent in both marine (depositional settings of the Upper Muschelkalk and the dolomite beds from Miedary) and terrestrial (depositional settings of most of the Lettenkeuper above Grenzbonebed and the M3 layer from Miedary) environments and flourished in the transitional zones between them, which are recorded in the glauconite beds of Miedary (layers M1-M2, and to some extent M4). This hypothesis is consistent with the general environmental conditions (shallow marine with a significant terrestrial input) present in the localities from the Aupa Valley, described by Dalla Vecchia (2006, 2010) and Dalla Vecchia and Simonetto (2018), which is the only other known site in which *Tanystropheus* is also quantitatively dominant among the tetrapod finds. Regarding the other sites that have yielded abundant material of *Tanystropheus*, the Besano Formation of Monte San Giorgio, from which most of the articulated skeletons of *Tanystropheus* are known, was deposited in a euryhaline marine intraplatform basin with

water depths between 30 and 130 m (Bernasconi and Riva 1993; Bernasconi 1994; Röhl et al. 2001; Beardmore and Furrer 2017). At first glance these characteristics could be viewed as inconsistent with the preferred habitat of *T. conspicuus* as reported here but the results of the taphonomic analysis of Beardmore and Furrer (2017) indicated that tanystropheid remains found in the Besano Formation have originated from nearshore settings, which has previously also been suggested by Renesto (2005) for specimens from other stratigraphic units of Monte San Giorgio. In China, the *Tanystropheus* cf. *T. hydroides* specimen GMPKU P 1527 described by Rieppel et al. (2010) originated from the Lower Assemblage of the Zhuganpo Member of the Falang Formation (Lu et al. 2018; Jiang et al. 2025). The general environmental and faunistic characteristics of this unit are similar to the Besano Formation. Washed-in articulated skeletons of the terrestrial tanystropheid *Macrocnemus fuyuanensis* are present in both units as well (Lu et al. 2018; Jiang et al. 2025), indicating a similar taphonomical history of *Tanystropheus* remains (Beardmore and Furrer 2017). In general, all known remains that can currently be confidently referred to *Tanystropheus* have been found in strata that were deposited in shallow aquatic environments, or slightly deeper basins with significant terrestrial material influx. The Miedary site is unique among them in recording the setting that was likely the closest to the original habitat of *Tanystropheus*, at least in some of its aspects. This hypothesis is supported by multiple lines of taphonomic evidence as well as the presence of individuals of different sizes – from early juveniles to old, including very large individuals affected by various skeletal pathologies (pers. obs. AR). Environmental preferences of *T. conspicuus* can, to some extent, be extrapolated to other species of *Tanystropheus* and are congruent with virtually all the data reported. Even though the sedimentary sequence accessible at Miedary is relatively short, it showcases which environments were preferred by this animal – not terrestrial, but not fully marine either, and in the very shallow nearshore ecosystems. Such conditions were present during the deposition of the glauconite beds from Miedary (M1-M2, see Czepiński et al. 2023), which serve as a good proxy for reconstructing the habitat of *Tanystropheus*.

Mode of life

The discussion on the mode of life of *Tanystropheus*, predominantly understood as its preferred habitat, hunting strategy and mode of locomotion, is as old as the "modern" understanding of the bauplan of this animal (Peyer 1930, 1931; but see Wild 1973 and Nosotti 2007 for a summary on the subject). Due to the lack of extant analogues for the unique anatomical features of this animal (see Rytel et al. 2024*a*), deciphering its biology has always been problematic.

Throughout the history of research on *Tanystropheus*, the views on its mode of life have changed markedly. Peyer (1931) did not find any adaptations for an aquatic lifestyle in the skeleton of this reptile, interpreting it as a fully terrestrial animal. Kuhn-Schnyder (1959) regarded the elongated fifth pedal digit of *Tanystropheus* as an indicator of aquatic locomotion. Wild (1973, 1980*a*) considered this animal to change its habitat preferences during ontogeny – from more terrestrial smaller forms to predominantly aquatic larger individuals, which used their long hindlimbs as the main source of propulsion. Tschanz (1986, 1988) argued that the anatomy of the elongate neck would be much more advantageous in an aquatic environment, which was therefore inferred to be the primary habitat of *Tanystropheus* regardless of ontogenetic stage. Contradicting with this view, based mostly on its lack of morphological adaptations towards an aquatic lifestyle, Renesto (2005) considered this animal to have mainly lived on land, as a shoreline dweller, similar to what Peyer (1931) suggested. Nosotti (2007) concurred with Tschanz (1986, 1988) in interpreting the functional anatomy of *Tanystropheus* as being unsuitable for terrestrial locomotion an pointing towards an aquatic mode of life. Rieppel et al. (2010, p. 1088) stated that *Tanystropheus* "might have only come on land to lay eggs, or perhaps not at all". The study of Jaquier and Scheyer (2017) showed that the histological characteristics of the bones of *Tanystropheus* indicate an amphibious lifestyle. Renesto and Saller (2018) revised the previous interpretations of Renesto (2005), and, based on a re-interpretation of its caudal musculature, considered *Tanystropheus* a semi-aquatic animal that lived in a shoreline and/or shallow-water environment. A description of the cranial anatomy of *T. hydroides* by Spiekman et al. (2020*a, b*) revealed several adaptations to hunting in water, but the morphology of the inner ear suggests this animal likely did not spend much time in open-marine environments.

In general, all recent findings are congruent with the interpretation of *Tanystropheus* as an animal strictly connected with a shallow marine habitat rather than open pelagic or terrestrial environments. From among the known specimens of *Tanystropheus*, only the

isolated cervical YPM VPPU.022000 (Sues and Olsen 2015, fig. 10; Sues et al. 2022, fig. 6A–B), referred to *Tanystropheus* sp. by Spiekman and Scheyer (2019) and Sues et al. (2022) has not originated from a marine-influenced environment but rather from a freshwater, fully terrestrial depositional setting of the Economy Member of the Wolfville Formation in Canada (Sues and Olsen 2015). This specimen, which is Middle Triassic (Anisian – Ladinian) in age, is currently the only record of *Tanystropheus* in North America (Spiekman and Scheyer 2019; Sues et al. 2022). Whereas the cervical is similar to the neck vertebrae of *Tanystropheus* in its overall proportions, it seems to lack the subcentral foramina, and its rib articulation facets are much more prominent than in other representatives of this genus. It might, therefore, represent a separate taxon. If so, it would additionally strengthen the connection of *Tanystropheus* with marine environments or brackish reservoirs with some marine influence (e.g., Miedary, Vellberg – see Pawlak et al. 2022). The recent contributions to the discussion on the mode of life of *Tanystropheus*, together with the data concerning the occurrence of its remains presented herein, support the (semi-)aquatic hypothesis. The novel anatomical data on *Tanystropheus conspicuus* give additional insight into this subject:

1) The large size of the nasolacrimal duct in *T. conspicuus* and *T. hydroides* and its presence within the maxilla contrasts with the configuration documented their Triassic relatives (Sookias et al. 2020; Sobral 2023; Forster et al. 2024). In archosauromorphs the nasolacrimal duct is narrow and usually enclosed by the lacrimal and sometimes by the prefrontal bones, but in some taxa it can pass along the medial surface of the maxilla (e.g., in crocodilians, see Rehorek et al. 2005; Witmer 1997). Placement of the canal in the maxilla of *T. hydroides* in a continuum with the foramen piercing the lacrimal strongly supports its interpretation as the nasolacrimal duct, although its passage through the maxilla itself is a highly unusual feature. The disparity between the characteristics of the nasolacrimal duct in *Tanystropheus* and other archosauromorphs might result from differences in their lifestyles. Adaptation to osmoregulation in haline environments is one of the most important aspects of transition from terrestrial to marine habitats, and several aquatic lineages of reptiles have convergently modified their lacrimal apparatus to accustom their physiology to this factor (Fernández and Gasparini 2008; Babonis and Brischoux 2012; Motani and Vermeij 2021; Cowgill et al. 2023). The diet of *Tanystropheus* consisted of food collected directly in sea (e.g., cephalopods, fish, Wild 1973), and recently Spiekman et al. (2020*b*) suggested that the large space of confluent external nares in in *T. hydroides* could have facilitated a salt gland, although no skeletal correlates were identified for it. The modifications of the nasolacrimal

duct morphology might serve as another example of adaptation of the osmoregulatory system of *Tanystropheus* to life in a marine environment. Further comparative data on the nasolacrimal duct morphology in archosauromorphs are, however, needed to evaluate this hypothesis in more detail;

2) Importantly, all non-tricuspid teeth of *Tanystropheus* are characterised by the presence of apicobasal dental ridges. The role of this trait is not clear, but it has evolved independently numerous times, almost exclusively in taxa that feed within the aquatic environment (McCurry et al. 2019; Mackenzie et al. 2024). Among non-archosauriform archosauromorphs, clearly outlined apicobasal ridges are present only in the fully aquatic trachelosaurid *Dinocephalosaurus orientalis* (Li 2003; Spiekman et al. 2024*a*);

3) If *Tanystropheus* could move on land, it would likely do so with a sprawling gait (Wild 1973; Nosotti 2007), which is further indicated by the three-dimensional morphology of the pelvic girdle, femur, tibia, and fibula of *T. conspicuus* presented here. This mode of locomotion is, however, not supported by the forelimb morphology in *Tanystropheus*. The neck of *Tanystropheus*, together with the expanded musculature at its base, would contribute significantly to the mass of the anterior part of the body of the animal, and yet the humerus is very simplified, with a barely discernible deltopectoral crest (Fig. 35), suggesting a decreased role of the *musculus pectoralis* and *musculus deltoideus clavicularis*. These muscles are generally expanded in Triassic reptiles for which a sprawling gate has been proposed (see Piechowski and Tałanda 2020). In *Macrocnemus*, a close relative of *Tanystropheus* that is widely considered a terrestrial reptile, the deltopectoral crest is noticeably more expanded and formed as a thin, long ridge (see Jaquier et al. 2017). This suggests a more prominent forelimb musculature in *Macrocnemus*, even though its neck was relatively much shorter than in *Tanystropheus* and therefore contributed significantly less to the relative weight of the anterior portion of the body. Moreover, the girdle elements of *Tanystropheus* are relatively delicate and transversely thin, with the thickness of the iliac and scapular blades decreasing distally and never exceeding 5 mm, and usually being much narrower. Furthermore, the girdle bones are generally relatively small, compared to the size of the animal (cf. Nosotti 2007), as in aquatic trachelosaurids (Spiekman et al. 2024*a*, *b*). These characteristics, together with the lack of well-developed muscle attachment sites on the humerus, are contra indicators of terrestrial locomotion. It is unlikely that the appendicular skeleton could support the body of *Tanystropheus* on land, at least for prolonged periods of

time, especially considering the large size of some individuals of *T. conspicuus* and *T. hydroides*.

The centre of body mass of *Tanystropheus* represents a further concern regarding the relatively increased mass of the anterior part of the body, when compared to other tanystropheids. In aquatic tetrapods the centre of body mass is located closer to the centre of buoyancy (usually located near the lungs), which allows for finer control of their body trim in water (Motani and Vermeij 2021). The mass of their forelimbs and the pectoral girdle are consequently increased, with the forelimb and the pelvic girdle being reduced simultaneously, to achieve the anterior displacement of the centre of body mass (see Motani and Vermeij 2021). In *Tanystropheus*, however, the hindlimb, and not the forelimb, was larger and better adapted for propulsion in water (Kuhn-Schnyder 1959; Wild 1973; Tschanz 1986; Nosotti 2007; Renesto and Saller 2018). Although this disagrees with the pattern outlined above, this configuration corresponds with some other long-lived marine reptile lineages that have transitioned into aquatic habitats from terrestrial ones. An excellent example is found within the Thalattosuchia, in which the early diverging forms still possessed relatively gracile limbs and a hindlimb much longer than the forelimb (as in *Tanystropheus*), and their adaptation to life in an (shallow) aquatic environment is undisputed (see Pierce and Benton 2006; Cowgill et al. 2023; Young et al. 2024; Johnson et al. 2025). Moreover, in some fully aquatic trachelosaurids, which are the closest relatives of tanystropheids, the pectoral girdle and forelimbs were not hypertrophied (Liu et al. 2017; Spiekman et al. 2024*a*, *b*). Instead, the anterior displacement of the centre of body mass might have been achieved predominantly through the elongation of the neck, and the resulting mass increase of the anterior portion of the body, as in *Tanystropheus* (see Rytel et al. 2024*b*). There are further similarities between *Dinocephalosaurus orientalis*, *T. conspicuus* and *T. hydroides*, which all had a transversely wide skull with long, conical or recurved teeth, undulating toothrows, an extremely long neck, and lacked an interclavicle (pers. obs. AR; Spiekman et al. 2020*b*, 2024*a*). A study by Gutarra et al. (2022) looked at the body dimensions of long-necked sauropterygians and shown that if trunk dimensions are kept constant while the neck is elongated up to double its length, drag does not significantly increase, although an even more elongate neck, with fixed trunk size, would incur some additional drag. In *Dinocephalosaurus orientalis*, *T. hydroides*, and *T. longobardicus* the neck is around two to three times longer than the torso (pers. obs. AR; Wild 1973; Spiekman et al. 2024*a*) but their trunk volume also increased during their evolution – in *Dinocephalosaurus orientalis* due to the increase in the count of dorsal vertebra, in

Tanystropheus due to the expanded musculature of the cervicodorsal transitional region, and possibly the pelvic region (see Renesto and Saller 2018). Both genera are, therefore, mirroring the body proportions obtained for similarly built aquatic sauropterygians, which would suggest convergence directly related to an aquatic lifestyle.

It is clear that *Tanystropheus* hunted aquatic prey as fish and cephalopod remains have been found in the stomach region of some individuals (Wild 1973). Wild (1973) stated that *Tanystropheus* was likely an extraordinarily efficient swimmer that could pursue even some fast-moving animals. Tschanz (1986) proposed "kinetic inertial feeding" (see Gans 1961, 1969), as seen in extant reptiles, to be the main mode of prey capture and manipulation in *Tanystropheus*. He considered the animal as an aquatic, slow moving ambush predator that caught its prey by suddenly lunging its head forward. Taylor (1989) emphasised that the ambush-strategy of prey capture would suit *Tanystropheus* best if it were not for the long, stiffened neck. Renesto (2005, following Peyer 1931) suggested that *Tanystropheus* hunted from land ("fishing rod hypothesis"), but the later study of Renesto and Saller (2018) concluded that the animal caught its prey in water. Due to the length of the neck, the main bulk of the body, which caused most of the water disturbance, would have been positioned some distance from the small head, allowing the animal to approach its prey by stealth (Renesto and Saller 2018). Spiekman et al. (2020*a*, *b*) and de Souza and Klein (2022) supported this interpretation, stating the active pursuit-predation was very unlikely employed by *Tanystropheus*. Suction feeding was also not considered a plausible mechanism for catching prey because of the presence of highly procumbent and elongate, fang-like teeth, which would interfere rather than aid during suction feeding (Spiekman et al. 2020*a*, *b*). Instead, based on the insights gained from the recently reconstructed skull of *T. hydroides*, Spiekman et al. (2020*a*, *b*) hypothesised that this taxon was an ambush predator which hunted using laterally directed snapping bites. The same strategy is also supported herein for *T. conspicuus*, which is characterised by a similar morphology of the jaws and teeth. Importantly, this hypothesis is not mutually exclusive with the "kinetic inertial feeding" proposed by Tschanz (1986). Nosotti (2007) found the latter strategy to be most plausible for *Tanystropheus*, but wondered whether the neck of the animal might have been too stiff to employ it. More recent studies refute the latter suggestion, as currently we know that there were 13, not 12, cervical vertebrae (Rieppel et al. 2010), and that the base of the neck was inclined and held by strong musculature at its base (see the discussion herein). The anatomy of the transitional cervicodorsal region would allow some flexion and a capacity for storage of

considerable amounts of elastic energy, which could be then released with a protraction of the neck during an attack on prey. It is, therefore, clear that the results of all recent studies on the subject, together with all the aforementioned correlates of an amphibious lifestyle, are congruent with the data provided. They point towards *Tanystropheus* being an ambush predator that caught its prey while fully submerged, employing either lateral snapping or forward lunges of the head.

Concerning the aquatic locomotion mode of *Tanystropheus*, there is currently no consensus on the main propulsion source of this animal. Various studies presented different hypotheses on the subject at various times. Kuhn-Schnyder (1959) was first to point out that the hindlimb was adapted to propelling the animal when it was submerged. Wild (1973) supported this view and suggested that the tail of the animal was only for steering. Tschanz (1986, 1988) considered *Tanystropheus* an axial-subundulational swimmer, in which undulations of the trunk and tail were responsible for most of the propelling force, and were only supported by paddling of the hindlimbs. Renesto (2005) concluded that neither the tail nor the hindlimbs were adapted for efficient swimming. Nosotti (2007) provided an elaborate discussion on the subject, and after analysing the functional morphology of the hindlimb, concurred with Tschanz (1986, 1988) in interpreting lateral undulations of the body as the main propulsion source in *Tanystropheus*. Renesto and Saller (2018) opposed this view, as their reconstruction of the caudal musculature provided arguments (primarily the dorsoventral flattening) against the tail being an efficient propulsion source during lateral undulation. Instead, Renesto and Saller (2018) suggested symmetrical rowing of the hindlimbs as the more likely mode of locomotion. Spiekman et al. (2020*b*) found this hypothesis unlikely, stating that strokes of the hind limbs alone would have not provided sufficient underwater propulsion, and undulatory movements of the posterior portion of the body of *Tanystropheus* must have also contributed to its locomotion. Sennikov (2023, p. 441) noted that tanystropheids had “an anteriorly wide and flat tail”, which could have made its vertical movements a probable source of propulsion in water.

The findings provided herein contribute further insights on the subaqueous propulsion of *Tanystropheus*. The most striking and distinct feature for *T. conspicuus* is the presence of a relatively tall, distally expanded neural spine in many of its vertebrae. This indicates that the tail skeleton of *Tanystropheus* was not dorsoventrally flattened, with the transverse processes and the neural spine in the proximal caudal vertebrae of at *T. conspicuus* being of subequal length (Fig. 26), and the neural spine in the distal tail vertebrae being relatively tall (Fig. 27).

Whereas the tail almost certainly contributed to some extent to the movement of the animal in water, in the absence of a biomechanical analysis its role should not be overstated. The suggestion of Sennikov (2023) concerning the possibility of the tail propelling the animal through vertical movements seems implausible for *Tanystropheus*, considering that in *T. conspicuus* the skeleton of the tail is more expanded dorsally than laterally. As already pointed out by Spiekman et al. (2020*b*), anterior caudal vertebrae with long transverse processes are common in (semi)aquatic reptiles, including those using lateral undulation of the tail, and reflect the presence of well-developed axial muscles. There is, thus, no evidence supporting the hypothesis of Sennikov (2023), especially when also considering that the ancestors of tanystropheids were terrestrial and relied on a sprawling gait for locomotion, which requires axial musculature capable of lateral, not vertical, undulation. Moreover, as mentioned by Renesto and Saller (2018), the complex of long postcloacal bones present in all species of *Tanystropheus* could have considerably impaired the vertical movements of the anterior portion of the tail, which also bears the longest transverse processes. Considering the shared bauplan, it is unlikely that *T. conspicuus* differed significantly from *T. hydroides* and *T. longobardicus* in its mode of underwater propulsion. This makes interpreting the adaptive role of the distal expansion of the neural spine more difficult.

It seems likely that the increased height of the vertebral column aided the lateral undulation of the body, supporting the hypotheses of Tschanz (1986, 1988), Nosotti (2007), and Spiekman et al. (2020*b*). The distal expansion of the neural spine is interpreted as a support structure for cingulate ligaments (Pritchard et al. 2015). The dorsal margin of the neural spine is transversely expanded, flat, and straight in lateral view in virtually all currently accessible dorsal, sacral, and anterior caudal vertebrae of *Tanystropheus*, excluding *T. conspicuus* (Wild 1973, 1980*a*; Dalla Vecchia 2000, 2006; Nosotti 2007; Renesto and Saller 2018). The anterior caudal vertebrae of *T. conspicuus* share this characteristic, but the dorsal margin in all its dorsal and sacral vertebrae is conspicuously dorsally expanded, rounded and strongly convex in lateral view (Figs. 20–21, 24–26). This trait likely arose from the modified neural spine table, which is a feature widely present among archosauromorphs, including many other tanysaurians (e.g., *Dinocephalosaurus orientalis*, *Macrocnemus* spp., *Trachelosaurus fischeri*; see Ezcurra 2016; Pritchard et al. 2015; Renesto and Saller 2018; Scheyer et al. 2020; Spiekman et al. 2021; Spiekman et al. 2024*a*, *b*; pers obs. AR). Renesto and Saller (2018) hypothesised that the expanded dorsal region of the neural spines of *Tanystropheus* supported a supraspinous ligament system that would have stiffened the trunk,

and possibly limited the lateral undulation of the body. Spiekman et al. (2020*b*, 2024*b*) opposed this interpretation, stating that the spine table might have indeed contributed to the ligament system, but the novel data concerning the aquatic trachelosaurids suggest that the stiffening might have stabilised the vertebral column, but likely did not severely affect the efficiency of lateral undulation for propulsion. In the morphology of the distal portion of the neural spine, *T. conspicuus* resembles the trachelosaurid *Trachelosaurus fischeri* more than other *Tanystropheus* species, with the first two tanysaurians sharing the general shape, extent of dorsal expansion, and the presence of distinct transverse rugosities, although the neural spines in *T. conspicuus* are relatively much taller. Whereas lateral undulation was speculated to be the main propulsive source for aquatic trachelosaurids (Spiekman et al. 2024*a*, *b*), these forms have a serpentine vertebral column, which is composed of a far greater number of vertebrae and in its post-cervical section is relatively much longer than in tanystropheids. The distinct neural spine morphology of *T. conspicuus* might, therefore, represent an adaptation to an aquatic lifestyle that is only partially shared by other species of *Tanystropheus*. Alternatively, the evolution of this feature might have been related to the size increase of the animal – *T. conspicuus* is the largest known tanystropheid. With increasing size, the mass of an animal increases exponentially, and further ligament support might have been needed to propel the animal in water and preserve finer control over the vertebral column, and especially the long neck, with the anterior dorsal vertebrae contributing to its movements. This would explain the greater extent of the distal expansion of the neural spine in *T. conspicuus*, but not the other, smaller, species of *Tanystropheus*.

Interestingly, in *T. hydroides* and *T. longobardicus* there is a strong positive correlation between vertebral height and length in the dorsal vertebrae (Fig. 23), similar to the observations of Wild (1973) and Tschanz (1986, 1988). In contrast, within *T. conspicuus* this correlation seems to be much weaker, with the neural spines reaching variable heights for the vertebrae of roughly identical length (Fig. 23). This might be due to larger height differences within a series, or due to more prominent intraspecific variation. Nevertheless, the relatively tall dorsal, sacral, and caudal vertebrae of *T. conspicuus* likely contributed to the more efficient lateral undulation of the body. Corresponding to Tschanz (1986, 1988), Nosotti (2007), and Spiekman et al. (2020*b*), I interpret *Tanystropheus* as an animal that propelled itself underwater mainly by the movements of its trunk and tail. The role of the hindlimbs in locomotion is difficult to assess, and in the future should be analysed through dedicated myological and biomechanical studies, which are feasible with the Miedary material. It can be

stated with confidence that *Tanystropheus* led an aquatic lifestyle within a shallow near-shore habitat, rather than a fully pelagic mode of life. Its skeletal adaptations to underwater propulsion are relatively subtle and do not support pelagic diving (Beardmore and Furrer 2017; Jaquier and Scheyer 2017; Nosotti 2007; Renesto and Saller 2018; Spiekman et al. 2020*a*; Spiekman and Mujal 2023).

Hypodigm of *Tanystropheus conspicuus*

The majority of tanystropheid remains from Miedary are isolated, yet they can all be confidently referred to *Tanystropheus conspicuus* due to their highly diagnostic morphology. The axis ZPAL V. 36/550 from Miedary, originally reported by Czepiński et al. (2023), was not referred to *Tanystropheus* due to several morphological differences compared with the known axes of *Tanystropheus*. With new, more complete, specimens from the same site having been prepared (Fig. 10), this morphological disparity can be attributed to the incomplete preservation of ZPAL V. 36/550, as the specimen falls within the range of intraspecific variation of *T. conspicuus*. Currently there is no evidence for the presence of more than one taxon within the association of tanystropheid remains from the M1, M2 and M4 layers of Miedary. The only non-tanystropheid archosauromorph fossils from these strata include rare isolated ziphodont teeth and an osteoderm of the doswellid *Jaxtasuchus* sp. (see Czepiński et al. 2023). The presence of skeletal elements of a new archosauromorph taxon mentioned by Czepiński et al. (2023) seems to be constrained to the M3 layer, which has not yielded any tanystropheid remains. Whereas the Miedary strata preserve a multitaxic assemblage of archosauromorphs, the remains of *T. conspicuus* are quantitatively dominant. Bones and teeth of this animal can be identified with high confidence due to the morphological similarity to the elements known from articulated individuals of other species of *Tanystropheus* (especially *T. hydroides*). Additionally, several specimens of *T. conspicuus* (Figs. 16, 20; SMNS 13337) preserve partially overlapping portions of the axial and appendicular skeletons between them, which together facilitate the identification of isolated remains based on shared diagnostic features (e.g., rugose distal portion of the neural spine). I refrain from detailed taxonomic identification of some less diagnostic bones (e.g., holocephalous ribs, gastralia, hemal arches, distal caudal vertebrae, autopodial elements) from the CEB, including Miedary, even though at least some likely belong to tanystropheids, as among early archosauromorphs many skeletal elements are morphologically similar and therefore hard to taxonomically identify in isolation. Thus, the hypodigm of *T. conspicuus* currently comprises most of the vertebral column, complete pelvic and pectoral girdles,

stylopodium, zeugopodium, postcloacal bones, ribs, gastralia, several cranial elements and teeth.

Some intraspecific variation is present in the Miedary assemblage, but it does not exceed what might be expected within individuals from one population. For example, some vertebrae of *T. conspicuus* from the same position in the vertebral column differ considerably in the height and curvature of their neural spine (compare Fig. 18A and B; Fig. 23), but they nevertheless share most other morphological characteristics, including the diagnostic distal expansion of the neural spine. No further major morphological deviations can be identified within the material of *T. conspicuus*, including the remains from outside Miedary, which predominantly comprise highly diagnostic elements – vertebrae, teeth, femora and humeri. Importantly, the material referred to this species that originated from Germany and France (including the type series) falls within the size range and the spectrum of morphological disparity seen in the specimens from Miedary. Therefore, specimens from the western part of the CEB, which have been gathered from a multitude of outcrops that record several millions years, do not seem to differ in any taxonomically distinct way from the remains of *T. conspicuus* from Miedary. Moreover, the only paralectotype of *T. conspicuus* known from the eastern part of the CEB, a partial vertebra MB.S.11, originated from Laryszów - a village directly adjacent to the Miedary site. The specimen was found in the Boruszowice Beds, which underlay the strata outcropping in Miedary (von Meyer 1847-1855; Czepiński et al. 2023). Thus, through parsimony and lack of any contrary evidence, all large-sized *Tanystropheus* remains known from the Muschelkalk and Lower Keuper of the CEB, together with all the tanystropheid material from Miedary, can be considered as belonging to one species, and are all referred to *T. conspicuus* herein (see Appendix I).

Re-identification of historic specimens

Through the long and convoluted research history on *Tanystropheus conspicuus* many isolated specimens has been referred to this species, or its junior synonyms. Through comparisons with the novel material described herein, their status is reevaluated, providing an updated and better defined hypodigm of *T. conspicuus*.

Wild (1973) and Spiekman and Scheyer (2019) considered *Chelyzoon blezingeri*, *Chelyzoon latum*, *Procerosaurus cruralis*, and *Thecodontosaurus latespinatus* subjective junior synonyms of *Tanystropheus conspicuus*, and these assessments are upheld here as there are no clear morphological differences between the type material of these taxa and the specimens referred to *T. conspicuus*. I consider two additional taxa as junior synonyms of *T. conspicuus* – *Nothosaurus blezingeri* and *Megacnemus grandis*. The former was erected on the basis of teeth and some postcranial remains, of which only one tooth was illustrated (Fraas 1896, fig. 4), making it the only specimen of the type series that can be reliably identified. I was able to recover this specimen, together with several other teeth labelled as originals of Fraas (1896), selected by R. Wild and registered under the number SMNS 52478. They all exhibited a long root and sparse, uneven, ridges on the crown, clearly belonging to *T. conspicuus* and not to any species of *Nothosaurus*, corresponding with the previous suggestion of Rieppel and Wild (1996) and Rieppel (2000).

Concerning *Megacnemus grandis*, new data on the three-dimensional morphology of tanystropheid limb-bones allow a re-assessment of the affinities of the holotype and the only known specimen (von Huene 1954) – the GPIH 253 humerus (Fig. 35B). This element falls within the known size range of humeri of *T. conspicuus*, being close in length to the largest specimens from Miedary (see Fig. 35). Moreover, despite some deformation, GPIH 253 preserves overall proportions and curvature congruent with the humeri of *T. conspicuus* and is also similar in the shape of the proximal and distal articular surfaces and the absence of a developed deltopectoral crest. The main feature which might differentiate *M. grandis* from *T. conspicuus* is the possible absence of the supinator process in the former (Fig. 35B). This characteristic might, however, be artificial and caused by the preservation of the specimen, with its proximal and distal ends being damaged and missing the portion that included the supinator process. Based on its preservation, von Huene (1954) hypothesized that GPIH 253 likely originated from the Triassic outcrops of Silesia. I agree with this interpretation as the preservation of the specimen is similar to those found in the Muschelkalk. Moreover, the few remaining labelled Triassic vertebrate specimens housed at GPIH, excluding the holotype of

Velocipes guerichi (see Czepiński et al. 2021), all come from Muschelkalk localities of modern-day Poland and Germany. These include specimens from the collections of M. Grunday and G. Gürich, who both gathered thousands of fossils from the Triassic localities of Silesia. Some of those GPIH specimens originated from the Upper Muschelkalk of Tarnowskie Góry ("Tarnowitz"), strata which were the subject of research for G. Gürich (1884, 1887) who worked at the University of Hamburg for many years, after moving there from Silesia. Outcrops of this unit in the area (Laryszów/Larischhof) have yielded cervical vertebrae of *T. conspicuus* including one of the paralectotypes (von Meyer 1847-1855; Langenhan 1903). Taking into account the morphology, size and preservation of GPIH 253 as well as the historic background of the other Triassic vertebrae specimens housed at GPIH, it is very likely that the humerus belongs to *T. conspicuus* and originated from the Upper Muschelkalk of Upper Silesia ("Rybnaer Kalk"), and not from the Lower Muschelkalk of Gogolin as suggested by von Huene (1954). *Megacnemus grandis* is here regarded as a subjective junior synonym of *T. conspicuus*.

Whereas most of the type material of the junior synonyms of *Tanystropheus conspicuus* is still accessible, the holotype of *Chelyzoon latum* was most likely destroyed during the Second World War while deposited in Munich (Wild, 1973; pers. obs. AR). However, I identified two casts of that specimen in the GPIT collection (GPIT-PV-60024 and GPIT-PV-60025). Spiekman and Scheyer (2019) mentioned that the type specimens of both species of *Chelyzoon* appear to be morphologically disparate from the known vertebrae of *Tanystropheus*, yet I concur with Wild (1973) in designating both *Ch. blezingeri* and *Ch. latum* as junior synonyms of *T. conspicuus*. Their type specimens are indistinguishable from the two posteriormost neck vertebrae of *T. conspicuus*, with SMNS 8728 (the holotype of *Ch. blezingeri*) being a twelfth cervical vertebra and the lost holotype of *Ch. latum* a thirteenth cervical vertebra. Specimen ZPAL V. 36/584 (Fig. 16) preserves both corresponding vertebrae from these positions in a tight association with some other remains of a single individual of *T. conspicuus*, which further strengthens the referral of the type material of both species of *Chelyzoon* to this species

Concerning the partial vertebra GPIT-PV-60014, the holotype of *Pectenosaurus strunzi* von Huene, 1902, I concur with R. Wild (specimen label) in reidentifying it as belonging to a sauropterygian, not to *Tanystropheus* (contra Kuhn 1963, 1971; Spiekman and Scheyer, 2019). The vertebra presents no clear archosauromorph features. *Pectenosaurus strunzi* is deemed a *nomen dubium* and not a synonym of *T. conspicuus*.

Von Huene (1902, plate 5; fig. 6) described a long bone of uncertain affinities, found near Bayreuth, which he later (von Huene 1931) considered likely to be a humerus of *Tanystropheus*. Wild (1973) rejected this hypothesis but stated that the bone could not be located. I was able to rediscover the specimen in question in the U-MO collection as an uncatalogued and unlabelled bone. I can confirm confidently that the specimen described by von Huene (1902, plate 5; fig. 6) is not an archosauromorph humerus but rather a partially preserved sauropterygian clavicle articulated with an interclavicle.

An unpublished fragmentary right hemimandible SMNS 56289, originally identified as belonging to *Tanystropheus conspicuus*, served as one of the sources of scoring for *Tanystropheus* in the phylogenetic analysis of Ezcurra (2016). The long, straight bone is indistinguishable from sauropterygian dentaries in its general morphology and proportions. Although the anteriormost part of the dentary is missing, the specimen preserves three large, laterally projecting alveoli and a row of smaller teeth of relatively homogenous size posterior to them. The same pattern is present in *Nothosaurus* (Rieppel and Wild 1996, fig. 63). Considering how closely the *T. conspicuus* dentaries from Miedary resemble those of the *T. hydroides* holotype, SMNS 56289, which differs from both of them significantly, can confidently be stated not to be referrable to *Tanystropheus*. Together with several unpublished ischia (see Appendix I) stored at SMNS and originally labelled as *T. conspicuus*, SMNS 56289 is regarded as belonging to an indeterminate sauropterygian.

Wild (1973) considered the lectotype specimen U-MO BT 740 to be a tenth cervical vertebra. As illustrated herein (Fig. 15), the main feature that differentiates the tenth cervical vertebra from the other neck vertebrae of *Tanystropheus conspicuus* is the continuous and relatively tall neural spine characterised by its undulating, thickened, distal edge. U-MO BT 740 lacks this feature, with its neural spine being well-preserved as a low, narrow ridge that increases in height only in its anterior portion (compare figs. 46 and 47 of Wild 1973). The neural spine height in the tenth vertebra of *T. conspicuus* seems to be affected by ontogeny, with the smallest known specimen SMF R 285 (erroneously identified as an eleventh cervical vertebra by Wild 1973) exhibiting a relatively straight distal edge. The morphology observed in U-MO BT 740 is, however, outside of this spectrum, and the specimen is regarded as a middle cervical vertebra instead. Whereas I find this particular minor reinterpretation worthy of mention due to the lectotype status of this cervical, the full list of specimens, their status, and current identification, can be found within the Appendix I.

Remarks on the characters included in the diagnosis of the genus

Presence of bifurcated ribs in the sacral vertebrae of Tanystropheus

The absence of bifurcated ribs of the second sacral vertebra was regarded as one of the diagnostic features of the genus *Tanystropheus* by Spiekman and Scheyer (2019), following Ezcurra (2016) and concurring with Rieppel (1989). There is no clear indication for the presence of this character in *Tanystropheus* species other than *T. conspicuus*, although in PIMUZ T 2817, one of the specimens referred to *T. hydroides* by Spiekman et al. (2020*b*), a miniscule hook-like posterior expansion of the left partially preserved second sacral rib can be observed (pers. obs. AR). The second sacral vertebra of *Tanystropheus conspicuus* unequivocally possesses a distinct triangular projection, extending posteriorly from the sacral ribs at the same vertical level as the dorsal margin of the posterior articular surface of the centrum. Thus, the absence of bifurcated ribs of the second sacral vertebra is not shared by all species of *Tanystropheus* and is not a diagnostic feature of the genus. The previous diagnosis was based on a misidentification of the sacral vertebra of *T. conspicuus* SMNS 54631 as a second sacral vertebra (Ezcurra 2016, fig. 35A), which is actually a first sacral vertebra (in accord with Wild 1973, fig. 55), and which does indeed lack the bifurcating sacral ribs.

Presence of an interclavicle in Tanystropheus

An ossified interclavicle is present in the majority of early-diverging archosauromorphs (see Spiekman et al. 2021). In *Tanystropheus*, however, no articulated specimen preserves an element that can be unequivocally identified as an interclavicle. Haas (1970) described an isolated interclavicle from Israel that he considered to likely be from *Tanystropheus*. The specimen was later found to belong to *Simosaurus* sp. (Rieppel et al. 1999). Wild (1973) noted the presence of an incomplete elongate bone in a partial skeleton PIMUZ T 2793 and interpreted it as an interclavicle, morphologically disparate from the one published in Haas (1970). This element (Wild 1973, fig. 64) is rod-like for most of its length, but widens to form a thin plate close to the edge of the rock slab. It overlays a proximal part of the third dorsal rib. Nosotti (2007) recognised a fragment of a tentative interclavicle in the *T. longobardicus* specimen MSNM BES SC 1018.

New morphological information provided herein allows for a reinterpretation of the "interclavicle" from PIMUZ T 2793 as one of the first dorsal ribs, which would explain its slight asymmetry as well. The element mentioned by Nosotti (2007) is likely of the same origin. Several partially preserved, isolated bones stored at SMNS, originally identified as

Tanystropheus interclavicles, are disparate in their morphology and their taxonomic affinities are highly uncertain. Therefore, with the multiple articulated and complete skeletons not preserving an interclavicle, and no archosauromorph interclavicle being found in Miedary so far, it can be unequivocally confirmed that the interclavicle in *Tanystropheus*, if it was present in any form, was not ossified. This corroborates the scorings of the phylogenetic analyses of Spiekman et al. (2021, 2024*a*). Among tanysaurians in which this character can be assessed, only *Dinocephalosaurus orientalis* and *Ozimek volans* Dzik and Sulej, 2016 lack an ossified interclavicle (Dzik and Sulej 2016; Spiekman et al. 2024*a*).

Presence of subcentral foramina in Tanystropheus

Spiekman et al. (2021) stated that among all archosauromorph taxa analysed therein for which this character could be assessed, conspicuous foramina on the ventral side of the cervical vertebrae are present only in *Tanystropheus conspicuus*, but their absence in other species of *Tanystropheus* cannot be confirmed either. These subcentral foramina were recently shown to be associated with intersegmental arteries that ran within the vertebrae (see Rytel et al. 2024*b*). The presence of this character can be unequivocally confirmed in the three-dimensionally preserved material referred to *Tanystropheus* sp., from the sites in Hungary (Ősi et al. 2020), NE Italy (Dalla Vecchia 2006; pers. obs. AR), Romania (Jurcsak 1975; pers. obs. AR) and small-sized vertebrae from the Lower Keuper of Germany (Schoch 2015, fig. 10.7C; Spiekman and Scheyer 2019, supp. inf.; pers. obs. AR). In the articulated specimens from Monte San Giorgio and China the existence of the subcentral foramina is difficult to assess due to the ventral side of the vertebrae rarely being visible. Interestingly, Wild (1980*a*) described PIMUZ T 3901 as having foramina on the lateral side of the cervical vertebrae, near the midpoints of their anteroposterior length. It is very likely that these foramina are homologous to subcentral foramina of other *Tanystropheus* species, and it is only due to diagenetic alteration of the original morphology that they appear as if located on the lateral side of the centrum. Similarly, PIMUZ T 2819 preserves some three-dimensional information and was prepared in such a way that deep pits are visible on the ventral side of the centra, at an identical relative location as the subcentral foramina in other species of *Tanystropheus*. PIMUZ T 3901 was referred to *T. longobardicus* by Spiekman and Scheyer (2019) and PIMUZ T 2819 was referred to *T. hydroides* by Spiekman et al. (2020*a*). Therefore, the existence of subcentral foramina on the ventral surface of postaxial cervical vertebrae can be confirmed for all three valid species of *Tanystropheus* as well as in most other specimens in which the presence of this character could be assessed.

Reduction of the neural spine in the cervical vertebrae of Tanystropheus

An extreme elongation of a vertebra is usually accompanied by a reduction in neural spine height, resulting in convergently similar morphologies. This is evident when comparing the cervical vertebrae of tanysaurians and azhdarchid pterosaurs, which, despite being comparable in general vertebral shape, exhibit clear differences in their internal anatomy, thereby indicating different biomechanical means for accommodating their extreme proportions (see Rytel et al. 2024*b*). Whereas the neural spine in the middle section of the middle cervical vertebrae of *Tanystropheus* is extremely low, histological and microanatomical studies prove that it was not lost, but rather embedded in a thick cortex (Rytel et al. 2024*b*). Thus, it cannot be regarded as "completely reduced" but rather only "virtually completely reduced", as interpreted in some studies (e.g., Pritchard et al. 2015). The neural spine is present along the entire length of the middle cervical vertebrae of *Tanystropheus*, despite not being outlined in the middle sections of some of them.

Femur/humerus length ratio in Tanystropheus

Whereas Spiekman et al. (2021) found the ratio of the total length of the humerus versus the total length of the femur between 0.84 and 0.91 to be one of the synapomorphies present in *Tanystropheus*, this character is not included in the emended diagnosis herein. The articulated specimens from Monte San Giorgio area display a different state for this character, with the mentioned ratio reaching values from around 0.63 to around 0.76 (pers. obs. AR). These values are generally congruent with the measurements of Spiekman et al. (2021, supplementary material) and are similar to those present in other early-diverging archosauromorphs studied therein, thus not constituting a diagnostic character for *Tanystropheus*.

Presence of the postcloacal bones in Tanystropheus

In some articulated and largely complete individuals of *Tanystropheus* of various size (GMPKU P 1527, PIMUZ T 1270, PIMUZ T 1277, PIMUZ T 1307, PIMUZ T 2817) four elongate elements arranged in two pairs are present posterior to the pelvic girdle. These ossifications are absent in several other similarly sized individuals with a well preserved pelvic region (e.g., MSNM BES SC 265, PIMUZ T 2483, PIMUZ T 2791, PIMUZ T 2818). Wild (1973, p. 123) already noted that the presence of this feature is due to sexual dimorphism, interpreting these "calcified cartilage rods" as "penile elements". Rieppel (1976)

suggested that they are likely post-cloacal bones, a hypothesis that Wild (1980*a*) later supported.

Post-cloacal elements, as defined by Russell et al. (2016), are subcutaneous, mineralised (or at least radio-opaque) structures located in the base of the tail of some squamates (geckos, xantusiids) and lissamphibians (caecilians). In extant animals only the males bear them. The postcloacal bones are used during copulation but their specific function remains relatively poorly understood (Rieppel 1976; Russell 1977; Russell et al. 2016). The study of Jaquier and Scheyer (2017) has shown that the postcloacal bones in *Tanystropheu*s have no cartilaginous precursor, and are bony elements, similar to structures that have been reported for the postcloacal bones of geckos, but unlike caecilians (Russell et al. 2016).

Among all archosauromorphs, only one other tanystropheid, *Tanytrachelos ahynis* Olsen, 1979, shares the presence of postcloacal bones with *Tanystropheus* (Olsen 1979; Casey et al. 2007). In both taxa there are two pairs of elongate, anteroposteriorly oriented elements. Whereas the complex postcloacal apparatus in Tanystropheidae has likely evolved only once, as *Tanystropheus* and *Tanytrachelos* seem to be closely related (see Spiekman et al. 2021), the later development of a similar anatomical feature in squamates appears to be convergent (contra Wild 1973). When compared to geckos, in which the postcloacal bones are relatively well-studied, the elements present in tanystropheids are relatively much larger, less mediolaterally expanded, and of more constant length within the whole apparatus (Wild 1973; Rieppel 1976; Russell 1977; Olsen 1979; Wild 1980*a*; Kluge 1982; Russell et al. 2016). The homology between the postcloacal bones in squamates and tanystropheids is likely purely functional, although further finds of early reptiles with associated postcloacal bones could change this interpretation.

Olsen (1979) suggested that the ossifications in *Tanytrachelos ahynis* were characteristic to females and might have served a role of an egg pouch support, but it seems more parsimonious to concur with Wild (1973, 1980*a*) in attributing them to males, as observed in the extant squamates. In an animal of such extraordinary proportions as *Tanystropheus*, copulation might have demanded an additional structure that would serve as an attachment point for tissues associated with the copulatory organ of the male. Regardless of their function and distribution between the sexes, the postcloacal bones documented in all three species of *Tanystropheus* and *Tanytrachelos ahynis* give additional insights into the dimorphic features found among the early members of Archosauromorpha. Further indications for sexual dimorphism have also been reported from all other major clades of non-

archosauriform archosauromorphs – some rhynchosaurians (different body proportions, see Chatterjee 1974; Benton 1983), the allokotosaurian *Shringasaurus indicus* Sengupta, Ezcurra and Bandyopadhyay, 2017 (presence of horns in some specimens), and possibly in the trachelosaurid *Dinocephalosaurus* (size difference between mature individuals; Liu et al. 2017; Spiekman et al. 2024*a*). Therefore, it seems that sexual dimorphism in Triassic archosauromorphs was not uncommon and was expressed in diverse osteological forms. In combination with the already described articulated specimens of *Tanystropheus* with the postcloacal apparatus preserved in situ, the newly reported isolated postcloacal bones from Miedary (Fig. 45) will allow for a more comprehensive analysis of the function of these elements in the future.

Biogeographic distribution of *Tanystropheus conspicuus*

The earliest described specimens of *Tanystropheus* originated from Europe, specifically France, Germany, Poland (von Meyer 1847-1855; von Huene 1907-1908), Italy, and Switzerland (Bassani 1886; Peyer 1931). Outside of the CEB and the sites of Monte San Giorgio, remains of *Tanystropheus* have so far been reported from Canada (Sues and Olsen 2015), China (Li 2007; Rieppel et al. 2010), Hungary (Ősi et al. 2020), Israel (Peyer 1955; Rieppel 2001), several further localities in Italy (Dalla Vecchia 2000, 2006, 2008; Dalla Vecchia and Avanzini 2002; Dalla Vecchia and Simonetto 2018), Romania (Jurcsak 1973, 1975, 1978) and Saudi Arabia (Vickers-Rich et al. 1999), giving the genus a Tethys-wide spatial range of occurrence (Spiekman and Scheyer 2019). The Polish sites constitute the northernmost confirmed occurrence of *Tanystropheus*, being located on higher palaeolatitudes than the sites from the western side of the CEB, due to the counterclockwise rotation of the tectonic plates that formed this portion of Pangaea relative to the modern day (see Nawrocki and Szulc 2000; Scotese 2014).

Whereas material of *T. hydroides* might potentially be present both in Europe and in China (Spiekman et al. 2020*a*), the finds of *Tanystropheus conspicuus* are palaeobiogeographically constrained to the CEB (Fig. 47). Remains of the latter species are widespread in the upper Anisian – upper Ladinian outcrops of the basin. The first appearance of *T. conspicuus* is near the base of the Upper Muschelkalk (lower Trochitenkalk Formation of Bad Sulza in Germany), and its last record can be found in the uppermost stratum of the Lower Keuper (Grenzdolomit, uppermost Erfurt Formation of Molsdorf and Hoheneck in Germany). Overall, the taxon is known from around 70 localities (see Appendix I). The prevailing majority of these sites are located in Germany, forming three clusters (Fig. 47) –

one north of Stuttgart, one in Bavaria (Upper Franconia, Bayreuth area), and the third in Thuringia (around Erfurt). From among other localities, an ilium and a vertebra have been found in north-western Germany (Horn-Bad Meinberg and near Göttingen), several specimens have been described from four sites in Alsace and Lorraine (France), and the material from Laryszów and Miedary in Upper Silesia (Poland) is reported herein. An additional vertebra potentially belonging to *T. conspicuus* has been found in an Upper Muschelkalk quarry in Lamerden in Hesse, near the border with North Rhine-Westphalia (Germany, see Diedrich 2015) and a Lettenkeuper outcrop in Kościelec (nowadays a part of Chrzanów, Lesser Poland) has yielded a large postzygapophysis with a prominent epipophysis ZPAL P. VIII (*partim*), reminiscent of that of *Tanystropheus*.

The remains of *Tanystropheus conspicuus* are, therefore, relatively evenly spatially spread within the accessible Upper Muschelkalk-Lettenkeuper sites of the CEB. They seem to be much less common in the northern part of Germany, possibly due to sampling bias, as some additional privately-held specimens (pers. obs. AR) suggest the occurrence of *T. conspicuus* is more common and widespread than documented by the material from public collections. Thus, throughout the existence of this taxon its range of occurrence likely covered most of the CEB. Among all the aforementioned material reported from outside of the CEB, no specimen is morphologically more similar to *T. conspicuus* than to *T. hydroides* or *T. longobardicus*, and none of them reached the size range of the larger individuals of *T. conspicuus*. This implies that the latter species might have been endemic to the CEB. Largely due to the sedimentary record in the region in the Middle Triassic, *T. conspicuus* is currently the species of *Tanystropheus* with the longest and most continuous unambiguous fossil record, encompassing several millions years from the late Anisian to the late Ladinian. This suggests that *Tanystropheus* was well adapted to living in the environments of the CEB (contra Wild 1980*b*).

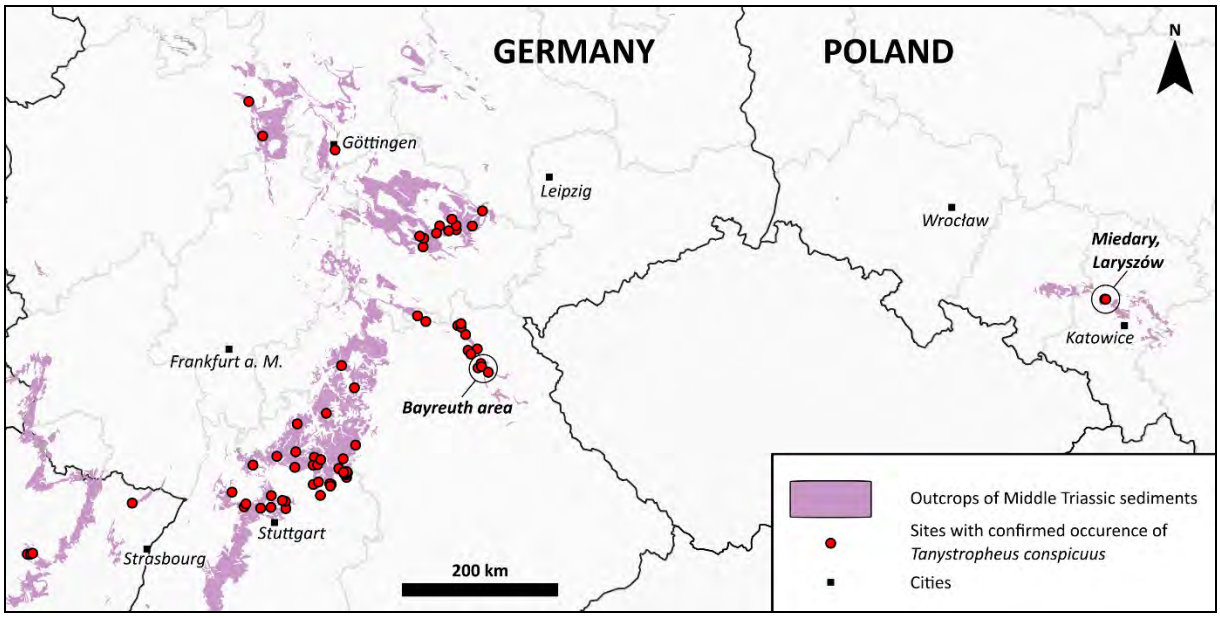

Fig. 47. Map of Central Europe with the outcrops of Middle Triassic sediments and the occurrences of *Tanystropheus conspicuus* marked. Outcrops in Poland based on Marks et al. (2022), and the rest on the Geologische Karte der Bundesrepublik Deutschland 1:1 000 000, created by the BGR (version 2024-04-23). For Poland the Middle Triassic outcrops are visible, and the rest of the marked area signifies the presence of the following strata, with the stratigraphy assigned by the BGR: Muschelkalk undivided, Upper Muschelkalk, Muschelkalk and Keuper undivided, Lower Keuper. Labelled localities represent the sites from which the type material derives (Bayreuth area, Laryszów) and the site with the largest amount of specimens (Miedary). For the full list of included localities refer to the Appendix I.

Co-occurrence of small and large sized individuals of *Tanystropheus* in the Central European Basin

To estimate the total body size of an animal, we have to consider the allometric growth of some of its body parts. Whereas in *T. hydroides* and *T. longobardicus* allometric growth can be noted for the cervical vertebrae (Tschanz 1986, 1988), humeral and femoral length seems to increase roughly isometrically to the total body length of the animal (pers. obs. AR). The largest limb bones of *Tanystropheus conspicuus* are around 1.5 times longer than those of the largest known complete and articulated individual of *T. hydroides*, PIMUZ T 2818, which measured slightly over 4 m in length. Thus, the known maximal total body length for *Tanystropheus* is estimated at over 6 m. This is also supported by the size of the vertebrae from Miedary, the largest of which (ZPAL V. 36/182) has a nearly 40 cm long centrum. The relatively smallest element referred to *T. conspicuus*, a cervical vertebra ZPAL V. 36/181, is around eight times smaller, with its centrum measuring 49 mm. It is likely a ninth or tenth

cervical vertebra as its neural spine is relatively tall in its mid-posterior portion (see Rytel et al. 2024*b*, fig. 7). Cervical vertebrae nine and ten of nearly the exact same size are present in the neotype of *T. longobardicus*, PIMUZ T 2791, a largely complete and articulated individual with an estimated total body length of around 85 cm (pers. obs. AR; Wild 1973). As the body proportions of all *Tanystropheus* species are generally similar, the individual to which the ZPAL V. 36/181 vertebra belonged was likely similar in size to PIMUZ T 2791. Hence, the estimated value of total body length ratio between the largest and the smallest known individuals of *T. conspicuus* equals around seven. In *T. hydroides* and *T. longobardicus* this value equals less than three – PIMUZ T 2792 (around 190 cm) versus PIMUZ T 2793 (around 5 meters) for the former and PIMUZ T 2481 (around 55 cm) versus PIMUZ T 1277 (around 145 cm) for the latter, based on estimates of Wild (1973) and complemented by the measurements made by the author. Most diagnostic features for *Tanystropheus* species from Monte San Giorgio refer to their cranium, and thus specimens not preserving the skull can only be referred to a species based on size (Spiekman and Scheyer 2019; Spiekman et al. 2020*b*). Hence, some size-overlap might exist but cannot be confirmed due to the preservation characteristics of this material.

The size range of *T. conspicuus* ranges from the equivalent of medium sized individuals of *T. longobardicus* (total body length under 1 m) to individuals larger than the largest known specimens referred to *T. hydroides* (total body length over 6 m). Some potential lines of arrested growth are already present in ZPAL V. 36/181 (Rytel et al. 2024*b*, fig. 8B), implying that this juvenile might have already gone through several cycles of growth, and the neonates were certainly even smaller. It is therefore possible that some of the specimens previously considered referable to *T. longobardicus* based on size, and lacking any associated cranial material, are in fact juveniles of *T. hydroides*. Further research on the ontogenetic variation of postcranial remains of all three species of *Tanystropheus* is needed to evaluate this hypothesis but should be preceded by broader studies on intra- and interspecific variation of these forms.

The Ladinian sediments of Germany have yielded small teeth, characterised by their tricuspid morphology – with one centrally located large central cusp flanked both distally and mesially by a small accessory cusp. Some of these specimens have been previously referred to ?Cynodontia, *T*. cf. *meridensis* (=*Tanystropheus* cf. *T. longobardicus*), or *Tanystropheus* sp. (Wild 1980*a*; Dorka 2002; Löffler et al. 2007; Schoch 2015; Schoch et al. 2018; Spiekman and Scheyer 2019). This tooth morphotype appears throughout the entire Lettenkeuper

sequence, from its lowermost (Grenzbonebed) to its uppermost (Grenzdolomit) strata, but it is currently not known from the underlaying Muschelkalk sediments (pers. obs. AR). Most of these specimens documented to date originated from the Vellberg-Eschenau locality in Baden-Württemberg, with Layer 6 of the Untere Graue Mergel being their most productive source. The same stratum at this site has yielded small *Tanystropheus* sp. vertebrae mentioned by Schoch (2015), Schoch et al. (2018) and Spiekman and Scheyer (2019). Importantly, a postcloacal bone and several teeth here referred to *Tanystropheus conspicuus* also originate from the Untere Graue Mergel of Vellberg-Eschenau. Another tooth morphotype represented by several specimens (e.g., SNSB-BSPG 1973 VII 85) found only in the western part of the CEB, is seemingly intermediate between the previously mentioned tricuspid teeth and the specimens referred to *T. conspicuus* herein. Most of the crown in this morphotype is indistinguishable from those of *T. conspicuus*, but miniscule mesial and distal cusps are present. The taxonomic affinities of these teeth might be revealed in future, if they are found preserved in jaw fragments.

Both the small cervical vertebrae of *Tanystropheus* sp. and the tricuspid teeth from the Lettenkeuper of Germany are reminiscent in size and morphology to those of *T. longobardicus*, as mentioned in previous studies (Wild 1980*a*; Dorka 2002; Schoch 2015; Schoch et al. 2018). Whereas the cervical vertebrae are not diagnostic to the species level in *Tanystropheus* (excluding *T. conspicuus*), the presence of tricuspid teeth is a clear autapomorphy of *T. longobardicus*. Although a dentitions of similar morphology were present in basal pterosaurs and some cynodont synapsids (Hahn et al. 1984; Dorka 2002; Schoch 2015; Schoch et al. 2018), only Hahn et al. (1984) compared teeth of these three groups directly. The chronostratigraphically youngest specimen referred to *T. longobardicus* originated from the Cassina beds of the Meride Limestone, on the Swiss side of Monte San Giorgio (Wild 1980*a*; Spiekman et al. 2021). The $^{206}Pb/^{238}U$ age of 240.63 ± 0.13 Ma was assigned to Cassina beds by Stockar et al. (2012), making this interval contemporaneous with the lower Lettenkeuper strata of the CEB (Hagdorn et al. 2015*a*; Hagdorn and Simon 2020). Thus, it would seem most parsimonious to assume that the association of the small-sized *Tanystropheus* sp. vertebrae and the tricuspid teeth is due to the presence of a form very similar to *T. longobardicus*, or this species itself, in the Ladinian of Germany. This animal would co-occur with *T. conspicuus* in the western part of the CEB, demonstrating that the presence of two different-sized forms of *Tanystropheus* in one environment was characteristic not only to Monte San Giorgio (Spiekman et al. 2020*a*). Other possible cases of this

phenomenon include the *Tanystropheus* material from Makhtesh Ramon in Israel (Rieppel 2001) and the Falang Formation in China (Li 2007; Rieppel et al. 2010).

In Miedary some small cervical vertebrae have been found but they represent juveniles of *Tanystropheus conspicuus*, as evidenced by their microanatomy (see Rytel et al. 2024*b*). No tricuspid teeth have been identified despite intensive research on the vertebrate microremains from the site (Pawlak et al. 2022). Miedary is, however, older than the Lettenkeuper sites in the western part of the CEB (see Czepiński et al. 2023) and more distant from the sites from which *T. longobardicus* is known. It is possible that migration of the smaller *Tanystropheus* form occurred later during the Ladinian. Its appearance might have been connected to the environmental turnover of the CEB during the Muschelkalk-Keuper sedimentation transition, during which terrestrial habitats became increasingly more prevalent (see Franz et al. 2013).

To verify the likely presence of a second, small, species of *Tanystropheus* in the CEB, future research should be carried out to determine the ontogenetic age of the small cervical vertebrae from Vellberg-Eschenau as well as the comparative analysis of the tricuspid teeth and dentary morphologies in the Middle Triassic taxa. If in future remains of the small-sized *Tanystropheus* from the Lettenkeuper of Germany are referred to *T. longobardicus*, and the Chinese specimen GMPKU P 1527 *Tanystropheus* cf. *T. hydroides* (see Rieppel et al. 2010; Spiekman et al. 2020*b*) can be referred to *T. hydroides*, then both of these species, together with *T. conspicuus*, would have a very similar temporal ranges – late Anisian to late Ladinian. For now, I refrain from reassessing the original taxonomic identification of the aforementioned specimens.

Conclusions

The novel early Ladinian site in Miedary (southern Poland) has yielded a diverse assemblage of bones and teeth, including hundreds of elements referred here to *Tanystropheus conspicuus*. Based on these remains, combined with all the previously published specimens of *T. conspicuus*, this species is here no longer regarded as a *nomen dubium*. It differs distinctly from other species of *Tanystropheus* in several important characters, including the expansion of the distal portion of the neural spines in the torso, the posterodorsal extension of the scapular blade, and its large size, with the longest individuals likely reaching over six meters in total body length. The newly reported cranial elements constitute the first record of skull bones of *Tanystropheus* from outside of Monte San Giorgio, and provide important insights into the interrelationships of *Tanystropheus conspicuus*, *Tanystropheus hydroides*, and

Tanystropheus longobardicus. Whereas *Tanystropheus conspicuus* appears to be closely related to *T. hydroides* if we only take into account the cranial features, *T. longobardicus* and *T. hydroides* are more similar to each other, and disparate from *T. conspicuus*, in many aspects of their postcranial morphology (Figs. 23, 34). This provides valuable insights into the interrelationships of these taxa, and demonstrates a mosaic of features present among the three valid species of *Tanystropheus*. Future studies should focus on studying their inter- and intraspecific variation, assessing which morphological characters result from ontogenetic or size differences, and which might be phylogenetically significant.

This work will facilitate the identification of archosauromorph remains from a broader range of geographical areas. The first comprehensive evaluation of the three-dimensional morphology of *Tanystropheus* remains from the CEB allows for a better assessment of similar material from other regions (e.g., Jurcsak 1973; Vickers-Rich et al. 1999; Rieppel 2001; Dalla Vecchia 2000, 2006, 2008; Sues and Olsen 2015; Ősi et al. 2020). For now, *Tanystropheus conspicuus* seems to be endemic to the CEB, but further detailed study on the aforementioned material might bring additional insights into the evolution and spread of *Tanystropheus* throughout the marine realm of the Tethys. Moreover, the material described here is also suitable for future research on myology, histology, pathologies, sexual dimorphism, biomechanics, propulsion style and other aspects of the biology of *Tanystropheus*, which were previously mostly constrained by the preservation characteristics of known remains.

The environmental characteristics recorded at the Miedary site (specifically within layers M1, M2, and M4, see Czepiński et al. 2023) are a good proxy for inferring the preferred habitat of *Tanystropheus*. The number of elements of this animal recovered at Miedary, their diversity, and state of preservation, all point towards over 20 individuals of *T. conspicuus* dying, and likely living, in close proximity to the current excavation site. Previously known localities from which the remains of *Tanystropheus* were reported seem to be positioned further away from the actual habitat of the animal (Renesto 2005; Beardmore and Furrer 2017). Studying the fossil assemblage of Miedary, and the faunistic components contained within it, will bring us closer to understanding the trophic connections between *Tanystropheus* and the other taxa coinhabiting this environment. It is still an open question how constrained the niches occupied by various Middle Triassic aquatic long-necked piscivorous reptiles (nothosaurids, pistosaurids, *Tanystropheus*, trachelosaurids) were, and how their convergent evolution affect their emergence, success, and later disappearance.

Thanks to the material from Miedary the status of *Tanystropheus conspicuus* changes from an obscure and dubious taxon based on fragmentary, isolated bones to one of the better documented Triassic archosauromorphs. It is known from over a thousand of specimens. These are mostly isolated elements, but they include some articulated remains. *Tanystropheus conspicuus* is the largest tanystropheid known to date, and one of the longest Middle Triassic reptiles. There are multiple lines of evidence for its aquatic lifestyle (e.g., depositional environment, dental morphology, reduced deltopectoral crest, etc.), and no clear indication for terrestrial locomotion. This is congruent with hypotheses from previous studies on *Tanystropheus* (Tschanz 1986; Nosotti 2007; Rieppel et al. 2010; Beardmore and Furrer 2017; Jaquier and Scheyer 2017; Renesto and Saller 2018; Spiekman et al. 2020*a*, *b*; Spiekman and Mujal 2023; Rytel et al. 2024*b*). Virtually all our current knowledge on this genus points towards it being a (semi)aquatic ambush predator that lived and hunted in shallow marine or brackish waters. Its ability to walk on land is difficult to assess – it might have reproduced on land but the evolution of viviparity in the slightly older, closely related taxon, *Dinocephalosaurus* (Li et al. 2017b; Liu et al. 2017), makes even this inference uncertain.

Chapter II

Unique internal anatomy of vertebrae as a key factor for neck elongation in Triassic archosauromorphs

Edited postprint version of the article: Rytel, A., Surmik, D., Szczygielski, T., Spiekman, S.N.F., Kamp, T. Van De, Zuber, M. and Scheyer, T.M. 2024b. Unique internal anatomy of vertebrae as a key factor for neck elongation in Triassic archosauromorphs. *Zoological Journal of the Linnean Society* 202 (3): zlae126.

Adam Rytel[1,2,*], Dawid Surmik[3,*], Tomasz Szczygielski[1], Stephan N.F. Spiekman[4], Thomas van de Kamp[5,6], Marcus Zuber[5], Torsten M. Scheyer[2]

[1] Institute of Paleobiology, Polish Academy of Sciences, Twarda 51/55, 00-818 Warsaw, Poland

[2] Department of Paleontology, University of Zurich, Karl Schmid-Strasse 4, 8006 Zurich, Switzerland

[3] Institute of Earth Sciences, Faculty of Natural Sciences, University of Silesia in Katowice, Będzińska 60, 41-200 Sosnowiec, Poland

[4] Staatliches Museum für Naturkunde Stuttgart, Rosenstein 1, 70191 Stuttgart, Germany

[5] Institute for Photon Science and Synchrotron Radiation (IPS), Karlsruhe Institute of Technology (KIT), Hermann-von-Helmholtz-Platz 1, 76344 Eggenstein-Leopoldshafen, Germany

[6] Laboratory for Applications of Synchrotron Radiation (LAS), Karlsruhe Institute of Technology (KIT), Kaiserstraße 12, 76131 Karlsruhe, Germany

* – corresponding authors: adam.rytel@twarda.pan.pl, dawid.surmik@us.edu.pl

Introduction

The period following the End-Permian Mass Extinction saw the appearance, diversification, and radiation of several vertebrate lineages that became major components of later faunas (e.g., Foth et al. 2016; Ezcurra and Butler 2018; Simões et al. 2018; Benton and Wu 2022; Laboury et al. 2023; Sues and Schoch 2023). Among the Mesozoic tetrapods, diapsids achieved the most extensive evolutionary success, giving rise to the lineages that dominated terrestrial (non-avian dinosaurs, pseudosuchians, non-mosasaur squamates),

aquatic (sauropterygians, ichthyosaurs, mosasaurs), and aerial (pterosaurs, birds) environments. Members of these groups evolved derived adaptations to the niches they occupied and adopted new, unique bauplans. In the Triassic, one the most ecologically diverse clades of vertebrates were the tanysaurians (Tanysauria), a group of early-diverging archosauromorphs (Spiekman et al. 2024*b*). The Tanysauria contained terrestrial (e.g., Rieppel 1989; Renesto 1994), aquatic (e.g., Spiekman et al. 2024*a, b*), and possibly gliding (Dzik and Sulej 2016) forms. Members of this group exhibited substantial neck elongation, achieved through either cervical vertebrae count increase (trachelosaurids, see Spiekman et al. 2024*a, b*) or the hyperelongation of the cervicals (tanystropheids, see Wild 1973; Nosotti 2007; Dzik and Sulej 2016; Spiekman and Scheyer 2019; Spiekman et al. 2021). The first described and widely known tanysaurian *Tanystropheus* demonstrated an extreme extent of the latter condition, with its cervicals being over 10 times longer than tall (Fig. 1A–B; Spiekman and Scheyer 2019; Spiekman et al. 2021) and its neck constituting about half of the total body length in large individuals (AR pers. obs.; Wild 1973; Tschanz 1988). The lifestyle of *Tanystropheus* spp. remains not fully resolved, with recent developments in the subject pointing towards it being a shallow marine ambush predator (Nosotti 2007; Beardmore and Furrer 2017; Renesto and Saller 2018; Spiekman et al. 2020*a, b*). Currently, the main skeletal feature not in keeping with the inferred aquatic habitat is the internal structure of the cervical vertebrae, which are preserved as hollow inside, potentially implying a more terrestrial lifestyle (Broili 1915; Edinger 1924; Renesto 2005; Jaquier and Scheyer 2017).

Despite the internal anatomy of tanysaurian cervicals being widely known and acknowledged as unique (von Meyer 1847– 1855; von Huene 1907–1908; Broili 1915; Edinger 1924; Wild 1973; Dalla Vecchia 2000; Rieppel 2001; Renesto 2005; Nosotti 2007; Dzik and Sulej 2016; Jaquier and Scheyer 2017; Formoso et al. 2019; Spiekman and Scheyer 2019; Miedema et al. 2020; Spiekman et al. 2020*a*), its function and evolution have never been investigated in detail. The distinct internal anatomy of the vertebrae was noted already in the original description of *Tanystropheus conspicuus* von Meyer, 1852. von Meyer (1847–1855) hypothesised that the internal cavity was filled with vascularised soft tissue, whereas the spinal cord developed as a series of intervertebral ganglia, located in the anterior and posterior concavities of the neural arch (see Edinger 1924). von Huene (1907–1908) corrected this interpretation, reporting on the neural canal being located more conservatively, between the centrum and the neural arch, and being ventrally floored by bone in its anteroposteriorly terminal sections, with only a hypothetical ‘delicate periosteum’ in the middle. Broili (1915)

described the internal vertebral anatomy in more detail, noting the presence of some bony trabeculae inside of one of the vertebrae, and hypothesising that the other specimens are devoid of them due to post-mortem alterations. Research on the subject was summarised by Edinger (1924), who stated that the spinal cord ran within the vertebral centra of *T. conspicuus*, a feature unique among vertebrates. All of these authors considered the vertebrae of *Tanystropheus* spp. to be 'dinosaur' caudals. It was not until the articulated specimens from Monte San Giorgio were described (Peyer 1931) that the true nature of these bones was revealed. Wild (1973) provided a comprehensive summary of previous studies on the biology of *Tanystropheus* spp., as well as many additional insights on this subject. According to Wild (1973), the spinal cord in the cervicals of *Tanystropheus* spp. ran within the centra, and its course changed ventrodorsally along the anteroposterior axis of the neck (like a 'garland'), reaching the ventral surface of the internal cavity shortly after entering the vertebra.

Jaquier and Scheyer (2017) were the first to comparatively investigate tanysaurian histology by sampling, among others, cervicals of *Macrocnemus bassanii* Nopcsa, 1930 *and Tanystropheus* spp., revealing the generally homogenous, compact structure of the bone walls of these vertebrae. Recent studies employing phase-contrast synchrotron computed tomography provide insights into the internal morphology of the axes of *Macrocnemus bassanii* and *Tanystropheus hydroides* Spiekman, Neenan, Fraser, Fernandez, Rieppel, Nosotti, & Scheyer, 2020, which revealed the tubular structure of the anteriormost postatlantal cervicals (Miedema et al. 2020; Spiekman et al. 2020*a*). Similar anatomy can also be observed in the elongate cervicals of other tanysaurians—*Augustaburiania vatagini* Sennikov, 2011 from the late Olenekian of Russia (AR pers. obs.; Sennikov 2011), *Czatkowiella harae* Borsuk-Białynicka & Evans, 2009 from the late Olenekian of Poland (T. Szczygielski pers. obs.; Borsuk-Białynicka and Evans 2009), a putative tanysaurian *Microcnemus efremovi* von Huene, 1940 from the Early Triassic of Russia (von Huene 1940), the Moenkopi Formation tanystropheid from the early Anisian of the USA (Formoso et al. 2019), *Ozimek volans* Dzik & Sulej, 2016 from the late Carnian of Poland (Dzik and Sulej 2016), and *Tanytrachelos ahynis* Olsen, 1979 from the late Carnian of the USA (Spiekman et al. 2021), as well as the Homestead tanystropheids from the early-mid Norian of the USA (Heidenfelder et al. 2023). Thus, the observed 'hollowness' of the cervicals is potentially a characteristic feature of all tanystropheids and possibly non-tanystropheid tanysaurians, despite their disparate lifestyles, as well as the wide temporal (Early to Late Triassic) and spatial (North America to China) range of occurrence of the mentioned taxa. Therefore, it can be hypothesized that this unique

vertebral anatomy was an important adaptation correlated with substantial neck elongation—a feature shared by all tanysaurians to at least some extent. Due to their elongation, the presence of the ‘shaft’ and internal cavity, the cervical vertebrae of some tanystropheids (e.g., *Tanystropheus* spp., *Ozimek volans*) are similar in their general structure to long bones of avemetatarsalians, not only in their superficial anatomy, but potentially also the internal structure and biomechanical properties. This resemblance allows for intriguing comparisons with extant and extinct animals, but to further explore this phenomenon and its origin, broader and more detailed sampling was needed. Previous studies have been constrained by the scarcity of available three-dimensionally (3D) preserved material (Broili 1915; Wild 1973; Jaquier and Scheyer 2017), but the newly identified material from Silesia in southern Poland (Surmik et al. 2016; Czepiński et al. 2023) allows for a more extensive and holistic approach. Herein, we describe the internal anatomy of the cervical vertebrae of *Tanystropheus* spp. and ‘*Protanystropheus*’ *antiquus*, employing both traditional sectioning and computed tomography (CT) scanning, to trace the evolution and function of the extensive modifications of the vertebral anatomy in tanysaurians.

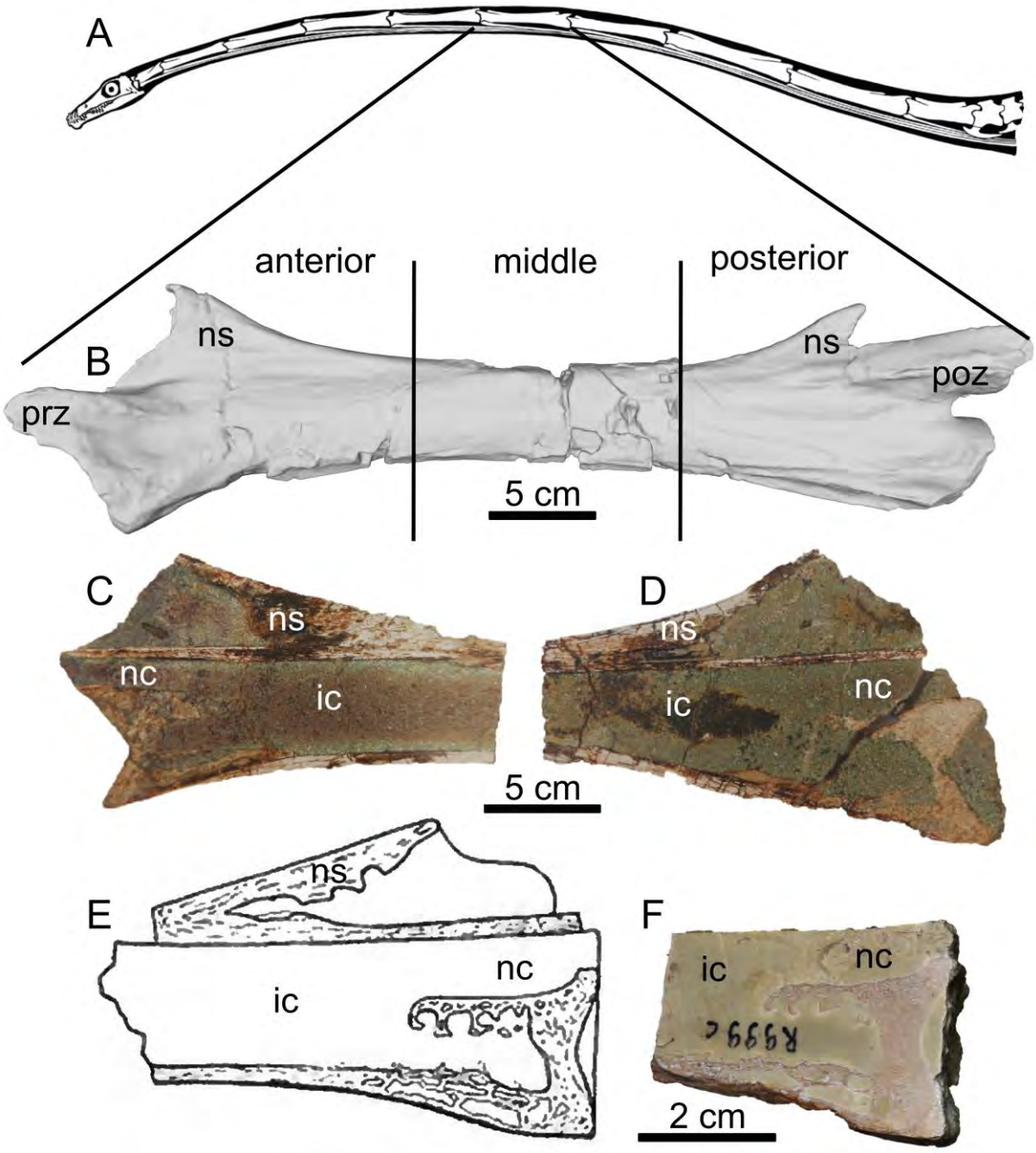

Fig. 1. Reconstruction of the neck of *T. hydroides* (**A**), after Spiekman et al. (2020*a*, changed; Author: Beat Scheffold) and some of the sampled middle cervicals of *Tanystropheus conspicuus* (**B**–**F**): (B) ZPAL V. 36/101, surface model in left lateral view; (C) ZPAL V. 36/1016/1, polished longitudinal cross section of an anterior portion of a vertebra; (D) ZPAL V. 36/1016/2, polished longitudinal section of a posterior portion of a vertebra; (E) SMF R 999c, a longitudinal cross section through a posterior portion of a vertebra as originally illustrated by von Huene (1907–1908: fig. 251) and (F) as currently preserved. Anatomical abbreviations: ic—internal cavity; nc—neural canal; ns—neural spine; poz—postzygapophysis; prz—prezygapophysis.

Material and methods

Tanystropheus conspicuus von Meyer, 1852 was erected on the basis of elongate vertebrae found in Germany and Poland. It shares its general anatomy with the more completely known *Tanystropheus hydroides* and *Tanystropheus longobardicus* (Bassani, 1886). These constitute all of the currently valid species of *Tanystropheus*. Taxonomic revisions of this taxon, combined with an extensive summary of referred material and its history, were provided by Wild (1973) and Spiekman and Scheyer (2019). Due to the lack of informative remains that would allow for a detailed comparison with the other *Tanystropheus* spp., Spiekman and Scheyer (2019) and Spiekman et al. (2021) considered *T. conspicuus* a *nomen dubium*. The newly uncovered locality of Miedary (southern Poland) has yielded abundant and diverse material of this species (see Czepiński et al. 2023). The majority of the studied specimens of *Tanystropheus* spp. (22 out of 30 cervicals, see Table 1) were recently excavated from the Miedary site (Czepiński et al. 2023). Similar to the typical preservational characteristics of this locality (Czepiński et al. 2023), these cervicals were found isolated and fully 3D preserved, but they quite often exhibited some degree of diagenetic alteration of their original morphology. Additionally, a well preserved 11th vertebra, SMNS 84821, described by Wild (1973, fig. 49), was CT scanned.

Unfortunately, the postaxial cervicals of *Tanystropheus* spp. exhibit a strikingly similar morphology from the 3rd to the 9th vertebra (Rytel et al. 2024*a*), and thus are extremely difficult to assign to their exact original position in the vertebral column (contra Wild 1973; see also Spiekman and Scheyer 2019). Therefore, only the posterior cervicals (vertebrae 10–13) could be confidently identified, and the postaxial vertebrae preceding them are referred to as ‘middle’ throughout the text. The sampled specimens varied in size, with the largest centra reaching over 35 cm in length (e.g., ZPAL V. 36/101—Fig. 1B) and the shortest being only 5 cm long (ZPAL V. 36/181). To better evaluate morphological change of the neck-torso transition, two well-preserved dorsal vertebrae of *Tanystropheus conspicuus* were also CT-scanned: SMNS 54628 and ZPAL V. 36/112. Moreover, specimens published by previous authors were reanalysed. These included a polished longitudinal section of a posterior portion of a middle cervical of *T. conspicuus* SMF R 999 (von Huene 1907–1908: fig. 251), polished transverse sections of an 11th cervical of *T. conspicuus* U-MO BT 738.00 (Broili 1915: plates 2 and 3), and thin sections of four cervical vertebrae of *Tanystropheus* spp.: PIMUZ T 2784, PIMUZ T 2799, MHI 1104, and an uncatalogued 10th cervical from SMNS (Jaquier and Scheyer 2017). Additionally, synchrotron CT scans of the holotype of *T. hydroides* PIMUZ T

2790 (see Spiekman et al. 2020*a*, *b*), as well as a thin section of a cervical from the same specimen, were used to evaluate the internal morphology of the anteriormost postatlantal vertebrae.

Protanystropheus was introduced as a generic name by Sennikov (2011) to encompass the original material of von Huene's (1907–1908) '*Tanystropheus*' *antiquus*, which included isolated cervical vertebrae originating from several Lower Muschelkalk localities in Silesia (southern Poland). Additional specimens were reported from the roughly contemporaneous strata of Germany and the Netherlands (Huene 1931; Wild and Oosterink 1984; Spiekman and Scheyer 2019; Spiekman et al. 2019), thus extending the biogeographic range of occurrence of the genus. To this day, the material referable to this taxon is constrained to scarce isolated cervicals, making any detailed interpretations of the biology of '*P*'. *antiquus* unattainable. These vertebrae are elongate, but proportionally much shorter than those of *Tanystropheus* spp. (Fig. 2). Morphologically, they are more reminiscent of those of other tanysaurians, e.g., *Amotosaurus rotfeldensis* Fraser and Rieppel 2006, *Augustaburiania vatagini*, or *Gracilicollum latens* Wang, Spiekman, Zhao, Rieppel, Scheyer, Fraser & Li, 2023 (AR pers. obs.; Fraser and Rieppel 2006; Sennikov 2011; Spiekman et al. 2021; Wang et al. 2023*b*). This disparity between the cervicals of '*P*'. *antiquus* and all other vertebrae referred to the genus *Tanystropheus* has been noted by previous authors, before Sennikov (2011) introduced the new combination, with some suggesting the non-congenerity of these taxa (Wild 1973, 1987; Evans 1988; Fraser and Rieppel 2006). Sennikov (2011) was unaware that the syntypes housed in MGUWr had survived World War II (see Skawiński et al. 2017). The most recent study of this material was performed by Spiekman and Scheyer (2019) and Spiekman et al. (2021), who summarised the available data and research on this taxon. '*Protanystropheus*' *antiquus* was included in one of the phylogenetic analyses of Spiekman et al. (2021), where it was recovered among 'dinocephalosaurids' (= trachelosaurids). '*Protanystropheus*' *antiquus* requires a taxonomical redescription including the syntype material, which will be addressed in a separate publication. Herein, we confidently consider it an early diverging tanysaurian.

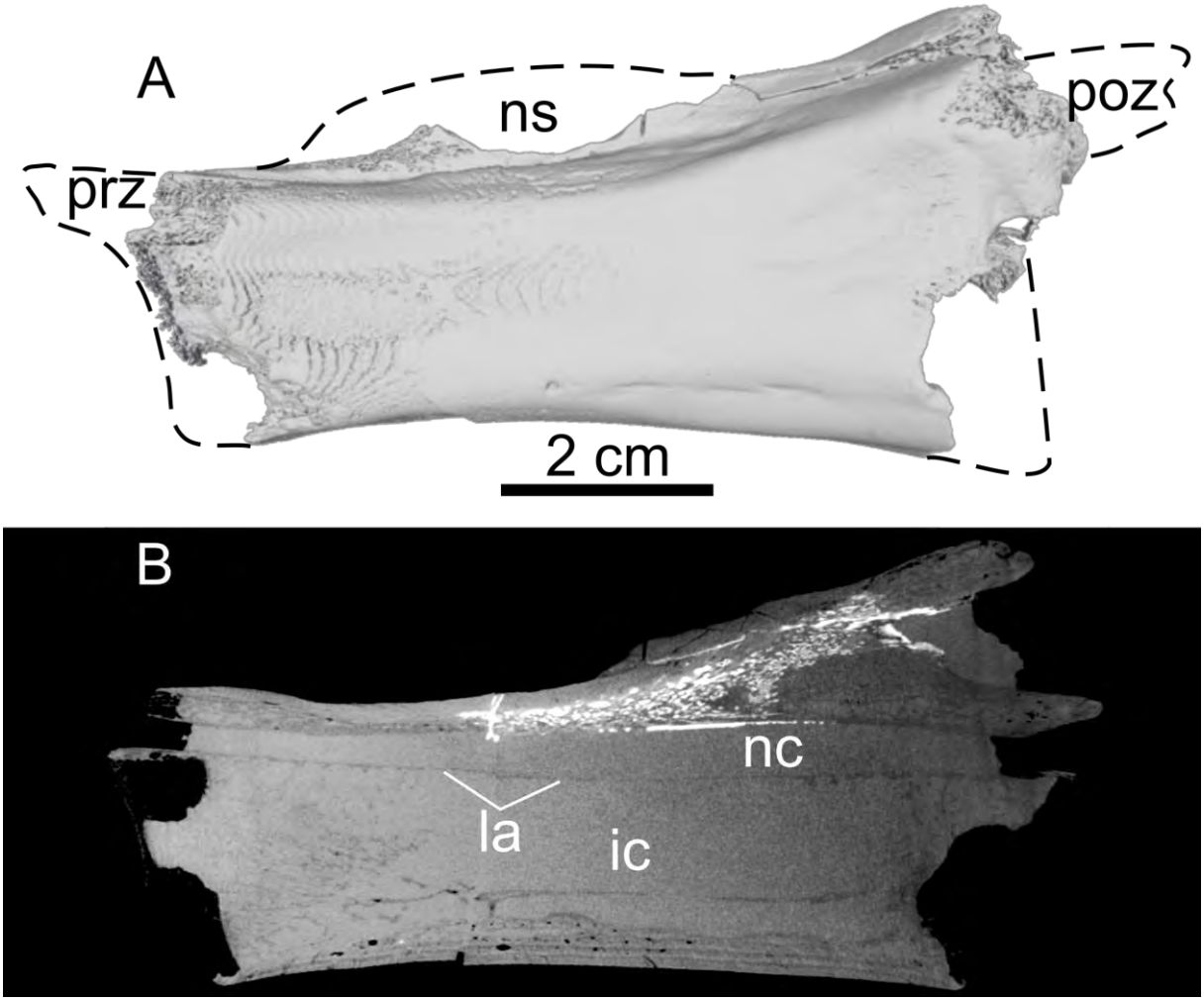

Fig. 2. GIUS-7-3674, cervical of '*Protanystropheus*' *antiquus*, surface model in left lateral view (**A**) and a longitudinal CT cross section (**B**). Notice the thin, but generally continuous neural canal floor. Anatomical abbreviations: ic—internal cavity; la—lamella that separates the neural canal from the internal cavity; nc—neural canal; ns—neural spine; poz—postzygapophysis; prz—prezygapophysis.

Seven cervicals of '*P*'. *antiquus* were analysed (Table 1)—these included the syntypes of von Huene (1907–1908): MGUWr 3889s, MGUWr 3895s, MGUWr 3902s, as well as three other vertebrae identified recently by the authors—GIUS-7-3674, SUT-MG/F/Tvert/2, and WNoZ/s/7-39. The specimens studied herein originated from both historic (Gogolin, Nakło Śląskie) and novel (Sosnowiec, Żyglin) sites located in south-western Poland. These localities represent a short time interval (early Anisian). Most, if not all, of the studied '*P*'. *antiquus* specimens were found in marine carbonates of the Gogolin Formation—the lower-most part of the Lower Muschelkalk (see Kowal-Linka 2008; Skawiński et al. 2017), although the exact stratigraphic provenience of GPIH 5194c and WNoZ/s/7-39 is not certain. All of the '*P*'.

antiquus vertebrae identified so far were found isolated, which, together with their scarcity and lack of research on their morphological disparity, precludes us from referring any of them to their exact original position in the vertebral column. Sampled specimens varied in size, with the largest centra reaching over 9 cm in length (WNoZ/s/7-39) and the shortest being only around 4 cm long (MGUWr 3889s). Even though these specimens are not fully complete, they are 3D preserved and virtually unaltered diagenetically, thus constituting material well suited for CT studies. The six mentioned vertebrae have been scanned, and subsequently GIUS-7-3674 and SUT-MG/F/Tvert/2 were thin sectioned transversely at the midpoint of their anteroposterior length. Two additional historical thin sections of a '*P*'. *antiquus* cervical vertebra were found in the collection of GPIH. The source specimen GPIH 5194c lost its original label, but additional notes on the sections indicate that it was collected by G. Gürich in Silesia, possibly in Gogolin. Thus, the analysed dataset includes all of the published material (including historical specimens) in which the internal anatomy of tanysaurian cervicals was well visible. New specimens sampled for this study were investigated to complement and expand the available data, allowing for a comprehensive de- scription of the internal morphology of these vertebrae. The full list of the studied specimens, including the sampling methods used for each of them, is provided in Table 1. CT data, specimen models, and photographs used in this study are available on MorphoSource: https://www.morphosource.org/pro- jects/000661974.

CT scans of the majority of the specimens studied herein were acquired using a GE Phoenix v|tome|x s CT scanner (GE Sensing and Inspection Technologies Phoenix|x-ray, Wunstorf, Germany), installed in the Faculty Laboratory of Computed Microtomography, Faculty of Science and Technology, University of Silesia in Katowice, Poland. Due to the elongation, fragility, and size of some of the vertebrae, several cervicals were scanned in parts, to preserve sufficient imaging resolution for their anterior and posterior portions. Reconstructed cross sections were used to generate 3D views of the whole specimens based on volume rendering. VG Studio Max 2.0 (Volume Graphics, Germany) and ImageJ (National Institutes of Health, USA) software was applied to visualize the internal structure of the samples. Finally, Mimics 14.11 (Materialise, Belgium) was used to model the surface of the internal cavities of '*P*'. *antiquus*. The smallest *Tanystropheus* spp. cervical (ZPAL V. 36/181) was analysed using μCT. These data were collected with a Zeiss XRadia MicroXCT-200 system equipped with a 90 kV/8 W tungsten X-ray, located in the Laboratory of Microtomography, Institute of Paleobiology, Polish Academy of Sciences, Warsaw. Radial

projections were reconstructed with XMReconstructor (Zeiss) software and viewed with XM3DViewer (Zeiss) soft- ware. Avizo Lite 2020.3.1 (Thermo Fisher Scientific, USA) was used to model the surface of the internal cavity of ZPAL V. 36/181. The vertebrae of *T. conspicuus* SMNS 54628 and SMNS 84821 were scanned in the laboratory of the Institute for Photon Science and Synchrotron Radiation at KIT. A microfocus X-ray tube (XWT-225, X-RAY WorX, Garbsen, Germany) with an acceleration voltage of 200 kV and a flat panel detector (XRD 1621 CN14 ES, PerkinElmer, Waltham, USA) with a physical pixel size of 200 μm and a DRZ + scintillator were employed. The spectrum was hardened with an additional copper filter. For both samples, the field of view, magnification, tube power, and exposure time were optimized, resulting in an effective pixel size of 63.9 μm for SMNS 54628 with an exposure time of 2 s and a tube power of 60 W, and 62.7 μm for SMNS 84821 with an exposure time of 3 s and a tube power of 50 W. Three full CT scans were acquired for both samples and then stitched together. Each scan consisted of 2048 projections acquired over an angular range of 360°. CT reconstruction was performed using Octopus 8.6 (Inside Matters, Ghent, Belgium). The new thin sections presented in this study (Table 1) were created in the laboratories of the Institute of Paleobiology, Polish Academy of Sciences, University of Silesia in Katowice, and the Laboratory of Electron Microscopy, Microanalysis and X-Ray Diffraction, Faculty of Geology, University of Warsaw, Warsaw. The specimens selected for sectioning were sampled transversely. To allow for a more extensive comparison with the CT scan data, the vertebrae were cut at different points along their anteroposterior length (predominantly near the midpoint) and the thin sections thickness varied from 40 to 80 μm, to underline different aspects of their histology. Additionally, two partially preserved, but diagenetically unaltered, middle cervical vertebrae of *Tanystropheus conspicuus*, ZPAL V. 36/1016/1 (anterior part) and ZPAL V. 36/1016/2 (posterior part), were cut along their sagittal plane (Fig. 1C–D). Subsequently, the longitudinal cross sections were polished, to allow for a detailed comparison with the CT scan data.

Thin sections were examined using a Nikon Eclipse 80i transmitted light microscope fitted with a DS-5Mc cooled camera head (ZPAL), an Olympus BX51 polarized microscope equipped with an Olympus SC30 camera and a halogen light source (GIUS), as well as two Keyence VHX-7000 digital micro- scopes with a VHX-7100 fully integrated head with two lens systems (20–100×; 100–500×) and a polarisation adapter, located at the University of Zurich and the University of Warsaw.

Table 1. Specimens analysed in this study.

Specimen	Taxon	Locality	Stratigraphy	Age	Sampling	References/notes
GIUS-7-3674	"P." *antiquus*	Żyglin (Poland)	Lower Muschelkalk	earliest Anisian?	CT scanned, sectioned	
GPIH 5194c	"P." *antiquus*	Gogolin? (Poland)	Lower Muschelkalk?	earliest Anisian?	Sectioned	two historic thin sections
MGUWr 3889s	"P." *antiquus*	Nakło (Poland)	Lower Muschelkalk	earliest Anisian?	CT scanned	von Huene 1907-1908
MGUWr 3895s	"P." *antiquus*	Gogolin (Poland)	Lower Muschelkalk	earliest Anisian?	CT scanned	von Huene 1907-1908
MGUWr 3902s	"P." *antiquus*	Gogolin (Poland)	Lower Muschelkalk	earliest Anisian?	CT scanned	von Huene 1907-1908
SUT-MG/F/Tvert/2	"P." *antiquus*	Gogolin (Poland)	Lower Muschelkalk	earliest Anisian?	CT scanned, sectioned	Surmik et al. 2016
WNoZ/s/7-39	"P." *antiquus*	Sosnowiec (Poland)	Lower Muschelkalk	earliest Anisian?	CT scanned	Surmik 2010
PIMUZ T 2790	*T. hydroides*	Punkt 902 (Switzerland)	Besano Formation	Anisian/Ladinian	CT scanned, sectioned	Spiekman et al. 2020*a*, *b*
PIMUZ T 2784	*Tanystropheus* sp.	Cave Tre Fontane (Switzerland)	Besano Formation	Anisian/Ladinian	Sectioned	Jaquier and Scheyer 2017
PIMUZ T 2799	*Tanystropheus* sp.	Valle Stelle (Switzerland)	Besano Formation	Anisian/Ladinian	Sectioned	Jaquier and Scheyer 2017
MHI 1104	*T. conspicuus*	Öhringen (Germany)	Upper Muschelkalk	early Ladinian	Sectioned	Jaquier and Scheyer 2017
SMF R 999a-c	*T. conspicuus*	Bindlach (Germany)	Upper Muschelkalk	early Ladinian	Cut and polished	von Huene 1907-1908
SMNS 54628	*T. conspicuus*	Hegnabrunn (Germany)	Upper Muschelkalk	early Ladinian	CT scanned	
SMNS 84821	*T. conspicuus*	Schwingen (Germany)	Upper Muschelkalk	early Ladinian	CT scanned	Wild 1973
SMNS uncat.	*T. conspicuus*	Crailsheim (Germany)	Upper Muschelkalk	early Ladinian	Sectioned	Jaquier and Scheyer 2017
U-MO BT 738.00	*T. conspicuus*	Bindlach (Germany)	Upper Muschelkalk	early Ladinian	Cut and polished	Broili 1915
ZPAL V. 36/101	*T. conspicuus*	Miedary (Poland)	Lettenkeuper	early Ladinian	CT scanned	Czepiński et al. 2023
ZPAL V. 36/102	*T. conspicuus*	Miedary (Poland)	Lettenkeuper	early Ladinian	CT scanned	
ZPAL V. 36/104	*T. conspicuus*	Miedary (Poland)	Lettenkeuper	early Ladinian	CT scanned	
ZPAL V. 36/105	*T. conspicuus*	Miedary (Poland)	Lettenkeuper	early Ladinian	CT scanned	
ZPAL V. 36/106	*T. conspicuus*	Miedary (Poland)	Lettenkeuper	early Ladinian	CT scanned	
ZPAL V. 36/107	*T. conspicuus*	Miedary (Poland)	Lettenkeuper	early Ladinian	CT scanned	
ZPAL V. 36/108	*T. conspicuus*	Miedary (Poland)	Lettenkeuper	early Ladinian	CT scanned	
ZPAL V. 36/110	*T. conspicuus*	Miedary (Poland)	Lettenkeuper	early Ladinian	CT scanned	
ZPAL V. 36/112	*T. conspicuus*	Miedary (Poland)	Lettenkeuper	early Ladinian	CT scanned	
ZPAL V. 36/126	*T. conspicuus*	Miedary (Poland)	Lettenkeuper	early Ladinian	Sectioned	
ZPAL V. 36/149	*T. conspicuus*	Miedary (Poland)	Lettenkeuper	early Ladinian	CT scanned	
ZPAL V. 36/150	*T. conspicuus*	Miedary (Poland)	Lettenkeuper	early Ladinian	Sectioned	
ZPAL V. 36/156	*T. conspicuus*	Miedary (Poland)	Lettenkeuper	early Ladinian	Sectioned	
ZPAL V. 36/166	*T. conspicuus*	Miedary (Poland)	Lettenkeuper	early Ladinian	Sectioned	
ZPAL V. 36/176	*T. conspicuus*	Miedary (Poland)	Lettenkeuper	early Ladinian	Sectioned	
ZPAL V. 36/181	*T. conspicuus*	Miedary (Poland)	Lettenkeuper	early Ladinian	CT scanned	
ZPAL V. 36/192	*T. conspicuus*	Miedary (Poland)	Lettenkeuper	early Ladinian	Sectioned	
ZPAL V. 36/193	*T. conspicuus*	Miedary (Poland)	Lettenkeuper	early Ladinian	Sectioned	
ZPAL V. 36/1016/1	*T. conspicuus*	Miedary (Poland)	Lettenkeuper	early Ladinian	Cut and polished	
ZPAL V. 36/1016/2	*T. conspicuus*	Miedary (Poland)	Lettenkeuper	early Ladinian	Cut and polished	
ZPAL V. 36/1071	*T. conspicuus*	Miedary (Poland)	Lettenkeuper	early Ladinian	Sectioned	
ZPAL V. 36/1090	*T. conspicuus*	Miedary (Poland)	Lettenkeuper	early Ladinian	Sectioned	
ZPAL V. 36/1099	*T. conspicuus*	Miedary (Poland)	Lettenkeuper	early Ladinian	Sectioned	

Results

Bone histology and internal structure of vertebrae of '*P*'. *antiquus*

The CT examination of vertebrae was performed to non- destructively investigate the internal structure of each specimen and to assess the thickness of compact and cancellous bone in the different regions of the vertebrae. Within the anteroposteriorly terminal portions of all scanned '*P*'. *antiquus* centra, the core was filled with dense cancellous bone (identified in CT images so of uncertain tissue composition) and the cortex was relatively thin (Figs. 2–4), whereas in the middle portion, where the internal cavity was revealed, the cortical bone was distinctly thicker. The transverse sections revealed the changes of the cortical bone thickness and the shape of internal cavities, with the mid-centrum being roughly cylindrical. The cortex was thinner near the anteroposteriorly terminal portions of the vertebrae and its thickness gradually increased up to approximately four times the original thickness (about 10% of bone diameter), near the midpoint (Fig. 3). The density of the cancellous bone of the anteroposteriorly terminal portions of the centrum decreased medially, with larger cavities being present closer to the mid- point. The transition to the empty internal cavity was relatively sharp. The anterior and posterior ends of the internal cavity were roughly hemispherical and surrounded circumferentially by marginalised trabeculae (Fig. 3).

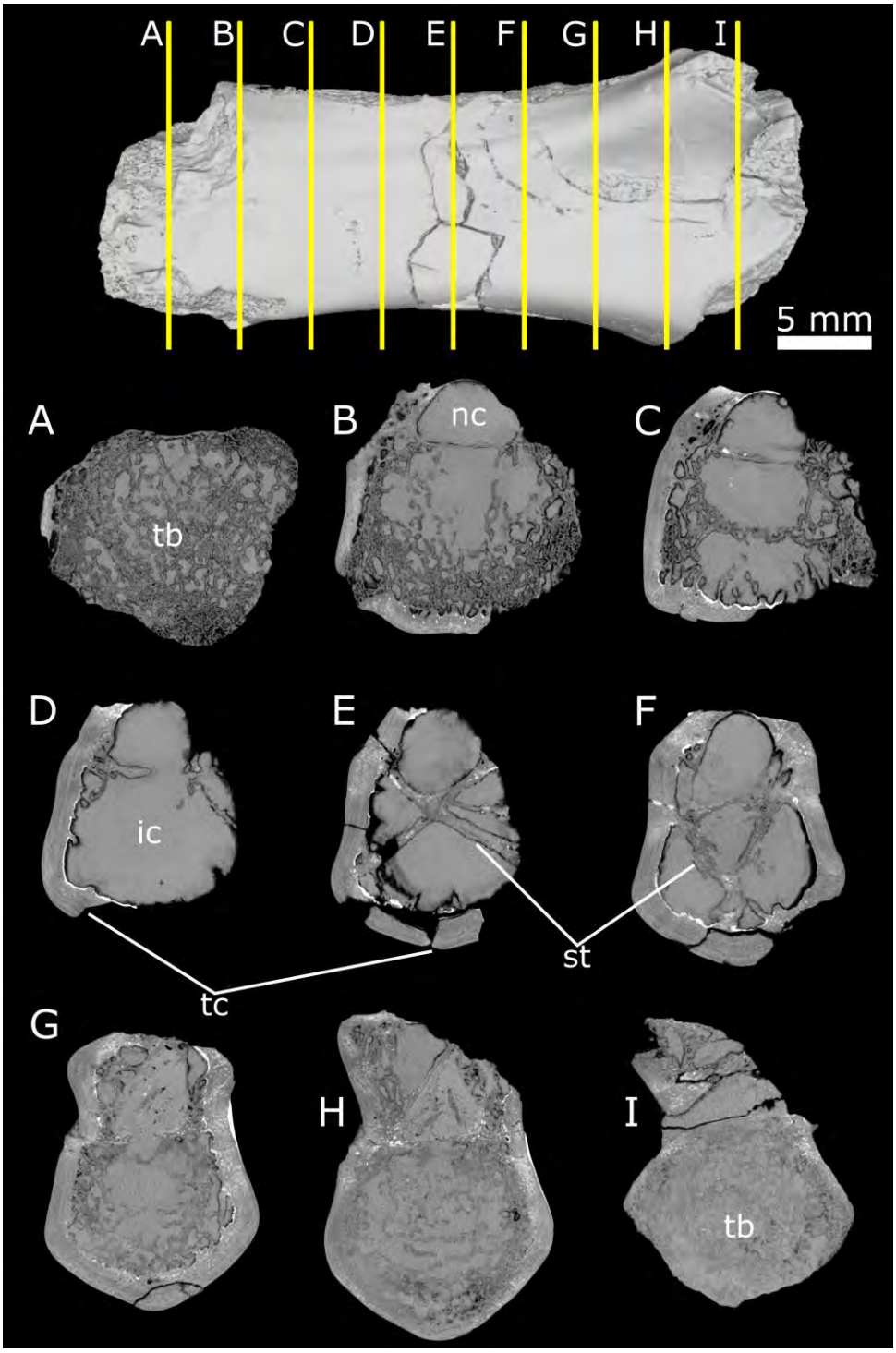

Fig. 3. CT transverse cross sections (from anterior to posterior) of '*Protanystropheus*' *antiquus* cervical MGUWr 3889s (surface model in left lateral view) showing internal structure of the vertebra. Sectioning planes are marked with lines. Note the presence of a large internal cavity (ic), thicker cortex layer (tc), and slanted trabeculae (st) spanning across the internal chamber. Trabecular bone (tb) is present in the anteroposteriorly terminal portions of the centrum.

Long intermittent trabeculae composed of parallel-fibred bone moderately remodelled with endosteal secondary lamellar bone (Fig. 4D) crossed the internal cavity in varied directions, mainly diagonally. In some vertebrae they divided the internal cavity into several smaller terminus-like pockets (Figs 2B, 3). The neural canal was separated ventrally from the internal cavity by a horizontal, plate-like lamella consisting of endosteal lamellar bone (Figs. 2B, 3, 4A–C), which was generally thinner than the internal trabeculae composed of the same tissue. This separation was not continuous, the neural canal floor was perforated by large openings in some specimens (Figs. 2B and 3C–G) and seemed to disappear completely in others. For example, in MGUWr 3889s at least two large openings were present in the lamella separating the neural canal from the internal cavity. In MGUWr 3902 and GPIH 5194c there appeared to be no bony separation between the neural canal and the internal cavity for most of the length of the centrum. Because no fragments of broken bone were present anywhere inside of the neural canal or the internal cavity of the centrum, and this condition was present in several specimens approximately in the same area, it appears not to be an artifact of preservation. The cortex was predominately composed of parallel-fibred matrix (Fig. 4), with locally (especially in the dorsolateral part) highly organized arrays of mineralized collagen fibres. No rest lines were present. The vascularisation was moderate, and its pattern was radial, which was especially evident in the ventral part of the vertebrae (Fig. 4A–C, H–I). Inside the neural arch, mostly dorsally to the neural canal (inside of the base of the neural spine) and in some specimens laterally to the neural canal there was a region of occurrence of secondary trabecular bone (Fig. 4J). Both the cavity and the neural canal were clear cut and lined with a thin layer of endosteal lamellar bone (Fig. 4E–J). Sharpey’s fibres could be seen extending throughout the cortex, especially in the dorsolateral and ventrolateral regions of the centrum (Fig. 4C, G–I).

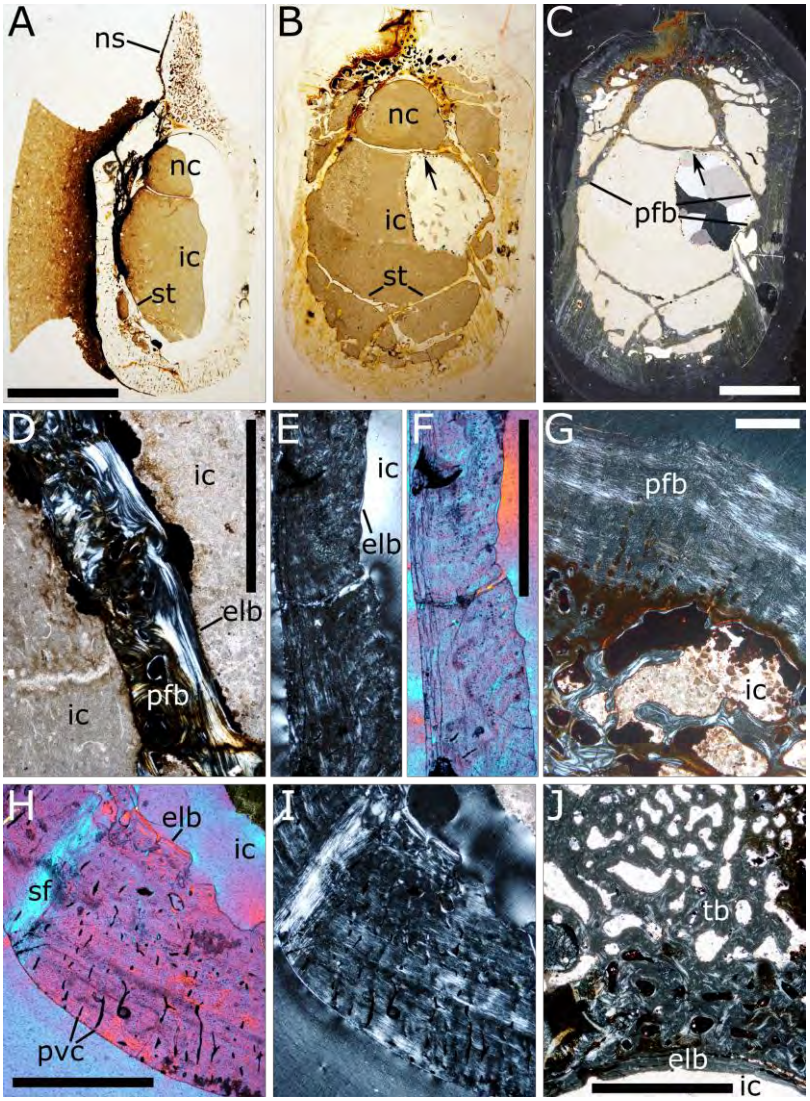

Fig. 4. Thin sections of '*Protanystropheus*' *antiquus* cervical vertebrae SUT-MG/F/Tvert/2 (**A, E, F, H, I**) and GIUS-7-3674 (**B–D, G, J**). A–C, thin sections in normal transmitted light (A, B) and in polarised light (C). D, close-up of the internal supporting trabeculae in polarised light, presenting heavy remodelling. E–F, the lateral cortex of the centrum in polarised light (E) and polarised light with lambda compensator (F) showing lack of distinctive zonation and loosely ordered bone structure. G, cortex of the dorsolateral region of the centrum displaying more pronounced zonation and dorsal internal slanted trabeculae in polarized light. H–I, cortex of the ventrolateral region of centrum showing radial vascularisation and a well-developed bundle of Sharpey's fibres in polarized light (H) and polarized light with lambda compensator (I). J, the trabecular bone of the neural arch in polarised light. Arrows indicate a perforation of the neural canal floor. Anatomical abbreviations: elb—endosteal lamellar bone; ic—internal cavity; nc—neural canal; ns—neural spine; pfb—parallel-fibred bone; pvc—primary vascular canals; sf—Sharpey's fibres; st—slanted trabeculae; tb—trabecular bone. Scale bars for panels A–C equal 5 mm and 0.5 mm for D–J.

Bone histology and internal structure of vertebrae of *Tanystropheus* spp.

Anatomy of the middle cervicals

Within all of the studied vertebrae, a large cavity could be identified, surrounded by relatively thick cortex composed of alternating layers of well-organized parallel-fibred to lamellar bone (Figs. 5–8). In the anterior and posterior terminal portions of the cervicals, discs of secondary cancellous bone of endosteal origin formed the articular regions of the centrum (Fig. 5B–D). Above them, the openings of the neural canal were present. In some of the middle cervicals the neural canal floor extended only slightly from the openings towards the middle of the vertebra, forming a shelf that partially separated the internal cavity from the neural canal (Figs. 5B–E, 6C, F), although in some other of these vertebrae the neural canal transitioned smoothly into the internal cavity (compare Fig. 6B to Fig. 5B; Fig. 7B). In the transverse cross section, the inner surface of the bone wall of the internal cavity was generally parallel to the circumferential outline of the vertebra (Fig. 8A–E). In most of the studied specimens, the dorsal part of the internal cavity seemed to preserve a semicircular shape in the transverse cross section, whereas tissue layout of its ventrolateral portion was usually much less uniform, with an irregular resorption front cutting through multiple annuli (Fig. 8A, C, E). This was especially evident in larger specimens, whereas in the smallest cervical, the regions of resorption were much less developed, and the outline of the internal cavity in the transverse cross section was more regularly oval (Fig. 8B).

The neural spine extended over two deep fossae, located on both of its anteroposteriorly terminal portions. They were triangular in longitudinal cross section and ventrally delimited by thin bone trabeculae, that also constituted the roof of the neural canal. The posterior cavity was larger, forming the ‘postzygapophyseal trough’ (Rieppel 2001). Contrary to what was observed for ‘*P*’. *antiquus*, in none of the studied sections of the *Tanystropheus* spp. middle cervicals did the internal cavity contain bony trabeculae extending internally from the surface of the bone wall. Some semi-symmetrical, slanted trabeculae of endosteal origin were present only incidentally in the anteroposteriorly terminal sections of the vertebrae (see Broili 1915: plate 3, fig. 4c). The roof of the neural canal was generally straight and parallel to the longitudinal axis of the vertebra. The ventral delimitation of the neural canal was seemingly absent for most of its length within a vertebra. Intriguingly, in one of the transverse polished sections from the anterior part of U-MO BT 738.00 (Fig. 8F), minute bony projections appeared symmetrically on each lateral side of the internal cavity. The colour of the limestone infill of the vertebra changed drastically at the same horizontal

level, at which these projections were situated. Similar characteristics could be noted for the transverse thin section of ZPAL V. 36/166 (Fig. 8E), in which corresponding projections composed of periosteal bone were also present in the dorsolateral regions of the internal cavity. Between them, there was a sharp transition in sediment fraction, with the more coarse-grained infill occupying the ventral-more space. Presence of this feature possibly shows the differences in taphonomical microenvironments of the ventral and dorsal portions of the internal cavity, which may have been caused by the original existence of a no longer preserved barrier between them. Near the anteroposterior midpoint of the middle cervicals, two symmetrically placed foramina were located on the ventral side of the centrum. They entered the internal cavity as straight canals (Fig. 8B, E), perforating the dense cortex. While in '*P*'. *antiquus* the neural spine was easily identifiable, it was much less recognisable in the middle cervicals of *Tanystropheus* spp. It was impossible to demarcate the border between the neural arch and the vertebral centrum—they were completely fused, with no preserved remnants of the suture between them, even in the smallest specimens, and little to no trabeculae within the neural arch.

Continuous layers of dense parallel-fibred tissue sheathed the internal cavity. In the middle section of the larger middle cervicals of *Tanystropheus* spp. the outermost of these zones formed complete rings, whereas the ones located innermost were discontinued only due to resorption of the region ventral into the internal cavity, as well as the presence of the neural spine (Fig. 8A, C, Fig. 9B). In some of the studied transverse thin sections, including the smallest specimens, the spinous process was developed only as a thin, vertically oriented plate. It was located directly above the internal cavity and emerged from the parallel-fibred tissue of the bone walls in the dorsalmost portion of the vertebra, projecting slightly from the smooth outline of the transverse cross section. In the smallest specimen from Miedary, ZPAL V. 36/181, the neural spine was never overlain by parallel-fibred bone (Fig. 8B). In all of the larger specimens from Miedary, the anteroposteriorly middle part of the spinous process was obscured by thick layers of tissue that formed the walls of the internal cavity. Compared to what was noted for '*P*'. *antiquus*, the dorsolateral regions of the *Tanystropheus* spp. cervicals were thickened (see Fig. 9). The neural spine was, thus, not relatively reduced in the latter, but rather embedded within the walls of the tubularly structured vertebra. As a result, the neural canal was located close to the middle of the height of the vertebra, as in '*P*'. *antiquus*. However, in *Tanystropheus* spp. there was more tissue dorsolaterally (see Fig. 9), due to the neural spine being hypertrophied along the middle section of its anteroposterior length.

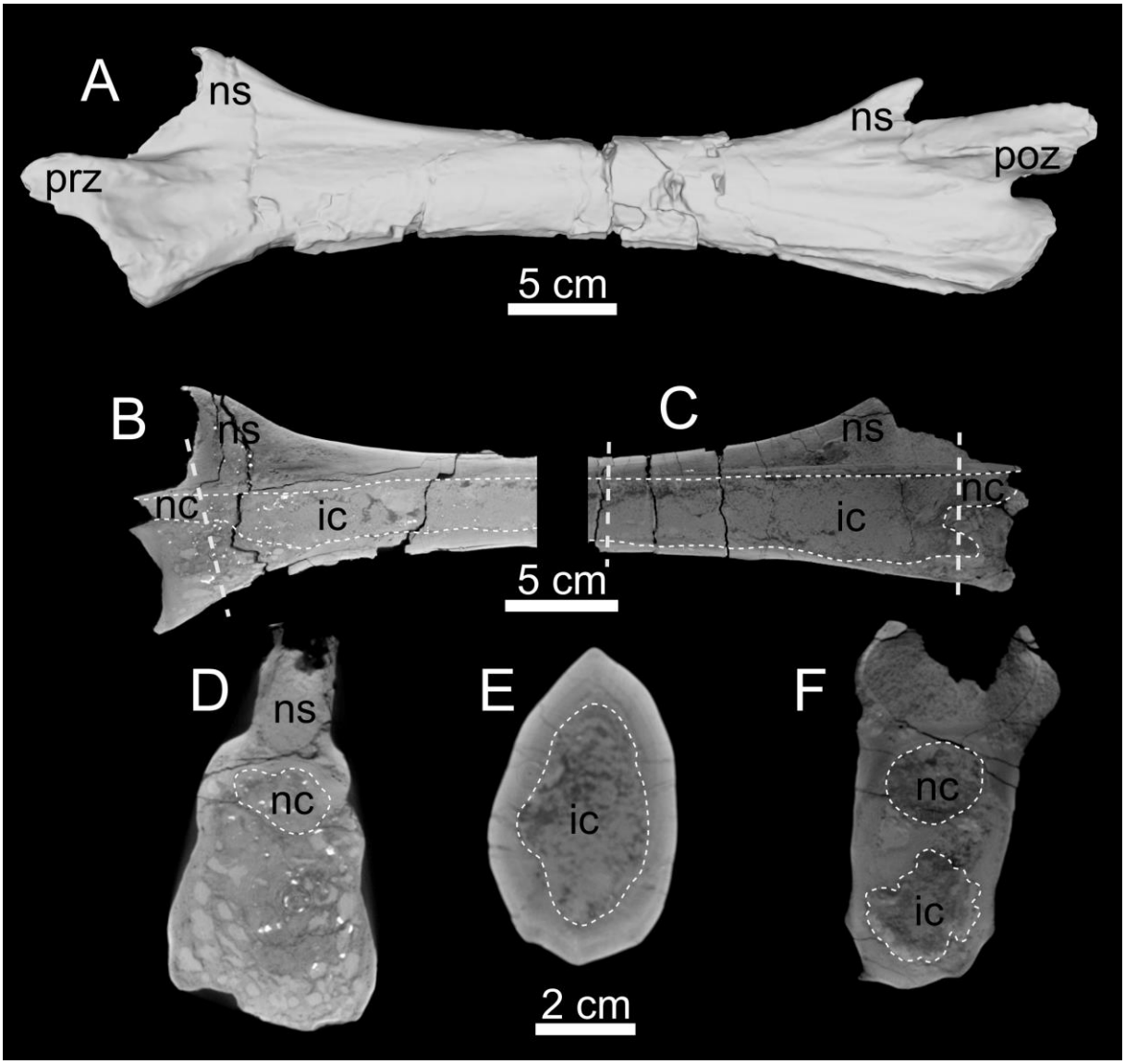

Fig. 5. Middle cervicals of *Tanystropheus conspicuus*: **A**, **B**, **D**—ZPAL V. 36/101; **C**, **E**, **F**—ZPAL V. 36/102; A is a surface model in left lateral view. B, C, longitudinal CT cross sections of an anterior (B) and a posterior portion (C) of the vertebra. D, E, F, transverse CT cross sections. Sectioning planes and walls of the neural canal and internal cavity have been outlined with white dashed lines, with the lines signifying the sectioning planes being thicker than the internal cavity outline. Anatomical abbreviations: ic—internal cavity; nc—neural canal; ns— neural spine; poz—postzygapophysis; prz—prezygapophysis.

Anatomy of the posterior cervicals

In *Tanystropheus*, the external morphology of the cervicals changed near the posterior subregion of the neck. The 10th and 11th vertebrae were still elongate, but, contrary to the middle cervicals, exhibited a well exposed, relatively tall and continuous neural spine (Fig. 6).

The two last cervicals were relatively much shorter (Fig. 6B, C), and more similar in proportions to the dorsals (Rieppel et al. 2010; Rytel et al. 2024). This transition was paired with the modifications in the internal structure of these elements. The relative volume occupied by the trabeculae within the centra increased caudally, especially along the neck-torso transition. In the middle cervicals the centrum was nearly devoid of trabecular bone, but this changed within the more posterior vertebrae, with the last two cervicals and the dorsals exhibiting sparse trabeculae occupying the space between the articular discs.

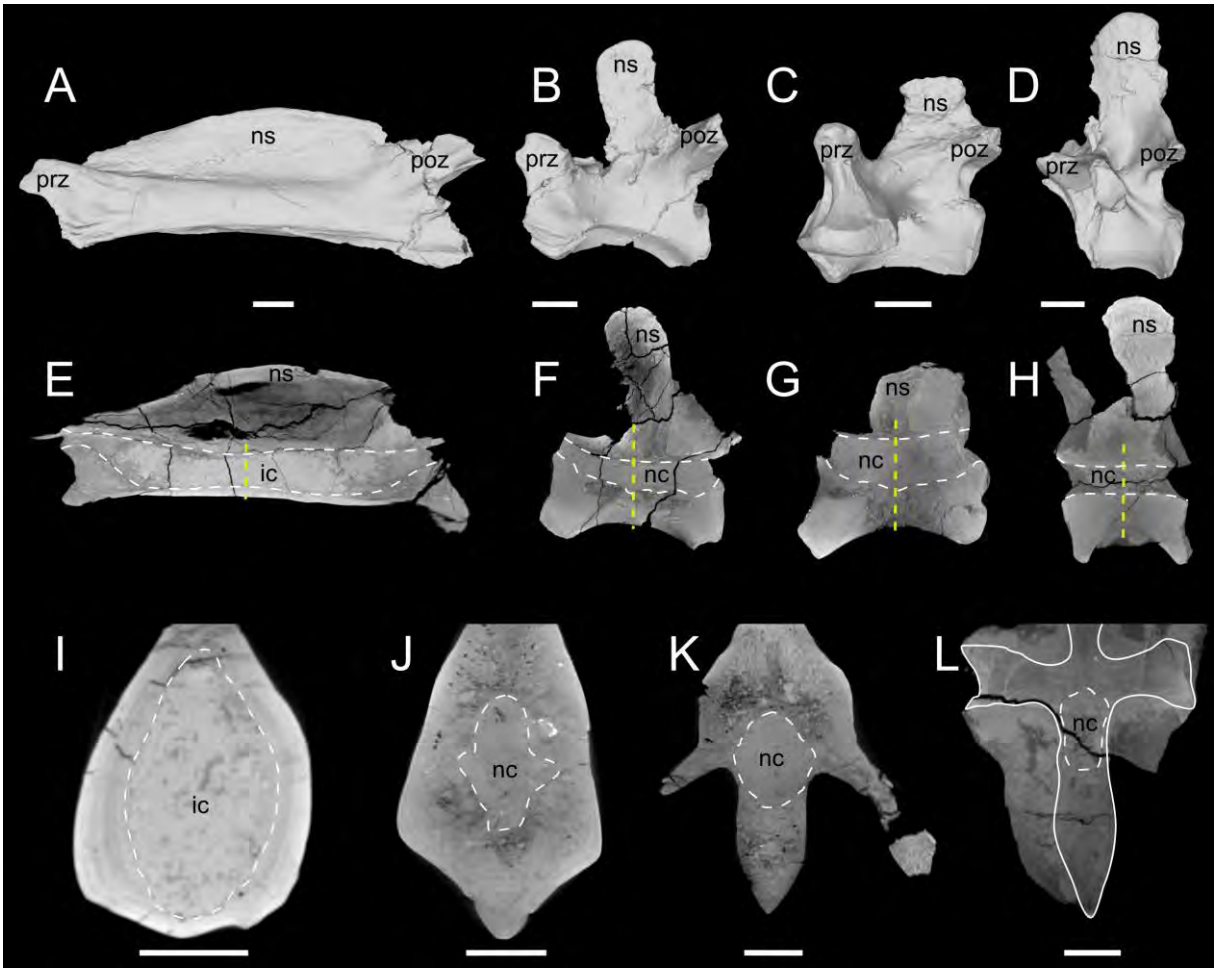

Fig. 6. Vertebrae of *Tanystropheus conspicuus*: **A**, **E**, **I**—ZPAL V. 36/106, 11th cervical; **B**, **F**, **J**—ZPAL V. 36/108, 12th cervical; **C**, **G**, **K**—ZPAL V. 36/110, 13th (last) cervical; **D**—ZPAL V. 36/1036, dorsal; **H**, **L**—ZPAL V. 36/112, dorsal. A–D, surface models in left lateral view. E–H, longitudinal CT cross sections. I–L, transverse CT cross sections. White dashed lines mark the sectioning planes (yellow) and walls of the neural canal and internal cavity (white). Anatomical abbreviations: ic—internal cavity; nc—neural canal; ns—neural spine; poz—postzygapophysis; prz—prezygapophysis. Scale bars equal 2 cm for A–H, and 1 cm for the other panels.

The 10th and 11th vertebrae were generally similar in their anatomy to the middle cervicals, with their internal cavities being surrounded by a dense cortex, forming a tube-like structure (Fig. 6I). However, in the succeeding vertebrae the internal cavity was greatly reduced and exhibited much thicker walls, composed of two regions: a relatively thin cortex and porous, cancellous bone encompassed by it. Especially in the middle portion of the centrum of the last two cervicals, there were several large chambers, similar to those present in the anteroposteriorly terminal portions of the more anteriorly located vertebrae (Fig. 8D). Some of them connected to the neural canal through its floor (Fig. 6E, F, H, I). The transverse cross sections of the posteriormost cervicals were less oval than in the preceding vertebrae, with the centrum being much more ventrally expanded, forming a distinct keel (Fig. 6J, K).

The diameter of the neural canal was relatively constant along the length of each of the two last vertebrae. In the longitudinal cross section, it had a sagging appearance, with its middle portion being located more ventrally. In the transverse cross section, it was oval, with its dorsolateral regions being roughly semicircular and symmetrical in outline (Fig. 6J, K). A similar shape could be noted in the anteroposteriorly terminal sections of the rest of the postaxial cervicals, in which the neural canal floor was still present (e.g. Fig. 8D), and also in the dorsal vertebrae (Fig. 6L). In each of the two posteriormost neck vertebrae of *Tanystropheus conspicuus*, up to two small subcentral foramina could be traced, with some specimens exhibiting only one subcentral for- amen or none at all. In the studied posteriormost cervical ZPAL V. 36/110, a straight, non-branching canal connected the one present foramen with the neural canal (Fig. 10). The dorsal vertebrae were generally similar to the posteriormost cervicals in their internal anatomy. They differed in a complete lack of subcentral foramina. Moreover, the neural canal of the dorsals extended anteroposteriorly straight, with its roof and floor remaining on a relatively constant horizontal level (Fig. 6H). Its transverse cross section was similar in shape to the posteriormost cervicals, but more regular. Congruently to what could be observed in the 12th and 13th cervical vertebrae, the internal portion of the centrum was composed of sparsely distributed trabeculae containing a large number of cavities, some of which opened to the neural canal through its floor.

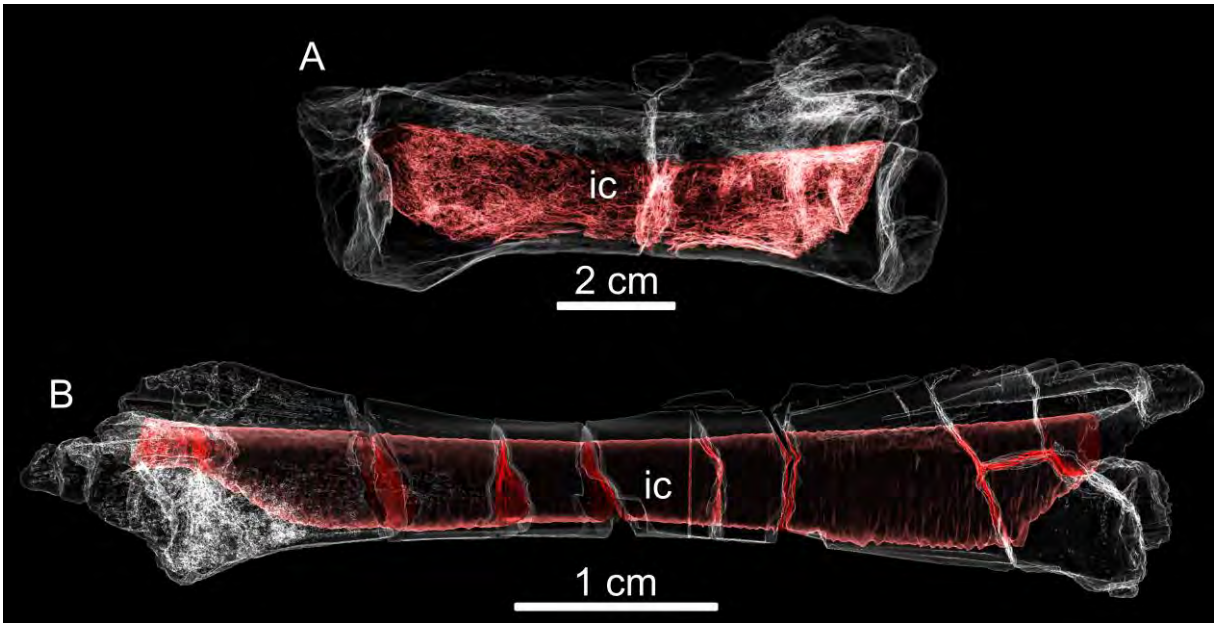

Fig. 7. Internal cavity volume in the cervical vertebrae of '*Protanystropheus*' *antiquus* MGUWr 3895s (**A**) and *Tanystropheus conspicuus* ZPAL V. 36/181 (**B**). ic—internal cavity. Images obtained using 'xray' shader in MeshLab v.2020.12 (Cignoni et al. 2008).

Vertebral histology

The histological characteristics of the studied vertebrae of *Tanystropheus* spp. were congruent with the results of the study performed by Jaquier and Scheyer (2017 and the supplemental data provided therein). New data presented herein expand our knowledge on the anteroposterior and ontogenetic variation of their structure. The walls of the internal cavity were built of primary compact lamellar to parallel-fibred matrix of periosteal origin. Some intervals with decreased vascularisation could be traced within these bone walls—they formed ellipsoidal annuli that alternated with more vascularized zones in parallel to the circumference of the vertebra (see Jaquier and Scheyer 2017). Closer to the terminal portions of the anteroposterior length of the cervicals, the tissue composition changed, with the internal cavity being dorsolaterally lined with secondary endosteal lamellar bone (Fig. 8H) and the ventrolateral portions of the bone centrum not exhibiting the regular annuli, but rather being nearly completely composed of endosteal lamellar bone scattered with secondary osteons and erosion cavities of varying size, forming a net of sparse trabeculae (Figs 5B–D, 8D, G). The core of the neural spine in larger specimens was highly remodelled with longitudinally oriented secondary osteons. Simple primary vascular canals extended radially in the middle part of the vertebrae, but became more longitudinally oriented, larger, and less organised in the anteroposteriorly terminal portions. The number of vascular canals was also smaller in the more compact sections of the cortex within a single cross section.

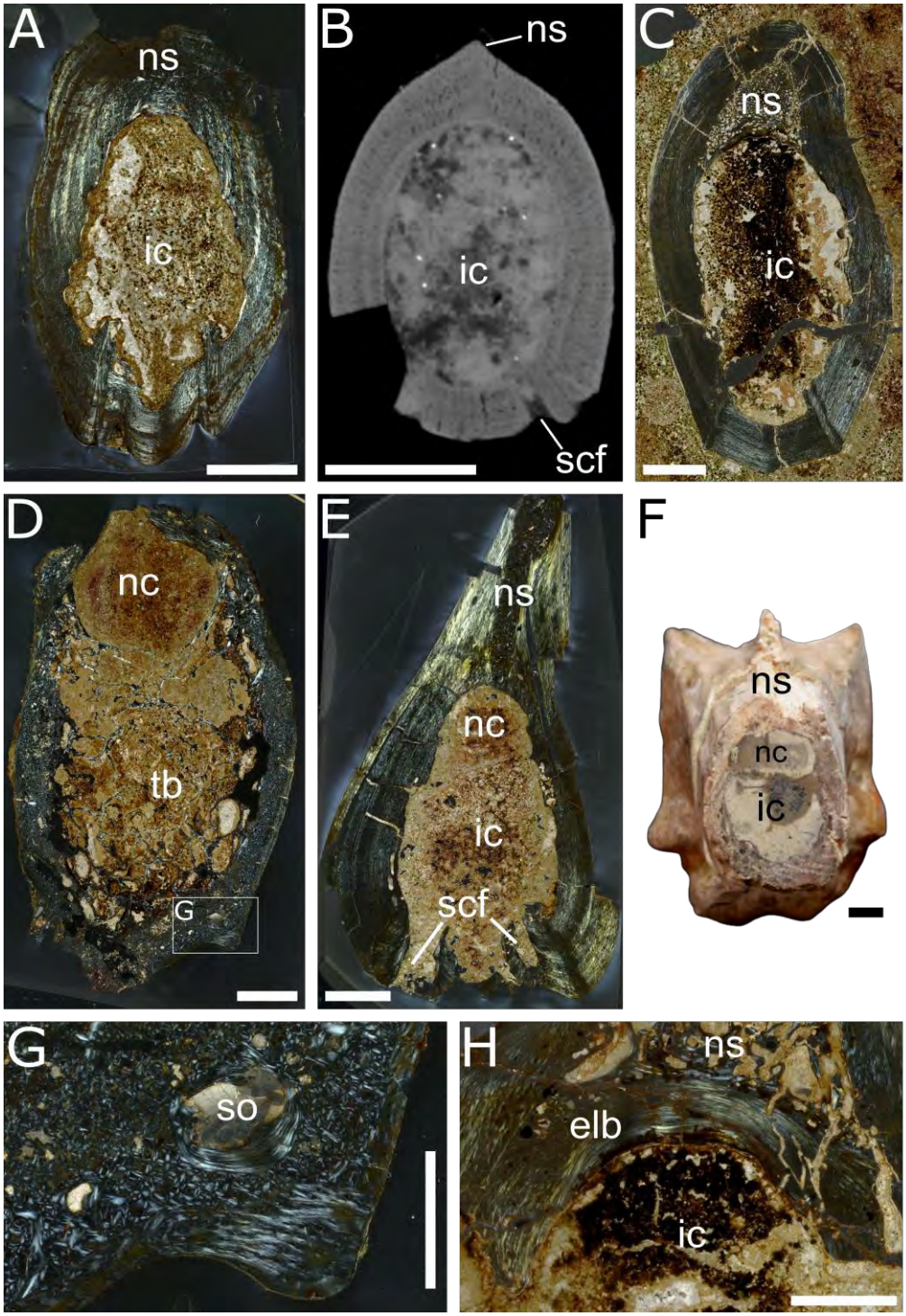

Fig. 8. Transverse cross sections through the cervicals of *Tanystropheus conspicuus*. (**A**), ZPAL V. 36/150, middle cervical, middle portion; (**B**) ZPAL V. 36/181, middle cervical, middle portion; (**C**) ZPAL V. 36/193, middle cervical, middle portion; (**D**) ZPAL V. 36/1099, 10th cervical, posterior portion; (**E**) ZPAL V. 36/166, 10th cervical, middle portion; (**F**) UMO BT 738.00, 11th cervical, anterior portion; (**G**) ZPAL V. 36/1099, 10th cervical, posterior portion, close-up on the right ventrolateral portion of the vertebra with bundles of longitudinally oriented secondary osteons; (*continued on the next page*)

(**H**) ZPAL V. 36/156, middle cervical, middle section, close-up on the base of neural spine with the endosteal bone lining. A, C, D, E, G, H, thin sections viewed in polarised light. B, μCT image. F, polished section. Anatomical abbreviations: elb—endosteal lamellar bone; ic—internal cavity; nc—neural canal; ns—neural spine; scf—subcentral foramen; so—secondary osteons; tb—trabecular bone. Scale bar equals 2 mm for B, G, H, and 5 mm for the other panels.

Discussion

Ontogenetic age of the studied specimens

Microanatomical characteristics of ZPAL V. 36/181, the smallest vertebra in the analysed *Tanystropheus* spp. sample, advocate for a young ontogenetic age of this individual. Even though some evident zonation can be identified throughout the transverse cross sections, the annuli are mostly preserved as nearly complete ellipsoids that extend parallel to the external outline of the bone. A much smaller extent of resorption of both the walls of the internal cavity and the highly vascularised tissue of the neural spine can be observed (compare Fig. 8B to the larger individuals in the same figure). Notably, ZPAL V. 36/181 is the only analysed representative of the genus *Tanystropheus* in which the vestigial neural spine is not overlain by the continuous parallel- fibred tissue layers at any point along its anteroposterior length. These characteristics are congruent with the interpretation of Jaquier and Scheyer (2017), who suggested that in the middle section of the vertebrae of older individuals the spinous process grew relatively slower than the rest of the vertebrae, and was overlain by additional periosteal bone, as we see in the larger vertebrae studied herein. Thus, it can be assumed that the size variation of the analysed cervicals is a result of presence of individuals at different ontogenetic stages, additionally broadening the scale of insights obtained from the sampled specimens. Detailed studies on microanatomical and histological changes throughout ontogeny, including skeletochronology, require more detailed sampling along the anteroposterior axis of the vertebrae and between each vertebra in a sequence.

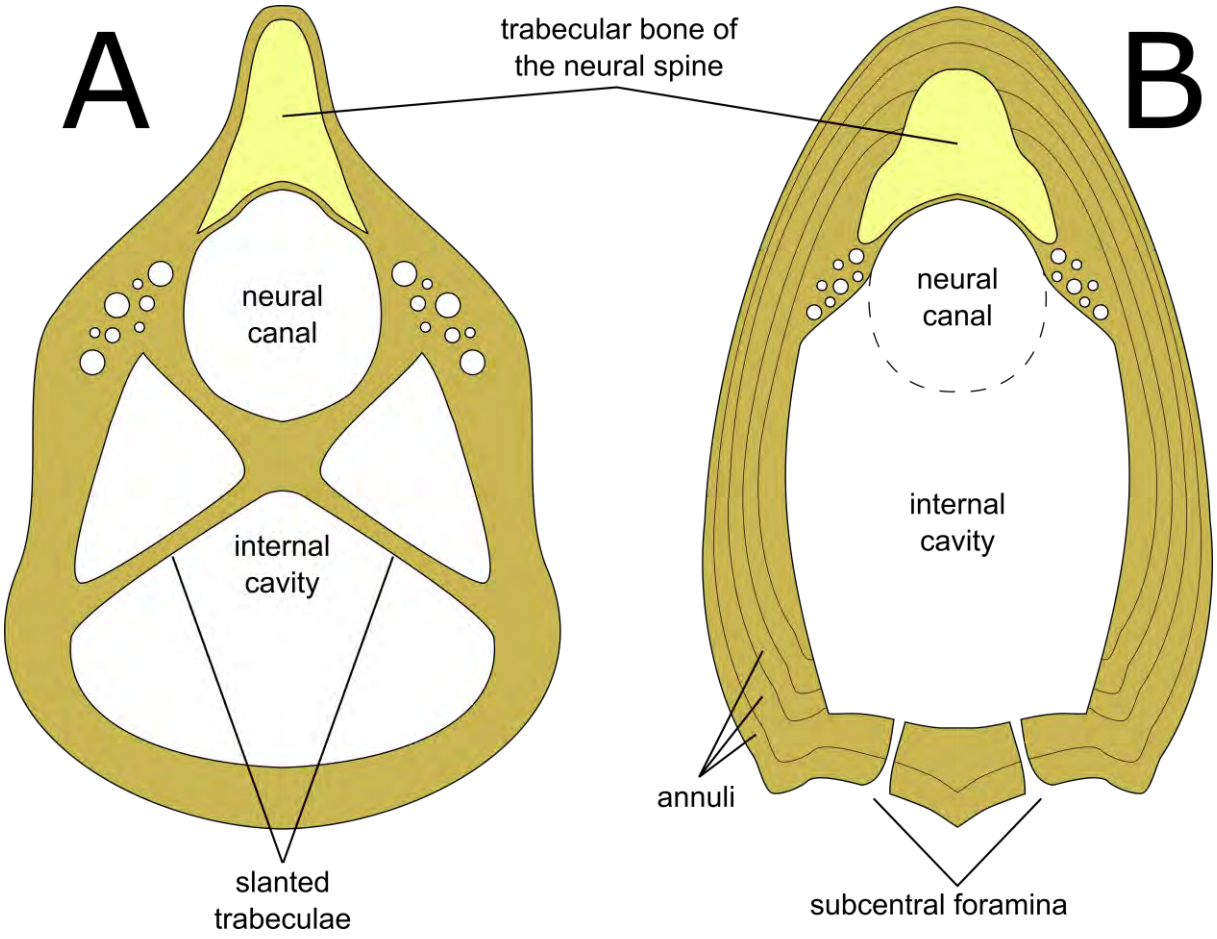

Fig. 9. Interpretative drawings of the internal anatomy of a cervical vertebra of '*Protanystropheus*' *antiquus* (**A**) and a middle cervical of an adult individual of *Tanystropheus* (**B**) shown in the transverse cross section near the midpoint of their anteroposterior length

Interpreting the internal anatomy of the tanysaurian cervicals

In accord with previous works (von Meyer 1847–1855; von Huene 1907–1908; Edinger 1924; Wild 1973; Spiekman et al. 2020*b*), our observations confirm the presence of a large, open cavity that occupies most of the volume of the centrum (see Fig. 7) within the cervical vertebrae of *Tanystropheus* spp. and '*P*'. *antiquus*. The presence of the cavity in all of the cervicals studied herein, together with the structure of the cortex and the state of preservation of continuous, undamaged slanted trabeculae spanning across the cavity (in '*P*'. *antiquus*) indicate that this empty space did not originate from the post mortem dissolution or destruction of the trabecular bone (contra Broili 1915). In *Tanystropheus* spp., the middle portion of the vertebral centra was not filled with spongiosa in vivo, as there are no signs of abrasion on the inner walls of the internal cavity, regardless of specimen size. In U-MO BT 738.00, previously described by Broili (1915), the trabeculae are present due to the sampling location—in the anteroposteriorly terminal portions of the posterior cervicals they occur much

more commonly (e.g., Fig. 8D). The neural canal floor seems to be non-continuous in some of the specimens studied herein. Many birds and some non-avian saurischian dinosaurs have foramina in the neural canal that connect to pneumatic chambers in the vertebrae (Wedel et al. 2014). They tend to be located in the lateral or dorsal walls of the canal, although small foramina in the ventral floor of the canal are occasionally present in pelicans (*Pelecanus*) and large ratites (*Struthio, Dromaius, Rhea*). Those foramina are proportionally smaller than the gaps in the floor of the neural canal in '*P*'. *antiquus*, and in the dorsals and posteriormost cervicals of *Tanystropheus* spp. We are unaware of large gaps in the walls of the neural canal in apneumatic vertebrae. This may be a feature unique to tanysaurians, although more work on the internal structure of vertebrae in other archosauromorphs will be required to adequately assess that possibility.

None of the studied middle cervicals of *Tanystropheus* spp. exhibit any traces of the bony neural canal floor being present within their anteroposteriorly middle portion. Some support for the neural canal being ventrally delimited from the internal cavity with soft tissue can be observed in two of the studied specimens—U-MO BT 738.00 and ZPAL V. 36/166. Despite different sedimentation characteristics of the two source localities (calcareous vs. argillaceous), their rock infill was preserved as if two taphonomic microenvironments were present in the internal cavity, indicating that it might have been horizontally partitioned by a barrier that diversified the rock infill. In both specimens the outline of the more dorsally located portion is ellipsoidal and resembles the shape and proportions that would be expected for a neural canal cross section. Thus, through parsimony and some taphonomic evidence, we hypothesise that the neural canal in *Tanystropheus* spp. was ventrally delimited from the internal cavity not with bony trabeculae, but rather by a functionally analogous non-mineralized tissue barrier. Even in the two posteriormost cervicals, the neural canal seems to have been underlain with a layer of soft tissue, as can be determined by its ventrally varying outline. The neural canal anatomy of '*P*'. *antiquus* might approach morphology intermediate between the plesiomorphic condition of diapsids (fully ossified neural canal floor) and the condition observed in *Tanystropheus* spp. The cervicals of '*P*'. *antiquus* exhibit different degrees of ossification of the neural canal floor, from mostly absent (e.g. MGUWr 3902s) to nearly fully ossified, but with some gaps (e.g. MGUWr 3889s). This reflects the presence of an already highly modified vertebral anatomy among the early branching tanysaurians, and even more derived features occurring in later forms (*Tanystropheus* spp.).

Comparison of the studied vertebrae with the cavernous bone of other animals

Cavernous bone tissue is widespread among different vertebrate groups. In avemetatarsalians, this type of bone contains pneumatic diverticula, which are extensions of the lungs and air-sac system (King 1966; Duncker 1971; O'Connor 2004, 2006, 2009; O'Connor and Claessens 2005; Butler et al. 2012). Cavernous bones occur also in the skulls of mammals and archosaurs (pneumatic spaces; e.g., paranasal and paratympanic sinuses), as well as in various postcranial skeletal elements in theropods, sauropods, and pterosaurs, especially in the vertebrae (Wedel 2003*a*, *b*, 2005; Cerda et al. 2012; Williams et al. 2021; Fronimos 2023; Aureliano et al. 2024). The vertebrae of the studied tanysaurians are distinct from the typical cavernous bone of tetrapods, and, despite sharing the presence of very considerable cavities, there are also several important differences between the internal anatomy of the cervicals of tanysaurians and avemetatarsalians. The chambers in the vertebrae studied herein grade evenly from the large central cavity that occupies virtually the entire centrum at its midpoint, through a complex network of trabeculae toward the anteroposteriorly terminal portions of the vertebrae. That level of heterogeneity in chamber size is not seen in pterosaurs (see Buchmann et al. 2021; Williams et al. 2021), nor in extant birds—the closest analogue among pneumatic vertebrae would be the polycamerate and semicamellate vertebrae of some sauropod dinosaurs, which have large open chambers at the mid-centrum (camerae) that grade into smaller, thin-walled chambers near the extremities of the centrum (camellae; Wedel et al. 2000; Wedel 2003*a*). In these sauropod vertebrae, the smallest pneumatic chambers are still much larger than the trabecular spaces of apneumatic vertebrae from the same taxa (e.g., Wedel 2005: fig. 7.7).

The smallest pneumatic spaces in the vertebrae of birds and pterosaurs approach the size of trabecular spaces in apneumatic, marrow-filled bone, but the size of the pneumatic spaces tends to be consistent throughout the internal structure, giving the vertebrae a honeycombed appearance—the fully camellate condition described by Britt (1993), Wedel et al. (2000), and Wedel (2003*a*). Criteria for diagnosing pneumaticity in fossil vertebrates have been reviewed by many authors (Janensch 1947; Britt 1993; Witmer 1997; Wedel 2003*a*, *b*, 2005, 2007; O'Connor 2006; Butler et al. 2012; Yates et al. 2012). Most of the uncertainty in diagnosing pneumaticity is in regard to external fossae, which are pneumatic in some cases, but may also be associated with other soft tissues, including muscle, adipose deposits, and cartilage (O'Connor 2006). All of the cited authors agree that the least ambiguous evidence of pneumaticity is the presence of large internal chambers connected to large external foramina.

Even here there is some uncertainty due to the considerable overlap in size between the largest neurovascular foramina and the smallest pneumatic foramina—see in particular the different views of Britt et al. (1998) and O'Connor (2006) on vertebral pneumaticity in *Archaeopteryx lithographica*. Butler et al. (2012) provided some clarification, noting that neurovascular foramina typically maintain the same diameter along their course (length exceeds diameter), whereas most pneumatic foramina open into chambers that are larger than the foramina (diameter exceeds length).

Foramina with possibly pneumatic affinities were not reported in any tanysaurians, nor in non-avemetatarsalian archosauromorphs as such (Spiekman et al. 2021 and the references cited therein). Numerous straight, narrow, not anastomosing canals, mostly located in the anteroventral region of the centrum, cross the cortical bone of the vertebrae of the studied tanysaurians and open into the internal trabecular spaces. In size, number, spacing, and geometry, they are more consistent with neurovascular foramina than with pneumatic foramina. On the ventral side of most of the postaxial cervicals of *Tanystropheus* spp., near their anteroposterior midpoint, one or two anteroposteriorly elongate foramina are present, occupying both lateral sides of the ventral keel (see Figs 8B, D, 9–11). In ZPAL V. 36/110, a posteriormost cervical of *Tanystropheus conspicuus*, a canal that forms from one of these foramina perforates the ventral surface of the centrum and the floor of the neural canal, with no visible branching along its tract. Thus, the mentioned foramen and, as an extension, all other similar openings in the cervicals of *Tanystropheus* spp. are not associated with pneumatisation. Moreover, the geometry of internal cavities in the taxa studied herein also suggests that they were not filled with air. Therefore, we recognize no evidence for the presence of pneumaticity in tanysaurians.

Apneumatic vertebrae with a heterogeneous internal structure like that of the tanysaurian vertebrae are known in other animals. In particular, Butler et al. (2012) documented very similar internal structures in the vertebrae of *Varanus komodoensis*, *Chelonoidis nigra*, and *Alligator mississippiensis*. Their description of the internal structure of the alligator vertebrae is strikingly similar to that of '*P*'. *antiquus*, as well as the posterior cervicals and dorsals of *Tanystropheus* spp. (see Butler et al. 2012: p. 4–6). Furthermore, the CT cross sections of vertebrae of *Varanus komodoensis* and *Chelonoidis nigra* show large cavities similar to those reported herein, which are apneumatic and filled with marrow in life. Thus, the internal cavities of tanysaurians were most likely filled with soft tissue, probably with bone marrow (Fig. 11), following the hypothesis of Dzik and Sulej (2016), who

suggested that the vertebrae were filled with fat. In many animals (including humans), the hematopoietic (blood-forming) ‘red marrow’ in the trabecular spaces of long bones grades into the ‘yellow marrow’ (with a high content of adipose tissue) in the shafts (Maniatis et al. 1971; Gurevitch et al. 2007). The composition (e.g., fat content) and volume of the soft tissue contained within the skeletal internal cavities might be dependent on lifestyle of an animal and changes through its ontogeny (see Krahl et al. 2013). Thus, with the currently available data, we cannot confidently identify the exact tissue that occupied the large vertebral internal cavities in tanysaurians. Importantly, Butler et al. (2012) have also demonstrated that at least in some other early non-tanysaurian, non-archosauriform archosauromorphs (e.g. the rhynchosaur *Stenaulorhynchus*) the interior of the vertebrae was composed of densely packed trabecular bone with no large empty spaces. Studies on the skeletal internal morphology of other non-archosauriform archosauromorphs are thus needed to further investigate the phylogenetic distribution, evolution, and function of the intervertebral cavities, as well as their connection with the origin of pneumatisation. Recent analyses have shown that vertebral pneumaticity has evolved independently in pterosaurs, theropods, and sauropods (Aureliano et al. 2022, 2024). It is perhaps possible that the large marrow-filled cavities observed in tanysaurians were more widespread in early archosauromorphs and only later, in certain lineages, were invaded by the diverticula of the air-sacs, thus potentially being a feature that was exapted for vertebral pneumaticity by some avemetatarsalians. A similar developmental process of bone marrow substitution by invading diverticula occurs postnatally in birds (Schepelmann 1990).

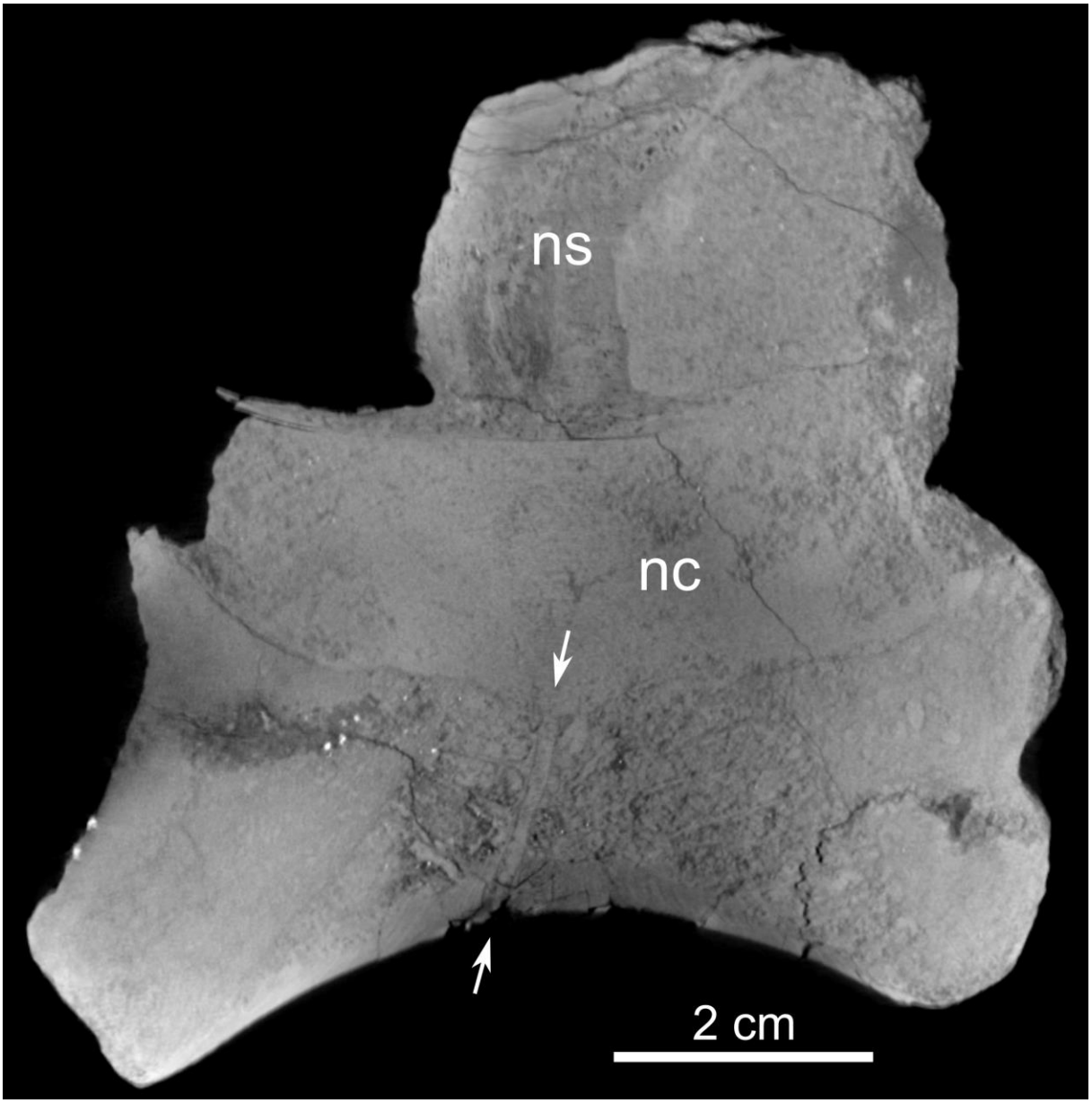

Fig. 10. Longitudinal cross section of ZPAL V. 36/110, 13th (last) cervical vertebra of *Tanystropheus conspicuus*, showing the course of the arterial canal (locations of its end sections are indicated with arrows). The anterior end of the vertebra points towards the left. Anatomical abbreviations: nc—neural canal; ns—neural spine.

Role of the subcentral foramina in *Tanystropheus* spp.

The foramina present on the ventral side of most of the postaxial cervicals of *Tanystropheus conspicuus* were already noticed by von Meyer (1847–1855). Wild (1973) described them in more detail, interpreting them as subcentral foramina. The 11th cervical is the last vertebra in which they are well outlined. In the much less elongate 12th and 13th cervicals, their size declines greatly, and in some specimens one or both of the foramina are

absent (AR pers. obs.). They are not present in the dorsals (AR pers. obs.). Therefore, some correlation can be noted between the elongation of a vertebra and the presence and size of the aforementioned foramina. Interestingly, paired foramina of vascular origin, located on the ventral side of cervical vertebrae are also characteristic of another group of long-necked aquatic reptiles—the pistosauroids, especially plesiosaurs (Wintrich et al. 2017). In plesiosaurs, these foramina are a result of the persistence of the intersegmental arteries (Wintrich et al. 2017), yet it would be difficult to confirm a similar interpretation in the middle cervicals of *Tanystropheus* spp. due to the course of the presumed arteries not being preserved in the hollow vertebrae. However, as previously mentioned, the CT-scan of the posteriormost cervical ZPAL V. 36/110 reveals that the canal originating from the foramen is straight and directly connects the ventral surface of the centrum with the neural canal. This demonstrates the existence of intersegmental arteries within the described specimen, and, as an extension, in all postaxial cervicals of *Tanystropheus* spp. in which the subcentral foramina are present. Similar interpretation of the genesis of these subcentral foramina was formulated by Wild (1973).

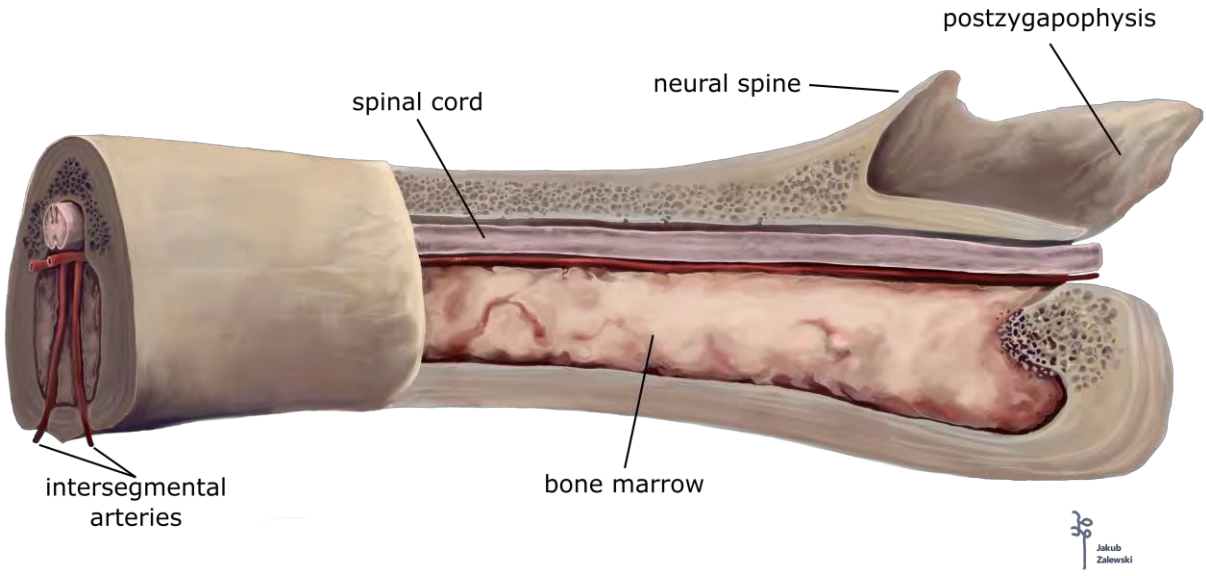

Fig. 11. Artistic reconstruction of a cross section through the posterior portion of a middle cervical vertebra of *Tanystropheus conspicuus* with hypothetical soft tissue layout included. Artwork by Jakub Zalewski.

It can also be hypothesised that the size and occurrence rate decrease of the subcentral foramina in the anteroposteriorly terminal cervicals of *Tanystropheus* spp. is connected with their relatively shorter length. It seems that there was a much stronger selective pressure towards consistent persistence of intersegmental arteries in the longest vertebrae. Convergent

evolution of this feature in *Tanystropheus* spp. and pistosauroids, two taxa of long-necked aquatic reptiles employing extremely disparate strategies of achieving neck elongation (see Rytel et al. 2024) is intriguing. Its adaptive role remains enigmatic, but could be connected with providing sufficient cerebral blood supply (see Wintrich et al. 2017). If the voluminous internal cavity of tanysaurian vertebrae was filled with soft tissue, an adequate vascularisation must have also been present there. This could additionally explain the size and occurrence rate decrease of the subcentral foramina in the shortest anterior- and posteriormost cervicals of *Tanystropheus* spp.— soft tissue volume was (relatively) much lower there than in the vertebrae from the middle section of the neck. Thus, the existence of large foramina on these elongate cervicals might be analogous to what can be observed in some appendicular bones (humeri, ulnae, femora, etc.) that also tend to have one or several larger nutrient foramina allowing access for the nutrient arteries and veins into the bone. Although no branching can be noted for the fully preserved arterial canal (Fig. 10), it cannot be ruled out that in the middle cervicals the vasculature entering the centrum though the subcentral foramina diverged into the tissue of the internal cavity.

Phylogenetic distribution and function of the unique cervical anatomy

Presence of a large internal cavity within the cervical vertebrae can be confirmed in all of the tanysaurian taxa in which the 3D preserved material was available for study—*Tanystropheus* spp., '*P*'. *antiquus*, *Augustaburiania vatagini*, *Macrocnemus bassanii*, *Ozimek volans*, *Tanytrachelos ahynis*, and the Moenkopi Formation and Homestead tanystropheids, as well as the putative tanysaurians *Czatkowiella* harae and *Microcnemus efremovi* (AR pers. obs.; von Huene 1940; Dzik and Sulej 2016; Formoso et al. 2019; Miedema et al. 2020; Spiekman et al. 2021; Heidenfelder et al. 2023). The tubular structure of the elongated cervical centra can therefore be regarded as a possible synapomorphy of Tanystropheidae. Absence of the internal cavity has been confirmed only in one known tanysaurian—*Dinocephalosaurus orientalis*, in which there seems to be no indication for hollow centra (Spiekman et al. 2024*a*). Thus, for now, the tubular structure of the cervicals cannot be unanimously regarded as ancestral for Tanysauria. Notably, *Dinocephalosaurus orientalis* exhibits the highest degree of adaptation to life in open water among the known non-archosauriform archosauromorphs—the internal anatomy of its vertebrae might therefore have also been secondarily modified, as in other aquatic amniotes (see Houssaye et al. 2016).

Interestingly, the presence of the large internal cavity in the vertebrae of tanystropheids does not seem to be affected by the disparity of their lifestyles, habitats, or spatial and temporal ranges of occurrence. Although, as exemplified herein, some variation in its relative size and anatomy should be noted, it would seem that the tubular structure of the cervicals is related to a character shared by all of the aforementioned taxa—neck elongation. A similar condition can be observed in another extinct clade of Mesozoic reptiles, the pterosaurs. Cervicals of tanystropheids, and especially *Tanystropheus* spp., resemble those of azhdarchid pterosaurs in their general external morphology (Renesto 2005), despite the obvious differences between the members of these groups. Shared features include the extent of vertebral elongation and the low neural spine. The internal vertebral cavities of '*P*'. *antiquus* are also structurally similar to the pneumatic bone chambers of pterosaurs in the presence of intermittent trabeculae spanning across the cavity (Fastnacht 2005; Williams et al. 2021) and marginal trabeculae surrounding the ends of the cavity, but disappearing towards the mid-shaft (Martin and Palmer 2014). A recent study using CT scanning has revealed that at least in some azhdarchids the cervicals were structured as a 'tube within a tube' (Williams et al. 2021). Due to their superficial similarity, comparison of the internal anatomy of the neck vertebrae of tanystropheids and pterosaurs is particularly intriguing, and available for the first time in detail through the data presented herein.

Our results demonstrate that azhdarchids converged on tanystropheids in the tubular structure of their cervicals, but detailed study reveals major differences between these elements. In the analysed vertebrae, the neural canal is wide and voluminous, the centrum is mostly hollow, with no (*Tanystropheus* spp.) or crossed ('*P*'. *antiquus*) trabeculae, a mostly thick and relatively compact cortex, and (in *Tanystropheus* spp.) an even thicker supraneural region. In azhdarchids the neural canal is relatively narrow and centrally located within an essentially hollow vertebra with helically arranged trabeculae roughly radiating away from the neural canal, a very thin cortex with no apparent differentiation between the centrum and neural arch, and no evidence of the neural spine (Williams et al. 2021). Thus, although some analogies exist between these two vertebral morphologies, it can be assumed that they mostly resulted from biomechanical limitations and plesiomorphic archosauromorph vertebral and muscular anatomy (general shape of the vertebra). The cervicals of both taxa evolved under conditions favouring neck elongation, which was achieved not by the adding to the cervical vertebrae count, but rather by increasing their relative length (Müller et al. 2010; Rytel et al. 2024). The resulting morphologies are a response to a similar biomechanical problem and

using similar resources but resulting in a very different solution. In tanysaurians, and especially in *Tanystropheus* spp., the tubular structure of the vertebrae was achieved by replacement of the bony trabeculae of the centrum with soft tissue, which resulted in the appearance of a large internal cavity, sheathed with a dense bone layer. The redistribution of bone mass towards the periphery of the vertebra most likely had a mechanical function, congruent with what was observed in pterosaurs (Fastnacht 2005; Williams et al. 2021). Hollow, cylindrical bones have increased bending and torsional strength, relative to their volume (Fastnacht 2005; Cuff and Rayfield 2013; Williams et al. 2021; Toyama et al. 2024). A heavy, compact cortex is also present in the long bones of birds, partially compromising their lightness but increasing their strength-to-weight and stiffness-to-weight ratios (Dumont 2010).

In '*P*'. *antiquus* the relatively thick internal slanted trabeculae spanning across the internal cavity most likely increased the resistance to buckling (see Williams et al. 2021). Taking into consideration the ordered layout and heavy remodelling of these trabeculae, their biomechanical importance is evident. Thus, it can be hypothesised that with the increasing relative neck length of early archosauromorphs, their vertebrae were adapted to withstand more and more considerable tensions resulting from bending and torsion on the cervical column. An extreme result of this trend is well exemplified in *Tanystropheus* spp., which among known tanystropheids possessed the (absolutely and relatively) longest neck and vertebrae. The cervicals of this animal demonstrate a higher degree of modification than its stratigraphically older or contemporaneous relatives (e.g., '*P*'. *antiquus*; compare Figs 1 and 2), exhibiting a centrum structured as a cylinder of dense parallel-fibred bone, devoid of trabeculae, and with a triangularly-ellipsoidal transverse cross section. The decrease of the amount of bony trabeculae in the middle section of the vertebra was not an apomorphy of *Tanystropheus* spp., but rather a character that was widespread among tanystropheids, which *Tanystropheus* spp. only expanded on. Although the cervicals of *Tanystropheus* spp. are substantially longer than in other tanysaurians, their internal anatomy does not seem to correlate with further bone mass reduction, but rather achieving a more resistant cylindrical outline of the centrum. Overall, it should be noted that if the tanysaurian vertebrae were adapted for minimising mass, the adaptation was probably in the material properties (especially the densities) of its compact bone and marrow, and not in the overall construction of the vertebrae, in contrast to the very light, pneumatic vertebrae of pterosaurs and saurischian dinosaurs.

Relationship of cervical anatomy to lifestyle in *Tanystropheus* spp.

Recent studies have nearly unequivocally supported a (semi) aquatic lifestyle for *Tanystropheus* spp. (Nosotti 2007; Renesto and Saller 2018; Spiekman et al. 2020*a, b*; Spiekman and Mujal 2023), but the lightly built cervicals of those animals could seem, at least at first glance, to contradict this hypothesis. The vertebrae of secondarily aquatic tetrapods such as cetaceans, ichthyosaurs, plesiosaurids, and mosasaurids are filled with dense trabecular bone and lack large open chambers (Dumont et al. 2013; Houssaye et al. 2016; 2018; Sander and Wintrich 2021). The cervicals of *Tanystropheus* spp. do not show internal vertebral microanatomy similar to fully aquatic tetrapods, and they also seem to lack the skeletal osteosclerosis, pachyostosis, or increased bone porosity in cortical bone that are present in numerous aquatic taxa, depending on the animal's lifestyle and habitat (Houssaye 2009; Houssaye et al. 2016). However, in most semi-aquatic taxa (e.g., crocodylians), the internal vertebral organisation is more similar to that in terrestrial animals (see Butler et al. 2012; Houssaye et al. 2016), so the lack of microanatomical characters traditionally associated with a (semi)aquatic lifestyle does not preclude it. Trachelosaurids, which are a sister group of tanystropheids (Spiekman et al. 2021, 2024*a, b*), exhibit a roughly similar (although considerably less elongate) cervical shape, and yet several taxa from this group are clearly extensively adapted to an aquatic lifestyle (Liu et al. 2017; Li et al. 2017*b*; Wang et al. 2023*a, b*; Spiekman et al. 2024*a, b*).

Interestingly, a large internal cavity is present in the core of some of the vertebral centra of Triassic eosauropterygians, especially in nothosaurids (Broili 1915; Klein et al. 2019; AR pers. obs.). This cavity is relatively smaller and less regular than the clear-cut internal cavities of tanystropheids, but, being ventrolaterally encompassed only by dense cortex, it follows similar patterns of reorganisation and redistribution of the mass of the vertebra to its periphery (Klein et al. 2019). Some eosauropterygian vertebrae are similar to those of '*P*'. *antiquus* in their internal anatomy and layout of the cavities (compare Fig. 9A with Klein et al. 2019: fig. 1C). Eosauropterygians exhibited extensive adaptations to an aquatic lifestyle (Klein et al. 2016). Therefore, it is evident that the presence of a large internal cavity in the vertebrae does not necessarily indicate a terrestrial lifestyle for an animal; contrastingly, Klein et al. (2019) interpreted it as a potential paedomorphic adaptation to life in an aquatic habitat. This constitutes another example of anatomical characters shared by *Tanystropheus* spp. and sauropterygians, the others including the hyperelongation of the neck, teeth layout, and morphology, as well as the here-proven retainment of the

intersegmental arteries in adult individuals. Notably, remains of *Tanystropheus* spp. are virtually always accompanied by remains of nothosaurids (AR pers. obs.). Thus, convergent evolution of the mentioned features in tanysaurians and early sauropterygians might have been related to them adapting to similar, or even overlapping, habitats.

Extensive 'cervicalisation' of the dorsal vertebrae throughout the evolution of *Tanystropheus* spp. resulted in only 12 dorsals being present in the vertebral column of this animal (Rieppel et al. 2010, Rytel et al. 2024). This number is very low for a non- avian archosauromorph (see supporting information in Müller et al. 2010; Rytel et al. 2024), possibly the lowest among non- archosauriform members of the Archosauromorpha, matched solely by *Pectodens zhenyuensis* Li, Fraser, Rieppel, Zhao & Wang, 2017 (Li et al. 2017a). Therefore, the trunk of *Tanystropheus* spp. was not only short when compared to its neck, but generally composed of relatively few vertebrae. With the decrease of the number of dorsals and the shoulder girdle shifting its location along the body axis, the position of the centre of body mass was almost certainly also affected. The elongate cervicals, together with the bundles of nearly completely avascular cervical ribs (Jaquier and Scheyer 2017), might have contributed to the weight of the anterior portion of the body in a major way. Some researchers have suggested that the neck of *Tanystropheus* spp. was lightly built, due to the 'hollowness' of the cervicals, and thus allowed for locomotion on land (Renesto 2005; Renesto and Saller 2018). However, the tubular anatomy of these vertebrae does not have to equate to their light weight, taking into consideration their relatively high compactness. Correspondingly, extant birds and bats exhibit relatively heavy skeletons (compared to volume) that are resistant to stress, despite their delicate, slender appearance, and hollow, thin walled long bones (Dumont 2010). Tanysaurians may serve as another, well-fitting example of this phenomenon. Importantly, anterior displacement of the centre of mass relative to its position in terrestrial ancestors is one of the key adaptations to an aquatic lifestyle in non-avian tetrapods (Motani and Vermeij 2021). Thus, the increase of cervical verte- brae count and length, when compared to other tanystropheids (Rytel et al. 2024), could be interpreted as an adaptation correlated with the transition to an aquatic environment. However, further studies taking into account the physical properties of the cervicals of the early diverging archosauromorphs are needed to fully explore this hypothesis.

Conclusions

In his original description of *Tanystropheus conspicuus* von Meyer (1847–1855) summarised his hypothesis on the neurology of its vertebral column as follows: 'It is hardly conceivable that a contraption like the one to which the fossil vertebrae [of *Tanystropheus conspicuus*] point should stand alone and have only existed in a prehistoric animal' [translated from German]. Contrastingly, research presented herein demonstrates that the cervicals of some tanysaurians, especially *Tanystropheus* spp., are characterised by anatomical features that are unparalleled in any other animals known. Morphology (both external and internal) of these vertebrae is unique among vertebrates, with some extinct groups (e.g., azhdarchid pterosaurs, sauropods, sauropterygians) being the most comparable. Strikingly, evolution of an anatomical modification of such a considerable extent and intensity proceeded quickly—in the time shortly after (< 10 Mya) the End-Permian Extinction, underlining the fast pace of morphological diversification of archosauromorphs during this period (Foth et al. 2016; Ezcurra and Butler 2018). The unique bauplan of *Tanystropheus* spp. is a result of extreme evolutionary trade-offs between cervical length, weight, and durability, induced by a selective pressure towards the transition to an aquatic lifestyle, but constrained by developmental and structural limitations. Interestingly, the hyperelongation of the neck vertebrae was not shared by all tanysaurians—in trachelosaurids, the sister group of tanystropheids, an entirely different strategy of neck elongation is exhibited. This is well exemplified in *Dinocephalosaurus orientalis*, a taxon much more extensively adapted to the aquatic lifestyle, which possessed over 60 presacral vertebrae (with only 25 in *Tanystropheus* spp.). Our findings provide further insights into the remarkable disparity of evolutionary innovations connected with neck elongation in early archosauromorphs. While in '*P*'. *antiquus* some trabecular support structures are present within the cervical centra, they are absent in the middle neck vertebrae of *Tanystropheus* spp.—with the latter being nearly perfectly cylindrical in transverse cross section. This tubular architecture, together with the high compactness of the bone walls in the cervicals of both studied taxa, provided durability and forced rigidity of the vertebral column. The large internal cavities present in these vertebrae were filled with soft tissue, most probably bone marrow. Some tanysaurians were similar to long-necked avemetatarsalians in lightening of their elongate cervicals. Interestingly, they did so not through vertebral pneumatisation, but rather by evolving a large internal cavity in the centrum, resulting in hollow, cylindrical verte- brae, morphologically unique among vertebrates. *Tanystropheus* serves as an extreme example of this feature, exhibiting major modifications of not only general vertebrae morphology, but also their histology and

associated soft tissue layout. Especially noteworthy is the persistence of the intersegmental arteries in the cervicals of adult individuals of *Tanystropheus* spp., a unique feature among archosauromorphs. This character, together with the presence of the large internal cavity within vertebrae, is shared with sauropterygians, revealing some potential parallels in their evolution and convergent adaptation to an aquatic life- style in these groups. The internal morphology of the cervicals of non-tanysaurian early archosauromorphs should be further explored to trace the evolution and development of the internal chambers within them, as well as their potential connection with the origin of bone pneumaticity in avemetatarsalians.

Chapter III

Biomechanics of the extremely elongated neck of the Triassic archosauromorph *Tanystropheus*

Adam Rytel[1,*], Pasha A. van Bijlert[2,3], Stephan Lautenschlager[4,5], Stephan N. F. Spiekman[6], Mateusz Tałanda[7], Tomasz Sulej[1]

[1]Institute of Paleobiology, Polish Academy of Sciences, Twarda 51/55, 00-818 Warsaw, Poland;

[2]Department of Earth Sciences, Faculty of Geosciences, Utrecht University, Vening Meinesz Building A, Princetonlaan 8A, 3584 CB Utrecht, Netherlands;

[3]Naturalis Biodiversity Center, Darwinweg 2, 2333 CR Leiden, Netherlands;

[4]School of Geography, Earth and Environmental Sciences, University of Birmingham, Birmingham B15 2TT, United Kingdom;

[5]Lapworth Museum of Geology, Birmingham B15 2TT, United Kingdom;

[6]Staatliches Museum für Naturkunde, Rosenstein 1, D-70191 Stuttgart, Germany;

[7]University of Warsaw, Faculty of Biology, Biological and Chemical Research Centre, Institute of Evolutionary Biology, ul. Żwirki i Wigury 101, 02089 Warsaw, Poland;

* – corresponding author: adam.rytel@twarda.pan.pl

Introduction

Extremely elongate necks have convergently evolved in several amniote lineages, including both aquatic and terrestrial forms (Fig. 1). The development of such a feature brings with it advantages in obtaining food items, but also biomechanical challenges, such as flexibility, stability, lift, and inertia. In *Tanystropheus*, a particularly long-necked Triassic archosauromorph, the neck is composed of only 13, mostly extraordinarily elongated and slender cervical vertebrae and accompanying rod-like, overlapping ribs, making it arguably the most extreme example of neck elongation in tetrapod evolution (Fig. 1; Wild 1973; Nosotti 2007, Rieppel et al. 2010; Rytel et al. 2024*a, b*; Chapter I). Understanding the function of this remarkable neck provides insights into the limits of neck elongation in amniotes and the evolution of morphological novelties in Triassic reptiles. Here we present the first quantitative biomechanical analysis of the *Tanystropheus* neck using a digital model based on three-dimensionally preserved bones. We assessed its range of motion (ROM) and performed finite element analysis (FEA) on the individual cervical ribs and the neck model in

different configurations. Our results indicate that the neck of *Tanystropheus* was not extremely stiff, as previously postulated, and the ribs likely did not impair its movements. They transferred tensile forces towards the base of the neck, similar to what hypothesised for sauropods (Christian and Dzemski 2007). This study elucidates the bauplan of an extremely specialised animal and brings us closer to understanding the patterns of achieving neck elongation in vertebrates.

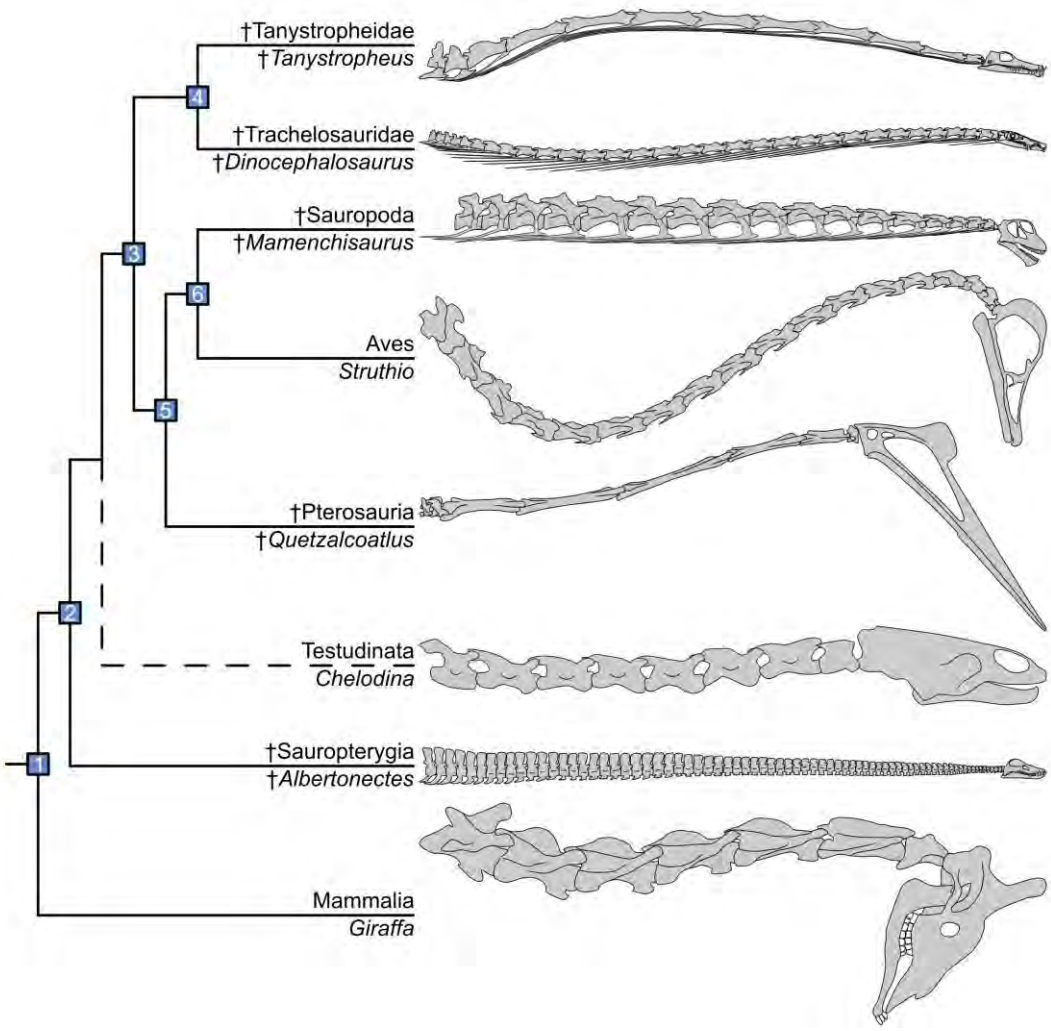

Fig. 1. Comparison of the cervical vertebral column anatomy of some long-necked tetrapods. Reconstructions not to scale. Based on: *Tanystropheus conspicuus* – Rytel (Chapter I); *Dinocephalosaurus orientalis* – Spiekman et al. (2024*a*); *Mamenchisaurus youngi* – Pi et al. (1996), Ouyang and Ye (2002); *Struthio camelus* – Mivart (1874); *Quetzalcoatlus* – Padian et al. (2021); *Chelodina longicollis* – Herrel et al. (2007); *Albertonectes vanderveldei* – Kubo et al. (2012), Sachs et al. (2018); *Giraffa camelopardalis* – Badlangana et al. (2009). The numbered nodes correspond to the following taxa: 1. Tetrapoda; 2. Diapsida; 3. Archosauromorpha; 4. Tanysauria; 5. Avemetatarsalia; and 6. Saurischia.

Materials and methods

Specimens

To analyse the neck biomechanics of *Tanystropheus* we gathered digital representations (watertight surface models) of the anterior portion of its axial skeleton. These include the skull, cervical vertebrae, the corresponding ribs, as well as the first dorsal vertebra, which originated from two species of *Tanystropheus*. The skull and the atlas-axis complex originated from PIMUZ T 2790, the holotype of *Tanystropheus hydroides* described by Spiekman et al. (2020*a*, *b*).

To differentiate the anterior, middle, and posterior subregions of the neck we followed Rytel et al. (2024*a*, but see also Chapter I). The models of ribs and most postaxial vertebrae derive from various specimens of *Tanystropheus conspicuus* from the Ladinian site of Miedary, Poland (Czepiński et al. 2023), and were first presented in Rytel (Chapter I; Appendix I). They are freely available at MorphoSource: https://www.morphosource.org/projects/000774422. The morphology of the 11th cervical vertebra of *T. conspicuus* was reconstructed based on SMNS 84821 from Schwingen, Germany (see Rytel et al. 2024*b*; https://www.morphosource.org/concern/media/000668709). All mentioned specimens, excluding PIMUZ T 2790, were isolated specimens with excellent three-dimensional preservation. Measurements of the angles between the articular surfaces of the centrum and its ventral margin in lateral view were taken from all postatlantal vertebrae used in the analyses. These data were compared with the curvature reconstructed in the model, to assess if the retrieved posture is supported by the osteological correlates.

Additionally, two cervical ribs of *Tanystropheus conspicuus* from Miedary (the shaft of ZPAL V. 36/1013 and the articular region of ZPAL V. 36/1092) were thin sectioned to gain insights into their internal anatomy. Their histology was then compared with other cervical rib thin sections available for *Tanystropheus* (Fig. 2).

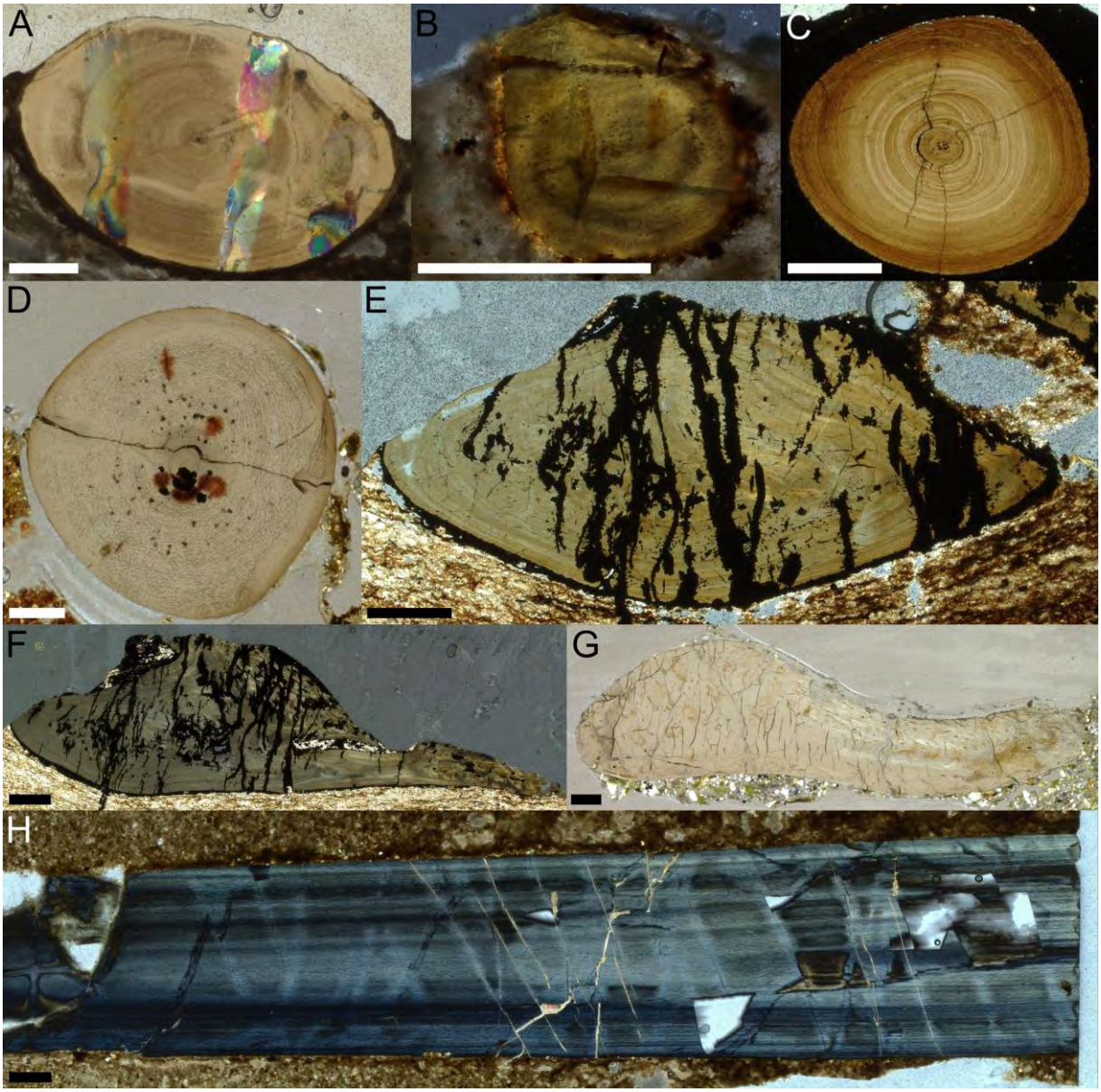

Fig. 2. Histology of the cervical ribs of *Tanystropheus*. Transverse (**A–G**) and longitudinal (**H**) cross sections through the shaft (A–D, H) and the articular portion of the rib (E–G) in normal transmitted (A, C–G) and cross-polarised light (B, H). A, H – SMNS 54057 (*T. conspicuus*). B - PIMUZ T 1277 (*T. longobardicus*). C – PIMUZ T 2789 (*Tanystropheus* sp.). D – ZPAL V. 36/1013 (*T. conspicuus*). E–F – PIMUZ T 2784 (*Tanystropheus* sp.). G – ZPAL V. 36/1092 (*T. conspicuus*). See Wild (1973), Jaquier & Scheyer (2017), and Appendix I for stratigraphic and topographic data concerning the specimens. Scale bars equal 5 mm.

Skeletal reconstruction

The anterior portion of the axial skeleton of *Tanystropheus* was reconstructed in Blender 4.5. Vertebral models were created by mirroring the better preserved lateral halves of the postatlantal vertebrae along the sagittal plane. Isolated middle cervical vertebrae of *Tanystropheus* cannot be unequivocally referred to a specific position in the vertebral column due to their similar morphology, and no specimen preserves all of them in three dimensions (Rytel et al. 2024*a*; Chapter I). Instead, ZPAL V. 36/1078 was used to represent the cervical vertebrae three to nine (the same model was used in different scales). Shafts of the rib pairs associated with the anterior eleven vertebrae were reconstructed by adding an elongated cylindrical extension to the articular head. The capitulum of the ZPAL V. 36/1000 rib was reconstructed, and the orientation of the capitulum of ZPAL V. 36/1251 was changed to counteract the slight compression of the specimen.

The size of all individual elements was scaled to fit the proportions present in the complete, large individual of *T. hydroides* PIMUZ T 2818 (Fig. 3), which preserves a nearly complete anterior part of the axial skeleton (see Table 1 for measurements). Measuring the total cervical rib lengths in *Tanystropheus* is difficult due to their fragility and preservation in bundles. In the reconstructed model the rib lengths were adjusted to mirror how many rib pairs are present along different sections of the neck of PIMUZ T 2818, even if the visible elements cannot be directly traced to their articulation with the associated vertebrae.

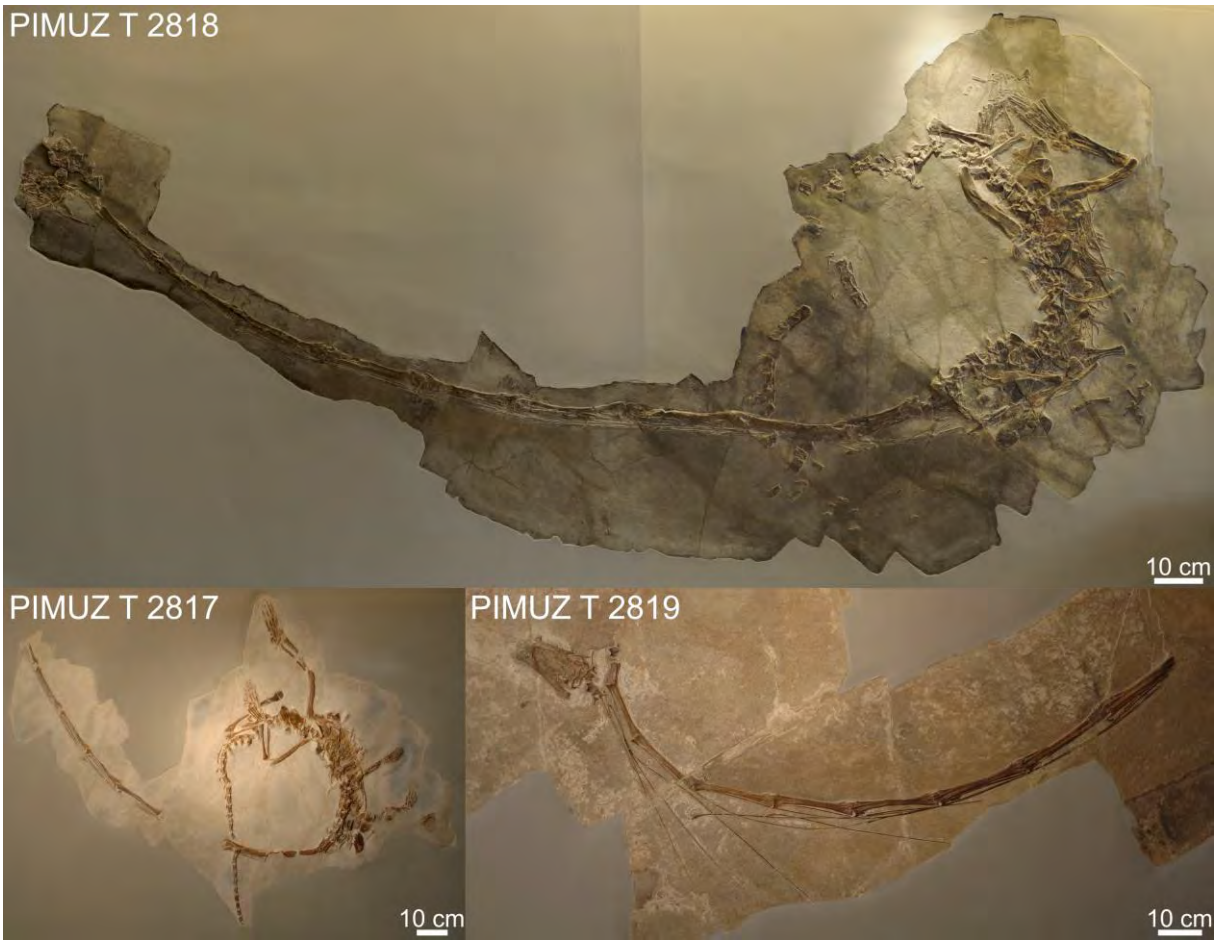

Fig. 3. Articulated specimens of *Tanystropheus* with varying curvature of the neck.

Positioning of the vertebrae was based on the orientation of the articular surfaces. We analysed the neck motions with respect to the first dorsal vertebra, which was kept immobile. Only two vertebrae were shown at a time to minimise preconceived notions (Mallison 2010; Vidal et al. 2024). Each cervical vertebra was positioned so that the articular surfaces of its postzygapophyses are aligned as parallel as possible to the corresponding surface of the prezygapophyses of the more posterior vertebra, and so that the overlap between them is maximised. The position of the vertebra was then further vertically adjusted, to make the corresponding articular surfaces of the centra face each other (to the maximal extent possible without the models intersecting). Ribs were articulated to the vertebrae and the morphology of their shaft was modified to mirror the curvature of the neck. The ribs from one lateral side of the vertebral column were then mirrored to the other. Each succeeding rib pair was positioned dorsolaterally to the pair preceding it. After assembling, the entire model was scaled to match the size of large *T. conspicuus* individuals (Chapter I), from which the isolated elements originated, and measured 325 cm in total anteroposterior length. The resulting model served as the osteological neutral pose for the analyses.

Table 1. Measurements of vertebrae and ribs of a large *T. hydroides* individual PIMUZ T 2818 and the corresponding specimens used to reconstruct them within the biomechanical model. Cervical ribs lengths include only the visible portion of the element (minimal length), usually without the distal end of the shaft.

Element	Length [mm]	Specimen model used	Notes
CV2	68	PIMUZ T 2790	
CV3	170	ZPAL V. 36/1078	
CV4	221	ZPAL V. 36/1078	
CV5	217	ZPAL V. 36/1078	
CV6	230	ZPAL V. 36/1078	
CV7	228	ZPAL V. 36/1078	
CV8	257	ZPAL V. 36/1078	
CV9	246	ZPAL V. 36/1078	
CV10	239	ZPAL V. 36/186a	
CV11	178	SMNS 84821	
CV12	78	ZPAL V. 36/1209	
CV13	51	ZPAL V. 36/2485	
DV1	43	ZPAL V. 36/1249	
CR2	345	ZPAL V. 36/2433	Shaft reconstructed
CR3	609	ZPAL V. 36/2433	
CR4	745	ZPAL V. 36/2433	
CR5	870	ZPAL V. 36/2433	
CR6	954	ZPAL V. 36/2433	
CR7	996	ZPAL V. 36/2433	
CR8	866	ZPAL V. 36/2433	
CR9	737	ZPAL V. 36/2433	
CR10	532	ZPAL V. 36/2433	
CR11	278	ZPAL V. 36/1019	
CR12	96	ZPAL V. 36/1000	Capitulum reconstructed
CR13	82	ZPAL V. 36/1251	Capitulum orientation adjusted

Rigid kinematic analysis

The ROM analysis was performed with a Blender plugin MuSkeMo (van Bijlert 2024; https://github.com/PashavanBijlert/MuSkeMo), using a rigid body kinematic approach. The aim of this analysis was to recover the general patterns of neck mobility in *Tanystropheus* and assess how it could be affected by the cervical ribs. A centre of rotation (joint) was created at the midpoints between each pair of centra. To uniformise the joint placement along the neck, landmarks were added to mark the most anterodorsal, anteroventral, posterodorsal, and posteroventral points on the centrum. The position of the centre of rotation was set to the average location of the four mentioned landmarks placed on the corresponding articular

surfaces. Joint axes were aligned with respect to each posterior vertebra from the pair as follows: positive x was aligned with the long axis of the vertebra and pointed anteriorly, positive z was oriented mediolaterally and pointed to the right, and positive y pointed dorsally. To achieve this, we fitted cylinders to the vertebral bodies using MuSkeMo's "Fit cylinder" function, and transferred these orientations to the joints. Bodies were created for each vertebra, and then tied with the joints as the child (preceding) and parent (succeeding) elements, to establish the proximodistal hierarchy of the vertebrae. The atlas-axis complex and the skull were treated as a single rigid element. Two variations of the resulting model were used - with and without the cervical ribs. The ribs were fused with the vertebra, with no movement allowed in the articulation between them.

ROM was checked by employing a script included in MuSkeMo that rotates the entire section of the neck anterior to a given joint around its centre of rotation by one degree at a time, until any meshes intersect. Script traversed anteriorly from the most posterior joint (first dorsal vertebra/13th cervical vertebra), recording the last rotation value reached before the intersection for each joint. Maximum ROM was tracked by summing the rotation values reached for the X (torsion), Y (lateral flexion), or Z (dorsoventral flexion) axes of each joint. The maxima were, thereby, the differences in rotation between the osteological neutral pose and the ending pose of the atlas-axis complex and the skull. If the results were asymmetric, the higher maximum ROM value was used.

Finite element analysis

In order to test the flexibility of the neck, three different biomechanical simulations were performed using FEA: (1) a simulation of an isolated cervical rib to test its bending properties, (2) a simulation of the entire neck with cervical ribs, and (3) the same as two but without cervical ribs. For the FEA of the isolated rib, two straight cervical rib models with different shaft length were tested. For analysis setup and pre-processing, the models were imported into Hypermesh (version 11, Altair Engineering). Solid mesh models were generated from surface models each consisting of ca. 1.5 million elements. In the absence of material properties for reptilian rib bone, properties derived from the biomechanical modelling of human ribs were used (García-Vilana et al. 2025). The latter is a common biomedical application of FEA and given the similarity to our study, we used corresponding material properties. To account for the likelihood that the ribs of *Tanystropheus* had somewhat different composition of cortical and trabecular bone, we performed sensitivity tests using a range of material properties (E = 10-20 GPa, υ = 0.1-0.35). As the variation of the material

properties did not result in any notable differences in bending behaviour, we used the material properties with the highest stiffness (E = 20 GPa, υ = 0.35). These values also fall within the average for most vertebrates (Erickson et al. 2002). Our results may underestimate the bending capability of the ribs and the flexibility of the neck may have been higher. The rib models were constrained from movement at eight nodes along the articular surface with the corresponding cervical vertebrae. A displacement force was applied to the distal end of the rib models in different directions (dorsal, ventral, and lateral). Results of these analyses were evaluated using overall bending when encountering different von Mises stress thresholds (50, 100, 200 MPa). Given the simplifications inherent in the FEA models, these thresholds represent general indicators of bone stress with bone failure around 200 MPa (Currey 2006).

For the two simulations of the full model, the surface model of the neck was imported into Hypermesh. Connective tissues were added in Blender between the centra of successive vertebrae corresponding to the extent of the articular surfaces of the centra. A Boolean operation was applied to remove overlapping surfaces of the connective tissue models with the vertebrae. A single solid mesh was generated for the entire neck model with different material properties applied to the individual components. For the vertebrae and ribs the same material properties as for the simulation of the isolated ribs was selected. For the connective tissue the Young's modulus was set to 1% of the bone (E = 0.2 GPa, υ = 0.35) similar to the upper range of values for material properties used for sutures studies in lizard biomechanics (Jones et al. 2017). Again, this may overestimate stiffness, but as the full neck simulations were performed in a comparative context, material properties were of negligible importance. The model was constrained from movement at 10 nodes at the first dorsal vertebra. The cervical vertebrae were free to rotate and translate about all three axes (six degrees of freedom per vertebra), and these motions were constrained through the material properties of the intervertebral tissue. A load force of 100 N was applied to the second cervical vertebra in different directions (dorsal, ventral, and lateral). This force was chosen to allow for sufficient displacement of the neck, as for this analysis we were interested in the effect of the cervical ribs in a comparative context rather than absolute values. The analyses were performed for each bending direction with and without the cervical ribs. Results were evaluated using von Mises stress and tensile/compressive stress distribution plots. In contrast to the FEAs for the individual rib models, we did not test for failure stress magnitudes but compared the stress distributions in the models with and without cervical ribs. Stress magnitudes recovered are therefore below the failure threshold.

Results

The reconstructed osteological neutral pose of the neck of *Tanystropheus* (see Methods) is curved, with its central portion located dorsally relative to both the skull and the base of the neck (Fig. 4B). This arch-like reconstruction is further supported by the orientations of the articular surfaces of the centra (Table 2). The anterior surface of the centrum of the 13th cervical vertebra and the posterior surface of the centra of the 12th and 11th cervical vertebrae were oriented distinctly more dorsally than in the other specimens. In all more anterior cervical vertebrae, the articular surfaces of the centrum are subvertical in lateral view, or slightly ventrally oriented. These characteristics indicate the dorsal inclination of the base of the neck (see Renesto 2005; Chapter I), which is also recovered within the model. The middle-anterior portion of the neck is recovered as gradually more ventrally bowing in the anterior direction. In the reconstructed model the distance between the articular surfaces of the articulating middle vertebral centra is considerable, supporting the presence of relatively large amounts of intervertebral tissue (Wild 1973; Tschanz 1986, 1988).

Table 2. Differences of angulation of the articular surfaces of the centrum in relation to its ventral edge.

Element	Specimen	Centrum articular surface angulation [°]	
		posterior	anterior
CV2	PIMUZ T 2790	96	91
Mid CV	ZPAL V. 36 1078	97	102
CV10	ZPAL V. 36 186	89	96
CV11	SMNS 84821	75	97
CV12	ZPAL V. 36 1209	72	92
CV13	ZPAL V. 36 2485	94	73

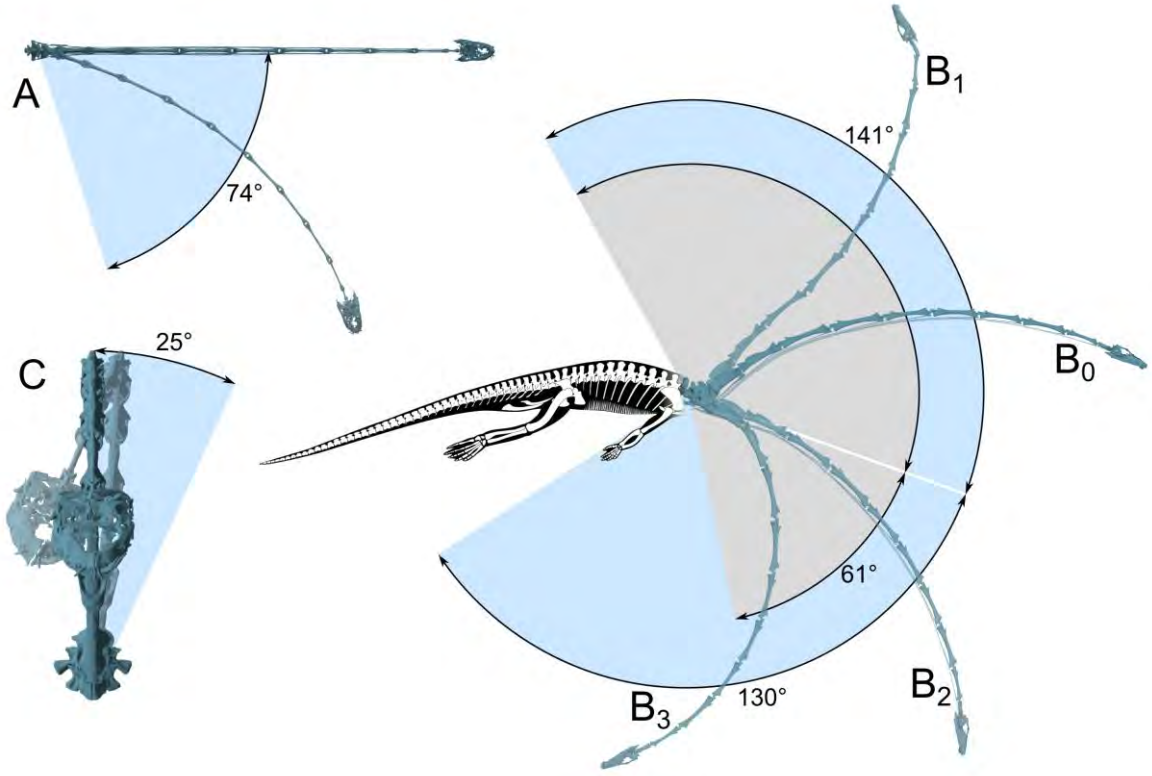

Fig. 4. *Tanystropheus* neck postures based on the ROM analysis. (A) Maximum lateral flexion without cervical ribs. (B) Postures within the dorsoventral osteological range of motion: the osteological neutral pose (B0); maximum dorsiflexion (B1) and maximum ventroflexion with (B2) and without cervical ribs (B3). (C) Maximum torsion without cervical ribs. Arcs described between the osteological neutral pose and the maximum flexion (of the skull) in a given plane are indicated in blue for the model including the cervical ribs and in grey for a model without them. All models in orthographic view. *Tanystropheus* reconstruction from Chapter I.

The results of the ROM analysis for torsion, dorsiflexion, and lateral flexion are nearly identical for the analytical iterations carried out on the model with and without cervical ribs (Table 3). Values for the lateral rotation vary between the joints, but no clear patterns can be noted when comparing between the subregions of the neck. The neck bends laterally in a gentle curve, up to a maximum angle of 73° with ribs and 74° without them (Fig. 4A). Torsion is very limited, with all joints being able to rotate by <5°, which results in a maximum torsion of 25° (Fig. 4C). Maximum dorsiflexion is achieved with the neck being anterodorsally oriented and relatively straight, and the skull pointing posterodorsally. There is a clear disparity between the maximum rotation values reached by the joints associated with the posterior and middle cervical vertebrae, with the former reaching much lower values (2-5°)

than the latter (12-17°). The neck is slightly ventrally curved in this posture, with the maximum dorsiflexion reaching 141° for the model with cervical ribs and 142° without them (Fig. 4B). Many articulated specimens of *Tanystropheus* are preserved with a dorsiflexion of the vertebral column (=opisthotonus, see Faux and Padian 2007; Fig. 3). In the specimens in which the ribs are predominantly still articulated and largely intact, the neck curvature does not exceed the maximum curvature recovered by the ROM analysis.

Table 3. Values of the maximal rotation of the joints achieved in the ROM analysis.

Joint	Total rotation [°]											
	Lateral (left)		Lateral (right)		Dorsal		Ventral		Torsion (clockwise)		Torsion (counterclockwise)	
	Without ribs	With ribs	Without ribs	With ribs	Without ribs	With ribs	Without ribs	With ribs	Without ribs	With ribs	Without ribs	With ribs
DV1/CV13	6	6	6	6	5	4	29	23	3	3	2	2
CV13/CV12	10	10	10	10	5	5	16	16	1	1	1	1
CV12/CV11	6	6	6	6	5	5	19	14	3	3	2	2
CV11/CV10	1	1	0	0	2	2	29	3	0	0	0	0
CV10/CV9	4	4	3	3	2	2	5	0	1	1	1	1
CV9/CV8	6	5	8	8	17	17	6	1	3	3	2	2
CV8/CV7	8	8	6	6	15	15	6	0	2	0	3	0
CV7/CV6	8	8	4	4	13	13	4	1	1	1	3	3
CV6/CV5	7	7	5	5	15	15	5	0	2	2	3	3
CV5/CV4	5	5	4	4	12	12	5	0	2	2	2	2
CV4/CV3	8	8	3	3	16	16	4	1	2	2	4	4
CV3/CV2	5	5	2	2	35	35	2	2	1	1	2	2
Sum	74	73	57	57	142	141	130	61	21	19	25	22

The maximum ventroflexion achieved by the neck is 130° when the ribs are included and 61° when the ribs are omitted. In both cases, the differences between the rotation achieved by the posterior joints and the anterior joints is opposite to what was noted for dorsiflexion – most of the mobility of the neck during ventroflexion originates from the base of the neck. The middle and posterior cervical vertebrae form distinct modules, mirroring the morphological regionalisation reported by Rytel et al. (2024*a*). The rigid ribs nearly completely constrain the movement of the anterior-middle portion of the cervical column. Some posterior vertebrae disarticulate slightly during ventroflexion.

Results of the FEA performed on the cervical ribs individually show that they can bend considerably in all directions before reaching failure stress (Fig. 5). A longer rib can achieve higher curvature at similar stress than a shorter rib. Nevertheless, the curvature of the ribs with peak stresses reaching 100-200 MPa is similar or higher than the curvature of the corresponding neck segments along which they would extend during the maximum rotation in all tested directions of the ROM analysis (compare Figs. 4 and 5). The bending capabilities of the ribs are further supported by the curvature preserved in a complete left fourth cervical rib of a *Tanystropheus hydroides* specimen PIMUZ T 2819 (see Fig. 3), which is similar to those achieved in the FEA model with peak stresses reaching 100-200 MPa (>70°).

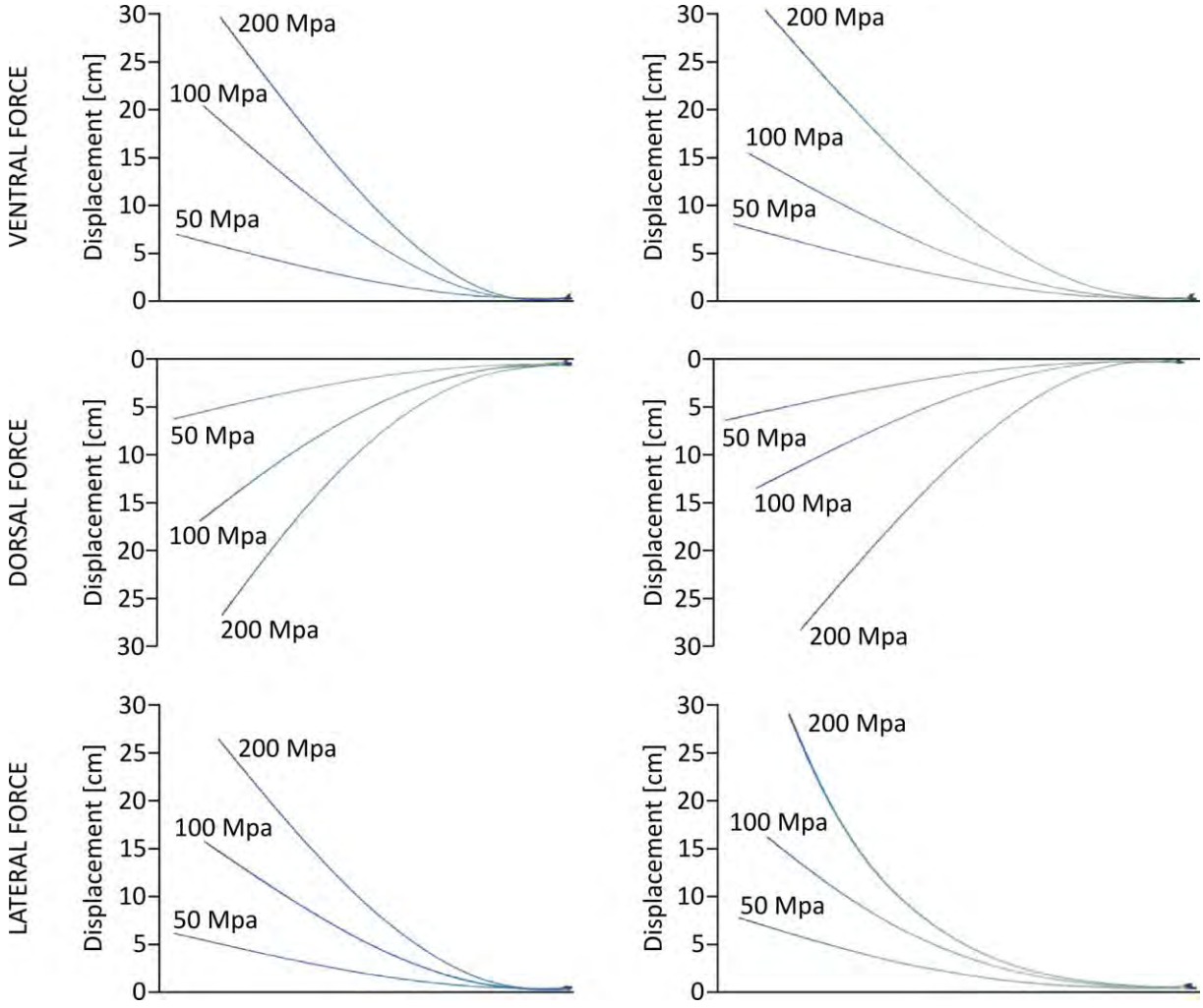

Fig. 5. Results of the FEA analysis performed on the cervical ribs of *Tanystropheus*. Colours indicate the Von Mises stress distribution [MPa], with the areas marked with brighter colour (red) being a subject to more stress than the areas marked with darker colours (blue). White indicates that the region is experiencing stress beyond the current scale.

Comparisons of the results from the FEA performed on the neck model with and without ribs reveal a major disparity between them in the Von Mises stress distribution pattern. When analysed without the cervical ribs, peak stresses are recorded mainly around the zygapophyseal articulations, the middle portion of the neural spine, and the ventral surface of the vertebrae, regardless of the direction of the force applied (Fig. 6). Some of the middle cervical vertebrae (five to ten) experience notably higher amounts of stress than the other elements. Direction of the applied force affects the distribution of compact and tensile stresses. With ventrally directed force the tensile stress is present across the ventral surfaces of the centrum and the zygapophyses, and the entire dorsal portions of the vertebrae are affected by compressive force (Fig. 6). The opposite pattern can be observed for the dorsally directed force. With laterally directed force the lateral side of the vertebral column oriented towards it is affected by tensile force, and the other lateral side by the compressive force. With the addition of the cervical ribs into the model the Von Mises stress distribution changes drastically. The middle cervical vertebrae, and especially their ventral portions, are a subject of much less stress, with some regions experiencing nearly none at all. The Von Mises stress distribution pattern becomes more homogenous when compared between the individual middle cervical vertebrae. Peak Von Mises stresses are observed in the areas around the neural spines of the cervical vertebrae nine to eleven. In *Tanystropheus* these are the only elongate vertebrae in which the neural spine is well-pronounced along its middle portion, being distinctly distally thickened in the two more posterior elements (Chapter I). The inclusion of the cervical ribs into the model also affects the distribution of tensile and compressive stresses. Regardless of the direction of the applied force, along the middle section of the neck the tensile stress is present nearly solely along the cervical ribs, but not the vertebrae with which they were associated (Fig. 6).

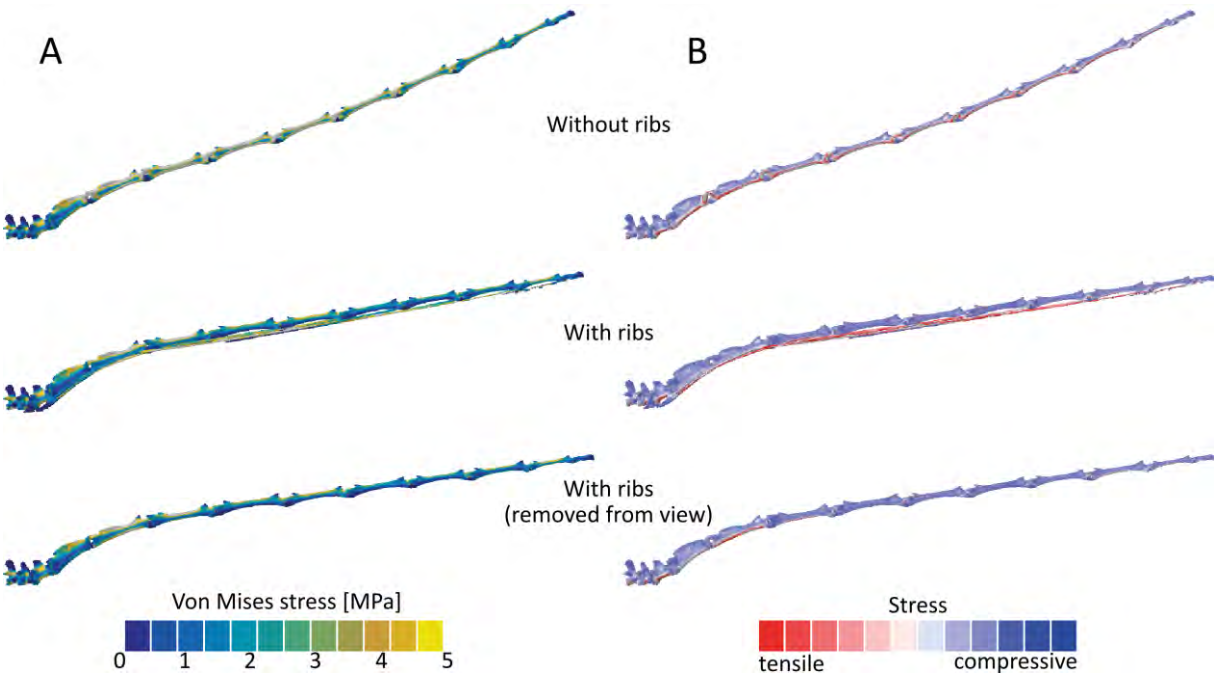

Fig. 6. Results of the FEA analysis in models with and without ribs with ventral force applied, in right lateral view. A – Von Mises stress distribution. B – Tensile/compressive stress distribution. For (A) colours indicate the Von Mises stress distribution [MPa], with the areas marked with brighter colour (red) being a subject to more stress than the areas marked with darker colours (blue). White indicates that the region is experiencing stress beyond the current scale. Postures achieved by the neck model do not reflect its maximum ROM.

Histological characteristics of the sectioned ribs are fully congruent with the results presented by Jaquier and Scheyer (2017). All analysed sections show that the shaft was extremely uniform in its internal composition, consisting of avascular compact lamellar bone (Fig. 2). Only the articular heads and the centre of the shaft near the articular region were a subject of remodelling.

Discussion

Neck of *Tanystropheus* – stiff or flexible?

Previous studies postulated contradictory hypotheses concerning the mobility of the neck of *Tanystropheus*. Peyer (1931), Wild (1973), and Kummer (1975) hypothesised that it was extraordinarily flexible. Tschanz (1986, 1988) opposed this view, arguing that the neck of *Tanystropheus* was stiffened by the bundled cervical ribs, which supported the vertebral column and reduced gravitational shearing stresses. In consequence, the neck had to be held horizontally. Renesto (2005) argued that the ribs reduced the neck movements to some extent, but did not render it stiff, as individual thin body rods would be relatively flexible. Nosotti

(2007) generally concurred with Tschanz (1986, 1988), interpreting the stiffening of the neck as an adaptation to cope with underwater propulsion, but noting that an immobile neck would make hunting for nektonic prey difficult. Rieppel et al. (2010) hypothesised that the neck of *Tanystropheus* could be elevated only slightly above the horizontal position, as the ribs severely restricted its movement. The results of the histological study of Jaquier and Scheyer (2017) on the ribs of *Tanystropheus* were also interpreted as indicating a relatively stiff neck.

Results of the ROM analysis provided here indicate that the neck of *Tanystropheus* was not immobile in any direction. The retrieved values are generally similar to those achieved in some directions for other long necked reptiles like plesiosaurs, pterosaurs, or sauropods, despite the comparatively modest number of cervical vertebrae in *Tanystropheus* (e.g., Wintrich et al. 2019; Vidal et al. 2020, 2024; Padian et al. 2021). Whereas the aim of this study is to provide general patterns, not definitive values of ROM, and differences in methodology make direct comparisons of the results less feasible, the similarity of the ROM results achieved here for *Tanystropheus* here and by Wintrich et al. (2019) for a plesiosaur *Cryptoclidus* is particularly intriguing.

With ribs included in the model, only the maximum ventroflexion value decreased substantially. The FEA results indicate that the ribs could bend enough to withstand the stress caused by being bent to the curvature present in the maximal positions of the ROM analysis carried out on the model without the cervical ribs (Fig. 4). Thus, if treated individually, the ribs would likely not restrict the motion of the neck (Wild 1973; Tschanz 1986; Renesto 2005). As already noted, and valid especially for long-necked taxa, interpretation of results obtained from purely osteological reconstructions not taking into account the effect of soft tissues should be approached with caution (e.g., Cobley 2013; Taylor and Wedel 2013*a*; Taylor 2014; Werneburg et al. 2014). Whereas the relatively small number of intervertebral articulations present in the neck of *Tanystropheus* makes this issue less consequential compared to animals with higher cervical vertebral counts, it is difficult to assess how the ribs would behave when bound by interosseous connective tissues and muscles. In articulated *Tanystropheus* specimens the overlapping cervical ribs are preserved in tight association, and likely formed bundles (Tschanz 1986). In life their ability to slide along each other could possibly be limited, together with the total ROM of the neck itself. Nevertheless, a huge part of the maximum ROM, especially during ventroflexion, originates from the base of the neck, which would not be affected by this issue, as the ribs exhibit limited overlap in this section of the column.

The role of the ribs was likely not to brace the neck (see below) and, therefore it still seems unlikely that the hyperelongate morphology of the vertebrae and the associated rod-like ribs stiffened the neck of *Tanystropheus* to the extent proposed by Tschanz (1986, 1988). The reconstructions presenting the neck as either rather immobile (Tschanz 1986, 1988; Nosotti 2007) or extremely flexible (Peyer 1931; Wild 1973; Kummer 1975) are not supported by the results of this study. The neck of *Tanystropheus* could bend in a relatively gentle curve, which would still allow for a considerable reach due its length (Fig. 4). The pose of the neck as restored here is congruent with the insights provided by Wild (1973), Renesto (2005), and Rytel (Chapter I), but in contrast to the hypotheses of Tschanz (1986, 1988) and Nosotti (2007), who favoured a much more horizontal orientation of the *Tanystropheus* neck. The morphology of the posterior cervical vertebrae differs between the species of *Tanystropheus*, with *T. conspicuus* showing more pronounced indicators for the dorsal inclination of the neck than *T. hydroides* and *T. longobardicus* (Renesto 2005; Rieppel et al. 2010; Chapter I). The curved posture may have stretched the cervical supraspinous ligaments, storing elastic energy that could have been released during a prey strike lunge (Tschanz 1986; Chapter I).

Role of the cervical ribs in *Tanystropheus*

The hyperelongate, thin and non-bifurcated cervical ribs of *Tanystropheus* are similar to those of the only other tanysaurian that has convergently achieved comparable neck elongation - *Dinocephalosaurus orientalis* (see Spiekman et al. 2024*a*). In other tanysaurians the ribs can be short and bifurcated (*Trachelosaurus fischeri*), hyperelongate and bifurcated (*Sclerostropheus fossai*), thin and relatively short (*Macrocnemus fuyuanensis*), or thick and short (*Tanytrachelos ahynis*) (Olsen 1979; Spiekman and Scheyer 2019; Scheyer et al. 2020; Spiekman et al. 2024*b*). *Tanystropheus* has proportionally the longest cervical ribs among all known vertebrates, which makes understanding their role in its bauplan particularly interesting. In some specimens the longest individual ribs reach >40% of the combined neck and skull lengths and >20% of total body length (PIMUZ T 2818, see Fig. 3; Wild 1973). This exceeds even the ratios estimated for sauropods (e.g., in *Mamenchisaurus* <35% and <20% respectively, see Taylor and Wedel 2013*b*; Moore et al. 2023), for which the role of the cervical rib elongation has been discussed extensively (e.g., Frey and Martin 1997; Martin et al. 1998; Christian and Dzemski 2007; Klein et al. 2012; Preuschoft and Klein 2013; Taylor and Wedel 2013*b*). The ribs were suggested to provide stabilization for the neck, resistance against torsion, and allowed for a transfer of the cervical musculature towards the base of the neck, which reduces the inertia (Taylor and Wedel 2013*b*). Two main hypotheses were

formulated – the ventral bracing hypothesis (Frey and Martin 1997; Martin et al. 1998) and the tensile member hypothesis (Christian and Dzemski 2007). The ventral bracing hypothesis suggests that the ribs supported the neck, transferred compression forces, and counteracted torque. This implies a rather inflexible, horizontally oriented neck, as recovered in the study of Tschanz (1986), who also interpreted the ribs of *Tanystropheus* as transferring compressive forces. In the tensile member hypothesis the tensile forces were transferred instead, and the weight of the neck was reduced by shifting the cervical musculature towards the trunk, allowing for more neck flexibility. In sauropods the ribs are partially composed of ossified tendons, in contrast to *Tanystropheus* in which they are built of avascular lamellar bone (Fig. 2; Klein et al. 2012; Jaquier and Scheyer 2017). The longitudinally oriented mineralized collagen fibres, presence of which supports the tensile member hypothesis in sauropods, are absent in *Tanystropheus* (Fig. 2; Klein et al. 2012; Jaquier and Scheyer 2017).

Despite the lack of preserved longitudinal mineralised collagen fibres associated with the cervical ribs, our model suggests that the ribs transferred tensile forces, as predicted by the tensile member hypothesis (contra Tschanz 1986). Therefore, it seems more likely that the main role of the hyperelongation of the cervical ribs of *Tanystropheus* was to allow for a shift of the associated musculature towards the torso. This is further supported by the distribution of the muscle attachment sites, which are greatly reduced along the middle portion of the neck, and expanded near its base (Wild 1973; Tschanz 1986, 1988; Chapter I). Furthermore, two *Tanystropheus* specimens in which the neck was bitten off by a predator or scavenger in a single bite further suggest that the central portion of the neck was remarkably slender (Spiekman and Mujal 2023). Finally, the majority of the ribs terminate distally around the same section of the neck, ventrally to the last cervical vertebra. Having long ribs and short tendons and muscles associated with them (instead of short ribs and long tendons) is viewed as an adaptation for a finer control of the neck movements (Taylor and Wedel 2013*b*). During movements of a neck with long (or very compliant) tendons, the muscle has to contract a greater distance to also account for the stretch in the tendons. The cervical rib morphology of *Tanystropheus* thus may have functioned more as very stiff tendons, allowing for greater control of the head position, which is necessitated by the extreme length of the neck. The shift of the cervical musculature posteriorly would have also reduced the inertia of the neck. Even considering that the gravitational stress was decreased in an aquatic medium, muscle mass reduction along the neck allowed for its better stabilisation, and might have reduced drag during lateral flexion.

Comparison with other long-necked animals

Although many taxa convergently evolved a long neck, the phylogenetic distribution of hyperelongate cervical ribs among long-necked tetrapods is constrained to archosauromorphs – tanysaurians (e.g., *Dinocephalosaurus*, *Tanystropheus*) and saurischians (some sauropods and non-avian theropods) (Fig. 1; Spiekman et al. 2024*a*; Taylor and Wedel 2013*b*). Their presence seems to be connected with certain specific patterns of neck elongation that appeared both in terrestrial herbivores and aquatic carnivores. *Tanystropheus* is the only known aquatic tetrapod with hyperelongate cervical vertebrae and hyperelongate cervical ribs. *Dinocephalosaurus*, a closely related tanysaurian, had more cervical vertebrae (which were relatively much less elongate than in *Tanystropheus*) than any other archosauromorph and hyperelongate ribs associated with them (Spiekman et al. 2024*a*). Its general bauplan resembled the plesiosaurs. Despite the similarity, in virtually all long-necked sauropterygians the cervical ribs are relatively short, stout, and rarely cross more than one intervertebral articulation. If the presence of elongate cervical ribs is constrained to archosauromorphs, what are the factors controlling their hypertrophy in some long-necked taxa, and atrophy in the others? Even within Sauropoda a major disparity exists in the morphology and length of the cervical ribs between the clades (Taylor and Wedel 2013*b*; Vidal et al. 2024), as in the tanysaurians. In long-necked pterosaurs and birds the cervical ribs are extremely reduced (Fig. 1).

Several factors should be considered when interpreting the causes of the observed phylogenetic distribution of the hyperelongated ribs. First, in some taxa the shift of musculature towards the torso might not have been advantageous – in azhdarchid pterosaurs the neck was likely relatively muscular, as it had to support a large head (Naish and Witton 2017; Buchmann and Rodrigues 2025). In all long-necked taxa with hyperelongated ribs the skull is relatively small, presumably due to the effects of gravity and drag (Fig. 1). Whereas in some plesiosaurs the neck to skull length proportions were similar to tanysaurians (Fig. 1), the necks of the former were likely much thicker, which would decrease drag during locomotion and feeding (Troelsen et al. 2019). This is also supported by taphonomic data – despite the rich fossil record of plesiosaurs, there is no unambiguous evidence for predatory targeting of their necks, which, in contrast, was documented for two specimens of *Tanystropheus* (see Spiekman and Mujal 2023). This indicates that the neck of the latter was much more slender. Moreover, the short cervical ribs in plesiosaurs served as osteological stops, which might have been energetically more advantageous than using muscle power to keep the neck straight

(Wintrich et al. 2019). Finally, the feeding strategy (duration and intensity of the head movements, as well as the neck flexibility required to achieve them) seems to play a major role in the extent of stiffening of the neck tendons (Dzemski and Christian 2007; Taylor and Wedel 2013*b*). In ostriches, the flexibility of the neck is paramount in obtaining the food items, as the animal tries to reach a large area without moving the trunk, minimising force and energy requirements during frequent changes of the position of the neck (Dzemski and Christian 2007). This is exactly the opposite to what is hypothesised for *Tanystropheus*, which was likely an ambush predator that relied on a limited number of precise strikes (Renesto and Saller 2018; Spiekman et al. 2020*a*, *b*; Chapter I). Thus, the presence and extent of elongation of the cervical ribs in long-necked animals can be correlated with several controlling factors – the relative skull size, the muscularity of the neck, the importance of its flexibility during locomotion and feeding, the preferred posture of the neck, and some other unique characters that are more difficult to assess (e.g., pneumacity). Within the mosaic of bauplans evolved by different long-necked animals, *Tanystropheus* is an important taxon that helps to disentangle the possible connections existing between different aspects of biology of distantly related taxa.

Conclusions

This study elucidates the appearance of one of the key anatomical features characteristic to some long-necked animals – the hyperelongated cervical ribs. Whereas they have previously been interpreted as a part of a bracing system that stiffened the neck, our results indicate that at least in *Tanystropheus* the main role of the cervical ribs was instead to transfer tensile forces and shift the mass of the neck towards the torso. This is the first quantitative evidence supporting the tensile member hypothesis, which was formulated for sauropods, but remains difficult to test due to the characteristics of their fossil record (Taylor 2022). The biomechanical analysis provided here suggests that the individual cervical ribs could bend considerably before breaking. They likely did not restrict the neck movements in *Tanystropheus* in a major way, and could enable finer control over the head movements. This is congruent with the interpretation of *Tanystropheus* as an aquatic ambush predator. These new insights show that despite being composed of a limited number of vertebrae, the neck of *Tanystropheus* could achieve a range of motion comparable to those of some of the long-necked plesiosaurs. This finding rejects previous hypotheses of either extreme stiffness and extraordinary flexibility of the *Tanystropheus* neck, and reveals that this morphological extreme in neck configuration formed a highly effective evolutionary adaptation.

Chapter IV

Bone infills reveal the parautochtonous origin of the Middle Triassic Miedary vertebrate assemblage

Adam Rytel[1,*], Wojciech Pawlak[2], Maciej R. Ruciński[3], Eudald Mujal[4,5], Paweł Bącal[1]

[1]Institute of Paleobiology, Polish Academy of Sciences, Twarda 51/55, 00818 Warszawa, Poland

[2]University of Warsaw, Faculty of Biology, Biological and Chemical Research Centre, Institute of Evolutionary Biology, Żwirki i Wigury 101, 02089 Warsaw, Poland

[3]Natural History Museum, University of Oslo, P.O. Box 1172 Blindern, NO-0318 Oslo, Norway

[4]Staatliches Museum für Naturkunde Stuttgart, Rosenstein 1, 70191 Stuttgart, Germany

[5]Institut Català de Paleontologia Miquel Crusafont (ICP-CERCA), Universitat Autònoma de Barcelona, Edifici ICTA-ICP, c/ Columnes s/n, Campus de la UAB, 08193 Cerdanyola del Vallès, Barcelona, Catalonia, Spain

* – corresponding author: adam.rytel@twarda.pan.pl

Introduction

Taphonomic data is a valuable source of information concerning the environmental conditions present during decomposition of organic matter, and its later diagenesis (e.g., Behrensmeyer 1975, 1978; Weigelt 1989). In vertebrate palaeontology, histotaphonomy has been used as a powerful tool for tracing the post-mortem histories of various remains, spanning fossil records across multiple stratigraphic intervals (e.g., Bodzioch and Kowal-Linka 2012, 2017; Bodzioch 2015; Kowal-Linka 2015; Mancuso and Previtera 2022; Laker 2024). When depositional and early diagenetic conditions cannot be directly assessed from fossil-bearing strata (e.g. due to transport of skeletal remains or overprinting by pedogenic processes, erosion, and bioturbation) the information contained within the bone itself might carry especially important evidence for deciphering the depositional context of the specimen. This can be valid for multitaxic mass accumulation of elements originating from different habitats, where the taphonomic studies can be key to unraveling the genesis of an assemblage (e.g., Bodzioch and Kowal-Linka 2012, 2017; Bodzioch 2015; Kowal-Linka 2015; Beardmore and Furrer 2017).

Many such cases have been documented from the Middle Triassic of the Central European Basin (CEB; e.g., Hagdorn and Reif 1988; Schoch and Seegis 2016; Schoch et al. 2022; Czepiński et al. 2023), also known as the Germanic Basin, which is dominated by marine deposits, overlaid with a thick unit of alternating siliciclastic-carbonate sedimentary succession - the Lower Keuper (Fig. 1). This heterogeneous unit represents a regressive trend of the Muschelkalk Sea, resulting in a mix of typically marine, continental and marginally marine environments of intermediate specificity (Hagdorn and Mutter 2011; Franz et al. 2013; Nitsch 2015; Schoch and Seegis 2016; Pawlak et al. 2022; Schoch et al. 2022). From the palaeontological perspective, a valuable feature of these deposits is the unusually high content of vertebrate fossils, resulting in numerous assemblages comprising dozens of fish, amphibian and reptile species (e.g., von Meyer 1847-1855; Fraas 1896; Böttcher 2015; Hagdorn et al. 2015; Schoch and Seegis, 2016; Pawlak et al. 2022; Schoch et al. 2022; Czepiński et al. 2023).

Miedary is a recently discovered vertebrate-bearing site of Lower Keuper strata in southern Poland (Fig. 1A), first deriving from the eastern part of the CEB conversely to previously reported assemblages from Germany (Czepiński et al. 2023). Fossils of more than 20 vertebrate species have been recorded from this site so far, including: reptiles (e.g., *Blezingeria* sp., *Jaxtasuchus* sp., *Nothosaurus* sp., *Tanystropheus conspicuus*), a chroniosuchian, temnospondyl amphibians (*Mastodonsaurus* sp., three plagiosaur species), and numerous fishes, including a lungfish (*Ptychoceratodus* sp.), actinopterygians (e.g., *Gyrolepis* sp., *Serrolepis* sp., *Saurichthys* sp.), and hybodontiform elasmobranchs (Czepiński et al. 2023). Besides the taxonomic diversity, the vertebrate remains also occur at exceptionally high concentrations. Interestingly, the German Lower Keuper (e.g., Schoch and Seegis 2016; Schoch et al. 2022) shows a similar pattern, with some equivalent vertebrate taxa, both fishes and tetrapods (Pawlak et al. 2022; Mujal et al. 2025). However, notable differences between the two regions also existed. The German Lower Keuper generally preserves more terrestrial taxa, with organisms interpreted from marine habitats being secondary. Instead Miedary shows a notoriously high abundance of remains of marine taxa, and particularly *Tanystropheus*.

Because of the uncommonly abundant remains of *Tanystropheus*, the Miedary locality is especially relevant for elucidating the habitat of this taxon (Chapter I). *Tanystropheus* is a bizarre long-necked archosauromorph reptile known predominantly from the Middle Triassic, characterised by a Tethys-wide distribution (Wild 1973; Rieppel et al. 2010; Spiekman and

Scheyer 2019). Its lifestyle and environmental preferences have been historically disputed, but virtually all recent studies point towards it being a shallow aquatic ambush predator (e.g., Nosotii 2007; Renesto and Saller 2018; Spiekman et al. 2020*a*, *b*; Chapter I). In the rest of the CEB *Tanystropheus* constitutes a widespread, but accessory faunistic element. This disparity is intriguing and indicates that data concerning the environmental conditions present in Miedary might correlate highly positively with the actual habitat of the animal.

However, the co-occurrence of typically marine and freshwater taxa in Miedary raises questions about the origin of this fossil assemblage, particularly biostratinomic pathways of accumulated remains. This pattern can be explained either by transport, mixing and subsequent deposition of freshwater and marine taxa originating from different habitats, or by their sympatric presence and parautochtonous deposition within a shared paralic ecosystem. To assess which hypothesis is more favourable, we analysed the sedimentary infill of several bones from multiple taxa. Due to the formation in isolated microenvironments, infilled internal cavities can retain information about the taphonomic history of the fossils, including: decay, transport, burial, and early diagenesis. We applied a suite of taphonomic approaches, including biostratinomic observations and histotaphonomic analyses, supported by SEM–EDS elemental mapping, to determine the possible accumulation pathways, and subsequent burial history of fossils from Miedary. These analyses are used to test the aforementioned hypotheses and to shed light on the origin of the mass accumulations of vertebrate remains.

Geological setting

The palaeontological locality in Miedary exposes an about 5-metre-thick section (Fig. 1C) dated to the early Ladinian (Middle Triassic) based on regional biostratigraphic and magnetostratigraphic correlations (Pawlak et al. 2022). Vertebrate fossils occur mainly within two intervals: dolostone beds characterised by typically marine faunistic assemblages, and glauconite beds yielding mixed communities of freshwater and marine taxa (Sulej et al. 2011; Pawlak et al. 2022; Czepiński et al. 2023). The material examined in this study was excavated from the three distinct layers within the glauconite beds *sensu* Pawlak et al. (2022): M1, M2a, M2b, and two strata directly overlaying them (M3, M4). The M1 and M2b layers share similar lithological features, including variegated green to reddish colouration and a composition of quartz-glauconitic sandstone cemented with calcium carbonate (Fig. 1C). However, they differ substantially in internal structure: the M1 layer is predominantly massive with none or poorly accented bedding, whereas the M2b layer displays horizontal bedding. In both layers, lensoidal intercalations of coarser, glauconite-dominated sandstone are present

but thicker and spatially broader interbeds occur in the M2b layer. Both layers host abundant root structures. The M2a layer is bounded by the M1 and M2b packages and is abruptly limited from the underlying M1 layer with an erosional surface. It consists of coarse-grained sandstone rich in glauconite with subordinate quartz, muscovite, locally high phosphatic microfossil content, bone fragments, and coprolites – components characteristic also for the interbeds within the M1 and M2b layers. These features combined with erosional lower boundaries point to the high-energetic origin of both the M2a layer and the interbeds within the directly overlaying and underlaying layers. This interpretation is further supported by the preservational characteristics of the vertebrate fossils, which are predominantly found isolated, and usually do not bear marks of prolonged erosion or weathering (*sensu* Behrensmeyer 1978). The M3 layer is composed of red, clayish and highly homogenous sediment with common grey-coloured, laterally discontinuous horizons, and desiccation cracks with strongly cemented mineral infill. It is separated from the underlying sediments by an inconspicuous erosional surface, which is traceable across the entire site. Its thickness ranges from five to fifteen cm. It is overlain by about 30 cm thick M4 layer composed of interbedding packages of reddish to greenish mudstone and sandstone. The coarser facies are composed of quartz- and glauconite-dominated beds similar to the M1 and M2b layers. The top of the M4 layer forms a conspicuously grey-coloured horizon, continuous across the excavation. It is characterised by numerous desiccation cracks filled with carbonate mineralisation and the presence of subspherical concretions. Despite notable differences between individual layers, they share several key features, such as grain types, sandy granulation, at least partially high-energetic origin, and root bioturbation. This implies that the entire glauconite beds formed in a similar or even the same depositional environment. An exact reconstruction of this palaeoenvironment requires a detailed examination of sedimentary structures, which is the subject of ongoing studies.

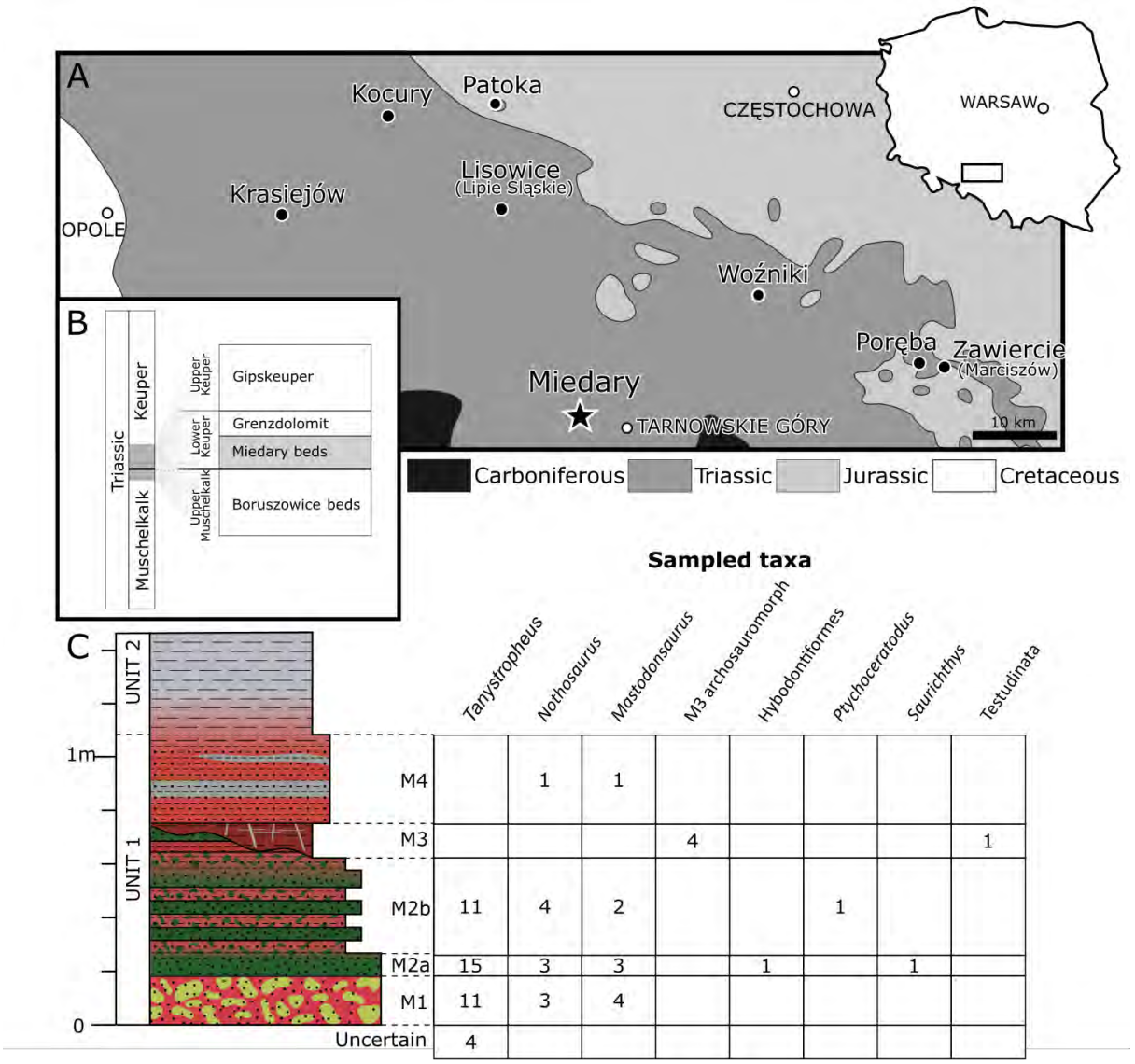

Fig. 1. Spatial and stratigraphic data of the Lower Keuper (lower Ladinian) site of Miedary (Poland) (modified after Czepiński et al. 2023) – map of southern Poland with the main fossil-bearing Keuper localities marked (**A**), placement of the Miedary Beds within the Triassic lithostratigraphic units of the Upper Silesia (**B**), and a simplified geological section of the site (**C**) with an associated table including the numbers of specimens studied per each taxon and stratum (for more details see Appendix II).

Material and Methods

Specimen thin sectioning

To analyse the infill characteristics of the bones from Miedary, 98 thin sections were made, out of 70 specimens (see Appendix II, Fig. 1C), all from the collection of the Institute of Paleobiology, Polish Academy of Sciences, Warsaw, Poland (ZPAL). These included isolated, but three-dimensionally preserved bones of eight taxa - four reptiles (*Nothosaurus* sp., *Tanystropheus conspicuus*, a testudinate, and a hitherto unnamed armoured archosauromorph - see Czepiński et al. 2023), three fishes (*Ptychoceratodus* sp., *Saurichthys* sp., and a hybodontiform shark), as well as the large-sized temnospondyl *Mastodonsaurus* sp. Only highly diagnostic bones were sampled. To reduce the possible bias originating from disparity in taphonomic characteristics of specimens with dissimilar shape and/or size, different skeletal elements were sectioned.

To take into account differences induced by varying depositional environments, all layers from a vertically short (1 m) section of Miedary were sampled (layers M1, M2a, M2b, M3, and M4; see Fig. 1C). For each of the three tetrapod taxa that are most abundant in the site (*Nothosaurus*, *Tanystropheus*, *Mastodonsaurus*) one specimen was sectioned per element type (vertebra, rib, pectoral/pelvic girdle bone), per the three main fossiliferous layers (M1, M2a, M2b), to ensure a more even sampling. Additionally, some elements from less common taxa (a toothplate of *Ptychoceratodus*, a lower jaw of *Saurichthys*, a fin spike hybodontiform shark, as well as osteoderms and ribs of an armoured archosauromorph from the M3 layer), and from significantly less fossil-yielding layers (M3 and M4) were also taken into account, to gain broader insights into the possible differences in taphonomic characteristics between strata and taxa. Moreover, further sections of the bones of *Tanystropheus*, previously acquired for histological studies (see Rytel et al. 2024*b*), were included in the dataset. All data concerning the taxonomy, stratigraphy, and element type of each specimen are contained within the Appendix II.

Specimen imaging

To illustrate the spatial layout of different chemical elements within a section, 15 thin sections were visualised, and either completely or partially mapped using Scanning Electron Microscope (SEM) with Energy Dispersive X-ray Spectrometry (EDS). The microscope was a Thermo Fisher Quattro S held in the Laboratory of Scanning Electron Microscopy, ZPAL. This SEM is coupled with the EDAX Octane Elect Plus EDS detector. This is an environmental SEM, which also allows for imaging and elemental analysis at higher than

typical pressure in a microscope chamber. Here, a H_2O vapour was used to maintain elevated pressure (50 Pa) in the chamber during measurements when non-conductive, non-sputtered/coated samples were investigated. The vast majority of both imaging and EDS measurements was done on Pt-sputtered samples or carbon coated samples, which allowed to minimise number of charging artifacts, and speed-up elemental distribution mapping and elemental analysis. The samples were thin coated with a carbon layer using CCU-10 Safematic sputter or thicker coated with Pt using Balt-Tec SCD 005 sputter. Photographs of the thin sections were taken with a Keyence VHX-7000 digital microscope with a VHX-7100 fully integrated head with two lens systems (20–100×; 100–500×) and a polarisation adapter, located at the University of Warsaw.

To visualise the whole area of thin section slides we employed MAPS3 software (Thermo Fisher Scientific) which automates the acquisition of large overviews by stitching multiple images. This software was used to image the whole area of the sample (up to several cm^2) maintaining high resolution. Imaging was done employing: secondary and backscatter electron detectors. A Directional Backscatter electron detector was used to enhance image contrast related to sample composition.

During imaging of large samples, the accelerating voltage was kept in the 5-20 kV range. The mapping measurements were performed at the accelerating voltage of 20 kV. All large area elemental distribution mapping were done using Montage Large Area Mapping, an add-in feature of APEX software (AMETEK Inc.) allowing precise large-area imaging and EDS. Elemental distribution maps of Al, C, Ca, Cl, Fe, K, Mg, Mn, Na, O, P, S, Si, Ti, and Pt (for Pt sputtered samples) within the thin sections were generated. Additional data concerning the chemical composition of specific authigenic minerals were gathered for five further specimens by single-point SEM-EDS analysis.

To differentiate various generations of calcareous infills of bones, thin sections from three specimens (ZPAL V. 36/877, ZPAL V. 36/1071, ZPAL V. 36/1185) were coated with carbon and examined with a cathodoluminescence microscope at ZPAL, which was equipped with a hot cathode and an integrated UV-VIS spectrograph.

Quantitative analyses

To quantify the observed disparity of the notable sedimentary infill features, we compiled a matrix of numerical characters (Appendix II). Observations included the the presence of various mineral phases and types of carbonate cements. Types of carbonate

cements follow the classification of Flügel (2010). These observations were semi-quantified, typically using a 0–2 scoring system (except for glauconite presence; see Appendix II for scoring details): 0—feature absent; 1—feature present but rare in the specimen; 2—feature abundant or pervasive within the sample. The absence of a score indicates uncertainty regarding the presence or degree of the corresponding feature. Although quantitatively limited, this approach enables uniform scoring of features with variable character, facilitating Non-metric Multidimensional Scaling (NMDS) and Correspondence Analysis (CA). Both analyses were performed by employing PAST v. 5.3 (Hammer et al. 2001). Only specimens with sufficiently preserved sedimentary infill could be properly scored within the matrix. Hence, 62 out of 70 sectioned bones were included in the analyses (see Appendix II).

Based on the preliminary results taking into account a version of the matrix expanded with histotaphonomic features, only the 20 characters concerning the infill characteristics, were included in the iterations of the analyses contained within this study. This resulted in a lower recorded stress value for NMDS (0.205 vs 0.277) and higher sum of variance values covered by CA1 and CA2 for CA (26.3% vs 37.8%). NMDS ordination was performed using Gower distance, which is appropriate for semi-quantitative ordinal data. This metric standardises variables and accommodates relative feature intensities, ensuring all attributes contribute equally to the analysis without assuming linear relationships between scores. Correspondence Analysis was performed on the same dataset.

Sampled skeletal elements varied in cortical bone thickness as well as in the size of nutrient foramina and the internal cavities, which affected the volume of natural void space that could be infilled within them. These anatomical differences likely influenced the ease with which sediment and, later during diagenesis, fluids could percolate into the bone, resulting in variable degrees of cementation and authigenic mineral formation. To be able to compare the effects of pre-diagenetical characteristics of the specimen that might have induced a different taphonomical pathway, the bones were classified into several groups. These included their taxonomic identification (eight taxa), stratigraphic origin (five strata), element shape (four morphological subclasses), and pore size (three subclasses). For exact groups assigned for each individual element see Appendix II. The results of the analyses were compared both within and between the groups, to visualise the possible correlations in specimen clustering, and its connection to the aforementioned characteristics.

Results

Taphonomical features

Sedimentary infills

Five distinct types of bone infill were identified. The clastic- and clay-dominated types represent sedimentary material transported into bone cavities from the external environment. The remaining infill types comprise authigenic minerals or their parageneses formed in situ within fossils. They are well exemplified in the cervical vertebra ZPAL V. 36/1071 (see EDS mapping results below), and the humerus ZPAL V. 36/1185 (Fig. 2B) of *Tanystropheus*.

- *Sulphides* (Fig. 2A) are represented mainly by pyrite or chalcopyrite with rare admixture of Ni sulphides. They rarely occur as the sole or dominant infill of pore cavities, except micropores. Most frequently, they are associated with other types of infills, either as embedded euhedral crystals or as linings of pore walls, both of authigenic origin.

- *Calcite* (Fig. 2B, D) occurs as authigenic cements filling spaces between allogenic material or other authigenic crystallisations, as well as the sole pore-filling phase. Four main types of calcitic cement can be distinguished: micrite, microsparite, peloidal microsparite, and sparite. The spartic cement is subdivided to: drusy, mosaic, granular and circumgranular based on crystal habit. All recognized cements show high content of divalent cations substituting Ca: Mg, Mn and Fe.

- *Ferrous-organic infill* (Fig. 2C) forms thin bands lining pore walls and is usually accompanied by other infill types. It most likely represents a mixture of organic compounds and ferrous oxides evidenced by high content of carbon and iron.

- *Clay-dominated sediment infill* (Fig. 2E): composed primarily of a massive matrix comprising mainly Fe-, Al- and Si- oxides and hydroxides, opaque in transmitted light. It commonly contains high amounts of embedded quartz grains revealing an external source of the material. Fe-Al-Si oxide pseudomorphs after glauconite grains are also present but less abundant.

- *Clast-dominated sediment infill* (Fig. 2F): composed mainly of quartz and glauconite grains reaching up to 0.25 mm in diameter. The quartz grains are sub-angular to angular in most samples, whereas the glauconite grains are typically sub-rounded. The glauconite grains display some differences of maturity, visually expressed by colour

range from light to dark green. Nonetheless, the vast majority of the grains represent the evolved stage, whereas initial or highly evolved stages are absent or exceptionally rare. Conversely to maturity, the weathering degree of glauconite shows the full spectrum, from nearly non-weathered, through partial substitution by reddish Fe- and Al-oxides, to complete replacement with preservation of a grain shape (pseudomorphs). The ratio of quartz to glauconite grains varies between samples from quartz- to glauconite-dominated sediment. Accessory grains include muscovite flakes and ilmenite grains.

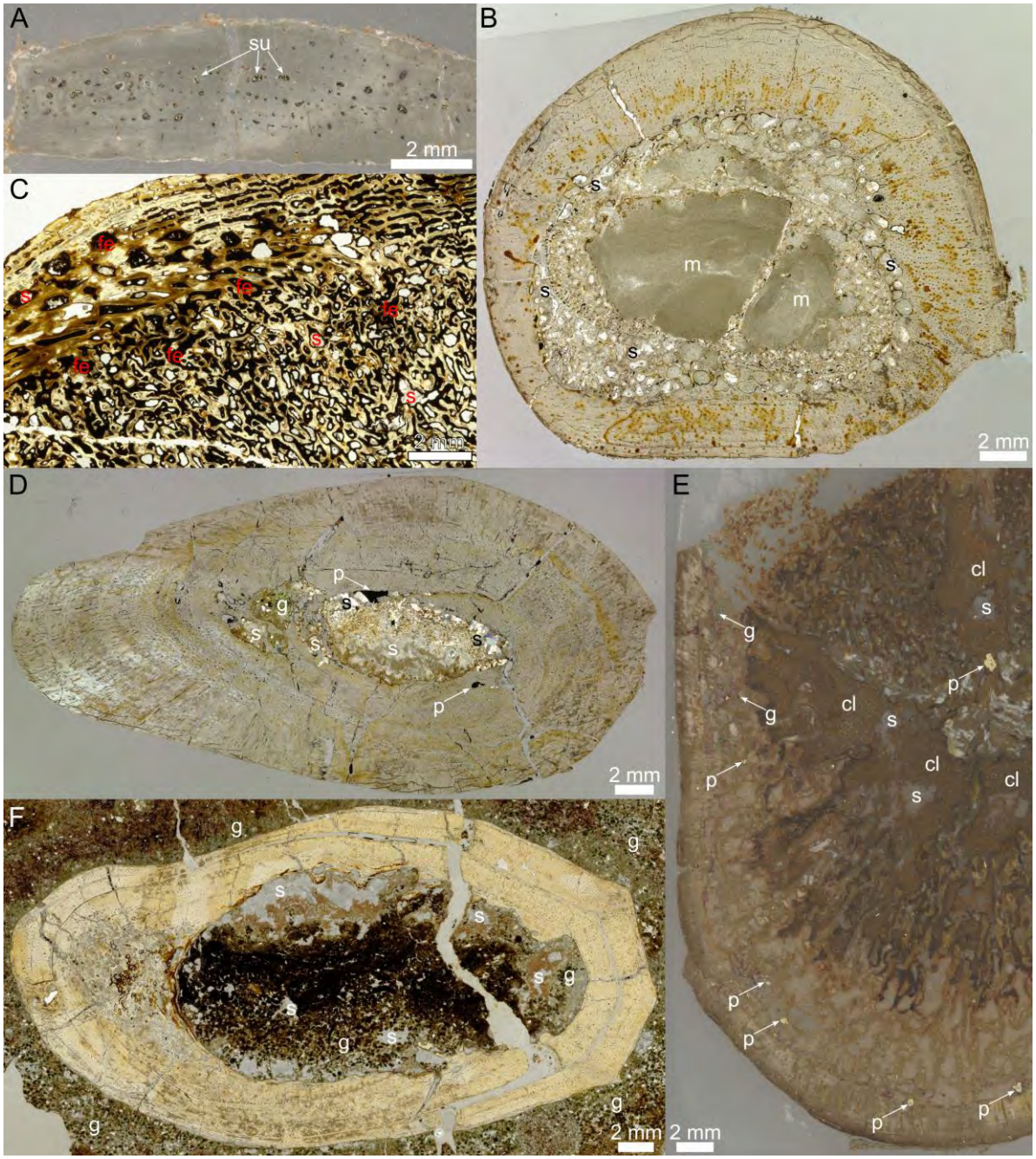

Fig. 2. Bone infill types from the Lower Keuper (lower Ladinian) of Miedary (Poland). Sulphide (**A**), calcite (**B**, **D**), ferrous-organic (**C**), clay (**E**), and clast (**F**) dominated sedimentary infills. Photographs with normal (A, E) or normal transmitted (B–D, F) light. All sections are transverse and represent: an osteoderm of the new archosauromorph (A – ZPAL V. 36/411/10), a *Tanystropheus* humerus (B – ZPAL V. 36/1185), a *Mastodonsaurus* vertebral centrum (C – ZPAL V. 36/324), a *Tanystropheus* femur (D – ZPAL V. 36/877), a *Nothosaurus* vertebral centrum (E – ZPAL V. 36/267), and a *Tanystropheus* cervical vertebra (F – ZPAL V. 36/193). Abbreviations: cl – clay-dominated infill; fe - fe-oxides lining; g – glauconite; m – micrite; p – pyrite; s – sparite; su – sulphides.

Other features

Bone staining is highly variable among different specimens (Figs. 2–3), with no noticeable correlation to their other characteristics. In some bones its extent is very local and patchy, whereas in some other specimens most of the original tissue is stained, often with clear zonation. Staining colours span from light grey to dark brown. Zones of stained tissue are sometimes associated with cracks. Cracking extent varies highly between the analysed specimens, with only few being pristine. In most of the specimens cracks extend both parallel and perpendicular to the bone margin, and are infilled with sediment (Fig. 3 E–F). Distinct generations of cracks can be observed in several specimens, with some originating after the fossilisation of the bone (Fig. 3F). Brecciation is usually relatively limited in the sample, although the largest internal cavities of some of the studied specimens are collapsed. Conspicuous patterns of microcracks are also present in the sample. Drying microcracks were observed only in one bone, with notable osteon separation due to collagen shrinkage (see Laker 2024) being widespread within the entire section (Fig. 3B). Waterlogging microcracks are less evident, but more common, with many minute cracks branching between osteons in several specimens (Fig. 3D). Evidence of bioerosion in the sample is nearly absent, with only one root structure being documented, penetrating the bone surface (Fig. 3A). Microbial tunneling traces and invertebrate burrows are seemingly absent. Clear geopetal structures are rare, and usually associated with the presence of pyrite localised only on one side of the cavity (Fig. 3C). Some specimens from the M4 layer are completely covered with a calcite crust (Fig. 3E).

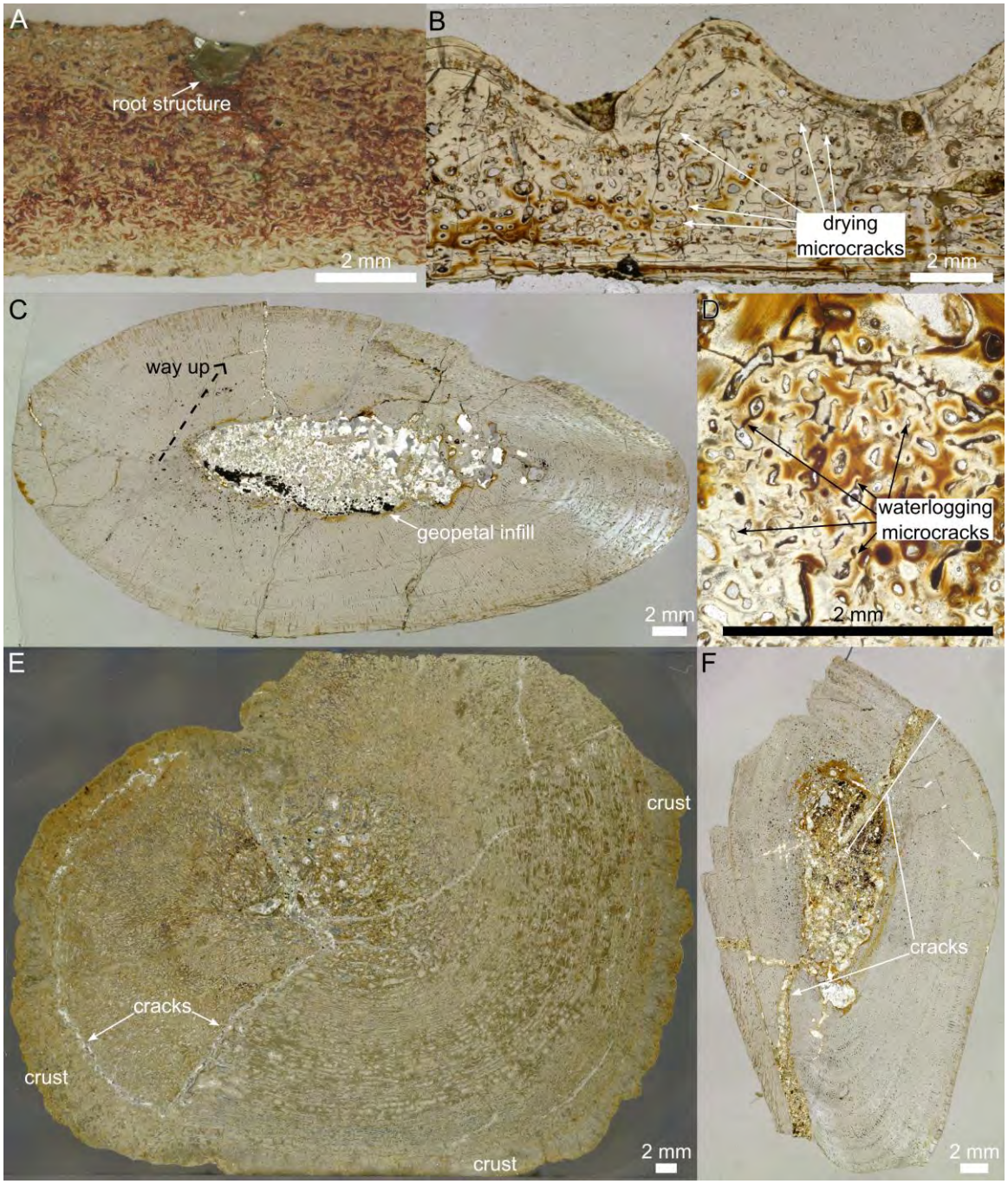

Fig. 3. Specific taphonomic features present in the studied specimens from the Lower Keuper (lower Ladinian) of Miedary (Poland). A root structure (**A**), drying microcracks (**B**), a geopetal structure (**C**), waterlogging microcracks (**D**), cracks running perpendicular and parallel to the bone surface, with the bone overlain by crust (**E**), and cracks generated after the fossilisation of the bone (**F**). Photographs with normal (A) or normal transmitted (B–F) light. All sections are transverse and represent: a *Tanystropheus* scapula (A – ZPAL V. 36/153), a *Mastodonsaurus* clavicle (B – ZPAL V. 36/927), a *Tanystropheus* femur (C – ZPAL V. 36/878), a *Tanystropheus* cervical vertebra (D – ZPAL V. 36/176), a *Mastodonsaurus* vertebral centrum (E – ZPAL V. 36/924), and a *Tanystropheus* femur (F – ZPAL V. 36/1003).

EDS mapping and cathodoluminescence

Results of the EDS mapping of the thin sections reveal a pattern of spatial layout of specific elements that is generally shared within all the studied bones, and is well exemplified in the *Tanystropheus* cervical vertebra ZPAL V. 36/1071 (Fig. 4). Abundance rate of several elements seems to be highly correlated with the regions within the specimen that they usually occupy. Fe is present in its highest concentrations in small intertrabecular spaces (Fig. 4K). In larger cavities it is more common peripherally, as a layer lining the walls of pore cavities. Towards the centre of the cavities, its concentration is lower, but rather consistent throughout the whole central infill, with only some detrital grains being completely devoid of it. The bone tissue can be easily distinguished from the sediment when observing the concentration of P (Fig. 4J). Unsurprisingly, similarly high levels of Ca are present within the bone (Fig. 4I). Moreover, Ca is generally absent from the smaller pores and the cracks that open towards the external surface of the bone, but present within most of the area of the larger cavities, usually being the most abundant element therein. Presence and abundance of Ca and Mg are clearly highly positively correlated within the mineral infill, with the latter being absent from the bone tissue itself (Fig. 4L). Sulfur is relatively widespread throughout the whole thin section, with visibly higher abundance within the bone, and forming some especially prominent angular concentrations associated with iron (Fig. 4G). The detrital grains are primarily composed of Si, Al, and O (not necessarily all three at the same time), and are most often deposited in the larger cavities, sometimes within the calcareous matrix (Fig. 4B, N, D). An especially high abundance of these elements can be noted within some cracks that open towards the bone external surface, which have an infill nearly devoid of Ca. The presence of C can be tied solely with the unfilled voids within the bone and the background area around it (Fig. 4F), which originated from resin residue in which the specimen was submerged during sample preparation. The remaining analysed elements were much less abundant, and their distribution did not seem to follow any significant patterns. Observed levels of spatial abundance and concentration of different elements give a more complete and quantitative view into the infill composition disparity within the dataset, supplementing the identifications made with the usage of light microscopy.

The results of cathodoluminescence were severely limited, as luminescence was revealed only in the bone tissue, and not the mineral infill. This is likely due to high Fe/Mn content ratios in the sectioned specimens (see Fig 4), and much higher concentrations of Fe in the sediment, than in the surrounding bone (Fig 4K).

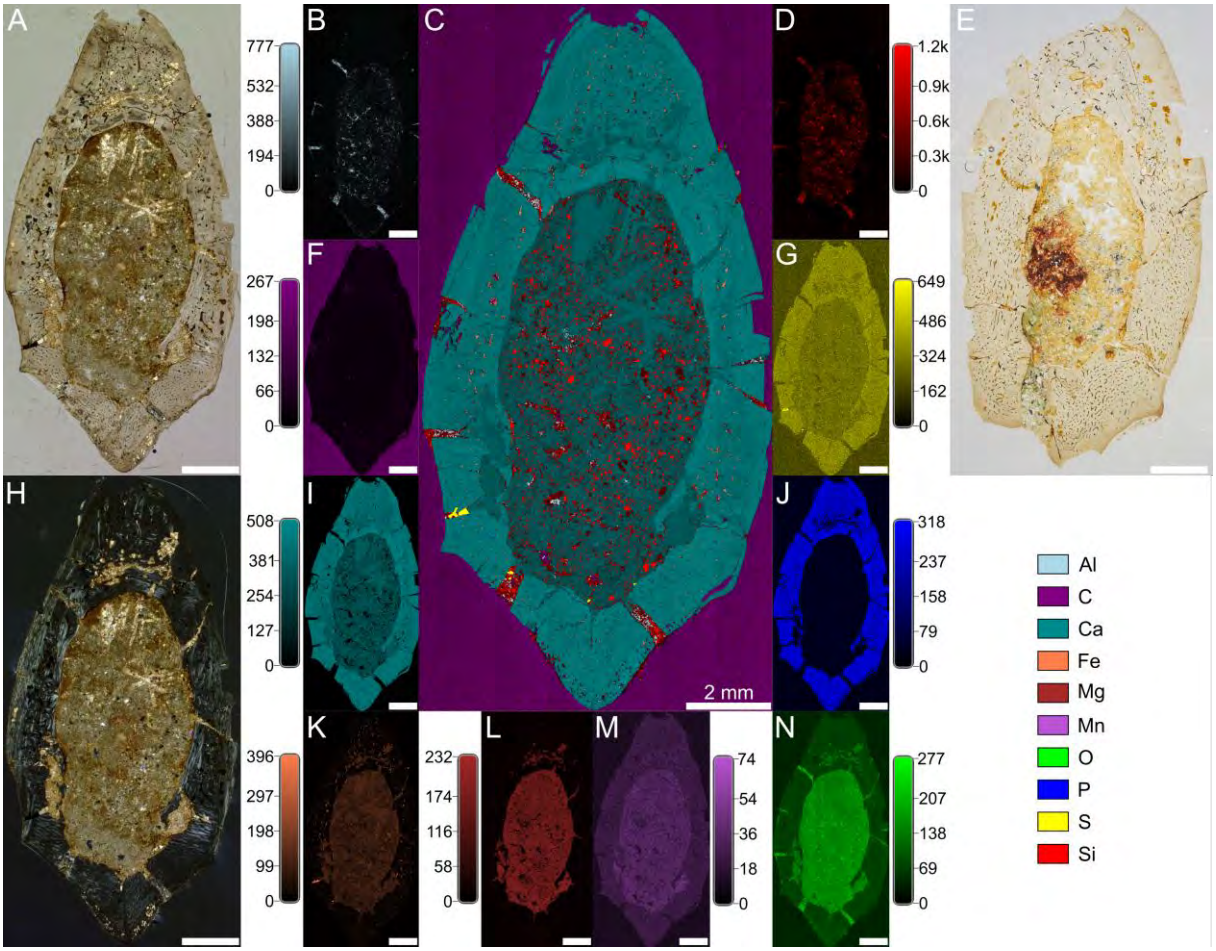

Fig. 4. Comparison between microscopic images of a transverse cross section through a *Tanystropheus* cervical vertebra ZPAL V. 36/1071 from the Lower Keuper (lower Ladinian) of Miedary (Poland). Photographs with normal transmitted light (**A**), normal light (**E**), and polarised light (**H**). SEM-EDS mapping results, with the distribution of Al (**B**), C (**F**), Ca (**I**), Fe (**K**), Mg (**L**), Mn (**M**), O (**N**), P (**J**), S (**G**), Si (**D**), and a composite map showing the dominant element in a given area (**C**). Scales associated with the panels mark the gradient of spatial abundance of the measured elements in average intensity/counts of signal per pixel. The thin section illustrated in the panel (**E**) comes from the opposite side of the cutting plane from which the sample shown in the other panel has originated. Scale equals 2 mm in all panels.

Comparative Taphonomy and Quantitative Analysis

Character matrix analysis

Both quantitative analyses (CA and NMDS) reveal considerable diversity in sediment infill and permineralisation patterns. Clustering is primarily controlled by variation in the proportions between three infill types: sedimentary infill, the Fe-rich mineral phases

(sulphides and ferrous-organic infill), and the carbonate cementation. The distribution of most samples is primarily driven by these three dominant infill components, whereas the rare occurrence of mica and Ni-rich sulphides characterises only some samples from the M3 layer. In contrast, mechanical alterations (e.g., cracking patterns and weathering) contributed less to the distribution of data points. Consequently, the proportion of each type of element largely (but not solely) reflects gradients in the type of void filling. CA1 and CA2 account for 23.2% and 14.6% of variance, respectively.

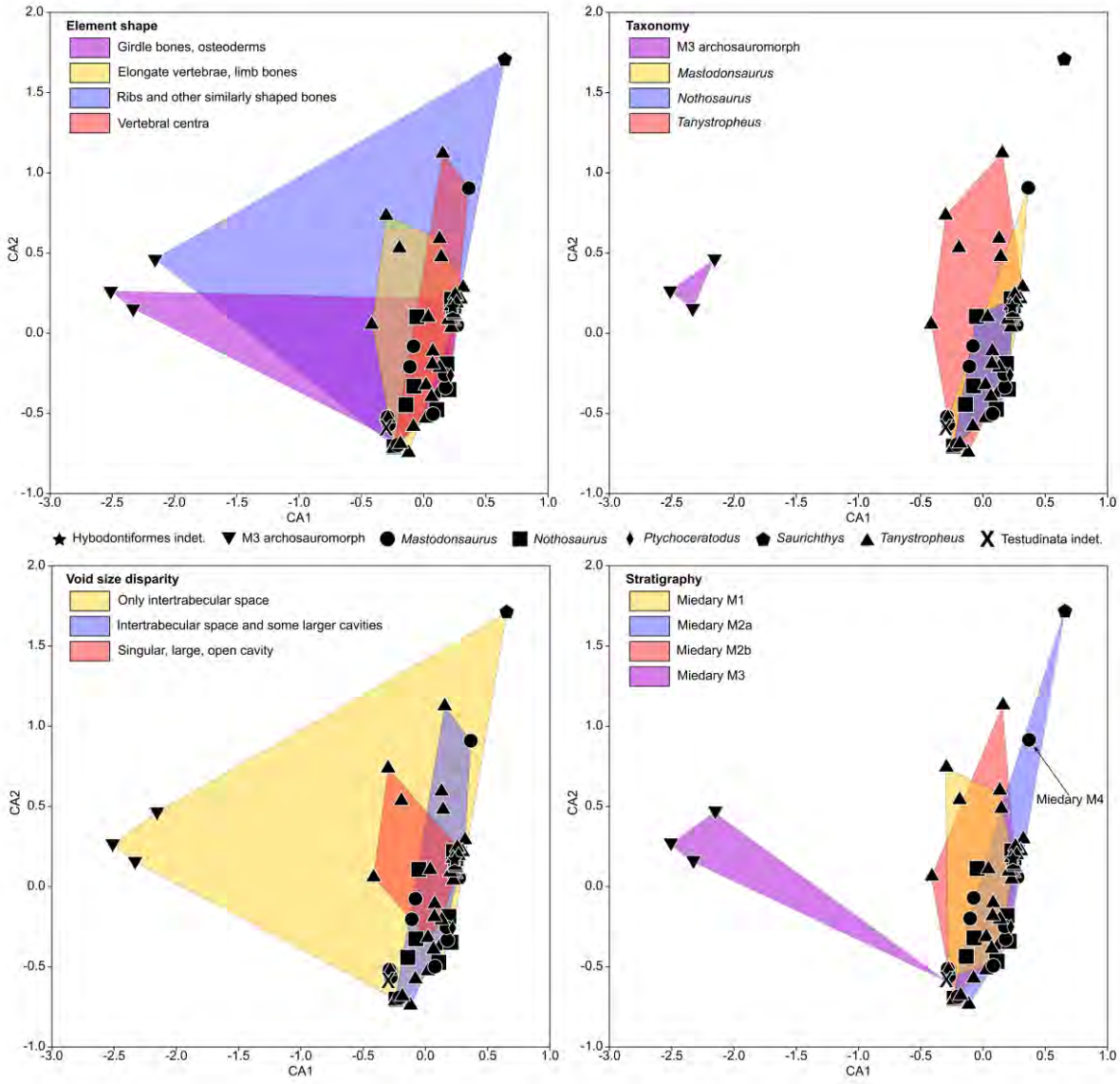

Fig. 5. Correspondence Analysis results. CA1 and CA2 account for 23.2% and 14.6% of variance, respectively.

Histotaphonomic patterns do not correlate with taxonomic assignment of the specimens, as each of the tetrapod species well-represented in the dataset occupies a substantial, largely overlapping portion of the order space (Figs. 5–6). From among the three most extensively studied taxa, *Tanystropheus* exhibits the highest apparent disparity, reflecting a high diversity of infill types in bone cavities. In both analyses, the M3 archosauromorph plots either at the margin of the overlapping taphospace (NMDS) or as a distinct cluster (CA), which is mainly driven by the unique abundance of mica and the presence of Cu- and Ni-rich sulphides. Overall, these analyses indicate that multiple taphonomic pathways can be distinguished, but they are not taxon-specific, with the potential exception of the M3 archosauromorph, the rostrum of *Saurichthys*, and outliers represented by *Tanystropheus* remains.

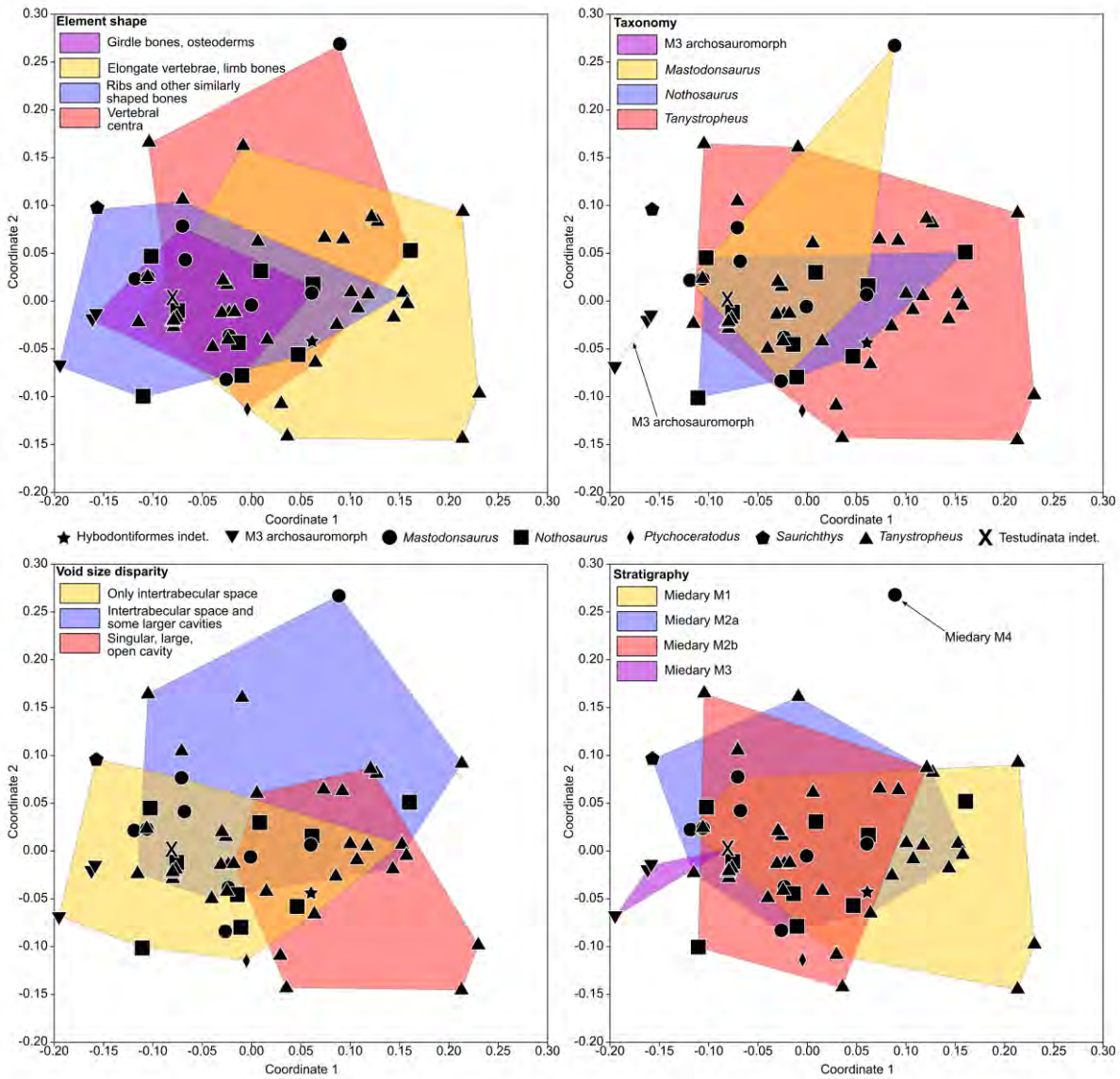

Fig. 6. Non-metric Multidimensional Scaling analysis results. The lowest recorded stress value equals 0.205.

Greater disparity is observed among different skeletal element types, which still form largely overlapping clusters but display a more pronounced spread across both CA and, more prominently, NMDS ordination spaces (Figs. 5–6). When classified according to pore size, a similar pattern is revealed, with most data points clustering centrally, indicating overall homogeneity in histotaphonomic patterns. However, despite substantial overlap, the cervical vertebrae of *Tanystropheus* are more clearly differentiated than in the taxon-based group comparison. Bones with small foramina (Subgroup 1) predominantly exhibit Fe-oxide linings or pyrite, and show low degrees of void filling by both siliciclastic material and carbonate cements. Elements with larger cavities (Subgroups 2 and 3) display less clearly defined trends, although conspicuously higher variability is observed in elements with large foramina compared to those with large, open cavities. In both cases, siliciclastic infill and carbonate cementation occur more frequently than in Subgroup 1 elements. Overall, these patterns indicate a measurable influence of pore size on bone infill patterns.

NMDS and CA yield slightly differing results with respect to the stratigraphic origin of the vertebrate remains (Figs. 5–6). In the NMDS order, fossil-bearing strata form highly overlapping clusters, with only a small number of data points from individual layers extending beyond the main overlap. CA similarly shows substantial overlap among stratigraphic layers; however, the M3 layer is plotted as a more distinct cluster, and the M2b layer exhibits a broader spectrum relative to the remaining layers. These patterns largely correspond to the presence of mica in the M3 layer and circumgranular cement in the M2b layer. Notably, three of the four sampled elements from the M3 layer are referred to the unnamed archosauromorph taxon, which was also distinct in the taxon-based CA. The fourth bone (ZPAL V. 36/404, Testudinata indet.) groups with the M1-M2 specimens. The M4 layer is somewhat distinct, with a *Mastodonsaurus* vertebra (Fig. 3E) plotting notably outside of the main cluster. Nevertheless, the ordinations indicate a lack of strong stratigraphic control on histotaphonomic patterns, with the potential exception of the M3 layer; however, this distinction remains uncertain given the similar pattern observed in the taxon-based analysis.

Discussion

Perminalisation sequence

The spatial relationships between bone pore infills and microstructural features allow the delineation of several potential taphonomic and early diagenetic pathways for the accumulated skeletal elements, defining a main permineralisation sequence, although multiple sequences appear to be represented (Fig. 7). Across the examined specimens, the earliest phase of permineralisation is consistently associated with formation of pyrite or accumulation of ferrous-organic matter, commonly occurring as pore linings or localised infill of minor voids (Fig. 2C). The systematic occurrence of pyrite along bone margins, later enclosed from the void side by clastic material or carbonate cement, supports its early diagenetic formation. Pyrite precipitation, whereas not exclusive, is widely recognised as a commonly early diagenetic process linked to microbial sulphate reduction under anoxic conditions during decay of organic matter (Shapiro and Spangler 2009; Pesquero et al. 2015; Vietti et al. 2015; Laker 2024). The former pyrite linings were likely subsequently oxidised to the Fe-oxides and hydroxides mixture, with organic matter content due to elevation of the oxidising potential within the microenvironment. Both types of linings often co-occur within a specimen indicating local significance of the redox potential changes.

The very early diagenetic stage also includes the development of microcracking within cortical bone, expressed as cracks between or around osteons (Fig. 3B, D). The concentric microcracking around osteons, found only in one *Mastodontosaurus* specimen (ZPAL V. 36/927), is associated with aerial or sub-aerial exposure of the carcass during decomposition (Pfretzschner 2000; Pfretzschner and Tütken 2011; Laker 2024). In contrast, microcracks extending between neighbouring osteons relate to collagen swelling during decomposition in subaqueous conditions (Pfretzschner 2000; Pfretzschner and Tütken 2011; Laker 2024). These features are, however, only clearly preserved in a limited number of specimens.

Subsequently, in elements containing siliciclastic infill (Fig. 2E–F), sediment likely entered bone pores, foramina, or cavities either via pre-existing weathering-related cracks or through infiltration associated with gas release during decomposition (Bodzioch 2015; Kowal-Linka 2015). A spectrum of sediment infills can be distinguished; however, they can be classified into two main types: clay-dominated and sand-dominated infills. Both share the same components (quartz, glauconite, mica, and clay) and differ mainly in their proportions and grain size. This suggests formation within the same depositional environment, although in different parts characterised by varying hydraulic energy and grain sorting. Alternatively, this

disparity might be due to the difference in size of the openings through which sediment entered the bone. Nearly all sedimentary infills contain glauconite, which is particularly interesting due to its typical formation in saline environments. Its in situ origin is usually favoured by microenvironments such as burrows, cracks, or skeletal fossils, which may lead to the formation of glauconite aggregates composed of pellets representing a wide range of maturation stages. In the studied bones, as well as in the surrounding sediment, glauconite is evenly dispersed and represented predominantly by moderately mature pellets, whereas both immature and highly mature pellets are absent. This strongly suggests that the glauconite grains originated from the erosion of older bedrock. Moreover, nearly all glauconite grains show varying degrees of weathering into Fe-Al oxides both inside and outside the bone cavities (Fig. 2F). Such glauconite decomposition has been observed in modern soil examples (REF/S?), which correlates with the common occurrence of root structures across the Miedary section. In sandy sediment, pellets are only partially weathered, which is expressed by reddish spots along their edges. A notably higher degree of glauconite weathering occurs in clay-rich sediment, where most pellets are nearly completely replaced by Fe-Al oxides, forming pseudomorphs rather than preserving the original glauconite. This disparity suggests the formation of the clay-rich facies in a more proximal environment characterised by lower hydraulic energy and more strongly affected by pedogenic alteration compared with the sandy sediment. The co-occurrence of both sediment types in some samples indicates that weathering, at least partially, took place before bone burial. Considering the pedogenic overprint expressed by younger root structures, ongoing soil formation in proximity to the simultaneous bone accumulation appears to be a plausible scenario.

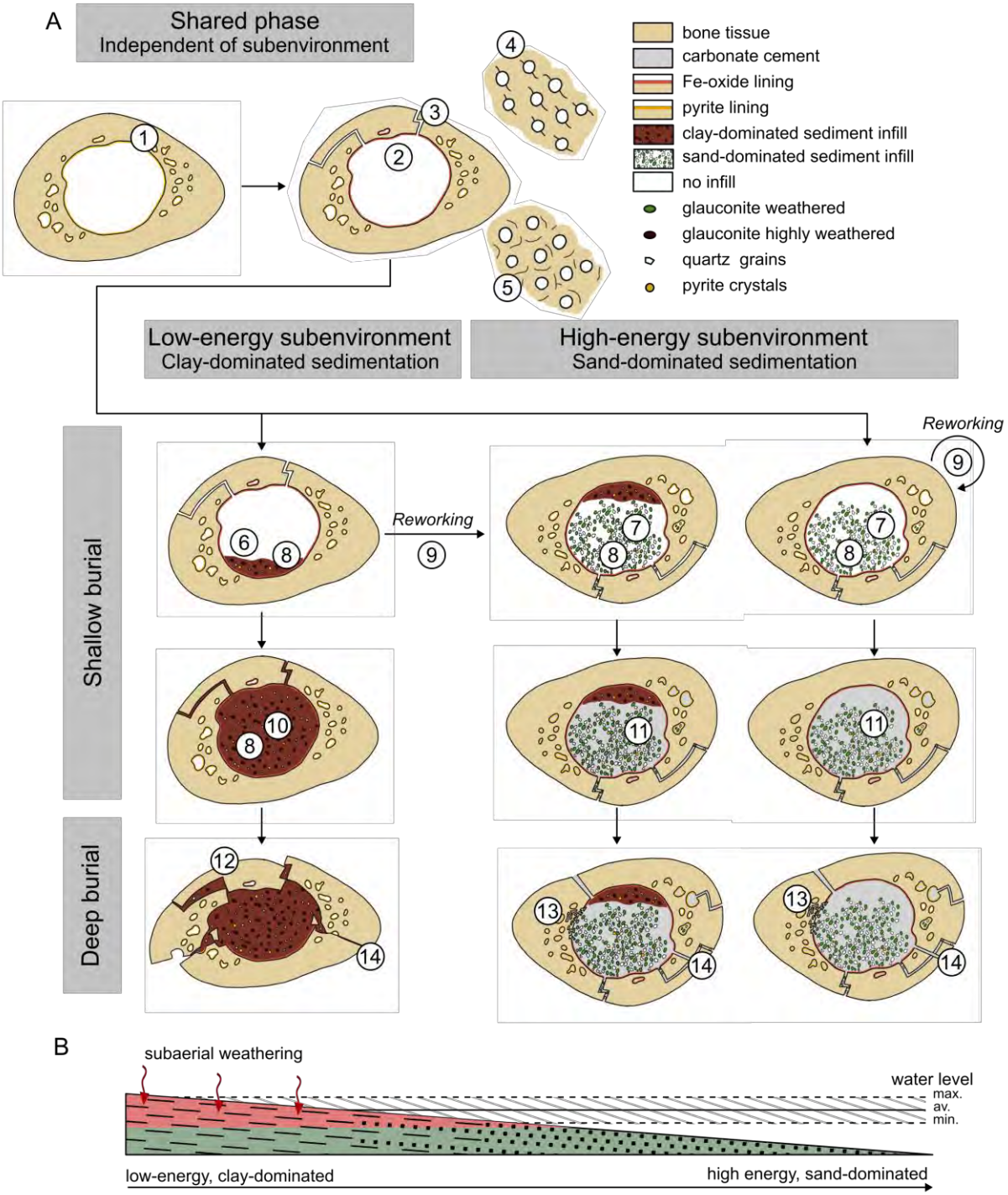

Fig. 7. A. Idealised scenarios of bone taphonomic trajectory in the Miedary assemblage. 1 - Microbial sulphate reduction at presence of organic matter in anoxic microenvironment - pyrite lining formation. 2 - Local oxidation of pyrite lining to Fe-oxides lining in oxidising microenvironment. 3 - Macrocracking related with mechanical damage, gas release or desiccation. 4 - Microcracking of osteons related with waterlogging in submerged conditions. 5 - Microcracking of osteons related to short term aerial exposure. 6 - Partial infill of porous spaces with sediment. *(continued on the next page)*

7 - Partial infill of interconnected porous spaces and macrocracks with sandy sediment, permeable for phreatic solutions. 8 - Reduction of Fe compounds and nucleation of pyrite crystals in reductive microenvironment. 9 - Possible reworking of bones within subenvironment or with short-distance transport to different subenvironment. Possible additional cracking and mixing of uncemented sedimentary infill. Reorientation. 10 - Complete infill of interconnected porous spaces and macrocracks with clayish sediment, non-permeable for phreatic solutions. 11 - Cementation of available porous and intergranular spaces with carbonate cement. 12 - Compaction and brecciation of bones infilled with soft uncemented clayish sediment. 13 - Limited brecciation of bones infilled with cemented sandy sediment. 14 - Late diagenetic macrocracking related to overload pressure or microtectonics. Infill of macrocracks with carbonate cement or sediment. **B**. Schematic representation of the Miedary environment during deposition of the Unit 1 bone assemblage.

Remaining void spaces were filled at a later diagenetic stage by carbonate cements under calcium-carbonate–saturated pore-water conditions (Kowal-Linka 2015). The carbonate cementation is common in specimens filled with highly porous, sand-dominated sediment (Fig. 4). By contrast, the carbonates rarely co-occur with clay infills, which probably reflects their poor permeability for phreatic fluids (Fig. 3E). Bones lacking siliciclastic infill show more extensive carbonate cementation occupying most of the available pore space (Figs. 2B, 3C). Carbonate cementation (at least some of its generations) appears to have occurred relatively early after burial, as indicated by the generally limited brecciation of bone tissue. Brecciation, where present, is likely linked to mechanical compaction related to increasing overburden during progressive burial, which could have been limited by void cementation; this is in line with the overall 3D preservation of most of skeletal remains from Miedary (Czepiński et al. 2023). The carbonate cementation itself is heterogeneous, including microsparitic, drusy, blocky, and mosaic spar, suggesting the multi-phase formation (Figs. 2B, 3C). The overall cement assemblage indicates that phreatic diagenetic conditions predominated, as evidenced by the abundance of coarse-grained mosaic and blocky sparry calcite cements (Flügel 2010; Alonso-Zarza 2003). Distinct cementation phases can be identified by contrasting cement infill patterns in secondary fractures relative to the main void spaces within individual specimens. However, the frequent co-occurrence of multiple carbonate cement textures within single voids, most commonly the central cavities, suggests that progressive recrystallisation (aggrading neomorphism) might have contributed to the observed textural variability (Freytet and Verrecchia 2002; Alonso-Zarza 2003; Flügel 2010).

Although such processes may also occur during deeper burial diagenesis, they are commonly associated with deposits that experienced subaerial exposure or very shallow burial conditions, which are conducive to neomorphic recrystallisation (Freytet and Verrecchia 2002; Alonso-Zarza 2003; Flügel 2010). Paedogenic alteration in the bone-bearing sediments is consistent with the neomorphism of carbonate cements under conditions of subaerial exposure. Yet, bone weathering (*sensu* Behrensmeyer 1978) is relatively low, indicating generally rather short periods of subaerial exposure, and/or an environment that did not prompt weathering.

Broader fractures crosscutting earlier infill phases, as well as older fractures (Fig. 3F), likely represent later-stage mechanical alteration, occurring during resedimentation of pre-fossilised bones, advanced diagenesis, or increasing burial compaction. These cracks are commonly filled with either carbonate cement or, less frequently, siliciclastic material that often differs from earlier pore infills, suggesting secondary infilling under different diagenetic conditions. This, in turn, suggests reworking of the portion of accumulated remains.

Some unfilled fractures may reflect relatively recent damage, including breakage during excavation or thin-section preparation. The timing of development of some features, such as pyrite and glauconite-rich sediment oxidation, remains uncertain, as these processes may reflect either a prolonged residence phase, an early exhumation episode, or more recent exposure of skeletal elements. However, the specimen-specific and spatially restricted occurrence of oxidised material, for example oxidation confined to the interior of bones while absent in the surrounding sediment, favours the former interpretation, suggesting oxidation during an early post-burial phase rather than recent exposure.

Origin of the bone assemblage

Overall, within the analysed sample we observe a relatively complex taphonomic history, with periods of reworking of skeletal elements, potentially also including reincorporation in the system of prefossilised elements (resedimentation). Interestingly, bone infill appears largely independent of stratigraphic position and taxonomy, but exhibits some degree of dependence on intraosseous void size. The frequent absence of both siliciclastic infill and carbonate cementation in bones with thick cortical walls and limited pore volume likely reflects restricted access for sediment and pore fluids, resulting in unfilled pores or pores occupied by pyrite associated with microbial degradation of organic matter. Conversely, the variable extent of siliciclastic and carbonate infill in bones with larger cavities and pore

networks may reflect differences in taphonomic histories, particularly the degree of fracturing that facilitated the ingress of external material. Despite the inclusion of taxa generally assumed to originate from different environments (freshwater vs marine), the variance noted between the majority of the analysed samples does not seem to be correlated with their stratigraphic origin or taxonomy. The only specimens that are excluded from the main cluster, encompassing the majority of studied taxa, are the remains of the unnamed archosauromorph from the M3 layer, the *Saurichthys* rostrum, and the *Mastodonsaurus* vertebral centrum from the M4 layer.

The co-occurrence of remains of taxa from principally different environments may stem from the original nature of these ecosystems. During the Middle Triassic, central Europe underwent profound environmental changes linked to sea level transgression-regression phases (e.g., Franz et al. 2013; Mujal et al. 2025). In particular, Lower Keuper successions resulted from the regression of the Muschelkalk Sea which triggered the expansion of terrestrialised settings and thus the expansion of biota adapted to these. This triggered a faunal turnover which witnessed the simultaneous disappearance of several vertebrate groups (e.g., most of sauropterygians, ichthyosaurs) and the dispersal of many other lineages (e.g., archosauriforms, dipnoans, temnospondyls) in the CEB (Hagdorn and Reif 1988; Rieppel and Hagdorn 1997; Hagdorn and Rieppel 1999; Hagdorn et al. 2015; Mujal et al. 2025; Sues and Shoch 2025). Miedary represents an exemplary case recording these changes, with a mixture of vertebrate faunas from primarily different habitats. Indeed, the same layers preserve taxa that usually do not co-occur, or if they do so, it is in great disparity. For example, plagiosaur temnospondyls in Miedary are represented in the same layers by at least three taxa (Czepiński et al. 2023); in particular, *Plagiosternum* sp. represents an exception in the assemblage, as this taxon is usually found in marine (or marine-influenced) horizons (Schoch et al. 2025). Remains of *Nothosaurus*, principally a marine taxon, are also much more common in Miedary than in the comparable Lower Keuper sites in the western part of the CEB (Hinz et al. 2019, 2020; Schoch and Seegis 2016; Schoch et al. 2022). Pawlak et al. (2022) documented the co-occurrence of marine-related and freshwater fish taxa within the M1–M2 layers, but considered some of them possibly allochthonous. Our results demonstrate that this is likely not the case.

Whereas the bone infills analysed here preserve a disparate array of different sedimentary characteristics, the observed patterns are not taxon-specific, with the exception of the M3 archosauromorph. Material from the glauconite beds (M1-M2) followed several

taphonomic pathways (Fig. 7) mirrored between the three main studied taxa (*Mastodonsaurus*, *Nothosaurus*, *Tanystropheus*). This strongly indicates that these remains shared the characteristics of their decomposition, depositional environment, and early diagenesis. We observed only limited evidence of post-mortem mixing and subsequent deposition of remains of taxa originating from different habitats in the same assemblage. The short transportation regime, quick burial, and the prevalence of characteristics suggesting subaqueous conditions have already indicated that the tetrapod remains in the glauconite beds (M1-M2) had likely originated from a spatially limited area. The new taphonomic data supports this concept. Our results point to the sympatric presence and parautochtonous deposition of freshwater and marine taxa within a shared paralic ecosystem. Only the M3 archosauromorph can be regarded as a possibly allochthonous element of this assemblage.

This interpretation bears further importance for resolving the question on the habitat of *Tanystropheus*. As noted by Rytel (Chapter I), *T. conspicuus* is rare or absent in both marine (depositional settings of the Upper Muschelkalk and the dolostone beds from Miedary) and terrestrial (depositional settings of most of the Lower Keuper and the M3 layer from Miedary) environments, but is common in the transitional zones between them, which are recorded in the M1–M2 layers of Miedary. The sedimentary infill of the analysed *Tanystropheus* remains does not differ from those of *Mastodonsaurus* and *Nothosaurus*. Otherwise, our analyses (Figs. 5–6) show that the remains of *Tanystropheus* exhibit more taphonomic diversity than *Mastodonsaurus* and *Nothosaurus*. This might be due to much more intensive sampling of *Tanystropheus*, or the presence of a unique subenvironment within its empty cervical vertebrae (Rytel et al. 2024*b*). Nevertheless, the general taphonomic homogeneity of the glauconite beds assemblage, contrasting with the preservation of the M3 archosauromorph, indicates a similar post-mortem history of the remains of the three main studied taxa. This supports the interpretation of *Tanystropheus* as an aquatic animal that lived in near-shore (shallow marine/brackish) environments (Nosotii 2007; Beardmore and Saller 2017; Renesto and Saller 2018; Spiekman et al. 2020*a*, *b*; Chapter I). This also agrees with the relatively higher proportion of remains of tetrapod taxa associated with marine habitats in this Lower Keuper site. Its environmental preferences were likely more strict than those of *Mastodonsaurus* or *Nothosaurus*, explaining its relative scarcity in the western part of the CEB, and its abundance in some of the Miedary layers. Similarly to the other studied taxa from the glauconite beds, *Tanystropheus* was not an allochthonous faunistic element, but a part of a complex ecosystem with co-acting marine and freshwater influences.

Conclusions

This study demonstrates how broad sampling of taphonomic characters and their subsequent holistic analysis can be crucial to deciphering the diverse individual biostratinomic pathways of vertebrate remains. Our results confirm that the massive bone accumulation from the glauconite beds of the Middle Triassic site of Miedary has not originated from transport and mixing of freshwater and marine taxa. Instead, the assemblage records taxa that principally do not co-occur, but were present in the same ecosystem in Miedary. The marine influence in the locality is especially more evident when compared to the sites from the western part of the CEB, with taxa like *Nothosaurus*, *Plagiosternum* or *Tanystropheus* being much more common in Miedary. This may be explained by the slightly older age of Miedary (early Ladinian) with respect to the German counterparts (late Ladinian), indicating a still strong influence of the Muschelkalk Sea in the former. This shows the diversity of these Middle Triassic ecosystems, especially during the major environmental turnover of the Lower Keuper. Finally, our study also confirms that the remains of *Tanystropheus* were deposited in subaqueous environments even at the earliest stage of their decomposition and diagenesis. Our study supports the interpretation of *Tanystropheus* as an aquatic animal that dwelled in shallow marine/brackish habitats and not on land. Future studies on the environmental conditions present during the deposition of the glauconite beds in Miedary are needed to establish the characteristics of this setting more precisely, and explain its distinct faunistic composition

Conclusions of the thesis

- The type species of *Tanystropheus*, *T. conspicuus*, is a valid taxon that can be distinguished from the other *Tanystropheus* spp. by the presence of a combination of features, including the expansion of the distal portion of the neural spines in the torso, the posterodorsal extension of the scapular blade, and its very transversely wide frontals. It is known only from the Central European Basin, but is reminiscent in its morphology to *T. hydroides* from Monte San Giorgio and China.

- The entire material of *Tanystropheus* from Miedary is referred to *T. conspicuus*, together with a far more limited number of specimens from other localities. The site has yielded remains of over 20 individuals of various sizes, including some juveniles. *Tanystropheus* from Miedary is the largest known tanystropheid and one of the longest Middle Triassic archosauromorphs, reaching over six meters in total maximal body length..

- The anatomy of the pectoral girdle and the humerus (especially the nearly complete reduction of the deltopectoral crest) strongly indicate that *Tanystropheus* was not capable of terrestrial locomotion.

- The environmental characteristics recorded at the Miedary site (specifically the glauconite beds) are a good proxy for inferring the preferred habitat of *Tanystropheus*. The number of elements of this animal recovered at Miedary, their diversity, and state of preservation, all point towards *T. conspicuus* dying, and likely living, in close proximity to the current excavation site. Previously known localities from which the remains of *Tanystropheus* were reported seem to be positioned further away from the actual habitat of the animal.

- Morphology of the cervical vertebrae of tanysaurians is unique among vertebrates. In contrast to the pneumatised vertebrae of the later avemetatarsalians, only one, large internal cavity was present in the tanysaurian vertebrae. This tubular architecture, together with the high compactness of the bone walls in the cervical vertebrae of the studied taxa, provided durability and forced rigidity of the vertebral column. The cavity was likely filled with soft tissue, most probably bone marrow. These results prove that the extensive internal modifications of the vertebrae were already present in the early archosauromorphs, and might have been later exapted for pneumatisation.

- The main role of the hyperelongate cervical ribs in *Tanystropheus* was to transfer tensile forces and shift the mass of the neck towards the torso. This is the first quantitative evidence supporting the tensile member hypothesis, which was formulated for sauropods. The individual cervical ribs could bend considerably before breaking. They likely did not restrict the neck movements in *Tanystropheus* in a major way, and could enable finer control over the head movements. Despite being composed of a limited number of vertebrae, the neck of *Tanystropheus* could achieve a range of motion comparable to those of some of the long-necked plesiosaurs. This finding rejects previous hypotheses of either extreme stiffness and extraordinary flexibility of the *Tanystropheus* neck.
- The massive bone accumulation from the glauconite beds of Miedary has not originated from long-distance transport and mixing of freshwater and marine taxa. Instead, the assemblage records taxa that principally do not co-occur, but were present in the same ecosystem in Miedary. The remains of *Tanystropheus* were deposited in subaqueous environments even at the earliest stage of their decomposition and diagenesis.
- The abovementioned factors underline some unique aspects of biology of *Tanystropheus*, but the conducted studies place these features in a broader research context and explain their role. Virtually all available data points towards *Tanystropheus* being an aquatic ambush predator that dwelled in shallow marine/brackish habitats.
- Further studies should result from the insights presented in this work. Several subjects are of particular importance in this context, such as: analysis of the inter- and intraspecific variation within *Tanystropheus* and its species; studying the myology and biomechanics of the limbs and tail of *Tanystropheus*; and improving our understanding of the causes of the convergent neck elongation in several marine reptile groups in the Middle Triassic.

References

Abel, O. 1919. *Die Stämme der Wirbeltiere*. 914 pp. Walter de Gruyter & Co., Berlin and Leipzig.

Adam, K.D. 1953. Ein *Tanystropheus*-Fund aus dem Hauptmuschelkalk bei Schloss Stetten (Kreis Künzelsau). *Neues Jahrbuch für Geologie und Paläontologie Monatshefte* 1: 40–43.

Alberti, F. von. 1864. *Ueberblick über die Trias, mit Berücksichtigung ihres Vorkommens in den Alpen*. 353 pp. Cottaschen Buchhandlung, Stuttgart.

Alonso-Zarza, A.M. 2003. Palaeoenvironmental significance of palustrine carbonates and calcretes in the geological record. *Earth-Science Reviews* 60: 261–298.

Assmann, P. 1913. Beitrag zur Kenntnis der Stratigraphie des oberschlesichen Muschelkalks. *Jahrbuch der Königlich Preussischen Geologischen Landesanstalt* 34: 268–340.

Assmann, P. 1944. Die Stratigraphie der oberschlesischen Trias: Teil 2: Der Muschelkalk. *Abhandlungen des Reichsamtes für Bodenforschung, Neue Folge* 208: 124 pp.

Aureliano, T., Ghilardi, A.M., Müller, R.T., Kerber, L., Fernandes, M.A., Ricardi-Branco, F. and Wedel, M.J. 2024. The origin of an invasive air sac system in sauropodomorph dinosaurs. *The Anatomical Record* 307 (4): 1084–1092.

Aureliano, T., Ghilardi, A.M., Müller, R.T., Kerber, L., Pretto, F.A., Fernandes, M.A., Branco, F.R. and Wedel, M.J. 2022. The absence of an invasive air sac system in the earliest dinosaurs suggests multiple origins of vertebral pneumaticity. *Scientific Reports* 12: 20844.

Babonis, L.S. and Brischoux, F. 2012. Perspectives on the convergent evolution of tetrapod salt glands. *Integrative and Comparative Biology* 52 (2): 245–256.

Badlangana, N.L., Adams, J.W. and Manger, P.R. 2009. The giraffe (*Giraffa camelopardalis*) cervical vertebral column: A heuristic example in understanding evolutionary processes? *Zoological Journal of the Linnean Society* 155: 736–757.

Bassani, F. 1886. Sui fossili e sull'eta degli schisti bituminosi triasici di Besano in Lombardia. *Atti Società Italiana di Scienze Naturali* 29: 15–72.

Beardmore, S.R. and Furrer, H. 2017. Land or water: using taphonomic models to determine the lifestyle of the Triassic protorosaur *Tanystropheus* (Diapsida, Archosauromorpha).

Palaeobiodiversity and Palaeoenvironments 98 (2): 243–258.

Behrensmeyer, A. 1975. The taphonomy and paleoecology of Plio-Pleistocene vertebrate assemblages east of Lake Rudolf, Kenya. *Bulletin of the Museum of Comparative Zoology* 146 (10): 473–578.

Behrensmeyer, A. 1978. Taphonomic and ecologic information from bone weathering. *Paleobiology* 4 (2): 150–162.

Benoit, J., Ford, D.P., Miyamae, J.A., and Ruf, I. 2021. Can maxillary canal morphology inform varanopid phylogenetic affinities? *Acta Palaeontologica Polonica* 66 (2): 389–393.

Benton, M.J. 1983. The Triassic reptile *Hyperodapedon* from Elgin: functional morphology and relationships. *Philosophical Transactions of the Royal Society of London, Series B* 302: 605–717.

Benton, M.J. 1986. The Late Triassic reptile *Teratosaurus* - a rauisuchian, not a dinosaur. *Palaeontology* 29 (2): 293–301.

Benton, M.J. and Allen, J.L. 1997. *Boreopricea* from the Lower Triassic of Russia, and the relationships of the prolacertiform reptiles. *Palaeontology* 40 (4): 931–953.

Benton, M.J. and Wu, F. 2022. Triassic Revolution. *Frontiers in Earth Science* 10: 899541.

Bergounioux, F.-M. 1955. Testudinata. *In*: Piveteau, J. (ed.), *Traite de Paleontologie. V. Amphibiens, Reptiles, Oiseaux*, 487–544. Masson et Cie, Paris.

Bernasconi, S.M. 1994. Geochemical and microbial controls on dolomite formation in anoxic environments. A case study from the Middle Triassic (Ticino, Switzerland). *Contributions to Sedimentology* 19: 109 pp.

Bernasconi, S.M. and Riva, A. 1993. Organic geochemistry and depositional environment of a hydrocarbon source rock: the Middle Triassic Grenzbitumenzone Formation, Southern Alps, Italy/Switzerland. *In*: Spencer, A.M. (ed.), *Generation, Accumulation and Production of Europe's Hydrocarbons*, 179–190. Springer, Berlin, Heidelberg.

Bertin, T.J.C., Thivichon-Prince, B., LeBlanc, A.R.H., Caldwell, M.W. and Viriot, L. 2018. Current perspectives on tooth implantation, attachment, and replacement in Amniota. *Frontiers in Physiology* 9: 1630.

Bijlert, P.A. van. 2024. MuSkeMo: Open-source software to construct, analyze, and visualize human and animal musculoskeletal models and movements in Blender. *BioRxiv*: doi.org/10.1101/2024.12.10.627828.

Blob, R.W., Espinoza, I., and Iijima, M. 2022. Anatomy informs geology: Hydrodynamic dispersal of alligator bones, with implications for taphonomic interpretations of fossil deposits of crocodylians, dinosaurs, and other morphologically novel taxa. *The Anatomical Record* 306 (7): 1618–1630.

Borsuk-Białynicka, M. and Evans, S.E. 2009. A long-necked archosauromorph from the early Triassic of Poland. *Palaeontologia Polonica* 65: 203–234.

Böttcher, R. 2015. 8. Fische des Lettenkeupers. *In*: Hagdorn, H., Schoch, R. and Schweigert, G. (eds.), *Der Lettenkeuper - Ein Fenster in Die Zeit vor Den Dinosauriern*, 141–202. Staatliches Museum für Naturkunde Stuttgart, Stuttgart.

Braun, F.W. 1840. *Verzeichnis der in der Kreis-Naturalien-Sammlung zu Bayreuth befindlichen Petrefakten*. 117 pp. Leopold Voss, Leipzig.

Braun, F.W. 1862. *Ueber* Placodus gigas*: Agassiz. und* Placodus Andriani*. Münster*. Programm zum Jahresbericht der königlisches Kreis-Landwirtschafts- und Gewerbeschule zu Bayreuth für das Schuljahr 1861/62. 16 pp. Theodor Burger T., Bayreuth.

Brignon, A. 2021*a*. *The collecting of Triassic vertebrate remains during the eighteenth century*. 72 pp. Arnaud Brignon, Bourg-la-Reine (France).

Brignon, A. 2021*b*. L'histoire de la paléontologie des vertébrés dans le Trias alsacien jusqu'au début du XXe siècle. *Bulletin de la Société d'Histoire naturelle et d'Ethnographie de Colmar* 77 (8): 70–136.

Britt, B.B. 1993. *Pneumatic postcranial bones in dinosaurs and other archosaurs*. 383 pp. D. Phil. Thesis, University of Calgary.

Britt, B.B., Makovicky, P.J., Gauthier, J.A. and Bonde, N. 1998. Postcranial pneumatization in *Archaeopteryx*. *Nature* 395: 374–376.

Broili, F. 1915. Beobachtungen an *Tanystropheus conspicuus* H. v. Meyer. *Neues Jahrbuch für Mineralogie, Geologie und Paläontologie* 2: 51–62.

Buchmann, R., Holgado, B., Sobral, G., dos Santos Avilla, L. and Rodrigues, T. 2021.

Quantitative assessment of the vertebral pneumaticity in an anhanguerid pterosaur using micro-CT scanning. *Scientific Reports* 11: 18718.

Buchmann, R. and Rodrigues, T. 2025. Resistance of cervical vertebrae in response to muscular stresses in pterosaurs: implications for foraging habits and skeletal pneumatization. *PeerJ* 13: e20388.

Butler, R.J., Barrett, P.M. and Gower, D.J. 2012. Reassessment of the evidence for postcranial skeletal pneumaticity in triassic archosaurs, and the early evolution of the avian respiratory system. *PLoS ONE* 7 (3): e34094.

Camp, C.L. 1945. *Prolacerta* and the protorosaurian reptiles; Part II. *American Journal of Science* 243 (2): 84–101.

Carroll, R.L. 1988. *Vertebrate paleontology and evolution*. 698 pp. W. H. Freeman and Company, New York.

Carter, Joseph, G., Altaba, C.R., Anderson, L.C., Campbell, D.C. and Fang, Z. 2015. The paracladistic approach to phylogenetic taxonomy. *Paleontological Contributions* 12: 1–9.

Case, E.C. 1932. On the caudal region of *Coelophysis* sp., and some new or little known forms from the Upper Triassic of Western Texas. *Contributions from the Museum of Paleontology. University of Michigan* 4 (3): 81–91.

Casey, M.M., Fraser, N.C., and Kowalewski, M. 2007. Quantitative taphonomy of a Triassic reptile *Tanytrachelos ahynis* from the Cow Branch Formation, Dan River basin, Solite Quarry, Virginia. *Palaios* 22: 598–611.

Cerda, I.A., Salgado, L. and Powell, J.E. 2012. Extreme postcranial pneumaticity in sauropod dinosaurs from South America. *Paläontologische Zeitschrift* 86: 441–449.

Chatterjee, S. 1974. A rhynchosaur from the Upper Triassic Maleri Formation of India. *Philosophical Transactions - Royal Society of London, Series B* 267: 209–261.

Chatterjee, S. 1980. *Malerisaurus*, a new eosuchian reptile from the Late Triassic of India. *Philosophical Transactions of the Royal Society of London, Series B* 291: 163–200.

Chatterjee, S. 1986. *Malerisaurus langstoni*, a new diapsid reptile from the Triassic of Texas. *Journal of Vertebrate Paleontology* 6 (4): 297–312.

Cignoni, P., Callieri, M., Corsini, M., Dellepiane, M., Ganovelli, F., and Ranzuglia, G. 2008. MeshLab: An open-source mesh processing tool. *6th Eurographics Italian Chapter Conference 2008 - Proceedings*: 29–36.

Cobley, M.J., Rayfield, E.J. and Barrett, P.M. 2013. Inter-vertebral flexibility of the ostrich neck: implications for estimating sauropod neck flexibility. *PLoS ONE* 8 (8): e72187.

Colbert, E.H. 1970. A saurischian dinosaur from the Triassic of Brazil. *American Museum Novitates* 2405: 1–39.

Cope, E.D. 1887. A contribution to the history of the Vertebrata of the Trias of North America. *Proceedings of the American Philosophical Society* 24 (126): 209–228.

Corroy, G. 1928. Les Vertébrés du Trias de Lorraine et le Trias Lorrain. *Annales de Paléontologie* 17: 81–136.

Cowgill, T., Young, M.T., Schwab, J.A., Walsh, S., Witmer, L.M., Herrera, Y., Dollman, K.N., Turner, A.H. and Brusatte, S.L. 2023. Cephalic salt gland evolution in Mesozoic pelagic crocodylomorphs. *Zoological Journal of the Linnean Society* 197 (3): 812–835.

Cuff, A.R. and Rayfield, E.J. 2013. Feeding mechanics in spinosaurid theropods and extant crocodilians. *PLoS ONE* 8 (5): e65295.

Currey, J. D. 2006. *BONES: Structure and Mechanics. Second ed.* 453 pp. Princeton University Press, Princeton.

Czepiński, Ł., Dróżdż, D., Szczygielski, T., Tałanda, M., Pawlak, W., Lewczuk, A., Rytel, A., and Sulej, T. 2021. An Upper Triassic terrestrial vertebrate assemblage from the forgotten Kocury locality in southern Poland with a new aetosaur taxon. *Journal of Vertebrate Paleontology* 41 (1): e1898977.

Czepiński, Ł., Pawlak, W., Rytel, A., Tałanda, M., Szczygielski, T., and Sulej, T. 2023. A new Middle Triassic vertebrate assemblage from Miedary (southern Poland). *Journal of Vertebrate Paleontology* 43 (2): e2265445.

Dalla Vecchia, F.M. 2000. *Tanystropheus* (Archosauromorpha, Prolacertiformes) remains from the Triassic of the northern Friuli (NE Italy). *Rivista Italiana di Paleontologia e Stratigrafia* 106 (2): 135–140.

Dalla Vecchia, F.M. 2006. Remains of *Tanystropheus*, sauropterygians and ‘rauisuchians’ (Reptilia) in the Middle Triassic of Aupa Valley (Udine, Friuli Venezia Giulia, NE

Italy). *Gortania Atti del Museo Friulano di Storia Naturale* 27 (2006): 25–48.

Dalla Vecchia, F.M. 2008. *Vertebrati fossili del Friuli – 450 milioni di anni di evoluzione*. 304 pp. Museo Friulano di Storia Naturale, Udine.

Dalla Vecchia, F.M. 2010. New ichthyosaurian (Amniota, ?Diapsida) remains in the Triassic of Friuli (NE Italy). *Gortania: Geologia, Paleontologia, Paletnologia* 31 (2009): 15–22.

Dalla Vecchia, F.M. 2020. *Raibliania calligarisi* gen. n., sp. n., a new tanystropheid (Diapsida, Tanystropheidae) from the Upper Triassic (Carnian) of northeastern Italy. *Rivista Italiana di Paleontologia e Stratigrafia* 126 (1): 197–222.

Dalla Vecchia, F.M. and Avanzini, M. 2002. New findings of isolated remains of Triassic reptiles from Northeastern Italy. *Bollettino della Societa Paleontologica Italiana* 41 (2–3): 215–235.

Dalla Vecchia, F.M. and Simonetto, L. 2018. Osteological remains of reptiles from Friuli region (NE Italy) in the palaeontological collections of the Museo Friulano di Storia Naturale. *Gortania: Geologia, Paleontologia, Paletnologia* 39 (2017): 27–70.

Dalle-Laste, V.Z., Garcia, M.S., Aureliano, T., Ghilardi, A.M., Kerber, L., and Müller, R.T. 2025. The first allokotosaurian from South America and the Gondwanan radiation of non-archosauriform archosauromorphs. *Zoological Journal of the Linnean Society* 204 (4): zlaf098.

Diedrich, C.G. 2009. The vertebrates of the Anisian/Ladinian boundary (Middle Triassic) from Bissendorf (NW Germany) and their contribution to the anatomy, palaeoecology, and palaeobiogeography of the Germanic Basin reptiles. *Palaeogeography, Palaeoclimatology, Palaeoecology* 273: 1–16.

Diedrich, C.G. 2012. The Middle Triassic marine reptile biodiversity in the Germanic Basin, in the centre of the Pangaean world. *Central European Journal of Geosciences* 4 (1): 9–46.

Diedrich, C.G. 2015. The vertebrates from the Lower Ladinian (Middle Triassic) bonebed of Lamerden (Germany) as palaeoenvironment indicators in the Germanic Basin. *Open Geosciences* 7 (1): 755–782.

Dilkes, D.W. 1998. The Early Triassic rhynchosaur *Mesosuchus browni* and the interrelationships of basal archosauromorph reptiles. *Philosophical Transactions of the*

Royal Society of London. Series B. Biological Sciences 353: 501–541.

Dorka, M. 2002. Tetrapod teeth from an Upper Ladinian bone bed, Schöningen (Lower Saxony, Germany). *Paläontologische Zeitschrift* 76 (2): 283–296.

Drevermann, F. 1915. Über *Placodus*. *Centralblatt für Mineralogie, Geologie und Paläontologie* 13 (13): 402–405.

Dumont, E.R. 2010. Bone density and the lightweight skeletons of birds. *Proceedings of the Royal Society B: Biological Sciences* 277: 2193–2198.

Dumont, M., Laurin, M., Jacques, F., Pelle, E., Dabin, W. and Buffrenil, V. De. 2013. Inner architecture of vertebral centra in terrestrial and aquatic mammals: A two-dimensional comparative study. *Journal of Morphology* 584: 570–584.

Duncker, H.-R. 1971. The lung air sac system of birds. *Advances in Anatomy and Embryology and Cell Biology* 45 (6): 171pp.

Dzemski, G. and Christian, A. 2007. Flexibility along the neck of the ostrich (*Struthio camelus*) and consequences for the reconstruction of dinosaurs with extreme neck length. *Journal of Morphology* 268: 701–714.

Dzik, J. and Sulej, T. 2016. An early Late Triassic long-necked reptile with a bony pectoral shield and gracile appendages. *Acta Palaeontologica Polonica* 61 (4): 805–823.

Eck, H. 1865. *Ueber die Formationen des bunten Sandsteins und des Muschelkalkes in Oberschlesien und ihre Versteinerungen*. 148 pp. J. F. Starcke, Berlin.

Edinger, T. 1921. Über *Nothosaurus*. PhD thesis. 82pp. Johann Wolfgang Goethe-Universität, Frankfurt a. M.

Edinger, T. 1923. Eine Bemerkung über *Tanystropheus*. *Senckenbergiana* 5: 143–144.

Edinger, T. 1924. Rückenmark im Wirbelkörper! *Anatomischer Anzeiger* 57 (23): 515–519.

Edinger, T. 1931. *Tanystropheus* aufgeklärt. *Die Naturwissenschaften* 19 (41): 846–847.

Emmert, U. and Horstig, G. von. 1972. *Geologische Karte von Bayern 1:25000. Erläuterungen zum Blatt Nr. 5734 Wallenfels*. 240 pp. Bayerisches Geologisches Landesamt, München.

Erickson, G. M., Catanese III, J., and Keaveny, T. M. 2002. Evolution of the biomechanical material properties of the femur. *The Anatomical Record* 268(2): 115–124.

Evans, S.E. 1988. The early history and relationships of the Diapsida. *In*: Benton, M.J. (ed.), *The Phylogeny and Classification of the Tetrapods, Volume 1: Amphibians, Reptiles, Birds*, 221–260. Oxford University Press.

Ezcurra, M.D. 2016. The phylogenetic relationships of basal archosauromorphs, with an emphasis on the systematics of proterosuchian archosauriforms. *PeerJ* 4: e1778.

Ezcurra, M.D. and Butler, R.J. 2018. The rise of the ruling reptiles and ecosystem recovery from the Permo-Triassic mass extinction. *Proceedings of the Royal Society B: Biological Sciences* 285: 20180361.

Ezcurra, M.D., Jones, A.S., Gentil, A.R., and Butler, R.J. 2020. Early Archosauromorphs: The Crocodile and Dinosaur Precursors. *In* Alderton, D. and Elias, S.A. (eds.), *Encyclopedia of Geology (Second Edition)*, 175–185. Elsevier Inc.

Ezcurra, M.D., Scheyer, T.M., and Butler, R.J. 2014. The origin and early evolution of Sauria: Reassessing the Permian saurian fossil record and the timing of the crocodile-lizard divergence. *PLoS ONE* 9 (2): e89165.

Ezcurra, M.D., Sues, H.-D. and Fröbisch, J. 2025. A new late Permian archosauromorph reptile from Germany enhances our understanding of the early diversity of the clade. *Journal of Systematic Palaeontology* 23 (1): 2509639.

Fastnacht, M. 2005. The first dsungaripterid pterosaur from the Kimmeridgian of Germany and the biomechanics of pterosaur long bones. *Acta Palaeontologica Polonica* 50 (2): 273–288.

Faux, C. M., and Padian, K. 2007. The opisthotonic posture of vertebrate skeletons: Postmortem contraction or death throes? *Paleobiology* 33(2), 201–226.

Fernández, M. and Gasparini, Z. 2008. Salt glands in the Jurassic metriorhynchid *Geosaurus*: implications for the evolution of osmoregulation in Mesozoic marine crocodyliforms. *Naturwissenschaften* 95: 79–84.

Flügel, E., 2010. *Microfacies of Carbonate Rocks. Analysis, Interpretation and Application. Second Edition*. 976 pp. Springer-Verlag, Berlin.

Ford, D.P. and Benson, R.B.J. 2018. A redescription of *Orovenator mayorum* (Sauropsida, Diapsida) using high-resolution μCT, and the consequences for early amniote phylogeny. *Papers in Palaeontology* 5 (2): 197–239.

Formoso, K.K., Nesbitt, S.J., Pritchard, A.C., Stocker, M.R., and Parker, W.G. 2019. A long-necked tanystropheid from the Middle Triassic Moenkopi Formation (Anisian) provides insights into the ecology and biogeography of tanystropheids. *Palaeontologia Electronica* 22.3.73: 1–15.

Foster, W., Gensbigler, P., Wilson, J.D., Smith, R.M.H., Lyson, T.R. and Bever, G.S. 2024. Cranial anatomy of the Triassic rhynchosaur *Mesosuchus browni* based on computed tomography, with a discussion of the vomeronasal system and its deep history in Reptilia. *Zoological Journal of the Linnean Society* 201 (4): zlae097.

Foth, C., Ezcurra, M.D., Sookias, R.B., Brusatte, S.L., and Butler, R.J. 2016. Unappreciated diversification of stem archosaurs during the Middle Triassic predated the dominance of dinosaurs. *BMC Evolutionary Biology* 16 : 188.

Fraas, E. 1896. *Die Schwäbischen Trias-Saurier nach dem Material der Königlichen Naturalien-Sammlung in Stuttgart zusammengestellt*. 18 pp. Schweizerbartsche Verlagsbuchhandlung, Stuttgart.

Franz, M., Henniger, M., and Barnasch, J. 2013. The strong diachronous Muschelkalk/Keuper facies shift in the Central European Basin: Implications from the type-section of the Erfurt Formation (Lower Keuper, Triassic) and basin-wide correlations. *International Journal of Earth Sciences* 102: 761–780.

Franz, M., Kaiser, S.I., Fischer, J., Heunisch, C., Kustatscher, E., Luppold, F.W., Berner, U., and Röhling, H.-G. 2015. Eustatic and climatic control on the Upper Muschelkalk Sea (late Anisian/Ladinian) in the Central European Basin. *Global and Planetary Change* 135: 1–27.

Fraser, N.C. and Rieppel, O. 2006. A new protorosaur (Diapsida) from the Upper Buntsandstein of the Black Forest, Germany. *Journal of Vertebrate Paleontology* 26 (4): 866–871.

Frey, E. and Martin, J. 1997. Long necks of sauropods. *In*: Currie, P.J. and & Padian, K. (eds.), *Encyclopedia of dinosaurs*, 406–409. Academic Press, San Diego.

Freytet, P. and Verrecchia, E.P. 2002. Lacustrine and palustrine carbonate petrography: an overview. *Journal of Paleolimnology* 27: 221–237.

Fritsch, K. von. 1894. Beitrag zur Kenntnis der Saurier des Halle'schen unteren Muschelkalkes. *Abhandlungen der naturforschenden Gesellschaft zu Halle* 20: 271–302.

Fronimos, J.A. 2023. Patterns and function of pneumaticity in the vertebrae, ribs, and ilium of a titanosaur (Dinosauria, Sauropoda) from the Upper Cretaceous of Texas. *Journal of Vertebrate Paleontology* 43 (2): e2259444.

Galton, P.M. and Cluver, M.A. 1976. *Anchisaurus capensis* (Broom) and a revision of the Anchisauridae (Reptilia, Saurischia). *Annals of the South African Museum* 69 (6): 121–159.

Gans, C. 1961. The feeding mechanism of snakes and its possible evolution. *American Zoologist* 1 (2): 217–227.

Gans, C. 1969. Comments on inertial feeding. *Copeia* 4: 855–857.

García-Vilana, S., Sánchez-Molina, D., and Llumà, J. 2025. Effect of strain rate on the mechanical properties of human ribs: Insights from complete rib bending tests. *Journal of the Mechanical Behavior of Biomedical Materials* 166: 106954.

Gervais, P. 1858. Description de l'*Aphelosaurus lutevensis*, saurien fossile des schistes permiens de Lodève. *Annales des Sciences Naturelles. Zoologie* 10 (4): 233–235.

Gervais, P. 1859. *Zoologie et paléontologie françaises: nouvelles recherches sur les animaux vertébrés dont on trouve les ossements enfouis dans le sol de la France et sur leur comparaison avec les espèces propres aux autres régions du globe*. 544 pp. Arthus Bertrand, Paris.

Gottmann-Quesada, A. and Sander, P.M. 2009. A redescription of the early archosauromorph *Protorosaurus speneri* Meyer, 1832, and its phylogenetic relationships. *Paleontographica A* 287: 123–220.

Gow, C. 1975. The morphology and relationships of *Youngina capensis* Broom and *Prolacerta broomi* Parrington. *Palaeontologia africana* 18: 89–131.

Gurevitch, O., Slavin, S. and Feldman, A.G. 2007. Conversion of red bone marrow into yellow – Cause and mechanisms. *Medical Hypotheses* 69: 531–536.

Gürich, G. 1884. Ueber einige Saurier oberschlesishen Muschelkalkes. *Zeitschrift der Deutschen Geologischen Gesellschaft* 36: 125–144.

Gürich, G. 1887. Über den Boruschowitzer Mergelschiefer. *Jahres-Bericht der Schlesischen Gesellschaft für Vaterländische Cultur* 63: 137–138.

Gutarra, S., Stubbs, T.L., Moon, B.C., Palmer, C., and Benton, M.J. 2022. Large size in aquatic tetrapods compensates for high drag caused by extreme body proportions. *Communications Biology* 5: 380.

Haas, G. 1970. Eine bemerkenswerte Interclavicula von (?) *Tanystropheus* aus dem Muschelkalk des Wadi Ramon, Israel. *Paläontologische Zeitschrift* 44 (3/4): 207–214.

Hagdorn, H. 1990. Das Muschelkalk/Keuper-Bonebed von Crailsheim. *Klassische Fundstellen der Paläontologie* 2 (23): 78–88.

Hagdorn, H. and Mutter, R.J. 2011. The vertebrate fauna of the Lower Keuper Albertibank (Erfurt Formation, Middle Triassic) in the vicinity of Schwäbisch Hall (Baden-Wurttemberg, Germany). *Paleodiversity* 4: 223–243.

Hagdorn, H. and Reif, W.-E. 1988. 'Die Knochenbreccie von Crailsheim' und weitere Mitteltrias-Bonebeds in Nordost-Württemberg - Alte und neue Deutungen. *In*: Hagdorn, H. (ed.), *Neue Forschungen zur Erdgeschichte von Crailsheim*, 116–143. Goldschneck, Korb.

Hagdorn, H. and Rieppel, O. 1999. Stratigraphy of marine reptiles in the Triassic of Central Europe. *Zentralblatt für Geologie und Paläontologie* 1 (7–8): 651–678.

Hagdorn, H. and Simon, T. (eds.) 2020. *Stratigraphie von Deutschland XIII: Muschelkalk Teil I + II*. 1256 pp. Schweizerbart, Hannover.

Hagdorn, H., Heunisch, C., and Schoch, R.R. 2015*a*. 4. Biostratigraphie und Alter des Lettenkeupers. *In*: Hagdorn, H., Schoch, R., and Schweigert, G. (eds.), *Der Lettenkeuper - Ein Fenster in Die Zeit vor den Dinosauriern*, 41–47. Staatliches Museum für Naturkunde Stuttgart, Stuttgart.

Hagdorn, H., Schoch, R.R., Seegis, D., and Werneburg, R. 2015*b*. 14. Wirbeltierlagerstätten im Lettenkeuper. *In*: Hagdorn, H., Schoch, R., and Schweigert, G. (eds.), *Der Lettenkeuper - Ein Fenster in Die Zeit vor den Dinosauriern*, 325–358. Staatliches Museum für Naturkunde Stuttgart, Stuttgart.

Hahn, G., Lepage, J.C. and Wouters, G. 1984. Cynodontier-Zähne aus der Ober-Trias von Medernach, Grossherzogtum Luxemburg. *Bulletin de la Société belge de Géologie* 93 (4): 357–373.

Hammer, Ø., Harper, D.A.T. and Ryan, P.D. 2001. PAST: Paleontological Statistics Software

Package for Education and Data Analysis. *Palaeontologia Electronica* 4 (1): 1–9.

Hauschke, N. and Wilde, V. (eds.) 1999. *Trias. Eine ganz andere Welt. Mitteleuropa im frühen Erdmittelalter*. 647 pp. Dr. Friedrich Pfeil, München.

Hauschke, N., Franz, M., and Bachmann, G.H. (eds.) 2021. *Trias. Aufbruch in das Erdmittelalter. Volume 1*. 356 pp. Dr. Friedrich Pfeil, München.

Heidenfelder, J., Heckert, A.B., Pugh, I., Nesbitt, S.J., Lauer, R. and Lauer, B. 2023. The morphology of tanystropheids (Reptilia Archosauromorpha) of the Upper Triassic (Revueltian early-mid Norian) Homestead site in east central New Mexico. *Program Guide of the Society of Vertebrate Paleontology 83rd Annual Meeting, October 18-21, 2023*: 209–210.

Herrel, A., Damme, J. Van and Aerts, P. 2007. Cervical anatomy and function in turtles. *In*: Wyneken, J., Godfrey, M.H. and Bels, V. (eds.), *Biology of Turtles*, 163–185. CRC Press, Boca Raton.

Hinz, J.K., Matzke, A.T. and Pfretzschner, H.U. 2019. A new nothosaur (Sauropterygia) from the Ladinian of Vellberg-Eschenau, southern Germany. *Journal of Vertebrate Paleontology* 39 (2): e1585364-12.

Hinz, J.K., Matzke, A.T., Augustin, F.J. and Pfretzschner, H.U. 2020. A *Nothosaurus* (Sauropterygia) skull from Kupferzell (Triassic, late Ladinian; SW Germany). *Neues Jahrbuch für Geologie und Paläontologie - Abhandlungen* 297 (1): 101–111.

Houssaye, A. 2009. 'Pachyostosis' in aquatic amniotes: a review. *Integrative Zoology* 4: 325–340.

Houssaye, A., Sander, P.M. and Klein, N. 2016. Integrative and comparative biology adaptive patterns in aquatic amniote bone microanatomy - more complex than previously thought. *Integrative and Comperative Biology* 56 (6): 1349–1369.

Houssaye, A., Nakajima, Y. and Sander, P.M. 2018. Structural, functional, and physiological signals in ichthyosaur vertebral centrum microanatomy and histology. *Geodiversitas* 40 (7): 161–170.

Hörandl, E. 2006. Paraphyletic versus monophyletic taxa – evolutionary versus cladistic classifications. *Taxon* 55 (3): 564–570.

Hörandl, E. and Stuessy, T.F. 2010. Paraphyletic groups as natural units of biological

classification. *Taxon* 59 (6): 1641–1653.

Huene, F. von. 1902. Übersicht über die Reptilien der Trias. *Geologische und Paläontologische Abhandlungen. Neue Folge* 6: 1–84.

Huene, F. von. 1905. Über die Trias-Dinosaurier Europas. *Zeitschrift der Deutschen Geologischen Gesellschaft* 57: 345–349.

Huene, F. von. 1906. Ueber die Dinosaurier der aussereuropäischen Trias. *Geologische und Paläontologische Abhandlungen. Neue Folge* 8 (2): 99–156.

Huene, F. von. 1907-1908. Die Dinosaurier der europäischen Triasformation. *Geologische und Paläontologische Abhandlungen. Supplement 1*: 419 pp.

Huene, F. von. 1910. Ein primitiver Dinosaurier aus der mittleren Trias von Elgin. *Geologische und Paläontologische Abhandlungen. Neue Folge* 8 (6): 317–321.

Huene, F. von. 1914*a*. Das natürliche System der Saurischia. *Centralblatt für Mineralogie, Geologie und Paläontologie* 5: 154–158.

Huene, F. von. 1914*b*. Saurischia et Ornitischia triadica ("Dinosauria" triadica). *In* Frech, F. (ed.), *Fossilium Catalogus. I: Animalia. Part 4*. 21 pp. W. Junk, Berlin.

Huene, F. von. 1914*c*. Coelurosaurier-Reste aus dem untern Muschelkalk. *Centralblatt für Mineralogie, Geologie und Paläontologie* 21: 670–672.

Huene, F. von. 1920*a*. Ein Parasuchier aus dem oberen Muschelkalk von Bayreuth. *Senckenbergiana* 2 (5): 143–145.

Huene, F. von. 1920*b*. Stammesgeschichtliche Ergebnisse einiger Untersuchungen an Trias-Reptilien. *Zeitschrift für Induktive Abstammungs- und Vererbungslehre* 24: 159–163.

Huene, F. von. 1931. Über *Tanystropheus* und verwandte Formen. *Neues Jahrbuch für Geologie und Paläontologie, Abteilung B* 67: 65–86.

Huene, F. von. 1932. Die fossile Reptil-Ordnung Saurischia, ihre Entwicklung und Geschichte. *Monographien zur Geologie und Paläontologie* 1 (4): 1–361.

Huene, F. von. 1940. Eine Reptilfauna aus der ältesten Trias Nordrußlands. *Neues Jahrbuch für Mineralogie, Geologie und Paläontologie, Beilage-Band, Abteilung B* 84: 1–23.

Huene, F. von. 1944. Beiträge zur Kenntnis der Protorosaurier. *Neues Jahrbuch für Mineralogie, Geologie und Paläontologie, Monatshefte, Abteilung B* 5: 120–131.

Huene, F. von. 1946. Die großen Stämme der Tetrapoden in den geologischen Zeiten. *Biologischen Zentralblatt* 65 (7): 268–275.

Huene, F. von. 1954. Ein neuer Protorosauridae. *Neues Jahrbuch für Geologie und Paläontologie, Monatshefte* 5: 228–230.

Huene, F. von. 1956. *Paläontologie und Phylogenie der Niederen Tetrapoden*. 716 pp. Gustav Fischer, Jena.

Huene, F. von. 1958*a*. Neue Vertebratenfunde aus dem Muschelkalk Württembergs. *Jahreshefte des Vereins für Vaterländische Naturkunde in Württemberg* 113: 316–319.

Huene, F. von. 1958*b*. Gleiche Parasuchier von Braunsehweig und Bristol. *Paläontologische Zeitschrift* 32 (1): 63–66.

Huxley, T. H. 1871. A Manual of the Anatomy of the Vertebrated Animals. 432 pp. J. & A. Churchill, London.

Jaekel, O. 1916. Die Wirbeltierfunde aus dem Keuper von Halberstadt. *Palaeontologische Zeitschrift* 2: 88–214.

Janensch, W. 1947. Pneumatizität bei Wirbeln von Sauropoden und anderen Saurischiern. *Palaeontographica - Supplement* 7 (1): 1–25.

Jaquier, V.P. and Scheyer, T.M. 2017. Bone histology of the Middle Triassic long-necked reptiles *Tanystropheus* and *Macrocnemus* (Archosauromorpha, Protorosauria). *Journal of Vertebrate Paleontology* 37 (2): e1296456.

Jaquier, V.P., Fraser, N.C., Furrer, H., and Scheyer, T.M. 2017. Osteology of a new specimen of *Macrocnemus* aff. *M. fuyuanensis* (Archosauromorpha, Protorosauria) from the middle triassic of Europe: Potential implications for species recognition and paleogeography of tanystropheid protorosaurs. *Frontiers in Earth Science* 5: 91.

Jiang, D., Tintori, A., Zhou, M., Motani, R., Ji, C., Rieppel, O., Fraser, N.C., Conedera, D., Yao, M., Wang, Y., and Sun, Z. 2025. Vertebrate diversity of the Middle Triassic Xingyi Fauna. *Diversity* 17: 453.

Johnson, M.M., Scheyer, T.M., Canoville, A., and Maxwell, E.E. 2025. Palaeohistology of *Macrospondylus bollensis* (Crocodylomorpha: Thalattosuchia: Teleosauroidea) from the Posidonienschiefer Formation (Toarcian) of Germany, with insights into life history and ecology. *The Anatomical Record* 308 (2): 342–368.

Jones, M. E., Gröning, F., Dutel, H., Sharp, A., Fagan, M. J., and Evans, S. E. 2017. The biomechanical role of the chondrocranium and sutures in a lizard cranium. *Journal of the Royal Society Interface* 14 (137): 20170637.

Jurcsak, T. 1973. Date noi asupra reptilelor mezozoice din Transilvania. *Nymphea* 1: 245–261.

Jurcsak, T. 1975. *Tanystropheus biharicus* n. sp. (Reptilia, Squamata) o noua specie pentru fauna Triasica Romaniei. *Nymphea* 3: 45–52.

Jurcsak, T. 1978. Rezultate noi în studiul saurienilor fosili de la Aleșd. *Nymphea* 6: 15–60.

King, A.S. 1966. Structural and functional aspects of the avian lungs and air sacs. *International Review of General and Experimental Zoology* 2: 171–267.

Klein, N., Canoville, A. and Houssaye, A. 2019. Microstructure of vertebrae, ribs, and gastralia of Triassic sauropterygians—new insights into the microanatomical processes involved in aquatic adaptations of marine peptiles. *Anatomical Record* 302 (10): 1770–1791.

Klein, N., Christian, A. and Sander, P.M. 2012. Histology shows that elongated neck ribs in sauropod dinosaurs are ossified tendons. *Biology Letters* 8 (6): 1032–1035.

Klein, N., Eggmaier, S., and Hagdorn, H. 2022. The redescription of the holotype of *Nothosaurus mirabilis* (Diapsida, Eosauropterygia) — a historical skeleton from the Muschelkalk (Middle Triassic, Anisian) near Bayreuth (southern Germany). *PeerJ* 10: e13818.

Klein, N., Sander, P.M., Krahl, A., Scheyer, T.M. and Houssaye, A. 2016. Diverse aquatic adaptations in Nothosaurus spp. (Sauropterygia) - Inferences from humeral histology and microanatomy. *PLoS ONE* 11 (7): e0158448.

Kluge, A. 1982. Cloacal bones and sacs as evidence of gekkonoid lizard relationships. *Herpetologica* 38 (3): 348–355.

Korte, C., Kozur, H.W., Bruckschen, P., and Veizer, J. 2003. Strontium isotope evolution of Late Permian and Triassic seawater. *Geochimica et Cosmochimica Acta* 67 (1): 47–62.

Kowal-Linka, M. 2008. Formalizacja litostatygafii formacji gogolińskiej (trias środkowy) na Śląsku Opolskim. *Geologos* 14 (2): 126–161.

Kowal-Linka, M. 2015. Analysis of marrow cavity fillings as a tool to recognise diverse taphonomic histories of fossil reptile bones: Implications for the genesis of the Lower Muschelkalk marine bone-bearing bed (Middle Triassic, Żyglin, S Poland). *Palaeogeography, Palaeoclimatology, Palaeoecology* 436 (October 2015): 64–76.

Kowal-Linka, M. and Bodzioch, A. 2017. Genesis of the Lower Triassic bonebeds from Gogolin (S Poland): The impact of microbial mats on trapping of vertebrate remains. *Palaeogeography, Palaeoclimatology, Palaeoecology* 466: 38–58.

Krahl, A., Klein, N. and Sander, P.M. 2013. Evolutionary implications of the divergent long bone histologies of *Nothosaurus* and *Pistosaurus* (Sauropterygia, Triassic). *BMC Evolutionary Biology* 13: 123.

Kubo, T., Mitchell, M.T. and Henderson, D.M. 2012. *Albertonectes vanderveldei*, a new elasmosaur (Reptilia, Sauropterygia) from the Upper Cretaceous of Alberta. *Journal of Vertebrate Paleontology* 32 (3): 557–572.

Kuhn-Schnyder, E. 1959. Hand und Fuss von *Tanystropheus longobardicus* (Bassani). *Ecologae geologicae Helvetiae* 52 (2): 921–941.

Kuhn-Schnyder, E. 1974. Die Triasfauna der Tessiner Kalkalpen. *Neujahrsblatt der Naturforschenden Gesellschaft in Zürich* 118: 119 pp.

Kuhn, O. 1934. Sauropterygia. *In* Quenstedt, W. (ed.), *Fossilium Catalogus. I: Animalia. Part 69*. 127 pp. W. Junk, ’s-Gravenhage.

Kuhn, O. 1939*a*. Beiträge zur Keuperfauna von Halberstadt. *Paläontologische Zeitschrift* 21 (4): 258–286.

Kuhn, O. 1939*b*. Saurischia. *In* Quenstedt, W. (ed.), *Fossilium Catalogus. I: Animalia. Part 87*. 124 pp. W. Junk, ’s-Gravenhage.

Kuhn, O. 1941. Testudinata triadica. *In* Quenstedt, W. (ed.), *Fossilium Catalogus. I: Animalia. Pars 94*. 12 pp. Gustav Feller, Neubrandenburg.

Kuhn, O. 1961*a*. Reptilia (Supplementum 1(2)). *In* Westphal, F. (ed.), *Fossilium Catalogus. I: Animalia. Pars 99*. 163 pp. W. Junk, ’s-Gravenhage.

Kuhn, O. 1961*b*. *Die Familien der rezenten und fossilen Amphibien und Reptilien*. 79 pp. Verlagshaus Meisenbach KG, Bamberg.

Kuhn, O. 1963. Sauria (Supplementum I). *In* Westphal, F. (ed.), *Fossilium Catalogus. I: Animalia. Pars 104*. 87 pp. W. Junk, 's-Gravenhage.

Kuhn, O. 1965. Saurischia (Supplementum 1). *In* Westphal, F. (ed.), *Fossilium Catalogus. I: Animalia. Part 109*. 94 pp. W. Junk, 's-Gravenhage.

Kuhn, O. 1969. *Encyclopedia of Paleoherpetology Part 9. Proganosauria, Bolosauria, Placodontia, Araeoscelidia, Trilophosauria, Weigeltisauria, Millerosauria, Rhynchocephalia, Protorosauria*. 74 pp. Gustav Fischer Verlag, Stuttgart.

Kuhn, O. 1971. *Die Saurier der deutschen Trias*. 105 pp. Gebr. Geiselberger, Altötting.

Kuhn, O. 1975. Die deutschen Saurier, Nachtrag II. *Bericht der naturforschenden Gesellschaft Bamberg* 50: 5–23.

Kummer, B. 1975. Biomechanik fossiler und rezenter Wirbeltiere. *Natur und Museum* 105 (5): 156–167.

Laboury, A., Scheyer, T.M., Klein, N., Stubbs, T.L. and Fischer, V. 2023. High phenotypic plasticity at the dawn of the eosauropterygian radiation. *PeerJ* 11: e15776.

Laker, R.M. 2024. Vertebrate fossil permineralization in a sequence stratigraphic context: Capsules of early diagenesis from shallow-marine siliciclastics (Eocene, Egypt). *Palaios* 39: 243–263.

Lang, M. and Huene, F. von. 1952. *Die Saurier Thüringens nach Erhebungen ihres centralen Betreuers Hugo Rühle von Lilienstern*. 44 pp. Gustav Fischer, Jena.

Langenhan, A. 1903. *Versteinerungen der deutschen Trias (des Buntsandsteins, Muschelkalks und Keupers)*. 22 pp. Scholz'sche Kunsthandlung, Liegnitz.

Langenhan, A. 1911. *Versteinerungen der deutschen Trias (des Buntsandsteins, Muschelkalks und Keupers)*. 10 pp. A. Langenhan, Friedrichroda.

Lapparent, A.-F. De and Lavocat, R. 1955. Dinosauriens. *In*: Piveteau, J. (ed.), *Traite de Paleontologie. V. Amphibiens, Reptiles, Oiseaux*, 785–902. Masson et Cie, Paris.

Laurenti, J. N. 1768. *Specimen Medicum, exhibens synopsin Reptilium emendatum cum experimentis circa venena et antidota Reptilium Austriacorum*. 214 pp. J. T. de Trattern, Vienna.

Li, C. 2003. First record of protorosaurid peptile (Order Protorosauria) from the Middle

Triassic of China. *Acta Geologica Sinica* 77 (4): 419–423.

Li, C. 2007. A juvenile *Tanystropheus* sp. (Protorosauria, Tanystropheidae) from the Middle Triassic of Guinzhou, China. *Vertebrata PalAsiatica* 45 (1): 37–42.

Li, C., Fraser, N.C., Rieppel, O.C., Zhao, L.-J. and Wang, L.-T. 2017a. A new diapsid from the Middle Triassic of southern China. *Journal of Paleontology* 91 (6): 1306–1312.

Li, C., Rieppel, O. and Fraser, N.C. 2017b. Viviparity in a Triassic marine archosauromorph reptile. *Vertebrata PalAsiatica* 55 (3): 210–217.

Li, C., Zhao, L.-J., and Wang, L.-T. 2007. A new species of *Macrocnemus* (Reptilia: Protorosauria) from the Middle Triassic of southwestern China and its palaeogeographical implication. *Science in China, Series D: Earth Sciences* 50 (11): 1601–1605.

Liu, J., Organ, C.L., Benton, M.J., Brandley, M.C., and Aitchison, J.C. 2017. Live birth in an archosauromorph reptile. *Nature Communications* 8: 14445.

Löffler, T., Thies, D., Vespermann, J., and Zellmer, H. 2007. Fauna, Sedimentologie und Geochemie des Unteren Keupers (Erfurt Formation) von Schöningen. *Berichte der Naturhistorischen Gesellschaft Hannover* 149: 3–39.

Lu, H., Jiang, D.-Y., Motani, R., Ni, P.G., Sun, Z.-Y., Tintori, A., Xiao, S.Z., Zhou, M., Ji, C., and Fu, W.L. 2018. Middle Triassic Xingyi Fauna: Showing turnover of marine reptiles from coastal to oceanic environments. *Palaeoworld* 27 (1): 107–116.

Lucas, S.G. 1995. Biochronology of Triassic marine reptiles. *Albertiana* 15: 92–97.

Mackenzie, A.S., Brock, G.A., and McCurry, M.R. 2024. The impact of apicobasal ridges on dental load-bearing capacity in aquatic-feeding predatory amniotes. *Paleobiology* 50: 346–363.

Mallison, H. 2010. The digital *Plateosaurus* II: An assessment of the range of motion of the limbs and vertebral column and of previous reconstructions using a digital skeletal mount. *Acta Palaeontologica Polonica* 55 (3): 433–458.

Mancuso, A.C. and Previtera, E. 2022. Bone diagenesis of tetrapods from the Middle Triassic Tarjados Formation: implication for depositional environment and palaeoclimate. *Palaeobiodiversity and Palaeoenvironments* 105: 205–221.

Maniatis, A., Tavassoli, M. and Crosby, W.H. 1971. Factors affecting the conversion of yellow to red marrow. *Blood* 37 (5): 581–586.

Marks, L., Grabowski, J., and Stępień, U. 2022. *Geological Map of Poland 1:500 000*. Polish Geological Institute – National Research Institute, Warsaw.

Martin, E.G. and Palmer, C. 2014. Air space proportion in pterosaur limb bones using computed tomography and its implications for previous estimates of pneumaticity. *PloS ONE* 9 (5): e97159.

Martin, J., Martin-Rolland, V. and Frey, E. 1998. Not cranes or masts, but beams: the biomechanics of sauropod necks. *Oryctos* 1: 113–120.

McCurry, M.R., Evans, A.R., Fitzgerald, E.M.G., McHenry, C.R., Bevitt, J., and Pyenson, N.D. 2019. The repeated evolution of dental apicobasal ridges in aquatic-feeding mammals and reptiles. *Biological Journal of the Linnean Society* 127 (2): 245–259.

Melville, R. V. 1981. Opinion 1186. *Tanystropheus* H. von Meyer, [1852] (Reptilia) conserved. *Bulletin of Zoological Nomenclature* 38: 188–190.

Mestriner, G., Funston, G.F., Marsola, J.C.A., Nesbitt, S.J., Langer, M.C., Evans, D.C., and Leblanc, A.R.H. 2025. Rethinking thecodonty: the influence of two centuries of comparative dental anatomy on our understanding of tooth evolution. *Biology Letters* 21: 20250316.

Meyer, H. von. 1832. *Palaeologica zur Geschichte der Erde und ihrer Geschopfe*, 560pp. Siegmund Schmerber, Frankfurt am Main.

Meyer, H. von. 1839. *Pistosaurus* im Bayreuther Muschelkalk. *Neues Jahrbuch für Mineralogie, Geognosie, Geologie und Petrefaktenkunde*: 699–701.

Meyer, H. von. 1847-1855. *Zur Fauna der Vorwelt. Die Saurier des Muschelkalkes mit Rücksicht auf die Saurier aus buntem Sandstein und Keuper*. 167 pp. Heinrich Keller, Frankfurt am Main.

Meyer, H. von. 1849. Fische, Crustaceen, Echinodermen und andere Versteinerungen aus dem Muschelkalk Oberschlesiens. *Palaeontographica* 1 (6): 216–242.

Meyer, H. von. 1854. Briefwechsel. *Neues Jahrbuch für Mineralogie, Geologie und Paläontologie* 61: 47–58.

Meyer, H. von. 1860. *Reptilien aus dem Litographischen Schiefer des Jura in Deutschland und Frankreich*. 162 pp. Heinrich Keller, Frankfurt am Main.

Miedema, F., Spiekman, S.N.F., Fernandez, V., Reumer, J.W.F. and Scheyer, T.M. 2020. Cranial morphology of the tanystropheid *Macrocnemus bassanii* unveiled using synchrotron microtomography. *Scientific Reports* 10: 12412.

Mivart, S.G. 1874. On the Axial Skeleton of the Ostrich (*Struthio camelus*). *The Transactions of the Zoological Society of London* 8 (7): 385–451.

Moore, A.J., Barrett, P.M., Upchurch, P., Liao, C., Ye, Y., Hao, B. and Xu, X. 2023. Re-assessment of the Late Jurassic eusauropod *Mamenchisaurus sinocanadorum* Russell and Zheng, 1993, and the evolution of exceptionally long necks in mamenchisaurids. *Journal of Systematic Palaeontology* 21 (1): 2171818.

Motani, R. and Vermeij, G.J. 2021. Ecophysiological steps of marine adaptation in extant and extinct non-avian tetrapods. *Biological Reviews* 96 (5): 1769–1798.

Mujal, E., Sues, H.-D., Moreno, R., Schaeffer, J., Sobral, G., Chakravorti, S., Spiekman, S.N.F. and Schoch, R.R. 2025. Triassic terrestrial tetrapod faunas of the Central European Basin, their stratigraphical distribution, and their palaeoenvironments. *Earth-Science Reviews* 264: 105085.

Müller, J., Scheyer, T.M., Head, J.J., Barrett, P.M., Werneburg, I., Ericson, P.G.P., Pol, D. and Sánchez-Villagra, M.R. 2010. Homeotic effects, somitogenesis and the evolution of vertebral numbers in recent and fossil amniotes. *Proceedings of the National Academy of Sciences of the United States of America* 107 (5): 2118–2123.

Naish, D. and Witton, M.P. 2017. Neck biomechanics indicate that giant Transylvanian azhdarchid pterosaurs were short-necked arch predators. *PeerJ* 5: e2908.

Nawrocki, J. and Szulc, J. 2000. The Middle Triassic magnetostratigraphy from the Peri-Tethys basin in Poland. *Earth and Planetary Science Letters* 182 (1): 77–92.

Nesbitt, S.J. 2011. The early evolution of archosaurs: Relationships and the origin of major clades. *Bulletin of the American Museum of Natural History* 352: 1–292.

Nesbitt, S.J., Flynn, J.J., Pritchard, A.C., Parrish, J.M., Ranivoharimanana, L., and Wyss, A.R. 2015. Postcranial osteology of *Azendohsaurus madagascarensis* (?Middle to Upper Triassic, Isalo Group, Madagascar) and its systematic position among stem archosaur

reptiles. *Bulletin of the American Museum of Natural History* 398: 126 pp.

Nitsch, E. 2015. 13. Fazies und Ablagerungsräume des Lettenkeupers. *In*: Hagdorn, H., Schoch, R. and Schweigert, G. (eds.), *Der Lettenkeuper - Ein Fenster in Die Zeit Vor Den Dinosauriern*, 285–324. Staatliches Museum für Naturkunde Stuttgart, Stuttgart.

Nopcsa, F. 1901. Synopsis und Abstammung der Dinosaurier. *Földtani Közlöny* 31: 247–288.

Nopcsa, F. 1930. Notizen uber *Macrochemus Bassanii* nov. gen. et spec. *Centralblatt für Mineralogie, Geologie und Paläontologie, Abteilung B: Geologie und Paläontologie* 7: 252–255.

Nosotti, S. 2007. *Tanystropheus longobardicus* (Reptilia, Protorosauria): Re-interpretations of the anatomy based on new specimens from the Middle Triassic of Besano (Lombardy, Northern Italy). *Memorie della Società Italiana di Scienze Naturali e del Museo Civico di Storia Naturale di Milano* 35 (3): 88 pp.

Novas, F.E. 1996. Dinosaur monophyly. *Journal of Vertebrate Paleontology* 16 (4): 723–741.

O'Connor, P.M. 2004. Pulmonary pneumaticity in the postcranial skeleton of extant Aves: A case study examining Anseriformes. *Journal of Morphology* 261: 141–161.

O'Connor, P.M. 2006. Postcranial pneumaticity: an evaluation of soft-tissue influences on the postcranial skeleton and the reconstruction of pulmonary anatomy in archosaurs. *Journal of Morphology* 267: 1199–1226.

O'Connor, P.M. 2009. Evolution of archosaurian body plans: skeletal adaptations of an air-sac-based breathing apparatus in birds and other archosaurs. *Journal of Experimental Zoology* 311A: 629–646.

O'Connor, P.M. and Claessens, L.P.A.M. 2005. Basic avian pulmonary design and flow-through ventilation in non-avian theropod dinosaurs. *Nature* 436: 253–256.

Olsen, P.E. 1979. A new aquatic eosuchian from the Newark Supergroup (Late Triassic-Early Jurassic) of North Carolina and Virginia. *Postilla* 176: 1–14.

Olshevsky, G. 1991. A revision of the parainfraclass Archosauria Cope, 1869, excluding the advanced Crocodylia. *Mesozoic Meanderings* 2: 196 pp.

Oosterink, H.W., Berkelder, W., de Jong, C., Lankamp, J., and Winkelhorst, H. 2003. Sauriers uit de Onder-Muschelkalk van Winterswijk. *Staringia* 11: 144 pp.

Osborn, H.F. 1903. On the primary division of the Reptilia into two sub-classes, Synapsida and Diapsida. *Science* 17 (424): 275–276.

Ősi, A., Szabó, M., and Botfalvai, G. 2020. *Tanystropheus* and other archosauromorph reptile remains from the Middle and Late Triassic of Villány (Villány Hills , Hungary). *Geologica Carpathica* 72 (3): 264–273.

Ouyang, H. and Ye, Y. 2002. *The first mamenchisaurian skeleton with complete skull:* Mamenchisaurus youngi. 111 pp. Sichuan Science and Technology Press, Chengdu.

Owen, R. 1860. *Palaeontology, or a systematic summary of extinct animals and their geological relations*. 420 pp. Adam and Charles Black, Edinburgh.

Padian, K., Cunningham, J.R., Langston Jr, W. and Conway, J. 2021. Functional morphology of *Quetzalcoatlus* Lawson 1975 (Pterodactyloidea: Azhdarchoidea). *Journal of Vertebrate Paleontology* 41 (sup1): 218–251.

Parrington, M.A. 1935. On *Prolacerta broomi*, gen. et sp. n., and the origin of lizards. *Journal of Natural History* 16 (92): 197–205.

Pawlak, W., Rozwalak, P., and Sulej, T. 2022. Triassic fish faunas from Miedary (Upper Silesia, Poland) and their implications for understanding paleosalinity. *Palaeogeography, Palaeoclimatology, Palaeoecology* 590: 110860.

Pesquero, M.D., Alcalá, L., Bell, L.S. and Fernández-Jalvo, Y. 2015. Bacterial origin of iron-rich microspheres in Miocene mammalian fossils. *Palaeogeography, Palaeoclimatology, Palaeoecology* 420: 27–34.

Peyer, B. 1930. *Tanystropbeus longobardicus* Bass. sp. *Centralblatt für Mineralogie, Geologie und Paläontologie, Abteilung B* 8: 336–337.

Peyer, B. 1931. Die Triasfauna der Tessiner Kalkalpen II. *Tanystropheus longobardicus* Bass. sp. *Abhandlungen der Schweizerischen Paläontologischen Gesellschaft* 50: 9–110.

Peyer, B. 1937. Die Lösung eines paläontologischen Rätsels. *In*: *Bericht über den Verlauf der Feier der 250. Wiederkehr des Tages der Erhebung der am 1. Jan. 1652 gegründeten usw.*, 83–93. Kaiserlich Leopoldinisch-Carolinisch Deutsche Akademie der Naturforscher, Halle (Salle).

Peyer, B. 1944. Die Reptilien von Monte San Giorgio. *Neujahrsblatt der Naturforschenden*

Gesellschaft in Zürich 146: 95 pp.

Peyer, B. 1955. Demonstration von Trias-Vertebraten aus Palästina. *Ecologae geologicae Helvetiae* 48 (2).

Peyer, B. and Kuhn-Schnyder, E. 1955. Squamates du Trias. *In*: Piveteau, J. (ed.), *Traité de Paléontologie, Vol. 5*, 578–605. Masson, Paris.

Pfretzschner, H.-U. 2000. Microcracks and fossilization of Haversian bone. *Neues Jahrbuch für Geologie und Paläontologie - Abhandlungen* 216 (3): 413–432.

Pfretzschner, H.-U. and Tütken, T. 2011. Rolling bones – Taphonomy of Jurassic dinosaur bones inferred from diagenetic microcracks and mineral infillings. *Palaeogeography, Palaeoclimatology, Palaeoecology* 310 (1–2): 117–123.

Pi, L., Ouyang, H. and Ye, Y. 1996. A new species of sauropod from Zigong, Sichuan, *Mamenchisaurus youngi*. *Proceedings of the 30th International Geological Congress*: 87–91.

Piechowski, R. and Tałanda, M. 2020. The locomotor musculature and posture of the early dinosauriform *Silesaurus opolensis* provides a new look into the evolution of Dinosauromorpha. *Journal of Anatomy* 236: 1044–1100.

Pierce, S.E. and Benton, M.J. 2006. *Pelagosaurus typus* Bronn, 1841 (Mesoeucrocodylia: Thalattosuchia) from the Upper Lias (Toarcian, Lower Jurassic) of Somerset, England. *Journal of Vertebrate Paleontology* 26 (3): 621–635.

Plieninger, T. 1846*a*. Über ein neues Sauriergenus und die Einreihung der Saurier mit flachen, schneidenden Zähnen in eine Familie. *Jahreshefte des Vereins für vaterländische Naturkunde in Württemberg* 1 (2): 148–154.

Plieninger, T. 1846*b*. Nachträgliche Bemerkungen zu dem Vortrage (S. 148 dieses Heftes) über ein neues Sauriergenus und die Einreihung der Saurier mit flachen, schneidenden Zähnen in Eine Familie. *Jahreshefte des Vereins für vaterländische Naturkunde in Württemberg* 2 (1): 247–255.

Preuschoft, H. and Klein, N. 2013. Torsion and bending in the neck and tail of sauropod dinosaurs and the function of cervical ribs: insights from functional morphology and biomechanics. *PloS ONE* 8 (10): e78574.

Pritchard, A.C., Turner, A.H., Nesbitt, S.J., Irmis, R.B., and Smith, N.D. 2015. Late Triassic

tanystropheids (Reptilia, Archosauromorpha) from northern New Mexico (Petrified Forest Member, Chinle Formation) and the biogeography, functional morphology, and evolution of Tanystropheidae. *Journal of Vertebrate Paleontology* 35 (2).

Quenstedt, W. 1963. Clavis bibliographica. *In* Westphal, F. (ed.), *Fossilium Catalogus. I: Animalia. Part 102*. 118 pp. W. Junk, 's-Gravenhage.

Rehorek, S.J., Legenzoff, E.J., Carmody, K., Smith, T.D. and Sedlmayr, J.C. 2005. Alligator tears: a reevaluation of the lacrimal apparatus of the crocodilians. *Journal of Morphology* 266 (3): 298–308.

Renesto, S. 1994. A new prolacertiform reptile from Late Triassic of northern Italy. *Rivista Italiana di Paleontologia e Stratigrafia* 100 (2): 285–306.

Renesto, S. 2005. A new specimen of *Tanystropheus* (Reptilia Protorosauria) from the Middle Triassic of Switzerland and the ecology of the genus. *Rivista Italiana di Paleontologia e Stratigrafia* 111 (3): 377–394.

Renesto, S. and Saller, F. 2018. Evidences for a semi aquatic life style in the Triassic diapsid reptile *Tanystropheus*. *Rivista Italiana di Paleontologia e Stratigrafia* 124 (1): 23–34.

Rieppel, O. 1976. On the presence and function of post-cloacal bones in the Lacertilia. *Monitore Zoologico Italiano - Italian Journal of Zoology* 10: 7–13.

Rieppel, O. 1989. The hind limb of *Macrocnemus bassanii* (Nopcsa) (Reptilia, Diapsida): Development and functional anatomy. *Journal of Vertebrate Paleontology* 9 (4): 373–387.

Rieppel, O. 2000. *Encyclopedia of Paleoherpetology. Part 12A. Sauropterygia I. Placodontia, Pachypleurosauria, Nothosauroidea, Pistosauroidea*. 134 pp. Dr. Friedrich Pfeil, München.

Rieppel, O. 2001. A new species of *Tanystropheus* (Reptilia: Protorosauria) from the Middle Triassic of Makhtesh Ramon, Israel. *Neues Jahrbuch für Geologie und Paläontologie - Abhandlungen* 221 (2): 271–287.

Rieppel, O. 2019. *Mesozoic Sea Dragons*. 340 pp. Indiana University Press.

Rieppel, O.C. and Hagdorn, H. 1997. Paleobiogeography of Middle Triassic Sauropterygia in Central and Western Europe. *Ancient Marine Reptiles* 5: 121–144.

Rieppel, O. and Wild, R. 1996. A revision of the genus *Nothosaurus* (Reptilia: Sauropterygia) from the Germanic Triassic, with comments on the status of *Conchiosaurus clavatus*. *Fieldiana - Geology* 34: 1–82.

Rieppel, O., Mazin, J.-M., and Tchernov, E. 1999. Sauropterygia from the Middle Triassic of Makhtesh Ramon, Negev, Israel. *Fieldiana - Geology* 40: 85 pp.

Rieppel, O.C., Fraser, N.C. and Nosotti, S. 2003. The monophyly of Protorosauria (Reptilia, Archosauromorpha): a preliminary analysis. *Atti della Società Italiana di Scienze Naturali e del Museo Civico di Storia Naturale in Milano* 144 (2): 359–382.

Rieppel, O., Jiang, D.-Y., Fraser, N.C., Hao, W.-C., Motani, R., Sun, Y.-L., and Sun, Z.-Y. 2010. *Tanystropheus* cf. *T. longobardicus* from the early Late Triassic of Guizhou Province, Southwestern China. *Journal of Vertebrate Paleontology* 30 (4): 1082–1089.

Roemer, F. 1870. *Geologie von Oberschlesien. Eine Erläuterung zu der im Auftrage des Königl. Preuss. Handels-Ministeriums von dem Verfasser bearbeiteten geologischen Karte von Oberschlesien in 12 Sektionen*. 587 pp. R. Nischowsky, Breslau.

Röhl, H.-J., Schmid-Röhl, A., Furrer, H., Frimmel, A., Oschmann, W., and Schwark, L. 2001. Microfacies, geochemistry and palaeoecology of the Middle Triassic Grenzbitumenzone from the Monte San Giorgio (Canton Ticino, Switzerland). *Geologia Insubrica* 6 (1): 1–13.

Romer, A.S. 1956. *Osteology of the Reptiles*. 772 pp. The University of Chicago Press, Chicago and London.

Russell, A.P. 1977. Comments concerning postcloacal bones in geckos (Reptilia: Gekkonidae). *Canadian Journal of Zoology* 55: 1201–1205.

Russell, A.P., Vickaryous, M.K., and Bauer, A.M. 2016. The phylogenetic distribution, anatomy and histology of the post-cloacal bones and adnexa of geckos. *Journal of Morphology* 277: 264–277.

Rytel, A., Böhmer, C., Spiekman, S.N.F., and Tałanda, M. 2024*a*. Extreme neck elongation evolved despite strong developmental constraints in bizarre Triassic reptiles—implications for neck modularity in archosaurs. *Royal Society Open Science* 11 (5): 240233.

Rytel, A., Surmik, D., Szczygielski, T., Spiekman, S.N.F., Kamp, T. Van De, Zuber, M., and

Scheyer, T.M. 2024*b*. Unique internal anatomy of vertebrae as a key factor for neck elongation in Triassic archosauromorphs. *Zoological Journal of the Linnean Society* 202 (3): zlae126.

Sachs, S., Lindgren, J. and Kear, B.P. 2018. Reassessment of the *Styxosaurus snowii* (Williston, 1890) holotype specimen and its implications for elasmosaurid plesiosaurian interrelationships. *Alcheringa* 42 (4): 560–574.

Sander, P.M. and Wintrich, T. 2021. Sauropterygia: Histology of Plesiosauria. *In*: Buffrénil, V. de, de Ricqlès, A., Zylberberg, L. and Padian, K. (eds.), *Vertebrate Skeletal Histology and Paleohistology*, 444–457. CRC Press, Boca Raton and London.

Schepelmann, K. 1990. Erythropoietic bone marrow in the Pigeon: Development of its distribution and volume during growth and pneumatization of bones. *Journal of Morphology* 203: 21–34.

Scheyer, T.M., Wang, W., Li, C., Miedema, F., and Spiekman, S.N.F. 2020. Osteological re-description of *Macrocnemus fuyuanensis* (Archosauromorpha, Tanystropheidae) from the Middle Triassic of China. *Vertebrata PalAsiatica* 58 (3): 169–187.

Schmidt, M. 1928. *Die Lebewelt unserer Trias*. 445 pp. Hohenlohe'sche Buchhandlung Ferdinand Rau, Öhringen.

Schmidt, M. 1938. *Die Lebewelt unserer Trias (Nachtrag)*. 144 pp. Hohenlohe’sche Buchhandlung Ferdinand Rau, Öhringen.

Schoch, R.R. 1999. Comparative osteology of *Mastodonsaurus giganteus* (Jaeger, 1828) from the Middle Triassic (Lettenkeuper: Longobardian) of Germany (Baden-Württemberg, Bayern, Thüringen). *Stuttgarter Beiträge zur Naturkunde. Serie B* 278: 175 pp.

Schoch, R.R. 2011. New archosauriform remains from the German Lower Keuper. *Neues Jahrbuch für Geologie und Paläontologie - Abhandlungen* 260 (1): 87–100.

Schoch, R.R. 2015. 10. Reptilien des Lettenkeupers. *In*: Hagdorn, H., Schoch, R., and Schweigert, G. (eds.), *Der Lettenkeuper - Ein Fenster in Die Zeit vor den Dinosauriern*, 231–264. Staatliches Museum für Naturkunde Stuttgart, Stuttgart.

Schoch, R.R. and Seegis, D. 2016. A Middle Triassic palaeontological gold mine: the vertebrate deposits of Vellberg (Germany). *Palaeogeography, Palaeoclimatology, Palaeoecology* 459: 249–267.

Schoch, R.R., Gastou, S., Steyer, J.-S., Mujal, E., Moreno, R. and Witzmann, F. 2025. Morphology and ontogeny of the plagiosaurid temnospondyl *Plagiosternum granulosum* from the Middle Triassic of Germany. *PalZ*.

Schoch, R.R., Seegis, D. and Mujal, E. 2022. The Middle Triassic vertebrate deposits of Kupferzell (Germany): Palaeoenvironmental evolution of complex ecosystems. *Palaeogeography, Palaeoclimatology, Palaeoecology* 603: 111181.

Schoch, R.R., Sues, H.-D., Sobral, G., Kurz, C., Gottmann-Quesada, A. and Spiekman, S.N.F. 2025. New data on the skull of *Protorosaurus speneri* (Reptilia: Archosauromorpha) and their phylogenetic significance. *Journal of Systematic Palaeontology* 23 (1): 1–20.

Schoch, R.R., Ullmann, F., Rozynek, B., Ziegler, R., Seegis, D., and Sues, H.-D. 2018. Tetrapod diversity and palaeoecology in the German Middle Triassic (Lower Keuper) documented by tooth morphotypes. *Palaeobiodiversity and Palaeoenvironments* 98 (4): 615–638.

Schubul, A.N., Marsh, A.D., and Kligman, B.T. 2025. A diverse assemblage of tanystropheid archosauromorphs from the continental interior of Late Triassic Pangea includes a new taxon (*Akidostropheus oligos* gen. et sp. nov.). *Palaeodiversity* 18 (1): 99–125.

Schwermann, A., Pauser, M. and Spiekman, S.N.F. 2025. *Tanystropheus* – Erstnachweis eines Giraffenhalssauriers für NRW. *Archäologie in Westfalen-Lippe (2024)* 16: 35–37.

Scotese, C.R. 2014. Atlas of Permo-Triassic Paleogeographic Maps (Mollweide Projection). *In*: *Maps 43 - 52, Volumes 3 & 4 of the PALEOMAP Atlas for ArcGIS, PALEOMAP Project*, Evanston.

Sengupta, S., Ezcurra, M.D., and Bandyopadhyay, S. 2017. A new horned and long-necked herbivorous stem-archosaur from the Middle Triassic of India. *Scientific Reports* 7: 8366.

Sengupta, S., Ezcurra, M.D., and Bandyopadhyay, S. 2024. The redescription of *Malerisaurus robinsonae* (Archosauromorpha: Allokotosauria) from the Upper Triassic lower Maleri Formation, Pranhita-Godavari. *Anatomical Record* 307 (4): 1315–1365.

Sennikov, A.G. 2005. A new specialized prolacertilian (Reptilia: Archosauromorpha) from the Lower Triassic of the Orenburg Region. *Paleontological Journal* 39 (2): 199–209.

Sennikov, A.G. 2011. New tanystropheids (Reptilia: Archosauromorpha) from the Triassic of

Europe. *Paleontological Journal* 45 (1): 90–104.

Sennikov, A.G. 2023. Some morphofunctional features of the tail of early archosaurs related to swimming adaptations. *Paleontological Journal* 57 (4): 432–451.

Shapiro, R.S. and Spangler, E. 2009. Bacterial fossil record in whale-falls: Petrographic evidence of microbial sulfate reduction. *Palaeogeography, Palaeoclimatology, Palaeoecology* 274 (3–4): 196–203.

Simões, T.R., Caldwell, M.W., Tałanda, M., Bernardi, M., Palci, A., Vernygora, O., Bernardini, F., Mancini, L. and Nydam, R.L. 2018. The origin of squamates revealed by a Middle Triassic lizard from the Italian Alps. *Nature* 557: 706–709.

Skawiński, T., Tałanda, M., and Sachs, S. 2015. *Megacnemus* – a forgotten reptile, presumably from the Triassic of Poland. *Poster. 13th Annual Meeting of the European Association of Vertebrate Palaeontologists Opole, Poland, 8-12 July 2015 – Abstracts*.

Skawiński, T., Ziegler, M., Czepiński, Ł., Szermański, M., Tałanda, M., Surmik, D., and Niedźwiedzki, G. 2017. A re-evaluation of the historical 'dinosaur' remains from the Middle-Upper Triassic of Poland. *Historical Biology* 29 (4): 442–472.

Sobral, G. 2023. The holotype of the basal archosauromorph *Prolacerta broomi* revisited. *Acta Palaeontologica Polonica* 68 (3): 393–413.

Sookias, R.B., Dilkes, D., Sobral, G., Smith, R.M.H., Wolvaardt, F.P., Arcucci, A.B., Bhullar, B.-A.S. and Werneburg, I. 2020. The craniomandibular anatomy of the early archosauriform *Euparkeria* capensis and the dawn of the archosaur skull. *Royal Society Open Science* 7 (7): 200116.

de Souza, R.B.B. and Klein, W. 2022. Modeling of the respiratory system of the long - necked Triassic reptile *Tanystropheus* (Archosauromorpha). *The Science of Nature* 109: 55.

Spiekman, S.N.F. and Mujal, E. 2023. Decapitation in the long-necked Triassic marine reptile *Tanystropheus*. *Current Biology* 33: R1–R2.

Spiekman, S.N.F. and Scheyer, T.M. 2019. A taxonomic revision of the genus *Tanystropheus* (Archosauromorpha, Tanystropheidae). *Palaeontologia Electronica* 22.3.80: 1–46.

Spiekman, S.N.F., Bleeker, R., Dorst, M., Haan, R. de, Winkelhorst, H., and Voeten, D.F.A.E. 2019. Tanystropheids from the Winterswijk quarry - rare but recurring elements. *Staringia* 16 (5/6): 208–215.

Spiekman, S.N.F., Butler, R.J. and Maidment, S.C.R. 2024. The postcranial anatomy and osteohistology of *Terrestrisuchus gracilis* (Archosauria, Crocodylomorpha) from the Late Triassic of Wales. *Papers in Palaeontology* 10 (4): e1577.

Spiekman, S.N.F., Ezcurra, M.D., Rytel, A., Wang, W., Mujal, E., Buchwitz, M., and Schoch, R.R. 2024*b*. A redescription of *Trachelosaurus fischeri* from the Buntsandstein (Middle Triassic) of Bernburg, Germany: the first European *Dinocephalosaurus*-like marine reptile and its systematic implications for long-necked early archosauromorphs. *Swiss Journal of Palaeontology* 143: 10.

Spiekman, S.N.F., Fraser, N.C., and Scheyer, T.M. 2021. A new phylogenetic hypothesis of Tanystropheidae (Diapsida, Archosauromorpha) and other "protorosaurs", and its implications for the early evolution of stem archosaurs. *PeerJ* 9: e11143.

Spiekman, S.N.F., Neenan, J.M., Fraser, N.C., Fernandez, V., Rieppel, O., Nosotti, S., and Scheyer, T.M. 2020*a*. Aquatic habits and niche partitioning in the extraordinarily long-necked Triassic reptile. *Current Biology* 30: 3889–3895.

Spiekman, S.N.F., Neenan, J.M., Fraser, N.C., Fernandez, V., Rieppel, O., Nosotti, S., and Scheyer, T.M. 2020*b*. The cranial morphology of *Tanystropheus hydroides* (Tanystropheidae, Archosauromorpha) as revealed by synchrotron microtomography. *PeerJ* 8: e10299.

Spiekman, S.N.F., Wang, W., Zhao, L.-J., Rieppel, O., Fraser, N.C., and Li, C. 2024*a*. *Dinocephalosaurus orientalis* Li, 2003: a remarkable marine archosauromorph from the Middle Triassic of southwestern China. *Earth and Environmental Science Transactions of the Royal Society of Edinburgh* 114 (3–4): 218–250.

Spielmann, J.A., Lucas, S.G., Heckert, A.B., Rinehart, L.F., and Richards, H.R.I. 2009. Redescription of *Spinosuchus caseanus* (Archosauromorpha: Trilophosauridae) from the Upper Triassic of North America. *Palaeodiversity* 2: 283–313.

Stockar, R., Baumgartner, P.O., and Condon, D. 2012. Integrated Ladinian bio-chronostratigraphy and geochrononology of Monte San Giorgio (Southern Alps, Switzerland). *Swiss Journal of Geosciences* 105 (1): 85–108.

Sues, H.-D. 1987. Postcranial skeleton of *Pistosaurus* and interrelationships of the Sauropterygia (Diapsida). *Zoological Journal of the Linnean Society* 90: 109–131.

Sues, H.-D. 2017. *Arctosaurus osborni*, a Late Triassic archosauromorph reptile from the

Canadian Arctic Archipelago. *Canadian Journal of Earth Sciences* 54: 129–133.

Sues, H.-D. 2024. Bernhard Peyer and his discoveries of Triassic vertebrates in Switzerland. *Swiss Journal of Palaeontology* 143: 8.

Sues, H.-D. and Olsen, P.E. 2015. Stratigraphic and temporal context and faunal diversity of Permian-Jurassic continental tetrapod assemblages from the Fundy rift basin, eastern Canada. *Atlantic Geology* 51 (2015): 139–205.

Sues, H.-D. and Schoch, R.R. 2023. The oldest known rhynchocephalian reptile from the Middle Triassic (Ladinian) of Germany and its phylogenetic position among Lepidosauromorpha. *Anatomical Record* 307 (4): 776–790.

Sues, H.-D. and Schoch, R.R. 2025. Synopsis of the Triassic reptiles from Germany. *Fossil Record* 28 (2): 411–483.

Sues, H.-D., Olsen, P.E., Fedak, T.J., and Schoch, R.R. 2022. Diverse assemblage of Middle Triassic continental tetrapods from the Newark Supergroup of Nova Scotia (Canada). *Journal of Vertebrate Paleontology* 41 (4): e2023168.

Sulej, T., Niedźwiedzki, G., Niedźwiedzki, R., Surmik, D., and Stachacz, M. 2011. Nowy zespół kręgowców z marginalnomorskich i lądowych osadów kajpru (ladyn, środkowy trias) z Miedar na Śląsku. *Przegląd Geologiczny* 59 (5): 426–430.

Surmik, D., Boczarowski, A., Balin, K., Dulski, M., Szade, J., Kremer, B. and Pawlicki, R. 2016. Spectroscopic studies on organic matter from Triassic reptile bones, Upper Silesia, Poland. *PLoS ONE* 11 (3): e0151143.

Szczygielski, T., Dróżdż, D., Chanthasit, P., Manitkoon, S., and Ditbanjong, P. 2025. The Triassic turtle of Thailand - revision of *'Proganochelys' ruchae*. *PLoS ONE* 20 (3): e0316338.

Taylor, M.A. 1989. Neck and neck. *Nature* 341: 688–689.

Taylor, M.P. and Wedel, M.J. 2013. The effect of intervertebral cartilage on neutral posture and range of motion in the necks of sauropod dinosaurs. *PLoS ONE* 8 (10): e78214.

Taylor, M.P. 2014. Quantifying the effect of intervertebral cartilage on neutral posture in the necks of sauropod dinosaurs. *PeerJ* 2: e712.

Taylor, M.P. 2022. Almost all known sauropod necks are incomplete and distorted. *PeerJ* 10:

e12810.

Taylor, M.P. and Wedel, M.J. 2013a. The effect of intervertebral cartilage on neutral posture and range of motion in the necks of sauropod dinosaurs. *PLoS ONE* 8 (10): e78214.

Taylor, M.P. and Wedel, M.J. 2013b. Why sauropods had long necks; and why giraffes have short necks. *PeerJ* 1: e36.

Toyama, K.S., Tinius, A. and Mahler, D.L. 2024. Evidence supporting an evolutionary trade-off between material properties and architectural design in *Anolis* lizard long bones. *Evolution* 782 (2): 315–328.

Troelsen, P. V., Wilkinson, D.M., Seddighi, M., Allanson, D.R. and Falkingham, P.L. 2019. Functional morphology and hydrodynamics of plesiosaur necks: Does size matter? *Journal of Vertebrate Paleontology* 39 (2): e1594850.

Tschanz, K. 1986. Funktionelle Anatomie der Halswirbelsäule von *Tanystropheus longobardicus* (Bassani) aus der Trias (Anis/Ladin) des Monte San Giorgio (Tessin) auf der Basis vergleichend morphologischer Untersuchungen an der Halsmuskulatur rezenter Echsen. PhD thesis. 109 pp. Univeristy of Zurich, Zurich.

Tschanz, K. 1988. Allometry, and heterochrony in the growth of the neck of Triassic prolacertiform reptiles. *Palaeontology* 31 (4): 997–1011.

Vickers-Rich, P., Rich, T.H., Rieppel, O., Thulborn, R.A., and McClure, H.A. 1999. A Middle Triassic Vertebrate Fauna from the Jilh Formation, Saudi Arabia. *Neues Jahrbuch für Geologie und Paläontologie - Abhandlungen* 213 (2): 201–232.

Vidal, D., Moncho, P., Sanz, J.L. and Ortega, F. 2020. Ontogenetic similarities between giraffe and sauropod neck osteological mobility. *PLOS One* 15 (1): e0227537.

Vidal, L.S., Bergqvist, L.P., Candeiro, C.R.A., Bandeira, K.L.N., Tavares, S., Brusatte, S.L. and Pereira, P.V.L.G.C. 2024. The axial biomechanics of *Trigonosaurus pricei* (Neosauropoda: Titanosauria) and the importance of the cervical–dorsal region to sauropod high-browser feeding strategy. *Zoological Journal of the Linnean Society* 201 (3): 1–33.

Vietti, L.A., Bailey, J.V., Fox, D.L. and Rogers, R.R. 2015. Rapid formation of framboidal sulfides on bone surfaces from a simulated marine carcass fall. *Palaios* 30: 327–334.

Wang, W., Lei, H. and Li, C. 2023a. A small-sized dinocephalosaurid archosauromorph from

the Middle Triassic of Yunnan, southwestern China. *Vertebrata Palasiatica* 62 (1): 13–32.

Wang, W., Spiekman, S.N.F., Zhao, L.-J., Rieppel, O.C., Scheyer, T.M., Fraser, N.C. and Li, C. 2023b. A new long-necked archosauromorph from the Guanling Formation (Anisian, Middle Triassic) of southwestern China and its implications for neck evolution in tanystropheids. *The Anatomical Record* 308 (10): 2548–2562.

Wedel, M.J. 2003a. The evolution of vertebral pneumaticity in sauropod dinosaurs. *Journal of Vertebrate Paleontology* 23 (2): 344–357.

Wedel, M.J. 2003b. Vertebral pneumaticity, air sacs, and the physiology of sauropod dinosaurs. *Paleobiology* 29 (2): 243–255.

Wedel, M.J. 2005. Postcranial skeletal pneumaticity in sauropods and its implications for mass estimates. *In*: Wilson, J.A. and Curry-Rogers, K. (eds.), *The Sauropods: Evolution and Paleobiology*, 201–228. University of California Press, Berkeley.

Wedel, M.J. 2007. What pneumaticity tells us about 'prosauropods', and vice versa. *Special Papers in Palaeontology* 77: 207–222.

Wedel, M.J., Cifelli, R.L. and Sanders, R.K. 2000. Osteology, paleobiology, and relationships of the sauropod dinosaur *Sauroposeidon*. *Acta Palaeontologica Polonica* 45 (4): 343–388.

Wedel, M.J., Fiorillo, A., Maxwell, D. and Tykoski, R. 2014. Pneumatic diverticula associated with the spinal cord in birds, sauropod dinosaurs, and other ornithodiran archosaurs. *62nd Symposium on Vertebrate Palaeontology and Comparative Anatomy, Meeting Proceedings*: 60.

Weigelt, J. 1989. *Recent vertebrate carcasses and their paleobiological implications*. *In* Schaefer, J. (ed.). 204 pp. University of Chicago Press, Chicago and London.

Werneburg, I., Hinz, J.K., Gumpenberger, M., Volpato, V., Natchev, N. and Joyce, W.G. 2014. Modeling neck mobility in fossil turtles. *Journal of Experimental Zoology* 324B: 230–243.

Wild, R. 1973. Die Triasfauna der Tessiner Kalkalpen XXII. *Tanystropheus longobardicus* (Bassani) (Neue Ergebnisse). *Schweizerische Paläontologische Abhandlungen* 95: 158 pp.

Wild, R. 1975*a*. *Tanystropheus* H. v. Meyer, 1855 (Reptilia): Request for conservation under the plenary powers. *Bulletin of Zoological Nomenclature* 32 (2): 124–126.

Wild, R. 1975*b*. Der Giraffenhals-Saurier. *Die Naturwissenschaften* 62 (4): 149–153.

Wild, R. 1976*a*. *Tanystropheus* H. v. Meyer, [1852] (Reptilia): Revised request for conservation under the plenary powers. *Bulletin of Zoological Nomenclature* 33 (2): 124–126.

Wild, R. 1976*b*. Neues über den Giraffenhalssaurier *Tanystropheus*. *Natur und Museum* 106 (1): 13–22.

Wild, R. 1977. Der Saurier mit dem Giraffenhals. *Umschau* 77 (20): 674–675.

Wild, R. 1980*a*. Neue Funde von *Tanystropheus* (Reptilia, Squamata). *Schweizerische Paläontologische Abhandlungen* 102: 1–43.

Wild, R. 1980*b*. *Tanystropheus* (Reptilia: Squamata) and its importance for stratigraphy. *Mémoires de la Société Géologique de France, Nouvelle Série* 139: 201–206.

Wild, R. 1987. An example of biological reasons for extinction: *Tanystropheus* (Reptilia: Squamata). *Mémoires de la Société Géologique de France, Nouvelle Série* 150: 37–44.

Wild, R. 1989. Erdwissenschaffliche forschung in Bayreuth - ein historischer überblick. *Berichte der Naturwissenschaftlichen Gesellschaft Bayreuth* 20: 31–53.

Wild, R. and Oosterink, H.W. 1984. *Tanystropheus* (Reptilia: Squamata) aus dem Unteren Muschelkalk von Winterswijk, Holland. *Grondboor en hamer* 5 (3): 142–148.

Williams, C.J., Pani, M., Bucchi, A., Smith, R., Kao, A., Keeble, W., Ibrahim, N. and Martill, D.M. 2021. Helically arranged cross struts in azhdarchid pterosaur cervical vertebrae and their biomechanical implications. *IScience* 24 (4): 102338.

Wintrich, T., Jonas, R., Wilke, H.J., Schmitz, L. and Sander, P.M. 2019. Neck mobility in the Jurassic plesiosaur *Cryptoclidus eurymerus*: Finite element analysis as a new approach to understanding the cervical skeleton in fossil vertebrates. *PeerJ* 7: e7658.

Wintrich, T., Scaal, M. and Sander, P.M. 2017. Foramina in plesiosaur cervical centra indicate a specialized vascular system. *Fossil Record* 20: 279–290.

Witmer, L.M. 1997. The evolution of the antorbital cavity of archosaurs: A study in soft-tissue reconstruction in the fossil record with an analysis of the function of Pneumaticity.

Journal of Vertebrate Paleontology 17 (S1): 1–76.

Yates, A.M., Wedel, M.J. and Bonnan, M.F. 2012. The early evolution of postcranial skeletal pneumaticity in sauropodomorph dinosaurs. *Acta Palaeontologica Polonica* 57 (1): 85–100.

Young, M.T., Wilberg, E.W., Johnson, M.M., Herrera, Y., Andrade, M.B. de, Brignon, A., Sachs, S., Abel, P., Foffa, D., Fernández, M.S., Vignaud, P., Cowgill, T., and Brusatte, S.L. 2024. The history, systematics, and nomenclature of Thalattosuchia (Archosauria: Crocodylomorpha). *Zoological Journal of the Linnean Society* 200: 547–617.

Zittel, K.A. von. 1887-1890. *Handbuch der Palaeontologie. I. Abteilung Palaeozoologie. III Band. Vertebrata*. 900 pp. Oldenburg R., Munich and Leipzig.

Zittel, K.A. von. 1932. *Text-book of Paleontology. Vol II*. *In* Eastman, C. and Woodward, A.S. (eds.). 464 pp. Macmillan and Co., London.

Appendix I

Specimens referred to *Tanystropheus conspicuus*.

Specimen number	Taxon	Contents	Locality	Stratigraphy	References	Notes
BGR-B-ORIG-000185673	*T. conspicuus*	Cervical vertebra	Hochstedt near Erfurt, Germany	Lettenkeuper, Lettenkohle	von Huene 1931 (fig. 6), Shmidt 1938 (fig. 1188b), Spiekman and Scheyer 2019 (supp. tab. 1)	
BGR-B-STGR-000073870	*T. conspicuus*	Tooth	Gehädrich near Weimar, Germany	Upper Muschelkalk	This study	
FG 484/2006	*T. conspicuus*	Tooth	Bayreuth, Germany	Upper Muschelkalk	This study	
GG 23/159	*T. conspicuus*	Tooth	Bibersfeld, Germany	Lowermost Lettenkeuper, Grenzbonebed	This study	
GPIH 253	*T. conspicuus?*	Humerus	Tarnowskie Góry area?, Poland?	Upper Muschelkalk?, "Rybnaer Kalk"?	von Huene 1954, Kuhn 1969 (fig. 24, 3), Kuhn 1971 (plate 21, fig. 1), Skawiński et al. 2015	*Megacnemus grandis* holotype
GPIT-PV-111898	*T. conspicuus*	Cervical vertebra	Öhlmühle near Crailsheim, Germany	Lowermost Lettenkeuper, Grenzbonebed?	Spiekman and Scheyer 2019 (supp. tab. 1)	Previous number GPIT/RE/00652
GPIT-PV-111928 and GPIT-PV-111929	*T. conspicuus*	Cervical vertebra	Öhlmühle near Crailsheim, Germany	Lowermost Lettenkeuper, Grenzbonebed?	Spiekman and Scheyer 2019 (supp. tab. 1)	Previous number GPIT/RE/00652, parts of the same vertebra under different numbers
GPIT-PV-111930 and GPIT-PV-111931	*T. conspicuus*	Cervical vertebra (11th)	Bayreuth, Germany	Upper Muschelkalk		Cast of U-MO BT 738
GPIT-PV-111932	*T. conspicuus*	Cervical vertebra	Bayreuth, Germany	Upper Muschelkalk		Cast of U-MO BT 740
GPIT-PV-111933	*T. conspicuus*	Cervical vertebra	Bayreuth, Germany	Upper Muschelkalk		Cast of U-MO BT 733 and U-MO BT 734 glued together
GPIT-PV-111934	*T. conspicuus*	Cervical vertebra	Bayreuth, Germany	Upper Muschelkalk		Cast of U-MO BT 736
GPIT-PV-42013	*T. conspicuus*	Cervical vertebrae	Bayreuth, Germany	Upper Muschelkalk		Casts of U-MO BT 733, U-MO BT 736, U-MO BT 740. Previous number GPIT/RE/03189
GPIT-PV-44254	*T. conspicuus*	Cervical vertebra (10th)	Bayreuth, Germany	Upper Muschelkalk		Cast of U-MO BT 737
GPIT-PV-44255	*T. conspicuus*	Cervical vertebra (9th?)	Bayreuth, Germany	Upper Muschelkalk		Cast of U-MO BT 739
GPIT-PV-44256	*T. conspicuus*	Cervical vertebra	Bayreuth, Germany	Upper Muschelkalk		Cast of U-MO BT 732
GPIT-PV-44257	*T. conspicuus*	Cervical vertebra	Öhlmühle near Crailsheim, Germany	Lowermost Lettenkeuper, Grenzbonebed?	Spiekman and Scheyer 2019 (supp. tab. 1)	Previous number GPIT/RE/00652

GPIT-PV-45657	*T. conspicuus*	Tooth	Bibersfeld, Germany	Lettenkeuper, Lettenkohle	This study	
GPIT-PV-45658	*T. conspicuus*	Tooth	Bibersfeld, Germany	Lettenkeuper, Lettenkohle	This study	
GPIT-PV-45822	*T. conspicuus*	Caudal vertebra (anterior)	Bayreuth, Germany	Upper Muschelkalk	Spiekman and Scheyer 2019 (supp. tab. 1)	Cast of SMF R 4092. Previous number GPIT/RE/03192
GPIT-PV-45901	*T. conspicuus*	Teeth (19)	Crailsheim, Germany	Lowermost Lettenkeuper, Grenzbonebed	This study	
GPIT-PV-45911	*T. conspicuus*	Tooth	Bibersfeld, Germany	Lettenkeuper	This study	Together in a box with a *Nothosaurus* tooth
GPIT-PV-45912	*T. conspicuus*	Teeth (at least 3)	Crailsheim, Germany	Lowermost Lettenkeuper, Grenzbonebed	This study	Mixed with *Nothosaurus* teeth within one box
GPIT-PV-46096	*T. conspicuus*	Teeth (multiple)	Crailsheim, Germany	Lowermost Lettenkeuper, Grenzbonebed	This study	Mixed with *Nothosaurus* teeth within one box
GPIT-PV-46100	*T. conspicuus*	Teeth (multiple)	Crailsheim, Germany	Lowermost Lettenkeuper, Grenzbonebed	This study	Mixed with *Nothosaurus* teeth within one box
GPIT-PV-46103	*T. conspicuus*	Tooth	Öhlmühle near Crailsheim, Germany	Lowermost Lettenkeuper, Grenzbonebed	This study	
GPIT-PV-46105	*T. conspicuus*	Teeth (at least 2)	Crailsheim, Germany	Lowermost Lettenkeuper, Grenzbonebed	This study	
GPIT-PV-46106	*T. conspicuus*	Tooth	Crailsheim, Germany	Lowermost Lettenkeuper, Grenzbonebed	This study	
GPIT-PV-60009	*T. conspicuus*	Femur	Öhlmühle near Crailsheim, Germany	Lowermost Lettenkeuper, Grenzbonebed	von Huene 1902 (plate 9, fig. 1), Schmidt 1928 (fig. 1190), von Huene 1931 (fig. 3), Spiekman and Scheyer 2019 (supp. tab. 1)	Previous number GPIT/RE/03193, *Procerosaurus cruralis* holotype
GPIT-PV-60011	*T. conspicuus*	Sacral vertebra (2nd)	Laineck, Germany	Upper Muschelkalk	von Huene 1902 (fig. 50, plate 6, fig. 6)	
GPIT-PV-60024 and GPIT-PV-60025	*T. conspicuus*	Cervical vertebra (13th)	Laineck, Germany	Upper Muschelkalk	von Huene 1902 (plate 7, fig. 2), Schmidt 1928 (fig. 1160), Kuhn 1971 (plate 17, fig. 1), Wild 1973 (p.147, 149) - references for the source specimen, which is now lost	Casts, original was deposited in Munich
GPIT-PV-60131	*T. conspicuus*	Caudal vertebra (posterior)	Bayreuth, Germany	Upper Muschelkalk	von Huene 1907-1908 (plate 91, fig. 2) - reference for the source specimen, which is now	Cast, original was deposited in Bayreuth

					lost	
GPIT-PV-60132	*T. conspicuus*	Caudal vertebra (posterior)	Bindlacher Berg, Germany	Upper Muschelkalk		Cast of SMF R 287
GPIT-PV-60133	*T. conspicuus*	Dorsal vertebra	Öhlmühle near Crailsheim, Germany	Lowermost Lettenkeuper, Grenzbonebed	von Huene 1907-1908 (plate 91, fig. 5), Spiekman and Scheyer 2019 (supp. tab. 1)	Syntype of *Thecodontosaurus latespinatus*
GPIT-PV-60134	*Tanystropheus?*	Dorsal vertebra	Öhlmühle near Crailsheim, Germany	Lowermost Lettenkeuper, Grenzbonebed	von Huene 1907-1908 (plate 91, fig. 6), Spiekman and Scheyer 2019 (supp. tab. 1)	Syntype of *Thecodontosaurus latespinatus*
GPIT-PV-60135	*T. conspicuus*	Dorsal vertebra	Bindlacher Berg, Germany	Upper Muschelkalk		Cast of U-MO BT 741
GPIT-PV-60136	*T. conspicuus*	Dorsal vertebra	Bayreuth, Germany	Upper Muschelkalk	von Huene 1907-1908 (plate 91, fig. 4) - reference for the source specimen, which is now lost	Cast, original was deposited in Munich
GPIT-PV-60137	*T. conspicuus*	Caudal vertebra (anterior)	Öhlmühle near Crailsheim, Germany	Lowermost Lettenkeuper, Grenzbonebed	von Huene 1907-1908 (plate 91, fig. 8), Wild 1973 (fig. 57), Spiekman and Scheyer 2019 (supp. tab. 1)	Syntype of *Thecodontosaurus latespinatus*
GPIT-PV-60138	*T. conspicuus*	Caudal vertebra (anterior)	Göttingen, Germany	Upper Muschelkalk, *nodosus*-Zone		Cast of GZG.V.318
GPIT-PV-60139	*T. conspicuus*	Caudal vertebra (anterior)	Bayreuth, Germany	Upper Muschelkalk	von Huene 1907-1908 (plate 92, fig. 4) - reference for the source specimen, which is now lost	Cast, original was deposited in Munich
GPIT-PV-60140	*T. conspicuus*	Caudal vertebra (anterior)	Bayreuth, Germany	Upper Muschelkalk	von Huene 1907-1908 (fig. 239; plate 92, fig. 2) - reference for the source specimen, which is now lost	Cast, original was deposited in Munich
GPIT-PV-60141	*T. conspicuus*	Caudal vertebra (anterior)	Öhlmühle near Crailsheim, Germany	Lowermost Lettenkeuper, Grenzbonebed	von Huene 1907-1908 (fig. 240; plate 92, fig. 3), Spiekman and Scheyer 2019 (supp. tab. 1)	Syntype of *Thecodontosaurus latespinatus*
GPIT-PV-60142	*T. conspicuus*	Caudal vertebra (anterior)	Bayreuth, Germany	Upper Muschelkalk		Cast of SMF R 283
GPIT-PV-60143	*T. conspicuus*	Caudal vertebra (anterior)	Öhlmühle near Crailsheim, Germany	Lowermost Lettenkeuper, Grenzbonebed	von Huene 1907-1908 (fig. 242; plate 92, fig.	Syntype of *Thecodontosaurus latespinatus*

					6), Spiekman and Scheyer 2019 (supp. tab. 1)	
GPIT-PV-60144	*T. conspicuus*	Caudal vertebra (anterior)	Öhlmühle near Crailsheim, Germany	Lowermost Lettenkeuper, Grenzbonebed	von Huene 1907-1908 (plate 92, fig. 7), Spiekman and Scheyer 2019 (supp. tab. 1)	Syntype of *Thecodontosaurus latespinatus*
GPIT-PV-60145	*T. conspicuus*	Cervical vertebra	Öhlmühle near Crailsheim, Germany	Lowermost Lettenkeuper, Grenzbonebed	von Huene 1907-1908 (plate 96, fig. 7), Spiekman and Scheyer 2019 (supp. tab. 1)	
GPIT-PV-60146	*T. conspicuus*	Cervical vertebra	Öhlmühle near Crailsheim, Germany	Lowermost Lettenkeuper, Grenzbonebed	von Huene 1907-1908 (plate 96, fig. 4), Spiekman and Scheyer 2019 (supp. tab. 1)	
GPIT-PV-60147	*T. conspicuus*	Cervical vertebra (11th)	Bindlacher Berg, Germany	Upper Muschelkalk	von Huene 1907-1908 (plate 96, fig. 2)	
GPIT-PV-60148	*T. conspicuus*	Cervical vertebra (10th)	Öhlmühle near Crailsheim, Germany	Lowermost Lettenkeuper, Grenzbonebed	von Huene 1907-1908 (plate 96, fig. 6), Spiekman and Scheyer 2019 (supp. tab. 1)	Previous number GPIT/RE/03191
GPIT-PV-60149	*T. conspicuus*	Cervical vertebra	Öhlmühle near Crailsheim, Germany	Lowermost Lettenkeuper, Grenzbonebed	von Huene 1907-1908 (plate 96, fig. 3), Spiekman and Scheyer 2019 (supp. tab. 1)	Previous number GPIT/RE/03190
GPUL uncatalogued	*T. conspicuus*	Tooth	Laineck, Germany	Upper Muschelkalk	This study	
GZG.V.306	*Tanystropheus?*	Caudal vertebra (anterior)	Hainberg?, Germany	?Lowermost Lettenkeuper, Grenzbonebed	This study	Original specimen label lost, provenance uncertain
GZG.V.316	*T. conspicuus*	Cervical vertebra	?Bayreuth, Germany	?Upper Muschelkalk	This study	
GZG.V.317	*T. conspicuus*	Cervical vertebra (11th)	Thuringia, Germany	?Lower Keuper	This study	
GZG.V.318	*T. conspicuus*	Caudal vertebra (anterior)	Göttingen (Tillyschanze), Germany	Upper Muschelkalk, *nodosus*-Zone	von Huene 1907-1908 (plate 92, fig. 1)	Syntype of *Thecodontosaurus latespinatus*
GZG.V.319	*T. conspicuus*	Femur	Coburg, Germany	Upper Muschelkalk, *nodosus*-Zone	This study	Fragments of at least one femur, which can be identified based on the characteristic curvature, transverse cross section shape, and internal anatomy

GZG.V.320	*T. conspicuus*	Femur	Weimar, Germany	Upper Muschelkalk, *nodosus*-Zone	This study	
MAN 2016.0.201	*T. conspicuus*	Tooth	Mont-sur-Meurthe, France	Upper Muschelkalk?	Corroy 1928 (p. 121; plate 3, fig. 2)	Unaccesioned
MAN 2016.0.202	*T. conspicuus*	Tooth	Rehainvillers, France	Upper Muschelkalk?	Corroy 1928 (p. 121; plate 3, fig. 7)	Unaccesioned
MB.1969.54.274	*T. conspicuus*	Cervical vertebra	Kleinwalbur, Germany	Upper Muschelkalk	Lang & von Huene 1952	
MB.1970.42.2	*T. conspicuus*	Cervical vertebra (12th)	Bayreuth, Germany	Upper Muschelkalk	von Huene 1931 (fig. 2), Shmidt 1938 (fig. 1188a:a), Kuhn 1971 (plate 21a, fig. 1a), Wild 1973 (fig. 50)	
MB.R.112	*T. conspicuus*	Tooth	Bayreuth, Germany	Upper Muschelkalk	This study	
MB.R.121	*T. conspicuus*	Tooth	Bayreuth, Germany	Upper Muschelkalk	This study	
MB.R.122	*T. conspicuus*	Tooth	Bayreuth, Germany	Upper Muschelkalk	This study	
MB.R.390.2	*T. conspicuus*	Caudal vertebra (anterior)	Bayreuth, Germany	Upper Muschelkalk	This study	
MB.S.11	*T. conspicuus*	Cervical vertebra	Laryszów (Larischhof), Poland	Upper Muschelkalk, *spinosus*-Zone?	von Meyer 1849 (p. 219), von Meyer 1847-1855 (s. 128, plate 27, figs 19, 20), Skawiński et al. 2016 (fig. 5O,P), Spiekman and Scheyer 2019 (supp. tab. 1)	Paralectotype
MHI 1/1	*T. conspicuus*	Tooth	Sattelweiler, Germany	Lowermost Lettenkeuper, Grenzbonebed	Spiekman and Scheyer 2019 (supp. tab. 1)	
MHI 1/2	*T. conspicuus*	Tooth	Crailsheim, Germany	Lowermost Lettenkeuper, Grenzbonebed	Spiekman and Scheyer 2019 (supp. tab. 1)	
MHI 1/3	*T. conspicuus*	Tooth	Crailsheim, Germany	Lowermost Lettenkeuper, Grenzbonebed	Spiekman and Scheyer 2019 (supp. tab. 1)	
MHI 1104	*T. conspicuus*	Cervical vertebra	Öhringen (Unterohrn), Germany	Upper Muschelkalk, *spinosus*-Zone	Jaquier and Scheyer 2017, Spiekman and Scheyer 2019 (supp. tab. 1)	
MHI 1142	*T. conspicuus*	Dorsal vertebra	Künzelsau-Garnberg, Germany	Upper Muschelkalk, *evolutus*-Zone	Spiekman and Scheyer 2019 (supp. tab. 1)	
MHI 1172	*T. conspicuus*	Caudal vertebra (anterior)	Satteldorf-Neidenfels, Germany	Upper Muschelkalk, *pulcher*-Zone	Spiekman and Scheyer 2019 (supp. tab. 1)	
MHI 1339	*T. conspicuus*	Cervical vertebra (12th)	Wittighausen near Schwäbisch Hall, Germany	Upper Muschelkalk, *nodosus*-Zone	Spiekman and Scheyer 2019 (supp. tab. 1)	
MHI 1426	*T. conspicuus*	Teeth (at least 2)	Kirchberg/Jagst, Germany	Lower Lettenkeuper, Anthrakonitbank	This study	
MHI 1966	*T. conspicuus*	Femur	Engelhardshausen near Crailsheim, Germany	Upper Muschelkalk	Spiekman and Scheyer 2019 (supp. tab. 1)	

MHI 2094	*T. conspicuus*	Caudal vertebra (anterior)	Neidenfels, Germany	Upper Muschelkalk, *robustus-compressus*-Zone	This study	
MHI 2136	*T. conspicuus*	Cervical vertebra	Tiefenbach, Germany	Lowermost Lettenkeuper, Grenzbonebed	Spiekman and Scheyer 2019 (supp. tab. 1)	
MHI 2194	*T. conspicuus*	Ischium	Ummenhofen near Vellberg, Germany	Lowermost Lettenkeuper, Grenzbonebed	This study	
MHI 2195	*T. conspicuus*	Cervical vertebra	Tiefenbach, Germany	Upper Muschelkalk, *spinosus*-Zone	This study	
MHI 2196/1, 2196/2, 2196/3	*T. conspicuus*	Teeth (3)	Tiefenbach, Germany	Lowermost Lettenkeuper, Grenzbonebed	This study	
MHI 2197	*T. conspicuus*	Tooth	Satteldorf, Germany	Lowermost Lettenkeuper, Grenzbonebed	This study	
MHI 2198	*T. conspicuus*	Tooth	Crailsheim area, Germany	Lowermost Lettenkeuper, Grenzbonebed	This study	
MHI 2199/1	*T. conspicuus*	Ischium	Dettelbach/Main, Germany	Upper Muschelkalk, *subleavigatus-nodosus*-Zone	This study	
MHI 2199/2	*T. conspicuus*	Caudal vertebra (first?)	Dettelbach/Main, Germany	Upper Muschelkalk, *subleavigatus-nodosus*-Zone	This study	
MHI 2200	*T. conspicuus*	Caudal vertebra (anterior)	Neidenfels, Germany	Upper Muschelkalk, *robustus*-zone	This study	
MHI 2201	*T. conspicuus*	Cervical vertebra	Kupferzell-Rüblingen, Germany	Lowermost Lettenkeuper, Grenzbonebed	This study	
MHI 276	*T. conspicuus*	Tooth	Sattelweiler, Germany	Lowermost Lettenkeuper, Grenzbonebed	This study	
MHI 67	*T. conspicuus*	Cervical vertebra	Dettelbach/Main, Germany	Upper Muschelkalk, *nodosus*-Discoceratiten-Zone	Spiekman and Scheyer 2019 (supp. tab. 1)	
MHI 788	*T. conspicuus*	Dorsal rib (anterior)	Wollmershausen I, Germany	Upper Muschelkalk, *pulcher*-Zone	Spiekman and Scheyer 2019 (supp. tab. 1)	
MLU.GeoS.2206	*T. conspicuus*	Cervical vertebra	Weimar, Germany	Upper Muschelkalk?	This study	
MLU.GeoS.2207	*T. conspicuus*	Tooth	Weimar, Germany	Upper Muschelkalk, mo2	This study	
MNG uncatalogued	*T. conspicuus*	Tooth	Weimar, Germany	Upper Muschelkalk	This study	
MNG-1161	*T. conspicuus?*	Femur	Molsdorf, Germany	Upper Lettenkeuper, Grenzdolomit	This study	
MNG-15960	*T. conspicuus*	Tooth	Neudietendorf, Germany	Lettenkeuper, Lettenkohle	This study	
MNG-15967	*T. conspicuus*	Tooth	Neudietendorf, Germany	Lettenkeuper, Lettenkohle	This study	
MNM 1037 (partim)	*T. conspicuus*	Cervical vertebra	Ettersberg near Weimar, Germany	Upper Muschelkalk	This study	
MSBO Pal 327—534	*Tanystropheus?*	Tooth	Bissendorf, Germany	Upper Muschelkalk, *compressus*-Zone	Diedrich 2009 (fig. 12)	Unaccesioned, might be of *Pistosaurus*

Muz. PGI-NRI uncatalogued	*T. conspicuus*	Cervical vertebrae (3), (?)dorsal vertebra	Miedary, Poland	Lower Lettenkeuper	This study	
NHMS-GT 836	*T. conspicuus*	Cervical vertebra	Bindlach, Germany	Upper Muschelkalk	This study	
NHMS-WT 1526	*T. conspicuus*	Tooth	Suhlequelle near Erfurt, Germany	Upper Muschelkalk, mo2	This study	
NHMS-WT 2720	*T. conspicuus*	Ilium	Molsdorf, Germany	Lettenkeuper	This study	
NHMS-WT 2721	*T. conspicuus*	Cervical vertebra	Molsdorf, Germany	Lettenkeuper	This study	
NHMS-WT 2722	*Tanystropheus?*	Cervical vertebra? (posterior part)	Molsdorf, Germany	Lettenkeuper	This study	
NHMS-WT 2723	*T. conspicuus*	Tooth	Molsdorf, Germany	Lettenkeuper	This study	
NHMS-WT 2773	*T. conspicuus*	Tooth	Molsdorf, Germany	Lettenkeuper	This study	
NHMS-WT 3048	*T. conspicuus*	Caudal vertebra (anterior)	Molsdorf, Germany	Lettenkeuper	This study	
NHMS-WT 585b	*Tanystropheus?*	Caudal vertebra	Legefeld near Weimar, Germany	Upper Muschelkalk, 1m over Cycloidesbank	This study	
NHMS-WT 736	*T. conspicuus*	Tooth	Arnstadt, Germany	Lettenkeuper	This study	
NHMS-WT 992	*T. conspicuus*	Cervical vertebra	Troistedt near Weimar, Germany	Upper Muschelkalk, mo1	This study	
NHMUK PV OR 48202	*T. conspicuus*	Caudal vertebra (posterior)	Bayreuth, Germany	Upper Muschelkalk	This study	
NHMUK PV R 4012	*T. conspicuus*	Cervical vertebra (10th)	Bindlach, Germany	Upper Muschelkalk		Cast of SMF R 285
NHMW 1839/0013/0215	*T. conspicuus*	Cervical vertebra	Bayreuth, Germany	Upper Muschelkalk	This study	
NME 93/133	*T. conspicuus*	Cervical vertebra	Kleinromstedt, Germany	Upper Muschelkalk, mo2?	This study	
NME uncatalogued	*T. conspicuus?*	Cervical vertebra	Unknown	Upper Muschelkalk?	This study	Specimen label lost
NME uncatalogued	*T. conspicuus*	Tooth	Crailsheim, Germany	Lowermost Lettenkeuper, Grenzbonebed	This study	
NME uncatalogued	*T. conspicuus*	Tooth	Unknown	Upper Muschelkalk?	This study	Specimen label lost
NMK Lam 1508b	*Tanystropheus?*	Vertebral fragment	Lamerden, Germany	Upper Muschelkalk, *enodis-posseckeri*-Zone	Diedrich 2015 (fig. 10C: 2)	Unaccesioned
PIMUZ A/III 0885	*T. conspicuus*	Cervical vertebra	Hegnabrunn, Germany	Upper Muschelkalk, *spinosus*-Zone		Cast of SMNS 54631
PIMUZ A/III 0886	*T. conspicuus*	Cervical vertebra	Bindlach, Germany	Upper Muschelkalk		Cast of SNSB-BSPG 1988 I 32
PIMUZ A/III 1371	*T. conspicuus*	Tooth	Vellberg-Eschenau, Germany	Lower Lettenkeuper, Esterienschichten	This study	
PIMUZ A/III 1372	*T. conspicuus*	Tooth	Kupferzell-Rüblingen, Germany	Lowermost Lettenkeuper, Grenzbonebed	This study	
PIMUZ A/III 1373	*T. conspicuus*	Tooth	Satteldorf, Germany	Lowermost Lettenkeuper, Grenzbonebed	This study	
PIMUZ uncatalogued	*T. conspicuus*	Caudal vertebra (posterior)	Eschenau, Germany	Upper Muschelkalk, mo3	This study	Coll. Ch. Klug

PMJ P 1185	*T. conspicuus*	Femur	Bad Sulza, Germany	Upper Muschelkalk?	This study	
PMU uncatalogued	*T. conspicuus*	Cervical vertebra (13th)	Germany	Upper Muschelkalk?/Lower Keuper?	This study	
RE 537.761.2 A318/1	*T. conspicuus*	Tooth	Crailsheim, Germany	Lowermost Lettenkeuper, Grenzbonebed	This study	
SMF R 1031	*T. conspicuus*	Cervical vertebra (posterior - ?12th)	Bayreuth, Germany	Upper Muschelkalk	This study	
SMF R 1058a	*T. conspicuus*	Cervical vertebra	Bayreuth, Germany	Upper Muschelkalk	This study	In a box together with a sauropterygian ilium
SMF R 1059	*T. conspicuus*	Cervical vertebra	Bayreuth, Germany	Upper Muschelkalk	Spiekman and Scheyer 2019 (supp. tab. 1)	
SMF R 1061	*T. conspicuus*	Cervical vertebra	Bayreuth, Germany	Upper Muschelkalk	Edinger 1924 (fig. 2), Spiekman and Scheyer 2019 (supp. tab. 1)	
SMF R 1063	*T. conspicuus*	Femur	Bayreuth, Germany	Upper Muschelkalk	Spiekman and Scheyer 2019 (supp. tab. 1)	
SMF R 1076	*Tanystropheus?*	Metacarpal?	Bayreuth, Germany	Upper Muschelkalk	Spiekman and Scheyer 2019 (supp. tab. 1)	
SMF R 2022	*T. conspicuus*	Sacral vertebra	Bayreuth, Germany	Upper Muschelkalk	Spiekman and Scheyer 2019 (supp. tab. 1)	
SMF R 282a	*T. conspicuus*	Caudal vertebra (anterior)	Laineck, Germany	Upper Muschelkalk, *semipartitus*-Zone	von Huene 1907-1908 (fig. 237), Wild 1973 (fig. 61), Diedrich 2012 (fig. 14, 12), Spiekman and Scheyer 2019 (supp. tab. 1)	Syntype of *Thecodontosaurus latespinatus*
SMF R 282b	*T. conspicuus*	Cervical vertebra	Bayreuth, Germany	Upper Muschelkalk	von Huene 1907-1908 (fig. 250), Wild 1973 (fig. 44), Spiekman and Scheyer 2019 (supp. tab. 1)	
SMF R 283	*T. conspicuus*	Caudal vertebra (anterior)	Laineck, Germany	Upper Muschelkalk, *semipartitus*-Zone	von Huene 1907-1908 (fig. 241; plate 92, fig. 5), Wild 1973 (p. 93), Spiekman and Scheyer 2019 (supp. tab. 1)	Syntype of *Thecodontosaurus latespinatus*
SMF R 285	*T. conspicuus*	Cervical vertebra (10th)	Bindlach, Germany	Upper Muschelkalk	von Huene 1907-1908 (plate 94, fig. 8), Edinger 1924 (fig.1), Wild 1973 (fig. 48, fig. 97b), Diedrich 2012 (fig. 14, 6), Spiekman and Scheyer 2019 (supp. tab. 1)	

SMF R 286	*T. conspicuus*	Caudal vertebra (anterior)	Laineck, Germany	Upper Muschelkalk, *semipartitus*-Zone	von Huene 1907-1908 (fig. 238), Spiekman and Scheyer 2019 (supp. tab. 1)	Syntype of *Thecodontosaurus latespinatus*. Wild 1973 (fig. 60) mentions this number but means SMF R 4092
SMF R 287	*T. conspicuus*	Caudal vertebra (posterior)	Laineck, Germany	Upper Muschelkalk, *semipartitus*-Zone	von Huene 1907-1908 (fig. 243, plate 91, fig. 1), Wild 1973 (fig. 62), Wild 1976 (fig. 3), Diedrich 2012 (fig. 14, 13), Spiekman and Scheyer 2019 (supp. tab. 1)	Syntype of *Thecodontosaurus latespinatus*
SMF R 4034	*T. conspicuus*	Humerus	Bindlach, Germany	Upper Muschelkalk	von Huene 1920 (fig. 1), von Huene 1958 (fig. 4), Wild 1973 (fig. 67), Spiekman and Scheyer 2019 (supp. tab. 1)	
SMF R 4092	*T. conspicuus*	Caudal vertebra (anterior)	Bindlach, Germany	Upper Muschelkalk	Wild 1973 (fig. 60), Diedrich 2012 (fig. 14, 10)	
SMF R 4182	*T. conspicuus*	Cervical vertebra	Bayreuth, Germany	Upper Muschelkalk	Spiekman and Scheyer 2019 (supp. tab. 1)	Cast of U-MO BT 740
SMF R 4183	*T. conspicuus*	Cervical vertebra	Bayreuth, Germany	Upper Muschelkalk	Spiekman and Scheyer 2019 (supp. tab. 1)	Cast of U-MO BT 732
SMF R 4748	*Tanystropheus?*	Cervical rib fragment	Bayreuth, Germany	Upper Muschelkalk	Spiekman and Scheyer 2019 (supp. tab. 1)	
SMF R 5138a	*T. conspicuus*	Tooth	Crailsheim, Germany	Lowermost Lettenkeuper, Grenzbonebed	This study	
SMF R 69	*T. conspicuus?*	Humerus	Bayreuth, Germany	Upper Muschelkalk	Spiekman and Scheyer 2019 (supp. tab. 1)	
SMF R 820	*T. conspicuus*	Dorsal vertebra	Bindlacher Berg, Germany	Upper Muschelkalk	Wild 1973 (fig. 54), Diedrich 2012 (fig. 14, 8), Spiekman and Scheyer 2019 (supp. tab. 1)	
SMF R 913	*T. conspicuus*	Cervical vertebra	Bayreuth, Germany	Upper Muschelkalk	This study	
SMF R 924	*T. conspicuus*	Cervical vertebra	Bayreuth, Germany	Upper Muschelkalk	This study	
SMF R 988	*T. conspicuus*	Tooth	Crailsheim, Germany	Lowermost Lettenkeuper, Grenzbonebed	This study	
SMF R 998	*T. conspicuus*	Cervical vertebra (11th)	Bindlach, Germany	Upper Muschelkalk	Wild 1973 (p. 79), Spiekman and Scheyer 2019 (supp. tab. 1)	

SMF R 999a-c	*T. conspicuus*	Cervical vertebra	Bindlach, Germany	Upper Muschelkalk	von Huene 1907-1908 (fig. 251), Edinger 1924 (fig. 3), Spiekman and Scheyer 2019 (supp. tab. 1), Rytel 2024b (fig. 1E-F)	
SMF R uncatalogued	*T. conspicuus*	Cervical vertebra	Bayreuth, Germany	Upper Muschelkalk		Two casts of U-MO BT 736
SMNK-PAL 34722	*T. conspicuus?*	Femur	Hoheneck, Germany	Upper Lettenkeuper, Grenzdolomit?	This study	
SMNK-PAL 34774	*T. conspicuus*	Tooth	Crailsheim, Germany	Lowermost Lettenkeuper, Grenzbonebed	This study	
SMNS 13337	*T. conspicuus*	Dorsal vertebrae (10 elements) and the first sacral vertebra in articulation	Tiefenbach, Germany	Upper Muschelkalk, *nodosus*-Discoceratiten-Zone?	This study	
SMNS 14731	*T. conspicuus*	Caudal vertebra (anterior)	Tiefenbach, Germany	Lowermost Lettenkeuper, Grenzbonebed	Spiekman and Scheyer 2019 (supp. tab. 1)	
SMNS 15891	*T. conspicuus*	Cervical vertebra	Neidenfels, Germany	Upper Muschelkalk, Trochitenkalk	Peyer 1931 (fig. 25), Spiekman and Scheyer 2019 (supp. tab. 1)	
SMNS 16364	*T. conspicuus*	Cervical vertebra	Crailsheim, Germany	Upper Muschelkalk, Discoceratitenschichten?	Peyer 1931 (fig. 24), Wild 1973 (s. 79), Spiekman and Scheyer 2019 (supp. tab. 1)	
SMNS 16643	*T. conspicuus*	Caudal vertebra (anterior)	Tiefenbach, Germany	Upper Muschelkalk, mo3	Spiekman and Scheyer 2019 (supp. tab. 1)	
SMNS 16737c	*T. conspicuus*	Cervical vertebra	Tiefenbach, Germany	Upper Muschelkalk, Discoceratitenschichten	Spiekman and Scheyer 2019 (supp. tab. 1)	
SMNS 19197	*T. conspicuus*	Cervical vertebra	Schloss Stetten near Crailsheim, Germany	Upper Muschelkalk, Glaukonitbank	Adam 1953 (fig. 1), Spiekman and Scheyer 2019 (supp. tab. 1)	
SMNS 50054	*Tanystropheus?*	Cervical rib fragment	Markgröningen, Germany	Lowermost Lettenkeuper, Grenzbonebed	This study	
SMNS 50092	*T. conspicuus*	Tooth	Markgröningen, Germany	Lower Lettenkeuper	This study	
SMNS 50154	*T. conspicuus*	Caudal vertebra (posterior)	Bayreuth, Germany	Upper Muschelkalk	von Huene 1907-1908 (plate 91, fig. 2) - reference for the source specimen, which is now lost	Cast, riginal was deposited in Bayreuth
SMNS 50154a	*T. conspicuus*	Caudal vertebra (posterior)	Bindlach, Germany	Upper Muschelkalk		Cast of SMF R 287
SMNS 50226	*T. conspicuus*	Axis	Grombach, Germany	Upper Muschelkalk, Discoceratitenschichten	Spiekman and Scheyer 2019 (supp. tab. 1)	
SMNS 50232	*T. conspicuus*	Tooth	Markgröningen, Germany	Lower Lettenkeuper, 'Untere Dolomit'	This study	

SMNS 50237	*T. conspicuus*	Tooth	Weiler zum Stein, Germany	Lower Lettenkeuper, Vitriolschiefer	This study	
SMNS 51064	*T. conspicuus*	Tooth	Rielingshausen, Germany	Lowermost Lettenkeuper, Grenzbonebed	This study	
SMNS 51749	*T. conspicuus*	Tooth	Zwingelhausen, Germany	Lower Lettenkeuper, Blaubank	This study	
SMNS 51860	*T. conspicuus*	Tooth	Gerichtstetten, Germany	Upper Muschelkalk, Glaukonitbank	This study	
SMNS 51862	*Tanystropheus?*	Cervical rib fragment	Rüblingen, Germany	Upper Muschelkalk, Discoceratitenschichten	This study	
SMNS 52063	*T. conspicuus*	Cervical vertebra	Knittlingen, Germany	Upper Muschelkalk, Discoceratitenschichten	Spiekman and Scheyer 2019 (supp. tab. 1)	
SMNS 52293	*T. conspicuus*	Tooth	Rüblingen, Germany	Lowermost Lettenkeuper, Grenzbonebed?	This study	
SMNS 52478	*T. conspicuus*	Teeth (4)	Crailsheim, Germany	Lowermost Lettenkeuper, Grenzbonebed	Fraas 1896 (fig. 4), Schmidt 1928 (fig. 1115), Rieppel and Wild 1996 (p. 61)	Syntypes of *Nothosaurus blezingeri*
SMNS 52479	*T. conspicuus*	Cervical vertebra	Tiefenbach, Germany	Upper Muschelkalk	Spiekman and Scheyer 2019 (supp. tab. 1)	
SMNS 52479a	*T. conspicuus*	Cervical vertebra	Tiefenbach, Germany	Upper Muschelkalk	This study	Morphology mostly artificial
SMNS 54055	*T. conspicuus*	Tooth	Mundelsheim, Germany	Upper Muschelkalk, Discoceratitenschichten	This study	
SMNS 54056	*T. conspicuus*	Cervical vertebra	Steinbach, Germany	Lowermost Lettenkeuper, Grenzbonebed	Spiekman and Scheyer 2019 (supp. tab. 1)	
SMNS 54057	*Tanystropheus?*	Cervical rib fragment	Großglattbach, Germany	Upper Muschelkalk	Jaquier and Scheyer 2017	
SMNS 54147	*T. conspicuus*	Tooth	Unterrodach, Germany	Upper Muschelkalk, *nodosus*-Zone	Ezcurra 2016 (fig. 14A-B)	
SMNS 54148	*T. conspicuus*	Tooth	Dettelbach/Main, Germany	Upper Muschelkalk, Discoceratitenschichten	This study	
SMNS 54620	*T. conspicuus*	Cervical vertebra	Unterrodach, Germany	Upper Muschelkalk, *nodosus*-Zone	Wild 1973 (fig. 51), Spiekman and Scheyer 2019 (supp. tab. 1)	
SMNS 54621	*T. conspicuus*	Femur	Hegnabrunn, Germany	Upper Muschelkalk, *spinosus*-Zone	Wild 1973 (fig. 73), Ezcurra 2016 (fig. 43A,B), Spiekman and Scheyer 2019 (supp. tab. 1)	
SMNS 54622	*T. conspicuus*	Femur	Bindlach, Germany	Upper Muschelkalk, *compressus-robustus*-Zone?	Jaquier and Scheyer 2017	

SMNS 54623	*T. conspicuus*	Femur	Hegnabrunn, Germany	Upper Muschelkalk, *spinosus-nodosus*-Zone	Spiekman and Scheyer 2019 (supp. tab. 1)	
SMNS 54624	*T. conspicuus*	Femur	Lessau, Germany	Upper Muschelkalk, *spinosus*-Zone	Spiekman and Scheyer 2019 (supp. tab. 1)	
SMNS 54626	*T. conspicuus*	Femur	Hegnabrunn, Germany	Upper Muschelkalk, *spinosus*-Zone	Spiekman and Scheyer 2019 (supp. tab. 1)	
SMNS 54627	*T. conspicuus*	Caudal vertebra (anterior)	Unterrodach, Germany	Upper Muschelkalk, *nodosus*-Zone	Spiekman and Scheyer 2019 (supp. tab. 1)	
SMNS 54628	*T. conspicuus*	Dorsal vertebra	Hegnabrunn, Germany	Upper Muschelkalk, *enodis-leavigatus*-Zone	Spiekman and Scheyer 2019 (supp. tab. 1), Rytel et al. 2024b	
SMNS 54629	*T. conspicuus*	Dorsal vertebra	Dörfles near Kronach, Germany	Upper Muschelkalk, *spinosus-nodosus*-Zone?	Wild 1973 (fig. 52), Spiekman and Scheyer 2019 (supp. tab. 1)	
SMNS 54630	*T. conspicuus*	Cervical vertebra (12th)	Hegnabrunn, Germany	Upper Muschelkalk, *nodosus*-Zone	Spiekman and Scheyer 2019 (supp. tab. 1)	
SMNS 54631	*T. conspicuus*	Sacral vertebra (1st)	Hegnabrunn, Germany	Upper Muschelkalk, *spinosus*-Zone	Wild 1973 (fig. 55), Ezcurra 2016 (fig. 35A), Spiekman and Scheyer 2019 (supp. tab. 1)	
SMNS 54632	*T. conspicuus*	Sacral vertebra (1st)	Bindlach, Germany	Upper Muschelkalk, *nodosus*-Zone?	Wild 1973 (fig. 56), Spiekman and Scheyer 2019 (supp. tab. 1)	
SMNS 54633	*T. conspicuus*	Cervical vertebra (11th)	Hegnabrunn, Germany	Upper Muschelkalk, *spinosus*-Zone?	Spiekman and Scheyer 2019 (supp. tab. 1)	
SMNS 54635	*Tanystropheus?*	Cervical rib fragment	Kirchenthumbach near Eschenbach, Germany	Lowermost Lettenkeuper, Grenzbonebed?	This study	
SMNS 54639	*T. conspicuus*	Dorsal vertebra	Unterrodach, Germany	Upper Muschelkalk, *nodosus*-Zone	Spiekman and Scheyer 2019 (supp. tab. 1)	
SMNS 54640	*T. conspicuus*	Dorsal vertebra	Bindlach, Germany	Upper Muschelkalk, *compressus*-Zone?	von Huene 1931 (fig. 1), Shmidt 1938 (fig. 1188a:b), Kuhn 1971 (plate 21a, fig. 1b), Wild 1973 (s. 84), Diedrich 2012 (fig. 14, 9), Spiekman and Scheyer 2019 (supp. tab. 1)	
SMNS 54641	*T. conspicuus*	Dorsal vertebra	Hegnabrunn, Germany	Upper Muschelkalk, *enodis-leavigatus*-Zone	Spiekman and Scheyer 2019 (supp. tab. 1)	
SMNS 54642	*T. conspicuus*	Sacral vertebra	Unterrodach, Germany	Upper Muschelkalk, *nodosus*-Zone	Spiekman and Scheyer 2019 (supp. tab. 1)	

SMNS 54643	*T. conspicuus*	Cervical vertebra	Hegnabrunn, Germany	Upper Muschelkalk, *spinosus*-*enodis*-Zone	Spiekman and Scheyer 2019 (supp. tab. 1)	
SMNS 54644	*T. conspicuus*	Cervical vertebra	Hegnabrunn, Germany	Upper Muschelkalk, *nodosus*-Zone?	Spiekman and Scheyer 2019 (supp. tab. 1)	
SMNS 54647	*T. conspicuus*	Cervical vertebra	Unterrodach, Germany	Upper Muschelkalk, *nodosus*-Zone	This study	
SMNS 54648	*T. conspicuus*	Cervical vertebra	Kübelhof near Kulmbach, Germany	Upper Muschelkalk, *nodosus*-Zone	Spiekman and Scheyer 2019 (supp. tab. 1)	
SMNS 54653	*T. conspicuus*	Cervical vertebra	Bindlach, Germany	Upper Muschelkalk, *pulcher*-*robustus*-Zone	Wild 1973 (fig. 40), Spiekman and Scheyer 2019 (supp. tab. 1)	
SMNS 54654	*T. conspicuus*	Cervical vertebra (12th)	Gänheim near Würzburg, Germany	Upper Muschelkalk	Ezcurra 2016 (fig. 33B), Spiekman and Scheyer 2019 (supp. tab. 1)	
SMNS 54662	*T. conspicuus*	Tooth	Hegnabrunn, Germany	Upper Muschelkalk, *nodosus*-Zone	This study	
SMNS 54665	*T. conspicuus*	Tooth	Forstlahm, Germany	Upper Muschelkalk, *spinosus*-Zone	This study	
SMNS 54666	*T. conspicuus*	Tooth	Schwingen, Germany	Upper Muschelkalk, upper Ceratitenschichten	This study	
SMNS 54667	*T. conspicuus*	Tooth	Bindlach, Germany	Upper Muschelkalk, *pulcher*-*robustus*-Zone	This study	
SMNS 54668	*T. conspicuus*	Tooth	Kübelhof near Kulmbach, Germany	Lowermost Lettenkeuper, Grenzbonebed	This study	
SMNS 55205	*T. conspicuus*	Tooth	Vellberg-Eschenau, Germany	Lower Lettenkeuper, Blaubank	This study	
SMNS 55341	*T. conspicuus*	Dorsal vertebra	Berlichingen, Germany	Upper Muschelkalk, *enodis*-*leavigatus*-Zone	Ezcurra et al. 2014 (figs 16D; 18C), Ezcurra 2016 (fig. 31B), Spiekman and Scheyer 2019 (supp. tab. 1), Ezurra et al. 2020 (fig. 1D)	
SMNS 56496	*T. conspicuus*	Tooth	Neudenau, Germany	Upper Muschelkalk, 7m over Cycloidesbank	This study	
SMNS 56516	*T. conspicuus*	Tooth	Neidenfels, Germany	Lowermost Lettenkeuper, Grenzbonebed	This study	
SMNS 56517	*T. conspicuus*	Tooth	Neidenfels, Germany	Lowermost Lettenkeuper, Grenzbonebed	This study	
SMNS 56518	*T. conspicuus*	Tooth	Neidenfels, Germany	Lowermost Lettenkeuper, Grenzbonebed	This study	
SMNS 56528	*T. conspicuus*	Tooth	Sattelweiler, Germany	Lowermost Lettenkeuper, Grenzbonebed	This study	

SMNS 56738	*T. conspicuus*	Tooth	Rüblingen, Germany	Upper Muschelkalk, Discoceratitenschichten	This study	
SMNS 57006	*T. conspicuus*	Tooth	Mundelsheim, Germany	Lower Lettenkeuper, Blaubank	This study	
SMNS 57016	*T. conspicuus*	Postcloacal bone (morphotype P)	Rothenburg ob der Tauber, Germany	Lowermost Lettenkeuper, Grenzbonebed	Jaquier and Scheyer 2017	
SMNS 57531	*T. conspicuus*	Cervical vertebra (13th?)	Mundelsheim, Germany	Lower Lettenkeuper, Blaubank	Spiekman and Scheyer 2019 (supp. tab. 1)	
SMNS 58906	*T. conspicuus*	Tooth	Mundelsheim, Germany	Lower Lettenkeuper, Vitriolschiefer	This study	
SMNS 58908	*T. conspicuus*	Tooth	Mundelsheim, Germany	Lower Lettenkeuper, Vitriolschiefer	This study	
SMNS 58909	*T. conspicuus*	Tooth	Mundelsheim, Germany	Lower Lettenkeuper, Vitriolschiefer	This study	Together in a box with a ?*Nothosaurus* tooth
SMNS 58914	*T. conspicuus*	Tooth	Mundelsheim, Germany	Lower Lettenkeuper, Vitriolschiefer	This study	
SMNS 59362	*T. conspicuus*	Cervical vertebra	Unterrodach, Germany	Upper Muschelkalk, *nodosus*-Zone	Spiekman and Scheyer 2019 (supp. tab. 1)	
SMNS 59380	*T. conspicuus*	Femur	Öhringen (Unterohrn), Germany	Lowermost Lettenkeuper, Grenzbonebed	Spiekman and Scheyer 2019 (supp. tab. 1)	
SMNS 59387	*T. conspicuus*	Tooth	Rothenburg ob der Tauber, Germany	Lowermost Lettenkeuper, Grenzbonebed	This study	
SMNS 59411	*T. conspicuus*	Cervical vertebra	Roßwag, Germany	Upper Muschelkalk, *nodosus*-Discoceratiten-Zone	Spiekman and Scheyer 2019 (supp. tab. 1)	
SMNS 81582	*T. conspicuus*	Tooth	Rüblingen, Germany	Upper Muschelkalk, Discoceratitenschichten	This study	
SMNS 81583	*T. conspicuus*	Cervical vertebra	Crailsheim, Germany	Upper Muschelkalk	von Huene 1907-1908 (plate 96, fig. 10), Spiekman and Scheyer 2019 (supp. tab. 1)	
SMNS 81721	*T. conspicuus*	Cervical vertebra	Hegnabrunn, Germany	Upper Muschelkalk, *nodosus*-Zone	Spiekman and Scheyer 2019 (supp. tab. 1)	
SMNS 81989	*T. conspicuus*	Postcloacal bone (morphotype Z)	Vellberg-Eschenau, Germany	Upper Lettenkeuper, Untere Graue Margel	This study	
SMNS 84816	*T. conspicuus*	Sacral vertebra	Bindlach, Germany	Upper Muschelkalk	Spiekman and Scheyer 2019 (supp. tab. 1)	Cast of GPIT-PV-60011
SMNS 84821	*T. conspicuus*	Cervical vertebra (11th)	Schwingen, Germany	Upper Muschelkalk, *enodis-leavigatus*-Zone	Wild 1973 (fig. 49), Hauschke and Wilde 1999 (fig. 13)	

SMNS 8728	*T. conspicuus*	Cervical vertebra (12th)	Öhlmühle near Crailsheim, Germany	Lowermost Lettenkeuper, Grenzbonebed	von Huene 1902 (plate 7, fig. 1), Schmidt 1928 (fig. 1161), Wild 1973 (s. 80), Spiekman and Scheyer 2019 (supp. tab. 1)	Holotype of *Chelyzoon blezingeri*
SMNS 91385 (?)	*T. conspicuus*	Tooth	Crailsheim, Germany	Lowermost Lettenkeuper, Grenzbonebed	Schoch 2015 (fig. 10.13:l), Schoch et al. 2018 (fig. 4q)	Specimen together in a box with SMNS 52478, without its own number, pictured by Schoch et al. (2018) under the same number as a dentary with tricuspid teeth
SMNS 91473	*T. conspicuus*	Cervical vertebra	Öhlmühle near Crailsheim, Germany	Lowermost Lettenkeuper, Grenzbonebed	von Huene 1907-1908 (plate 96, fig. 5), Spiekman and Scheyer 2019 (supp. tab. 1)	
SMNS 91891	*Tanystropheus?*	Tooth	Vellberg-Eschenau, Germany	Upper Lettenkeuper, Layer 6a of Untere Graue Mergel	Spiekman and Scheyer 2019 (supp. tab. 1)	
SMNS 97273	*T. conspicuus*	Cervical vertebra	Dörfles near Kronach, Germany	Upper Muschelkalk	Emmert and von Horstig 1972 (plate 2, fig. 4), Wild 1973 (fig. 43)	Unaccesioned, formerly F. Martin's collection
SMNS 97801	*T. conspicuus*	Cervical vertebra	Kupferzell, Germany	Lower Lettenkeuper, Vitriolschiefer	This study	Unaccesioned, formerly F. Gustke's collection
SMNS 9863	*T. conspicuus*	Cervical vertebra	Crailsheim, Germany	Upper Muschelkalk, Discoceratitenschichten	von Huene 1907-1908 (plate 96, fig. 1), Wild 1973 (fig. 43), Spiekman and Scheyer 2019 (supp. tab. 1)	
SMNS uncatalogued	*T. conspicuus*	Cervical vertebra (10th)	Crailsheim, Germany	Upper Muschelkalk	Jaquier and Scheyer 2017	Specimen label notes "?Beleg zu von Huene? aus alten beständen"
SMNS uncatalogued	*Tanystropheus?*	Caudal vertebra	Kübelhof near Kulmbach, Germany	Upper Muschelkalk?	This study	Unaccesioned, formerly F. Martin's collection
SMNS uncatalogued	*T. conspicuus*	Caudal vertebra (anterior)	Roßlach near Kronach, Germany	Upper Muschelkalk?	This study	Unaccesioned, formerly F. Martin's collection
SMNS uncatalogued	*Tanystropheus?*	Caudal vertebra (posterior)	Kübelhof near Kulmbach, Germany	Upper Muschelkalk?	This study	Unaccesioned, formerly F. Martin's collection

SMNS uncatalogued	*T. conspicuus*	Cervical vertebra	Dörfles near Kronach, Germany	Upper Muschelkalk?	This study	Unaccesioned, formerly F. Martin's collection
SMNS uncatalogued	*Tanystropheus?*	Cervical vertebra	Kübelhof near Kulmbach, Germany	Upper Muschelkalk?	This study	Unaccesioned, formerly F. Martin's collection
SMNS uncatalogued	*T. conspicuus*	Cervical vertebra (11th)	Dörfles near Kronach, Germany	Upper Muschelkalk?	This study	Unaccesioned, formerly F. Martin's collection
SMNS uncatalogued	*T. conspicuus*	Cervical vertebra (12th)	Dörfles near Kronach, Germany	Upper Muschelkalk?	This study	Unaccesioned, formerly F. Martin's collection
SMNS uncatalogued	*T. conspicuus*	Coracoid	Roßlach near Kronach, Germany	Upper Muschelkalk?	This study	Unaccesioned, formerly F. Martin's collection
SMNS uncatalogued	*T. conspicuus*	Dorsal rib (3rd)	Dörfles near Kronach, Germany	Upper Muschelkalk?	This study	Unaccesioned, formerly F. Martin's collection
SMNS uncatalogued	*Tanystropheus?*	Dorsal vertebra	Unterrodach, Germany	Upper Muschelkalk?	This study	Unaccesioned, formerly F. Martin's collection
SMNS uncatalogued	*Tanystropheus?*	Dorsal vertebra	Unterrodach, Germany	Upper Muschelkalk?	This study	Unaccesioned, formerly F. Martin's collection
SMNS uncatalogued	*Tanystropheus?*	Dorsal vertebra	Unterrodach, Germany	Upper Muschelkalk?	This study	Unaccesioned, formerly F. Martin's collection
SMNS uncatalogued	*Tanystropheus?*	Dorsal vertebra	Unterrodach, Germany	Upper Muschelkalk?	This study	Unaccesioned, formerly F. Martin's collection
SMNS uncatalogued	*T. conspicuus*	Tooth	Neidenfels, Germany	Lowermost Lettenkeuper, Grenzbonebed	This study	"Collection Diem"
SMNS uncatalogued	*Tanystropheus?*	Tooth	Roßlach near Kronach, Germany	Upper Muschelkalk?	This study	Unaccesioned, formerly F. Martin's collection
SNSB-BSPG 1954 VI 37	*T. conspicuus*	Tooth	Crailsheim, Germany	Lowermost Lettenkeuper, Grenzbonebed	This study	
SNSB-BSPG 1973 VII 587	*T. conspicuus*	Tooth	Crailsheim, Germany	Lowermost Lettenkeuper, Grenzbonebed	This study	
SNSB-BSPG 1973 VII 76	*T. conspicuus*	Tooth	Heldenmühle near Crailsheim, Germany	Lowermost Lettenkeuper, Grenzbonebed	This study	
SNSB-BSPG 1988 I 32	*T. conspicuus*	Cervical vertebra	Bindlach, Germany	Upper Muschelkalk	Wild 1973 (fig. 42)	
SNSD BaTr 1	*T. conspicuus*	Cervical vertebra	Bayreuth, Germany	Upper Muschelkalk	This study	
SUT uncatalogued	*Tanystropheus?*	Cervical vertebra? (posterior part)	Crailsheim, Germany	Lowermost Lettenkeuper, Grenzbonebed?	This study	
SUT uncatalogued	*T. conspicuus*	Femur	Bindlach, Germany	Upper Muschelkalk	This study	

SUT uncatalogued	*T. conspicuus*	Tooth	Crailsheim, Germany	Lowermost Lettenkeuper, Grenzbonebed?	This study	
SUT uncatalogued	*T. conspicuus*	Tooth	Crailsheim, Germany	Lowermost Lettenkeuper, Grenzbonebed?	This study	
U-MO BT 2171	*T. conspicuus*	Caudal vertebra (anterior)	Bindlach, Germany	Upper Muschelkalk	Braun 1840 (plate 20, fig. 3), Wild 1973 (fig. 59), Diedrich 2012 (fig. 14, 11), Spiekman and Scheyer 2019 (supp. tab. 1)	
U-MO BT 3079	*T. conspicuus*	Humerus	Bayreuth, Germany	Upper Muschelkalk	Braun 1840 (plate 11, fig. 6), von Meyer 1847-1855 (plate 49, fig. 3), Diedrich 2012 (fig. 14, 14)	
U-MO BT 732	*T. conspicuus*	Cervical vertebra	Bindlacher Berg, Germany	Upper Muschelkalk	von Meyer 1847-1855 (plate 30, fig. 5), von Huene 1907-1908 (fig. 351), Wild 1973 (fig. 39), Diedrich 2012 (fig. 14, 2), Spiekman & Scheyer 2019 (fig. 6A)	Paralectotype
U-MO BT 733	*T. conspicuus*	Cervical vertebra	Bindlacher Berg, Germany	Upper Muschelkalk	Braun 1840 (plate 11, fig. 1), von Meyer 1847-1855 (plate 30, fig. 1), von Huene 1907-1908 (plate 95, fig. 2), Broili 1915 (p. 52-53), Peyer 1931 (fig. 2), Shmidt 1938 (fig. 1188a:c), Kuhn 1971 (plate 21a, fig. 1c), Wild 1973 (fig. 41), Spiekman & Scheyer 2019 (fig. 6B), Spiekman et al. 2021 (figs 24B, 26B)	Paralectotype
U-MO BT 734	*T. conspicuus*	Cervical vertebra	Bindlacher Berg, Germany	Upper Muschelkalk	Braun 1840 (plate 11, fig. 1), von Meyer 1847-1855 (plate 30, fig. 1), von Huene 1907-1908 (plate 95, fig. 2), Broili 1915 (p. 52-53), Spiekman and Scheyer 2019 (supp. tab. 1)	Paralectotype

U-MO BT 735	*T. conspicuus*	Caudal vertebra (anterior)	Bindlacher Berg, Germany	Upper Muschelkalk	Wild 1973 (fig. 58), Spiekman and Scheyer 2019 (supp. tab. 1)	
U-MO BT 736	*T. conspicuus*	Cervical vertebra (10th)	Bindlacher Berg, Germany	Upper Muschelkalk	von Huene 1907-1908 (plate 95, fig. 3), Wild 1973 (fig. 46), Wild 1975 (fig. 1), Wild 1977 (fig. 1a), Diedrich 2012 (fig. 14, 5), Spiekman & Scheyer 2019 (fig. 6C)	
U-MO BT 737	*T. conspicuus*	Cervical vertebra (10th)	Bindlacher Berg, Germany	Upper Muschelkalk	Braun 1840 (plate 9, fig. 5), von Meyer 1847-1855 (plate 46, fig. 1), von Huene 1907-1908 (plate 95, fig. 4), Spiekman & Scheyer 2019 (fig. 6D)	Paralectotype
U-MO BT 738	*T. conspicuus*	Cervical vertebra (11th)	Bindlacher Berg, Germany	Upper Muschelkalk	von Huene 1907-1908 (plate 94, figs 6,7; plate 96, fig. 9), Broili 1915 (plate 2, figs 2-3; 3), Edinger 1924 (fig. 2), Schmidt 1928 (fig. 1188b), Kuhn 1971 (plate 41b, fig. 12), Spiekman & Scheyer 2019 (fig. 6F), Rytel et al. 2024b (fig. 8F)	
U-MO BT 739	*T. conspicuus*	Cervical vertebra (9th?)	Bindlacher Berg, Germany	Upper Muschelkalk	von Huene 1907-1908 (plate 94, fig. 9), Wild 1973 (fig. 45), Diedrich 2012 (fig. 14, 4), Spiekman & Scheyer 2019 (fig. 6E)	

U-MO BT 740	*T. conspicuus*	Cervical vertebra	Bindlacher Berg, Germany	Upper Muschelkalk	von Meyer 1847-1855 (plate 30, figs 2-4), Zittel 1887-1890 (fig. 514), von Huene 1907-1908 (plate 95, fig. 1), Broili 1915 (plate 2, fig. 1), Schmidt 1928 (fig. 1188a), Peyer 1931 (fig. 1), Peyer 1937b (fig. 1), Peyer 1944 (fig. 49), Peyer & Kuhn-Schnyder 1955 (figs 1, 21), von Huene 1956 (fig. 657e), Romer 1956 (122M), Kuhn 1969 (plate. 19, fig. 18), Kuhn 1971 (plate 21, fig. 11; 41b, fig. 11), Wild 1973 (fig. 47), Diedrich 2012 (fig. 14, 3), Spiekman & Scheyer 2019 (fig. 5), Spiekman et al. 2021 (fig. 25B), Sues and Schoch 2025 (fig. 8C)	Lectotype
U-MO BT 741	*T. conspicuus*	Dorsal vertebra	Laineck, Germany	Upper Muschelkalk, *semipartitus*-Zone	Braun 1840 (plate 21, fig. 6), von Huene 1907-1908 (plate 91, fig. 7), Wild 1977 (fig. 1b), Wild 1973 (fig. 53), Diedrich 2012 (fig. 14, 7), Spiekman and Scheyer 2019 (supp. tab. 1)	Syntype of *Thecodontosaurus latespinatus*
U-MO uncatalogued	*T. conspicuus*	Cervical vertebra	Bayreuth, Germany	Upper Muschelkalk	This study	
U-MO uncatalogued	*T. conspicuus*	Cervical vertebra	Bayreuth, Germany	Upper Muschelkalk	This study	
U-MO uncatalogued	*T. conspicuus*	Cervical vertebra	Bayreuth, Germany	Upper Muschelkalk	This study	
U-MO uncatalogued	*T. conspicuus*	Cervical vertebra	Bayreuth, Germany	Upper Muschelkalk	This study	
U-MO uncatalogued	*T. conspicuus*	Cervical vertebra	Bayreuth, Germany	Upper Muschelkalk	This study	
U-MO uncatalogued	*T. conspicuus*	Cervical vertebra (11th)	Bayreuth, Germany	Upper Muschelkalk	This study	
U-MO uncatalogued	*T. conspicuus*	Femur	Bayreuth, Germany	Upper Muschelkalk	This study	
U-MO uncatalogued	*T. conspicuus*	Femur (distal head)	Bindlach, Germany	Upper Muschelkalk	This study	

U-MO uncatalogued	*T. conspicuus*	Postcloacal bone (morphotype Z)	Bayreuth, Germany	Upper Muschelkalk	This study	
U-MO uncatalogued	*T. conspicuus*	Tooth	Bayreuth, Germany	Upper Muschelkalk	This study	
U-MO uncatalogued	*T. conspicuus*	Tooth	Bayreuth?, Germany	Upper Muschelkalk?	This study	
WMNM P 117508	*T. conspicuus*	Cervical vertebra	Willebadessen, Niesen	Upper Muschelkalk?	Schwermann et al. 2025	
WMNM P 19420	*T. conspicuus*	Ilium	Horn-Bad Meinberg, Germany	Upper Muschelkalk	This study	
ZPAL P. VIII (partim)	*Tanystropheus?*	Cervical vertebra (postzygapophysis with a long epiphysis)	Kościelec, Poland	Lowermost Lettenkeuper, Grenzbonebed?	This study	
ZPAL V. 36/100	*T. conspicuus*	Six semiarticulated cervical vertebrae	Miedary, Poland	Lower Lettenkeuper	Rytel et al. 2024a	
ZPAL V. 36/1000	*T. conspicuus*	Cervical rib (12th)	Miedary, Poland	Lower Lettenkeuper	This study	
ZPAL V. 36/1001	*T. conspicuus*	Cervical rib (12th)	Miedary, Poland	Lower Lettenkeuper	This study	
ZPAL V. 36/1002	*T. conspicuus*	Cervical vertebra (12th)	Miedary, Poland	Lower Lettenkeuper	This study	
ZPAL V. 36/1003	*T. conspicuus*	Femur	Miedary, Poland	Lower Lettenkeuper	This study	
ZPAL V. 36/1004	*T. conspicuus*	Humerus	Miedary, Poland	Lower Lettenkeuper	This study	
ZPAL V. 36/1006	*T. conspicuus*	Ischium	Miedary, Poland	Lower Lettenkeuper	This study	
ZPAL V. 36/1007	*T. conspicuus*	Ischium	Miedary, Poland	Lower Lettenkeuper	This study	
ZPAL V. 36/1008	*T. conspicuus*	Pubis	Miedary, Poland	Lower Lettenkeuper	This study	
ZPAL V. 36/1009	*T. conspicuus*	Pubis	Miedary, Poland	Lower Lettenkeuper	This study	
ZPAL V. 36/101	*T. conspicuus*	Cervical vertebra	Miedary, Poland	Lower Lettenkeuper	Czepiński et al. 2023 (fig. 6A), Rytel et al. 2024a, Rytel et al. 2024b (figs. 1A; 5A,B,D)	
ZPAL V. 36/1010	*T. conspicuus*	Scapula	Miedary, Poland	Lower Lettenkeuper	This study	
ZPAL V. 36/1011	*T. conspicuus*	Cervical rib (11th)	Miedary, Poland	Lower Lettenkeuper	This study	
ZPAL V. 36/1012	*T. conspicuus*	Cervical ribs (2)	Miedary, Poland	Lower Lettenkeuper	This study	
ZPAL V. 36/1013	*T. conspicuus*	Cervical ribs (2)	Miedary, Poland	Lower Lettenkeuper	This study	
ZPAL V. 36/1014	*T. conspicuus*	Ischium	Miedary, Poland	Lower Lettenkeuper	This study	
ZPAL V. 36/1015	*T. conspicuus*	Pubis, dorsal vertebra	Miedary, Poland	Lower Lettenkeuper	This study	
ZPAL V. 36/1016/1	*T. conspicuus*	Cervical vertebra	Miedary, Poland	Lower Lettenkeuper	Rytel et al. 2024b (fig. 1C)	
ZPAL V. 36/1016/2	*T. conspicuus*	Cervical vertebra	Miedary, Poland	Lower Lettenkeuper	Rytel et al. 2024b (fig. 1D)	
ZPAL V. 36/1017	*T. conspicuus*	Cervical vertebrae (2)	Miedary, Poland	Lower Lettenkeuper	This study	
ZPAL V. 36/1018	*T. conspicuus*	Cervical vertebrae (2), dorsal vertebra	Miedary, Poland	Lower Lettenkeuper	This study	
ZPAL V. 36/1019	*T. conspicuus*	Cervical rib (11th)	Miedary, Poland	Lower Lettenkeuper	This study	

ZPAL V. 36/102	*T. conspicuus*	Cervical vertebra (9th)	Miedary, Poland	Lower Lettenkeuper	Rytel et al. 2024a, Rytel et al. 2024b (fig. 5C,E,F)	
ZPAL V. 36/1020	*T. conspicuus*	Pubis	Miedary, Poland	Lower Lettenkeuper	This study	
ZPAL V. 36/1021	*T. conspicuus*	Dorsal vertebra	Miedary, Poland	Lower Lettenkeuper	This study	
ZPAL V. 36/1022	*T. conspicuus*	Dorsal vertebra	Miedary, Poland	Lower Lettenkeuper	This study	
ZPAL V. 36/1023	*T. conspicuus*	Dorsal vertebra	Miedary, Poland	Lower Lettenkeuper	This study	
ZPAL V. 36/1024	*T. conspicuus*	Cervical rib (13th)	Miedary, Poland	Lower Lettenkeuper	This study	
ZPAL V. 36/1025	*T. conspicuus*	Cervical rib (12th), cervical ribs (2)	Miedary, Poland	Lower Lettenkeuper	This study	
ZPAL V. 36/1026	*T. conspicuus*	Dorsal rib (1st?)	Miedary, Poland	Lower Lettenkeuper	This study	
ZPAL V. 36/1027	*T. conspicuus*	Cervical rib (12th?)	Miedary, Poland	Lower Lettenkeuper	This study	
ZPAL V. 36/1028	*T. conspicuus*	Cervical rib (posterior)	Miedary, Poland	Lower Lettenkeuper	This study	
ZPAL V. 36/1029	*T. conspicuus*	Cervical rib (posterior)	Miedary, Poland	Lower Lettenkeuper	This study	
ZPAL V. 36/103	*T. conspicuus*	Cervical vertebra	Miedary, Poland	Lower Lettenkeuper	Rytel et al. 2024a	
ZPAL V. 36/1030	*T. conspicuus*	Dorsal rib (2nd?)	Miedary, Poland	Lower Lettenkeuper	This study	
ZPAL V. 36/1031	*T. conspicuus*	Dorsal rib (2nd?)	Miedary, Poland	Lower Lettenkeuper	This study	
ZPAL V. 36/1032	*T. conspicuus*	Dorsal rib (1st)	Miedary, Poland	Lower Lettenkeuper	This study	
ZPAL V. 36/1033	*T. conspicuus*	Dorsal vertebra	Miedary, Poland	Lower Lettenkeuper	This study	
ZPAL V. 36/1034	*T. conspicuus*	Cervical vertebra	Miedary, Poland	Lower Lettenkeuper	This study	
ZPAL V. 36/1035	*T. conspicuus*	Dorsal vertebrae (3), caudal vertebra (anterior), tooth	Miedary, Poland	Lower Lettenkeuper	This study	
ZPAL V. 36/1036	*T. conspicuus*	Dorsal vertebra	Miedary, Poland	Lower Lettenkeuper	Rytel et al. 2024b (fig. 6D)	
ZPAL V. 36/1037	*T. conspicuus*	Sacral vertebra	Miedary, Poland	Lower Lettenkeuper	This study	
ZPAL V. 36/1038	*T. conspicuus*	Cervical rib (11th)	Miedary, Poland	Lower Lettenkeuper	This study	
ZPAL V. 36/1039	*T. conspicuus*	Cervical rib	Miedary, Poland	Lower Lettenkeuper	This study	
ZPAL V. 36/104	*T. conspicuus*	Cervical vertebra (10th)	Miedary, Poland	Lower Lettenkeuper	Rytel et al. 2024a, Rytel et al. 2024b	
ZPAL V. 36/1040	*T. conspicuus*	Cervical rib	Miedary, Poland	Lower Lettenkeuper	This study	
ZPAL V. 36/1041	*T. conspicuus*	Cervical rib	Miedary, Poland	Lower Lettenkeuper	This study	
ZPAL V. 36/1042	*T. conspicuus*	Cervical rib	Miedary, Poland	Lower Lettenkeuper	This study	
ZPAL V. 36/1043	*T. conspicuus*	Cervical rib	Miedary, Poland	Lower Lettenkeuper	This study	
ZPAL V. 36/1044	*T. conspicuus*	Dorsal vertebra	Miedary, Poland	Lower Lettenkeuper	This study	
ZPAL V. 36/1045	*T. conspicuus*	Caudal vertebra (anterior)	Miedary, Poland	Lower Lettenkeuper	This study	
ZPAL V. 36/1046	*T. conspicuus*	Dorsal vertebra	Miedary, Poland	Lower Lettenkeuper	This study	

ZPAL V. 36/1047	*T. conspicuus*	Dorsal vertebra	Miedary, Poland	Lower Lettenkeuper	This study	
ZPAL V. 36/1048	*T. conspicuus*	Dorsal vertebra	Miedary, Poland	Lower Lettenkeuper	This study	
ZPAL V. 36/1049	*T. conspicuus*	Cervical vertebra (13th)	Miedary, Poland	Lower Lettenkeuper	This study	
ZPAL V. 36/105	*T. conspicuus*	Cervical vertebra (10th)	Miedary, Poland	Lower Lettenkeuper	Rytel et al. 2024a, Rytel et al. 2024b	
ZPAL V. 36/1050	*T. conspicuus*	Caudal vertebra (anterior)	Miedary, Poland	Lower Lettenkeuper	This study	
ZPAL V. 36/1051	*T. conspicuus*	Dorsal vertebra?	Miedary, Poland	Lower Lettenkeuper	This study	
ZPAL V. 36/1052	*T. conspicuus*	Sacral vertebra	Miedary, Poland	Lower Lettenkeuper	This study	
ZPAL V. 36/1053	*T. conspicuus*	Dorsal vertebra	Miedary, Poland	Lower Lettenkeuper	This study	
ZPAL V. 36/1054	*T. conspicuus*	Dorsal vertebra?	Miedary, Poland	Lower Lettenkeuper	This study	
ZPAL V. 36/1055	*T. conspicuus*	Dorsal vertebra	Miedary, Poland	Lower Lettenkeuper	This study	
ZPAL V. 36/1056	*T. conspicuus*	Dorsal vertebra	Miedary, Poland	Lower Lettenkeuper	This study	
ZPAL V. 36/1057	*T. conspicuus*	Dorsal vertebra	Miedary, Poland	Lower Lettenkeuper	This study	
ZPAL V. 36/1058	*T. conspicuus*	Dorsal vertebra	Miedary, Poland	Lower Lettenkeuper	This study	
ZPAL V. 36/1059	*T. conspicuus*	Cervical vertebra (10th)	Miedary, Poland	Lower Lettenkeuper	This study	
ZPAL V. 36/106	*T. conspicuus*	Cervical vertebra (11th)	Miedary, Poland	Lower Lettenkeuper	Rytel et al. 2024a, Rytel et al. 2024b (fig. 6A,E,I)	
ZPAL V. 36/1061	*T. conspicuus*	Scapula	Miedary, Poland	Lower Lettenkeuper	This study	
ZPAL V. 36/1062	*T. conspicuus*	Coracoid	Miedary, Poland	Lower Lettenkeuper	This study	
ZPAL V. 36/1063	*T. conspicuus*	Caudal vertebra (anterior)	Miedary, Poland	Lower Lettenkeuper	This study	
ZPAL V. 36/1064	*T. conspicuus*	Femur	Miedary, Poland	Lower Lettenkeuper	This study	
ZPAL V. 36/1065	*T. conspicuus*	Femur	Miedary, Poland	Lower Lettenkeuper	This study	
ZPAL V. 36/1066	*T. conspicuus*	Humerus	Miedary, Poland	Lower Lettenkeuper	This study	
ZPAL V. 36/1067	*T. conspicuus*	Caudal vertebra (posterior)	Miedary, Poland	Lower Lettenkeuper	This study	
ZPAL V. 36/1068	*T. conspicuus*	Caudal vertebra (anterior)	Miedary, Poland	Lower Lettenkeuper	This study	
ZPAL V. 36/1069	*T. conspicuus*	Cervical vertebra	Miedary, Poland	Lower Lettenkeuper	This study	
ZPAL V. 36/107	*T. conspicuus*	Cervical vertebra (11th)	Miedary, Poland	Lower Lettenkeuper	Rytel et al. 2024a, Rytel et al. 2024b	
ZPAL V. 36/1070	*T. conspicuus*	Caudal vertebra (posterior)	Miedary, Poland	Lower Lettenkeuper	This study	
ZPAL V. 36/1071	*T. conspicuus*	Cervical vertebra	Miedary, Poland	Lower Lettenkeuper	Rytel et al. 2024b	
ZPAL V. 36/1072	*T. conspicuus*	Cervical vertebra	Miedary, Poland	Lower Lettenkeuper	This study	
ZPAL V. 36/1073	*T. conspicuus*	Cervical vertebra (10th)	Miedary, Poland	Lower Lettenkeuper	This study	
ZPAL V. 36/1074	*T. conspicuus*	Dorsal vertebra?	Miedary, Poland	Lower Lettenkeuper	This study	
ZPAL V. 36/1075	*T. conspicuus*	Dorsal vertebra?	Miedary, Poland	Lower Lettenkeuper	This study	
ZPAL V. 36/1076	*T. conspicuus*	Dorsal vertebra?	Miedary, Poland	Lower Lettenkeuper	This study	

ZPAL V. 36/1077	*T. conspicuus*	Cervical vertebra (11th)	Miedary, Poland	Lower Lettenkeuper	This study	
ZPAL V. 36/1078	*T. conspicuus*	Cervical vertebra	Miedary, Poland	Lower Lettenkeuper	This study	
ZPAL V. 36/1079	*T. conspicuus*	Coracoid	Miedary, Poland	Lower Lettenkeuper	This study	
ZPAL V. 36/108	*T. conspicuus*	Cervical vertebra (12th)	Miedary, Poland	Lower Lettenkeuper	Rytel et al. 2024a, Rytel et al. 2024b (fig. 6B,F,J)	
ZPAL V. 36/1080	*T. conspicuus*	Coracoid	Miedary, Poland	Lower Lettenkeuper	This study	
ZPAL V. 36/1081	*T. conspicuus*	Caudal vertebra (anterior)	Miedary, Poland	Lower Lettenkeuper	This study	
ZPAL V. 36/1082	*T. conspicuus*	Scapula	Miedary, Poland	Lower Lettenkeuper	This study	
ZPAL V. 36/1083	*T. conspicuus*	Scapula	Miedary, Poland	Lower Lettenkeuper	This study	
ZPAL V. 36/1084	*T. conspicuus*	Ilium	Miedary, Poland	Lower Lettenkeuper	This study	
ZPAL V. 36/1085	*T. conspicuus*	Ischium	Miedary, Poland	Lower Lettenkeuper	This study	
ZPAL V. 36/1086	*T. conspicuus*	Femur, cervical vertebra (10th), cervical vertebra, pubis, dorsal vertebra, caudal vertebra (anterior)	Miedary, Poland	Lower Lettenkeuper	This study	
ZPAL V. 36/1087	*T. conspicuus*	Cervical vertebra	Miedary, Poland	Lower Lettenkeuper	This study	
ZPAL V. 36/1088	*T. conspicuus*	Cervical vertebra (11th)	Miedary, Poland	Lower Lettenkeuper	This study	
ZPAL V. 36/1089	*T. conspicuus*	Cervical vertebrae (2)	Miedary, Poland	Lower Lettenkeuper	This study	
ZPAL V. 36/109	*T. conspicuus*	Cervical vertebra (12th)	Miedary, Poland	Lower Lettenkeuper	Rytel et al. 2024a	
ZPAL V. 36/1090	*T. conspicuus*	Cervical vertebra	Miedary, Poland	Lower Lettenkeuper	Rytel et al. 2024b	
ZPAL V. 36/1091	*T. conspicuus*	Dorsal vertebrae (2)	Miedary, Poland	Lower Lettenkeuper	This study	
ZPAL V. 36/1092	*T. conspicuus*	Cervical rib	Miedary, Poland	Lower Lettenkeuper	This study	
ZPAL V. 36/1093	*T. conspicuus*	Dorsal rib (2nd)	Miedary, Poland	Lower Lettenkeuper	This study	
ZPAL V. 36/1094	*T. conspicuus*	Dorsal rib (anterior)	Miedary, Poland	Lower Lettenkeuper	This study	
ZPAL V. 36/1095	*T. conspicuus*	Dorsal vertebra	Miedary, Poland	Lower Lettenkeuper	This study	
ZPAL V. 36/1096	*T. conspicuus*	Dorsal rib (anterior)	Miedary, Poland	Lower Lettenkeuper	This study	
ZPAL V. 36/1097	*T. conspicuus*	Dorsal rib (anterior)	Miedary, Poland	Lower Lettenkeuper	This study	
ZPAL V. 36/1098	*T. conspicuus*	Coracoid	Miedary, Poland	Lower Lettenkeuper	This study	
ZPAL V. 36/1099	*T. conspicuus*	Cervical vertebra (10th)	Miedary, Poland	Lower Lettenkeuper	Rytel et al. 2024b (fig. 8D,G)	
ZPAL V. 36/110	*T. conspicuus*	Cervical vertebra (13th)	Miedary, Poland	Lower Lettenkeuper	Rytel et al. 2024a, Rytel et al. 2024b (figs. 6C,G,K; 10)	
ZPAL V. 36/1100	*T. conspicuus*	Scapula	Miedary, Poland	Lower Lettenkeuper	This study	
ZPAL V. 36/1101	*T. conspicuus*	Coracoid, cervical rib	Miedary, Poland	Lower Lettenkeuper	This study	
ZPAL V. 36/1102	*T. conspicuus*	Coracoid, cervical vertebra	Miedary, Poland	Lower Lettenkeuper	This study	

ZPAL V. 36/1103	*T. conspicuus*	Ischium	Miedary, Poland	Lower Lettenkeuper	This study	
ZPAL V. 36/1104	*T. conspicuus*	Dorsal vertebra	Miedary, Poland	Lower Lettenkeuper	This study	
ZPAL V. 36/1105	*T. conspicuus*	Cervical rib (11th)	Miedary, Poland	Lower Lettenkeuper	This study	
ZPAL V. 36/1106	*T. conspicuus*	Cervical rib	Miedary, Poland	Lower Lettenkeuper	This study	
ZPAL V. 36/1107	*T. conspicuus*	Sacral vertebra	Miedary, Poland	Lower Lettenkeuper	This study	
ZPAL V. 36/1108	*T. conspicuus*	Dorsal rib (1st)	Miedary, Poland	Lower Lettenkeuper	This study	
ZPAL V. 36/1109	*T. conspicuus*	Dorsal vertebra with articulated ribs	Miedary, Poland	Lower Lettenkeuper	This study	
ZPAL V. 36/111	*T. conspicuus*	Dorsal vertebra	Miedary, Poland	Lower Lettenkeuper	This study	
ZPAL V. 36/1110	*T. conspicuus*	Cervical vertebra	Miedary, Poland	Lower Lettenkeuper	This study	
ZPAL V. 36/1111	*T. conspicuus*	Tooth	Miedary, Poland	Lower Lettenkeuper	This study	
ZPAL V. 36/1112	*T. conspicuus*	Teeth (2)	Miedary, Poland	Lower Lettenkeuper	This study	
ZPAL V. 36/1113	*T. conspicuus*	Dorsal vertebra	Miedary, Poland	Lower Lettenkeuper	This study	
ZPAL V. 36/1114	*T. conspicuus*	Cervical ribs (2)	Miedary, Poland	Lower Lettenkeuper	This study	
ZPAL V. 36/1115	*T. conspicuus*	Coracoid?	Miedary, Poland	Lower Lettenkeuper	This study	
ZPAL V. 36/1116	*T. conspicuus*	Cervical vertebra	Miedary, Poland	Lower Lettenkeuper	This study	
ZPAL V. 36/1117	*T. conspicuus*	Caudal vertebra (anterior)	Miedary, Poland	Lower Lettenkeuper	This study	
ZPAL V. 36/1118	*T. conspicuus*	Femur	Miedary, Poland	Lower Lettenkeuper	This study	
ZPAL V. 36/1119	*T. conspicuus*	Coracoid	Miedary, Poland	Lower Lettenkeuper	This study	
ZPAL V. 36/112	*T. conspicuus*	Dorsal vertebra	Miedary, Poland	Lower Lettenkeuper	Rytel et al. 2024b (fig. 6H,L)	
ZPAL V. 36/1120	*T. conspicuus*	Two dorsal vertebrae in articulation, pubis	Miedary, Poland	Lower Lettenkeuper	This study	
ZPAL V. 36/1121	*T. conspicuus*	Caudal vertebra (anterior)	Miedary, Poland	Lower Lettenkeuper	This study	
ZPAL V. 36/1122	*T. conspicuus*	Dorsal vertebra	Miedary, Poland	Lower Lettenkeuper	This study	
ZPAL V. 36/1123	*T. conspicuus*	Cervical vertebra	Miedary, Poland	Lower Lettenkeuper	This study	
ZPAL V. 36/1124	*T. conspicuus*	Caudal vertebra (anterior)	Miedary, Poland	Lower Lettenkeuper	This study	
ZPAL V. 36/1125	*T. conspicuus*	Cervical vertebra	Miedary, Poland	Lower Lettenkeuper	This study	
ZPAL V. 36/1126	*T. conspicuus*	Tooth	Miedary, Poland	Lower Lettenkeuper	This study	
ZPAL V. 36/1127	*T. conspicuus*	ilium	Miedary, Poland	Lower Lettenkeuper	This study	
ZPAL V. 36/1128	*T. conspicuus*	Cervical vertebra (11th)	Miedary, Poland	Lower Lettenkeuper	This study	
ZPAL V. 36/1129	*T. conspicuus*	Cervical vertebra	Miedary, Poland	Lower Lettenkeuper	This study	
ZPAL V. 36/113	*T. conspicuus*	Caudal vertebra (anterior)	Miedary, Poland	Lower Lettenkeuper	This study	
ZPAL V. 36/1130	*T. conspicuus*	Dorsal vertebra	Miedary, Poland	Lower Lettenkeuper	This study	

ZPAL V. 36/1131	*T. conspicuus*	Scapula	Miedary, Poland	Lower Lettenkeuper	This study	
ZPAL V. 36/1132	*T. conspicuus*	Cervical vertebra (12th)	Miedary, Poland	Lower Lettenkeuper	This study	
ZPAL V. 36/1133	*T. conspicuus*	Cervical vertebra (13th)	Miedary, Poland	Lower Lettenkeuper	This study	
ZPAL V. 36/1134	*T. conspicuus*	Sacral vertebra?	Miedary, Poland	Lower Lettenkeuper	This study	
ZPAL V. 36/1135	*T. conspicuus*	Caudal vertebra (posterior)	Miedary, Poland	Lower Lettenkeuper	This study	
ZPAL V. 36/1136	*T. conspicuus*	Cervical vertebra	Miedary, Poland	Lower Lettenkeuper	This study	
ZPAL V. 36/1137	*T. conspicuus*	Postcloacal bone	Miedary, Poland	Lower Lettenkeuper	This study	
ZPAL V. 36/1138	*T. conspicuus*	Postcloacal bone	Miedary, Poland	Lower Lettenkeuper	This study	
ZPAL V. 36/1139	*T. conspicuus*	Postcloacal bone	Miedary, Poland	Lower Lettenkeuper	This study	
ZPAL V. 36/114	*T. conspicuus*	Caudal vertebra (anterior)	Miedary, Poland	Lower Lettenkeuper	This study	
ZPAL V. 36/1140	*T. conspicuus*	Postcloacal bone	Miedary, Poland	Lower Lettenkeuper	This study	
ZPAL V. 36/1141	*T. conspicuus*	Postcloacal bone	Miedary, Poland	Lower Lettenkeuper	This study	
ZPAL V. 36/1142	*T. conspicuus*	Postcloacal bone	Miedary, Poland	Lower Lettenkeuper	This study	
ZPAL V. 36/1143	*T. conspicuus*	Postcloacal bone	Miedary, Poland	Lower Lettenkeuper	This study	
ZPAL V. 36/1144	*T. conspicuus*	Cervical rib (11th)	Miedary, Poland	Lower Lettenkeuper	This study	
ZPAL V. 36/1146	*T. conspicuus (partim)*	Ischium, ilium, cervical vertebra	Miedary, Poland	Lower Lettenkeuper	This study	
ZPAL V. 36/1147	*T. conspicuus*	Postcloacal bone	Miedary, Poland	Lower Lettenkeuper	This study	
ZPAL V. 36/1148	*T. conspicuus*	Postcloacal bone	Miedary, Poland	Lower Lettenkeuper	This study	
ZPAL V. 36/1149	*T. conspicuus*	Postcloacal bone	Miedary, Poland	Lower Lettenkeuper	This study	
ZPAL V. 36/115	*T. conspicuus*	Caudal vertebra (posterior)	Miedary, Poland	Lower Lettenkeuper	This study	
ZPAL V. 36/1150	*T. conspicuus*	Postcloacal bone	Miedary, Poland	Lower Lettenkeuper	This study	
ZPAL V. 36/1151	*T. conspicuus*	Postcloacal bone	Miedary, Poland	Lower Lettenkeuper	This study	
ZPAL V. 36/1152	*T. conspicuus*	Postcloacal bone	Miedary, Poland	Lower Lettenkeuper	This study	
ZPAL V. 36/1153	*T. conspicuus*	Ilium, cervical vertebra	Miedary, Poland	Lower Lettenkeuper	This study	
ZPAL V. 36/1154	*T. conspicuus*	Dorsal rib (1st)	Miedary, Poland	Lower Lettenkeuper	This study	
ZPAL V. 36/1155	*T. conspicuus*	Dorsal rib	Miedary, Poland	Lower Lettenkeuper	This study	
ZPAL V. 36/1156	*T. conspicuus*	Dorsal rib (anterior)	Miedary, Poland	Lower Lettenkeuper	This study	
ZPAL V. 36/1157	*T. conspicuus*	Dorsal rib?	Miedary, Poland	Lower Lettenkeuper	This study	
ZPAL V. 36/1158	*T. conspicuus*	Dorsal vertebra	Miedary, Poland	Lower Lettenkeuper	This study	
ZPAL V. 36/1159	*T. conspicuus*	Cervical vertebra	Miedary, Poland	Lower Lettenkeuper	This study	
ZPAL V. 36/116	*T. conspicuus*	Caudal vertebra (posterior)	Miedary, Poland	Lower Lettenkeuper	This study	
ZPAL V. 36/1160	*T. conspicuus*	Caudal vertebra (anterior)	Miedary, Poland	Lower Lettenkeuper	This study	
ZPAL V. 36/1161	*T. conspicuus*	Dorsal rib (2nd)	Miedary, Poland	Lower Lettenkeuper	This study	

ZPAL V. 36/1162	*T. conspicuus*	Cervical rib	Miedary, Poland	Lower Lettenkeuper	This study	
ZPAL V. 36/1163	*T. conspicuus*	Ischium	Miedary, Poland	Lower Lettenkeuper	This study	
ZPAL V. 36/1164	*T. conspicuus*	Scapula	Miedary, Poland	Lower Lettenkeuper	This study	
ZPAL V. 36/1165	*T. conspicuus*	Coracoid?	Miedary, Poland	Lower Lettenkeuper	This study	
ZPAL V. 36/1166	*T. conspicuus*	Femur	Miedary, Poland	Lower Lettenkeuper	This study	
ZPAL V. 36/1167	*T. conspicuus*	Cervical vertebra (10th)	Miedary, Poland	Lower Lettenkeuper	This study	
ZPAL V. 36/1168	*T. conspicuus*	Dorsal rib (1st)	Miedary, Poland	Lower Lettenkeuper	This study	
ZPAL V. 36/1169	*T. conspicuus*	Humerus	Miedary, Poland	Lower Lettenkeuper	This study	
ZPAL V. 36/117	*T. conspicuus*	Sacral vertebra	Miedary, Poland	Lower Lettenkeuper	This study	
ZPAL V. 36/1170	*T. conspicuus*	Axis	Miedary, Poland	Lower Lettenkeuper	This study	
ZPAL V. 36/1171	*T. conspicuus*	Cervical vertebra (11th)	Miedary, Poland	Lower Lettenkeuper	This study	
ZPAL V. 36/1172	*T. conspicuus*	Femur	Miedary, Poland	Lower Lettenkeuper	This study	
ZPAL V. 36/1173	*T. conspicuus*	Cervical vertebra	Miedary, Poland	Lower Lettenkeuper	This study	
ZPAL V. 36/1174	*T. conspicuus*	Dorsal rib (anterior)	Miedary, Poland	Lower Lettenkeuper	This study	
ZPAL V. 36/1175	*T. conspicuus*	Cervical vertebra	Miedary, Poland	Lower Lettenkeuper	This study	
ZPAL V. 36/1176	*T. conspicuus*	Fibula	Miedary, Poland	Lower Lettenkeuper	This study	
ZPAL V. 36/1177	*T. conspicuus*	Coracoid	Miedary, Poland	Lower Lettenkeuper	This study	
ZPAL V. 36/1178	*T. conspicuus*	Dorsal rib	Miedary, Poland	Lower Lettenkeuper	This study	
ZPAL V. 36/1179	*T. conspicuus*	Dorsal rib (anterior), cervical vertebra	Miedary, Poland	Lower Lettenkeuper	This study	
ZPAL V. 36/118	*T. conspicuus*	Cervical vertebra (9th)	Miedary, Poland	Lower Lettenkeuper	This study	
ZPAL V. 36/1180	*T. conspicuus*	Dorsal vertebra	Miedary, Poland	Lower Lettenkeuper	This study	
ZPAL V. 36/1181	*T. conspicuus*	Tooth	Miedary, Poland	Lower Lettenkeuper	This study	
ZPAL V. 36/1182	*T. conspicuus*	Tooth	Miedary, Poland	Lower Lettenkeuper	This study	
ZPAL V. 36/1183	*T. conspicuus*	Tooth	Miedary, Poland	Lower Lettenkeuper	This study	
ZPAL V. 36/1185	*T. conspicuus*	Humerus	Miedary, Poland	Lower Lettenkeuper	This study	
ZPAL V. 36/1186	*T. conspicuus*	Caudal vertebra (anterior)	Miedary, Poland	Lower Lettenkeuper	This study	
ZPAL V. 36/1187	*T. conspicuus*	Sacral vertebra	Miedary, Poland	Lower Lettenkeuper	This study	
ZPAL V. 36/1188	*T. conspicuus*	Femur	Miedary, Poland	Lower Lettenkeuper	This study	
ZPAL V. 36/1189	*T. conspicuus*	Coracoid	Miedary, Poland	Lower Lettenkeuper	This study	
ZPAL V. 36/119	*T. conspicuus*	Cervical vertebra	Miedary, Poland	Lower Lettenkeuper	This study	
ZPAL V. 36/1190	*T. conspicuus*	Ilium	Miedary, Poland	Lower Lettenkeuper	This study	
ZPAL V. 36/1191	*T. conspicuus*	Tooth, cervical rib	Miedary, Poland	Lower Lettenkeuper	This study	
ZPAL V. 36/1192	*T. conspicuus*	Cervical vertebra (13th)	Miedary, Poland	Lower Lettenkeuper	This study	

ZPAL V. 36/1193	*T. conspicuus*	Pubis	Miedary, Poland	Lower Lettenkeuper	This study	
ZPAL V. 36/1194	*T. conspicuus*	Femur, dorsal vertebra, caudal vertebra (anterior), pubis	Miedary, Poland	Lower Lettenkeuper	This study	
ZPAL V. 36/1195	*T. conspicuus*	Cervical vertebra	Miedary, Poland	Lower Lettenkeuper	This study	
ZPAL V. 36/1196	*T. conspicuus*	Dorsal vertebra	Miedary, Poland	Lower Lettenkeuper	This study	
ZPAL V. 36/1197	*T. conspicuus*	Cervical vertebra	Miedary, Poland	Lower Lettenkeuper	This study	
ZPAL V. 36/1198	*T. conspicuus*	Scapula	Miedary, Poland	Lower Lettenkeuper	This study	
ZPAL V. 36/1199	*T. conspicuus*	Fibula	Miedary, Poland	Lower Lettenkeuper	This study	
ZPAL V. 36/120	*T. conspicuus*	Cervical vertebra	Miedary, Poland	Lower Lettenkeuper	This study	
ZPAL V. 36/1200	*T. conspicuus*	Tibia	Miedary, Poland	Lower Lettenkeuper	This study	
ZPAL V. 36/1201	*T. conspicuus*	Ilium	Miedary, Poland	Lower Lettenkeuper	This study	
ZPAL V. 36/1202	*T. conspicuus*	Cervical vertebra (9th)	Miedary, Poland	Lower Lettenkeuper	This study	
ZPAL V. 36/1203	*T. conspicuus*	Tooth	Miedary, Poland	Lower Lettenkeuper	This study	
ZPAL V. 36/1204	*T. conspicuus*	Tooth	Miedary, Poland	Lower Lettenkeuper	This study	
ZPAL V. 36/1205	*T. conspicuus*	Tooth	Miedary, Poland	Lower Lettenkeuper	This study	
ZPAL V. 36/1206	*T. conspicuus*	Cervical rib (posterior)	Miedary, Poland	Lower Lettenkeuper	This study	
ZPAL V. 36/1207	*T. conspicuus*	Postcloacal bone	Miedary, Poland	Lower Lettenkeuper	This study	
ZPAL V. 36/1208	*T. conspicuus*	Dorsal rib (anterior)	Miedary, Poland	Lower Lettenkeuper	This study	
ZPAL V. 36/1209	*T. conspicuus*	Cervical vertebra (12th)	Miedary, Poland	Lower Lettenkeuper	This study	
ZPAL V. 36/121	*T. conspicuus*	Ischium	Miedary, Poland	Lower Lettenkeuper	This study	
ZPAL V. 36/1210	*T. conspicuus*	Dentary	Miedary, Poland	Lower Lettenkeuper	This study	
ZPAL V. 36/1211	*T. conspicuus*	Tibia	Miedary, Poland	Lower Lettenkeuper	This study	
ZPAL V. 36/1213	*T. conspicuus*	Maxilla	Miedary, Poland	Lower Lettenkeuper	This study	
ZPAL V. 36/1214	*T. conspicuus*	Tooth	Miedary, Poland	Lower Lettenkeuper	This study	
ZPAL V. 36/1215	*T. conspicuus*	Tooth	Miedary, Poland	Lower Lettenkeuper	This study	
ZPAL V. 36/1216	*T. conspicuus*	Tooth	Miedary, Poland	Lower Lettenkeuper	This study	
ZPAL V. 36/1217	*T. conspicuus*	Tooth	Miedary, Poland	Lower Lettenkeuper	This study	
ZPAL V. 36/1218	*T. conspicuus*	Caudal vertebra (posterior)	Miedary, Poland	Lower Lettenkeuper	This study	
ZPAL V. 36/1219	*T. conspicuus*	Tooth	Miedary, Poland	Lower Lettenkeuper	This study	
ZPAL V. 36/122	*T. conspicuus*	Cervical vertebra	Miedary, Poland	Lower Lettenkeuper	This study	
ZPAL V. 36/1220	*T. conspicuus*	Tooth	Miedary, Poland	Lower Lettenkeuper	This study	
ZPAL V. 36/1221	*T. conspicuus*	Fibula, humerus, femur	Miedary, Poland	Lower Lettenkeuper	This study	
ZPAL V. 36/1222	*T. conspicuus*	Tooth	Miedary, Poland	Lower Lettenkeuper	This study	

ZPAL V. 36/1223	*T. conspicuus*	Tooth	Miedary, Poland	Lower Lettenkeuper	This study	
ZPAL V. 36/1224	*T. conspicuus*	Tooth	Miedary, Poland	Lower Lettenkeuper	This study	
ZPAL V. 36/1225	*T. conspicuus*	Tooth	Miedary, Poland	Lower Lettenkeuper	This study	
ZPAL V. 36/1226	*T. conspicuus*	Tooth	Miedary, Poland	Lower Lettenkeuper	This study	
ZPAL V. 36/1227	*T. conspicuus*	Tooth	Miedary, Poland	Lower Lettenkeuper	This study	
ZPAL V. 36/1228	*T. conspicuus*	Tooth	Miedary, Poland	Lower Lettenkeuper	This study	
ZPAL V. 36/1229	*T. conspicuus*	Tooth	Miedary, Poland	Lower Lettenkeuper	This study	
ZPAL V. 36/123	*T. conspicuus*	Dorsal rib (1st)	Miedary, Poland	Lower Lettenkeuper	This study	
ZPAL V. 36/1230	*T. conspicuus*	Tooth	Miedary, Poland	Lower Lettenkeuper	This study	
ZPAL V. 36/1231	*T. conspicuus*	Tooth	Miedary, Poland	Lower Lettenkeuper	This study	
ZPAL V. 36/1232	*T. conspicuus*	Tooth	Miedary, Poland	Lower Lettenkeuper	This study	
ZPAL V. 36/1233	*T. conspicuus*	Tooth	Miedary, Poland	Lower Lettenkeuper	This study	
ZPAL V. 36/1234	*T. conspicuus*	Tooth	Miedary, Poland	Lower Lettenkeuper	This study	
ZPAL V. 36/1235	*T. conspicuus*	Tooth	Miedary, Poland	Lower Lettenkeuper	This study	
ZPAL V. 36/1236	*T. conspicuus*	Tooth	Miedary, Poland	Lower Lettenkeuper	This study	
ZPAL V. 36/1237	*T. conspicuus*	Tooth	Miedary, Poland	Lower Lettenkeuper	This study	
ZPAL V. 36/1238	*T. conspicuus*	Tooth	Miedary, Poland	Lower Lettenkeuper	This study	
ZPAL V. 36/1239	*T. conspicuus*	Tooth	Miedary, Poland	Lower Lettenkeuper	This study	
ZPAL V. 36/124	*T. conspicuus*	Cervical vertebra, dorsal vertebra, caudal vertebra (anterior)	Miedary, Poland	Lower Lettenkeuper	This study	
ZPAL V. 36/1240	*T. conspicuus*	Tooth	Miedary, Poland	Lower Lettenkeuper	This study	
ZPAL V. 36/1241	*T. conspicuus*	Tooth	Miedary, Poland	Lower Lettenkeuper	This study	
ZPAL V. 36/1242	*T. conspicuus*	Dorsal rib (anterior)	Miedary, Poland	Lower Lettenkeuper	This study	
ZPAL V. 36/1243	*T. conspicuus*	Cervical rib (13th)	Miedary, Poland	Lower Lettenkeuper	This study	
ZPAL V. 36/1244	*T. conspicuus*	Skull roof - fused parietals, frontals (2), fragmentary postorbitals (2)	Miedary, Poland	Lower Lettenkeuper	This study	
ZPAL V. 36/1245	*T. conspicuus*	Cervical vertebra	Miedary, Poland	Lower Lettenkeuper	This study	
ZPAL V. 36/1246	*T. conspicuus*	Fibula	Miedary, Poland	Lower Lettenkeuper	This study	
ZPAL V. 36/1247	*T. conspicuus*	Cervical rib (12th)	Miedary, Poland	Lower Lettenkeuper	This study	
ZPAL V. 36/1248	*T. conspicuus*	Cervical vertebra	Miedary, Poland	Lower Lettenkeuper	This study	
ZPAL V. 36/1249	*T. conspicuus*	Dorsal vertebra	Miedary, Poland	Lower Lettenkeuper	This study	

ZPAL V. 36/125	*T. conspicuus*	Articulated or associated: 11 dorsal vertebrae, two sacral vertebrae, three caudal vertebrae, dorsal ribs, gastralia, scapula, ilium, pubis	Miedary, Poland	Lower Lettenkeuper	This study	
ZPAL V. 36/1250	*T. conspicuus*	Cervical rib (13th)	Miedary, Poland	Lower Lettenkeuper	This study	
ZPAL V. 36/1251	*T. conspicuus*	Cervical rib (13th)	Miedary, Poland	Lower Lettenkeuper	This study	
ZPAL V. 36/1252	*T. conspicuus*	Dorsal vertebra	Miedary, Poland	Lower Lettenkeuper	This study	
ZPAL V. 36/1253	*T. conspicuus*	Cervical ribs (5)	Miedary, Poland	Lower Lettenkeuper	This study	
ZPAL V. 36/1254	*T. conspicuus*	Dorsal vertebra	Miedary, Poland	Lower Lettenkeuper	This study	
ZPAL V. 36/1255	*T. conspicuus*	Dorsal vertebra	Miedary, Poland	Lower Lettenkeuper	This study	
ZPAL V. 36/1256	*T. conspicuus*	Cervical vertebra (13th)	Miedary, Poland	Lower Lettenkeuper	This study	
ZPAL V. 36/1257	*T. conspicuus*	Dorsal vertebra	Miedary, Poland	Lower Lettenkeuper	This study	
ZPAL V. 36/1258	*T. conspicuus*	Cervical vertebra	Miedary, Poland	Lower Lettenkeuper	This study	
ZPAL V. 36/1259	*T. conspicuus*	Dorsal vertebra	Miedary, Poland	Lower Lettenkeuper	This study	
ZPAL V. 36/126	*T. conspicuus*	Cervical vertebra	Miedary, Poland	Lower Lettenkeuper	Rytel et al. 2024b	
ZPAL V. 36/1260	*T. conspicuus*	Dorsal vertebra	Miedary, Poland	Lower Lettenkeuper	This study	
ZPAL V. 36/1261	*T. conspicuus*	Caudal vertebra (anterior)	Miedary, Poland	Lower Lettenkeuper	This study	
ZPAL V. 36/1262	*T. conspicuus*	Dorsal vertebra	Miedary, Poland	Lower Lettenkeuper	This study	
ZPAL V. 36/1263	*T. conspicuus*	Dorsal vertebra	Miedary, Poland	Lower Lettenkeuper	This study	
ZPAL V. 36/1264	*T. conspicuus*	Dorsal vertebra	Miedary, Poland	Lower Lettenkeuper	This study	
ZPAL V. 36/1265	*T. conspicuus*	Dorsal vertebra	Miedary, Poland	Lower Lettenkeuper	This study	
ZPAL V. 36/1266	*T. conspicuus*	Tibia	Miedary, Poland	Lower Lettenkeuper	This study	
ZPAL V. 36/1267	*T. conspicuus*	Tibia	Miedary, Poland	Lower Lettenkeuper	This study	
ZPAL V. 36/1268	*T. conspicuus*	Fibula	Miedary, Poland	Lower Lettenkeuper	This study	
ZPAL V. 36/1269	*T. conspicuus*	Tibia	Miedary, Poland	Lower Lettenkeuper	This study	
ZPAL V. 36/127	*T. conspicuus*	Cervical vertebra	Miedary, Poland	Lower Lettenkeuper	This study	
ZPAL V. 36/1270	*T. conspicuus*	Tibia	Miedary, Poland	Lower Lettenkeuper	This study	
ZPAL V. 36/1272	*T. conspicuus*	Dorsal vertebra	Miedary, Poland	Lower Lettenkeuper	This study	
ZPAL V. 36/1273	*T. conspicuus*	Cervical vertebra	Miedary, Poland	Lower Lettenkeuper	This study	
ZPAL V. 36/1274	*T. conspicuus*	Dorsal vertebra	Miedary, Poland	Lower Lettenkeuper	This study	
ZPAL V. 36/1275	*T. conspicuus*	Cervical vertebra	Miedary, Poland	Lower Lettenkeuper	This study	
ZPAL V. 36/1276	*T. conspicuus*	Cervical vertebra (13th)	Miedary, Poland	Lower Lettenkeuper	This study	

ZPAL V. 36/1277	*T. conspicuus*	Cervical vertebra	Miedary, Poland	Lower Lettenkeuper	This study	
ZPAL V. 36/1278	*T. conspicuus*	Cervical vertebra	Miedary, Poland	Lower Lettenkeuper	This study	
ZPAL V. 36/1279	*T. conspicuus*	Dorsal vertebra	Miedary, Poland	Lower Lettenkeuper	This study	
ZPAL V. 36/128	*T. conspicuus*	Cervical vertebra	Miedary, Poland	Lower Lettenkeuper	This study	
ZPAL V. 36/1280	*T. conspicuus*	Dorsal vertebra	Miedary, Poland	Lower Lettenkeuper	This study	
ZPAL V. 36/1281	*T. conspicuus*	Cervical vertebra	Miedary, Poland	Lower Lettenkeuper	This study	
ZPAL V. 36/1282	*T. conspicuus*	Cervical vertebra (12th)	Miedary, Poland	Lower Lettenkeuper	This study	
ZPAL V. 36/1283	*T. conspicuus*	Caudal vertebra (anterior)	Miedary, Poland	Lower Lettenkeuper	This study	
ZPAL V. 36/1284	*T. conspicuus*	Cervical vertebra (10th), ischium	Miedary, Poland	Lower Lettenkeuper	This study	
ZPAL V. 36/1285	*T. conspicuus*	Cervical vertebra	Miedary, Poland	Lower Lettenkeuper	This study	
ZPAL V. 36/1286	*T. conspicuus*	Cervical vertebra	Miedary, Poland	Lower Lettenkeuper	This study	
ZPAL V. 36/1287	*T. conspicuus*	Cervical vertebra	Miedary, Poland	Lower Lettenkeuper	This study	
ZPAL V. 36/1288	*T. conspicuus*	Cervical vertebra (11th)	Miedary, Poland	Lower Lettenkeuper	This study	
ZPAL V. 36/1289	*T. conspicuus (partim)*	Cervical vertebra (11th)	Miedary, Poland	Lower Lettenkeuper	This study	
ZPAL V. 36/129	*T. conspicuus*	Cervical vertebra (13th)	Miedary, Poland	Lower Lettenkeuper	This study	
ZPAL V. 36/1290	*T. conspicuus*	Dorsal vertebra	Miedary, Poland	Lower Lettenkeuper	This study	
ZPAL V. 36/1291	*T. conspicuus*	Caudal vertebra (anterior)	Miedary, Poland	Lower Lettenkeuper	This study	
ZPAL V. 36/1292	*T. conspicuus*	Caudal vertebra (anterior)	Miedary, Poland	Lower Lettenkeuper	This study	
ZPAL V. 36/1293	*T. conspicuus*	Caudal vertebra (anterior)	Miedary, Poland	Lower Lettenkeuper	This study	
ZPAL V. 36/1294	*T. conspicuus*	Caudal vertebra (anterior)	Miedary, Poland	Lower Lettenkeuper	This study	
ZPAL V. 36/1295	*T. conspicuus*	Cervical vertebra (11th)	Miedary, Poland	Lower Lettenkeuper	This study	
ZPAL V. 36/1296	*T. conspicuus*	Cervical vertebra	Miedary, Poland	Lower Lettenkeuper	This study	
ZPAL V. 36/1297	*T. conspicuus*	Cervical vertebra	Miedary, Poland	Lower Lettenkeuper	This study	
ZPAL V. 36/1298	*T. conspicuus*	ischium	Miedary, Poland	Lower Lettenkeuper	This study	
ZPAL V. 36/1299	*T. conspicuus*	Caudal vertebra (anterior)	Miedary, Poland	Lower Lettenkeuper	This study	
ZPAL V. 36/130	*T. conspicuus*	Caudal vertebra (anterior)	Miedary, Poland	Lower Lettenkeuper	This study	
ZPAL V. 36/1308	*T. conspicuus*	Clavicle	Miedary, Poland	Lower Lettenkeuper	This study	
ZPAL V. 36/131	*T. conspicuus*	Caudal vertebra (anterior)	Miedary, Poland	Lower Lettenkeuper	This study	
ZPAL V. 36/132	*T. conspicuus*	Caudal vertebra (anterior)	Miedary, Poland	Lower Lettenkeuper	This study	
ZPAL V. 36/133	*T. conspicuus*	Axis	Miedary, Poland	Lower Lettenkeuper	This study	
ZPAL V. 36/134	*T. conspicuus*	Caudal vertebra (posterior)	Miedary, Poland	Lower Lettenkeuper	This study	
ZPAL V. 36/1340	*T. conspicuus (partim)*	Ischium	Miedary, Poland	Lower Lettenkeuper	This study	
ZPAL V. 36/135	*T. conspicuus*	Dorsal vertebra	Miedary, Poland	Lower Lettenkeuper	This study	

ZPAL V. 36/1350	*T. conspicuus*	Quadratum	Miedary, Poland	Lower Lettenkeuper	This study	
ZPAL V. 36/136	*T. conspicuus*	Caudal vertebra (posterior)	Miedary, Poland	Lower Lettenkeuper	This study	
ZPAL V. 36/137	*T. conspicuus*	Cervical vertebra	Miedary, Poland	Lower Lettenkeuper	This study	
ZPAL V. 36/138	*T. conspicuus*	Cervical vertebra	Miedary, Poland	Lower Lettenkeuper	This study	
ZPAL V. 36/139	*T. conspicuus*	Caudal vertebra (posterior)	Miedary, Poland	Lower Lettenkeuper	This study	
ZPAL V. 36/140	*T. conspicuus*	Cervical vertebra (10th)	Miedary, Poland	Lower Lettenkeuper	This study	
ZPAL V. 36/141	*T. conspicuus*	Dorsal vertebra	Miedary, Poland	Lower Lettenkeuper	This study	
ZPAL V. 36/142	*T. conspicuus*	Caudal vertebra (anterior)	Miedary, Poland	Lower Lettenkeuper	This study	
ZPAL V. 36/143	*T. conspicuus*	Dorsal vertebra	Miedary, Poland	Lower Lettenkeuper	This study	
ZPAL V. 36/144	*T. conspicuus*	Dorsal vertebra	Miedary, Poland	Lower Lettenkeuper	This study	
ZPAL V. 36/145	*T. conspicuus*	Dorsal vertebra	Miedary, Poland	Lower Lettenkeuper	This study	
ZPAL V. 36/146	*T. conspicuus*	Dorsal vertebra	Miedary, Poland	Lower Lettenkeuper	This study	
ZPAL V. 36/147	*T. conspicuus*	Pubis	Miedary, Poland	Lower Lettenkeuper	This study	
ZPAL V. 36/148	*T. conspicuus*	Caudal vertebra (anterior)	Miedary, Poland	Lower Lettenkeuper	This study	
ZPAL V. 36/149	*T. conspicuus*	Cervical vertebra (11th)	Miedary, Poland	Lower Lettenkeuper	Rytel et al. 2024b	
ZPAL V. 36/150	*T. conspicuus*	Cervical vertebra	Miedary, Poland	Lower Lettenkeuper	Rytel et al. 2024b (fig. 8A)	
ZPAL V. 36/151	*T. conspicuus*	Cervical vertebra (11th)	Miedary, Poland	Lower Lettenkeuper	This study	
ZPAL V. 36/152	*T. conspicuus*	Cervical vertebra	Miedary, Poland	Lower Lettenkeuper	This study	
ZPAL V. 36/153	*T. conspicuus*	Scapula	Miedary, Poland	Lower Lettenkeuper	This study	
ZPAL V. 36/154	*T. conspicuus*	Cervical vertebra (9th)	Miedary, Poland	Lower Lettenkeuper	This study	
ZPAL V. 36/155	*T. conspicuus*	Cervical vertebra	Miedary, Poland	Lower Lettenkeuper	This study	
ZPAL V. 36/156	*T. conspicuus*	Cervical vertebra	Miedary, Poland	Lower Lettenkeuper	Rytel et al. 2024b (fig. 8H)	
ZPAL V. 36/157	*T. conspicuus*	Postcloacal bone	Miedary, Poland	Lower Lettenkeuper	This study	
ZPAL V. 36/158	*T. conspicuus*	Cervical vertebra (11th)	Miedary, Poland	Lower Lettenkeuper	This study	
ZPAL V. 36/159	*T. conspicuus*	Tooth	Miedary, Poland	Lower Lettenkeuper	This study	
ZPAL V. 36/160	*T. conspicuus*	Tooth	Miedary, Poland	Lower Lettenkeuper	This study	
ZPAL V. 36/161	*T. conspicuus*	Tooth	Miedary, Poland	Lower Lettenkeuper	This study	
ZPAL V. 36/162	*T. conspicuus*	Tooth	Miedary, Poland	Lower Lettenkeuper	This study	
ZPAL V. 36/163	*T. conspicuus*	Tooth	Miedary, Poland	Lower Lettenkeuper	This study	
ZPAL V. 36/164	*T. conspicuus*	Tooth	Miedary, Poland	Lower Lettenkeuper	This study	
ZPAL V. 36/165	*T. conspicuus*	Tooth	Miedary, Poland	Lower Lettenkeuper	This study	
ZPAL V. 36/166	*T. conspicuus*	Cervical vertebra (10th)	Miedary, Poland	Lower Lettenkeuper	Rytel et al. 2024b (fig. 8E)	

ZPAL V. 36/167	*T. conspicuus*	Caudal vertebra (posterior)	Miedary, Poland	Lower Lettenkeuper	This study	
ZPAL V. 36/168	*T. conspicuus*	Dorsal vertebra	Miedary, Poland	Lower Lettenkeuper	This study	
ZPAL V. 36/169	*T. conspicuus*	Caudal vertebra (posterior)	Miedary, Poland	Lower Lettenkeuper	This study	
ZPAL V. 36/170	*T. conspicuus*	Caudal vertebra (anterior)	Miedary, Poland	Lower Lettenkeuper	This study	
ZPAL V. 36/1700	*T. conspicuus*	Cervical vertebrae (2)	Miedary, Poland	Lower Lettenkeuper	This study	
ZPAL V. 36/1701	*T. conspicuus*	Coracoid	Miedary, Poland	Lower Lettenkeuper	This study	
ZPAL V. 36/1702	*T. conspicuus*	Coracoid, caudal vertebra (anterior)	Miedary, Poland	Lower Lettenkeuper	This study	
ZPAL V. 36/1703	*T. conspicuus*	Coracoid	Miedary, Poland	Lower Lettenkeuper	This study	
ZPAL V. 36/1704	*T. conspicuus*	Cervical rib (13th)	Miedary, Poland	Lower Lettenkeuper	This study	
ZPAL V. 36/1705	*T. conspicuus*	Cervical vertebra, caudal vertebra (anterior)	Miedary, Poland	Lower Lettenkeuper	This study	
ZPAL V. 36/1706	*T. conspicuus*	Coracoid	Miedary, Poland	Lower Lettenkeuper	This study	
ZPAL V. 36/1707	*T. conspicuus*	Caudal vertebra (anterior), cervical vertebra	Miedary, Poland	Lower Lettenkeuper	This study	
ZPAL V. 36/1708	*T. conspicuus*	Cervical vertebra	Miedary, Poland	Lower Lettenkeuper	This study	
ZPAL V. 36/1709	*T. conspicuus*	Dorsal vertebra	Miedary, Poland	Lower Lettenkeuper	This study	
ZPAL V. 36/171	*T. conspicuus*	Scapula	Miedary, Poland	Lower Lettenkeuper	This study	
ZPAL V. 36/1710	*T. conspicuus*	Dorsal vertebra	Miedary, Poland	Lower Lettenkeuper	This study	
ZPAL V. 36/1711	*T. conspicuus*	Cervical rib (13th)	Miedary, Poland	Lower Lettenkeuper	This study	
ZPAL V. 36/1712	*T. conspicuus*	Dorsal vertebra	Miedary, Poland	Lower Lettenkeuper	This study	
ZPAL V. 36/1713	*T. conspicuus*	Dorsal vertebrae (2)	Miedary, Poland	Lower Lettenkeuper	This study	
ZPAL V. 36/1714	*T. conspicuus*	Caudal vertebra (anterior)	Miedary, Poland	Lower Lettenkeuper	This study	
ZPAL V. 36/1715	*T. conspicuus*	Cervical vertebra	Miedary, Poland	Lower Lettenkeuper	This study	
ZPAL V. 36/1716	*T. conspicuus*	Dorsal vertebra	Miedary, Poland	Lower Lettenkeuper	This study	
ZPAL V. 36/1717	*T. conspicuus*	Dorsal vertebra	Miedary, Poland	Lower Lettenkeuper	This study	
ZPAL V. 36/1718	*T. conspicuus*	Caudal vertebra (anterior)	Miedary, Poland	Lower Lettenkeuper	This study	
ZPAL V. 36/1719	*T. conspicuus*	Dorsal vertebra	Miedary, Poland	Lower Lettenkeuper	This study	
ZPAL V. 36/172	*T. conspicuus*	Coracoid	Miedary, Poland	Lower Lettenkeuper	This study	
ZPAL V. 36/1720	*T. conspicuus*	Cervical vertebra	Miedary, Poland	Lower Lettenkeuper	This study	
ZPAL V. 36/1721	*T. conspicuus*	Caudal vertebra (posterior)	Miedary, Poland	Lower Lettenkeuper	This study	
ZPAL V. 36/1722	*T. conspicuus*	Cervical vertebra	Miedary, Poland	Lower Lettenkeuper	This study	
ZPAL V. 36/1723	*T. conspicuus*	Caudal vertebra (anterior)	Miedary, Poland	Lower Lettenkeuper	This study	
ZPAL V. 36/1724	*T. conspicuus*	Dorsal vertebra	Miedary, Poland	Lower Lettenkeuper	This study	
ZPAL V. 36/1725	*T. conspicuus*	Cervical vertebra	Miedary, Poland	Lower Lettenkeuper	This study	

ZPAL V. 36/1726	*T. conspicuus*	Sacral vertebra, three caudal vertebrae (anterior)	Miedary, Poland	Lower Lettenkeuper	This study	
ZPAL V. 36/1727	*T. conspicuus*	Dorsal vertebra	Miedary, Poland	Lower Lettenkeuper	This study	
ZPAL V. 36/1728	*T. conspicuus*	Cervical rib (13th)	Miedary, Poland	Lower Lettenkeuper	This study	
ZPAL V. 36/1729	*T. conspicuus*	Caudal vertebra (anterior)	Miedary, Poland	Lower Lettenkeuper	This study	
ZPAL V. 36/173	*T. conspicuus*	Dorsal vertebra	Miedary, Poland	Lower Lettenkeuper	This study	
ZPAL V. 36/1730	*T. conspicuus*	Dorsal vertebra	Miedary, Poland	Lower Lettenkeuper	This study	
ZPAL V. 36/1731	*T. conspicuus*	Caudal vertebra (anterior)	Miedary, Poland	Lower Lettenkeuper	This study	
ZPAL V. 36/1732	*T. conspicuus*	Caudal vertebrae (anterior, 2)	Miedary, Poland	Lower Lettenkeuper	This study	
ZPAL V. 36/1733	*T. conspicuus*	Cervical vertebra	Miedary, Poland	Lower Lettenkeuper	This study	
ZPAL V. 36/1734	*T. conspicuus*	Caudal vertebra (anterior)	Miedary, Poland	Lower Lettenkeuper	This study	
ZPAL V. 36/1735	*T. conspicuus*	Caudal vertebra (posterior)	Miedary, Poland	Lower Lettenkeuper	This study	
ZPAL V. 36/1736	*T. conspicuus*	Caudal vertebra (anterior)	Miedary, Poland	Lower Lettenkeuper	This study	
ZPAL V. 36/1737	*T. conspicuus*	Caudal vertebra (anterior)	Miedary, Poland	Lower Lettenkeuper	This study	
ZPAL V. 36/1738	*T. conspicuus*	Caudal vertebra (posterior), caudal vertebra (anterior), cervical vertebra (13th)	Miedary, Poland	Lower Lettenkeuper	This study	
ZPAL V. 36/1739	*T. conspicuus*	Caudal vertebra (anterior)	Miedary, Poland	Lower Lettenkeuper	This study	
ZPAL V. 36/174	*T. conspicuus*	Dorsal vertebra	Miedary, Poland	Lower Lettenkeuper	This study	
ZPAL V. 36/1740	*T. conspicuus (partim)*	Dorsal vertebra	Miedary, Poland	Lower Lettenkeuper	This study	
ZPAL V. 36/1741	*T. conspicuus*	Caudal vertebra (anterior), dorsal vertebra	Miedary, Poland	Lower Lettenkeuper	This study	
ZPAL V. 36/1742	*T. conspicuus*	Dorsal vertebra	Miedary, Poland	Lower Lettenkeuper	This study	
ZPAL V. 36/1743	*T. conspicuus*	Caudal vertebra (anterior)	Miedary, Poland	Lower Lettenkeuper	This study	
ZPAL V. 36/1744	*T. conspicuus*	Caudal vertebra (anterior)	Miedary, Poland	Lower Lettenkeuper	This study	
ZPAL V. 36/1745	*T. conspicuus*	Cervical vertebra (11th)	Miedary, Poland	Lower Lettenkeuper	This study	
ZPAL V. 36/1746	*T. conspicuus*	Dorsal vertebra	Miedary, Poland	Lower Lettenkeuper	This study	
ZPAL V. 36/1747	*T. conspicuus*	Caudal vertebra (anterior)	Miedary, Poland	Lower Lettenkeuper	This study	
ZPAL V. 36/1748	*T. conspicuus*	Caudal vertebra (anterior), postcloacal bone	Miedary, Poland	Lower Lettenkeuper	This study	
ZPAL V. 36/1749	*T. conspicuus*	Caudal vertebra (anterior)	Miedary, Poland	Lower Lettenkeuper	This study	
ZPAL V. 36/175	*T. conspicuus*	Cervical vertebra	Miedary, Poland	Lower Lettenkeuper	This study	
ZPAL V. 36/1750	*T. conspicuus*	Cervical vertebra (13th)	Miedary, Poland	Lower Lettenkeuper	This study	
ZPAL V. 36/1751	*T. conspicuus*	Caudal vertebra (anterior)	Miedary, Poland	Lower Lettenkeuper	This study	

ZPAL V. 36/1752	*T. conspicuus*	Dorsal vertebra	Miedary, Poland	Lower Lettenkeuper	This study	
ZPAL V. 36/1753	*T. conspicuus*	Cervical vertebra (12th)	Miedary, Poland	Lower Lettenkeuper	This study	
ZPAL V. 36/1754	*T. conspicuus*	Dorsal vertebra	Miedary, Poland	Lower Lettenkeuper	This study	
ZPAL V. 36/1755	*T. conspicuus*	Dorsal vertebra	Miedary, Poland	Lower Lettenkeuper	This study	
ZPAL V. 36/1756	*T. conspicuus*	Caudal vertebra (anterior)	Miedary, Poland	Lower Lettenkeuper	This study	
ZPAL V. 36/1757	*T. conspicuus*	Cervical vertebra	Miedary, Poland	Lower Lettenkeuper	This study	
ZPAL V. 36/1758	*T. conspicuus*	Dorsal vertebra	Miedary, Poland	Lower Lettenkeuper	This study	
ZPAL V. 36/1759	*T. conspicuus*	Cervical vertebra (12th)	Miedary, Poland	Lower Lettenkeuper	This study	
ZPAL V. 36/176	*T. conspicuus*	Cervical vertebra	Miedary, Poland	Lower Lettenkeuper	Rytel et al. 2024b	
ZPAL V. 36/1760	*T. conspicuus*	Caudal vertebra (anterior)	Miedary, Poland	Lower Lettenkeuper	This study	
ZPAL V. 36/1761	*T. conspicuus*	Caudal vertebrae (anterior, 2)	Miedary, Poland	Lower Lettenkeuper	This study	
ZPAL V. 36/1762	*T. conspicuus*	Caudal vertebra (anterior)	Miedary, Poland	Lower Lettenkeuper	This study	
ZPAL V. 36/1763	*T. conspicuus*	Cervical vertebra	Miedary, Poland	Lower Lettenkeuper	This study	
ZPAL V. 36/1764	*T. conspicuus*	Quadratum	Miedary, Poland	Lower Lettenkeuper	This study	
ZPAL V. 36/1766	*T. conspicuus*	Sacral vertebra (1st)	Miedary, Poland	Lower Lettenkeuper	This study	
ZPAL V. 36/1767	*T. conspicuus*	Ilium	Miedary, Poland	Lower Lettenkeuper	This study	
ZPAL V. 36/1768	*T. conspicuus*	Tooth	Miedary, Poland	Lower Lettenkeuper	This study	
ZPAL V. 36/1769	*T. conspicuus*	Tooth	Miedary, Poland	Lower Lettenkeuper	This study	
ZPAL V. 36/177	*T. conspicuus*	Ilium	Miedary, Poland	Lower Lettenkeuper	This study	
ZPAL V. 36/1770	*T. conspicuus*	Tooth	Miedary, Poland	Lower Lettenkeuper	This study	
ZPAL V. 36/1771	*T. conspicuus*	Tooth	Miedary, Poland	Lower Lettenkeuper	This study	
ZPAL V. 36/1772	*T. conspicuus*	Tooth	Miedary, Poland	Lower Lettenkeuper	This study	
ZPAL V. 36/1773	*T. conspicuus*	Tooth	Miedary, Poland	Lower Lettenkeuper	This study	
ZPAL V. 36/1774	*T. conspicuus*	Tooth	Miedary, Poland	Lower Lettenkeuper	This study	
ZPAL V. 36/1775	*T. conspicuus*	Cervical rib	Miedary, Poland	Lower Lettenkeuper	This study	
ZPAL V. 36/1776	*T. conspicuus*	Cervical vertebra	Miedary, Poland	Lower Lettenkeuper	This study	
ZPAL V. 36/1777	*T. conspicuus*	Dorsal vertebra	Miedary, Poland	Lower Lettenkeuper	This study	
ZPAL V. 36/1778	*T. conspicuus*	Cervical rib	Miedary, Poland	Lower Lettenkeuper	This study	
ZPAL V. 36/1779	*T. conspicuus*	Cervical vertebra (12th)	Miedary, Poland	Lower Lettenkeuper	This study	
ZPAL V. 36/178	*T. conspicuus*	Pubis	Miedary, Poland	Lower Lettenkeuper	This study	
ZPAL V. 36/1780	*T. conspicuus*	Tooth	Miedary, Poland	Lower Lettenkeuper	This study	
ZPAL V. 36/1781	*T. conspicuus*	Tooth	Miedary, Poland	Lower Lettenkeuper	This study	
ZPAL V. 36/1782	*T. conspicuus*	Dorsal vertebra	Miedary, Poland	Lower Lettenkeuper	This study	

ZPAL V. 36/1783	*T. conspicuus*	Dorsal vertebra	Miedary, Poland	Lower Lettenkeuper	This study	
ZPAL V. 36/1784	*T. conspicuus*	Femur	Miedary, Poland	Lower Lettenkeuper	This study	
ZPAL V. 36/1785	*T. conspicuus*	Caudal vertebra (anterior)	Miedary, Poland	Lower Lettenkeuper	This study	
ZPAL V. 36/1786	*T. conspicuus*	Dorsal vertebra	Miedary, Poland	Lower Lettenkeuper	This study	
ZPAL V. 36/1787	*T. conspicuus*	Dorsal vertebra	Miedary, Poland	Lower Lettenkeuper	This study	
ZPAL V. 36/1788	*T. conspicuus*	Dorsal vertebra	Miedary, Poland	Lower Lettenkeuper	This study	
ZPAL V. 36/1789	*T. conspicuus*	Coracoid	Miedary, Poland	Lower Lettenkeuper	This study	
ZPAL V. 36/179	*T. conspicuus*	Premaxilla	Miedary, Poland	Lower Lettenkeuper	This study	
ZPAL V. 36/1790	*T. conspicuus*	Femur	Miedary, Poland	Lower Lettenkeuper	This study	
ZPAL V. 36/1791	*T. conspicuus*	Cervical vertebra	Miedary, Poland	Lower Lettenkeuper	This study	
ZPAL V. 36/1792	*T. conspicuus*	Tooth	Miedary, Poland	Lower Lettenkeuper	This study	
ZPAL V. 36/1793	*T. conspicuus*	Cervical rib	Miedary, Poland	Lower Lettenkeuper	This study	
ZPAL V. 36/1794	*T. conspicuus*	Cervical vertebra	Miedary, Poland	Lower Lettenkeuper	This study	
ZPAL V. 36/1795	*T. conspicuus*	Pubis	Miedary, Poland	Lower Lettenkeuper	This study	
ZPAL V. 36/1796	*T. conspicuus*	Tooth	Miedary, Poland	Lower Lettenkeuper	This study	
ZPAL V. 36/1797	*T. conspicuus*	Tooth	Miedary, Poland	Lower Lettenkeuper	This study	
ZPAL V. 36/1798	*T. conspicuus*	Ischium	Miedary, Poland	Lower Lettenkeuper	This study	
ZPAL V. 36/1799	*T. conspicuus*	Dentary	Miedary, Poland	Lower Lettenkeuper	This study	
ZPAL V. 36/180	*T. conspicuus*	Tooth	Miedary, Poland	Lower Lettenkeuper	This study	
ZPAL V. 36/181	*T. conspicuus*	Cervical vertebra	Miedary, Poland	Lower Lettenkeuper	Rytel et al. 2024b (figs. 7B; 8B)	
ZPAL V. 36/182	*T. conspicuus*	Cervical vertebra	Miedary, Poland	Lower Lettenkeuper	This study	
ZPAL V. 36/183	*T. conspicuus*	Two dorsal vertebrae in articulation, caudal vertebra (posterior)	Miedary, Poland	Lower Lettenkeuper	This study	
ZPAL V. 36/184	*T. conspicuus*	Dorsal vertebra	Miedary, Poland	Lower Lettenkeuper	This study	
ZPAL V. 36/185	*T. conspicuus*	Dorsal vertebra	Miedary, Poland	Lower Lettenkeuper	This study	
ZPAL V. 36/186/1	*T. conspicuus*	Cervical vertebra (10th)	Miedary, Poland	Lower Lettenkeuper	This study	
ZPAL V. 36/186/2	*T. conspicuus*	Cervical vertebra	Miedary, Poland	Lower Lettenkeuper	This study	
ZPAL V. 36/187	*T. conspicuus*	Humerus, two cervical vertebrae	Miedary, Poland	Lower Lettenkeuper	This study	
ZPAL V. 36/188	*T. conspicuus*	Cervical vertebra (10th), cervical vertebra	Miedary, Poland	Lower Lettenkeuper	This study	
ZPAL V. 36/189	*T. conspicuus*	Dorsal vertebra	Miedary, Poland	Lower Lettenkeuper	This study	
ZPAL V. 36/190	*T. conspicuus*	Ilium	Miedary, Poland	Lower Lettenkeuper	This study	
ZPAL V. 36/191	*T. conspicuus*	Ischium	Miedary, Poland	Lower Lettenkeuper	This study	

ZPAL V. 36/192	*T. conspicuus*	Cervical vertebra	Miedary, Poland	Lower Lettenkeuper	Rytel et al. 2024b	
ZPAL V. 36/193	*T. conspicuus*	Cervical vertebrae (2)	Miedary, Poland	Lower Lettenkeuper	Rytel et al. 2024b (fig. 8C)	
ZPAL V. 36/194	*T. conspicuus*	Dorsal vertebrae (2)	Miedary, Poland	Lower Lettenkeuper	This study	
ZPAL V. 36/195	*T. conspicuus*	Cervical vertebra	Miedary, Poland	Lower Lettenkeuper	This study	
ZPAL V. 36/196	*T. conspicuus*	Cervical vertebra	Miedary, Poland	Lower Lettenkeuper	This study	
ZPAL V. 36/197	*T. conspicuus*	Cervical vertebra (11th)	Miedary, Poland	Lower Lettenkeuper	This study	
ZPAL V. 36/198	*T. conspicuus*	Dorsal vertebra	Miedary, Poland	Lower Lettenkeuper	This study	
ZPAL V. 36/199	*T. conspicuus*	Tooth	Miedary, Poland	Lower Lettenkeuper	This study	
ZPAL V. 36/221	*T. conspicuus (partim)*	Dorsal vertebra	Miedary, Poland	Lower Lettenkeuper	This study	
ZPAL V. 36/2400	*T. conspicuus*	Cervical rib (13th)	Miedary, Poland	Lower Lettenkeuper	This study	
ZPAL V. 36/2401	*T. conspicuus*	Tooth	Miedary, Poland	Lower Lettenkeuper	This study	
ZPAL V. 36/2402	*T. conspicuus*	Cervical rib	Miedary, Poland	Lower Lettenkeuper	This study	
ZPAL V. 36/2403	*T. conspicuus*	Tooth	Miedary, Poland	Lower Lettenkeuper	This study	
ZPAL V. 36/2404	*T. conspicuus*	Tooth	Miedary, Poland	Lower Lettenkeuper	This study	
ZPAL V. 36/2405	*T. conspicuus*	Tooth	Miedary, Poland	Lower Lettenkeuper	This study	
ZPAL V. 36/2406	*T. conspicuus*	Dorsal rib (anterior)	Miedary, Poland	Lower Lettenkeuper	This study	
ZPAL V. 36/2407	*T. conspicuus*	Pubis	Miedary, Poland	Lower Lettenkeuper	This study	
ZPAL V. 36/2408	*T. conspicuus*	Tibia	Miedary, Poland	Lower Lettenkeuper	This study	
ZPAL V. 36/2409	*T. conspicuus*	Pubis	Miedary, Poland	Lower Lettenkeuper	This study	
ZPAL V. 36/2410	*T. conspicuus*	Caudal vertebra (anterior)	Miedary, Poland	Lower Lettenkeuper	This study	
ZPAL V. 36/2411	*T. conspicuus*	Caudal vertebra (anterior)	Miedary, Poland	Lower Lettenkeuper	This study	
ZPAL V. 36/2412	*T. conspicuus*	Cervical vertebra (12th)	Miedary, Poland	Lower Lettenkeuper	This study	
ZPAL V. 36/2413	*T. conspicuus*	Tooth	Miedary, Poland	Lower Lettenkeuper	This study	
ZPAL V. 36/2414	*T. conspicuus*	Tooth	Miedary, Poland	Lower Lettenkeuper	This study	
ZPAL V. 36/2415	*T. conspicuus*	Tooth	Miedary, Poland	Lower Lettenkeuper	This study	
ZPAL V. 36/2416	*T. conspicuus*	Cervical rib	Miedary, Poland	Lower Lettenkeuper	This study	
ZPAL V. 36/2417	*T. conspicuus*	Cervical rib (posterior)	Miedary, Poland	Lower Lettenkeuper	This study	
ZPAL V. 36/2418	*T. conspicuus*	Caudal vertebra (anterior)	Miedary, Poland	Lower Lettenkeuper	This study	
ZPAL V. 36/2419	*T. conspicuus*	Tooth	Miedary, Poland	Lower Lettenkeuper	This study	
ZPAL V. 36/2420	*T. conspicuus*	Cervical rib	Miedary, Poland	Lower Lettenkeuper	This study	
ZPAL V. 36/2422	*T. conspicuus*	Caudal vertebra (anterior)	Miedary, Poland	Lower Lettenkeuper	This study	
ZPAL V. 36/2423	*T. conspicuus*	Caudal vertebra (anterior)	Miedary, Poland	Lower Lettenkeuper	This study	
ZPAL V. 36/2424	*T. conspicuus*	Dorsal vertebra	Miedary, Poland	Lower Lettenkeuper	This study	

ZPAL V. 36/2425	*T. conspicuus*	Cervical vertebra (10th)	Miedary, Poland	Lower Lettenkeuper	This study	
ZPAL V. 36/2426	*T. conspicuus*	Scapula	Miedary, Poland	Lower Lettenkeuper	This study	
ZPAL V. 36/2427	*T. conspicuus*	Cervical vertebrae (2)	Miedary, Poland	Lower Lettenkeuper	This study	
ZPAL V. 36/2428	*T. conspicuus*	Dentary	Miedary, Poland	Lower Lettenkeuper	This study	
ZPAL V. 36/2429	*T. conspicuus*	Dorsal vertebra	Miedary, Poland	Lower Lettenkeuper	This study	
ZPAL V. 36/2430	*T. conspicuus*	Cervical rib (11th)	Miedary, Poland	Lower Lettenkeuper	This study	
ZPAL V. 36/2431	*T. conspicuus*	Dorsal rib (anterior)	Miedary, Poland	Lower Lettenkeuper	This study	
ZPAL V. 36/2432	*T. conspicuus*	Caudal vertebra (anterior)	Miedary, Poland	Lower Lettenkeuper	This study	
ZPAL V. 36/2433	*T. conspicuus*	Cervical rib	Miedary, Poland	Lower Lettenkeuper	This study	
ZPAL V. 36/2434	*T. conspicuus*	Humerus	Miedary, Poland	Lower Lettenkeuper	This study	
ZPAL V. 36/2435	*T. conspicuus*	Dorsal vertebra	Miedary, Poland	Lower Lettenkeuper	This study	
ZPAL V. 36/2436	*T. conspicuus*	Cervical ribs (5)	Miedary, Poland	Lower Lettenkeuper	This study	
ZPAL V. 36/2437	*T. conspicuus*	Cervical rib	Miedary, Poland	Lower Lettenkeuper	This study	
ZPAL V. 36/2438	*T. conspicuus*	Cervical vertebra	Miedary, Poland	Lower Lettenkeuper	This study	
ZPAL V. 36/2439	*T. conspicuus*	Caudal vertebra (anterior)	Miedary, Poland	Lower Lettenkeuper	This study	
ZPAL V. 36/2440	*T. conspicuus*	Dorsal vertebra	Miedary, Poland	Lower Lettenkeuper	This study	
ZPAL V. 36/2441	*T. conspicuus*	Cervical vertebra, ilium	Miedary, Poland	Lower Lettenkeuper	This study	
ZPAL V. 36/2442	*T. conspicuus*	Caudal vertebra (anterior)	Miedary, Poland	Lower Lettenkeuper	This study	
ZPAL V. 36/2443	*T. conspicuus*	Ilium	Miedary, Poland	Lower Lettenkeuper	This study	
ZPAL V. 36/2444	*T. conspicuus (partim)*	Scapula	Miedary, Poland	Lower Lettenkeuper	This study	
ZPAL V. 36/2445	*T. conspicuus*	Dorsal vertebra	Miedary, Poland	Lower Lettenkeuper	This study	
ZPAL V. 36/2446	*T. conspicuus*	Caudal vertebra (anterior)	Miedary, Poland	Lower Lettenkeuper	This study	
ZPAL V. 36/2447	*T. conspicuus (partim)*	Dorsal vertebra	Miedary, Poland	Lower Lettenkeuper	This study	
ZPAL V. 36/2448	*T. conspicuus*	Ilium	Miedary, Poland	Lower Lettenkeuper	This study	
ZPAL V. 36/2449	*T. conspicuus*	Clavicle	Miedary, Poland	Lower Lettenkeuper	This study	
ZPAL V. 36/2451	*T. conspicuus*	Caudal vertebra (anterior)	Miedary, Poland	Lower Lettenkeuper	This study	
ZPAL V. 36/2452	*T. conspicuus*	Cervical vertebra (12th)	Miedary, Poland	Lower Lettenkeuper	This study	
ZPAL V. 36/2453	*T. conspicuus*	Cervical rib	Miedary, Poland	Lower Lettenkeuper	This study	
ZPAL V. 36/2454	*T. conspicuus*	Coracoid	Miedary, Poland	Lower Lettenkeuper	This study	
ZPAL V. 36/2455	*T. conspicuus*	Pubis	Miedary, Poland	Lower Lettenkeuper	This study	
ZPAL V. 36/2456	*T. conspicuus*	Dorsal rib (3rd)	Miedary, Poland	Lower Lettenkeuper	This study	
ZPAL V. 36/2457	*T. conspicuus*	Dorsal rib	Miedary, Poland	Lower Lettenkeuper	This study	
ZPAL V. 36/2458	*T. conspicuus*	Pubis	Miedary, Poland	Lower Lettenkeuper	This study	

ZPAL V. 36/2459	*T. conspicuus*	Cervical vertebra	Miedary, Poland	Lower Lettenkeuper	This study	
ZPAL V. 36/2460	*T. conspicuus*	Tooth	Miedary, Poland	Lower Lettenkeuper	This study	
ZPAL V. 36/2461	*T. conspicuus*	Tooth	Miedary, Poland	Lower Lettenkeuper	This study	
ZPAL V. 36/2462	*T. conspicuus*	Tooth	Miedary, Poland	Lower Lettenkeuper	This study	
ZPAL V. 36/2463	*T. conspicuus*	Tooth	Miedary, Poland	Lower Lettenkeuper	This study	
ZPAL V. 36/2464	*T. conspicuus*	Tooth	Miedary, Poland	Lower Lettenkeuper	This study	
ZPAL V. 36/2465	*T. conspicuus*	Tooth	Miedary, Poland	Lower Lettenkeuper	This study	
ZPAL V. 36/2466	*T. conspicuus*	Postcloacal bone	Miedary, Poland	Lower Lettenkeuper	This study	
ZPAL V. 36/2467	*T. conspicuus*	Ischium, cervical vertebra	Miedary, Poland	Lower Lettenkeuper	This study	
ZPAL V. 36/2468	*T. conspicuus*	Cervical vertebra (11th), cervical vertebra	Miedary, Poland	Lower Lettenkeuper	This study	
ZPAL V. 36/2469	*T. conspicuus*	Femur	Miedary, Poland	Lower Lettenkeuper	This study	
ZPAL V. 36/2470	*T. conspicuus*	Cervical rib (posterior)	Miedary, Poland	Lower Lettenkeuper	This study	
ZPAL V. 36/2471	*T. conspicuus*	Cervical rib	Miedary, Poland	Lower Lettenkeuper	This study	
ZPAL V. 36/2472	*T. conspicuus*	Dorsal vertebra	Miedary, Poland	Lower Lettenkeuper	This study	
ZPAL V. 36/2473	*T. conspicuus*	Scapula?	Miedary, Poland	Lower Lettenkeuper	This study	
ZPAL V. 36/2474	*T. conspicuus*	Maxilla	Miedary, Poland	Lower Lettenkeuper	This study	
ZPAL V. 36/2475	*T. conspicuus*	Dorsal rib (anterior)	Miedary, Poland	Lower Lettenkeuper	This study	
ZPAL V. 36/2476	*T. conspicuus*	Cervical rib	Miedary, Poland	Lower Lettenkeuper	This study	
ZPAL V. 36/2477	*T. conspicuus*	Dorsal vertebrae (2)	Miedary, Poland	Lower Lettenkeuper	This study	
ZPAL V. 36/2478	*T. conspicuus*	Caudal vertebra (posterior)	Miedary, Poland	Lower Lettenkeuper	This study	
ZPAL V. 36/2479	*T. conspicuus*	Cervical vertebra	Miedary, Poland	Lower Lettenkeuper	This study	
ZPAL V. 36/2480	*T. conspicuus*	Dorsal vertebra	Miedary, Poland	Lower Lettenkeuper	This study	
ZPAL V. 36/2481	*T. conspicuus*	Dorsal vertebra	Miedary, Poland	Lower Lettenkeuper	This study	
ZPAL V. 36/2482	*T. conspicuus*	Cervical vertebra	Miedary, Poland	Lower Lettenkeuper	This study	
ZPAL V. 36/2483	*T. conspicuus*	Dorsal vertebra?	Miedary, Poland	Lower Lettenkeuper	This study	
ZPAL V. 36/2484	*T. conspicuus*	Dorsal vertebra	Miedary, Poland	Lower Lettenkeuper	This study	
ZPAL V. 36/2485	*T. conspicuus*	Cervical vertebra (13th)	Miedary, Poland	Lower Lettenkeuper	This study	
ZPAL V. 36/2486	*T. conspicuus*	Cervical vertebra, dorsal vertebra	Miedary, Poland	Lower Lettenkeuper	This study	
ZPAL V. 36/2487	*T. conspicuus*	Premaxilla	Miedary, Poland	Lower Lettenkeuper	This study	
ZPAL V. 36/2488	*T. conspicuus*	Radius	Miedary, Poland	Lower Lettenkeuper	This study	
ZPAL V. 36/2489	*T. conspicuus*	Caudal vertebra (anterior)	Miedary, Poland	Lower Lettenkeuper	This study	
ZPAL V. 36/2490	*T. conspicuus*	Caudal vertebra (anterior)	Miedary, Poland	Lower Lettenkeuper	This study	
ZPAL V. 36/2491	*T. conspicuus*	Caudal vertebra (anterior)	Miedary, Poland	Lower Lettenkeuper	This study	

ZPAL V. 36/2492	*T. conspicuus*	Maxilla	Miedary, Poland	Lower Lettenkeuper	This study	
ZPAL V. 36/2493	*T. conspicuus*	Tooth	Miedary, Poland	Lower Lettenkeuper	This study	
ZPAL V. 36/2494	*T. conspicuus*	Fibula	Miedary, Poland	Lower Lettenkeuper	This study	
ZPAL V. 36/2495	*T. conspicuus*	Fibula	Miedary, Poland	Lower Lettenkeuper	This study	
ZPAL V. 36/2496	*T. conspicuus*	Caudal vertebra (anterior)	Miedary, Poland	Lower Lettenkeuper	This study	
ZPAL V. 36/2541	*T. conspicuus*	Pterygoid	Miedary, Poland	Lower Lettenkeuper	This study	
ZPAL V. 36/302/04	*T. conspicuus (partim)*	Caudal vertebra (anterior)	Miedary, Poland	Lower Lettenkeuper	This study	
ZPAL V. 36/341	*T. conspicuus (partim)*	Dorsal vertebra	Miedary, Poland	Lower Lettenkeuper	This study	
ZPAL V. 36/525	*T. conspicuus (partim)*	Caudal vertebra (anterior), dorsal vertebra	Miedary, Poland	Lower Lettenkeuper	This study	
ZPAL V. 36/537	*T. conspicuus (partim)*	Dorsal vertebra, cervical rib head	Miedary, Poland	Lower Lettenkeuper	This study	
ZPAL V. 36/550	*T. conspicuus*	Axis	Miedary, Poland	Lower Lettenkeuper	Czepiński et al. 2023 (fig. 6B)	
ZPAL V. 36/551	*T. conspicuus*	Cervical vertebra (12th)	Miedary, Poland	Lower Lettenkeuper	This study	
ZPAL V. 36/574	*T. conspicuus*	Quadratum	Miedary, Poland	Lower Lettenkeuper	This study	
ZPAL V. 36/579	*T. conspicuus (partim)*	Cervical rib (12th), tooth	Miedary, Poland	Lower Lettenkeuper	This study	
ZPAL V. 36/584	*T. conspicuus (partim)*	Femur, seven associated dorsal vertebrae, cervical vertebrae (11th-13th), ribs (12th, 13th, anterior dorsal)	Miedary, Poland	Lower Lettenkeuper	This study	
ZPAL V. 36/585a+b	*T. conspicuus (partim)*	Scapula, caudal vertebra (anterior)	Miedary, Poland	Lower Lettenkeuper	This study	
ZPAL V. 36/586	*T. conspicuus (partim)*	Dorsal vertebrae (2), caudal vertebrae (2)	Miedary, Poland	Lower Lettenkeuper	This study	
ZPAL V. 36/587	*T. conspicuus (partim)*	Cervical vertebra, two caudal vertebrae (anterior), dorsal vertebra	Miedary, Poland	Lower Lettenkeuper	This study	
ZPAL V. 36/589	*T. conspicuus (partim)*	Coracoid, dorsal vertebra	Miedary, Poland	Lower Lettenkeuper	This study	
ZPAL V. 36/597	*T. conspicuus (partim)*	Postcloacal bone (P), caudal vertebra (posterior)	Miedary, Poland	Lower Lettenkeuper	This study	
ZPAL V. 36/800	*T. conspicuus*	Tooth	Miedary, Poland	Lower Lettenkeuper	This study	
ZPAL V. 36/801	*T. conspicuus*	Femur	Miedary, Poland	Lower Lettenkeuper	This study	
ZPAL V. 36/802	*T. conspicuus*	Tooth	Miedary, Poland	Lower Lettenkeuper	This study	
ZPAL V. 36/803	*T. conspicuus*	Cervical vertebrae (3), humerus	Miedary, Poland	Lower Lettenkeuper	This study	
ZPAL V. 36/804	*T. conspicuus*	Ilium	Miedary, Poland	Lower Lettenkeuper	This study	
ZPAL V. 36/805	*T. conspicuus*	Ilium, ischium, cervical vertebra (11th)	Miedary, Poland	Lower Lettenkeuper	This study	

ZPAL V. 36/806	*T. conspicuus*	Scapula	Miedary, Poland	Lower Lettenkeuper	This study	
ZPAL V. 36/807	*T. conspicuus*	Femur	Miedary, Poland	Lower Lettenkeuper	This study	
ZPAL V. 36/808	*T. conspicuus*	Scapula	Miedary, Poland	Lower Lettenkeuper	This study	
ZPAL V. 36/809	*T. conspicuus*	Cervical vertebra (13th)	Miedary, Poland	Lower Lettenkeuper	This study	
ZPAL V. 36/810	*T. conspicuus*	Coracoid	Miedary, Poland	Lower Lettenkeuper	This study	
ZPAL V. 36/811	*T. conspicuus*	Scapula	Miedary, Poland	Lower Lettenkeuper	This study	
ZPAL V. 36/812	*T. conspicuus*	Ilium	Miedary, Poland	Lower Lettenkeuper	This study	
ZPAL V. 36/813	*T. conspicuus*	Ilium	Miedary, Poland	Lower Lettenkeuper	This study	
ZPAL V. 36/814	*T. conspicuus*	Coracoid	Miedary, Poland	Lower Lettenkeuper	This study	
ZPAL V. 36/815	*T. conspicuus*	Pubis	Miedary, Poland	Lower Lettenkeuper	This study	
ZPAL V. 36/816	*T. conspicuus*	Scapula	Miedary, Poland	Lower Lettenkeuper	This study	
ZPAL V. 36/817	*T. conspicuus*	Coracoid?	Miedary, Poland	Lower Lettenkeuper	This study	
ZPAL V. 36/818	*T. conspicuus*	Ischium	Miedary, Poland	Lower Lettenkeuper	This study	
ZPAL V. 36/819	*T. conspicuus*	Cervical vertebra	Miedary, Poland	Lower Lettenkeuper	This study	
ZPAL V. 36/820	*T. conspicuus*	Dorsal vertebra?	Miedary, Poland	Lower Lettenkeuper	This study	
ZPAL V. 36/821	*T. conspicuus*	Dorsal vertebra	Miedary, Poland	Lower Lettenkeuper	This study	
ZPAL V. 36/822	*T. conspicuus*	Dorsal vertebra	Miedary, Poland	Lower Lettenkeuper	This study	
ZPAL V. 36/823	*T. conspicuus*	Dorsal vertebra	Miedary, Poland	Lower Lettenkeuper	This study	
ZPAL V. 36/824	*T. conspicuus*	Dorsal vertebra, dorsal rib (anterior)	Miedary, Poland	Lower Lettenkeuper	This study	
ZPAL V. 36/825	*T. conspicuus*	Dorsal vertebra?	Miedary, Poland	Lower Lettenkeuper	This study	
ZPAL V. 36/826	*T. conspicuus*	Dorsal vertebra?	Miedary, Poland	Lower Lettenkeuper	This study	
ZPAL V. 36/827	*T. conspicuus*	Dorsal vertebra?	Miedary, Poland	Lower Lettenkeuper	This study	
ZPAL V. 36/828	*T. conspicuus*	Caudal vertebra (anterior)	Miedary, Poland	Lower Lettenkeuper	This study	
ZPAL V. 36/829	*T. conspicuus*	Ulna	Miedary, Poland	Lower Lettenkeuper	This study	
ZPAL V. 36/830	*T. conspicuus*	Radius	Miedary, Poland	Lower Lettenkeuper	This study	
ZPAL V. 36/831	*T. conspicuus*	Fibula	Miedary, Poland	Lower Lettenkeuper	This study	
ZPAL V. 36/832	*T. conspicuus*	Femur	Miedary, Poland	Lower Lettenkeuper	This study	
ZPAL V. 36/833	*T. conspicuus*	Tibia	Miedary, Poland	Lower Lettenkeuper	This study	
ZPAL V. 36/834	*T. conspicuus*	Fibula	Miedary, Poland	Lower Lettenkeuper	This study	
ZPAL V. 36/835	*T. conspicuus*	Humerus	Miedary, Poland	Lower Lettenkeuper	This study	
ZPAL V. 36/836	*T. conspicuus*	Femur	Miedary, Poland	Lower Lettenkeuper	This study	
ZPAL V. 36/837	*T. conspicuus*	Femur	Miedary, Poland	Lower Lettenkeuper	This study	
ZPAL V. 36/838	*T. conspicuus*	Femur	Miedary, Poland	Lower Lettenkeuper	This study	

ZPAL V. 36/839	*T. conspicuus*	Cervical vertebra (10th)	Miedary, Poland	Lower Lettenkeuper	This study	
ZPAL V. 36/840	*T. conspicuus*	Caudal vertebra (anterior?)	Miedary, Poland	Lower Lettenkeuper	This study	
ZPAL V. 36/841	*T. conspicuus*	Dorsal vertebra	Miedary, Poland	Lower Lettenkeuper	This study	
ZPAL V. 36/843	*T. conspicuus*	Cervical vertebra (13th), dorsal vertebrae (2)	Miedary, Poland	Lower Lettenkeuper	This study	
ZPAL V. 36/844	*T. conspicuus*	Cervical vertebra	Miedary, Poland	Lower Lettenkeuper	This study	
ZPAL V. 36/845	*T. conspicuus*	Cervical vertebra (12th)	Miedary, Poland	Lower Lettenkeuper	This study	
ZPAL V. 36/846	*T. conspicuus*	Cervical vertebra (10th)	Miedary, Poland	Lower Lettenkeuper	This study	
ZPAL V. 36/847	*T. conspicuus*	Axis	Miedary, Poland	Lower Lettenkeuper	This study	
ZPAL V. 36/848	*T. conspicuus*	Cervical vertebra (13th)	Miedary, Poland	Lower Lettenkeuper	This study	
ZPAL V. 36/849	*T. conspicuus*	Cervical vertebra (12th)	Miedary, Poland	Lower Lettenkeuper	This study	
ZPAL V. 36/850	*T. conspicuus*	Cervical vertebra	Miedary, Poland	Lower Lettenkeuper	This study	
ZPAL V. 36/851	*T. conspicuus*	Cervical vertebra (11th)	Miedary, Poland	Lower Lettenkeuper	This study	
ZPAL V. 36/852	*T. conspicuus*	Cervical vertebra (10th)	Miedary, Poland	Lower Lettenkeuper	This study	
ZPAL V. 36/853	*T. conspicuus*	Cervical vertebra (12th), caudal vertebra (anterior)	Miedary, Poland	Lower Lettenkeuper	This study	
ZPAL V. 36/854	*T. conspicuus*	Cervical vertebra	Miedary, Poland	Lower Lettenkeuper	This study	
ZPAL V. 36/855	*T. conspicuus*	Cervical vertebra	Miedary, Poland	Lower Lettenkeuper	This study	
ZPAL V. 36/856	*T. conspicuus*	Cervical vertebra	Miedary, Poland	Lower Lettenkeuper	This study	
ZPAL V. 36/857	*T. conspicuus*	Cervical vertebra	Miedary, Poland	Lower Lettenkeuper	This study	
ZPAL V. 36/858	*T. conspicuus*	Cervical vertebra	Miedary, Poland	Lower Lettenkeuper	This study	
ZPAL V. 36/859	*T. conspicuus*	Cervical vertebra	Miedary, Poland	Lower Lettenkeuper	This study	
ZPAL V. 36/860	*T. conspicuus*	Cervical vertebra (11th)	Miedary, Poland	Lower Lettenkeuper	This study	
ZPAL V. 36/862	*T. conspicuus*	Cervical vertebrae (2)	Miedary, Poland	Lower Lettenkeuper	This study	
ZPAL V. 36/863	*T. conspicuus*	Cervical vertebrae (2)	Miedary, Poland	Lower Lettenkeuper	This study	
ZPAL V. 36/864	*T. conspicuus*	Cervical vertebra	Miedary, Poland	Lower Lettenkeuper	This study	
ZPAL V. 36/865	*T. conspicuus*	Sacral vertebra	Miedary, Poland	Lower Lettenkeuper	This study	
ZPAL V. 36/866	*T. conspicuus*	Cervical vertebra (13th)	Miedary, Poland	Lower Lettenkeuper	This study	
ZPAL V. 36/867	*T. conspicuus*	Caudal vertebra (anterior)	Miedary, Poland	Lower Lettenkeuper	This study	
ZPAL V. 36/868	*T. conspicuus*	Caudal vertebra (anterior)	Miedary, Poland	Lower Lettenkeuper	This study	
ZPAL V. 36/869	*T. conspicuus*	Caudal vertebra (posterior)	Miedary, Poland	Lower Lettenkeuper	This study	
ZPAL V. 36/870	*T. conspicuus*	Dorsal vertebra	Miedary, Poland	Lower Lettenkeuper	This study	
ZPAL V. 36/871	*T. conspicuus*	Sacral vertebra (2nd?)	Miedary, Poland	Lower Lettenkeuper	This study	
ZPAL V. 36/872	*T. conspicuus*	Sacral vertebra?	Miedary, Poland	Lower Lettenkeuper	This study	

ZPAL V. 36/873	*T. conspicuus*	Cervical vertebra (13th)	Miedary, Poland	Lower Lettenkeuper	This study	
ZPAL V. 36/874	*T. conspicuus*	Caudal vertebra (posterior)	Miedary, Poland	Lower Lettenkeuper	This study	
ZPAL V. 36/875	*T. conspicuus*	Dorsal vertebra	Miedary, Poland	Lower Lettenkeuper	This study	
ZPAL V. 36/876	*T. conspicuus*	Femur	Miedary, Poland	Lower Lettenkeuper	This study	
ZPAL V. 36/877	*T. conspicuus*	Femur	Miedary, Poland	Lower Lettenkeuper	This study	
ZPAL V. 36/878	*T. conspicuus*	Femur	Miedary, Poland	Lower Lettenkeuper	This study	
ZPAL V. 36/879	*T. conspicuus*	Femur	Miedary, Poland	Lower Lettenkeuper	This study	
ZPAL V. 36/880	*T. conspicuus*	Femur	Miedary, Poland	Lower Lettenkeuper	This study	
ZPAL V. 36/881	*T. conspicuus*	Humerus	Miedary, Poland	Lower Lettenkeuper	This study	
ZPAL V. 36/882	*T. conspicuus*	Humerus	Miedary, Poland	Lower Lettenkeuper	This study	
ZPAL V. 36/883	*T. conspicuus*	Sacral vertebra	Miedary, Poland	Lower Lettenkeuper	This study	
ZPAL V. 36/884	*T. conspicuus*	Sacral vertebra	Miedary, Poland	Lower Lettenkeuper	This study	
ZPAL V. 36/885	*T. conspicuus*	Tibia	Miedary, Poland	Lower Lettenkeuper	This study	
ZPAL V. 36/886	*T. conspicuus*	Cervical vertebra (11th)	Miedary, Poland	Lower Lettenkeuper	This study	
ZPAL V. 36/887	*T. conspicuus*	Cervical vertebra, cervical rib	Miedary, Poland	Lower Lettenkeuper	This study	
ZPAL V. 36/888	*T. conspicuus*	Caudal vertebra (anterior)	Miedary, Poland	Lower Lettenkeuper	This study	
ZPAL V. 36/889	*T. conspicuus*	Dorsal vertebra	Miedary, Poland	Lower Lettenkeuper	This study	
ZPAL V. 36/890	*T. conspicuus*	Tooth	Miedary, Poland	Lower Lettenkeuper	This study	
ZPAL V. 36/891	*T. conspicuus*	Dorsal vertebra	Miedary, Poland	Lower Lettenkeuper	This study	
ZPAL V. 36/892	*T. conspicuus*	Caudal vertebra (anterior)	Miedary, Poland	Lower Lettenkeuper	This study	
ZPAL V. 36/893	*T. conspicuus*	Cervical vertebra	Miedary, Poland	Lower Lettenkeuper	This study	
ZPAL V. 36/894	*T. conspicuus*	Axis?	Miedary, Poland	Lower Lettenkeuper	This study	
ZPAL V. 36/895	*T. conspicuus*	Cervical vertebra	Miedary, Poland	Lower Lettenkeuper	This study	
ZPAL V. 36/896	*T. conspicuus*	Scapula	Miedary, Poland	Lower Lettenkeuper	This study	
ZPAL V. 36/897	*T. conspicuus (partim)*	Cervical vertebra (13th), anterior dorsal rib	Miedary, Poland	Lower Lettenkeuper	This study	
ZPAL V. 36/898	*T. conspicuus*	Cervical vertebra (10th)	Miedary, Poland	Lower Lettenkeuper	This study	
ZPAL V. 36/899	*T. conspicuus*	Cervical vertebra (13th)	Miedary, Poland	Lower Lettenkeuper	This study	

Measurements of the bones referred to *Tanystropheus conspicuus*.

Specimen number	Taxon	Contents	Length (centrum) [mm]	Length (maximal) [mm]	Height (at midpoint) [mm]	Height (maximal) [mm]
GPIH 253	*T. conspicuus?*	Humerus		216		
MB.1970.42.2	*T. conspicuus*	Cervical vertebra (12th)	87			
MHI 1142	*T. conspicuus*	Dorsal vertebra	47			
MHI 1172	*T. conspicuus*	Caudal vertebra (anterior)	34	49		67
MHI 1339	*T. conspicuus*	Cervical vertebra (12th)	55			
MHI 2094	*T. conspicuus*	Caudal vertebra (anterior)	41			
MHI 2194	*T. conspicuus*	Ischium	147			158
MHI 2199/2	*T. conspicuus*	Sacral vertebra	17	26		
MHI 2200	*T. conspicuus*	Caudal vertebra (anterior)	16	23		
MHI 2201	*T. conspicuus*	Cervical vertebra	118	133	13	
MHI 788	*T. conspicuus*	Dorsal rib (anterior)		124		
NHMS-WT 2720	*T. conspicuus*	Ilium	105			79
NHMW 1839/0013/0215	*T. conspicuus*	Cervical vertebra		153		
NHMUK PV OR 48202	*T. conspicuus*	Caudal vertebra (posterior)	33			
SMF R 2022	*T. conspicuus*	Sacral vertebra	30			
SMF R 282a	*T. conspicuus*	Caudal vertebra (anterior)	30	42		51
SMF R 283	*T. conspicuus*	Caudal vertebra (anterior)	38			
SMF R 285	*T. conspicuus*	Cervical vertebra (10th)	136	149	31	37
SMF R 286	*T. conspicuus*	Caudal vertebra (anterior)	46			
SMF R 287	*T. conspicuus*	Caudal vertebra (posterior)	36	44		30
SMF R 4034	*T. conspicuus*	Humerus		196		
SMF R 4092	*T. conspicuus*	Caudal vertebra (anterior)	43	55		
SMF R 69	*T. conspicuus?*	Humerus		76		
SMF R 820	*T. conspicuus*	Dorsal vertebra	42	52		79
SMNS 13337	*T. conspicuus*	Dorsal vertebra (10th)	26	40		71
SMNS 13337	*T. conspicuus*	Dorsal vertebra (11th)	26	35		69
SMNS 13337	*T. conspicuus*	Dorsal vertebra (12th)	24	35		62
SMNS 13337	*T. conspicuus*	Dorsal vertebra (4th)		39		
SMNS 13337	*T. conspicuus*	Dorsal vertebra (5th)	33	43		72
SMNS 13337	*T. conspicuus*	Dorsal vertebra (6th)	33	40		75
SMNS 13337	*T. conspicuus*	Dorsal vertebra (7th)	34	43		74
SMNS 13337	*T. conspicuus*	Dorsal vertebra (8th)	33	40		72
SMNS 13337	*T. conspicuus*	Dorsal vertebra (9th)	31	39		75
SMNS 13337	*T. conspicuus*	Sacral vertebra (1st)	24			
SMNS 15891	*T. conspicuus*	Cervical vertebra	167	193	19	33
SMNS 16643	*T. conspicuus*	Caudal vertebra (anterior)		50		
SMNS 50226	*T. conspicuus*	Axis	88	109	39	46
SMNS 54621	*T. conspicuus*	Femur		184		
SMNS 54624	*T. conspicuus*	Femur		277		
SMNS 54627	*T. conspicuus*	Caudal vertebra (anterior)	42			94
SMNS 54628	*T. conspicuus*	Dorsal vertebra	41	56		119
SMNS 54629	*T. conspicuus*	Dorsal vertebra	58	67		
SMNS 54630	*T. conspicuus*	Cervical vertebra (12th)	77	87		
SMNS 54631	*T. conspicuus*	Sacral vertebra	19	31		

SMNS 54632	*T. conspicuus*	Sacral vertebra	14	26		
SMNS 54633	*T. conspicuus*	Cervical vertebra	97	109		
SMNS 54639	*T. conspicuus*	Dorsal vertebra	36			
SMNS 54640	*T. conspicuus*	Dorsal vertebra	38	51		80
SMNS 54654	*T. conspicuus*	Cervical vertebra (12th)	40	44		43
SMNS 55341	*T. conspicuus*	Dorsal vertebra	44	62		131
SMNS 57531	*T. conspicuus*	Cervical vertebra (13th?)	44	54		
SMNS 59380	*T. conspicuus*	Femur		253		
SMNS 81989	*T. conspicuus*	Post-cloacal bone (morphotype Z)		210		
SMNS 84821	*T. conspicuus*	Cervical vertebra (11th)	191	213	69	72
SMNS 8728	*T. conspicuus*	Cervical vertebra (12th)	82	97		
SNSB-BSPG 1988 I 32	*T. conspicuus*	Cervical vertebra	209		21	
U-MO BT 2171	*T. conspicuus*	Caudal vertebra (anterior)	35	48		63
U-MO BT 3079	*T. conspicuus*	Humerus		146		
U-MO BT 732	*T. conspicuus*	Cervical vertebra	189		15	
U-MO BT 735	*T. conspicuus*	Caudal vertebra (anterior)	36	43		
U-MO BT 736	*T. conspicuus*	Cervical vertebra	287	309	36	42
U-MO BT 739	*T. conspicuus*	Cervical vertebra	266	284	25	
U-MO BT 740	*T. conspicuus*	Cervical vertebra	252	272	26	
U-MO BT 741	*T. conspicuus*	Dorsal vertebra	46	57		
ZPAL V. 36/100/3	*T. conspicuus*	Cervical vertebra (3rd)	223	245	21	30
ZPAL V. 36/100/4	*T. conspicuus*	Cervical vertebra (4th)	221	257	25	36
ZPAL V. 36/100/5	*T. conspicuus*	Cervical vertebra (5th)	221	257	28	42
ZPAL V. 36/100/6	*T. conspicuus*	Cervical vertebra (6th)	220	257	28	53
ZPAL V. 36/100/7	*T. conspicuus*	Cervical vertebra (7th)	241	278	26	57
ZPAL V. 36/1000	*T. conspicuus*	Cervical rib (12th)		151		36
ZPAL V. 36/1001	*T. conspicuus*	Cervical rib (12th)		115		32
ZPAL V. 36/1006	*T. conspicuus*	Ischium		126		130
ZPAL V. 36/1008	*T. conspicuus*	Pubis		107	58	37
ZPAL V. 36/101	*T. conspicuus*	Cervical vertebra	330	375	40	70
ZPAL V. 36/102	*T. conspicuus*	Cervical vertebra	252	286	28	55
ZPAL V. 36/103	*T. conspicuus*	Cervical vertebra	244	268	21	44
ZPAL V. 36/1033	*T. conspicuus*	Dorsal vertebra	36	64		121
ZPAL V. 36/1034	*T. conspicuus*	Cervical vertebra	272		27	39
ZPAL V. 36/1036	*T. conspicuus*	Dorsal vertebra	45	60		117
ZPAL V. 36/1037	*T. conspicuus*	Sacral vertebra	44	56		97
ZPAL V. 36/104	*T. conspicuus*	Cervical vertebra (10th)	284	312	46	52
ZPAL V. 36/105	*T. conspicuus*	Cervical vertebra (10th)	291	331	54	67
ZPAL V. 36/106	*T. conspicuus*	Cervical vertebra (11th)	204	230		68
ZPAL V. 36/1062	*T. conspicuus*	Coracoid		161		125
ZPAL V. 36/1065	*T. conspicuus*	Femur		302		
ZPAL V. 36/107	*T. conspicuus*	Cervical vertebra (11th)	200	225		60
ZPAL V. 36/1070	*T. conspicuus*	Caudal vertebra (posterior)	42	39		29
ZPAL V. 36/1078	*T. conspicuus*	Cervical vertebra	266	307	38	66
ZPAL V. 36/108	*T. conspicuus*	Cervical vertebra (12th)	83	92		103
ZPAL V. 36/1081	*T. conspicuus*	Caudal vertebra (anterior)	43	63		85
ZPAL V. 36/1105	*T. conspicuus*	Dorsal vertebra		54		113
ZPAL V. 36/112	*T. conspicuus*	Dorsal vertebra	50			112

ZPAL V. 36/1128	*T. conspicuus*	Cervical vertebra (11th)	163			65
ZPAL V. 36/113	*T. conspicuus*	Caudal vertebra (anterior)	44	66		96
ZPAL V. 36/1137	*T. conspicuus*	Post-cloacal bone (morphotype Z)		301		
ZPAL V. 36/114	*T. conspicuus*	Caudal vertebra (anterior)	33	53		87
ZPAL V. 36/1146	*T. conspicuus*	Ischium		113		114
ZPAL V. 36/1147	*T. conspicuus*	Post-cloacal bone (morphotype Z)		253		
ZPAL V. 36/1148	*T. conspicuus*	Post-cloacal bone (morphotype P)		296		
ZPAL V. 36/115	*T. conspicuus*	Caudal vertebra (posterior)	40	41		33
ZPAL V. 36/116	*T. conspicuus*	Caudal vertebra (posterior)	43	49		42
ZPAL V. 36/1170	*T. conspicuus*	Axis	86	99		36
ZPAL V. 36/1171	*T. conspicuus*	Cervical vertebra (11th)	153	167		62
ZPAL V. 36/1173	*T. conspicuus*	Cervical vertebra	73		11	
ZPAL V. 36/1176	*T. conspicuus*	Fibula		189		
ZPAL V. 36/1177	*T. conspicuus*	Coracoid		158		115
ZPAL V. 36/1186	*T. conspicuus*	Caudal vertebra (anterior)	41	49		73
ZPAL V. 36/1187	*T. conspicuus*	Sacral vertebra	30	37		98
ZPAL V. 36/1192	*T. conspicuus*	Cervical vertebra (13th)	70	97		123
ZPAL V. 36/1193	*T. conspicuus*	Pubis		126	53	40
ZPAL V. 36/1200	*T. conspicuus*	Tibia		202		
ZPAL V. 36/1202	*T. conspicuus*	Cervical vertebra	287	333	34	59
ZPAL V. 36/1209	*T. conspicuus*	Cervical vertebra (12th)	100	100		92
ZPAL V. 36/123	*T. conspicuus*	Dorsal rib (anterior)		262		
ZPAL V. 36/124	*T. conspicuus*	Caudal vertebra (anterior)	36	53		74
ZPAL V. 36/1248	*T. conspicuus*	Cervical vertebra	230		28	53
ZPAL V. 36/1249	*T. conspicuus*	Dorsal vertebra	58	73		104
ZPAL V. 36/125	*T. conspicuus*	Dorsal vertebra (11th)	44			
ZPAL V. 36/125	*T. conspicuus*	Ilium				91
ZPAL V. 36/125	*T. conspicuus*	Sacral vertebra (1st)	44			98
ZPAL V. 36/125	*T. conspicuus*	Dorsal rib (3rd)		265		
ZPAL V. 36/125	*T. conspicuus*	Dorsal vertebra (10th)	44			103
ZPAL V. 36/125	*T. conspicuus*	Dorsal vertebra (12th)	44			
ZPAL V. 36/125	*T. conspicuus*	Dorsal vertebra (2nd)	63			108
ZPAL V. 36/125	*T. conspicuus*	Dorsal vertebra (3rd)	60			105
ZPAL V. 36/125	*T. conspicuus*	Dorsal vertebra (4th)	63			113
ZPAL V. 36/125	*T. conspicuus*	Dorsal vertebra (5th)	59			113
ZPAL V. 36/125	*T. conspicuus*	Dorsal vertebra (6th)	60			108
ZPAL V. 36/125	*T. conspicuus*	Dorsal vertebra (7th)	61			119
ZPAL V. 36/125	*T. conspicuus*	Dorsal vertebra (8th)	59			115
ZPAL V. 36/125	*T. conspicuus*	Dorsal vertebra (9th)	54			115
ZPAL V. 36/125	*T. conspicuus*	Scapula		172		128
ZPAL V. 36/1251	*T. conspicuus*	Cervical rib (13th)		127		47
ZPAL V. 36/1267	*T. conspicuus*	Tibia		127		
ZPAL V. 36/127	*T. conspicuus*	Cervical vertebra	270	308	30	60
ZPAL V. 36/133	*T. conspicuus*	Axis	84	89		30
ZPAL V. 36/139	*T. conspicuus*	Caudal vertebra (posterior)	41	49		45
ZPAL V. 36/141	*T. conspicuus*	Dorsal vertebra	57			117
ZPAL V. 36/142	*T. conspicuus*	Caudal vertebra (anterior)	44			90
ZPAL V. 36/143	*T. conspicuus*	Dorsal vertebra	50	65		119

ZPAL V. 36/145	*T. conspicuus*	Dorsal vertebra	57			113
ZPAL V. 36/146	*T. conspicuus*	Dorsal vertebra	44	65		137
ZPAL V. 36/148	*T. conspicuus*	Caudal vertebra (anterior)	34	50		93
ZPAL V. 36/154	*T. conspicuus*	Cervical vertebra	275	312	34	56
ZPAL V. 36/1721	*T. conspicuus*	Caudal vertebra (posterior)	44	57		50
ZPAL V. 36/173	*T. conspicuus*	Dorsal vertebra	54	63		96
ZPAL V. 36/178	*T. conspicuus*	Pubis		99	51	36
ZPAL V. 36/181	*T. conspicuus*	Cervical vertebra	49	56	6	11
ZPAL V. 36/182	*T. conspicuus*	Cervical vertebra	374		40	
ZPAL V. 36/183	*T. conspicuus*	Caudal vertebra (posterior)	48			48
ZPAL V. 36/183	*T. conspicuus*	Dorsal vertebra	54	73		114
ZPAL V. 36/1834	*T. conspicuus*	Fibula		194		
ZPAL V. 36/186	*T. conspicuus*	Cervical vertebra	214	241	16	41
ZPAL V. 36/186	*T. conspicuus*	Cervical vertebra (10th)	297	327	50	60
ZPAL V. 36/187	*T. conspicuus*	Humerus		198		
ZPAL V. 36/196	*T. conspicuus*	Cervical vertebra	285	350	44	74
ZPAL V. 36/198	*T. conspicuus*	Dorsal vertebra	57			135
ZPAL V. 36/2400	*T. conspicuus*	Cervical rib (13th)		129		50
ZPAL V. 36/2408	*T. conspicuus*	Tibia		201		
ZPAL V. 36/2418	*T. conspicuus*	Caudal vertebra (anterior)	45	64		78
ZPAL V. 36/2459	*T. conspicuus*	Cervical vertebra	237	277	27	63
ZPAL V. 36/2434	*T. conspicuus*	Humerus		203		
ZPAL V. 36/2485	*T. conspicuus*	Cervical vertebra (13th)	70	73		108
ZPAL V. 36/2488	*T. conspicuus*	Radius		131		
ZPAL V. 36/2489	*T. conspicuus*	Caudal vertebra (anterior)	49	58		56
ZPAL V. 36/2490	*T. conspicuus*	Caudal vertebra (anterior)	43	55		55
ZPAL V. 36/2490	*T. conspicuus*	Caudal vertebra (anterior)	48	57		52
ZPAL V. 36/597	*T. conspicuus*	Post-cloacal bone (morphotype P)		262		
ZPAL V. 36/801	*T. conspicuus*	Femur		319		
ZPAL V. 36/805	*T. conspicuus*	Cervical vertebra (11th)		183		69
ZPAL V. 36/805	*T. conspicuus*	Ilium		97		67
ZPAL V. 36/806	*T. conspicuus*	Scapula		185		140
ZPAL V. 36/807	*T. conspicuus*	Femur		240		
ZPAL V. 36/808	*T. conspicuus*	Scapula		184		133
ZPAL V. 36/811	*T. conspicuus*	Scapula		182		133
ZPAL V. 36/813	*T. conspicuus*	Ilium		98		80
ZPAL V. 36/814	*T. conspicuus*	Coracoid		189		143
ZPAL V. 36/816	*T. conspicuus*	Scapula		162		113
ZPAL V. 36/829	*T. conspicuus*	Ulna		131		
ZPAL V. 36/830	*T. conspicuus*	Radius		132		
ZPAL V. 36/833	*T. conspicuus*	Tibia		201		
ZPAL V. 36/835	*T. conspicuus*	Humerus		187		
ZPAL V. 36/838	*T. conspicuus*	Femur		314		
ZPAL V. 36/847	*T. conspicuus*	Axis	75	94		28
ZPAL V. 36/849	*T. conspicuus*	Cervical vertebra (12th)	83	96		76
ZPAL V. 36/867	*T. conspicuus*	Caudal vertebra (anterior)	34	46		91
ZPAL V. 36/881	*T. conspicuus*	Humerus		219		
ZPAL V. 36/882	*T. conspicuus*	Humerus		169		

ZPAL V. 36/884	*T. conspicuus*	Sacral vertebra	41	52		86
ZPAL V. 36/885	*T. conspicuus*	Tibia		125		
ZPAL V. 36/886	*T. conspicuus*	Cervical vertebra (11th)	182			64
ZPAL V. 36/887	*T. conspicuus*	Cervical vertebra	273	309	36	63
ZPAL V. 36/888	*T. conspicuus*	Caudal vertebra (anterior)	42	61		91

Lost specimens of (or possibly referrable to) *Tanystropheus conspicuus*.

Taxon	Contents	Locality	Stratigraphy	Casts	References	History
Tanystropheus conspicuus	Postcloacal bone (morphotype P)	Bayreuth, Germany	Upper Muschelkalk		Braun 1840 (plate 12, bottom left)	Figured in Braun (1840) as an indeterminate reptile bone. Could not be located at U-MO.
?*Tanystropheus*	Femur, tibia, fibula	Mont-sur-Meurthe, France	Upper Muschelkalk		Corroy 1928 (fig. 12, plate 4, fig. 11), Wild 1973, Spiekman & Scheyer 2019	Partial articulated hindlimb described and assigned to *Thecodontosaurus latespinatus* by Corroy (1928), assigned to *Tanystropheus conspicuus* by Wild (1973). In possession of the University of Strasbourg at the time of Corroy (1928), later in the Museum and Aquarium Nancy under the number MAN 2016.0.213, original labels present, but current location of the specimen unknown (pers. comm. Thibaut Keinerknecht 01.2023)
?*Tanystropheus*	Vertebra	Kleinromstedt near Jena, Germany	Upper Muschelkalk		Lang & von Huene 1952 (p. 22)	Mentioned in Lang & von Huene (1952). In a private collection of K. Walther (Univeristy of Jena) at the time of H. Rühle von Lilienstern's mention (around 1940). Could not be located.
Tanystropheus conspicuus	Cervical vertebra (11th)	Laryszów (Larischhof), Poland	Upper Muschelkalk		Langenhan 1903 (plate 15, fig. 8), Langenhan 1911 (plate 20, fig. 30)	Described by Langenhan (1903; 1911), found by Eck. Could not be located.
Tanystropheus conspicuus	Dorsal vertebra	Gaildorf, Germany	Lettenkeuper		Plieninger 1846 (fig. 4), von Huene 1907-1908 (figs 201-202), von Huene 1931, Wild 1973, Spiekman & Scheyer 2019 (supp. tab. 1)	Dorsal vertebra, one of the paralectotypes of *Zanclodon laevis* Plieninger, 1846, assigned to *Tanystropheus* by von Huene (1931) and to *Tanystropheus conspicuus* by Wild (1973, p. 149-150). Could not be located.
Tanystropheus conspicuus	Cervical vertebra (13th)	Laineck, Germany	Upper Muschelkalk	GPIT-PV-60024, GPIT-PV-60025	von Huene 1902 (plate 7, fig. 2), Schmidt 1928 (fig. 1160), Kuhn 1971 (plate 17, fig. 1), Wild 1973 (p. 147, 149), , Spiekman & Scheyer 2019	The holotype of *Chelyzoon latum* von Huene, 1902; stored in Munich at the time of description. Could not be located.
Tanystropheus conspicuus	Caudal vertebra (anterior)	Laineck, Germany	Upper Muschelkalk, *semipartitus*-Zone	GPIT-PV-60140	von Huene 1907-1908 (fig. 239; plate 92, fig. 2), Broili 1915 (plate 3, fig. 3)	Described by von Huene (1907-1908), a syntype of *Thecodontosaurus latespinatus*, later assigned to *Tanystropheus conspicuus* by von Huene (1931). Originally stored in Munich, but could not be located there.
Tanystropheus conspicuus	Caudal vertebra (posterior)	Laineck, Germany	Upper Muschelkalk, *semipartitus*-Zone	GPIT-PV-60131, SMNS 50154	von Huene 1907-1908 (plate 91, fig. 2), Schmidt 1928 (fig. 1213), Kuhn 1969 (plate 21, fig. 22), Kuhn 1971 plate 21, fig. 26)	Described by von Huene (1907-1908), a syntype of *Thecodontosaurus latespinatus*, later assigned to *Tanystropheus conspicuus* by von Huene (1931). Could not be located at U-MO.
Tanystropheus conspicuus	Dorsal vertebra	Blainville-sur-l'Eau, France	Upper Muschelkalk, *semipartitus*-Zone		von Huene 1907-1908 (plate 91, fig. 3)	Described by von Huene (1907-1908), a syntype of *Thecodontosaurus latespinatus*, later assigned to *Tanystropheus conspicuus* by von Huene (1931). Originally in possession of the University of Stasbourg but could not be located there (pers. comm. Kévin Janneau 01.2023).
Tanystropheus conspicuus	Dorsal vertebra	Laineck, Germany	Upper Muschelkalk, *semipartitus*-Zone	GPIT-PV-60136	von Huene 1907-1908 (plate 91, fig. 4)	Described by von Huene (1907-1908), a syntype of *Thecodontosaurus latespinatus*, later assigned to *Tanystropheus conspicuus* by von Huene (1931). Originally stored in Munich, but could not be located there.
Tanystropheus conspicuus	Caudal vertebra (anterior)	Laineck, Germany	Upper Muschelkalk, *semipartitus*-Zone	GPIT-PV-60139	von Huene 1907-1908 (plate 92, fig. 4)	Described by von Huene (1907-1908), a syntype of *Thecodontosaurus latespinatus*, later assigned to *Tanystropheus conspicuus* by von Huene (1931). Originally stored in Munich, but could not be located there.
Tanystropheus conspicuus	Cervical vertebra	Oberbronn, France	Upper Muschelkalk		von Huene 1907-1908 (plate 96, fig. 8), Brignon 2021 (fig. 34B), Spiekman & Scheyer 2019 (supp. tab. 1)	Described by von Huene (1907-1908) and in possession of the University of Stasbourg at that time. Could not be located there (pers. comm. Kévin Janneau 01.2023). Most probably destroyed (see Wild 1973, p. 80).

?*Tanystropheus*	Tibia?	Wesseln near Bad Salzdetfurt, Germany	Upper Muschelkalk, "middle Ceratitenschichten"		von Huene 1958 (fig. 1)	A limb bone described as a parasuchian radius by von Huene (1958). In Museum Braunshweig at that time. Could not be located (pers. comm. R. Kosma; Naturkundemuseum der 3Landesmuseen Braunschweig; 10.2024).
Tanystropheus conspicuus	Cervical vertebra	Bindlacher Berg, Germany	Upper Muschelkalk		von Meyer 1847-1855 (plate 30, fig. 6), Peyer 1931 (fig. 2), Shmidt 1938 (fig. 1188a:c), Kuhn 1971 (Plate 21a, fig. 1c)	Paralectotype of *T. conspicuus*. Could not be located at U-MO.
Tanystropheus conspicuus	Cervical vertebra	Bindlacher Berg, Germany	Upper Muschelkalk		von Meyer 1847-1855, (plate 46, fig. 2)	Paralectotype of *T. conspicuus*. Could not be located at U-MO.
Tanystropheus conspicuus	Cervical vertebra	Bindlacher Berg, Germany	Upper Muschelkalk		von Meyer 1847-1855, (plate 46, fig. 3)	Paralectotype of *T. conspicuus*. Could not be located at U-MO.
Tanystropheus conspicuus	Cervical vertebra	Bindlacher Berg, Germany	Upper Muschelkalk		von Meyer 1847-1855, (plate 46, fig. 4)	Paralectotype of *T. conspicuus*. Could not be located at U-MO.

Measurements of the dorsal vertebrae of *Tanystropheus* spp. (see Fig. 23).

Species	Specimen	Vertebra	Dorsal vertebra centrum length [mm]	Dorsal vertebra height [mm]
T. conspicuus	SMF R 820	Uncertain	42	79
T. conspicuus	SMNS 13337	DV10	26	71
T. conspicuus	SMNS 13337	DV11	26	69
T. conspicuus	SMNS 13337	DV12	24	62
T. conspicuus	SMNS 13337	DV5	33	72
T. conspicuus	SMNS 13337	DV6	33	75
T. conspicuus	SMNS 13337	DV7	34	74
T. conspicuus	SMNS 13337	DV8	33	72
T. conspicuus	SMNS 13337	DV9	31	75
T. conspicuus	SMNS 54628	Uncertain	41	119
T. conspicuus	SMNS 54640	Uncertain	38	80
T. conspicuus	SMNS 55341	Uncertain	44	131
T. conspicuus	ZPAL V. 36/1033	Uncertain	36	121
T. conspicuus	ZPAL V. 36/1036	Uncertain	45	117
T. conspicuus	ZPAL V. 36/112	Uncertain	50	112
T. conspicuus	ZPAL V. 36/1249	Uncertain	58	104
T. conspicuus	ZPAL V. 36/125	DV10	44	103
T. conspicuus	ZPAL V. 36/125	DV2	63	108
T. conspicuus	ZPAL V. 36/125	DV3	60	105
T. conspicuus	ZPAL V. 36/125	DV4	63	113
T. conspicuus	ZPAL V. 36/125	DV5	59	113
T. conspicuus	ZPAL V. 36/125	DV6	60	108
T. conspicuus	ZPAL V. 36/125	DV7	61	119
T. conspicuus	ZPAL V. 36/125	DV8	59	115
T. conspicuus	ZPAL V. 36/125	DV9	54	115
T. conspicuus	ZPAL V. 36/141	Uncertain	57	117
T. conspicuus	ZPAL V. 36/143	Uncertain	50	119
T. conspicuus	ZPAL V. 36/145	Uncertain	57	113
T. conspicuus	ZPAL V. 36/146	Uncertain	44	137
T. conspicuus	ZPAL V. 36/173	Uncertain	54	96
T. conspicuus	ZPAL V. 36/183	Uncertain	54	114
T. conspicuus	ZPAL V. 36/198	Uncertain	57	135
T. hydroides	PIMUZ T 2480	DV12	25	30
T. hydroides	PIMUZ T 2483	DV8	25	27
T. hydroides	PIMUZ T 2483	DV10	22	28
T. hydroides	PIMUZ T 2483	DV3	25	25
T. hydroides	PIMUZ T 2483	DV4	27	27
T. hydroides	PIMUZ T 2483	DV5	25	26
T. hydroides	PIMUZ T 2483	DV6	26	25
T. hydroides	PIMUZ T 2483	DV7	24	24
T. hydroides	PIMUZ T 2787	DV1	29	32
T. hydroides	PIMUZ T 2787	DV2	28	32
T. hydroides	PIMUZ T 2787	DV3	27	31
T. hydroides	PIMUZ T 2787	DV4	28	31
T. hydroides	PIMUZ T 2798	DV4	29	31

T. hydroides	PIMUZ T 2817	DV1	32	33
T. hydroides	PIMUZ T 2817	DV2	32	32
T. hydroides	PIMUZ T 2817	DV3	30	32
T. hydroides	SNSB-BSPG 1953 XV	DV2	21	20
T. hydroides	SNSB-BSPG 1953 XV	DV3	21	20
T. hydroides	SNSB-BSPG 1953 XV	DV4	21	20
T. longobardicus	MCSN 4451	DV7	12	10
T. longobardicus	MCSN 4451	DV8	12	10
T. longobardicus	MCSN 4451	DV9	12	10
T. longobardicus	MSNM BES SC 265	DV1	11	11
T. longobardicus	MSNM BES SC 265	DV10	10	10
T. longobardicus	PIMUZ T 1277	DV2	14	12
T. longobardicus	PIMUZ T 1277	DV5	15	13
T. longobardicus	PIMUZ T 1277	DV7	14	13
T. longobardicus	PIMUZ T 1277	DV8	15	13
T. longobardicus	PIMUZ T 2791	DV8	10	9
T. longobardicus	PIMUZ T 2791	DV9	10	9
T. longobardicus	PIMUZ T 2795	DV11	13	11

Specimens no longer considered to be referrable to *Tanystropheus conspicuus*.

Specimen number	Original taxon identification	Original element identification	Revised taxon identification	Revised element identification	Locality	Stratigraphy	Notes	References
GPIT-PV-117177	*Tanystropheus* sp.	Ilium	Sauropterygia indet.	Scapula	Kirchberg/Jagst, Germany	Upper Muschelkalk		von Huene 1958 (fig. 3), Wild 1973 (p. 114)
GPIT-PV-44258	*T. conspicuus*	Cervical vertebra	*Mastodonsaurus* sp.	Rib	Öhlmühle, Germany	Lowermost Lettenkeuper, Grenzbonebed ?		
GPIT-PV-60014	*Pectenosaurus strunzi*	Caudal vertebra?	Sauropsida indet.	Vertebra	Bayreuth, Germany	Upper Muschelkalk	Vertebra, the holotype of *Pectenosaurus strunzi von Huene*, 1902, assigned to *Tanystropheus* by Romer (1956) and to *Tanystropheus conspicuus* by Spiekman & Scheyer (2019)	von Huene 1902 (plate 6, 5ig. 5)
Lost specimen	*Zanclodon laevis*	Vertebra	Archosaurmorpha indet.	Vertebra	Gaildorf, Germany	Lettenkeuper	Vertebra, a paralectotype of *Zanclodon laevis* Plieninger, 1846, assigned to *Tanystropheus* by von Huene (1931) and to *Tanystropheus conspicuus* by Wild (1973, p. 149-150)	Plieninger 1846 (fig. 6), von Huene 1907-1908 (fig. 200), von Huene 1931, Wild 1973
Lost specimen	*Tanystropheus*	Claw	?Archosauromorpha indet.	Claw	Bayreuth, Germany	Upper Muschelkalk		von Huene 1931 (fig. 5)
MAN 2016.0.215	*T. conspicuus*	Neural spine?	Sauropsida indet.	Indeterminate bone	Mont-sur-Meurthe, France	Upper Muschelkalk?	Possibly an anterior dorsal rib of *Tanystropheus* sp., but too incomplete for identification. Unaccessioned	
MB. uncatalogued	*?Tanystropheus*	Metatarsal	Sauropsida indet.	Limb bone	Bayreuth, Germany	Upper Muschelkalk	Possibly a ?tibia of *Tanystropheus* sp., but would have to be prepared to check	
MB.uncatalogued	*Tanystropheus*	Cervical vertebra	?Sauropterygia indet.	Sacral rib?	Bayreuth, Germany	Upper Muschelkalk		
MHI 2202	*Tanystropheus/Nothosaurus*	Tooth	Sauropsida indet.	Tooth	Rüblingen, Germany	Lowermost Lettenkeuper, Grenzbonebed		
NHMW 1852/0001/0684	*Nothosaurus mirabilis*	Tooth	Sauropsida indet.	Tooth	Laineck, Germany	Upper Muschelkalk	Possibly of *Tanystropheus* sp., but would have to be prepared to check	
NME 93/132	*T. conspicuus*	Cervical rib fragment	Sauropsida indet.	Gastralium?	Bischleben, Germany	Upper Muschelkalk, mo2		
NME 93/134	*T. conspicuus*	Cervical vertebra	Tetrapoda indet.	Indeterminate bone	Mobisburg, Germany	Upper Muschelkalk, mo2		
SMNS 50067	*Tanystropheus*	Cervical rib	Tetrapoda	Indeterminate	Rüblingen,	Upper		

	sp.	fragment	indet.	bone	Germany	Muschelkalk, *nodosus*-Zone		
SMNS 50222	?*Tanystropheus* sp.	Interclavicle fragment?	Tetrapoda indet.	Indeterminate bone	Gaildorf, Germany	Upper Muschelkalk, *nodosus*-Zone		
SMNS 50825	*Tanystropheus* sp.	Tooth	Sauropsida indet.	Tooth	Roßwag, Germany	Lower Lettenkeuper, dolomite over Blaubank		
SMNS 51578	*T. conspicuus?*	Caudal vertebra?	Sauropsida indet.	Caudal vertebra	Wechrieden, Germany	Lowermost Lettenkeuper, Grenzbonebed		
SMNS 51975	*?Tanystropheus*	Tooth	Tetrapoda indet.	Tooth	Stuttgart-Untertü...heim, Germany	Upper Lettenkeuper, Anoplophora-Dolomite		
SMNS 52288	*Tanystropheus* sp.	Gastralium	Sauropsida indet.	Gastralium	Burgstall, Germany	Upper Muschelkalk		
SMNS 52323	*T. conspicuus?*	Tooth	Sauropsida indet.	Tooth	Seeholz near Herdtlingshagen, Germany	Upper Lettenkeuper, Anthrakonitbank	Possibly of *Tanystropheus* sp., but would have to be prepared to check	
SMNS 52985	*Tanystropheus* sp.	Tooth	Sauropsida indet.	Tooth	Eschenau, Germany	Lower Lettenkeuper, Hauptsandstein		
SMNS 54146	*?Tanystropheus*	Tooth	Sauropsida indet.	Tooth	Kübelhof, Germany	Upper Muschelkalk, *nodosus*-Zone	Possibly of *Tanystropheus* sp., but too incomplete for identification	
SMNS 54149	Not specified	Teeth	Sauropsida indet.	Teeth	Not specified	Not specified	Within a "*Tanystropheus*" drawer	
SMNS 54152	Not specified	Teeth	Sauropsida indet.	Teeth	Not specified	Not specified	Within a "*Tanystropheus*" drawer	
SMNS 54625	*T. conspicuus*	Ischium	Sauropterygia indet.	Pubis/ischium	Hegnabrunn, Germany	Upper Muschelkalk, *enodis-leavigatus*-Zone		Spiekman and Scheyer 2019 (supp. tab. 1)
SMNS 54634	*?Tanystropheus*	Interclavicle	Sauropsida indet.	Skull bone	Hegnabrunn, Germany	Upper Muschelkalk		
SMNS 54636	?*Tanystropheus* sp.	Interclavicle fragment?	Sauropsida indet.	Skull bone	Feldbuch, Germany	Lowermost Lettenkeuper, Grenzbonebed		
SMNS 54637	*?Tanystropheus*	Interclavicle fragment?	Sauropsida indet.	Skull bone?	Hegnabrunn, Germany	Upper Muschelkalk, *spinosus-nodosus*-Zone		
SMNS 54638	*Tanystropheus*	Partial neural spine	Archosaurmorpha indet.	Partial neural spine	Bindlach, Germany	Upper Muschelkalk	Possibly of *Tanystropheus* sp., but too incomplete for identification	
SMNS 54645	*Tanystropheus*	Caudal vertebra	Archosaurmorpha indet.	Caudal vertebra	Unterrodach, Germany	Upper Muschelkalk, *nodosus*-Zone	Possibly of *Tanystropheus* sp., but too incomplete for identification	
SMNS 54646	*Tanystropheus* sp.	Cervical rib fragment	Sauropsida indet.	Cervical rib fragment	Bindlach, Germany	Upper Muschelkalk, *pulcher*-Zone	Possibly of *Tanystropheus* sp., but too incomplete for identification	
SMNS 54649	*Tanystropheus*	Partial neural spine	?Archosauromorpha indet.	Partial neural spine	Hegnabrunn, Germany	Upper Muschelkalk, *evolutus*-Zone		
SMNS 54651	*Tanystropheus* sp.	Cervical rib fragment	Sauropsida indet.	Cervical rib fragment	Hegnabrunn?, Germany	Upper Muschelkalk, *nodosus*-Zone	Possibly of *Tanystropheus* sp., but too incomplete for	

							identification	
SMNS 54652	*?Tanystropheus*	Interclavicle fragment	Sauropsida indet.	Skull bone	Dörfles near Kronach, Germany	Upper Muschelkalk, *spinosus-nodosus*-Zone?		Spiekman and Scheyer 2019 (supp. tab. 1)
SMNS 54655	*Tanystropheus*	Caudal vertebra	Archosaurmorpha indet.	Dorsal vertebra	Unterrodach, Germany	Upper Muschelkalk, *nodosus*-Zone	Possibly of *Tanystropheus* sp., but too incomplete for identification	
SMNS 54656	*?Tanystropheus*	Cervical vertebra (2 fragments)	Tetrapoda indet.	Indeterminate bone	Hegnabrunn, Germany	Upper Muschelkalk, *spinosus-nodosus*-Zone		
SMNS 54657	*Tanystropheus*	Long bone	Tetrapoda indet.	Limb bone	Unterrodach, Germany	Upper Muschelkalk, *nodosus*-Zone	Possibly an autopodal element of *Tanystropheus* sp., but not diagnostic enough for identification	
SMNS 54658	*Tanystropheus* sp.	Cervical rib fragment	Sauropsida indet.	Cervical rib fragment	Kübelhof, Germany	Upper Muschelkalk, *nodosus*-Zone	Possibly of *Tanystropheus* sp., but too incomplete for identification	
SMNS 54659	*Tanystropheus* sp.	Cervical rib fragment	Sauropsida indet.	Cervical rib fragment	Kulm?, Germany	Unreadable		
SMNS 54660	?*Tanystropheus* sp.	Interclavicle fragment?	Sauropsida indet.	Skull bone	Hegnabrunn, Germany	Upper Muschelkalk, *spinosus*-Zone		
SMNS 54661	*T. conspicuus*	Tooth	Sauropsida indet.	Tooth	Unreadable	Upper Muschelkalk, *nodosus*-Zone	Possibly of *Tanystropheus* sp., but too incomplete for identification	
SMNS 55002	*T. conspicuus*	Ischium	Sauropterygia indet.	Ischium	Vaihingen, Germany	Upper Muschelkalk, *Trigonodus*-Zone		Spiekman and Scheyer 2019 (supp. tab. 1)
SMNS 56289	*T. conspicuus*	Dentary	?Sauropterygia indet.	Dentary	Nitzenhausen, Germany	Upper Muschelkalk, *dorsoplanus*-Zone		Ezcurra 2016, Spiekman and Scheyer 2019 (supp. tab. 1)
SMNS 56488	*Tanystropheus* sp.	Cervical rib fragment	Sauropsida indet.	Cervical rib fragment	Rüblingen, Germany	Upper Muschelkalk, mo2	Possibly of *Tanystropheus* sp., but too incomplete for identification	
SMNS 56589	*?Tanystropheus*	Interclavicle	Tetrapoda indet.	Indeterminate bone	Neckarrens?, Germany	Upper Muschelkalk		
SMNS 56594	*Tanystropheus* sp.	Tooth	Sauropsida indet.	Tooth	Bettenfeld, Ansbach, Germany	Lowermost Lettenkeuper, Grenzbonebed	Possibly of *Tanystropheus* sp., but too incomplete for identification	
SMNS 56687	*Tanystropheus* sp.	Tooth	Sauropsida indet.	Tooth	Zwingelhausen, Germany	Lowermost Lettenkeuper, Grenzbonebed		
SMNS 56875	*T. conspicuus*	Tooth	Sauropsida indet.	Tooth	Steinbach near Hall, Germany	Upper muschelkalk, Discoceratiten schichten	Possibly of *Tanystropheus* sp., but too incomplete for identification	
SMNS 58912	*Tanystropheus* sp.	Tooth	Sauropsida indet.	Tooth	Mundelsheim, Germany	Lower Lettenkeuper, Vitriolschiefer		
SMNS 59814	*?Tanystropheus*	Teeth	Sauropsida indet.	Teeth	Crailsheim, Germany	Lowermost Lettenkeuper, Grenzbonebed	Possibly of *Tanystropheus* sp., but too incomplete for	

							identification	
SMNS 80089	*?Tanystropheus* sp.	Dentary	?Sauropterygia indet.	Dentary	Schmalfelden, Germany	Upper Muschelkalk, Discoceratiten schichten		
SMNS 80359	*Tanystropheus* sp.	Parasphenoid	Tetrapoda indet.	Indeterminate bone	Kirchberg/Jagst, Germany	Upper Muschelkalk, Frankische Grenzschichten		
SMNS 81250	*Tanystropheus* sp.	Cervical rib fragment	Tetrapoda indet.	Indeterminate bone	Rüblingen, Germany	Upper muschelkalk, Discoceratiten schichten		
SMNS 81251	*T. conspicuus*	Partial neural spine	?Archosauromorpha indet.	Partial neural spine	Rüblingen, Germany	Upper muschelkalk, Discoceratiten schichten	Possibly of *Tanystropheus* sp., but too incomplete for identification	
SMNS 81371	*T. conspicuus*	Metatarsal	Tetrapoda indet.	Limb bone	Rüblingen, Germany	Upper muschelkalk, Discoceratiten schichten	Possibly an autopodal element of *Tanystropheus* sp., but not diagnostic enough for identification	
SMNS 84799	*Tanystropheus* sp.	Tooth	Sauropsida indet.	Tooth	Crailsheim, Germany	Lowermost Lettenkeuper, Grenzbonebed	Possibly of *Tanystropheus* sp., but too incomplete for identification	
SMNS 84813	*Tanystropheus* sp.	Claw	?Archosauromorpha indet.	Claw	Kulmbach, Germany	Upper Muschelkalk, *spinosus*-Zone		
SMNS 84814	*?Tanystropheus*	Caudal vertebra (posterior)	Archosaurmorpha indet.	Caudal vertebra	Dörfles near Kronach, Germany	Upper Muschelkalk	Possibly of *Tanystropheus* sp., but too incomplete for identification	
SMNS 84817	*T. conspicuus*	Ischium	Sauropterygia indet.	Pubis/ischium	Hegnabrunn, Germany	Upper Muschelkalk, *spinosus*-Zone		Spiekman and Scheyer 2019 (supp. tab. 1)
SMNS 84819	*Tanystropheus*	Limb bone	Tetrapoda indet.	Limb bone	Eschenbach, Germany	?"Geougschichten"		
SMNS 91592	*Tanystropheus* sp.	Teeth (6)	Sauropsida indet.	Teeth (6)	Crailsheim, Germany	Lowermost Lettenkeuper, Grenzbonebed	Possibly of *Tanystropheus* sp., but too incomplete for identification	
SMNS uncatalogued	*T. conspicuus?*	Cervical vertebra fragment	Tetrapoda indet.	Indeterminate bone	Tiefenbach, Germany	Lowermost Lettenkeuper, Grenzbonebed		
SMNS uncatalogued	*T. conspicuus*	Ischium	Sauropterygia indet.	Pubis/ischium	Hegnabrunn, Germany	Upper Muschelkalk, *enodis-leavigatus*-Zone		
SMNS uncatalogued	Not specified	Teeth	Sauropsida indet.	Teeth	Not specified	Not specified	Within a "*Tanystropheus*" drawer. Collection of A. Sailacher. Some possibly of *Tanystropheus* sp., but too incomplete for identification	
SMNS uncatalogued	*Tanystropheus* sp.	Tooth	Indeterminate	Indeterminate	Crailsheim, Germany	Lowermost Lettenkeuper, Grenzbonebed	No specimen present in the box with the specimen card	
SMNS	*T. conspicuus*	Tooth	Sauropsida	Tooth	Crailsheim,	Lowermost	Possibly of	

uncatalogued			indet.		Germany	Lettenkeuper, Grenzbonebed	*Tanystropheus* sp., but too incomplete for identification	
SMNS uncatalogued	*Tanystropheus* sp.	Tooth	Sauropsida indet.	Tooth	… a. Weidenbach, Germany	Lettenkeuper	Possibly of *Tanystropheus* sp., but too incomplete for identification	
SMNS uncatalogued	*Tanystropheus* sp.	Tooth	Sauropsida indet.	Tooth	Crailsheim, Germany	Lowermost Lettenkeuper, Grenzbonebed	Possibly of *Tanystropheus* sp., but too incomplete for identification	
SMNS uncatalogued	*Tanystropheus* sp.	Tooth	Sauropsida indet.	Tooth	Tiefenbach, Germany	Lowermost Lettenkeuper, Grenzbonebed	Possibly of *Tanystropheus* sp., but too incomplete for identification	
SMNS uncatalogued	*Tanystropheus* sp.	Tooth	Sauropsida indet.	Tooth	Kornwestheim, Germany	Upper Muschelkalk	Possibly of *Tanystropheus* sp., but too incomplete for identification	
U-MO BT 3078	*T. conspicuus*	Tooth	?*Pistosaurus*	Tooth	Bindlacher Berg, Germany	Upper Muschelkalk		Diedrich 2012 (fig. 14, 1)
U-MO uncatalogued	*Tanystropheus*	Humerus	Sauropterygia indet.	Shoulder girdle fragment - ?partial clavicle articulated with an interclavicle	Laineck, Germany	Upper Muschelkalk		von Huene 1902 (plate 5, fig. 6), von Huene 1931 (fig. 4), Shmidt 1938 (fig. 1188a:d), Kuhn 1971 (plate 21a, fig. 1d), Wild 1973 (p. 109)

Appendix II

Character matrix used in the histotaphonomic analyses.

Specimen # (ZPAL V. 36/xxxx)	Miedary layer	Taxon	Element	Numerical analysis	Element shape	Taxon	Pore size	Lithological disparity between bone infill and the surrounding sediment	Glauconite	Glauconite weathering stage	Fe. Oxides or Fe rich sediment	Fe. Oxides lining	Pyrite lining	Pyrite crystals	Non-pyrite sulphide	Chlorite	Mica	Geopetal	Microsparite	Peloidal microsparite	Sparite drusy	Sparite mosaic	Sparite blocky	Sparite granular	Circumgranular	Micrite	Quartz grains
126	1	*Tanystropheus*	vertebra cervical	YES	2	1	3	**0**	**2**	**1**	**2**	**1**	**0**	**1**	**0**	**0**	**0**	**0**	**1**	**0**	**0**	**0**	**1**	**1**	**0**	**0**	**2**
150	2	*Tanystropheus*	vertebra cervical	YES	2	1	3		**2**	**2**	**1**	**1**	**0**	**2**	**0**	**0**	**0**		**2**	**0**	**0**	**0**	**0**	**0**	**0**	**0**	**1**
153	3	*Tanystropheus*	scapula	YES	1	1	1		**1**	**2**	**2**			**2**	**0**	**0**	**0**		**1**	**0**	**0**	**0**	**0**	**0**	**0**	**0**	**1**
156	3	*Tanystropheus*	vertebra cervical	YES	2	1	3	**1**	**2**	**4**	**2**	**2**	**1**	**2**	**0**	**0**	**0**	**0**	**2**	**0**	**1**	**1**	**0**	**0**	**0**	**1**	**1**
166	1	*Tanystropheus*	vertebra cervical	YES	2	1	3		**2**	**2**	**2**	**2**	**1**	**2**	**0**	**0**	**0**	**0**	**0**	**0**	**0**	**0**	**0**	**0**	**0**	**0**	**1**
176	3	*Tanystropheus*	vertebra cervical	YES	2	1	3		**2**	**4**	**2**	**2**	**1**	**2**	**0**	**0**	**0**	**0**	**0**	**0**	**0**	**0**	**0**	**1**	**0**	**0**	**1**
192	2	*Tanystropheus*	vertebra cervical	YES	2	1	3	**1**	**2**	**4**	**2**	**2**	**1**	**2**	**0**	**0**	**0**	**0**	**2**	**0**	**1**	**0**	**0**	**0**	**0**	**1**	**1**
193	2	*Tanystropheus*	vertebra cervical	YES	2	1	3	**0**	**2**	**4**	**2**	**2**	**0**	**2**	**0**	**0**	**0**	**0**	**2**	**0**	**1**	**1**	**2**	**1**	**0**	**1**	**1**
231	1	*Nothosaurus*	ischium	YES	1	2	1	**0**	**2**		**2**	**2**	**0**	**2**	**0**	**0**	**0**	**0**	**2**	**0**	**1**	**0**	**0**	**1**	**0**	**0**	**1**
250	3	*Nothosaurus*	pubis	YES	1	2	1		**0**	**0**	**2**	**2**	**1**	**2**	**0**	**0**	**0**	**0**	**1**	**0**	**0**	**0**	**2**	**0**	**0**	**0**	**0**
252	3	*Nothosaurus*	vertebral centrum	YES	4	2	2		**0**	**0**	**2**	**2**	**1**	**2**	**0**	**0**	**0**	**0**	**0**	**0**	**0**	**0**	**2**	**0**	**0**	**0**	**0**
261	2	*Nothosaurus*	ischium	YES	1	2	1	**0**	**2**	**2**	**2**	**2**	**0**	**0**	**0**	**0**	**0**	**0**	**0**	**0**	**1**	**0**	**2**	**0**	**0**	**0**	**0**
262	2	*Nothosaurus*	rib	YES	3	2	1	**0**	**2**	**3**	**2**	**2**	**0**	**2**	**0**	**0**	**0**	**0**	**0**	**0**	**1**	**0**	**2**	**1**	**0**	**0**	**1**
263	3	*Nothosaurus*	rib	YES	3	2	1	**1**	**0**	**0**	**2**	**2**	**0**	**0**		**0**	**0**	**0**	**0**	**0**	**0**	**0**	**2**	**1**	**0**	**0**	**1**
267	1	*Nothosaurus*	vertebral centrum	YES	4	2	2	**1**	**2**	**3**	**2**	**2**	**0**	**2**		**0**	**0**	**0**	**2**	**0**	**1**	**1**	**2**	**1**	**0**	**1**	**0**
270	1	*Nothosaurus*	rib	YES	3	2	1	**0**	**2**	**4**	**2**	**2**	**1**	**2**	**0**	**0**	**0**	**0**	**0**	**0**	**0**	**0**	**2**	**0**	**0**	**0**	**0**
274	2	*Nothosaurus*	vertebral centrum	YES	4	2	2	**1**	**2**	**4**	**2**	**2**		**2**	**0**	**0**	**0**	**0**	**0**	**0**	**1**	**0**	**0**	**0**	**0**	**0**	**0**
324	3	*Mastodonsaurus*	vertebral centrum	YES	4	3	2		**0**	**0**	**2**	**2**		**2**	**0**	**0**	**0**	**0**	**0**	**0**	**0**	**0**	**2**	**0**	**0**	**0**	**0**
347	2	*Mastodonsaurus*	vertebral centrum	YES	4	3	2		**0**	**0**	**2**	**2**		**2**	**0**	**0**	**0**	**0**	**0**	**0**	**1**	**0**	**0**	**1**	**0**	**0**	**0**
404	4	Testudinata indet.	rib	YES	3	8	1	**0**	**0**	**0**	**2**	**2**	**0**	**2**	**0**	**0**	**0**	**0**	**0**	**0**	**0**	**0**	**0**	**0**	**0**	**0**	**0**
410/11	4	Reptilia indet.	rib	NO	3	4	1	**0**	**0**	**0**	**0**	**0**	**0**	**1**	**0**	**2**	**0**	**0**	**0**	**0**	**0**	**0**	**0**	**0**	**0**	**0**	**0**
410/12	4	Reptilia indet.	rib	YES	3	4	1	**0**	**0**	**0**	**2**	**2**	**1**	**2**	**1**	**1**	**2**	**0**	**0**	**0**	**0**	**0**	**0**	**0**	**0**	**0**	**1**
410/13	4	Reptilia indet.	osteoderm	YES	1	4	1		**0**	**0**	**2**	**2**	**1**	**2**	**1**	**0**	**2**	**0**	**0**	**0**	**0**	**0**	**0**	**0**	**0**	**0**	**0**
411/10	4	Reptilia indet.	osteoderm	YES	1	4	1		**0**	**0**	**2**	**2**	**0**	**2**	**1**	**0**	**2**	**0**	**0**	**0**	**0**	**0**	**0**	**0**	**0**	**0**	**0**
576	5	*Nothosaurus*	rib	YES	3	2	1	**0**	**0**	**0**	**1**	**2**	**1**	**1**	**0**	**0**	**0**	**0**	**2**	**0**	**0**	**0**	**0**	**0**	**0**	**0**	**0**
599	3	*Nothosaurus*	rib	NO	3	2	1																				
611	2	Hybodontiformes	fin spine	YES	3	5	1	**0**	**2**	**3**	**2**	**2**	**0**	**2**	**0**	**0**	**0**	**0**	**2**	**0**	**0**	**0**	**0**	**1**	**0**	**0**	**2**
700	3	*Ptychoceratodus*	toothplate	YES	4	7	1		**2**	**4**	**2**			**0**	**0**	**0**	**0**	**0**	**0**	**0**	**0**	**0**	**2**	**0**	**0**	**0**	**2**
740	2	*Saurichthys*	mandibular ramus	YES	3	6	1		**0**	**0**	**0**	**0**	**0**	**0**	**0**	**0**	**0**	**0**	**2**	**0**	**0**	**0**	**0**	**0**	**0**	**0**	**0**
877	2	*Tanystropheus*	femur	YES	2	1	2		**2**	**4**	**2**	**2**	**1**	**2**	**0**	**0**	**0**		**2**	**0**	**1**	**1**	**0**	**0**	**0**	**1**	**1**
878	2	*Tanystropheus*	femur	YES	2	1	2	**1**	**0**	**0**	**2**	**2**	**1**	**2**	**0**	**0**	**0**	**1**	**2**	**0**	**0**	**1**	**2**	**0**	**0**	**1**	**0**
879	2	*Tanystropheus*	femur	YES	2	1	2		**2**	**3**	**2**	**2**	**1**	**2**	**0**	**0**	**0**	**0**	**2**	**0**	**1**	**0**	**2**	**0**	**0**	**1**	**2**
880	2	*Tanystropheus*	femur	YES	2	1	2		**2**	**4**	**2**	**2**	**0**	**2**	**0**	**0**	**0**	**0**	**2**	**1**	**1**	**0**	**0**	**0**	**0**	**0**	**1**
913	1	*Mastodonsaurus*	rib	YES	3	3	1		**0**	**0**	**1**	**1**	**0**	**1**	**0**	**0**	**0**	**0**	**0**	**0**	**0**	**0**	**0**	**0**	**0**	**0**	**0**
918	1	*Mastodonsaurus*	flat bone	YES	1	3	1	**1**	**0**	**0**	**2**	**2**	**0**	**2**	**0**	**0**	**0**	**0**	**0**	**0**	**1**	**1**	**0**	**0**	**0**	**0**	**0**
920	3	*Mastodonsaurus*	clavicle	YES	1	3	1	**0**	**2**	**4**	**2**	**2**	**0**	**2**	**0**	**0**	**0**	**0**	**2**	**0**	**1**	**0**	**1**	**0**	**0**	**0**	**1**
921	2	*Mastodonsaurus*	rib	YES	3	3	1	**0**	**2**	**2**	**2**	**2**	**0**	**2**	**0**	**0**	**0**	**0**	**0**	**0**	**0**	**0**	**2**	**0**	**0**	**0**	**0**
922	1	*Mastodonsaurus*	rib	YES	3	3	1		**0**	**0**	**0**	**2**	**0**	**2**	**0**	**0**	**0**	**0**	**0**	**0**	**0**	**0**	**0**	**0**	**0**	**0**	**0**
923	1	*Mastodonsaurus*	vertebral centrum	YES	4	3	2	**1**	**2**	**4**	**2**	**2**	**0**	**2**	**0**	**0**	**0**	**0**	**0**	**0**	**0**	**0**	**0**	**1**	**0**	**0**	**0**
924	5	*Mastodonsaurus*	vertebral centrum	YES	4	3	2	**0**	**0**	**0**	**0**	**0**	**0**	**2**		**0**	**0**	**0**	**2**	**1**	**1**	**1**	**2**	**1**	**0**	**1**	**0**
927	2	*Mastodonsaurus*	flat bone	YES	1	3	1	**0**	**2**	**2**	**0**	**2**	**0**	**2**	**0**	**0**	**0**	**0**	**0**	**0**	**0**	**0**	**2**	**1**	**0**	**0**	**0**
1003		*Tanystropheus*	femur	YES	2	1	2		**2**	**4**	**2**	**2**	**1**	**2**	**0**	**0**	**0**	**0**	**2**	**0**	**1**	**0**	**2**	**1**	**0**	**1**	**2**
1004	1	*Tanystropheus*	humerus	YES	2	1	2		**2**	**2**	**2**	**2**	**1**	**2**	**0**	**1**	**0**	**0**	**2**	**1**	**1**	**1**	**0**	**0**	**0**	**1**	**2**
1013		*Tanystropheus*	rib	NO	3	1	1																				
1026	3	*Tanystropheus*	rib	YES	3	1	1		**0**	**0**	**2**	**2**	**1**	**2**	**0**	**0**	**0**	**0**	**0**	**0**	**0**	**0**	**2**	**0**	**0**	**0**	**0**
1051	1	*Tanystropheus*	vertebra dorsal	YES	4	1	2	**0**	**2**	**1**	**2**	**2**	**0**	**2**	**0**	**0**	**0**	**0**	**2**	**0**	**1**	**0**	**2**	**0**	**0**	**1**	**2**
1061	2	*Tanystropheus*	scapula	YES	1	1	1		**0**	**0**	**2**	**2**	**0**	**2**	**0**	**0**	**0**	**0**	**0**	**0**	**0**	**0**	**2**	**0**	**0**	**0**	**0**
1066	2	*Tanystropheus*	humerus	YES	2	1	2	**0**	**0**	**0**	**2**	**2**	**1**	**2**	**0**	**0**	**0**	**0**	**0**	**0**	**0**	**0**	**2**	**0**	**0**	**0**	**0**
1071	3	*Tanystropheus*	vertebra cervical	YES	2	1	3	**0**	**2**	**2**	**2**	**2**	**1**	**2**	**0**	**1**	**1**	**0**	**0**	**0**	**0**	**0**	**2**	**1**	**0**	**0**	**2**
1090	1	*Tanystropheus*	vertebra cervical	YES	2	1	3		**2**	**3**	**2**	**2**	**1**	**2**	**0**	**1**	**1**	**0**	**2**	**0**	**1**	**1**	**2**	**1**	**1**	**0**	**2**
1091	3	*Tanystropheus*	vertebra dorsal	YES	4	1	2		**2**	**1**	**2**	**2**	**2**	**2**	**0**	**0**	**0**	**0**	**0**	**0**	**0**	**0**	**2**	**0**	**0**	**0**	**0**
1092	3	*Tanystropheus*	rib	NO	3	1	1																				
1093	1	*Tanystropheus*	rib	NO	3	1	1																				
1094	3	*Tanystropheus*	rib	NO	3	1	1																				
1096	3	*Tanystropheus*	rib	YES	3	1	1		**0**	**0**	**2**	**2**	**1**	**2**	**0**	**0**	**0**	**0**	**0**	**0**	**0**	**0**	**2**	**0**	**0**	**0**	**0**
1097	2	*Tanystropheus*	rib	YES	3	1	1	**0**	**2**	**2**	**2**	**2**	**1**	**2**	**0**	**0**	**0**	**0**	**0**	**0**	**0**	**0**	**2**	**0**	**0**	**0**	**0**
1098	2	*Tanystropheus*	coracoid	YES	1	1	1	**0**	**2**	**2**	**2**	**2**	**0**	**2**	**0**	**0**	**0**	**0**	**0**	**0**	**0**	**0**	**0**	**0**	**0**	**0**	**0**
1099	1	*Tanystropheus*	vertebra cervical	YES	2	1	3	**0**	**2**	**0**	**2**	**2**	**0**	**2**	**0**	**1**	**1**	**0**	**2**	**0**	**0**	**1**	**2**	**1**	**1**	**1**	**2**
1100	1	*Tanystropheus*	scapula	NO	1	1	1																				
1108		*Tanystropheus*	rib	YES	3	1	1		**0**	**0**	**0**	**2**	**0**	**2**	**0**	**0**	**0**	**0**	**0**	**0**	**0**	**0**	**0**	**0**	**0**	**0**	**0**
1119	3	*Tanystropheus*	coracoid	YES	1	1	1	**0**	**2**	**3**	**2**	**2**	**0**	**2**	**0**	**0**	**0**	**0**	**0**	**0**	**0**	**0**	**0**	**0**	**0**	**0**	**0**
1141	2	*Tanystropheus*	postcloacal bone	YES	3	1	2		**0**	**0**	**0**	**2**	**0**	**2**	**0**	**0**	**0**	**0**	**2**	**0**	**0**	**0**	**0**	**0**	**0**	**1**	**0**
1154	2	*Tanystropheus*	rib	YES	3	1	1	**0**	**2**	**3**	**2**	**2**	**1**	**2**	**0**	**0**	**0**	**0**	**2**	**1**	**1**	**0**	**2**	**0**	**0**	**1**	**2**
1158	3	*Tanystropheus*	vertebra dorsal	YES	4	1	2		**0**	**0**	**0**	**2**	**0**	**1**	**0**	**0**	**0**	**0**	**2**	**0**	**1**	**0**	**0**	**1**	**1**	**0**	**0**
1160	2	*Tanystropheus*	vertebra caudal	YES	4	1	1	**0**	**2**	**3**	**2**	**2**	**0**	**2**	**0**	**0**	**0**	**0**	**2**	**0**	**0**	**0**	**2**	**1**	**0**	**0**	**2**
1161	1	*Tanystropheus*	rib	YES	3	1	1		**2**		**2**	**2**	**0**	**2**	**0**	**0**	**0**	**0**	**0**	**0**	**0**	**1**	**0**	**0**	**0**	**0**	**0**
1165	1	*Tanystropheus*	coracoid	NO	1	1	1																				
1168		*Tanystropheus*	rib	YES	3	1	1		**2**	**3**	**2**	**2**	**0**	**2**	**0**	**0**	**0**	**0**	**2**	**0**	**0**	**0**	**2**	**0**	**0**	**1**	**2**
1169	2	*Tanystropheus*	humerus	YES	2	1	2		**0**	**0**	**1**	**1**	**0**	**1**	**0**	**0**	**0**	**0**	**0**	**0**	**0**	**0**	**2**	**0**	**0**	**0**	**0**
1185	1	*Tanystropheus*	humerus	YES	2	1	2		**2**		**2**	**2**	**0**	**2**	**0**	**0**	**0**	**0**	**2**	**0**	**1**	**0**	**2**	**1**	**0**	**1**	**0**

Scoring: Miedary layer: 1 – M1; 2 – M2a; 3 – M2b; 4 – M3; 5 – M4. Element shape: 1 – flat bone; 2 – massive long bone; 3 – delicate long bone; 4 – compact bones. Pore size: 1 – only small nutrient foramina; 2 – one or more larger foramina; 3 – neural canal openings (*Tanystropheus* cervical vertebra). Glauconite weathering stage: 0 – absent; 1 – mixed evolved absent; 2 – mixed evolved present; 3 – mixed weathered present; 4 – mixed higly weathered present.

POLSKA AKADEMIA NAUK
INSTYTUT PALEOBIOLOGII
im. Romana Kozłowskiego

ul. Twarda 51/55, 00-818 Warszawa
phone: (4822) 697-88-50; fax: (4822) 620-62-25
e-mail address: paleo@twarda.pan.pl; http://www.paleo.pan.pl

Warszawa, 20 marca 2026 r.

Adam Rytel
Instytut Paleobiologii PAN
Twarda 51/55
00-818 Warszawa
adam.rytel@twarda.pan.pl

OŚWIADCZENIE / DECLARATION

Rozprawa pod tytułem „Osteologia, tryb życia i biomotoryka triasowego archozauromorfa *Tanystropheus* z Miedar" składa się z czterech rozdziałów. Jestem jedynym autorem pierwszego rozdziału. Pozostałe trzy są rozdziałami współautorskimi, a mój wkład w każdy z nich został wyszczególniony na kolejnych stronach niniejszego oświadczenia

This dissertation titled "Osteology, lifestyle, and biomechanics of the Triassic archosauromorph *Tanystropheus* from Miedary" consists of four chapters. I am the sole author of the first chapter. The remaining three chapters are co-authored, and my contribution to them was specified in the following pages of this declaration.

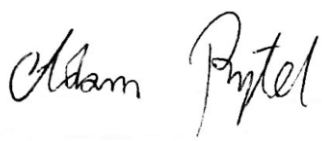

Adam Rytel

Rozdział II/Chapter II

Rozdział II powstał we współpracy z Dawidem Surmikiem (Uniwersytet Śląski w Katowicach), Tomaszem Szczygielskim (Instytut Paleobiologii PAN), Stephanem Spiekmanem (Staatliches Museum für Naturkunde Stuttgart), Torstenem Scheyerem (University of Zurich), Thomasem van de Kampem i Marcusem Zuberem (obaj z Karlsruhe Institute of Technology).

Projekt powstał częściowo na bazie danych tomograficznych i histologicznych *Protanystropheus antiquus* pozyskanych przez D. Surmika i T. Szczygielskiego, a także dwóch okazów *Tanystropheus conspicuus* zeskanowanych przy użyciu tomografii komputerowej przez T. van de Kampa, S. Spiekmana i M. Zubera. Wszystkie pozostałe dane powstały z mojej inicjatywy i pod moją koordynacją (zgłady, szlify histologiczne, skany tomograficzne, ilustracja z Figury 11), lub zostały utworzone przeze mnie (zdjęcia i modele okazów). Byłem autorem wszystkich Figur poza 4 i 11, a także całego tekstu manuskryptu poza częścią opisów histologicznych. Część danych porównawczych została pozyskana w czasie mojego stażu w Zurychu pod opieką T. Scheyera. Wszyscy autorzy uczestniczyli w dyskusji nad interpretacją uzyskanych wyników i nanieśli poprawki do tekstu i figur.

Chapter II was developed in collaboration with Dawid Surmik (University of Silesia in Katowice), Tomasz Szczygielski (Institute of Paleobiology PAS), Stephan Spiekman (Staatliches Museum für Naturkunde Stuttgart), Torsten Scheyer (University of Zurich), Thomas van de Kamp and Marcus Zuber (both from Karlsruhe Institute of Technology).

The project was partly based on tomographic and histological data of *Protanystropheus antiquus* obtained by D. Surmik and T. Szczygielski, as well as on two specimens of *Tanystropheus conspicuus* scanned using computed tomography by T. van de Kamp, S. Spiekman, and M. Zuber. All remaining data were generated on my initiative and under my coordination (thin sections, histological slides, tomographic scans, and the illustration in Figure 11), or were produced by me (photographs and specimen models). I was the author of all figures except Figures 4 and 11, as well as the entire manuscript text except for part of the histological descriptions. Some of the comparative data were obtained during my research stay in Zurich under the supervision of T. Scheyer. All authors participated in discussions on the interpretation of the results and contributed to the text and figures.

Oświadczam, że mój wkład w przygotowaniu rozdziału wynosi około 70%.

I declare that my contribution to the chapter is approximately 70%.

Podpisy współautorów / signatures of the co-authors:

Dawid Surmik 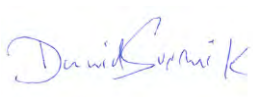

Tomasz Szczygielski 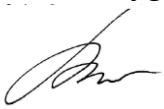

Stephan Spiekman 

Torsten Scheyer 

Thomas van de Kamp 

Marcus Zuber 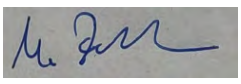

Rozdział III/Chapter III

Rozdział III powstał we współpracy z Pashą van Bijlertem (Utrecht University), Stephanem Lautenschlagerem (University of Birmingham), Stephanem Spiekmanem (Staatliches Museum für Naturkunde), Mateuszem Tałandą (Uniwersytet Warszawski) i Tomasz Sulej (Instytut Paleobiologii PAN).

Projekt rozpocząłem z własnej inicjatywy. Wyselekcjonowałem okazy które zostały użyte w modelu (poza czaszką, a także pierwszym, drugim i jedenastym kręgiem), koordynowałem ich preparację i stworzyłem ich modele. Część analityczna została zaplanowana przede mnie, P. van Bijlerta i S. Lautenschlagera. S. Lautenschlager utworzył pierwszą wersję modelu, która później modyfikowana była przeze mnie, pod opieką P. van Bijlerta. Analizy zasięgu ruchu szyi wykonałem samemu, korzystając z narzędzi autorstwa P. van Bijlerta. Analizy elementów skończonych przeprowadził S. Lautenschlager. Byłem autorem wszystkich figur i praktycznie całości tekstu manuskryptu. Wszyscy autorzy uczestniczyli w dyskusji nad interpretacją uzyskanych wyników i nanieśli poprawki do tekstu i figur.

Chapter III was developed in collaboration with Pasha van Bijlert (Utrecht University), Stephan Lautenschlager (University of Birmingham), Stephan Spiekman (Staatliches Museum für Naturkunde), Mateusz Tałanda (University of Warsaw), and Tomasz Sulej (Institute of Paleobiology PAS).

I initiated the project on my own initiative. I selected the specimens used in the model (except for the skull and the first, second, and eleventh vertebrae), coordinated their preparation, and created their models. The analytical part was planned by P. van Bijlert, S. Lautenschlager, and myself. S. Lautenschlager created the first version of the model, which was later modified by me under the supervision of P. van Bijlert. I performed the neck range of motion analyses myself using tools developed by P. van Bijlert. The finite element analyses were conducted by S. Lautenschlager. I was the author of all figures and virtually the entire manuscript. All authors participated in discussions on the interpretation of the obtained results and contributed to the text and figures.

Oświadczam, że mój wkład w przygotowaniu rozdziału wynosi około 60%.

I declare that my contribution to the chapter is approximately 60%.

Podpisy współautorów / signatures of the co-authors:

Pasha van Bijlert 

Stephan Lautenschlager 

Stephan Spiekman 

Mateusz Tałanda 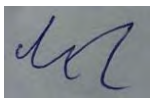

Tomasz Sulej 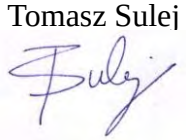

Rozdział IV/Chapter IV

Rozdział IV powstał we współpracy z Wojciechem Pawlakiem (Uniwersytet Warszawski), Maciejem Rucińskim (University of Oslo), Eudaldem Mujalem (Staatliches Museum für Naturkunde Stuttgart) i Pawłem Bącalem (Instytut Paleobiologii PAN).

Projekt powstał z inicjatywy mojej i W. Pawlaka. Dokonałem selekcji analizowanych okazów, koordynowałem ich preparację i utworzenie z nich szlifów, a także wykonałem ich zdjęcia. M. Ruciński zaprojektował macierz danych i jej analizę. Ja, W. Pawlak i M. Ruciński wspólnie uzupełniliśmy macierz. P. Bącal przeprowadził obrazowanie przy użyciu skaningowego mikroskopu elektronowego. E. Mujal porównał uzyskane wyniki z danymi dostępnymi dla stanowisk niemieckich podobnych do Miedar. Utworzyłem Figury 1–6 i znaczną część tekstu manuskryptu. Porównanie cech tafonomicznych przeprowadzili przede wszystkim W. Pawlak i M. Ruciński. Wszyscy autorzy uczestniczyli w dyskusji nad interpretacją uzyskanych wyników i nanieśli poprawki do tekstu i figur.

Chapter IV was developed in collaboration with Wojciech Pawlak (University of Warsaw), Maciej Ruciński (University of Oslo), Eudald Mujal (Staatliches Museum für Naturkunde Stuttgart), and Paweł Bącal (Institute of Paleobiology PAS).

The project was initiated by W. Pawlak and myself. I selected the specimens analysed in the study, coordinated their preparation and the production of thin sections, and took their photographs. M. Ruciński designed the data matrix and its analysis. W. Pawlak, M. Ruciński, and I jointly completed the matrix. P. Bącal performed imaging using a scanning electron microscope. E. Mujal compared the obtained results with data available from German sites similar to Miedary. I created Figures 1–6 and a substantial portion of the manuscript text. The comparison of taphonomic features was carried out primarily by W. Pawlak and M. Ruciński. All authors participated in discussions on the interpretation of the obtained results and contributed to the text and figures.

Oświadczam, że mój wkład w przygotowaniu rozdziału wynosi około 40%.

I declare that my contribution to the chapter is approximately 40%.

Podpisy współautorów / signatures of the co-authors:

Wojciech Pawlak	Maciej Ruciński	Eudald Mujal	Paweł Bącal